Characterising CG5846 (Peep) in *Drosophila melanogaster* neural function

A thesis presented in partial fulfilment of the requirements for the degree of

Doctor of Philosophy
in
Biochemistry

at Massey University, Manawatū,
New Zealand

Sarah Jean Wilson
2024

Abstract

Histone deacetylase 4 (HDAC4) is a transcriptional regulator that has been implicated in a number of neurodevelopmental and neurodegenerative diseases that are associated with intellectual disability, cognitive defects, and/or memory loss. Both the accumulation of nuclear HDAC4 and its loss-of-function have been linked to these conditions, therefore exploring HDAC4's role in neuronal function is essential to understand the molecular mechanisms underlying these diseases.

In *Drosophila*, overexpression of HDAC4 results in defects in morphogenesis of axons in the mushroom body, a structure essential for memory formation, as well as long-term memory defects and disruption to the development of the compound eye. The molecular mechanisms underlying these HDAC4-induced phenotypes are currently unknown. RNA-sequencing on fly heads in which HDAC4 was overexpressed has previously been performed and showed few genes were transcriptionally regulated by HDAC4. In addition, an enhancer/suppressor rough eye phenotype screen has also been performed which identified a number of genes that interact genetically in the same molecular pathway as *HDAC4*.

To further investigate the molecular mechanisms underlying HDAC4 dysfunction, an RNA interference (RNAi) based candidate screen for potential HDAC4-interactors was performed, which involved quantification of developmental defects in the mushroom body and eye following RNAi knockdown of each candidate. It was hypothesised that if a phenotype resulting from RNAi knockdown was similar to that induced by HDAC4 overexpression, that candidate may function in similar molecular pathways. A single candidate-interactor was selected (CG5846, named Peep) for further investigation. On overexpression, Peep and HDAC4 co-distribute in nuclei of mushroom body neurons, however no physical interaction was detected. Furthermore, overexpression of Peep did not rescue the HDAC4-induced mushroom body or eye defects.

Due to the uncharacterised nature of Peep, a thorough investigation was performed to assess the importance of Peep in survival, longevity, motor function, brain development, courtship learning and memory, and wing development. Peep was observed to be essential for survival of glial cells and for normal mushroom body development, which warrants further investigation.

Reduced expression of Peep also resulted in a unique severe necrotic eye phenotype, and through this, Peep was shown to play a potential role in processes involved in regulating mitochondrial and proteasomal function, apoptosis and oxidative stress.

These data provide the first documented characterisation of the functional role of Peep in *Drosophila* development and provide the basis for further investigation into the underlying molecular mechanisms involved in mushroom body and eye development.

Acknowledgements

I would first and foremost like to express my gratitude to my main supervisor, Dr Helen Fitzsimons. I am beyond grateful for the opportunity to have worked on this project and all the experiences that have come along with it. Your support, guidance, and enthusiasm for the research we do has been instrumental in helping me become the Scientist I am today. The depth of your knowledge and understanding is inspiring, and I cannot thank you enough for everything you have done and continue to do, and needless to say it has been an absolute pleasure to be a part of your lab over the course of my post-graduate career.

To my co-supervisor Dr Tracy Hale, thank you for all your feedback over the years, your outside perspective on this subject has been invaluable.

To the past members of the Neurogenetics Lab Group, Ana, Maddie, Patrick, Raoul, and Wei, thank you for your feedback during lab meetings, your comments and suggestions were greatly appreciated.

A special shout out to Hannah, my lab twin look-a-like, I really could not have gotten through these last years without your support, feedback, and camaraderie, I couldn't have asked for a better person to cross that finish line with. It has been a pleasure to have you as a friend both inside and outside of the lab, from conferences to movie days, wedding dress shopping and cake decorating (which has gotten significantly better over the course of the many creative cake pursuits), we have gone through and accomplished a lot together.

Aseel, thanks for being someone I can count on to brighten my day, you're always ready with a new one-liner, and you made wedding dress shopping a blast.

I would like to thank the Dr Matthew Savoian and the team at the Manawatu Microscopy and Imaging Centre for maintaining the equipment and patience with the old confocal microscope, without which, a significant proportion of the data in this thesis would not have been possible.

To the past members of the admin team, thank you for all that you did during my time here, you made the school run smoothly and getting stationary or a room key was always paired with a friendly chat.

Acknowledgements

To Massey University in which I was fortunate to receive a Massey University Māori Doctoral Scholarship which has funded my studies over the past 3 years and a Massey University Travel Grant to attend the Asia Pacific *Drosophila* Research Conference 2023 in Cairns Australia, which was informative and exciting to present my research to the wider *Drosophila* community.

To my family and friends, thank you for always being around when I needed advice or just a good distraction, for always being proud of me and your endless love and support.

Last but certainly not least I would like to thank my wonderful loving and patient fiancée, soon to be husband, Glen. Your support and encouragement of my career pursuits have been immeasurable. Your hard work and dedication to work and life is inspiring and I cannot thank you enough for all that you do, and I am beyond excited to see what the next chapter of our future holds.

This project was funded by the Royal Society New Zealand Marsden Fund.

Table of Contents

List of Figures

List of Tables

Abbreviations

AD	Activation domain
ADHD	Attention Deficit Hyperactivity Disorder
Adj P	Adjusted P value
AF	Antennal field
AGO2	Argonaute2
AIS	Axon initial segment
AL	Antennal lobe
AMC	7-amino-4-methylcoumarin
Ank2	Ankyrin2
ANKRA2	Ankyrin repeat family A member 2
AOUT	Anterior optic tubercle
APF	After pupal formation
APP	Amyloid Precursor Protein
ARBD	Ankyrin repeat binding domain
Arm	Armadillo
ASD	Autism Spectrum Disorder
ATM	Ataxia telangiectasia mutated
ATP	Adenine triphosphate
AVLP	Anterior ventrolateral protocerebrum
BDSC	Bloomington *Drosophila* Stock Centre
B	Bristle cell
Bl	*Bristle*
BLS	Bare lymphocyte syndrome
BMP	Bone morphogenetic protein
bp	Base pair
brp	Bruchpilot
C	Cone cell
Ca^{2+}	Calcium
CaMKII	Calcium/calmodulin-dependent kinase II
cAMP	Cyclic AMP
CBP	CREB binding protein

CCAP	Crustacean cardioactive peptide
Cdkl5	Cyclin dependent kinase-like 5
Cer	Crammer
CI	Courtship index
cm	Centimetre
CO_2	Carbon dioxide
Co-IP	Co-immunoprecipitation
Coq8	Coenzyme Q8
CPEB	Cytoplastic polyadenylation element-binding protein
CREB	cAMP response element-binding protein
CS	Canton Special
cVA	cis-vaccenyl acetate
CyO	*Curly of Oster*
Da	Daughterless
DBD	DNA binding domain
Dcp-1	Death caspase-1
dEGFR	*Drosophila* Epidermal Growth Factor Receptor
dfmr1	*Drosophila* fragile-X mental retardation1
dH_2O	Distilled water
DIAP1	Death-associated inhibitor of apoptosis-1
Dlg-1	Disc-large 1
DmHDAC4	*Drosophila* HDAC4
DMSO	Dimethylsulfoxide
DNA	Deoxyribonucleic acid
DopR1	Dopamine receptor R1
Dpp	Decapentaplegic
Drice	Death related ICE-like caspase
Dronc	Death regulator Nedd2-like caspase
dsDNA	Double stranded DNA
DSHB	Developmental Studies Hybridoma Bank
EDTA	Ethylenediaminetetraacetic acid
EF	Eye field
EGFP	Enhanced GFP
Eh	Eclosion hormone

Elav	Embryonic lethal abnormal visual system
En	Engrailed
ERM	Ezrin-radixin-moesin
EtBr	Ethidium bromide
ETC	Electron transport chain
Eth	Ecdysis-triggering hormone
ex/em	excitation/emission
Ey	Eyeless
FasII	FasciclinII
Foxo	Forkhead box, sub-group O
fwd	Forward
g	Gram
$GAL80^{ts}$	Temperature sensitive GAL80
GC3Ai	GFP-based variant of caspase 3-like proteases activity indicator
GFP	Green fluorescent protein
GMR	Glass multimer reporter
GNG	Gnathal ganglia
H_2O_2	Hydrogen peroxide
HAT	Histone acetyl transferase
HDAC	Histone deacetylase
$HDAC4^{\Delta Ank}$	*Drosophila* HDAC4 with mutated Ankyrin repeat binding domain
$HDAC4^{3SA}$	*Drosophila* nuclear-restricted HDAC4 mutant
$HDAC4^{WT}$	*Drosophila* wild-type HDAC4
HDAC4	Histone deacetylase 4
HsHDAC4	Human HDAC4
Hid	Head involution defective
HRP	Horseradish peroxidase
Hz	Horizontal secondary pigment cell
IHC	Immunohistochemistry
IP	Immunoprecipitation
IPC	Interommatidial pigment cell
JNK	c-Jun N-terminal kinase
KAc	Potassium acetate
kb	Kilobase

KC	Kenyon cell
kDa	Kilodalton
Kdm5	Lysine demethylase 5
Kek2	Kekkon 2
Kra	Krasavietz
L	Litre
L1-CAM	L1 cell adhesion molecule
LI	Learning index
LTM	Long-term memory
M	Molar
Marf	Mitochondrial associated regulatory factor
MAPK	Mitogen-activated protein kinase
MEF2	Myocyte enhancer factor 2
MF	Morphogenetic furrow
Mg^{2+}	Magnesium
mg	Milligram
MHC	Major histocompatibility complex
MI	Memory index
mL	Millilitre
mM	Millimolar
mm	Millimetre
MND	Motor neuron disease
Moldex	methyl 4-hydroxybenzoate
MPP+	1-methyl-4-phenylpyridinium
MPPP	1-methyl-4-phenyl-4-propionoxypiperdine
MPTP	1-methly-4-phenyl-1,2,3,6-tetrahydropyridine
mRNA	Messenger RNA
ms	Millisecond
Mthl8	Methuselah-like 8
n	Number
N-CoR	Nuclear receptor co-repressor
NES	Nuclear export sequence
NetB	Netrin-B
NIID	Neuronal intranuclear inclusion disease

NLS	Nuclear localisation sequence
nm	Nanometre
NMDAR	N-Methyl-D-Aspartic acid receptors
NPC2	Niemann-Pick Type C2
Npc2g	Niemann-Pick type C-2g
nSyb	neuronal Synaptobrevin
nt	Nucleotides
Ob	Oblique secondary pigment cell
OL	Optic lobe
ORF	Open reading frame
OS	Optic stalk
PBS	Phosphate buffered saline
PCR	Polymerase chain reaction
$Peep^{OE}$	Overexpression of Peep
PENP	Periesophageal
Per	Period
PI	Pars intercerebralis
Pink1	PTEN-induced kinase 1
PKA	Protein kinase A
PMSF	Phenylmethylsulfonyl fluoride
PP2A	Protein phosphatase 2A
PPL1	Posterior inferiolateral protocerebrum
PPL3	Posterior lateral protocerebrum
PPM	Posterior inferiomedial protocerebrum
PPM1	Posterior superiomedial protocerebrum
PSLPNI	Ankyrin repeat binding motif
R	Rhabdomere
Repo	Reversed polarity
rev	Reverse
RFXANK	Regulatory factor X associated ankyrin containing protein
RISC	RNA-induced silencing complex
RNA	Ribonucleic acid
RNAi	RNA interference
RNA-seq	RNA-sequencing

ROS	Reactive oxygen species
Rpd3	Reduced potassium dependency 3
Rpm	Revolutions per minute
Rpn	Regulatory particle of non-ATPase
Rpr	Reaper
Rpt	Regulatory particle of triple-ATPase
RT-qPCR	Reverse-transcriptase quantitative PCR
Sb	*Stubble*
Sco	*Scutoid*
SDS-PAGE	Sodium dodecyl sulfate-polyacrylamide gel electrophoresis
SEM	Standard error of the mean
Ser	Serrated
Sev	Sevenless
SEZ	Suboesophageal zone
Shn	Schnurri
Sik3	Salt-inducible kinase 3
siRNA	Short interfering RNA
SMA	Spinal muscular atrophy
SMN	Survival motor neuron
SMP	Superior medial protocerebrum
SMRT	Silencing mediation for retinoid and thyroid hormone receptor
SOD1	Superoxide dismutase 1
STM	Short-term memory
Suc-LLVY-AMC	N-succinyl-leucine-leucine-valine-tyrosine-7-amino-4-methylcoumain
TARGET	Temporal and regional gene expression targeting
Tb	*Tubby*
TM2	*Third Multiple 2*
TM3	*Third Multiple 3*
TM6B	*Third Multiple 6B*
TNF	Tumour necrosis factor
Tub	Tubulin
UAS	Upstream activating sequence
UTR	Untranslated region
V	Volts

v	Volume
VDRC	Vienna *Drosophila* Resource Centre
VM	Ventral medial
w	Weight
w+	mini-*white* gene
WB	Western blot
w(CS10)	White Canton Special
YFP	Yellow fluorescent protein
°C	Degrees Celsius
1°	Primary
2°	Secondary
3°	Tertiary
α	Alpha
α’	Alpha prime
β	Beta
β’	Beta prime
γ	Gamma
µg	Microgram
µL	Microlitre
µm	Micrometre

1 Introduction

1.1 Neurodevelopmental and neurodegenerative disorders

The proper functioning of the central nervous system relies on precise regulatory mechanisms that coordinate the organisation of neurons into complex neuronal networks. Genetic and epigenetic dysregulation of these processes can result in abnormalities and impairments, giving rise to neurodevelopmental and neurodegenerative disorders.

Neurodevelopmental disorder is an umbrella term for a wide range of neurological conditions primarily characterised by impairments in cognition, motor skills, communication, and behaviour. Such disorders include autism spectrum disorder (ASD), attention deficit hyperactivity disorder (ADHD), and intellectual disability (American Psychiatric Association, 2013).

Neurodegenerative disease is characterised by the progressive dysfunction and death of particular neuronal cell populations, resulting in clinical symptoms such as impaired motor function and loss of cognitive abilities. Alzheimer's and Parkinson's diseases are the most prevalent disorders (Neugroschl & Wang, 2011; Spillantini *et al.*, 1998), however there are many other well-known disorders that fall under the neurodegenerative disorder umbrella, including Huntington's disease (MacDonald *et al.*, 1993; Ridley *et al.*, 1991) and Amyotrophic Lateral Sclerosis (Masrori & Van Damme, 2020).

There are a few neurodegenerative disorders that have a well-established genetic cause, one example being Huntington's disease, which is caused by familial inheritance of a mutated form of the *huntingtin* gene (MacDonald *et al.*, 1993; Ridley *et al.*, 1991). The majority of neurodegenerative disorders are thought to be caused by a combination of genetic, epigenetic, and environmental factors that together contribute to the manifestation of neuropathological phenotypes. At a molecular level, neurodegenerative disease results from multiple molecular alterations within neurons, including mitochondrial dysfunction, synaptic dysfunction, and impaired protein clearance via aberrant accumulation of misfolded proteins leading to degeneration of specific neuronal cell populations, increased ubiquitination, oxidative stress induced apoptosis, and inflammation (Atkin & Paulson, 2014; Giasson *et al.*, 2000; Taylor *et al.*, 2002).

Dementia is the most common form of neurodegenerative disease with an individual developing dementia every 3 seconds. According to the World Alzheimer's Report of 2021, across the globe approximately 55 million individuals are living with dementia; costing an estimated total of $1.3 trillion USD worldwide. By 2030 this number is expected to reach 78 million, costing an estimated $2.8 trillion USD (Gauthier *et al.*, 2021), with the number of individuals almost tripling to 152 million by 2050 (Patterson, 2018).

Of particular interest for New Zealand, the prevalence of dementia has been shown to disproportionally increase in Māori compared to Europeans, and due to an ever-ageing population, the predicted number of Māori aged 65 years and over is set to increase by 197%, compared to the 59% increase for Europeans in the same age bracket between the years 2018 and 2043 (*National ethnic population projections, by age and sex, 2018(base)-2043*). An Alzheimers New Zealand report in 2016 identified that of the total population diagnosed with dementia, 5.1% were Māori and this figure is predicted to increase to 8% by 2038 (*Dementia economic impact report 2016*, 2017). A recent study from datasets across New Zealand between the years 2016 and 2020, at age 60+ and 80+, Māori have a 34-46% and 16-29% higher prevalence of dementia in each age group respectively compared to Europeans (Cheung *et al.*, 2022). Furthermore, Māori on average are 7.4 years younger when diagnosed with Dementia compared to Europeans (Ma'u *et al.*, 2022).

Alzheimer's disease is the most common form of dementia worldwide and is associated with progressive neurodegeneration (Neugroschl & Wang, 2011). Clinical hallmarks of this disease include intracellular neurofibrillary hyperphosphorylated tau tangles, extracellular amyloid beta (Aβ) plaques, a loss of neurons and synapses, neuroinflammation, and ultimate cell death (Alonso *et al.*, 1996; Alzheimer, 1907; Shen *et al.*, 2016; Taylor *et al.*, 2002). Tau is a protein localised to the axon where it facilitates axon transport and microtubule assembly and stability. During Alzheimer's disease progression, Tau translocates to the somatodendritic region of the neuron and becomes hyperphosphorylated resulting in neurofibrillary aggregated tangles (Alonso *et al.*, 1996; Li & Gotz, 2017). Short Aβ peptides, which include Aβ40 and Aβ42, are derived from the amyloid precursor protein (APP) and are secreted into the brain's extracellular space as soluble molecules. Accumulation of these peptides result in oligomers that are unable to be removed by the vascular system and therefore form insoluble toxic plaques (Brothers *et al.*, 2018) with Aβ42 implicated as the more pathological species in Alzheimer's disease (Miller *et al.*, 1993).

Lewy body diseases encompass a range of genetic disorders, a hallmark of which is the presence of Lewy bodies, which are cytoplasmic neuronal inclusions (Spillantini *et al.*, 1998). Parkinson's disease is described as a Lewy body neurodegenerative disorder, phenotypically characterised by a loss of motor function and coordination, tremor and the onset of dementia, with clinical features that include Lewy body inclusions, neuronal α-synuclein deposits, and neuroinflammation (Polymeropoulos *et al.*, 1997), all of which ultimately contribute to death of dopaminergic neurons in the substantia nigra, a region of the brain that controls movement (Przedborski, 2005). As there is currently a lack of treatments for neurodevelopmental and neurodegenerative diseases, research that increases understanding of the molecular mechanisms which underly these disorders is imperative.

1.1.1 Glia play pivotal roles in supporting neuronal health and in neurodegenerative disease

Glia are non-neuronal cells of the central and peripheral nervous systems that play important roles in maintaining the health of neurons. In the context of neurodevelopmental and neurodegenerative disorders, glia are increasingly recognised for their role in supporting the formation and maintenance of the central nervous system as well as in disease progression (Rahman *et al.*, 2022). Glia maintain and support neuronal function by providing cues through the secretion of neurotropic factors for neuronal conduction, axon guidance, neurotransmitter recycling, cell morphology, and the overall maintenance of homeostasis. The central nervous system is composed of two main types of glia, microglia and macroglia. Microglia comprise 7% of all non-neuronal cells in the mammalian brain (Dos Santos *et al.*, 2020) and are distributed non uniformly throughout the central nervous system (Lawson *et al.*, 1990). Microglia play a role in immune response whereby quiescent microglia are activated upon central nervous system injury, including infection and neurodegenerative disease. Microglia activation results in a proinflammatory response and release of cytokines from neighbouring cells (Yang *et al.*, 2010). Microglia also have a role in regulating brain development and neuronal network connectivity by shaping neuronal synapses (Roumier *et al.*, 2004; Wake *et al.*, 2009) by engaging in synaptic pruning through the process of trogocytosis of synaptic material (Paolicelli & Gross, 2011; Weinhard *et al.*, 2018).

Synaptic pruning is important in generating mature synapses to maintain synaptic plasticity, an essential process for memory acquisition and consolidation (Guan *et al.*, 2002). Synaptic pruning by trogocytosis (Weinhard *et al.*, 2018) during synapse establishment and elimination is associated with maintaining synaptic transmission and neuronal network connectivity. In a mouse model, dysfunction of synaptic pruning, due to a loss of microglia, resulted in a decline in brain function, impaired social interactions, and an increase in the time spent grooming, which represents an increase in repetitive behaviours (Zhan *et al.*, 2014), all of which have been previously associated with neurodevelopmental disorders, specifically ASD (American Psychiatric Association, 2013).

Central nervous system macroglia contain two main subgroups: astrocytes and oligodendrocytes. Star-shaped astrocytes play major roles in neurotransmission by regulating the balance between neurotransmitter uptake and release. Glutamate is the most studied excitatory neurotransmitter in the central nervous system and glutamate release is important for normal neuronal activity. However, excess glutamate can result in neuronal hyperexcitation, leading to neuronal death, therefore maintaining the balance of glutamate uptake and release by astrocytes is important in regulating neurotransmission (Mahmoud *et al.*, 2019).

The primary function of oligodendrocytes is myelination of axons, which generates electrical insulation to aid in propagation of action potentials and reduces ion leakage from axons (Tasaki, 1939). Oligodendrocytes develop predominantly during embryogenesis, from oligodendrocyte progenitor cells, the characteristics of which persist in the adult brain (Bergles & Richardson, 2015). Oligodendrocytes are only present in the central nervous system, whereas Schwann cells, which retain the same capacity for axon myelination, are predominantly localised to the peripheral nervous system. Upon damage, resulting in axon demyelination and destruction of both oligodendrocytes and astrocytes in the central nervous system, Schwann cells have been shown to spontaneously invade the central nervous system and remyelinate axons (Blakemore, 1975).

Glia have been implicated in neurodegenerative diseases such as Parkinson's and Alzheimer's disease, and multiple sclerosis. The predominant hallmark of Parkinson's disease is the generation and accumulation of pathogenic α-synuclein deposits, which activates microglia, resulting in an exacerbated neuroinflammatory response, leading to the release of cytotoxic factors and an increase in reactive oxygen species (ROS), eventuating in dopaminergic neuronal cell death and Parkinson's disease progression (Cinar *et al.*, 2022). In astrocytes, the

physiological level of α-synuclein is low. A Parkinson's disease mouse model inducing an accumulation of α-synuclein lead to astrocyte uptake of α-synuclein deposits and the generation of toxic inclusions. This resulted in disruption to normal astrocyte function, activation of microglia and subsequent inflammatory response, dopaminergic and motor neuron cell death, and paralysis. These results provide an example of non-autonomous neuronal cell death due to astrocyte-specific α-synuclein accumulation (Gu *et al.*, 2010).

Accumulation of Aβ is a clinical hallmark of Alzheimer's disease, and similarly to the accumulation of α-synuclein deposits in Parkinson's disease, rapid and continuous accumulation of Aβ results in prolonged uncontrollable microglia activation, leading to neuroinflammation, synaptic dysfunction, and neuronal degradation, all of which are characteristics associated with Alzheimer's disease (Zhang *et al.*, 2021).

Multiple sclerosis is a debilitating autoimmune neurodegenerative disease of the central nervous system with varied effects on both movement (Ghosh *et al.*, 2022) and cognitive function (Chiaravalloti & DeLuca, 2008). The most common clinical hallmark of multiple sclerosis is demyelination and degradation of the myelin sheath, which insulates the axon to provide strength and rapid action potential propagation, and occurs due to inflammatory lesions and demyelinating plaques (Frohman *et al.*, 2006). Oligodendrocytes myelinate axons and are therefore targeted for disease pathogenesis (Tasaki, 1939). It has recently been hypothesised that oligodendrocyte dysfunction may also be implicated in both Parkinson's and Alzheimer's disease due to either accumulation of α-synuclein or Aβ in oligodendrocytes. This then could result in activation of microglia and astrocytes, leading to demyelination of axons, disease progression, and cognitive decline (Han *et al.*, 2022).

1.2 Mechanisms of learning and memory

A common clinical feature of many neurodevelopmental and neurodegenerative disorders is cognitive dysfunction that manifests as impairments in learning and memory consolidation and recall (Budson, 2009; Y. Li *et al.*, 2019). Learning is the acquisition of information from environmental surroundings, whereas memory is the process of storing this information for later retrieval (Bailey & Kandel, 1993), both of which require transmission of electrochemical signals between neurons.

A neuron is composed of a nucleus-containing cell body, dendrites, and axon. The axon is a long synaptic structure, and the basic process of neurotransmission involves initiation of an action potential, at the axon initial segment (AIS), in response to a stimulus (Foust *et al.*, 2010). This action potential propagates down the axon to the presynaptic axon terminal and triggers an influx of calcium (Ca^{2+}) into the presynaptic terminal via voltage gated Ca^{2+} channels, resulting in movement and fusion of synaptic vesicles to the plasma membrane and the release of a neurotransmitter into the synaptic cleft, which is the junction between the presynaptic terminal of one neuron and postsynaptic terminal of a second neuron (Sudhof & Malenka, 2008). The neurotransmitter then binds to receptors on the postsynaptic dendrite of the following neuron (Sidiropoulou *et al.*, 2006), which alters the membrane potential and if the membrane is depolarised sufficiently, this triggers a new action potential (Reece *et al.*, 2014; van der Kloot & Kita, 1974) (Figure 1.1).

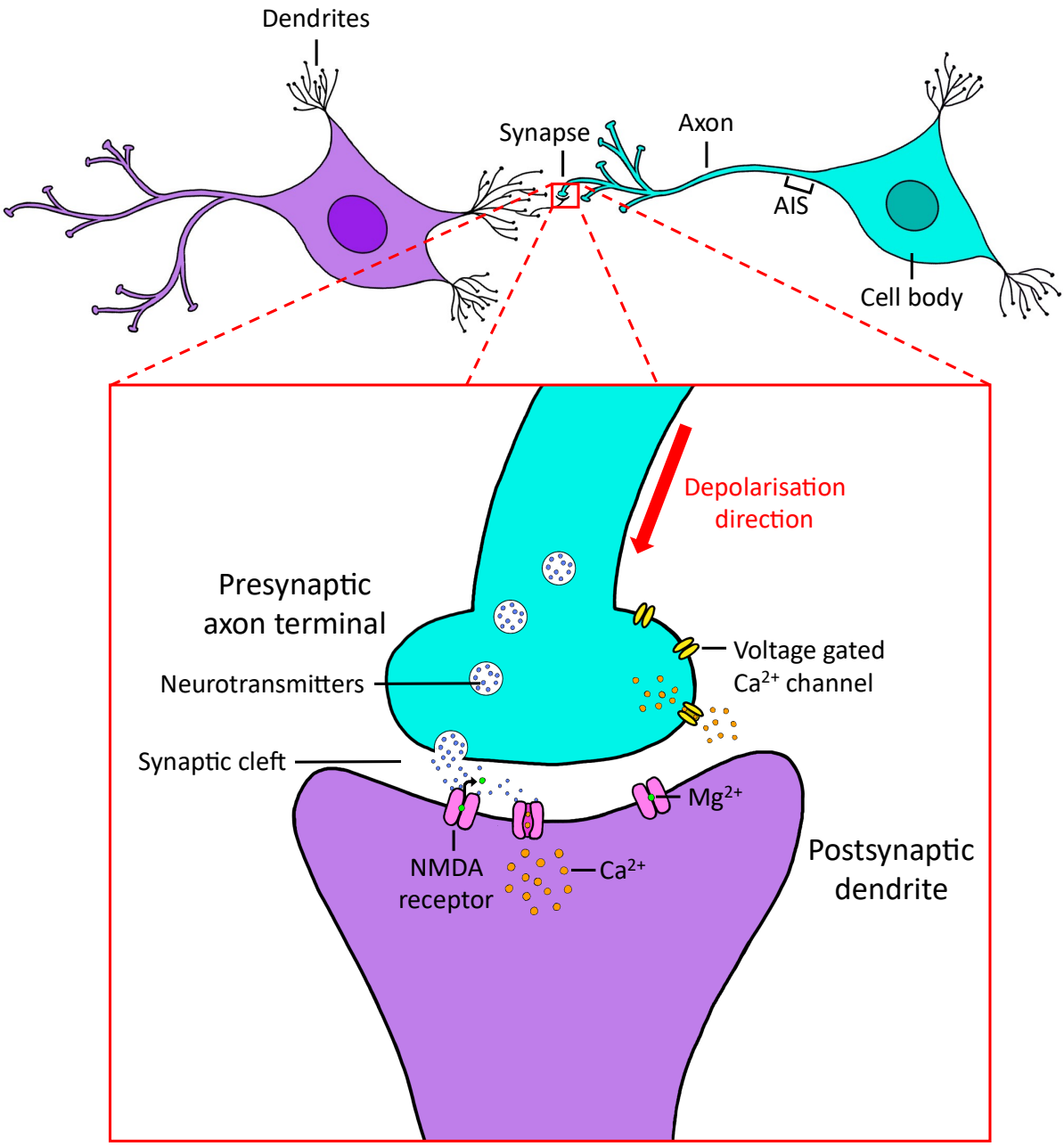

Figure 1.1. Synaptic connection between an axon and dendrite. Neurotransmitters enter the presynaptic terminal where they are bundled into synaptic vesicles. These neurotransmitters are released into the synaptic cleft following membrane depolarisation caused by the firing of an action potential which is initiated at the AIS and triggers the voltage-gated Ca^{2+} channels to open and flood the presynaptic terminal with Ca^{2+} ions. This flood of Ca^{2+} leads to movement and fusion of the synaptic vesicles to the plasma membrane, resulting in the release of neurotransmitters into the synaptic cleft which bind to NMDA receptors on the postsynaptic dendrite, leading to membrane depolarisation and firing of a subsequent action potential. Neurotransmitter binding also causes displacement of Mg^{2+} allowing for Ca^{2+} to flood the postsynaptic dendrite resulting in activation of downstream gene transcription pathways. AIS = Axon initial segment, Ca^{2+} = calcium, Mg^{2+} = magnesium. *Original figure created with reference to Barco et al. (2006); Sudhof and Malenka (2008).*

Learning occurs when the initial action potential results in an increase in neurotransmitter release (ie. an increased postsynaptic response), which is referred to as an increase in synaptic strength between neurons (Cajal, 1894).

It was not until the 1960's and 1970's that the molecular pathways that underlie learning and the formation of memory were elucidated, as model systems were developed that allowed insight into the molecular basis of learning and memory. The first of which involved the gill reflex response of the sea slug *Aplysia* to study short-term memory (STM). This learned behaviour is a result of tactile stimulation of the siphon which results in a defensive withdrawal response of the gill (Kupfermann & Kandel, 1969). This is associated with an increase of cyclic AMP (cAMP) in the cytoplasm that activates protein kinase A (PKA) resulting in covalent modifications of pre-existing proteins. This leads to an increase in neurotransmitter release, ion channel clustering, and transient alterations in synaptic strength lasting minutes to an hour (Kandel *et al.*, 2014; Kennedy, 2013).

Long-term memory (LTM) relies on new protein synthesis to store information for hours and even years. The process of LTM formation requires transcription and translation of new proteins in order to create new synaptic connections (Lamprecht & LeDoux, 2004). Neurotransmitters bind to N-Methyl-D-Aspartic acid receptors (NMDAR), which leads to membrane depolarisation and release of the inhibitory magnesium ion (Mg^{2+}) allowing for Ca^{2+} to flood the postsynaptic neuron (Evans *et al.*, 2012) (Figure 1.1). This influx of Ca^{2+} then results in activation of biochemical signalling cascades, in particular the mitogen-activated protein kinase (MAPK) pathway (Rosen & Greenberg, 1996; Wu *et al.*, 1993). Upon repeated stimulation, cAMP levels increase which results in activation of PKA to a critical threshold leading to recruitment of MAPK. PKA and MAPK then translocate into the nucleus, where they are responsible for phosphorylating cAMP response element-binding protein (CREB) to transcribe plasticity-related genes for the growth of new synaptic connections (Kandel *et al.*, 2014; Martin *et al.*, 1997; Yamamoto *et al.*, 1988), resulting in memory consolidation (Alberini, 2011).

1.3 The use of *Drosophila* as a model system for neuroscientific exploration

Since Thomas Hunt Morgan confirmed the linkage of inheritance of a specific trait with a chromosome in 1911 (Morgan, 1911), *Drosophila melanogaster* has been making a significant contribution to scientific knowledge for the last 110 years. Aside from classical genetic studies, *Drosophila* has also proved to be an ideal model system for dissecting the molecular mechanisms underlying neurodevelopmental and neurodegenerative disease. Importantly, approximately 75% of disease associated human genes are conserved in *Drosophila* (Lloyd & Taylor, 2010; Pandey & Nichols, 2011; Reiter *et al.*, 2001) and the *Drosophila* genome, which spans a total of four chromosome pairs, has been fully sequenced and characterised (Adams *et al.*, 2000), allowing the development of *Drosophila* models of Alzheimer's and Parkinson's diseases as well as intellectual disability (Crowther *et al.*, 2006; Feany & Bender, 2000; Oortveld *et al.*, 2013).

Drosophila melanogaster is an ideal model due to its short and rapid lifecycle, inexpensive maintenance and most importantly, its tractability for genetic manipulation. Over the last three decades, an abundant genetic toolkit has been developed that allows for the manipulation of gene expression in a temporal and spatial manner (Brand & Perrimon, 1993; Dukas, 2008; McGuire *et al.*, 2004).

1.3.1 The *Drosophila* brain

The *Drosophila* brain has been increasingly used to model neurodevelopmental and neurodegenerative diseases of the human brain. The central nervous system is divided into two regions: the cortical region and neuropil region. The cortical region harbours the neuronal cell bodies on the external surface of the brain and central nerve chord and connects the central nervous system to the peripheral nervous system. The neuropil region consists of the synaptic connectivity network enclosed by the cortical region in the protocerebrum at the centre of the brain, as well as the lobular, medulla, and lamina complexes of the optic lobes and the central region of the ventral nerve chord. All neuropiles are joined through axon tracts that trace throughout the brain (Freeman, 2015; Kremer *et al.*, 2017). Although the *Drosophila* brain is small, it consists of a highly organised network of neuronal processes and contains 200,000

neurons (Chiang *et al.*, 2011; Huang *et al.*, 2018; Raji & Potter, 2021). The brain is comprised of two optic lobes that flank the central brain, which houses bisymmetric antennal lobes and the mushroom body, both of which are highly specialised neuropils. The antennal lobes receive input from olfactory neurons, while the mushroom body receives olfactory input from the antennal lobe projection neurons (Turner *et al.*, 2008) (Figure 1.2).

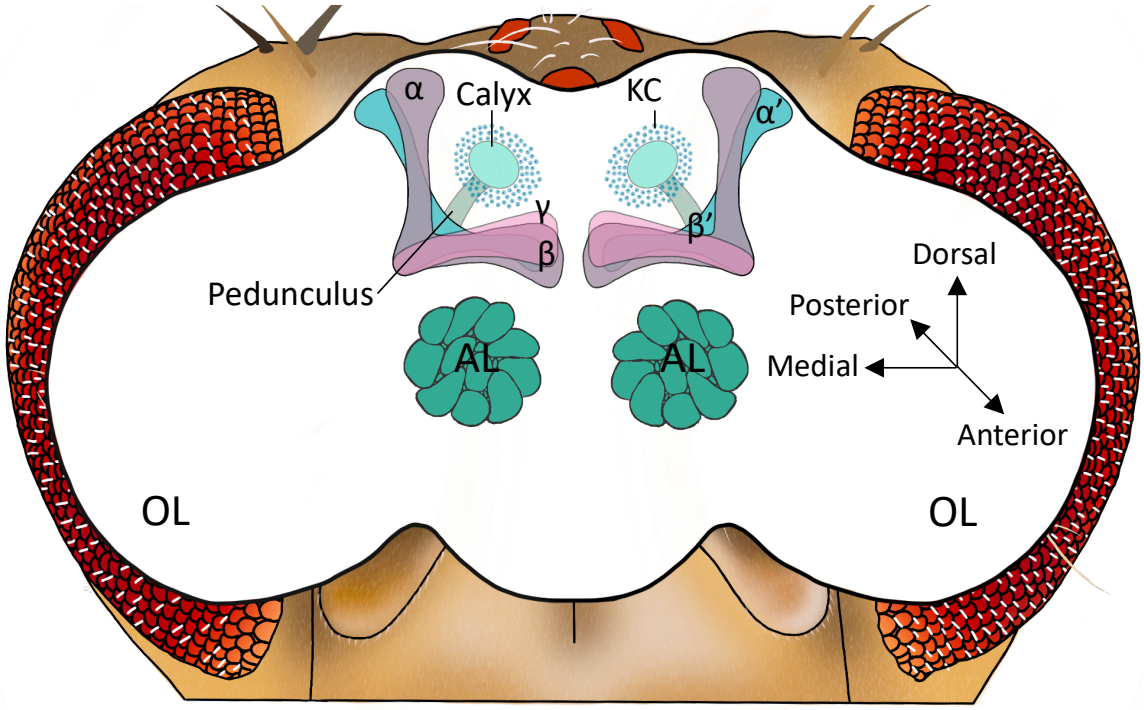

Figure 1.2. *Drosophila* brain structures. Anterior depiction of the *Drosophila* brain. Intrinsic Kenyon cells (KC) are localised at the posterior dorsal region of the brain and extend their dendrites anteriorly into the calyx. Axons extend to form the ventral projecting pedunculus that bifurcates forming the dorsal projecting α (purple)/α'(cyan) and medial projecting β (purple)/β' (cyan) and γ (magenta) lobes. Optic lobes (OL) receive visual sensory cues and the antennal lobes (AL) (teal) receive olfactory input.

1.3.1.1 The mushroom body

The mushroom body was first identified in 1850 by Félix Dujardin and is a symmetric bilateral structure, located in the centre of the brain in insects and other arthropods (Strausfeld *et al.*, 1998). Studies have shown that mutations and chemical ablations resulting in defects in the *Drosophila* mushroom body lead to impairments in STM and LTM (McBride *et al.*, 1999).

The approximately 2500 intrinsic neurons (Aso *et al.*, 2014) of the mushroom body are referred to as Kenyon cells and are clustered at the posterior dorsal region of the brain. There are three different subpopulations of Kenyon cells, which are derived from four neuroblasts (Ito *et al.*,

1997), alpha/beta (α/β), alpha prime/beta prime (α'/β'), and gamma (γ), with their extended dendrites forming the central calyx. Kenyon cell axons are bundled to form the ventral projecting peduncle that bifurcates forming the characteristic L-shaped mushroom body lobes (Crittenden *et al.*, 1998). Although there are only three subpopulations of Kenyon cells, these project to form five distinct lobes in a sequential highly regulated manner during larval and pupal development. The γ neurons are the first to form, their axons are bundled and begin extending both dorsally and medially at the initial larval stage and are fully extended by the mid-third instar larval stage (Armstrong *et al.*, 1998; Technau & Heisenberg, 1982). Following this, the α'/β' neurons are formed and extend their bundled axons both dorsally (α') and medially (β') from the mid-third instar larval stage through to pupation (Lee *et al.*, 1999). Upon pupation, rearrangement and degeneration of the γ lobe axons occurs and 24 hours after pupal formation (APF) the adult observed medial γ lobe has fully extended (Armstrong *et al.*, 1998; Technau & Heisenberg, 1982). Lastly, the α/β neurons are born and also extend their bundled axons dorsally (α) and medially (β) following pupation (Lee *et al.*, 1999) (Figure 1.2).

The extrinsic neurons of the brain allow for communication of signals to and from the mushroom body lobes, calyx, and peduncle and other regions of the brain (Ito *et al.*, 1998) establishing a key role in synaptic processing. During studies of learning and memory, one such group of extrinsic neurons, the dopaminergic neurons, release dopamine which bind dopamine receptors on Kenyon cells (Ichinose *et al.*, 2015; Yamagata *et al.*, 2015). Dopamine is an important neuromodulator in reward learning and motivation, and also in aversion (Bromberg-Martin 2011). These dopaminergic neurons are regulated by sensory cue inputs and the subsequent dopaminergic neuron response, to distinct brain regions, results in the related reward or aversive behavioral output (Kato *et al.*, 2023). In *Drosophila*, clusters of dopaminergic neurons innervate the mushroom body and modulate the output from Kenyon cells, which is an essential process for *Drosophila* courtship memory (Ichinose *et al.*, 2015; Yamagata *et al.*, 2015).

The structure and function of the mushroom body makes for an ideal model to assess genes involved in neuronal development and memory formation, as an intact mushroom body is essential for normal long-term courtship memory (McBride *et al.*, 1999). Axonal growth and guidance are imperative to generate a functional nervous system, where neuronal processes reach their target destinations, and this is controlled by signalling cues and cell surface receptors (O'Donnell *et al.*, 2009). A Fragile X syndrome model has been generated in *Drosophila* as

defects in the conserved *fragile-X mental retardation 1* (*dfmr1*) gene result in similar behavioural phenotypes to those observed in patients with Fragile X, including cognitive impairments displayed as courtship memory deficits (McBride *et al.*, 2005), described further in Section 1.3.3.1 and 1.3.3.2, and mushroom body defects of the β lobe due to a failure in axon termination, resulting in β lobe fusion (Michel *et al.*, 2004). Defects to long-term depression and potentiation, which are indicators of changes to synaptic strength, were observed in a Fragile X mouse model caused by mis-regulation of a metabotropic glutamate receptor, necessary in modulating synaptic plasticity (Huber *et al.*, 2002). Treatment with antagonists of metabotropic glutamate receptors rescued the courtship memory and β lobe fusion defects induced in the Fragile X *Drosophila* model (McBride *et al.*, 2005). The mushroom body has also been used in additional studies to demonstrate the requirement of Netrins (Kang *et al.*, 2019), cytoskeletal proteins including Ankyrin2 (Wilson, 2021; Wilson *et al.*, 2023), and Moesin (Freymuth & Fitzsimons, 2017), and the transcriptional regulator HDAC4 (Fitzsimons *et al.*, 2013; Main *et al.*, 2021; Tan *et al.*, 2024), for neuronal development and memory formation.

1.3.1.2 Glia in the *Drosophila* brain

The glia of the central nervous system are subdivided based on location, shape, size, and function. Cortex glia reside in the cortical region of the brain and ventral nerve chord, while ensheathing and astrocyte-like glia localise to the neuropil regions. Cortex glia generate a niche around the neuronal cells that reside within the cortical region (Dumstrei *et al.*, 2003). These glia are essential for neuronal metabolic support and synaptic transmission (Delgado *et al.*, 2018). Surface glia are comprised of two subgroups, perineurial and subperineurial glia, which generate two thin overlapping layers on the surface surrounding the entire central nervous system, forming the blood brain barrier (Freeman, 2015; Kremer *et al.*, 2017). Neuropil associated astrocyte-like glia and ensheathing glia both regulate synaptic processing through synapse pruning and remodelling (Doherty *et al.*, 2009; Hakim *et al.*, 2014; Paolicelli & Gross, 2011; Tasdemir-Yilmaz & Freeman, 2014), as previously discussed in Section 1.1.1. Astrocyte-like glia play a role in clearing axon debris from γ neurons upon mushroom body rearrangement, indicating the importance of astrocyte-like glia in neuronal activity and subsequent memory acquisition and consolidation (Hakim *et al.*, 2014; Tasdemir-Yilmaz & Freeman, 2014). Ensheathing glia flatten and extend their processes to surround the neuropil and have been

shown to phagocytose degenerating axonal debris (Doherty *et al.*, 2009) and have functional similarities to mammalian Schwann cells and oligodendrocytes (Yildirim *et al.*, 2019). The central nervous system glia function in unison with neurons to provide tropic factors and synaptic transmission support to modulate neuronal activity, similarly to the role that Astrocytes play in the mammalian central nervous system (Freeman, 2015).

1.3.2 The *Drosophila* compound eye

The *Drosophila* eye is also an ideal model for neuroscientific research as both disruption of neurodevelopmental pathways and neurodegeneration can be observed as perturbations in the regular ommatidial arrangement and bristle patterning (Cagan, 2009). The *Drosophila* eye is composed of approximately 800 hexagonal ommatidia. These ommatidial facets are comprised of eight rhabdomeric (R) photoreceptors which are specialised neurons the convert light into electrical signals. Individual photoreceptors differentiate based on signals from neighbouring fully differentiated photoreceptors (Freeman, 1996), and each cluster of photoreceptors are surrounded by cone, pigment, and bristle accessory cells (Cagan & Ready, 1989a).

1.3.2.1 *Drosophila* larval eye development

The development of the *Drosophila* eye begins during embryogenesis (Garcia-Bellido & Merriam, 1969) when a pair of eye imaginal disc primordia emerge from specific cell clusters (Beira & Paro, 2016). This pair of eye-antennal imaginal discs connect to the larval brain (Figure 1.3A) and give rise to external adult head structures, including the compound eyes and ocelli which encompass the *Drosophila* visual system, and the antennae and maxillary palps which encompass the olfactory system (de Bruyne *et al.*, 1999; Nayak & Singh, 1985; Venkatesh & Singh, 1984). The eye-antennal disc is a monolayer epithelium generated by invagination of the blastoderm to create a lumen encased epithelium sac. It is composed of three layers of different cell compositions; the peripodial epithelium, which gives rise to head structures and is comprised of low lying flat squamous cells lies atop the disc proper, which gives rise to the adult retina and is comprised of long columnar cells, the peripodial epithelium and disc proper are joined together at the edges by the marginal cuboidal cells (Figure 1.3B) (Haynie & Bryant, 1986; McClure & Schubiger, 2005; Weasner & Kumar, 2022). The posterior

eye region of each eye-antennal disc is connected to the brain by the optic stalk providing a link between the eye and brain allowing for photoreceptor axons to project through to innervate the brain (Murakami *et al.*, 2007).

Following embryogenesis, the nascent eye disc contains approximately 70 cells (Mandaravally & Schneiderman, 1977). Rapid proliferation results in enlargement and conformational changes to the eye disc during the first and second instar larval stages, followed by organised cell differentiation during the third instar larval stage (Kumar, 2018). A physical dorsoventral indentation in the eye disc termed the morphogenetic furrow forms at the posterior edge of the eye field, close to the optic stalk and sweeps anteriorly towards the antennal field (Ready *et al.*, 1976; Tomlinson, 1985; Tomlinson & Ready, 1987) (Figure 1.3C). The initiation of furrow migration in a posterior to anterior manner and subsequent photoreceptor differentiation occurs through a highly regulated pathway.

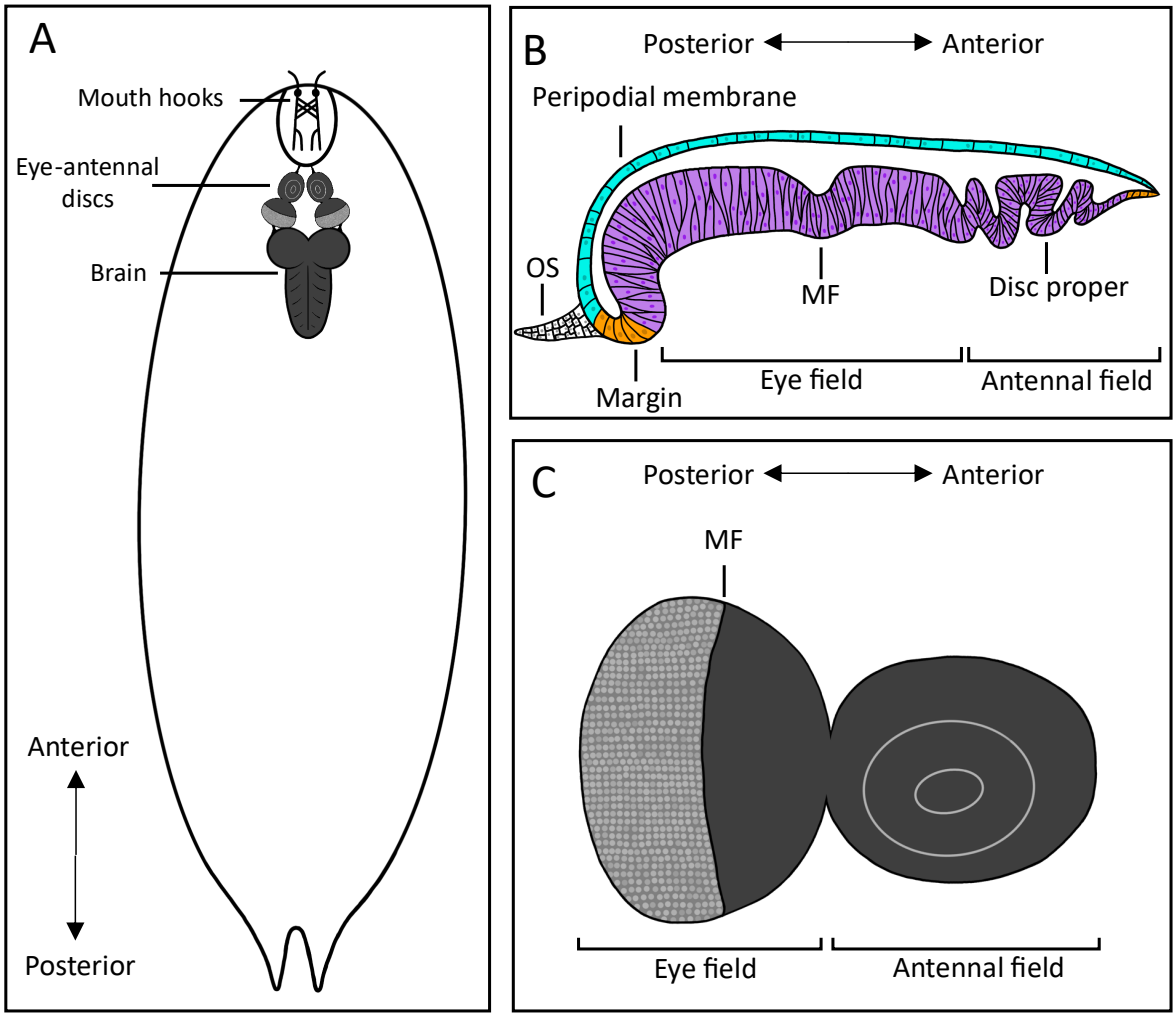

Figure 1.3. Schematic depiction of the *Drosophila* larval eye-antennal disc. A. The optic lobes of the third instar larval brain are attached to two identical eye-antennal discs at the anterior of the larva. B.

The eye-antennal disc is comprised of three cell types, the low-lying squamous cells (teal) that generate the peripodial membrane, the long columnar cells (purple) that generate the disc proper, and the cuboidal cells (orange) of the margin that join the peripodial membrane and disc proper. The morphogenetic furrow (MF) generates a dorsoventral indentation in the disc proper. The cells that generate the optic stalk (OS) are located at the posterior of the eye-antennal disc. C. The eye-antennal disc is comprised of a posterior localised eye field in which the MF sweeps from posterior to anterior, leaving a wake of differentiated cells, and at the anterior of the disc is the antennal field. OS = optic stalk, MF = morphogenetic furrow. *Original figures, B. generated with reference to Gibson and Schubiger (2001); Warren and Kumar (2023); Weasner et al. (2020).*

Two important proteins in this pathway are Hedgehog and Decapentaplegic (Dpp). Hedgehog is a signalling molecule that is initially expressed at the very posterior edge of the eye primordium and as photoreceptor differentiation begins, during the third instar larval stage, it is secreted by differentiating photoreceptors posterior to the morphogenetic furrow. In contrast, prior to initiation of the furrow, Dpp is expressed at the lateral posterior margin of the eye, flanking either side of Hedgehog and as photoreceptor differentiation begins, Hedgehog expression in photoreceptors promotes the expression of Dpp in the furrow (Chanut & Heberlein, 1997; Chawla *et al.*, 2003; Greenwood & Struhl, 1999). Migration of the morphogenetic furrow towards the anterior region of the eye disc leaves a wake of differentiated cells as cells just anterior to the furrow arrest in G1 resulting in an organised array of ommatidial units (Ready *et al.*, 1976). Neuronal adult precursor cells destined to become polarised adult photoreceptor cells differentiate posterior to the furrow and through cell-cell contact signalling and positional effects, the fate of each photoreceptor neuron (R cell) is determined. Initially during the first wave of mitosis a five-cell neuronal pre-cluster is formed, the first R cell born is R8, closely followed by two pairs of R cells, R2/R5 and R3/R4 (Figures 1.4A). These five-cell pre-clusters are observed to closely follow the furrow. During the second wave of mitosis the eight-cell photoreceptor cluster is complete and positioned posterior to the differentiating five-cell pre-cluster (Ready *et al.*, 1976; Tomlinson, 1985; Tomlinson & Ready, 1987). The R7 precursor belongs to the R7 equivalence group, which, aside from giving rise to the R7 photoreceptor, also gives rise to R1 and R6 as well as the four non-neuronal glial-like cone cells (further discussed in Section 1.3.2.2). Prior to differentiation, the R7 precursor expresses Tramtrack, a transcription factor that when expressed represses photoreceptor fate, allowing for differentiation of a cone cell. Upon downregulation of Tramtrack, a photoreceptor is born, and the fate of each photoreceptor, R1, R6, and R7 is dependent on the position within the photoreceptor cluster that is occupied (Li *et al.*, 1997; Mavromatakis & Tomlinson, 2016; Tang *et al.*, 1997). Each photoreceptor cluster is organised with the central R8 photoreceptor

surrounded by seven other photoreceptor cells (Figure 1.4B). The axons of all photoreceptors are ensheathed by a subset of glia called ensheathing glia (Section 1.3.2.1.1) where these axons then project posteriorly through the optic stalk and innervate the optic lobe of the brain (Cameron *et al.*, 2016; Chang *et al.*, 2018; Chen *et al.*, 2017; Ready *et al.*, 1976; Tomlinson & Ready, 1987).

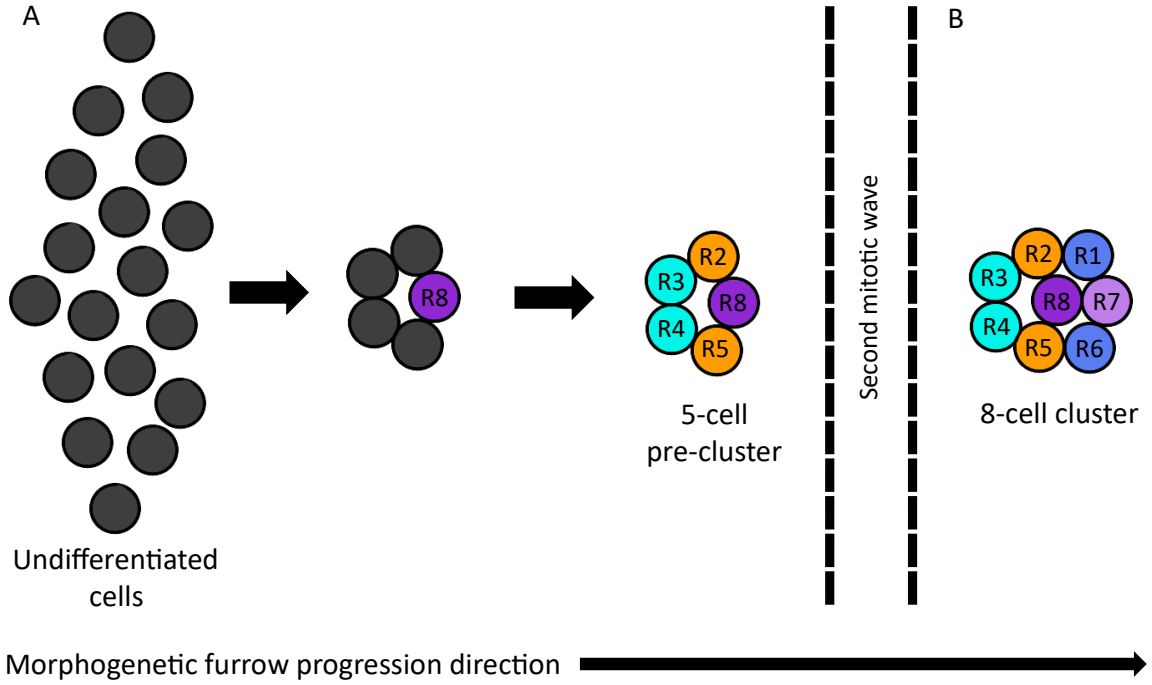

Figure 1.4. Differentiation and organisation of photoreceptor clusters in the larval eye disc. A. The R8 photoreceptor is first to be born followed by differentiation of the R2/R5, R3/R4 pairs of photoreceptors generating the 5-cell pre-cluster. Following the second mitotic wave, B. the R1, R6, and R7 photoreceptors differentiate, and the mature 8-cell cluster is formed. *Original figure generated with reference to Kumar (2020).*

1.3.2.1.1 Glia in the larval eye disc

In the third instar larval eye disc, the retinal basal glia migrate into the differentiating eye field via the optic stalk connecting the eye to the brain. Initiation of migration is dependent on photoreceptor differentiation posterior to the morphogenetic furrow, and establishment of the axon scaffold in order for retinal basal glia to migrate and populate the eye disc a few rows behind the newly differentiated photoreceptors (Choi & Benzer, 1994). Retinal basal glia are separated into three distinct groups; surface glia (perineurial), carpet glia (subperineurial), and ensheathing glia (Tsao *et al.*, 2020). Each eye disc contains two large carpet glia that migrate through the optic stalk and position their polyploid nuclei at the very posterior edge of the eye

disc, where their membranes create a septate junction at the dorsoventral midline and cover half of the eye disc posterior to the morphogenetic furrow. These carpet cell membranes create a divide between the photoreceptor cell bodies emerging at the apical surface and their axons projecting through the basal region of the eye disc (Silies *et al.*, 2007). Surface glia are the most prominent subtype of retinal basal glia and have a circular morphology. Surface glia migrate from the optic stalk and populate the eye field and are the only glial sub-group that undergo replication and cell division which initiates from two migratory cells (Silies *et al.*, 2007). Recently it was discovered that there are two distinct lineages of surface glia, those that populate the basal region below the carpet glia membrane and those that populate the apical surface. Those that reside at the basal surface only proliferate to generate more surface glia, however those at the apical surface receive signals to differentiate to generate the pool of ensheathing glia (Tsao *et al.*, 2020). Ensheathing glia differ in both shape and function, as they have an elongated morphology in order to wrap their membrane around the photoreceptor axons, (Tsao *et al.*, 2020) and aid in projection through the optic stalk.

1.3.2.2 Pupal eye development

Early in pupation the morphogenetic furrow completes its journey across the eye disc, everting the eye and reversing the invagination that occurred during embryogenesis, beginning the metamorphosis into the adult eye and antennal structures (Cagan & Ready, 1989a). As discussed in Section 1.3.2.1, the R7 precursor gives rise not only to photoreceptors but also four non-neuronal glial-like cone cells early in pupal development (Li *et al.*, 1997; Mavromatakis & Tomlinson, 2016; Tang *et al.*, 1997). During the final stages of retinal development these glial-like cone cells (Chaturvedi *et al.*, 2014) secrete the corneal lens and extend their processes to the floor of the retina. Each cone cell is named according to its position within the ommatidium and emerge in pairs. The anterior and posterior cone cells are first to emerge and contact at the retina floor, which blocks contact between the equatorial and polar cone cells which emerge later and contact at the apical region of the retina below the pseudocone (Cagan & Ready, 1989a; Tomlinson, 1985; Tomlinson & Ready, 1987). The nuclei of the cone cells remain at the apical region, above the photoreceptor cluster (Charlton-Perkins & Cook, 2010; Tomlinson, 1985) and at the basal region large cone cell processes, denoted as feet are positioned above the fenestrated membrane and accumulate brown ommochrome pigment granules that act as basal

insulators to block light scattering at the basal region of the retina and allow adequate lens transparency at the apical surface (Tomlinson, 2012) (Figure 1.5A).

During early pupation the interommatidial mechanosensory bristles begin to emerge and radiate from the centre of the eye. Each ommatidium shares three bristles, positioned at alternating vertices. Each bristle is comprised of four different cell types, the socket secreting tormogen, the bristle secreting trichogen, the sensory neuron, and supporting glial thecogen (Cagan & Ready, 1989a).

During mid to late pupal development, rhabdomeres begin to form inside of each photoreceptor. The rhabdomere is a specialised compartment located in the apical region of the photoreceptor neuron, and is comprised of approximately 30,000 microvili which absorb light and organise phototransduction machinery for processing of visual stimuli (Juusola & Hardie, 2001). Rapid rhabdomere growth results in retinal deepening as the rhabdomeres of R1-R6 continue to extend while the R7 rhabdomere is positioned above the R8 rhabdomere, each of these are half the length of the other six rhabdomeres (Cagan & Ready, 1989a; Tomlinson, 1985) (Figure 1.5A, C, D) and the rhabdomeres of each ommatidial unit form a regular repeating trapezoid cluster (Figure 1.5C'). The photoreceptor axons extend basally and squeeze through the fenestrated membrane, which is comprised of cells that lose contact with the apical surface of the eye disc upon differentiation and reside at the basal membrane providing a structure between the retina and the optic lobe (Cagan & Ready, 1989a). The photoreceptor axons then project through the optic stalk and innervate the optic lobe. R1-R6 axons innervate the lamina, while R7 and R8 axons bypass the lamina and innervate in two distinct layers of the medulla (Campos-Ortega & Strausfeld, 1972; Kolodziejczyk *et al.*, 2008; Trujillo-Cenóz, 1965).

Glial-like pigment cells (Chaturvedi *et al.*, 2014) ensheath the photoreceptor/cone cell cluster by spanning the apical tip of the pseudocone through to the fenestrated membrane (Figure 1.5A). Primary pigment cells can be identified 22 hours APF at 20°C. Two prospective primary pigment cells each surround the cone cells at the apical region of the retina with regulated posterior to anterior organisation (Figure 1.5B). Primary pigment cells are the only cell type in the ommatidia that do not extend their processes to the floor of the retina (Cagan & Ready, 1989a) (Figure 1.5A). Secondary and tertiary pigment cells give rise to the final ommatidial lattice and provide structural boundaries between individual ommatidial facets. A total of six secondary pigment cells form and are divided into two groups, oblique (Ob) and horizontal (Hz). There are four oblique secondary pigment cells and these are first to emerge. As the

primary pigment cells encase the cone cells, additional cells that contact two adjacent primary pigment cells with four other developing ommatidial units will emerge as the four oblique secondary pigment cells. Other cells that contact three different ommatidial primary pigment cells emerge as interommatidial tertiary pigment cells which form at alternating vertices to the bristle cells groups. Two horizontal secondary pigment cells then emerge and reside adjacent to the attachment site of the two primary pigment cells of two ommatidial clusters to generate the precise hexagonal ommatidial lattice (Figure 1.5B'). Secondary and tertiary pigment cells project their axons basally where a tight basal retina boundary is formed with the cone cell feet allowing only photoreceptor and bristle cell axons through the fenestrated membrane to the underlying subretinal pigment layer (Cagan & Ready, 1989a) (Figure 1.5A). Secondary and tertiary pigment cells contain two different pigment granules, brown ommochrome and long red pteridine, both function as optical sheathing and assemble from the apical lens through to the subretinal pigment layer, located below the fenestrated membrane to provide further insulation (Tomlinson, 2012). This insulation occludes lateral light transfer between ommatidia and a study on flies with pigmentation deficiencies resulted in reduced visual responses (Kalmus, 1943), demonstrating the importance of pigment granules in the eye.

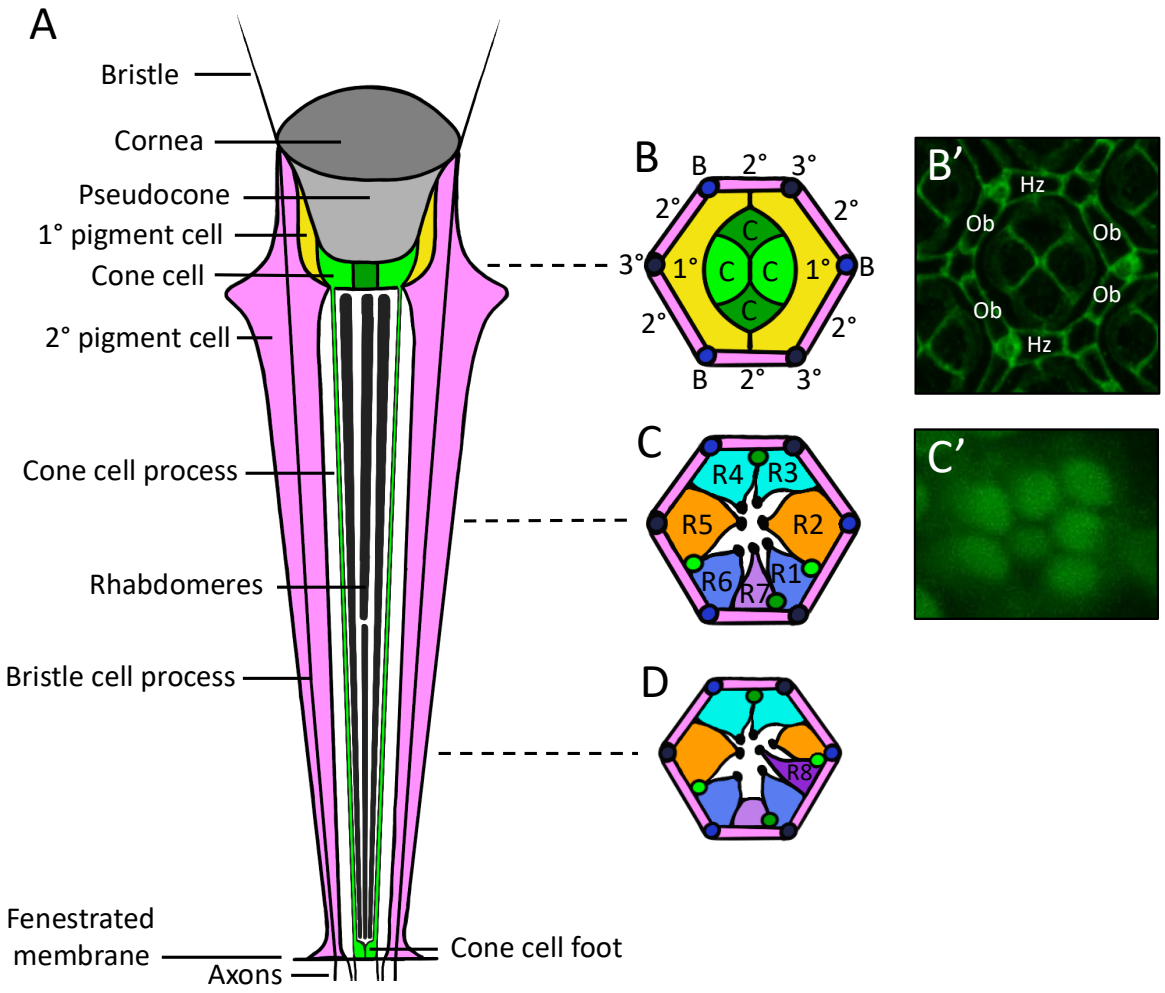

Figure 1.5. The *Drosophila* retina. A. The apical top of the retina is comprised on the cornea, which sits above the pseudocone, with three surrounding mechanosensory bristles. These structures lie atop the cone cells, which are encapsulated by primary (1°) pigment cells which are surrounded by secondary (2°) pigment cells. Bristle processes (axons) plunge through the fenestrated membrane, while the 2° pigment and cone cell processes sit atop the fenestrated membrane. B. Located basal to the cornea and pseudocone are the four cone cells (C) (green, dark green) of a single ommatidium which are encased by two 1° pigment cells (yellow). These are surrounded by six elongated 2° pigment cells (pink), which are shared with six additional ommatidia, and three tertiary (3°) pigment cells (navy) and three bristle (B) cells (blue) located at alternating vertices, which are shared with three additional ommatidia. B' Immunohistochemistry of an ommatidium with identical cell placement as depicted in B, with two horizontal (Hz) and four oblique (Ob) 2° pigment cells. C. Further basal the R1-R7 cells are located and C' form a trapezoid structure. D. Above the fenestrated membrane the R1-R6 and R8 rhabdomeres are observed. 1° = primary, 2° = secondary, 3° = tertiary, C = cone cell, B = bristle cell, Hz = horizontal, Ob = oblique, R = rhabdomere. *Original figure generated with reference to Wolff and Ready (1993).*

Throughout pupal development approximately 2000 excess cells in the retina fail to terminally differentiate. When cells fail to form appropriate contacts they are eliminated in one of the two waves of apoptosis that occurs uniformly across the eye disc with no particular directional influence (Wolff & Ready, 1991). After the primary pigment cells have enwrapped the cone

cells and allowed for potential secondary and tertiary pigment cells to make important cell-cell contacts the first wave of apoptosis occurs, resulting in maximal cell death and tightening of the hexagonal ommatidial lattice (Cagan & Ready, 1989a). A second wave of prolonged cell death follows later in pupal development to further refine the array (Cordero *et al.*, 2004). The onset of apoptosis is dependent on many signalling pathways, including the *Drosophila* Epidermal Growth Factor Receptor (dEGFR), Notch, and wingless pathways. dEGFR and Ras signalling promotes cell survival through regulation of the expression and activity of the pro-apoptotic gene *head involution defective* (*hid*) (Kurada & White, 1998), whose function is to repress Death-associated inhibitor of apoptosis-1 (DIAP1) resulting in the activation of initiator caspase Death regulator Nedd2-like caspase (Dronc). This in turn activates effector caspase cleavage proteins Death related ICE-like caspase (Drice) and Death caspase-1 (Dcp-1) (S. L. Wang *et al.*, 1999). Notch signalling is required for removal of interommatidial cells not fated to become secondary and tertiary pigment or bristle cells (Cagan & Ready, 1989b). Wingless signalling has also been implicated in differentiation and patterning of cells in the *Drosophila* eye, as expression of a wingless null mutant upon initiation of apoptosis resulted in a significant decrease in cell death (Cordero *et al.*, 2004). These results indicate that both the Notch and wingless pathways are required to induce apoptosis.

1.3.2.3 The adult *Drosophila* eye

After adult eclosion, the precise, invariant organisation of ommatidia and bristles (Figure 1.6A) allows disruption to ommatidial alignment, and bristle patterning to be easily visualised. Defects to the eye result in what is commonly referred to as a “rough eye” phenotype (Basler *et al.*, 1990) and in addition to pigmentation loss and rare occurrences of necrosis, these defects can be visually assessed and semi-quantitatively scored (Figure 1.6B) (Kaplow *et al.*, 2007; Schwartz *et al.*, 2016; Wilson, 2021).

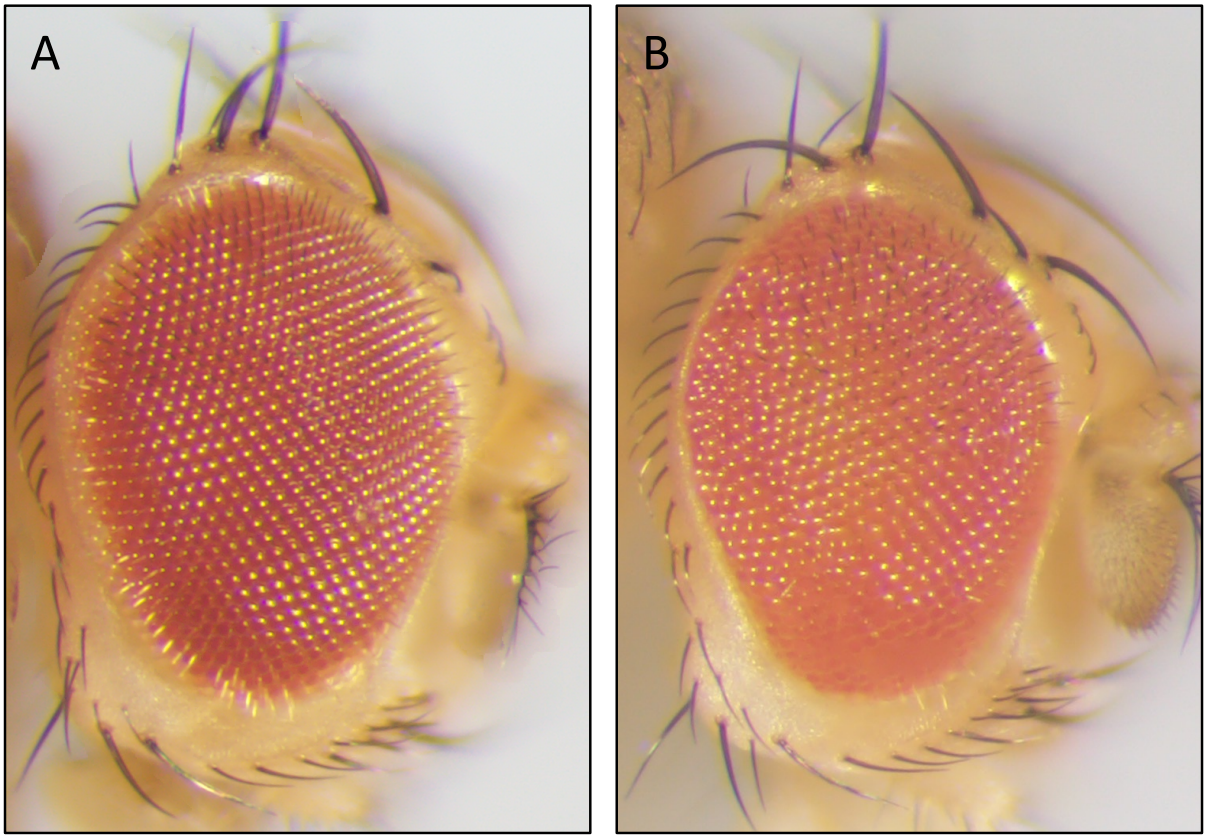

Figure 1.6. The use of the *Drosophila* eye to visually assess perturbations. Light microscopy on adult eyes show A. the uniform retinal array which B. upon disruption to neural pathways required for the generation of a normal eye can be visually assessed as a rough eye phenotype.

The wealth of knowledge regarding the development of the eye along with a well-established scoring system makes the *Drosophila* eye an ideal model for screening genetic interactions. A genetic interaction occurs when two genes act in the same molecular pathway and is observed as a synergistic interaction when the combination of two independent mutations results in a more severe phenotype than the additive effect of each mutation independently (Perez-Perez *et al.*, 2009).

1.3.3 *Drosophila* are ideal for behavioural analyses

The *Drosophila* model is ideal for dissecting behavioural paradigms and modelling clinical hallmarks associated with neurodegenerative disease. *Drosophila* respond to a number of stimuli including pheromones (Kurtovic *et al.*, 2007), light (Juusola & Hardie, 2001), temperature (Barbagallo & Garrity, 2015; Miquel *et al.*, 1976), and gravity (Inagaki *et al.*, 2010;

Kamikouchi *et al.*, 2009; Sun *et al.*, 2009), and their behavioural outputs can be quantitatively assessed. Due to the consistency of the fly' behavioural repertoire, and their amenability for genetic manipulation, the effects of gene expression changes can be assessed through changes in behaviour.

Neuronal circuity and the processes of learning and memory can be studied in the fly as the basic underlying mechanisms involved are conserved among species, making *Drosophila* an excellent model for understanding neurodegenerative disease, including Alzheimer's disease, where memory and cognitive decline are a predominant pathology (Chakraborty *et al.*, 2011; Goguel *et al.*, 2011).

Motor coordination and function can be studied in the fly via locomotor assays that are widely used to model neurodegenerative diseases, including Parkinson's disease, where a loss of motor function is a clinical hallmark of disease (Feany & Bender, 2000).

1.3.3.1 *Drosophila* courtship

Male *Drosophila* display a repertoire of courtship behaviours to attract a female and accomplish successful reproduction. These include orientation towards the female (Figure 1.7A), tapping of the female's abdomen by an outstretched leg (Figure 1.7B), performing a courtship song through wing vibrations (Figure 1.7C), tasting of the female genitalia (Figure 1.7D), and attempted (Figure 1.7E), followed by successful copulation (Figure 1.7F) (Anholt *et al.*, 2020; Sokolowski, 2001). Courtship is a hard-wired process, and a number of genes and neuronal circuitries are important for these behaviours to ensue.

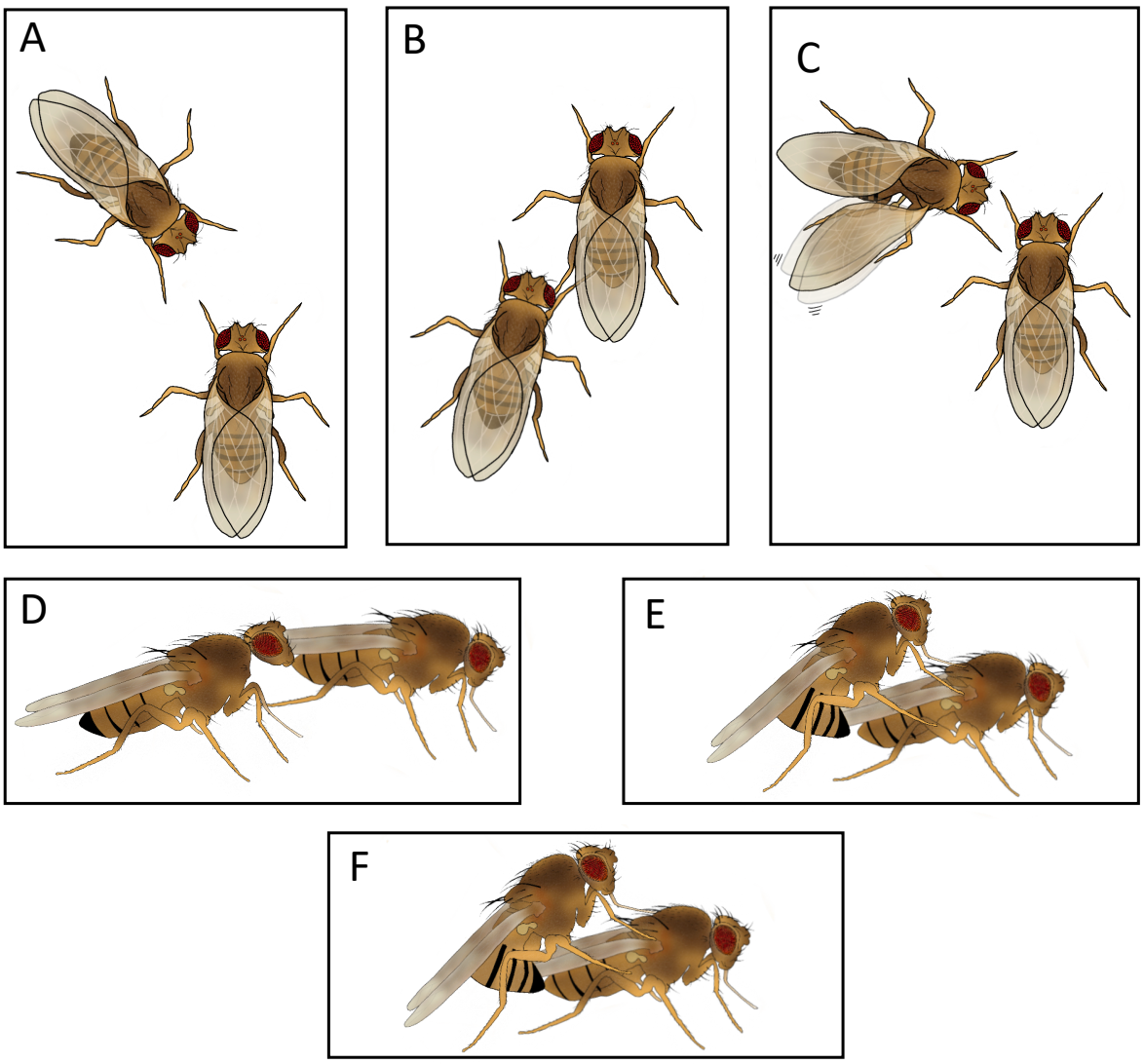

Figure 1.7. *Drosophila* courtship behaviours. A male *Drosophila* performs a number of ritualistic courtship behaviours before successfully mating with a female, these include, A. orientation toward the female, B. tapping the females abdomen with a leg, C. producing a song through vibrations of an outstretched wing, D. tasting the female's genitalia, E. attempting to copulate with the female, and finally F. successful copulation. *Original figure generated with reference to Sokolowski (2001).*

A wild-type male fly that has previously been rejected by a mated female fly demonstrates a decrease in courtship behaviours in the presence of a new mated female (Siegel & Hall, 1979). This suppression of courtship is in response to the male-specific pheromone cis-vaccenyl acetate (cVA) that is deposited by the male onto the female's abdomen during mating, therefore this type of courtship memory is called cVA-retrievable memory. All newly mated females harbour cVA (Ejima *et al.*, 2007), and this pheromone has been shown to elicit an anti-aphrodisiac response, which reduces male courtship behaviour (Ejima *et al.*, 2007; Zawistowski & Richmond, 1986). The olfactory neuron receptor Or67d in antennae detects cVA, this

activates projection neurons in the antennal lobe and mushroom body and facilitates higher order processing to control and repress courtship behaviour (Raun *et al.*, 2021).

This experience-dependent behaviour can be used as a robust and quantifiable assay to test STM and LTM by training a male with a freshly mated female for a defined period of time (60 minutes for STM and 5-7 hours for LTM). Following a rest period (0 to 60 minutes for STM and 24 hours for LTM), males are then exposed to a new freshly mated female and courtship activity is measured. A male with intact learning and memory displays an enhanced response to cVA and thus reduces his courtship activity (Raun *et al.*, 2021).

1.3.3.2 *Drosophila* courtship memory processes

The γ lobe has been shown to be important for learning and memory in *Drosophila*, as proteins expressed in the γ lobe play crucial roles in regulating synaptic plasticity. Mutations in the Cytoplasmic polyadenylation element-binding protein (CPEB) Orb2 have shown a reduction specifically in LTM (Keleman *et al.*, 2007; Kozlov *et al.*, 2023), while overexpression of Orb2 in the mushroom body γ neurons is able to restore LTM formation. Orb2 has two established isoforms, Orb2A and Orb2B, both of which harbour vastly different N-terminal domains with no conserved regions, and a glutamine rich domain (Q domain) shown to be important in LTM formation (Keleman *et al.*, 2007). Orb2A and Orb2B form higher order multimer complexes that are dependent on an intact Orb2A Q domain (Kruttner *et al.*, 2012). These complexes have been shown to localise to neuronal synapses (Kozlov *et al.*, 2023; Kruttner *et al.*, 2015), however these isoforms have non-redundant functions. The aSP13 presynaptic terminus is located at the tip of the γ lobe and activity from the aSP13 dopaminergic neurons up to 11 hours following training with a mated female, as detailed in Section 1.3.3.1, is required for LTM consolidation. Memory acquisition and consolidation are achieved through activation of the Dopamine receptor R1 (DopR1) that receives input from these aSP13 dopaminergic neurons and acts upstream of Orb2, which is a target of calcium/calmodulin-dependent protein kinase II (CaMKII) involved signalling pathways important for generating persistent memories (Keleman *et al.*, 2012; Kruttner *et al.*, 2015).

1.3.3.3 Adult *Drosophila* climbing activity

An adult *Drosophila's* innate behavioural response to gravitational stimuli is to move against gravity (negative geotaxis), therefore when trapped in a small vial, the fly will move against gravitational cues to the top of the vial (Kamikouchi *et al.*, 2009). To assay locomotor behaviour a negative geotaxis climbing assay can be employed, whereby the startle-induced behavioural response of a fly can be measured by how rapidly a fly will climb a specified distance against gravity (Madabattula *et al.*, 2015). A Parkinson's disease fly model expressing mutant forms of α-synuclein showed a marked decrease in climbing ability compared to control. This decrease in climbing activity, however, was only observed after 23 days and showed a progressive degenerative decline (Feany & Bender, 2000). In addition to being used as a model for neurodegenerative disease, climbing activity is also negatively affected by ageing (Le Bourg & Lints, 1992).

1.3.4 The *Drosophila* toolbox for gene manipulation

The appeal of *Drosophila* as a model system lies in the wide range of tools and techniques that have been developed for genetic manipulation. The generation of transgenic flies has allowed for tissue-specific transgene expression to assess gene function, protein interactomes, and overall neuronal systematics. To that end, the development of the UAS/GAL4 and the temporal and regional gene expression targeting (TARGET) system facilitated the ease of targeted gene expression in a spatial and/or temporal manner by pairing any tissue-specific promoter with expression of any transgene (Brand & Perrimon, 1993; McGuire *et al.*, 2004).

1.3.4.1 UAS/GAL4 system

The UAS/GAL4 system is a bipartite system utilising the exogenous yeast transcriptional transactivator GAL4, which binds an upstream activating sequence (UAS) to initiate downstream transgene expression. The GAL4 activator can be placed under the control of any tissue specific enhancer, creating a GAL4 'driver' line, to allow for tissue specific expression. Crossing virgin female driver flies to a male transgenic fly line harbouring a UAS fused to a downstream transgene of interest, will result in F1 progeny where GAL4 will bind the UAS and

drive tissue specific expression of the downstream transgene (Brand & Perrimon, 1993) (Figure 1.8).

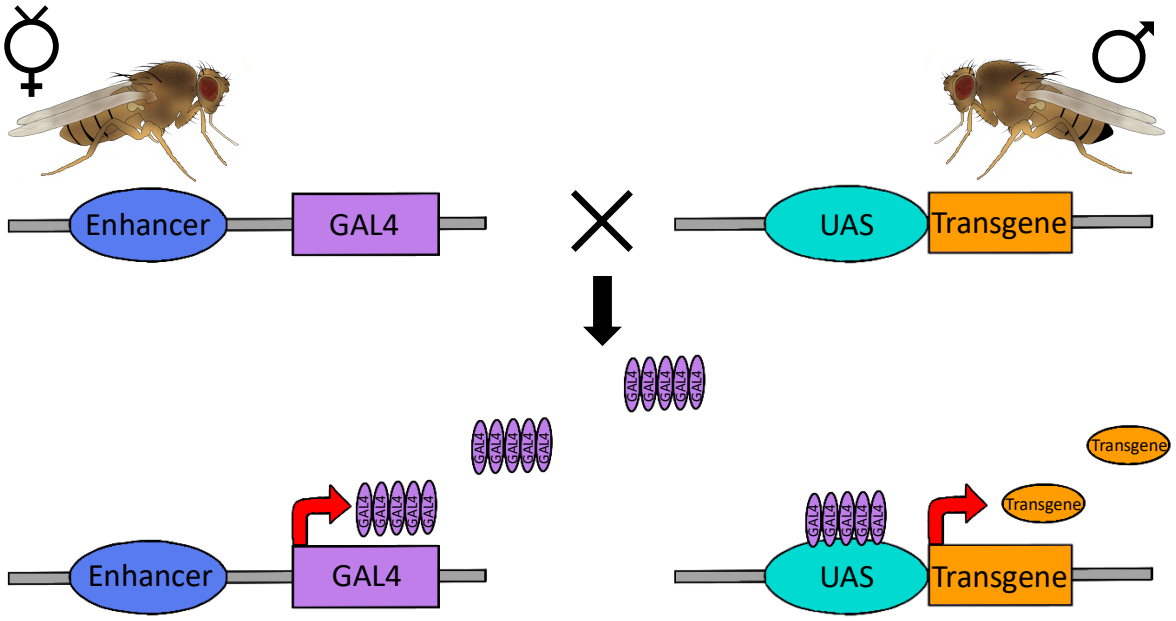

Figure 1.8. UAS/GAL4 bipartite system. Virgin females carrying the transcriptional transactivator GAL4 positioned downstream of a tissue specific enhancer are crossed to males harbouring a UAS fused to a downstream transgene. The F1 progeny express tissue-specific GAL4 which binds the UAS, initiating tissue specific downstream transgene expression. *Original figure generated with reference to Brand and Perrimon (1993).*

Drosophila stock centres such as the Bloomington *Drosophila* Stock Centre (BDSC), Vienna *Drosophila* Resource Centre (VDRC), and the Kyoto Stock Centre carry a range of GAL4 driver lines to induce transgene expression in most tissues and cell types. The expression pattern and levels of pan-neuronal *embryonic lethal abnormal visual system-GAL4,* (*elav-GAL4*) (Armstrong *et al.*, 2011; Hawley *et al.*, 2023) and *neuronal Synaptobrevin-GAL4* (*nSyb-GAL4*) (Hawley *et al.*, 2023; Weaver *et al.*, 2020); mushroom body-specific *OK107-GAL4* (Bates *et al.*, 2010; Hawley *et al.*, 2023); and eye-specific *glass multimer reporter-GAL4* (*GMR-GAL4*) (Escobedo *et al.*, 2021; Freeman, 1996; W. Z. Li *et al.*, 2012; Ray & Lakhotia, 2015) have been verified by expressing a fluorescent protein and examining the distribution. In addition, there are UAS-transgene libraries for expression of many *Drosophila* genes, UAS-RNAi lines for RNAi-mediated knock down of most *Drosophila* genes, further described in Section 1.3.4.3, and UAS-guideRNA lines for CRISPR/Cas9 knockout are also becoming widely available (Zirin *et al.*, 2020).

1.3.4.2 TARGET system

Spatial targeted gene expression using the UAS/GAL4 system can be further refined by the addition of a temporal element. GAL80 binds to GAL4 to repress GAL4 transcriptional activity, resulting in no downstream transgene expression. The TARGET system utilises a temperature sensitive mutant GAL80 ($GAL80^{ts}$) that allows for temporal control of transgene expression via temperature regulation. In this system, $GAL80^{ts}$ is ubiquitously expressed under the control of the *tubulin* promoter to induce ubiquitous expression. When flies are raised at a permissive temperature (19°C), $GAL80^{ts}$ binds GAL4 and masks the activation domain (AD), inhibiting transgene expression (Figure 1.9A). An increase to a non-permissive temperature (30°C) results in a conformation change of $GAL80^{ts}$, leading to GAL4 release and AD unmasking, resulting in GAL4 mediated downstream transgene expression (Figure 1.9B) (McGuire *et al.*, 2004; Suster *et al.*, 2004).

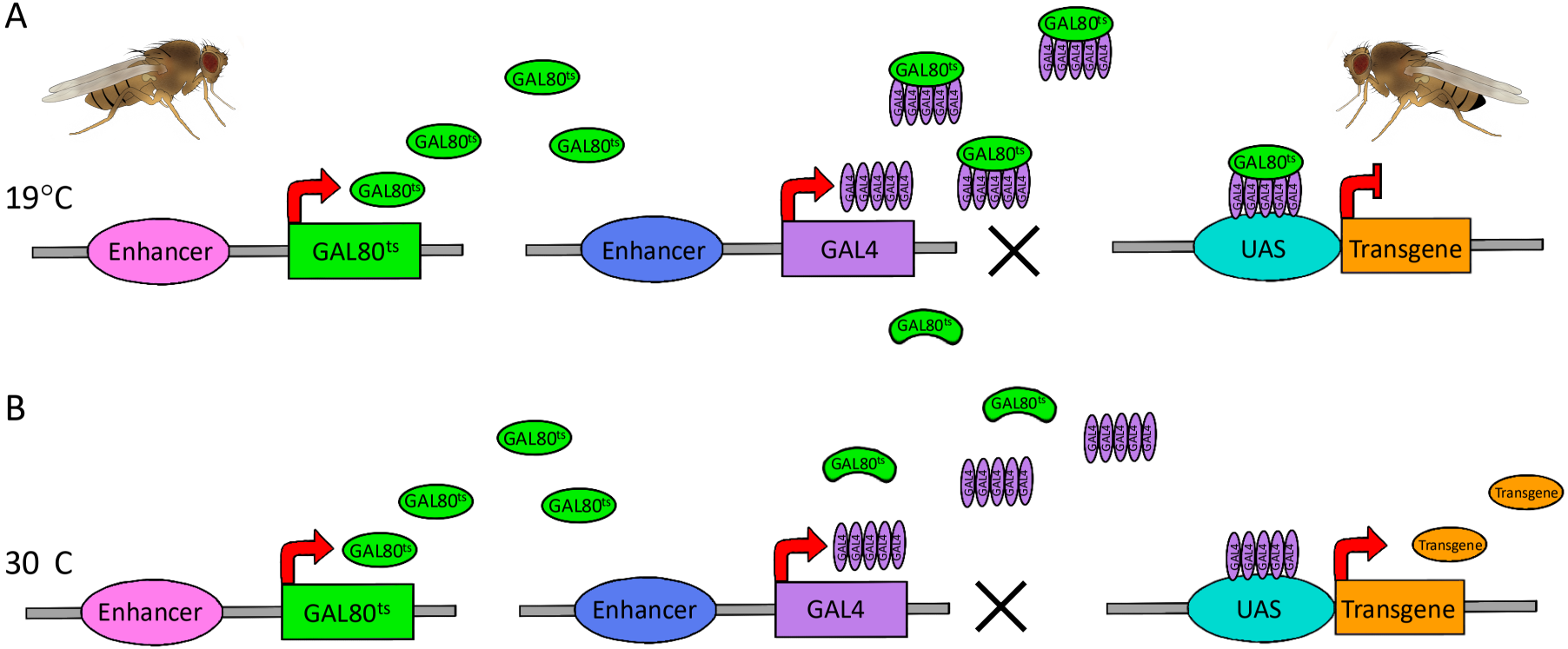

Figure 1.9. The *Drosophila* TARGET system. A. When raised at 19°C, GAL80^{ts} driven by a ubiquitous enhancer binds to GAL4 driven by a tissue specific enhancer and masks the GAL4 AD, preventing transgene expression. B. Upon a rise in temperature to 30°C, GAL80^{ts} has a shift in conformation, resulting in GAL4 release and AD unmasking , leading to downstream transgene expression. *Original figure generated with reference to McGuire et al. (2004).*

1.3.4.3 RNA interference

RNAi is a popular method for reducing the expression of a gene by targeting its mRNA for degradation. In *Drosophila,* this involves using the UAS/GAL4 system to drive expression of an inverted repeat double stranded RNA designed to target the mRNA of interest. Dicer-2 cleaves long inverted repeat hairpin RNA to generate double stranded short interfering RNAs (siRNA) that are 21-23 nucleotides in length (Elbashir *et al.*, 2001; Lee *et al.*, 2004). The siRNA is then loaded onto argonaute2 (AGO2) with the R2D2 cofactor to form a pre-RNA-induced silencing complex (RISC). Both strands of the siRNA have the capacity to be the guide RNA silencing strand based on functional asymmetry. The strand that is used as the guide will most often be the strand whose 5' end has the strongest interaction with its complementary 3' strand end. The other strand with the weaker pairing, the passenger strand, is ejected and degraded (Schwarz *et al.*, 2003). The guide strand then targets the complementary mRNA which is then cleaved and degraded by AGO2 (Figure 1.10).

The knockdown efficacy of RNAi stocks from VDRC often differ. This can be dependent on sequence specificity and the site of RNAi insertion in the genome. RNAi libraries have been constructed either by P-element-mediated insertion of the inverted repeat construct into the genome, which is semi-random, or by PhiC31-mediated integration where the RNAi construct is inserted into specific genomic locations via homologous recombination. RNAi expression can therefore be subject to different positional effects depending on the site of insertion, resulting in different levels of expression. Furthermore, all inverted repeat constructs are bioinformatically assessed to minimise the possibility of off-target effects and demonstrate gene target specificity (Dietzl *et al.*, 2007). UAS-RNAi lines can be crossed to a tissue specific enhancer GAL4 driver for tissue-specific knockdown of the gene of interest (Figure 1.10).

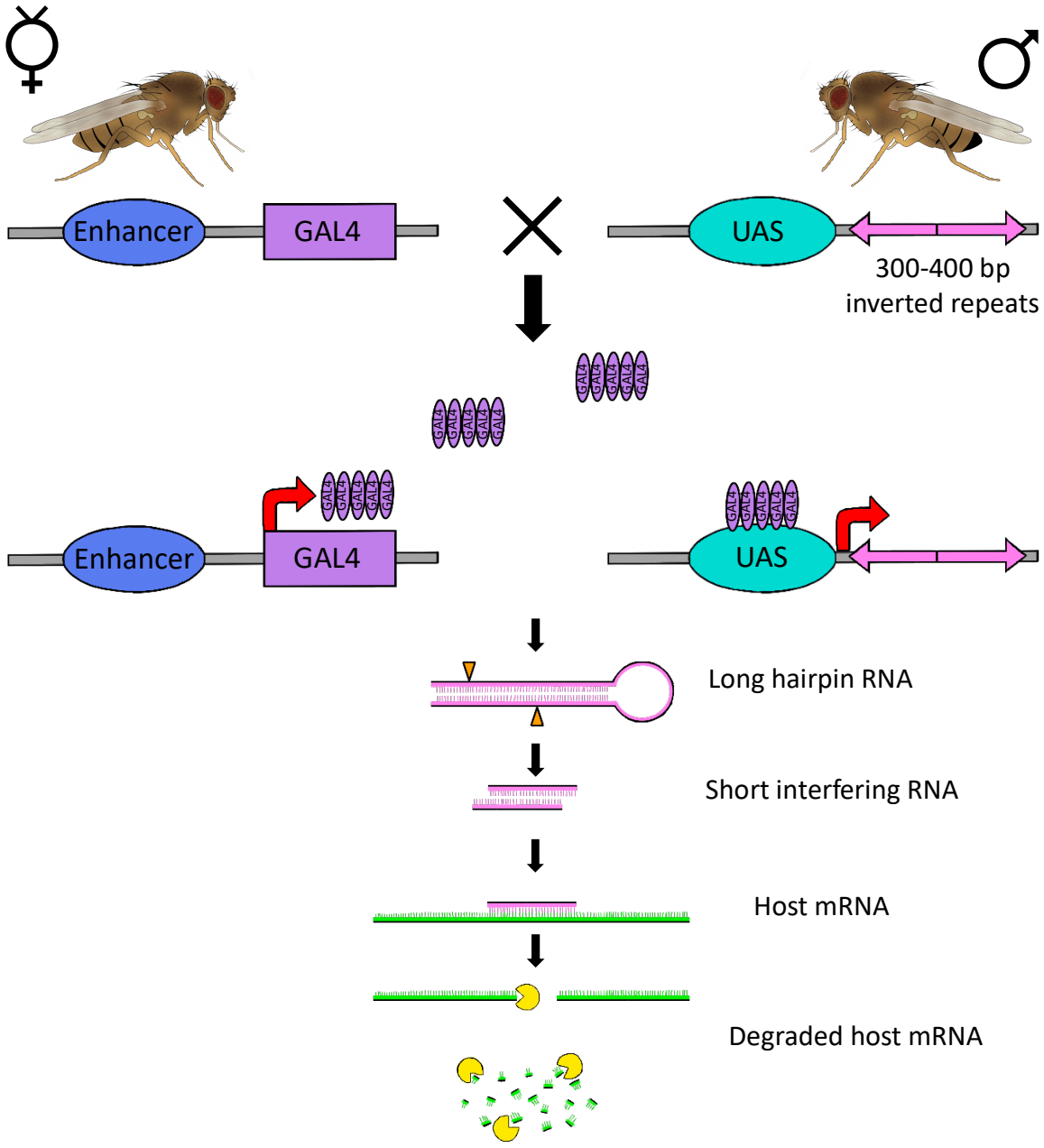

Figure 1.10. RNA interference. The UAS/GAL4 system is used to tissue specifically express the long inverted repeat hairpin RNAs of approximately 300-400 bp (pink). This is then cleaved by Dicer-2 (orange) to generate many siRNA transcripts which target a specific site on the host mRNA (green) resulting in degradation of the endogenous host mRNA by AGO2 (yellow). bp = base pair. *Original figure created with reference to Brand and Perrimon (1993); Petrova et al. (2013).*

1.4 Regulation of gene expression

Precise temporal and spatial expression of plasticity-related genes is essential for synaptic plasticity and memory formation (Zovkic *et al.*, 2013). This is regulated by accessibility of transcriptional regulators to promoter and enhancer regions in DNA. Within eukaryotic cells,

DNA is organised into chromatin, whereby it is wrapped around an octamer of core histones to form a nucleosome and arrays of nucleosomes undergo further higher order folding to compact the chromatin (Heslop-Harrison & Schwarzacher, 2013; Reiter *et al.*, 2001; Verreault, 2000).

Epigenetic regulation refers to changes in gene expression without altering the DNA sequence. Among the most commonly studied epigenetic mechanisms are acetylation/deacetylation, methylation/demethylation, and phosphorylation/dephosphorylation (Nowak & Corces, 2004; Sterner & Berger, 2000; Zhang & Reinberg, 2001). These modifications can alter promoter accessibility by modifying histone tails, which protrude from the histone cores. This alters the binding properties of DNA and histones, resulting in conformational changes in chromatin packing, which can lead to either activation or repression of transcription (Handy *et al.*, 2011; Jaenisch & Bird, 2003).

Histone acetylation involves the transfer of an acetyl group from acetyl coenzyme A to N-terminal lysine residues in core histone tails by a histone acetyl transferase (HAT). This transfer neutralises the positive charge of lysine residues to weaken the interaction with negatively charged DNA, resulting in transcription activation due to the relaxed open chromatin conformation (Verdone *et al.*, 2005). On the contrary, histone deacetylation involves the removal of the previously mentioned activating acetyl marks by a histone deacetylase (HDAC), resulting in a condensed chromatin conformation leading to transcriptional repression due to inaccessibility for transcription factors to bind to the DNA (Cho *et al.*, 2005; Foglietti *et al.*, 2006; Gallinari *et al.*, 2007).

1.4.1 HDACs

In humans there are a total of eleven highly conserved HDACs which are split into four different classes based on sequence similarity to yeast HDACs. Primarily localised in the nucleus, class I HDACs consist of HDAC1, 2, 3, and 8 which share homology with yeast *Reduced potassium dependency 3* (*Rpd3*). This class of HDACs all contain a single highly active deacetylase domain, contributing to the vast majority of HDAC deacetylation activity *in vivo* (Grozinger *et al.*, 1999; Grozinger & Schreiber, 2002; Hildmann *et al.*, 2006; Kao *et al.*, 1999; Morris & Monteggia, 2013; Somoza *et al.*, 2004). Class II HDACs share homology with yeast *Hda1* and are further divided into Class IIa, and Class IIb. Class IIa consists of HDAC4, 5, 7, and 9, and all are found in both the nucleus and cytoplasm. This class of HDACs undergo dynamic

nucleocytoplasmic shuttling that is regulated by phosphorylation of three conserved serine residues and binding of myocyte enhancer factor 2 (MEF2) to the conserved MEF2 binding domain at the N-terminus (Bertos *et al.*, 2001; Chawla *et al.*, 2003; Fischle *et al.*, 2001; Grozinger *et al.*, 1999; Grozinger & Schreiber, 2000; Grozinger & Schreiber, 2002; Hildmann *et al.*, 2006; Kao *et al.*, 1999; Schlumm *et al.*, 2013). Class IIb consists of HDAC6 and HDAC10 which are primarily localised to the cytoplasm. HDAC6 contains dual deacetylase domains, and a C-terminal zinc finger domain, whereas HDAC10 contains a single deacetylase domain and a C-terminal leucine rich region. Class III consists of seven Sirtuins which are homologous to yeast *Sir2* and are expressed in a variety of tissues and have varied subcellular localisation. Sirtuins differ from other HDAC classes based on cofactor dependence, all other HDACs rely on Zinc whereas Sirtuins require NAD^+ (Grozinger & Schreiber, 2002; Imai *et al.*, 2000). The final class of HDACs is Class IV and contains only HDAC11, which harbours a single deacetylase domain, resides primarily in the nucleus, and is the least characterised of all the HDACs.

1.5 Vertebrate HDAC4

Histone deacetylase 4 (HDAC4) is a Class IIa HDAC that undergoes nucleocytoplasmic shuttling in response to synaptic activation (Chawla *et al.*, 2003), however in humans, HDAC4 predominantly localises to the cytoplasm. The conserved features of the HDAC4 protein include an N-terminal MEF2 binding domain that, along with a nuclear localisation sequence (NLS), facilitates nuclear import (Chawla *et al.*, 2003; Wang & Yang, 2001). This is dependent on the presence of three conserved serine residues (Ser^{246}, Ser^{467}, and Ser^{632}) (Chawla *et al.*, 2003; Grozinger & Schreiber, 2000), that when dephosphorylated by Protein phosphatase 2A (PP2A) facilitate an interaction with the transcription factor MEF2A, which is required for successful nuclear import (Paroni *et al.*, 2008) as the NLS alone is relatively inefficient (Borghi *et al.*, 2001; Wang & Yang, 2001). Within the nucleus the HDAC4-MEF2 interaction results in repression of MEF2-dependent gene transcription (Chawla *et al.*, 2003). Upon influx of Ca^{2+}, CaMKII is activated and phosphorylates the three serine residues (Bolger & Yao, 2005; Chawla *et al.*, 2003; Grozinger & Schreiber, 2000; Wang & Yang, 2001). This recruits 14-3-3 chaperone proteins causing dissociation of the HDAC4-MEF2 repressive complex in the nucleus. This exposes a nuclear export sequence (NES) located toward the C-terminus that facilitates nuclear export of HDAC4 and sequestration in the cytoplasm (Bertos *et al.*, 2001;

Chawla *et al.*, 2003; Grozinger & Schreiber, 2000; McKinsey *et al.*, 2001; Wang & Yang, 2001; Wang *et al.*, 2014). The N-terminal ankyrin repeat binding domain is also conserved (Xu *et al.*, 2012) and facilitates binding to ankyrin repeat containing proteins, discussed further in Section 1.7.2. Furthermore, within this region is an additional serine residue (Ser^{350}) that when phosphorylated promotes nuclear shuttling (Xu *et al.*, 2012) (Figure 1.11). HDAC4 is catalytically inactive due to a single tyrosine to histidine point mutation in the C-terminal deacetylase domain (Lahm *et al.*, 2007), however, by interacting with HDAC3, which has active deacetylation capacity, HDAC4 can indirectly regulate histone deacetylation. HDAC3 forms a stable complex with the silencing mediator for retinoid and thyroid hormone receptor (SMRT) and nuclear receptor co-repressor (N-CoR) co-repressors. Both N-CoR and SMRT mediate HDAC3 deacetylation via a deacetylase activating domain and specific motifs located on N-CoR and SMRT (Guenther *et al.*, 2001; Li *et al.*, 2000). The N-CoR-SMRT complex has also been shown to interact with class II HDACs to repress transcription in reporter assays. Further studies have demonstrated that the N-CoR-SMRT co-repressor complex, bridges the interaction between catalytically inactive HDAC4 and catalytically active HDAC3 in order to exert deacetylase activity to repress transcription in an HDAC4 dependent manner (Fischle *et al.*, 2001; Grozinger *et al.*, 1999).

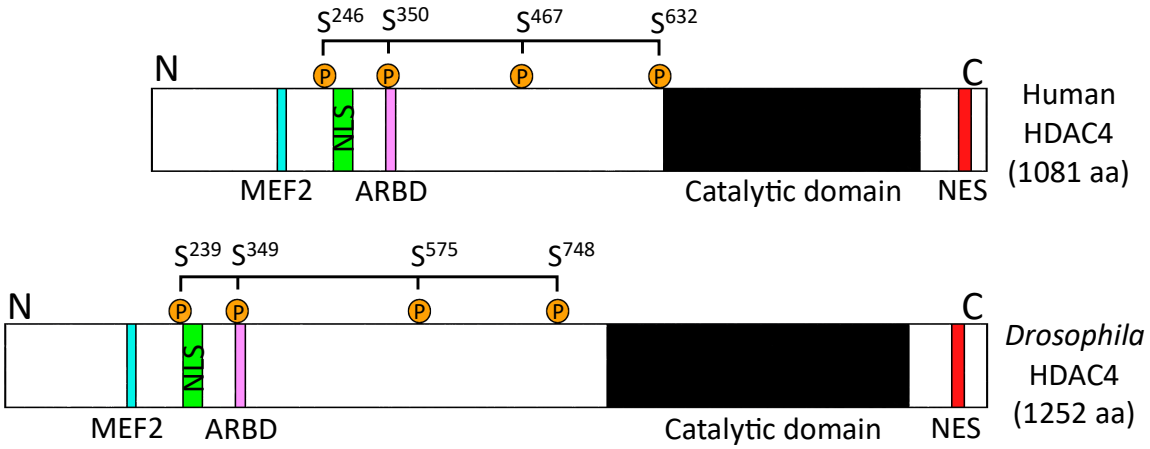

Figure 1.11. Domain structures conserved between human and *Drosophila* HDAC4. HDAC4 domain structures (Human HDAC4 GenBank accession NP_006028 and *Drosophila* HDAC4 GenBank accession NP_572868). Both human and *Drosophila* HDAC4 harbour an N-terminal MEF2 binding domain (cyan), NLS (green), ankyrin repeat binding domain (ARBD) (pink), and four conserved serine residues that when phosphorylated recruit 14-3-3 (orange). Both human and *Drosophila* HDAC4 also harbour a C-terminal deacetylase domain (black) and NES (red). MEF2 = MEF2 binding domain, NLS = nuclear localisation sequence, ARBD = ankyrin repeat binding domain, P = phosphorylated serine, NES = nuclear export sequence. *Original artwork created with reference to Fitzsimons et al. (2013); Tan et al. (2024); Wilson (2021).*

In vertebrates, HDAC4 expression in the brain is widespread (Darcy *et al.*, 2010; Grozinger *et al.*, 1999; Wang & Zeng, 2000) however, the subcellular distribution varies widely across different brain regions and even within specific subpopulations of cells. For example, in the dentate granule cells of the mouse hippocampus, a brain region important for learning and memory, HDAC4 localises to the postsynaptic density at dendritic shafts and spines with minor immunoreactivity in neuronal nuclei (Darcy *et al.*, 2010). In contrast, in the CA3 region of the hippocampus, to which the dentate granule cells project (Scharfman, 2007), HDAC4 distribution is heterogeneous, with presence in some nuclei but not others, indicative of dynamic shuttling (Darcy *et al.*, 2010).

1.5.1 HDAC4 and neuronal dysfunction

An increasing number of studies have implicated HDAC4 in neurodevelopmental and neurodegenerative diseases. Chromosomal deletion of 2q37, a region of chromosome 2 where *HDAC4* is located, results in 2q37 deletion syndrome (previously known as Brachydactyly Mental Retardation Syndrome). Individuals with a deletion or mutations within this region display clinical features that can include ASD, intellectual disability, and behavioral issues as well as phenotypic distinctions observed as craniofacial dysmorphism and metacarpal/metatarsal defects. These phenotypic differences are widely varied as a result of altered *HDAC4* dosage, as it has been hypothesised that HDAC4 deletion has incomplete penetrance therefore, these differences could be attributed to contribution from other genes (Morris *et al.*, 2012; Williams *et al.*, 2010). The role that HDAC4 plays in the manifestation of this disorder is currently unknown.

More recently, individuals carrying heterozygous *de novo* missense mutations of the *HDAC4* gene were identified and all presented with intellectual disability (Wakeling *et al.*, 2021). Of the seven unrelated cases, five involved a mutation of Proline^{248}, which is important in 14-3-3 chaperone binding and cytoplasmic HDAC4 shuttling. Two individuals had mutations in either Threonine^{244} or Glutamate^{247}, both of which lie within the 14-3-3 binding motif. It is likely that in these individuals, HDAC4 would have reduced 14-3-3 binding either due to conformational changes of the binding motif or reduced phosphorylation of Ser^{246} (the closest phosphorylation site to all point mutations). This lack of 14-3-3 binding is expected to result in a loss of nucleocytoplasmic shuttling of HDAC4, leading to reduced cytoplasmic retention and increased

nuclear accumulation (Wakeling *et al.*, 2021). Further, disruption of HDAC4 nucleocytoplasmic shuttling has been associated with mutations in the *cyclin dependent kinase-like 5* (*Cdkl5*) gene, which leads to CDKL5 disorder, the hallmarks of which include deficits in motor function, seizure onset, and intellectual disability (Trazzi *et al.*, 2016).

Loss of HDAC4 has been associated with cognitive impairment in a mouse model. A conditional forebrain neuron-specific HDAC4 knockout mouse strain resulted in defects in spatial learning and memory (Kim *et al.*, 2012). A parallel study documented impairments to spatial memory on overexpression of an HDAC4 mutant. Sando *et al.* (2012) generated a mouse strain harbouring an *HDAC4*-transgene lacking the C-terminal domain, which includes the deacetylase domain and the NES, resulting in aberrant nuclear accumulation of HDAC4. Expression of this mutant specifically in the mouse forebrain resulted in deficits in the Barnes maze, a model of spatial learning and memory (Bach *et al.*, 1995; Sando *et al.*, 2012).

Increased abundance of HDAC4 in the nucleus has also been associated with several neurodegenerative disorders, including Alzheimer's disease (Herrup *et al.*, 2013; Shen *et al.*, 2016), Ataxia telangiectasia (J. Li *et al.*, 2012), Neuronal intranuclear inclusion disease (NIID) (Takahashi-Fujigasaki *et al.*, 2006), and Lewy body dementia and Parkinson's disease (Takahashi-Fujigasaki *et al.*, 2006; Takahashi-Fujigasaki & Fujigasaki, 2006). Examination of the subcellular distribution of HDAC4 in both a mouse model expressing APP, and in 27 post-mortem brains from individuals with Alzheimer's disease revealed a significant increase in nuclear HDAC4 in the hippocampal sections of post-mortem brains from individuals with Alzheimer's disease compared to unaffected individuals, and the progressive severity of the disease had a positive correlation with the level of nuclear HDAC4 (Herrup *et al.*, 2013; Shen *et al.*, 2016).

Ataxia telangiectasia is a neurodegenerative disease caused by mutations in the *ataxia telangiectasia mutated* (*ATM*) gene, a molecular feature of which is accumulation of nuclear HDAC4 (J. Li *et al.*, 2012). Interestingly, the increased level of nuclear HDAC4 in Alzheimer's disease brains correlated with a mutation of the *ATM* gene, suggesting Alzheimer's disease could be linked to ataxia telangiectasia (Shen *et al.*, 2016). In wild-type mouse brains HDAC4 is largely cytoplasmic, however, in *ATM* deficient mice HDAC4 accumulates in the nucleus, a result of hypophosphorylation, leading to decreased 14-3-3 binding and thus reduced nuclear export. *ATM* deficient mice have cerebral dysfunction characterised by motor abnormalities, however, the introduction of cytoplasmic HDAC4 rescued these neurological phenotypes by

preventing cell cycle re-entry and caspase activation, suggesting cytoplasmic HDAC4 confers a neuroprotective role (J. Li *et al.*, 2012).

The characteristic hallmarks of the most common Lewy body disease, Parkinson's disease, have been discussed in Section 1.1 and accumulation of HDAC4 in the nuclei of dopaminergic neurons has been observed following exposure to Parkinsonism inducing environmental toxins (Ballard *et al.*, 1985; Wu *et al.*, 2017). One such compound that induces the effects of Parkinson's disease is the neurotoxin 1-methly-4-phenyl-1,2,3,6-tetrahydropyridine (MPTP), which is a precursor to 1-methyl-4-phenylpyridinium (MPP+), and an accidental by-product in the production of the psychoactive synthetic opioid 1-methyl-4-phenyl-4-propionoxypiperdine (MPPP). Several case studies have shown permanent Parkinsonism in those who injected MPTP (Ballard *et al.*, 1985). Cultured primary neurons harbouring a point mutation in the *α-synuclein* gene (A53T) display higher sensitivity to neurotoxins, and when exposed to MPP^+, HDAC4 accumulated in the nucleus of dopaminergic neurons. This translocation and nuclear accumulation resulted in repression of MEF2 and CREB transcriptional activity and dopaminergic cell death (Wu *et al.*, 2017).

The above-mentioned studies together indicate that HDAC4 is required for normal neurodevelopment, and that nuclear accumulation of HDAC4 is associated with neurodegeneration in several diseases. While it is not clear whether nuclear HDAC4 accumulation is a cause or a consequence of neurodegeneration, research into the mechanisms through which HDAC4 functions in normal brains and the molecular consequences of increased nuclear accumulation of HDAC4 warrants further investigation.

1.6 *Drosophila* HDAC4

HDAC4 is the sole *Drosophila* Class IIa HDAC. *Drosophila* HDAC4 (DmHDAC4) and human HDAC4 (HsHDAC4) share 59% sequence similarity and 35% identity across the entire protein, with high conservation through the deacetylase domain (84% sequence similarity and 57% identity) (Fitzsimons *et al.*, 2013). Although this domain is highly conserved, DmHDAC4 does not contain the tyrosine to histidine mutation that inactivates the deacetylase activity of HsHDAC4 (Lahm *et al.*, 2007), therefore, DmHDAC4 remains catalytically active.

As mentioned in Section 1.5, additional domains conserved between HsHDAC4 and DmHDAC4 include the N-terminal MEF2 binding domain, the NLS, for nuclear import, as well as the three serine phosphorylation sites (Ser^{239}, Ser^{573}, and Ser^{748}), and the NES, that are required for nuclear export (Main *et al.*, 2021; Mihaylova *et al.*, 2011; Wang & Yang, 2001). The ankyrin repeat binding domain is 100% conserved and therefore harbours an additional serine residue (Ser^{349}) to further promote nuclear entry (Xu *et al.*, 2012) (Figure 1.11).

DmHDAC4 is expressed throughout the brain, and its subcellular distribution is similar to that of mouse HDAC4, which is predominantly cytoplasmic. Analyses of the expression of HDAC4 in whole brains has revealed that it is abundantly distributed to the axons that bundle to form the mushroom body lobes (Fitzsimons *et al.*, 2013; Main *et al.*, 2021; Schwartz *et al.*, 2016; Tan *et al.*, 2024; Wilson, 2021). DmHDAC4 localises to only a subset of nuclei in Kenyon cells (Fitzsimons *et al.*, 2013; Main *et al.*, 2021; Tan *et al.*, 2024), indicative of differentially regulated subcellular distribution in specific neuronal cell populations, also observed in the mouse brain (Darcy *et al.*, 2010). Domain structure similarities and expression profiles suggest that the study of DmHDAC4 may contribute to further understanding the role of HDAC4 in vertebrate neuronal development and disease.

1.6.1 DmHDAC4 in neurodevelopment and memory

DmHDAC4 is required for normal mushroom body formation, with reduced expression resulting in mild deficits in axon elongation (Tan *et al.*, 2024). Increased expression of DmHDAC4 resulted in a more severe impairment to axon morphogenesis, observed as reduced axon elongation and deficits in guidance and termination of axons. The predominant phenotype was β lobe fusion which is due to a lack of axon termination signaling resulting in axons aberrantly extending and crossing the midline (Hawley, 2020; Main *et al.*, 2021; Tan *et al.*, 2024). These data indicate that not only is the presence of HDAC4 essential for normal mushroom body development, but that in excess HDAC4 is also neuro-disruptive.

Although DmHDAC4 distributes to both the nucleus and cytoplasm in Kenyon cells (the neuronal cell bodies of the mushroom body axons), upon overexpression of wild-type HDAC4, HDAC4 nuclear aggregates appear (Tan *et al.*, 2024) similar to what was observed in NIH3T3 cells (Wang *et al.*, 2005) and COS cells (McKinsey *et al.*, 2006) upon co-expression of HDAC4 and Ankyrin repeat family A member 2 (ANKRA2) or Regulatory factor X associated ankyrin

containing protein (RFXANK) (McKinsey *et al.*, 2006; Wang *et al.*, 2005) discussed further in Section 1.7.2. As discussed in Section 1.5.1, nuclear accumulation of HDAC4 has been implicated in a range of neurodegenerative diseases, therefore, both human and *Drosophila* HDAC4 mutants with altered subcellular distribution were generated to investigate the contribution of the different subcellular pools of HDAC4 to the neurodevelopmental defects (Main *et al.*, 2021; Tan *et al.*, 2024).

An HDAC4 cytoplasmic-restricted mutant, generated by mutating the MEF2 binding domain, resulted in a loss of MEF2 binding and MEF2-dependent nuclear import, leading to cytoplasmic retention (Wang & Yang, 2001). Expression of this mutant with *elav-GAL4* and *OK107-GAL4* resulted in minimal mushroom body defects and nuclear aggregates, respectively (Tan *et al.*, 2024), suggesting that nuclear HDAC4 was responsible for the defects observed in the mushroom body upon overexpression of wild-type DmHDAC4. To confirm this, a nuclear-restricted mutant was also generated by substituting the three conserved serine residues (Ser^{239}, Ser^{573}, Ser^{748}), required for HDAC4 nuclear export, to alanine. Expression in mushroom body neurons significantly impaired mushroom body development and a significant increase in nuclear aggregate formation was observed (Tan *et al.*, 2024).

These mutations were also tested with HsHDAC4 and mushroom body defects were assessed. The cytoplasmic-restricted mutant $HsHDAC4^{L175A}$, was generated by substituting $Lysine^{175}$, a residue located within the MEF2 binding region, to alanine, thereby restricting expression to the cytoplasm (Main *et al.*, 2021), as $HsHDAC4^{L175A}$ impairs MEF2 binding and nuclear import (Salma & McDermott, 2012). Expression of this mutant had very little impact on neurodevelopment with 15% of brains displaying defects in mushroom body development (Main *et al.*, 2021). A nuclear-restricted mutant, $HsHDAC4^{3SA}$, was similarly generated to the nuclear-restricted DmHDAC4 mutant, by mutating the conserved three serine residues (Ser^{246}, Ser^{467}, and Ser^{632}), important for 14-3-3 mediated nuclear export, to alanine (Chawla *et al.*, 2003; Grozinger & Schreiber, 2000). Expression of $HsHDAC4^{3SA}$ resulted in a significant increase in mushroom body defects (Main *et al.*, 2021), confirming that an increase of either human or *Drosophila* HDAC4 in the nucleus results in neurodevelopmental defects, providing further evidence of the conservation of HDAC4 function.

The mushroom body is a critical structure for memory formation, as its ablation completely abolishes the formation of long-term courtship memory (McBride *et al.*, 1999). The presence of wild-type levels of HDAC4 are critically required for normal memory formation as

knockdown and overexpression of HDAC4 in the brain resulted in impairments in long-term courtship memory. Given that both knockdown and overexpression of HDAC4 impairs the development of the mushroom body and since an intact mushroom body is required for LTM formation, expression was induced or knocked down in the adult brain using the TARGET system (Section 1.3.4.2) to avoid any developmental effects (Fitzsimons *et al.*, 2013). These results suggest that normal levels of HDAC4 are required for normal memory acquisition, and too much or too little is detrimental (Fitzsimons *et al.*, 2013; Main *et al.*, 2021).

As previously described in Section 1.5.1, overexpression of the mammalian truncated *HDAC4* mutant lacking the inactive C-terminal deacetylase domain, resulted in impairments in spatial memory (Sando *et al.*, 2012), suggesting that catalytic activity is not required for the impairment in memory induced by HDAC4 overexpression. Although vertebrate HDAC4 is catalytically inactive, it can interact with HDAC3 via the deacetylase domain to facilitate deacetylase activity to repress transcription in an HDAC4-dependent manner (Fischle *et al.*, 2001; Grozinger *et al.*, 1999). As DmHDAC4 retains its catalytic activity a catalytically inactive mutant was generated with a histidine^{968} substitution to alanine. This residue was equivalent to a histidine residue at position 803 that was shown, when substituted to leucine, diminished deacetylase activity (A. H. Wang *et al.*, 1999). Overexpression of this mutant resulted in defects to LTM suggesting that the abolishment of LTM by overexpression of HDAC4 is independent of its catalytic activity (Fitzsimons *et al.*, 2013).

Increased abundance of DmHDAC4 also resulted in severe deficits in photoreceptor development, resulting in a rough eye phenotype. Expression was induced in photoreceptor neurons posterior to the morphogenetic furrow by the eye-specific *GMR-GAL4* driver (Freeman, 1996). Overexpression of a single copy of wild-type DmHDAC4 resulted in a mild rough eye phenotype consisting of ommatidia disorganisation and alterations to regular bristle patterning, a defect that results in more than one bristle emerging from a single bristle pore (Schwartz *et al.*, 2016; Wilson, 2021). This rough eye phenotype was exacerbated upon expression of a second copy of DmHDAC4, inducing widespread depigmentation and ommatidial fusion (Tan *et al.*, 2024)

In summary, these data show that the predominant features of HDAC4 are recapitulated in *Drosophila*, including similar expression and subcellular distribution patterns in the brain, and the requirement for HDAC4 in *Drosophila* neuronal development, and that increased nuclear accumulation of HDAC4 is neurotoxic, resulting in neurodevelopmental defects and impaired

cognition. Together these provide strong rationale that the study of HDAC4 function in *Drosophila* is likely to be informative.

1.7 Investigating the HDAC4 molecular pathway

Recent studies have shed light on the mechanisms through which HDAC4 acts, and is itself regulated, to modulate neuronal function during development and in the adult brain, highlighting that it is complex and involves regulation of transcription as well as non-transcriptional mechanisms. This section will discuss evidence from mammalian and *Drosophila* studies relevant to the work carried out in this thesis.

Nuclear HDAC4 expression in cultured neurons resulted in a total of 214 differentially regulated genes via Microarray analysis, 40% of which were repressed. Of these genes, half were essential for synaptic function, suggesting a role for nuclear HDAC4 in synaptic function. The regulation of these synaptic genes was shown to be specific to nuclear HDAC4 as few overlapping transcriptionally regulated genes were observed upon expression of nuclear HDAC7 (Sando *et al.*, 2012). On the contrary, RNA-sequencing (RNA-seq) on flies overexpressing wild-type DmHDAC4 in the brain resulted in a total of only 26 differentially regulated genes (Schwartz *et al.*, 2016). A subsequent RNA-seq analysis was performed in which different subcellular pools of HsHDAC4 were investigated to determine whether the subcellular distribution of HsHDAC4 affected gene expression. Similarly to DmHDAC4, overexpression of nuclear- and cytoplasmic-restricted HsHDAC4 in the brain shared a total of 29 differentially regulated genes (Main *et al.*, 2021). It is hypothesised that HDAC4 may therefore be acting, at least in part, through non-transcriptional mechanisms.

To that end, in order to identify genes that act in the same molecular pathways as *HDAC4*, an enhancer/suppressor rough eye phenotype screen was performed in the *Drosophila* eye (Schwartz *et al.*, 2016). The eye consists of specialised photoreceptor neurons (Freeman, 1996) which are presumed to have conserved molecular pathways to that of other neuronal cell populations, including those involved in development and memory formation. In this screen, HDAC4 was overexpressed in the eye, resulting in a mild rough eye phenotype. A total of 124 RNAi lines that targeted candidate HDAC4-interacting genes were screened for enhancement or suppression of the HDAC4-induced phenotype. A genetic interaction is observed when the

combination of two independent mutations results in a more severe phenotype than is expected if the two mutations were additive (see Section 1.3.2.3) (Perez-Perez *et al.*, 2009). Knockdown of several genes enhanced the HDAC4-induced phenotype, and 18 novel genetic interactions with HDAC4 were identified, these included transcriptional regulators, components of the SUMOylation machinery, and cytoskeletal regulators (Schwartz *et al.*, 2016). This data suggests that these genes act in the same molecular pathway as HDAC4, the majority of which are yet to be characterised.

1.7.1 HDAC4 interacts with transcription factors

A number of transcription factors that interact with HDAC4 have been identified, including Runt-related transcription factor two (Vega *et al.*, 2004), activating transcription factor four (Zhang *et al.*, 2014), CREB (J. Li *et al.*, 2012), and MEF2 (Wang & Yang, 2001). The interaction with CREB and MEF2 has been extensively studied and as previously mentioned in Section 1.5.1, nuclear accumulation of HDAC4 in cultured primary neurons harbouring mutant α-synuclein, when exposed to MPP+ resulted in a repression of CREB and MEF2-mediated transcription and ultimate dopaminergic neuron death (Wu *et al.*, 2017).

1.7.1.1 HDAC4 interacts with CREB

CREB is a transcription factor that plays a key role in the formation of LTM in Aplysia, *Drosophila*, and mammals (Yin & Tully, 1996). Induction of LTM involves activation of CREB via phosphorylation which ultimately recruits the acetyltransferase CREB binding protein (CBP) to promoters of genes involved in synaptic plasticity and neuronal growth (Barco *et al.*, 2006).

CREB has been shown to bind to HDAC4 in an ATM null mutant model where HDAC4 translocated to the nucleus and repressed CREB-dependent transcription (J. Li *et al.*, 2012). Furthermore, CREB has been found to interact with HDAC4 in an anaesthetic induced mouse model. It was observed that the administration of anaesthetic lead to an accumulation of nuclear HDAC4 and a decrease in the formation of the CREB/CBP complex, resulting in repression of

CREB-dependent transcription of pro-neuronal genes. The repression of CREB was shown to be responsible for the cognitive impairments observed in the mouse (Sen & Sen, 2016).

1.7.1.2 HDAC4 interacts with MEF2

MEF2 is a highly conserved transcription factor that plays an important role in cell division and differentiation (Lilly *et al.*, 1995). HDAC4 directly interacts with MEF2 *in vivo* through an N-terminal MEF2 binding domain and has been verified through co-immunoprecipitation experiments (Miska *et al.*, 1999). Nuclear import and export of HDAC4 requires the NLS (Borghi *et al.*, 2001; Wang & Yang, 2001) and NES respectively (Bertos *et al.*, 2001; Chawla *et al.*, 2003; Grozinger & Schreiber, 2000; McKinsey *et al.*, 2001; Wang *et al.*, 2014). However, nuclear import is also MEF2-dependent as deletion mutants demonstrated that HDAC4 is directed into the nucleus through an interaction with MEF2. This interaction is dependent on an intact MEF2 binding domain as a single point mutation (L175A) located within this domain, resulted in a loss of MEF2 binding and cytoplasmic retention of HDAC4, observed to be independent of the NLS (Borghi *et al.*, 2001; Main *et al.*, 2021; Wang & Yang, 2001). The interaction between HDAC4 and MEF2 and subsequent nuclear import results in the repression of MEF2-dependent transcription (Chawla *et al.*, 2003). Mammalian MEF2 consists of four isoforms (MEF2A-D) and a recent study has demonstrated the nature of the HDAC4-MEF2A-DNA interaction to induce HDAC4-mediated MEF2 transcriptional repression (Dai *et al.*, 2024). The N-terminus of a MEF2A dimer binds to the N-terminal MEF2 binding domain on HDAC4, however, to mediate MEF2A transcriptional repression, HDAC4 dimerises in an antiparallel manner through the N-terminal glutamate rich alpha helix domain (residues 62-129). Therefore, each HDAC4-MEF2A complex contains two dimers of MEF2A, bridged by an antiparallel dimer of HDAC4. MEF2A binds DNA, in a sequence specific manner and through HDAC4 dimerisation and availability of the MEF2 binding domain, two positions on the DNA are bound by MEF2A resulting in conformational changes to chromatin, leading to transcriptional repression (Dai *et al.*, 2024).

In mammalian cell culture, HDAC4 has been shown to harbour E3 SUMO ligase activity and SUMOylates MEF2 (Zhao *et al.*, 2005), this activity however, is repressed upon SUMOylation of HDAC4 itself (Gregoire & Yang, 2005). The addition of a SUMO peptide at lysine^{424} on

MEF2 regulates MEF2-dependent transcription, in contrast this residue is also subject to acetylation by CBP to promote transcriptional activation (Zhao *et al.*, 2005).

In *Drosophila*, HDAC4 was shown to genetically interact with SUMOylation machinery (Schwartz *et al.*, 2016), however co-localisation in Kenyon cells was not observed upon expression of the nuclear-restricted mutant of HsHDAC4 (Main *et al.*, 2021). Furthermore, knockdown of Ubc9, an E2 SUMO-conjugating enzyme, impaired long-term courtship memory and when co-expressed with DmHDAC4, this memory impairment was further enhanced (Schwartz *et al.*, 2016).

The interaction between HDAC4 and MEF2 is conserved in *Drosophila*, as an increase in nuclear DmHDAC4 resulted in sequestration of MEF2 into nuclear HDAC4 aggregates (Fitzsimons *et al.*, 2013) and a genetic interaction was observed via a rough eye enhancer screen (Schwartz *et al.*, 2016). Furthermore, an HDAC4 mutant, with point mutations within the MEF2 binding region (HDAC4$^{\Delta MEF2}$) resulted in a loss of MEF2 binding and cytoplasmic retention of HDAC4 (Tan *et al.*, 2024). This also led to a reduction in nuclear aggregate accumulation and rescued the mushroom body β lobe fusion defects induced by both wild-type (Tan *et al.*, 2024) and nuclear-restricted HDAC4 (Main *et al.*, 2021). To differentiate defects induced by cytoplasmic localisation and MEF2 binding inhibition, an additional cytoplasmic-localised mutant with point mutations within the NLS (HDAC4$^{\Delta NLS}$) was generated and resulted in a significantly more severe mushroom body phenotype compared to HDAC4$^{\Delta MEF2}$ which was attributed to the availability of the MEF2 binding region. Therefore, the developmental defects induced by HDAC4 are dependent on the presence of and interaction with MEF2 (Tan *et al.*, 2024).

1.7.2 HDAC4 interacts with cytoskeletal regulators

It has been well characterised that the N-terminus of HDAC4 is capable of binding to the MEF2 transcription factor to regulate gene expression (Chawla *et al.*, 2003; Miska *et al.*, 1999). However, less is known about the MEF2-independent mechanisms of HDAC4 transcriptional regulation. Wang *et al.* (2005) and McKinsey *et al.* (2006) discovered physical interactions between HDAC4 and two ankyrin repeat containing proteins, ANKRA2 and RFXANK in mammalian cell culture via yeast-two-hybrid, co-immunoprecipitation, and co-localisation

studies. ANKRA2 interacts with the cytoplasmic tail of Megalin, which is a member of the low-density lipoprotein receptor family, in kidney cells and glomerular vesicles (Rader *et al.*, 2000). RFXANK is a positive regulator of the major histocompatibility complex (MHC) class I and II gene expression. Genes transcribed by this complex encode transmembrane proteins that have vital roles in the development and control of the adaptive immune system (Maternak *et al.*, 1998). While mutations in components of the MHC that lead to a loss of MHC class II antigen presentation, resulting in an immune deficiency disorder referred to as Bare lymphocyte syndrome (BLS) (Mach *et al.*, 1996; Wang *et al.*, 2005), MHC class I gene deficiency results in a loss of neuronal function, synaptic plasticity, and memory consolidation due to dendritic atrophy (Lazarczyk *et al.*, 2016). Recently it has been reported that a splice site loss of function mutation of RFXANK resulted in BLS immunodeficiency that presented with a novel case of late-onset neurodegenerative disease (Alharby *et al.*, 2021), implicating immune deficiency with neurological dysfunction.

Both ANKRA2 and RFXANK contain five ankyrin repeats at the C-terminus (Xu *et al.*, 2012). Each ankyrin repeat motif consists of two α helices connected by loops, and as there is no full consensus sequence for these repeats, mediating protein-protein interactions via the ankyrin repeat motif relies on protein folding and sufficient hydrophobic interactions (Mosavi *et al.*, 2004; Xu *et al.*, 2012). Given this, there are conserved residues at eight sites within the repeat, half of which are located at the beginning of the repeat, with the other half residing at the end of the repeat, all of which are necessary to generate the structure of the repeat (Mosavi *et al.*, 2004). These conserved residues are located within repeats two and four for both ANKRA2 and RFXANK. ANKRA2 (GenBank accession Q9H9E1) and RFXANK (GenBank accession O14593) share 60.6% sequence identity and 73.1% overall similarity with 66% sequence identity and 78.4% overall similarity across the ankyrin repeats (Pairwise Sequence Alignment, EMBOSS Water).

ANKRA2 was identified as a binding partner of HDAC4 in a yeast-two hybrid screen of human foetal brain cDNA. An *in vitro* binding assay substantiated these findings and demonstrated that the ankyrin repeats of ANKRA2 were responsible for mediating this interaction with an N-terminal region of HDAC4. As discussed above, ANKRA2 and RFXANK share homology, therefore binding assays were also performed between RFXANK and HDAC4 with results confirming that binding is mediated by the ankyrin repeats (Wang *et al.*, 2005; Xu *et al.*, 2012). A parallel study showed an interaction between ANKRA2 and HDAC5 using mouse embryo cDNA. Luciferase reporter and co-immunoprecipitation assays using ANKRA2 deletion

mutants confirmed the interaction with HDAC5 and showed that the first ankyrin repeat sequence was sufficient for stabilising the interaction with HDAC5, however when RFXANK deletion mutants were subject to co-immunoprecipitation assays with HDAC4, the first ankyrin repeat was insufficient in maintaining the interaction and either repeats one and two or repeats three and four were required for stable binding to HDAC4, as RFXANK showed lower binding affinity compared to ANKRA2 for HDAC4 (McKinsey *et al.*, 2006). To map the binding site of ankyrin repeats on HDAC4, both *in vivo* and *in vitro*, RFXANK was used. An *in vitro* binding assay was performed where a maltose binding protein (MBP) was fused to RFXANK and immobilised on amylose agarose. This complex was then incubated with labelled HDAC4-deletion mutants, followed by elution and identification of bound proteins. RFXANK was shown to interact with full length HDAC4, and residues 118-279 were shown to be essential for this interaction (Wang *et al.*, 2005).

To test the interaction *in vivo*, co-immunoprecipitation assays with HEK293 cells co-transfected with RFXANK and HDAC4 deletion mutants showed binding to residues 315-666, with lowered binding when reduced to residues 448-666, suggesting ankyrin repeat binding between residues 315-666 (Wang *et al.*, 2005). Further studies have since characterised what is commonly referred to as the ankyrin repeat binding domain, a highly conserved hydrophobic leucine- and proline-rich PxLPxI/L motif (Xu *et al.*, 2012). This motif is not only present in HDAC4, but also other binding partners of ANKRA2 and RFXANK, including CCDC8 which interacts with ANKRA2 and when mutated results in the 3M growth disorder syndrome (Nie *et al.*, 2015), Megalin which interacts with ANKRA2 (Rader *et al.*, 2000), RFX5 which interacts with RFXANK and is an important component of the MHC (Xu *et al.*, 2012), and RFX7 which interacts with both ANKRA2 and RFXANK and is also an important component of the MHC (Gao & Xu, 2020). The human HDAC4 ankyrin repeat binding motif (PSLPNI) is located within the range described above at residues 349-354 (Wang *et al.*, 2005). The recognition and binding of proteins via the PSLPNI motif stems from the ability of the sidechains of the HDAC4 motif to fit seamlessly into the hydrophobic pockets formed above the α helix of the ankyrin repeats as substitution mutations of leu^{351} or ile^{354} to glycine abolished, and pro^{349} substituted to glycine significantly diminished the binding capacity of ANKRA2 (Xu *et al.*, 2012). Interestingly, HDAC4-deletion mutants 315-1084, 208-1084, and 189-1084 showed stronger binding to RFXANK than full length HDAC4 and deletion mutant 146-1084, indicative of a region within residues 146-189 that inhibits binding to RFXANK (Wang *et al.*, 2005). These studies show that there are two potential binding sites of RFXANK to HDAC4, one within

residues 118-279 and the other within 315-666, and an autoinhibitory site located within residues 146-189 (Wang *et al.*, 2005). As the PSLPNI motif is located within residues 315-666 (Xu *et al.*, 2012), it is likely to be the predominant binding region as it is a highly conserved motif among proteins that interact with ankyrin repeat containing proteins, and across species where it is 100% conserved in DmHDAC4 (Xu *et al.*, 2012). Co-transfection of HDAC4 with either ANKRA2 in NIH3T3 cells (Wang *et al.*, 2005) or with ANKRA2 or RFXANK in COS cells (McKinsey *et al.*, 2006) show both redistribute to the nucleus, and are sequestered into HDAC4 nuclear aggregates (McKinsey *et al.*, 2006; Wang *et al.*, 2005). In neurons this regulation is not mediated through transcriptional changes, as ANKRA2 and RFXANK were not significantly up or down regulated following RNA-seq analyses on brains expressing either nuclear or cytoplasmic-restricted HsHDAC4 mutants (Main *et al.*, 2021), suggesting HDAC4 is not acting at a transcriptional level. Therefore, uncovering non-transcriptional mechanisms through which HDAC4 acts, warrants further investigation.

1.8 Aims and objectives

HDAC4 has been demonstrated to play a role in neurodevelopment (Schwartz *et al.*, 2016; Tan *et al.*, 2024; Wilson, 2021) and memory formation (Fitzsimons *et al.*, 2013; Main *et al.*, 2021) and has also been implicated in a range of neurodevelopmental (Morris *et al.*, 2012; Wakeling *et al.*, 2021; Williams *et al.*, 2010) and neurodegenerative diseases (Herrup *et al.*, 2013; J. Li *et al.*, 2012; Shen *et al.*, 2016; Wu *et al.*, 2017). The accumulation of nuclear HDAC4 as well as loss-of-function mutations of HDAC4 are key features of these diseases, many of which are associated with intellectual disability, cognitive defects, and memory loss.

Thus far the mechanisms through which nuclear HDAC4 promotes impaired neuronal development and LTM remain unclear. RNA-seq on flies expressing wild-type or nuclear-restricted HDAC4 showed few transcriptional changes (Main *et al.*, 2021; Schwartz *et al.*, 2016), therefore it is believed that nuclear HDAC4 may be acting, at least in part, through non-transcriptional mechanisms. A *Drosophila* rough eye enhancer screen identified a number of genes that interact with *HDAC4* (Schwartz *et al.*, 2016), but the molecular mechanisms underlying these interactions are yet to be identified. Investigating the interaction between candidate interactor(s) and HDAC4 to determine their roles in neuronal development,

morphogenesis, and memory may lead to discoveries in the HDAC4 molecular pathway that could help to uncover mechanism(s) through which HDAC4 regulates neurological processes.

The aim of this study is to identify and characterise candidate HDAC4-interactor(s) to investigate the molecular mechanisms through which HDAC4 may regulate neuronal development.

This project will attempt to address these gaps in knowledge through the following objectives:

1. **Selection of HDAC4 candidate interactor(s)**
   A number of proteins with different functional roles have previously been identified to interact with HDAC4, specifically in the nucleus (Chawla *et al.*, 2003; Miska *et al.*, 1999; Wang & Yang, 2001). Candidate *HDAC4*-interactors will be selected from the previous rough eye enhancer screen (Schwartz *et al.*, 2016); for genes that interact with *HDAC4*, from RNA-seq data (Main *et al.*, 2021; Schwartz *et al.*, 2016); for genes that were differentially regulated by *HDAC4*, and from a literature review for genes that have been shown to interact with *HDAC4* in other organisms. Expression of each candidate interactor will be depleted via RNAi and the *Drosophila* mushroom body and compound eye will both be analysed for defects. If candidate gene depletion results in similar defects in development as HDAC4 overexpression, these results would suggest they may act in similar molecular pathways. In addition, expression analyses in the *Drosophila* brain will be performed to demonstrate whether expression of the candidate(s) is in similar pattern to HDAC4, and from this screen, candidate interactor(s) will be selected for further investigation.

2. **Investigating the interaction of the candidate interactor(s) with HDAC4**
   A range of well-established assays in the *Drosophila* brain and eye will be carried out to investigate the nature of the interaction between the candidate interactor(s) and HDAC4 via immunohistochemistry, co-immunoprecipitation, and genetic analysis.

3. **Dissection of the role candidate interactor(s) play in *Drosophila* neural function**

   In order to understand the role that the candidate interactor(s) play in *Drosophila* development and function, morphological analyses of the *Drosophila* brain, eye, and wing will be assessed along with behavioural analyses including survival, longevity, locomotor function, and courtship learning and memory.

   If depletion of the candidate interactor(s) results in a disruptive phenotype in either the mushroom body or eye, further analyses will be carried out in these tissues. These analyses may elucidate the role the candidate interactor(s) play in regulating development in different neural cell types by investigating different stages of development and assessing the potential molecular pathways in which the candidate interactor(s) may function.

2 Methodology

2.1 *Drosophila melanogaster* fly strains

Drosophila melanogaster fly strains used in this study are listed in Table 2.1. For the sake of clarity and consistency, all fly strains will be mentioned throughout by name rather than genotype unless otherwise stated in the text.

Table 2.1. *Drosophila melanogaster* strains used throughout this study

Stock	Fly strains (Shorthand names)	Genotype	Chromosome	Source location
1	**w(CS10)**	*w[CS10]*		R.Davis
H83	**elav-GAL4**	*w[CS10],P{w[+mW.hs]=GawB}elav[C155]*	1	BDSC 458
H565	**OK107-GAL4**	*w[*]; P{w[+mW.hs]=GawB}OK107 ey[OK107]*	4	BDSC 854
H84	**GMR-GAL4**	*w[CS10]; P{w[+mC]=GAL4-ninaE.GMR}12*	2	BDSC 1104
H554	**CG5846^{RNAi1}/ peep^{RNAi1}**	*w[CS10]; P{GD10737}v21645 CG5846*	3	VDRC 21645
H555	**CG5846^{RNAi2}/ peep^{RNAi2}**	*w[CS10]; P{attP,y[+],w[3`v107793] CG5846*	2	VDRC 107793
H640	**crammer^{RNAi1}**	*w[1118];P{GD12961}v22752 CG10460*	3	VDRC 22752
H680	**crammer^{RNAi2}**	*y[1] v[1]; P{y[+t7.7] v[+t1.8]=TRiP.JF01914}attP2*	3	BDSC 25875
H655	**forked^{RNAi1}**	*w[1118];P{GD1443}v33200 CG42864*	2	VDRC 33200
H656	**forked^{RNAi2}**	*y,w[1118];P{attP,y[+],w[3`]}C G42864*	2	VDRC 103813
H661	**foxo^{RNAi1}**	*y,w[1118];P{attP,y[+],w[3`]}C G3143*	2	VDRC 106097
H662	**foxo^{RNAi2}**	*y,w[1118];P{attP,y[+],w[3`]}C G3143*	2	VDRC 107786
H553	**Kank^{RNAi}**	*w[CS10]; P{GD6584}v15009 CG10249*	2	VDRC 15009
H648	**Kdm5^{RNAi1}**	*w[1118];P{GD14113}v42203 CG9088*	3	VDRC 42203
H649	**Kdm5^{RNAi2}**	*w[1118];P{GD14113}v42204 CG9088*	3	VDRC 42204
H651	**kek2^{RNAi1}**	*w[1118];P{GD9}v42450 CG4977*	2	VDRC 42450
H652	**kek2^{RNAi2}**	*w[1118];P{GD2505}v4745 CG4977*	3	VDRC 4745

H641	**kra^{RNAi1}**	*w[1118];P{GD8839}v25166 CG2922*	2	VDRC 25166
H642	**kra^{RNAi2}**	*y,w[1118];P{attP,y[+],w[3`]}C G2922*	2	VDRC 102609
H646	**mthl8^{RNAi1}**	*w[1118];P{GD2227}v4071 CG32475*	3	VDRC 4071
H647	**mthl8^{RNAi2}**	*y,w[1118];P{attP,y[+],w[3`]}C G32475*	2	VDRC 100246
H657	**NetB^{RNAi1}**	*w[1118];P{VDRCsh60200}attP 40, CG10521*	2	VDRC 330183
H658	**NetB^{RNAi2}**	*y,w[1118];P{attP,y[+],w[3`]}C G10521*	2	VDRC 100840
H558	**Npc2g^{RNAi1}**	*w[CS10]; P{GD17722}v50721 CG11314*	2	VDRC 50721
H559	**Npc2g^{RNAi2}**	*w[CS10]; P{GD17722}v6523 CG11314*	3	VDRC 6523
H560	**Npc2g^{RNAi3}**	*w[CS10]; P{attP,y[+],w[3`v104942] CG11314*	2	VDRC 104942
H666	**rogdi^{RNAi1}**	*y,w[1118];P{attP,y[+],w[3`]}C G7725*	2	VDRC 107310
H667	**rogdi^{RNAi2}**	*w[1118];P{KK108321}VIE-260B CG7725*	3	VDRC 107310
H654	**Scamp^{RNAi1}**	*y,w[1118];P{attP,y[+],w[3`]}C G9195*	2	VDRC 106761
H682	**Scamp^{RNAi2}**	*y[1] sc[*] v[1] sev[21]; P{y[+t7.7] v[+t1.8]=TRiP.HMS01728}attP 40*	2	BDSC 38277
H653	**shn^{RNAi}**	*y,w[1118];P{attP,y[+],w[3`]}C G7734*	2	VDRC 105643
H663	**Sik3^{RNAi1}**	*y,w[1118];P{attP,y[+],w[3`]}C G42856*	2	VDRC 107458
H664	**Sik3^{RNAi2}**	*y,w[1118];P{attP,y[+],w[3`]}C G42856*	2	VDRC 106268
H665	**Sik3^{RNAi3}**	*y,w[1118];P{attP,y[+],w[3`]}C G42856*	3	VDRC 39866
H643	**Thor^{RNAi1}**	*w[1118];P{GD12533}v35439+ G83 CG8846*	3	VDRC 35439
H644	**Thor^{RNAi2}**	*w[1118];P{GD12533}v35440 CG8846*	3	VDRC 35440
H645	**Thor^{RNAi3}**	*y,w[1118];P{attP,y[+],w[3`]}C G8846*	2	VDRC 100739
H50	**UAS-CD8::GFP**	*y1w*; P{UAS-mCD8::GFP.L}LL5*	2	BDSC 5137
H693	**Kank-GAL4**	*y[1] w[*]; Mi{Trojan-GAL4.1}Kank[MI13070-TG4.1]/SM6a*	2	BDSC 76748
H691	**kra-GAL4**	*w[1118]; PBac{w[+mC]=IT.GAL4}kra[0506-G4]/TM6B, Tb[1]*	3	BDSC 63366
H695	**mthl8-GAL4**	*w[*]; TI{2+D302:D319A-GAL4}mthl8[2A-GAL4]/TM3, Sb[1]*	3	BDSC 84661

H688	**rogdi::GFP**	*y[1] w[*]; Mi{PT-GFSTF.0}rogdi[MI06667-GFSTF.0]/TM6C, Sb[1] Tb[1]*	3	BDSC 59299
H689	**shn::GFP**	*y[1] w[67c23]; Mi{PT-GFSTF.1}shn[MI01496-GFSTF.1]/SM6a*	2	BDSC 59403
H617	**Peep^{OE}**	*w[CS10]; PBac{y+-attP-3B}VK22, UAS-CG5846-HA. Insert into VK22(2R) 57F5*	2	Genetivision, USA
H741	**HDAC4^{WT}**	*w[CS10]; P{y[+t7.7]=CaryP}attP2, UAS-DmHDAC4(WT)-myc. Insert into P2:(3L) 68A4*	3	Genetivision, USA
H473	**HDAC4$^{\Delta Ank}$**	*y[1] w[67c23]; P{y[+t7.7]=CaryP}attP2, UAS-DmHDAC4-ΔAnk)-myc. Insert into P2:(3L) 68A4*	3	Genetivision, USA
H634	**GFP-HDAC4^{WT}, HDAC4^{WT}**	*w[CS10]; PBac{y+-attP-3B}VK37, UAS-GFP-DmHDAC4, P{y[+t7.7]=CaryP}attP2, UAS-DmHDAC4(WT)-myc/TM3, Sb Insert into P2:(3L) 68A4*	3	Genetivision, USA
H502	**Cy/Bl;TM2/ TM6B, Tb**	*w[1118]/Dp(1;Y)y[+]; CyO/Bl[1]; TM2/TM6B, Tb[1]*	2,3	BDSC 3704
H807	**HDAC4^{WT}; Peep^{OE}**	*w[CS10]; PBac{y+-attP-3B}VK22, UAS-CG5846-HA. Insert into VK22(2R) 57F5; P{y[+t7.7]=CaryP}attP2, UAS-DmHDAC4(WT)-myc. Insert into P2:(3L) 68A4*	2,3	Genetivision, USA
H808	**HDAC4$^{\Delta Ank}$; Peep^{OE}**	*w[CS10]; PBac{y+-attP-3B}VK22, UAS-CG5846-HA. Insert into VK22(2R) 57F5; P{y[+t7.7]=CaryP}attP2, UAS-DmHDAC4-dAnk)-myc. Insert into P2:(3L) 68A4*	2,3	Genetivision, USA
H622	**GMR; HDAC4^{WT}**	*w[CS10]; P{w[+mC]=GAL4-ninaE.GMR}12; P{y[+t7.7]=CaryP}attP2/CyO, UAS-DmHDAC4(WT)-myc. Insert into P2:(3L) 68A4*	2,3	BDSC 1104 Genetivision, USA
H595	**GMR; HDAC4$^{\Delta Ank}$**	*w[CS10]; P{w[+mC]=GAL4-ninaE.GMR}12/CyO; P{y[+t7.7]=CaryP}attP2, UAS-DmHDAC4-ΔAnk)-myc. Insert into P2:(3L) 68A4*	2,3	BDSC 1104 Genetivision, USA
H591	**GMR; HDAC4^{3SA}**	*w[CS10]; P{w[+mC]=GAL4-ninaE.GMR}12/CyO; P{y[+t7.7]=CaryP}attP2, UAS-DmHDAC4-3SA-myc. Insert into P2:(3L) 68A4*	2,3	BDSC 1104 Genetivision, USA
H806	**Peep-Myc**	*w[1118]; PBac{y+-attP-3B}VK22, CG5846p-CG5846*	2	Genetivision, USA

H742	**HDAC4^{3SA}**	*w[CS10]; P{y[+t7.7]=CaryP}attP2, UAS-DmHDAC4-3A-myc. Insert into P2:(3L) 68A4*	3	Genetivision, USA
H805	**Peep-GAL4**	*w[1118]; PBac{y+-attP-3B}VK22, CG5846p-GAL4*	2	Genetivision, USA
7	**CS**	*Wild-type CS strain*		R.Davis
H810	**GMR/Peep^{OE}**	*w[CS10]; P{w[+mC]=GAL4-ninaE.GMR}12, P{w+mC=UAS-2xEGFP}AH2/CyO*	2	BDSC 1104 Genetivision, USA
H393	**arm-GAL4**	*w[CS10]; P{w[+mW.hs]=GAL4-arm.S}4a P{w[+mW.hs]=GAL4-arm.S}4b/TM3, Sb[1] Ser[1]*	3	BDSC 1561
H407	**da-GAL4**	*w[*]; P{w[+mW.hs]=GAL4-da.G32}2; P{w[+mW.hs]=GAL4-da.G32}UH1*	2,3	BDSC 55849
H55	**Tub-GAL4**	*w[CS10]; P{w[+mC]=tubP-GAL4}LL7/TM3, Sb[1] Ser[1]*	3	BDSC 5138
H687	**nSyb-GAL4**	*y[1] w[1118]; P{y[+t7.7] w[+mC]=nSyb-GAL4.P}attP2*	3	BDSC 51941
H425	**repo-GAL4**	*w[1118]; P{w[+m*]=GAL4}repo/TM3, Sb[1]*	3	BDSC 7415
H484	**elav;Dicer-2**	*P{w[+mW.hs]=GawB}elav[C155] w[1118]; P{w[+mC]=UAS-Dcr-2.D}2*	X,2	BDSC 25750
H184	**elav-GAL80^{ts}**	*w[CS10]; P{w[+mW.hs]=GawB}elav[C155], P{w+mC=tubP-GAL80ts}10*	X,2	BDSC 458 R.Davis (BDSC 7108)
H758	**en-GAL4**	*y[1] w[*]; P{w[+mW.hs]=en2.4-GAL4}e16E*	2	BDSC 30564
H179	**ey-GAL4**	*w[*]; P{w[+m*]=GAL4-ey.H}4-8/CyO*	2	BDSC 5535
H753	**DIAP1**	*w[*]; P{w[+mC]=UAS-DIAP1.H}3*	3	BDSC 6657
H809	**GMR/GFP**	*w[CS10]; P{w[+mC]=GAL4-ninaE.GMR}12, P{w+mC=UAS-2xEGFP}AH2/CyO*	2	BDSC 1104 BDSC 6874
H567	**sev-GAL4**	*w[1118]; P{w[+mW.hs]=sevEP-GAL4.B}7*	2	BDSC 5793
H738	**GMR-GAL80^{ts}**	*w[CS10]; P{w[+mC]=GAL4-ninaE.GMR}12, P{w+mC=tubP-GAL80ts}10/CyO*	2	BDSC 1104 R.Davis (BDSC 7108)
4	**w(CS10);CyO**	*w[CS10];CyO/Sco*	2	R.Davis
H811	**GMR-GAL80^{ts}; peep^{RNAi1}**	*w[CS10]; P{w[+mC]=GAL4-ninaE.GMR}12,*	2,3	BDSC 1104 R.Davis (BDSC 7108)

		P{w+mC=tubP-GAL80ts}10; P{GD10737}v21645 CG5846		VDRC 21645
H812	**GMR-GAL80^{ts}, peep^{RNAi2}**	*w[CS10]; P{w[+mC]=GAL4-ninaE.GMR}12, P{w+mC=tubP-GAL80ts}10, P{attP,y[+],w[3`v107793] CG5846*	2	BDSC 1104 R.Davis (BDSC 7108) VDRC 107793
H694	**Catalase**	*y[1] w[*]; PBac{y[+mDint2] w[+mC]=UAS-hCAT.HA}VK00037/SM6a*	2	BDSC 78471
H764	**Marf**	*y[1] w[*]; P{w[+mC]=UAS-Marf.HA.S}3/T(2;3)TSTL, CyO: TM6B, Tb[1]*	3	BDSC 67157
H692	**SOD1**	*w[*]; P{y[+t7.7] w[+mC]=UAS-hSOD1.HA}attP40*	2	BDSC 64387

Abbreviations; R.Davis = Prof Ron Davis. The Scripps Institute, Jupiter, Florida, USA. BDSC = Bloomington *Drosophila* Stock Centre. VDRC = Vienna *Drosophila* Resource Centre.

2.1.1 Nomenclature

Nomenclature of the genes and proteins in this report is consistent with established protocols outlined in https://wiki.flybase.org/wiki/FlyBase:Nomenclature approved by FlyBase. These protocols disclose that if a gene name begins with an uppercase letter, the gene is dominant to the normal wild-type, on the contrary, if a gene name begins with a lowercase letter, the gene is recessive to the normal wild-type, in all cases the gene is named after the mutant phenotype. Both *Drosophila* and mammalian gene names are written all in italics, whereas proteins are not written in italics and begin with a capital letter.

2.1.2 Plasmid design

As there is currently no antibody available to accurately detect CG5846, the following three plasmids were designed by Dr Helen Fitzsimons. The plasmids were synthesised and cloned into the pUASTattB fly transformation vector by GenScript (Figure 8.1, Appendix 8.1).

CG5846-HA consists of the open reading frame (ORF) of *CG5846* (nucleotides 27-728 of NCBI reference sequence NM_135489.4) minus the stop codon, followed by a 3x glycine linker and

a 3x HA tag and flanked with a 5' NotI linker and a 3' XbaI linker (Figure 8.2, Appendix 8.2). The sequence was synthesised by Genscript into NotI and XbaI of the pUASTattB.

CG5846-Promoter-*CG5846-Myc* consists of 591 nucleotides (nt) of *CG5846* promoter (Figure 8.3, Appendix 8.3) upstream of the start codon and the ORF, minus the stop codon (nucleotides 995629-9957587, antisense strand of NCBI reference sequence CP121984.1). A 3x glycine linker and 6x Myc tag were added downstream. 5' SphI and 3' NotI linkers were added for insertion into SphI and NotI of pUASTattB, which replaces the UAS of pUAST with the *CG5846* promoter and coding region (Figure 8.4, Appendix 8.4).

CG5846-GAL4 consists of the same region of the *CG5846* promoter as in the *CG5846*-Promoter-*CG5846-Myc* construct above but without the *CG5846* coding region (nucleotides 9957587-9956995, antisense strand of NCBI reference sequence CP121984.1), instead *CG5846* was replaced with the *GAL4* ORF (nucleotides 443-3088 of NCBI reference sequence LN997417.1). 5' SphI and 3' NotI linkers were added for insertion into SphI and NotI of pUASTattB, which replaces the UAS of pUAST with the *CG5846* promoter and *GAL4* coding region (Figure 8.5, Appendix 8.5).

2.1.2.1 Plasmid transformation

Plasmids were transformed into *Escherichia coli* (*E. coli*) MAX Efficiency DH5α Competent cells (Invitrogen, Cat No. 18258-012). Competent cells were thawed completely on ice before 25 ng of plasmid DNA was added and incubated on ice for 30 minutes. The plasmid DNA and competent cells were then heat shocked for 45 seconds at 42°C before immediately being plunged back onto ice for a further two minutes. The addition of 900 µL of room temperature LB broth was followed by a one-hour incubation at 37°C at 220 revolutions per minute (rpm). *E. coli* was then spread onto an LB agar plate containing 100 µg/mL ampicillin and incubated overnight at 37°C.

2.1.2.2 Plasmid DNA Midi-Prep

A single colony was picked from the plate and a day culture consisting of 500 µL LB with 100 µg/mL ampicillin was incubated at 37°C for eight hours at 220 rpm. The day culture was then

added to an overnight culture in a 1 L flask containing 100 mL LB with 100 µg/mL ampicillin and incubated overnight at 37°C at 220 rpm. For high quality plasmid DNA purification, the PureLink HiPure Midiprep kit (Invitrogen) was used according to the manufacturer's instructions. The concentration of double stranded DNA (dsDNA) was measured using the Denovix DNA reader.

2.1.2.3 Transgenic fly generation

Plasmids were sent to Genetivision (Houston, TX, USA) where transgenic flies were produced via PhiC31 intergrase-mediated germline transformation. The presence of mini-*white* gene (w^+) allowed for transformant selection via eye colour. The attB site on the plasmid was recombined into the attP landing site on chromosome 2R at position 57F5 in the VK22 strain via homologous recombination. Tagged constructs were verified by size via western blot (Figures 3.13A and 4.3).

2.1.3 *Drosophila* stock maintenance

In all experiments flies were raised in a 12-hour light/dark cycle on standard fly media at 25°C, unless otherwise stated. To make 1 L of standard fly media, 10 g agar, 40 g yeast, and 110 g polenta were combined with 1 L of dH_2O in a large pot over a hot flame. This mixture was brought to the boil with intermittent stirring and boiled for 2 minutes. The pot was then removed from the heat and 130 g white sugar was added along with 20 mL molasses and 3.3 g methyl 4-hydroxybenzoate (Moldex) first dissolved in 37 mL 95% absolute ethanol and mixed thoroughly. Approximately 8 mL of standard fly media was poured into 30 mL vials (LabServ) and for larger experiments where more progeny were required, 40 mL of standard fly media was poured into 100 mL Schott bottles. Once the fly media was set, vials and bottles were sprinkled with additional yeast and plugged with mite resistant foam plugs.

2.1.4 Genetic crosses

In order to produce progeny containing specific targeted gene expression, virgin female flies of one genotype were crossed to male flies of another genotype. To collect virgin females, stock bottles housing the genotype of interest were emptied of adult flies in the morning. Females with a prominent abdominal meconium were collected as this is indicative of a newly eclosed adult. Additional virgin females were collected within an eight-hour timeframe following clearance of the bottle, as newly eclosed female flies do not mate within the first eight hours. Genetic crosses were set in either a vial, with 8 mL of standard fly media with five female virgins and five males or in a bottle, containing 40 mL of standard fly media with 10-15 virgin females and 10-15 males. Between three-seven days post cross the adults were removed, with progeny eclosing after 11 days (25°C), 19 days (23°C), or 28 days (19°C).

2.2 Isolation of *Drosophila* tissues and immunohistochemistry

2.2.1 *Drosophila* adult brain isolation

Flies were pre-fixed in PFAT/DMSO (4% paraformaldehyde in 1x phosphate buffered saline (PBS), 0.1% Triton X-100 and 5% Dimethylsulfoxide (DMSO)) at room temperature for 1 hour. All tissue isolation and immunohistochemistry incubation steps were performed with constant agitation on an Eppendorf tube rocker. Flies were washed three times for five minutes each in 1x PBT (1x PBS, 0.5% Triton X-100) before being dissected in a watch glass filled with ice cold 1x PBT using a pair of Dumont #5 sharpened forceps. Brains were isolated and transferred using a pipette to a PCR tube containing fresh 1x PBT on ice. Following isolation of the final brain, brains were then post fixed in PFAT/DMSO for 20 minutes at room temperature. Finally, brains were washed twice for five minutes at room temperature with 100% methanol and stored long-term in 100% methanol at -20°C.

2.2.2 *Drosophila* larval brain and eye imaginal disc isolation

Wandering third instar larvae were removed from vials with a paintbrush wet with 1x PBS and placed into a dissecting watch glass filled with 1x PBS for five minutes to clean larvae of excess

fly media. Careful isolation of the mouth hooks, eye imaginal discs and brain hemispheres were performed ensuring all tissues remained as a single unit for ease of further dissection. Tissues were then post-fixed in PFAT/DMSO for 20 minutes at room temperature before being washed and stored long-term as stated in Section 2.2.1.

2.2.3 *Drosophila* pupal eye isolation

To visualise the fully formed accessory cell lattice following two waves of programmed cell death, pupae were dissected 48 hours APF. White newly formed pupae were carefully removed from vials with a sterilised toothpick and incubated in open PCR tubes at 25°C for 48 hours. Following this incubation, pupae were removed from the PCR tubes and placed onto a piece of double-sided tape on a black surface with the dorsal side of the pupae facing up (Figure 2.1A). Using a pair of Dumont #5 sharpened forceps the operculum (head capsule) was removed exposing the pupal head (Figure 2.1B). An incision was then made down the length of the dorsal side of the pupal case to expose the thorax (Figure 2.1C). The whole pupa was then transferred to a watch glass filled with ice-cold 1x PBS. The head was removed from the remainder of the body and the pupal brain with attached eyes were isolated (Figure 2.1D) and transferred to a PCR tube filled with 1x PBS on ice. Tissues were post-fixed in 4% formaldehyde in 1X PBS for 30 minutes at room temperature before being washed and stored long-term as stated in Section 2.2.1.

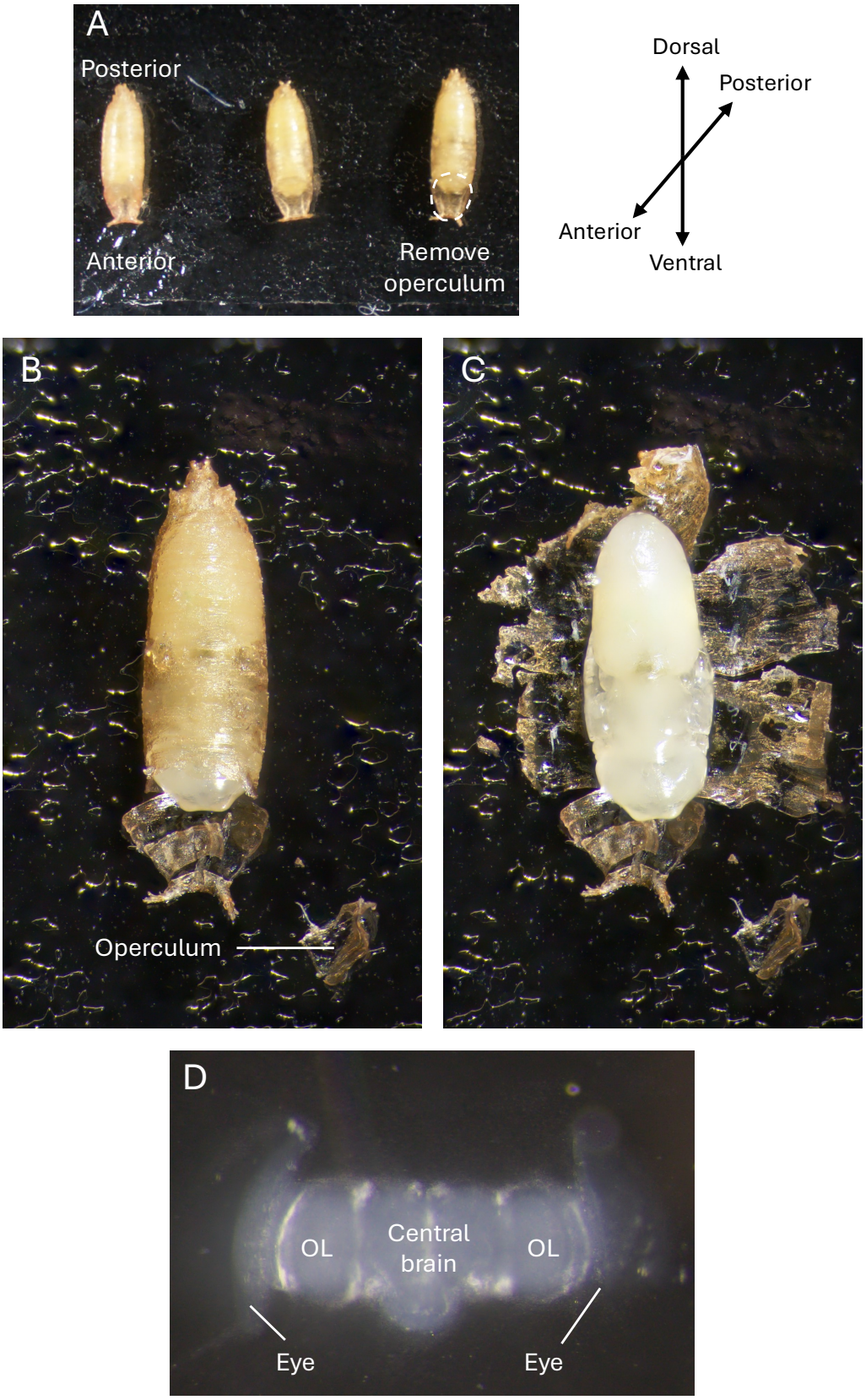

Figure 2.1. Pupal dissection. At 48-hours APF pupae were dissected and the eye-brain complex was isolated. A. 48-hour pupae were placed on doubled sided tape on a black background dorsal side facing up. B. The operculum was removed to expose the head, C. an anterior to posterior incision on the dorsal

side of the pupal case was made and the whole pupa was exposed. D. The whole pupa was transferred to a dissecting dish for isolation of the brain with eyes attached to either optic lobe. OL = optic lobe.

2.2.4 Immunohistochemistry on isolated *Drosophila* tissues

Dissected tissues (Section 2.2.1, 2.2.2, 2.2.3) were rehydrated for five minutes at room temperature in 50% methanol/1x PBT. Subsequent to this, all tissues were washed four times for five minutes each in 1x PBT before being blocked in immunobuffer (5% normal goat serum in 1x PBT). Adult brains and larval tissues were blocked for three hours, and pupal tissues were blocked for 1.5 hours at room temperature. All tissues were then incubated overnight at room temperature with appropriate primary antibody diluted in immunobuffer (Table 2.2). All tissues were then washed with 1x PBT for two quick washes then three times for five minutes each at room temperature before being incubated overnight at 4°C with appropriate secondary antibody diluted in immunobuffer (Table 2.3). Pupal tissues were then fixed for a second time in 4% formaldehyde in 1x PBS for 30 minutes at room temperature. All tissues were then washed with 1x PBT for two quick washes then three 20-minute washes at room temperature. Larval and pupal tissues were further dissected to isolate the eye tissues from the brain before being transferred to a drop of Antifade (1 mL 10x PBS, 9 mL glycerol and 0.2 mg/mL n-propyl gallate) on a prepared microscope slide. Adult brains were incubated in approximately 30 µL Antifade before being mounted onto a microscope slide. A coverslip was then placed over all tissues and sealed with clear nail varnish.

Table 2.2 Primary antibodies used for immunohistochemistry

Name	Catalogue number	Class	Host	Source	Dilution
Anti-FasII	1D4	Monoclonal	Mouse	DSHB	**IHC** – 1:20
Anti-GFP	Ab290	Polyclonal	Rabbit	Abcam	**IHC** – 1:20,000
Anti-HA	C29F4 clone 3724	Monoclonal	Rabbit	Cell Signalling	**IHC** – 1:200
Anti-DLG-1	4F3	Monoclonal	Mouse	DSHB	**IHC** – 1:200
Anti-bruchpilot	nc82	Monoclonal	Mouse	DSHB	**IHC** – 1:100
Anti-repo	8D12	Monoclonal	Mouse	DSHB	**IHC** – 1:20
Anti-Myc	9E10	Monoclonal	Mouse	DSHB	**IHC** – 1:100
Anti-Myc	Ab9106	Polyclonal	Rabbit	Abcam	**IHC** – 1:100
Anti-CG5846	-	-	Rabbit	Genscript	**IHC** – 1:2

DSHB = Developmental Studies Hybridoma Bank, IHC = immunohistochemistry

Table 2.3 Secondary antibodies used for immunohistochemistry

Name	Catalogue number	Host Species	Source	Dilution
Alexa Anti-Mouse 555	A-21422	Goat	Sigma Aldrich	**IHC** – 1:500
Alexa Anti-Rabbit 647	A-21244	Goat	Sigma Aldrich	**IHC** – 1:500

2.2.4.1 DAPI staining on adult brains

For brains stained with DAPI, following the overnight incubation with appropriate secondary antibody, brains were washed three times for five minutes each in 1x PBT before being incubated with 1:20,000 dilution of DAPI in 1x PBT for 20 minutes at room temperature. Brains were then washed three times for 20-minutes each before being mounted on a microscope slide as described in Section 2.2.4.

2.2.5 Confocal microscopy and image processing

Adult brains, larval eye discs, and pupal eyes were all imaged, under appropriate fluorescence spectra, using a Leica SP5 DM60000B Confocal Microscope (Manawatu Microscopy and Imaging Centre). Image Z-stacks were collected with an optical section size ranging from 0.5 µm for Kenyon cell and pupal eye images, 0.5 – 1µm for larval eye disc images, and 1 – 2 µm

for whole brain images. Images were analysed using the ImageJ software, where maximum projections and single slice images were attained. All phenotypic scoring was performed by a blinded observer.

2.2.6 Quantification and statistical analyses

For mushroom body phenotypes a scoring system outlined in Section 3.2.1 was employed ($n \geq 18$). To assess level of β lobe fusion, a one-tailed Fisher's exact test was used to confirm significance of notable RNAi lines compared to control where statistical significance was attained.

For Kenyon cell aggregate counting, maximum projections were produced (n=4) and each HDAC4 and HDAC4/CG5846 containing speckle were counted using the Cell Counter ImageJ plugin. Graphs were displayed as the mean ± standard error of the mean (SEM) and statistical significance was assessed via one-way ANOVA with post-hoc Tukey HSD analysis.

For quantification of the number of retinal basal glia in the larval eye disc (n=6) each Repo-labelled cell from every 2-4 optical sections of the Z-stack were counted using the Cell Counter ImageJ plugin and displayed in a box-and-whisker plot with statistical significance assessed via one-way ANOVA with post-hoc Tukey HSD analysis.

For pupal eye analyses (n=4) the number of accessory cells were identified and counted per ommatidium in four regions of each eye (posterior, anterior, dorsal, and ventral) using Procreate for iOS. Accessory cells included four cone cells, two primary pigment cells, six secondary pigment cells, three tertiary pigment cells, and three bristle cells, equating to a total of 18 accessory cells in a normal ommatidium. Violin plots showing the distribution of data were presented.

2.2.7 Nile Red staining of adult retina

Whole flies were pre-fixed as detailed in Section 2.2.1, and whole retina were isolated. Retina were post-fixed and stored as detailed in Section 2.2.1. Following this, retina were rehydrated in 50% methanol/1x PBT for five minutes at room temperature before being washed three times

five minutes each in 1x PBT. Wash buffer was removed and a 1:1000 dilution of a 1 mg/mL stock solution of Nile Red (Sigma Aldrich) in 1x PBT was added to the retina for 20 minutes at room temperature. Retina were then washed three times five minutes in 1x PBT and mounted as described in Section 2.2.4. Single optical section images were immediately taken at and excitation wavelength of 554 nm and emission wavelength of 638 nm (ex/em) using the Lecia SP5 DM60000B Confocal Microscope.

2.2.7.1 Quantification and statistical analyses of rhabdomere area

Rhabdomeres 1-7 were situated in the plane of focus in a single optical section image. The area of each rhabdomere was measured using the oval section tool and measure function in ImageJ. The measured sum of the seven visible rhabdomeres were graphed as the mean ± SEM. Statistical significance was assessed via one-way ANOVA with post-hoc Tukey HSD analysis.

2.3 *Drosophila* protein extraction

2.3.1 *Drosophila* head separation

Drosophila were anaesthetised with CO_2 and stored in 15 mL tubes (Greiner) and frozen at -80°C. Prior to total protein isolation (Section 2.3.7), flies were subject to multiple rounds of vortexing to snap off heads. Heads and bodies were transferred onto a piece of transparency over dry ice and heads were quickly sorted from the bodies using a fine paintbrush. Heads were then placed into an awaiting 1.7 mL Eppendorf tube on ice, and for experiments that require the fly body, these were also placed into a separate awaiting 1.7 mL Eppendorf tube on ice, followed by total protein isolation as described in Section 2.3.7.

2.3.2 *Drosophila* embryo protein isolation

One-day prior to egg collection, adult flies were moved to a new bottle containing standard fly media with approximately 5 mL yeast paste (dried yeast combined with dH_2O to create a peanut-butter texture) spread on top of the food, to encourage rapid egg laying. Egg laying

media was made by combining 4 g agar, 12 g polenta, 8 g molasses, and 200 mL dH_2O. This mixture was brought to a boil before being removed from the heat and 0.66 g Moldex dissolved in 7.4 mL ethanol was added and mixed thoroughly. Plastic plates measuring 55 mm in diameter were filled with approximately 15 mL egg laying media. Once the media was set, 2-3 mL of yeast paste was added to the centre of the plate prior to the addition of flies to further encourage egg laying. Flies were deposited into a 100 mL plastic beaker with airholes and taped to a plate containing egg laying media. Flies were incubated at 25°C for one hour to allow females to deposit all newly fertilised embryos onto the plate, adult flies were then discarded. Early-stage 0-2 hour old embryos were removed from plates and transferred using a dry paintbrush to an awaiting 1.7 mL Eppendorf tube on ice, followed by total protein isolation as described in Section 2.3.7.

2.3.3 *Drosophila* larval tissue protein extraction

Wandering third instar larvae were collected and dissected as described in Section 2.2.2. The whole eye/brain complex was placed into an awaiting 1.7 mL Eppendorf tube on ice, followed by total protein isolation as described in Section 2.3.7.

2.3.4 *Drosophila* brain protein extraction

Following adult brain dissection described in Section 2.2.1, brains were placed into an awaiting 1.7 mL Eppendorf tube on ice, followed by total protein isolation as described in Section 2.3.7.

2.3.5 *Drosophila* pupal tissue protein extraction

At 48 hours APF, whole pupae were isolated as described in Section 2.2.3 and observed in Figure 2.1C. Whole pupae were placed into an awaiting 1.7 mL Eppendorf tube on ice, followed by total protein isolation as described in Section 2.3.7.

2.3.6 *Drosophila* adult eye isolation

Adult *Drosophila* were anaesthetised using Flynap (Carolina) and individual eyes were removed with a new scalpel blade. Following removal of 30 pairs of eyes, these were either placed into a 1.7 mL Eppendorf tube on ice, followed by total protein isolation (Section 2.3.7), or snap-frozen in a dry-ice ethanol bath and stored at -80°C.

2.3.7 Total protein isolation and quantification

Whole cell lysates were generated by adding 100 µL RIPA buffer (150 mM sodium chloride, 0.1% Triton X-100, 0.5% sodium deoxycholate, 0.1% SDS, 50 mM Tris, pH 8.0, and 1x cOmplete mini EDTA-free protease inhibitor (Roche)) to 50 heads, 20 µL to 20 embryos, 10 µL to 10 larval tissues, 10 µL to 10 pupae, or 30 µL to 30 pairs of eyes in separate 1.7 mL Eppendorf tubes and homogenised with a motorised mortar and disposable plastic pestle for 30 seconds on ice. Lysates were cleared by centrifugation at 13,000 g for two minutes at 4°C. Supernatants were transferred to a new 1.7 mL Eppendorf tube on ice and total protein was quantified using the Pierce BCA Protein Assay Kit (ThermoFisher) according to the manufacturer's instructions. Absorbances were read using the BioTek PowerWave XS plate reader and a standard curve was generated in Excel to determine protein concentrations.

2.3.8 SDS-Page and western blotting

Following sample preparation and quantification (Section 2.3.7), proteins were separated by size via sodium dodecyl sulfate-polyacrylamide gel electrophoresis (SDS-PAGE). A total of 30 µg of protein diluted in RIPA buffer was added to 5x Laemmli sample buffer (2% SDS, 5% 2-mercaptoethanol, 10% glycerol, 0.01% bromophenol blue, 60 mM Tris HCl, pH 6.8) to a concentration of 1x and boiled at 95°C for five minutes. Samples were then cooled on ice and loaded into an assembled pre-cast polyacrylamide gel (Mini Protean TGX 4%-20%, Bio-Rad) in a buffer tank filled with 1x Running buffer (25 mM Tris, 190 mM glycine, 0.1% SDS). Samples were electrophoresed at 200 volts (V) for approximately 35 minutes, until the dye front reached the bottom of the gel. Proteins were then transferred to a nitrocellulose membrane (Amersham Protran premium 0.45 µm nitrocellulose, GE Healthcare LifeScience) in ice cold

1x Transfer buffer (25 mM Tris, 190 mM glycine, 0.1% SDS, 20% methanol) maintained at 4°C for one hour at 100 V. Nitrocellulose membranes were then incubated in 5% blocking buffer (5% w/v skim milk powder diluted in 1x TBST (20 mM Tris, 150 mM NaCl, 0.1% Tween-20)) for one-two hours at room temperature. For all incubation steps and washes, membranes were placed on an orbital shaker with gentle agitation. Membranes were washed three times for five minutes each in 1x TBST at room temperature before being incubated with appropriate primary antibody (Table 2.4) diluted in 1% blocking buffer overnight at 4°C. The membranes were then washed three times for five minutes each in 1x TBST at room temperature before being incubated with appropriate secondary antibody (Table 2.5) diluted in 1% blocking buffer for one hour at room temperature. Membranes were then washed three times for five minutes each in 1x TBST at room temperature. Proteins were then detected with the Amersham ECL Prime Western Blotting Detection Reagent (Cytiva) and imaged using the Azure Biosystems c600 imaging system.

Table 2.4 Primary antibodies used for immunoprecipitation and western blotting

Name	Catalogue number	Class	Host	Source	Dilution
Anti-HA	C29F4 clone 3724	Monoclonal	Rabbit	Cell Signalling	**IP** - 2 µL
Anti-Myc	Ab9106	Polyclonal	Rabbit	Abcam	**IP** - 2 µL **WB** - 1:1000
Anti-HA	3F10 clone 11867423001	Monoclonal	Rat	Merck (Roche)	**WB** – 1:1000
Anti-GFP	Ab290	Polyclonal	Rabbit	Abcam	**WB** – 1:4000
Anti-Tubulin	12G10	Monoclonal	Mouse	DSHB	**WB** – 1:500

IP = immunoprecipitation, WB = western blot

Table 2.5 Secondary antibodies used for western blotting

Name	Catalogue number	Target Species	Host Species	Source	Dilution
Rat HRP	Ab97057	Rat	Goat	Abcam	**WB** – 1:10,000
Mouse HRP	NA931VS	Mouse	Sheep	Sigma Aldrich	**WB** – 1:20,000
Rabbit HRP	NA934VS	Rabbit	Donkey	Sigma Aldrich	**WB** – 1:40,000
Veriblot for IP Detection reagent	Ab131366	Rabbit total IgG	-	Sigma Aldrich	**WB** – 1:4000

WB = western blot

2.3.9 Co-Immunoprecipitation (Co-IP)

Following head separation as detailed in Section 2.3.1, 300 µL of immunoprecipitation (IP) buffer (25 mM Tris pH 7.05, 50 mM sodium chloride, 30 mM sodium pyrophosphate, 50 mM sodium fluoride, 10% glycerol, 0.5% Triton X-100, 0.5 mM phenylmethylsulfonyl fluoride (PMSF), and 1x cOmplete mini EDTA-free protease inhibitor (Roche)) was added and heads were homogenised for 30 seconds, using a motorised mortar and disposable plastic pestle. Lysates were cleared and quantified as detailed in Section 2.3.7.

Immunoprecipitation was performed using the Surebeads Protein A magnetic beads (BioRad), 100 µL were resuspended and washed four times in 1 mL 1x PBS-T (1x PBS, 0.1% Tween-20). Per Co-IP, 2 µL of appropriate antibody (Table 2.4) diluted in 200 µL IP buffer was added to the magnetic beads and rotated at room temperature for 10 minutes. Beads were washed four times in 1 mL of 1x PBS-T before 2 mg of lysate diluted in 500 µL IP buffer was added to the beads and incubated overnight at 4°C while rotating. The beads were washed four times in 1 mL of IP buffer before proteins were eluted off the beads in 1x Laemmli buffer at 70°C for 10 minutes. IP samples alongside 30 µg inputs, were loaded and proteins were separated by SDS-PAGE, transferred to a nitrocellulose membrane and detected as detailed in Section 2.3.8.

2.4 Light microscopy

2.4.1 Light microscopy image acquisition and processing

To analyse *Drosophila* eye and wing morphology both were imaged using an Olympus SZX16 Stereo Microscope with DP74 camera and cellSens Dimension imaging software. Image Z-stacks were taken with an optical section size of 10 µm with approximately 30 slices being taken per eye and 12 slices being taken per wing. Images were taken with a 25.5 ms exposure and 115x magnification. Z-stacks were aligned and blended using the auto-align and auto-blend functions on Adobe Photoshop to gain clear maximum projections.

2.4.2 *Drosophila* initial adult eye phenotype screen

Crosses between five virgin female *GMR-GAL4* driver flies and five male flies harbouring the appropriate *UAS-RNAi* construct were raised on standard fly media at 25°C. In all experiments, a driver control cross between virgin female *GMR-GAL4* flies and male *w(CS10)* were included. *w(CS10)* carries the *w* (white-eyed) mutant in a Canton S background that was generated by outcrossing w^{1118} to Canton S for 10 generations. Adults were allowed to mate for four days before being removed. Once all adult progeny had emerged, flies were anaesthetised with CO_2 and placed in 15 mL tubes (Grenier) and stored at -80°C. All progeny subject to light microscopy were stored via this method unless otherwise stated. Up to ten randomly selected males and ten randomly selected females were then imaged under light microscopy as described in Section 2.4.1. A semi-quantitative scoring system was produced based on perturbations to the regular array of ommatidia, bristle organisation, pigment disturbances and appearance of necrosis (Table 2.6), and all eyes were scored by a blinded observer. Each eye required at least one of the phenotypic appearances for the corresponding score to be given. A one-tailed Fisher's exact test was used to confirm statistical significance.

Table 2.6 Semi-quantitative rough eye phenotype scoring system

Phenotype level	**No defects**	**Mild**	**Moderate**	**Severe**
Appearance	Wild-type appearance	- Mild ommatidia disorganisation - Mild bristle abnormalities	- Moderate ommatidia disorganisation - Moderate bristle abnormalities -Mild fusion - Mild loss of pigmentation	- Severe ommatidia disorganisation - Loss of bristle patterning - Severe fusion - Severe loss of pigmentation - Necrosis
Score	-	+	++	+++

2.4.3 *Drosophila* eye degeneration screen

Crosses were set and flies were raised as detailed in Section 2.4.2. Once emerged one-day old adult flies were housed in individual plastic vials containing 8 mL standard fly media. Flies were anaethetised with CO_2 and imaged as described in Section 2.4.1 on a white flypad diffusing CO_2 on days one, three, five, seven, and 14 to assess eye phenotype degeneration. The

progressive area of necrosis was measured in ImageJ by freehand tracing around all necrotic areas and using the measure function. The percentage of necrosis was attained by dividing the area of necrosis by the total area of the eye and was displayed as the mean ± SEM. Statistical significance was assessed via one-way ANOVA with post-hoc Tukey HSD analysis.

2.4.4 Necrosis-inducing eye phenotype analyses

Following the initial rough eye phenotype screen inclusive of all candidate genes, the remainder of the eye phenotypes assessed consisted of differing levels of necrosis on the eye, which were imaged according to Section 2.4.1. An updated semi-quantitative scoring system (Table 2.7) was put in place when assessing CG5846 and HDAC4 mutant-induced eye phenotypes which were more heavily weighted toward teasing out small differences in the spread of necrosis. The area of necrosis was measured in ImageJ by freehand tracing around all necrotic areas and using the measure function. The percentage of necrosis was attained by dividing the area of necrosis by the total area of the eye and was displayed as the mean ± SEM. Statistical significance was assessed via one-way ANOVA with post-hoc Tukey HSD analysis.

Table 2.7 Necrosis-inducing semi-quantitative scoring system for rough eye phenotype

	No defects	Mild	Moderate	Major	Severe
Bristles	No bristle disruption	Missing bristles/many emerging from a single pore over a small area	Missing bristles/many emerging from a single pore over equivalent to quarter of the eye	Missing bristles/many emerging from a single pore over equivalent to half eye	Missing bristles/many emerging from a single pore over entire eye
Ommatidia organisation	Normal	Mild dis-organisation	Moderate dis-organisation and fusion	Major dis-organisation and fusion	Severe dis-organisation and fusion
Pigmentation	Normal for number of transgenes present	Mild de-pigmentation in small areas	Moderate de-pigmentation across a quarter of the eye	Major de-pigmentation across half the eye	Severe de-pigmentation across entire eye
Necrosis	No necrosis	Small spot/s of necrosis	Larger spot/s of necrosis	Quarter of the eye covered in necrosis	Half the eye covered in necrosis
Score for each phenotype	0	0.25	0.5	0.75	1

2.4.5 Wing morphology screen

To assess wing morphology the *engrailed-GAL4* (*en-GAL4*) driver was used to drive expression of each *UAS-RNAi*. Once progeny emerged, wings were dissected from five randomly selected males and females. The wings were arranged on a microscope slide and a coverslip was gently placed on top to flatten each wing and imaged as described in Section 2.4.1.

2.5 Survival, longevity, and negative geotaxis assays

2.5.1 Survival assay

Survival assays were performed using the following drivers: *armadillo-GAL4* (*arm-GAL4*), *daughterless-GAL4* (*da-GAL4*), and *tubulin-GAL4* (*tub-GAL4*) for ubiquitous expression, *elav-GAL4* and *nSyb-GAL4* for pan-neuronal expression, and *reversed polarity-GAL4* (*repo-GAL4*) for pan-glial expression. A total of 10 virgin females of these drivers were each crossed to 10 males of the indicated UAS line and raised on 40 mL standard fly media in bottles. For the

crosses with *tub-GAL4* five virgin females were crossed to five males of the indicated UAS line and raised on 8 mL standard fly media in vials. All crosses were raised at 25°C, with adults removed after three days. Following eclosion of control progeny, all adults from all crosses were collected and counted. For *da-GAL4* crosses, images of the bottles were taken following collection of adult progeny, and pupal case counts were then taken, which accounted for those that had emerged as adults and those that had not emerged due to pupal lethality. Three independent biological replicates were analysed per genotype, unless otherwise stated, and the mean ± SEM were displayed and statistical significance was assessed via one-way ANOVA with post-hoc Tukey HSD analysis.

2.5.2 Lifespan assay

At 25°C a typical well maintained and healthy *Drosophila* will have an average lifespan of more than 50 days, with a maximum of approximately 80 days (Linford *et al.*, 2013). In order to determine how a gene is involved in the survival of a fly throughout development and adulthood, the ubiquitous driver *arm-GAL4* was used to drive expression. *arm-GAL4* was first outcrossed for five generations into the *w(CS10)* genetic background. A total of 10 virgin female *arm-GAL4* flies were crossed to 10 males of the indicated UAS line and raised on standard fly media at 23°C. This temperature was selected as knockdown of CG5846 with *da-GAL4* at 25°C was observed to be semi-lethal, therefore a lower expression level was desired. Adults were removed after five days. Once 50 flies (25 male and 25 female) had emerged, all were placed into new vials containing standard fly media and maintained at 23°C. Dead flies were tallied every two-three days and the surviving flies were turned onto new fly media every seven days until all flies were dead. The temperature of 23°C was further selected to induce minimal disruption to the fly's lifespan by way of turning flies onto new fly media, which would have been more frequent if raised at a higher temperature. Three independent biological replicates were analysed per genotype the total number of alive flies per day were graphed on a dot plot and statistical significance was assessed via Log rank test with post-hoc Bonferroni analysis.

2.5.3 Negative geotaxis assay

Locomotor function can be assessed via the negative geotaxis assay. The innate response of *Drosophila* to being trapped at the bottom of an enclosed container is to escape from the top (Kamikouchi *et al.*, 2009), therefore climbing ability can be monitored. The following protocol was modified based on Patel and Tamanoi (2006). For each genotype, three independent crosses were set and ten progeny (five females, five males) from each replicate at approximately five days post-eclosion were anaesthetised with CO_2 and placed into three respective flat bottomed climbing vials, devoid of food to avoid inducing distracting variables, and plugged with a foam plug. Flies were allowed to recover for 30 minutes at room temperature before testing. Flies were gently tapped to the bottom of the vial and the number of flies that climbed above 5 cm in a 10 second timeframe were quantified (Figure 2.2). A total of 10 rounds were completed for each genotype with a rest period of 4 minutes between rounds to allow flies time to recover. The mean ± SEM was displayed and statistical significance was assessed via one-way ANOVA with post-hoc Tukey HSD analysis.

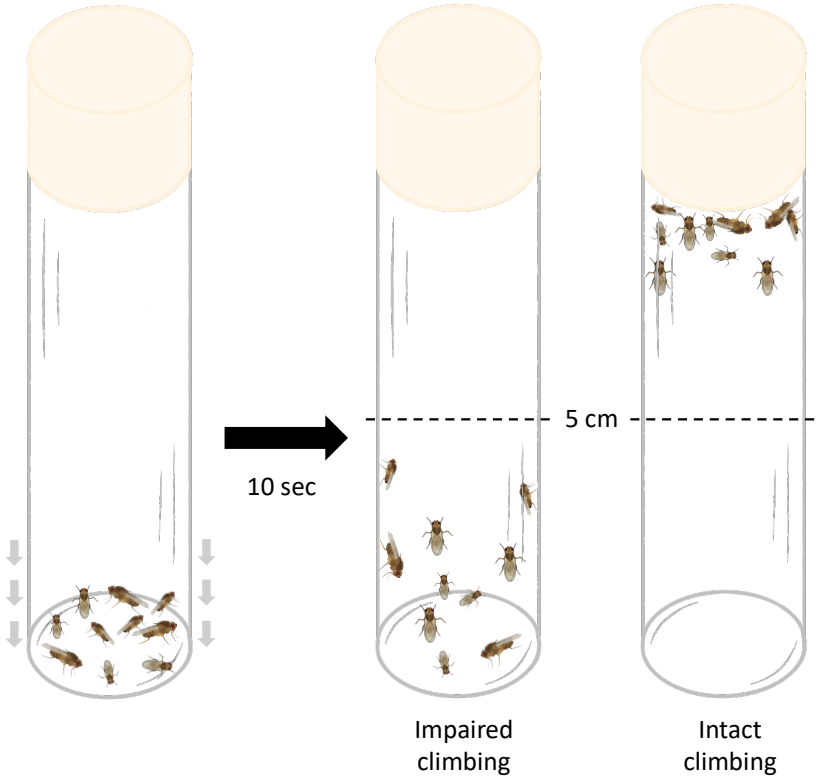

Figure 2.2. Negative geotaxis assay. Flies were gently tapped to the bottom of the vial and the number of flies observed above and below the 5 cm mark after 10 seconds were quantified. If the majority of flies were observed below the 5 cm mark, this was indicative of impaired climbing ability, whereas if the majority of flies were observed above the 5 cm mark, this was indicative of intact climbing ability.

2.6 Induction of reactive oxygen species

2.6.1 Developmental exposure to hydrogen peroxide (H_2O_2)

To test susceptibility to increased levels of ROS in the environment during development, H_2O_2 was added to standard fly media. To determine whether this increase in ROS affected the necrotic eye phenotype induced by CG5846 knockdown, 10 *GMR-GAL4* virgin females were crossed to 10 UAS-*CG5846*^{RNAi} males and raised at 25°C on 40 mL standard fly media in a bottle supplemented with and without 1% H_2O_2. Adult flies were removed after seven days. Enclosed pupae and dead pupal counts were taken 20 days following initial mating, and this assay was performed in triplicate. The mean ± SEM of total pupal counts were graphed and statistical significance was assessed via one-way ANOVA with post-hoc Tukey's HSD analysis. The proportion of eclosed and dead pupae were also graphed and statistical significance was assessed via one tailed Fisher's exact test.

2.6.2 Post-developmental exposure to H_2O_2

To test susceptibility to increased levels of reactive oxygen species on lifespan post-developmentally, ten male and ten female five day old flies were transferred to a vial containing a long thin rectangular piece of Whatman paper soaked in either 5% sucrose or 5% sucrose supplemented with 1% H_2O_2 (Johnmark & Kinyi, 2021).There were five vials of each treatment per genotype, totalling 50 flies per treatment and 100 flies per genotype. Whatman paper was replaced every 2-3 days and dead adults were also counted until all flies fed H_2O_2 were dead. The total number of alive flies per day were graphed on a dot plot and statistical significance was assessed via Log rank test with post-hoc Bonferroni analysis.

2.7 Courtship suppression assay

To test learning and memory in the *Drosophila*, cVA-retrievable courtship training was employed as described in Section 1.3.3.1. As the mushroom body is an important structure for normal memory formation (McBride *et al.*, 1999) the TARGET system, as described in Section

1.3.4.2 was employed to avoid any learning and memory deficits induced by developmental defects of the mushroom body.

All fly lines used for courtship suppression learning and memory testing were outcrossed for five generations into the *w(CS10)* genetic background. A total of 15 *elav-GAL80^{ts}* virgin females were crossed to 15 UAS-*CG5846*^{RNAi} males. A total of 15 Canton Special (CS) virgin females were crossed to 15 UAS-*CG5846*^{RNAi} males as a UAS-line control and 15 virgin *elav-GAL80^{ts}* virgin females were crossed to 15 CS males as a driver control. All crosses were raised at 19°C on 40 mL standard fly media in bottles and adult flies were removed after seven days. Newly emerged puffy, white virgin male progeny from each genotype were collected and housed in individual vials containing 4 mL of standard fly media. Vials were plugged with cotton wool and maintained at 19°C for up to four days. Males were transferred to 30°C for 72 hours which triggered a conformational change in GAL80^{ts}, resulting in the release of GAL4 and unmasking of the AD, leading to GAL4-mediated expression (Figure 1.9). Two days prior to training/testing virgin female and male CS (control) flies were mated for 48 hours to attain unreceptive mated females. Before training/testing ensued, the mated female flies were anaesthetised and housed in a new vial containing 8 mL standard fly media and allowed to recover for one hour at room temperature (learning assay) or 25°C (memory assays). Following the 72-hour incubation at 30°C, the learning and memory assays were carried out. The tester was blinded to the genotype and trained/naïve (sham) status of the flies.

2.7.1 Courtship activity

The male fly exhibits a repertoire of physical movements when courting a female fly which can be broken down into a series of discrete steps described in Section 1.3.3.1 (Figure 1.7). Each male was aspirated into a shallow transparent acrylic testing chamber followed by a mated female, and testing was performed at room temperature. The male's courtship behaviour as detailed in Section 1.3.3.1 was recorded using a GoPro Hero6 camera and scored over the first 10 minutes (pre-training) of the hour and the last 10 minutes (post-training) of the hour, allowing the males to learn and immediately recall the mated females rejection behaviour over a 50 minute timespan. A new mated female was used for each testing instance and the testing chambers were rinsed with 95% ethanol between bouts of testing to remove any pheromone residue. For normal courtship activity, the activity pre-training is higher than the activity post-

training. The courtship index was calculated for both pre-training and post-training by the proportion of time spent courting over the 10-minute timeframe.

$$\text{Courtship Index (CI)} \quad \frac{\text{Courting time}}{\text{10 min}}$$

2.7.2 Learning assay

The learning index was calculated from the courtship indices pre- and post-training, between zero and one ($n \geq 19$). A learning index closer to one indicates a high level of learning with the male spending less time courting the female whereas a learning index closer to zero indicates little to no learning has occurred, meaning that the male did not learn to associate the rejection behaviour with a mated female.

$$\text{Learning Index (LI)} = \left(\frac{\text{Post-training}}{\text{Pre-training}} \right)$$

2.7.3 Memory assays

To measure memory acquisition, male flies were trained with a mated female before being tested with a new mated female, the time between training and testing differed depending on the type of memory being assessed. For training, all males were aspirated into individual transparent acrylic training chambers filled with 1 mL standard fly medium, from here each genotype was split into two groups, trained and sham, with the trained males being housed with a mated female and the sham males being housed alone. The trained males with mated females and sham males alone were all incubated at 30°C for one hour for STM training or seven hours for LTM training. For STM, following the one-hour incubation, the mated females were discarded and the males were aspirated into individual testing chambers. A new mated female was then aspirated into each chamber with either a trained or sham male in which the test administer was blind to. Courtship was recorded on a GoPro Hero6 and courtship activity was scored over a ten-minute period, at 25°C. For LTM, multiple bouts of courtship advances and

mating rejection occurred in the training chambers housing the trained males during the seven-hour training session. Following this the females were discarded and the males were returned to 30°C and testing as detailed above occurred after 24 hours in testing chambers, at 25°C, with new mated females. A courtship index for both trained and sham STM and LTM was calculated as detailed in Section 2.7.1. The memory index for both STM and LTM was calculated based on the courtship indices of the trained (n≥19) and sham males (n≥20) to give a number between zero and one. Consistent with the learning index, a memory index closer to one indicates intact STM/LTM whereas a memory index closer to zero indicates little to no STM/LTM retention.

$$\text{Memory Index (MI)} = 1 - \left(\frac{\text{Trained}}{\text{Sham}} \right)$$

2.7.4 Courtship suppression statistical analyses

The raw courtship data (minutes) was converted into seconds. The courtship, learning and memory indices were calculated from this data and used to create graphs by plotting the mean ± SEM. This data was then subject to arcsine transformation in order to attain a normal distribution for statistical testing via one-way ANOVA with post-hoc Tukey HSD analysis.

2.8 Polymerase Chain Reaction (PCR)

2.8.1 *Drosophila* genomic DNA extraction

To prepare for DNA extraction, 10-15 flies were anaesthetised with FlyNap (Carolina) and their heads were removed using a scalpel blade. Heads were transferred into an Eppendorf tube on ice, and 250 µL of solution A (0.1 M Tris HCL pH 9.0, 0.1 M EDTA, 1% SDS) was added followed by homogenisation with a motorised mortar and disposable plastic pestle for 30 seconds. Samples were incubated for 30 minutes at 70°C prior to the addition of 35 µL KAc (8 M potassium acetate) followed by vigorous shaking. Samples were then incubated on ice for 30 minutes and debris pelleted by centrifuging for 15 minutes at 16,000 g at 4°C. All following centrifugation steps occurred at 4°C. The supernatant was transferred to a new tube with the addition of 250 µL Phenol-Chloroform and thoroughly shaken. The samples were then

centrifuged for 5 minutes at 16,000 g and the Phenol-Chloroform step was repeated a second time. The final sample supernatant was transferred to a new tube, 150 µL Isopropanol was added and the tube was shaken thoroughly before being centrifuged for five minutes at 13,000 g. The pellet was washed in 1 mL 70% Ethanol before being centrifuged for five minutes at 16,000 g. The pellet was then air dried completely before being resuspended in 100 µL TE buffer. The concentration of dsDNA was measured using the Denovix DNA reader.

2.8.2 PCR confirmation of RNAi construct identity

CG5846 RNAi (henceforth denoted as *CG5846*^{RNAi}) constructs were imported from VDRC and their identity was confirmed via PCR.

Genomic DNA was diluted to 50 ng/µL and a 20 µL reaction mixture was prepared that contained: 12.5 µL OneTaq 2x Master Mix (NEB) at a final concentration of 1x, 0.5 µL of each appropriate primer (Stock 100 µM, Sigma Aldrich, Tables 2.7, 2.8), 2 µL template DNA (50 ng/µL), and 9.5 µL dH_2O. Standard cycling consisted of an initial enzyme activation step at 94°C for 30 seconds followed by 38 cycles of denaturation at 94°C for 30 seconds, then annealing at 55°C (*CG5846*^{RNAi1}) or 60°C (*CG5846*^{RNAi2}) for 30 seconds and finally elongation at 68°C for one minute. These cycles were completed with a five minute extended elongation step at 68°C, then cooled to 4°C.

2.8.3 Agarose gel electrophoresis

Following amplification of PCR products (Section 2.8.2), agarose gel electrophoresis was performed in order to separate DNA fragments based on size. A 1% agarose gel was produced by melting 0.5 g agarose in 50 mL 1x TAE (Tris-base, acetic acid, EDTA 0.5 M). Once cooled, 1 µL of ethidium bromide (EtBr) (Stock 10 mg/mL) was added and the gel was poured. Once set, a total of 5 µL of each PCR product, diluted in 0.5 µL 10x loading buffer (final concentration 4% (v/v) glycerol, 0.05% (w/v) SDS, 0.1 mM EDTA, 0.025% (w/v) bromophenol blue, 0.0025% (w/v) xylene cyanol) were loaded alongside a 1 kb plus DNA ladder (Invitrogen). The tank was filled with 250 mL 1x TAE and 2.5 µL EtBr (Stock 10 mg/mL), and

the gel was run at 100 V for one hour, or until the dye front was three-quarters of the way through the gel. Following this, the gel was imaged using the GelDoc Imaging system (BioRad).

2.8.4 Verification of *CG5846*^{RNAi1}

Primers for verification of the *CG5846*^{RNAi1} (GD10737) line were synthesised (Sigma-Aldrich). These included the specific CG5846 primer (CG5846 rev) used during cloning and a common Hsp7_2 primer (Hsp2_7 fwd) which binds upstream of the transgene insertion in the pMF3 vector (Table 2.8) in which the *CG5846*^{RNAi1} (GD10737) construct was cloned (Dietzl *et al.*, 2007) (Figure 2.3A).

One half of the *CG5846*^{RNAi1} inverted repeat sequence from where the CG5846 rev primer bound was 315 bp and the section of the vector that was also amplified from where the Hsp7_2 fwd primer bound to the vector was 247 bp, therefore the total expected size of the product was 562 bp, which was observed following gel electrophoresis (Figure 2.3B).

Table 2.8 Primers used for *CG5846*^{RNAi1} PCR

Oligo name	Oligo number	Direction	Sequence 5'-3'
CG5846 rev	3029046409-000010	Reverse	CGCGGATCCGGCACCAGCAAACACAATCCAAA
Hsp7_2 fwd	3029046409-000020	Forward	GAGGCGCTTCGTCTACGGAGCGAC

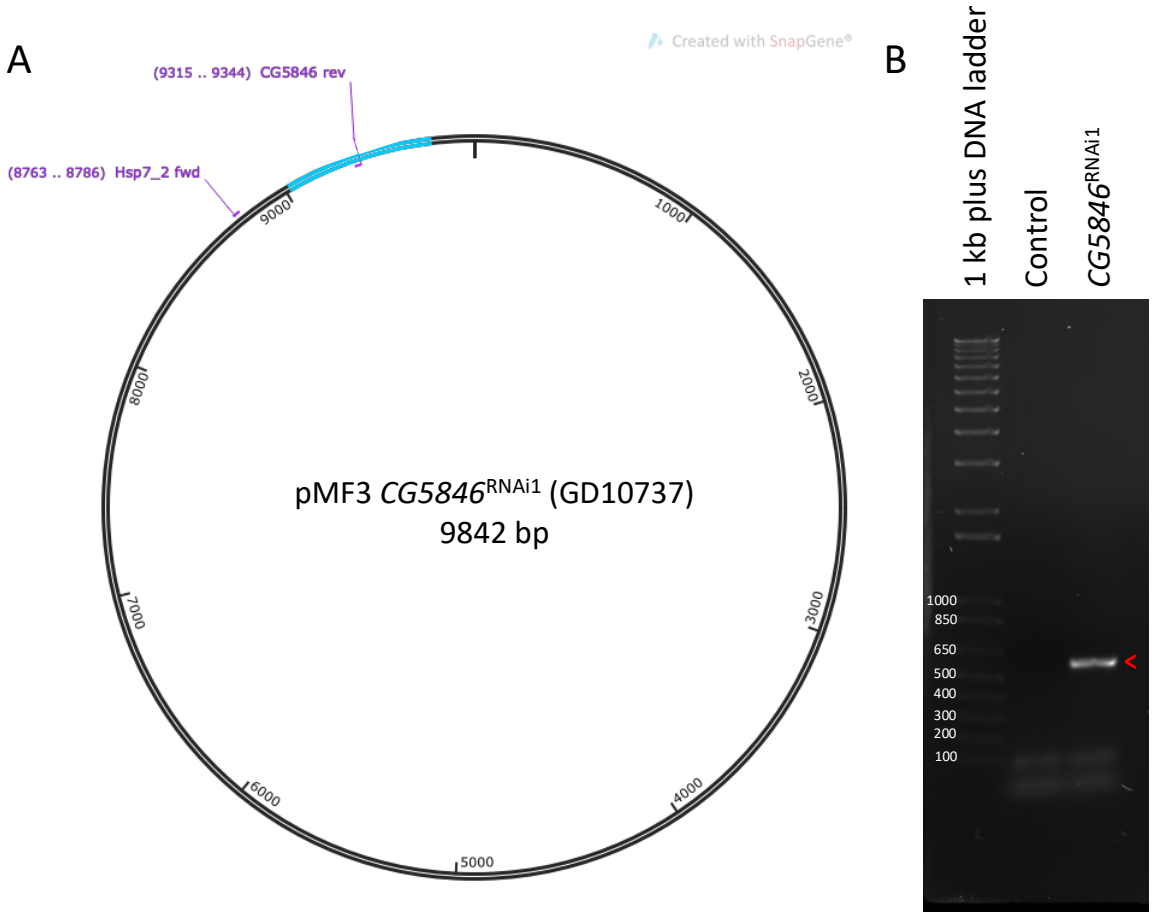

Figure 2.3. Validating the *CG5846*^{RNAi1} construct. A. The *CG5846*^{RNAi1} insert is an inverted repeat (blue) and the CG5846 rev primer binds at the centre of the inverted repeat. The Hsp7_2 fwd primer binds to the pMF3 vector. B. The *CG5846*^{RNAi1} construct was verified by amplifying the specific *CG5846*^{RNAi1} sequence. The resulting PCR product was run on an agarose gel and was confirmed to be of the expected size (red arrowhead).

2.8.5 The *CG5846*^{RNAi2} line

Three combinations of primer pairs were used to confirm the identity of the *CG5846*^{RNAi2} (KK105728) line. These consisted of the vector binding Hsp7_2 fwd and KK line sequence verification GTU rev primers, the vector binding SV2 rev and GTU fwd primers, and lastly the Hsp7_2 fwd and SV2 rev primers (Table 2.9). Hsp7_2 and SV2 bind to regions of the pKC26 vector on either side of the *CG5846*^{RNAi2} inverted repeat insert, whereas the GTU primer, a generic KK sequence verification primer, binds at the centre of the inverted repeats (Figure 2.4A).

Table 2.9 Primers used for *CG5846*^{RNAi2} PCR

Oligo name	Oligo number	Direction	Sequence 5'-3'
Hsp7_2 fwd	3029046409-000020	Forward	GAGGCGCTTCGTCTACGGAGCGAC
GTU	3029046409-000030	Forward/ Reverse*	GCGCAGATCTTGGCGCCCCTAGATG
SV2 rev	3029046409-000040	Reverse	CACAGAAGTAAGGTTCCTTCACAAAGATCC

* This primer recognises a palindromic region of the KK105728 insert and therefore can bind to both the sense and antisense DNA strand

A PCR product of expected size was not amplified with either the GTU and SV2 primer pair (504 bp), or with the GTU and Hsp7_2 primer pair (727 bp), both of which were tested with different annealing temperatures. A PCR product of expected size was attained through amplification with the SV2 and Hsp7_2 primer pair (1221 bp) (Figure 2.4B), however, it should be noted that a smaller PCR product of 850 bp was preferentially amplified and was indicated by primer binding software to be a second binding site for Hsp7_2.

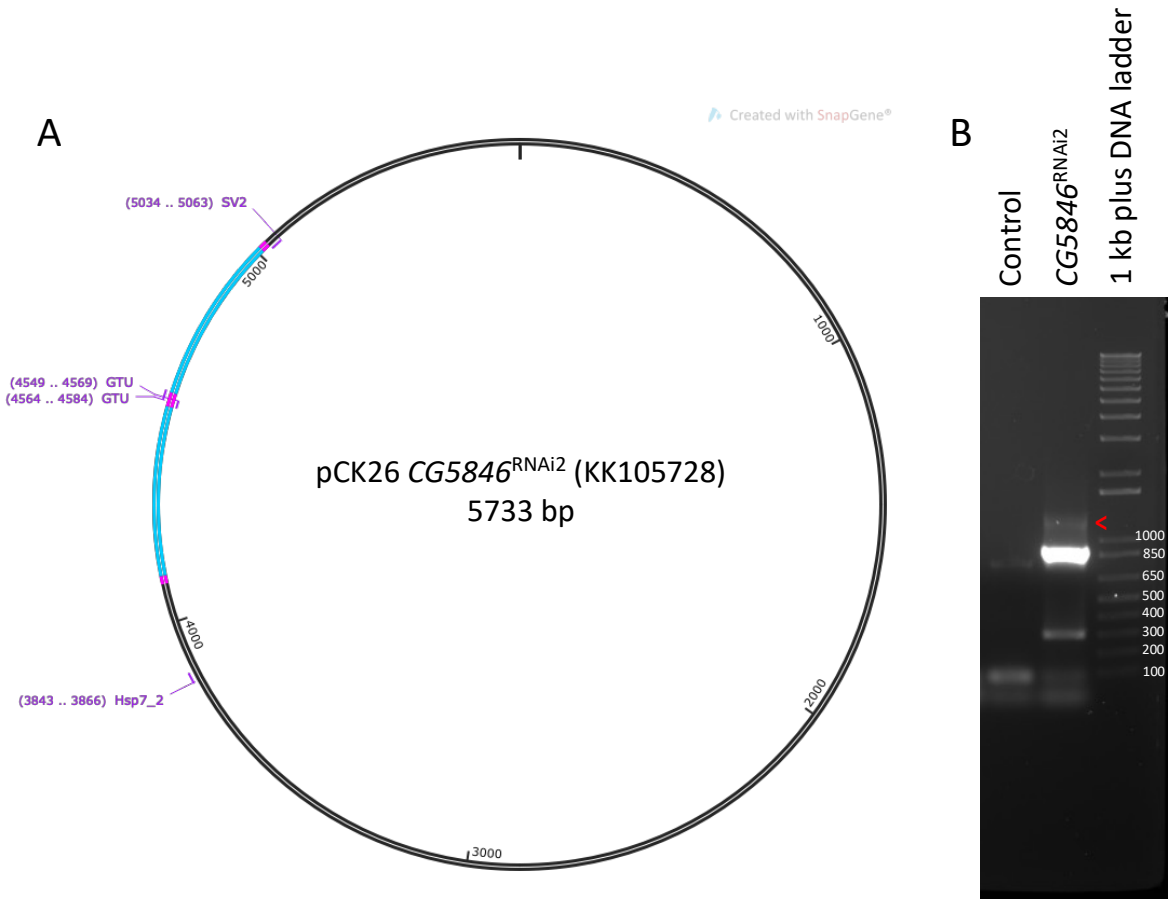

Figure 2.4. Validating the *CG5846*^{RNAi2} construct. A. The *CG5846*^{RNAi2} insert is an inverted repeat (blue) with palindromic sequences at the centre and at either ends of the inverted repeat (magenta). The GTU primer binds to a palindromic region at the centre of the insert. The Hsp7_2 fwd primer binds to the pCK26 vector upstream of the inverted repeat insert, the SV2 rev primer binds to the pCK26 vector downstream of the inverted repeat insert. B. The *CG5846*^{RNAi2} construct was verified using the Hsp7_2 fwd and SV2 rev primers. The resulting PCR product was run on an agarose gel and was confirmed to be of the expected size (red arrowhead). A smaller PCR product (850 kb) was amplified in abundance as a second primer binding site was preferential for Hsp7_2 binding.

Due to the possibility of off-target effects, standard practice is to verify phenotypic results generated by RNAi knockdown with more than one RNAi line; similar phenotypes were observed in the brain and eye with both *CG5846*^{RNAi1} and *CG5846*^{RNAi2}. Moreover, the rough eye phenotype observed for both knockdowns, with necrosis localised to the posterior of the eye is relatively unique and was not observed in a previous screen of over 100 RNAi lines (Schwartz *et al.*, 2016). Efficient knockdown of CG5846 was also confirmed for both lines (Section 4.2). Together, these data provide confidence that the phenotypes resulting from expression of *CG5846*^{RNAi} are a specific result of depletion of CG5846.

2.9 Proteasome activity

Proteasomal activity was analysed using the fluorogenic N-succinyl-leucine-leucine-valine-tyrosine-7-amino-4-methylcoumain (Suc-LLVY-AMC, Abcam) peptide which is used to measure chymotrypsin-like peptidase activity. The current protocol was adapted from Ikeda *et al.* (2019). Each sample was prepared from 30 heads, attained as detailed in Section 2.3.1, and lysed in 60 µL ice-cold homogenisation buffer (25 mM Tris-HCl pH 7.5). Cell lysis was achieved via 30 seconds of homogenisation with a motorised mortar and disposable plastic pestle. Cell lysates were centrifuged at 4°C for 10 minutes at a speed of 16,000 g, the supernatants were then transferred to a new Eppendorf tube on ice. Protein concentrations were measured via BCA assay as described in Section 2.3.6. The proteasome chymotrypsin-like activity was measured using the fluorogenic peptide, where 20 µg cell lysate was added to 100 µL of the fluorogenic assay buffer (25 mM Tris-HCl pH 7.5, 20 µM Suc-LLVY-AMC). Control samples for each genotype were also incubated with 20 µM of the proteasome inhibitor MG132 (Abcam AB147047). Protein and assay buffer with or without inhibitor were placed in a black walled, clear flat bottomed 96-well microplate (Invitrogen). The plate was incubated in the dark at 37°C for five minutes. Fluorescence of the cleaved 7-amino-4-methylcoumarin (AMC) was measured using the POLARstar Omega at 355 nm/460 nm (ex/em) at 37°C every two minutes over a 30 minute timeframe. The change in fluorescence per µg of protein was calculated for three biological replicates each assayed in triplicate after being subtracted by the values of each MG132-treated sample, and were displayed in box-and-whisker plots. Statistical significance was assessed via one-way ANOVA with post-hoc Tukey's HSD analysis.

3 Selection of HDAC4 candidate interactors and characterisation in the *Drosophila* brain and eye

HDAC4 is a transcriptional regulator and has been shown to play an important role in neurodevelopment, where overexpression of HDAC4 results in abnormal mushroom body and adult compound eye development (Fitzsimons *et al.*, 2013; Hawley, 2020; Main *et al.*, 2021; Schwartz *et al.*, 2016; Tan *et al.*, 2024; Wilson, 2021). To further the understanding of the molecular mechanisms that underlie HDAC4-overexpression-induced phenotypes, a candidate screen was carried out to identify genes that induce similar phenotypes to *HDAC4* in the brain and eye. The predominant brain phenotype induced by overexpression of HDAC4 is fusion of the mushroom body β lobes (Hawley, 2020; Main *et al.*, 2021; Tan *et al.*, 2024), which may result from a loss of axon termination or axon repulsion failure (Michel *et al.*, 2004). In the eye, overexpression of HDAC4 induces a mild rough eye phenotype with loss of the uniform ommatidial array (Schwartz *et al.*, 2016; Tan *et al.*, 2024; Wilson, 2021). The rationale for this screening approach is that if a reduction in expression of a candidate gene results in a similar phenotype to that induced by *HDAC4* overexpression, this would indicate that this candidate and HDAC4 may function in similar molecular pathways and therefore overexpression of the candidate may rescue the HDAC4-overexpression-induced phenotype by overcoming the pathway disruption.

3.1 Selection of candidate HDAC4-interactors

Candidate HDAC4-interactors were selected from a previous genetic interaction study and RNA-seq analyses that were carried out in this laboratory, as well as via a review of recent literature that identified candidate HDAC4-interactors that were not included in the genetic screen.

The rough eye enhancer screen for genes that interact with *HDAC4* ((Schwartz *et al.*, 2016), as described in Section 1.7) identified 18 novel genes that interacted genetically with *HDAC4*. Of these, seven genes were chosen for the initial screen: *CG5846*, *crammer* (*cer*), *krasavietz* (*kra*),

Netrin-B (*NetB*), *rogdi*, *Scamp*, and *schnurri* (*shn*). None of these candidates have been shown to interact physically with HDAC4 and were primarily selected based on evidence showing a function in LTM and/or involvement in axon growth and guidance in the mushroom body (Table 3.1).

In the same study, RNA-seq was conducted on fly heads overexpressing wild-type DmHDAC4 in the brain which identified 28 genes that were differentially expressed (Schwartz *et al.*, 2016). A follow up RNA-seq experiment was then conducted to analyse transcriptional changes associated with nuclear and cytoplasmic pools of HDAC4 via the expression of cytoplasmic- and nuclear-restricted mutants of HsHDAC4 in the brain (Main *et al.*, 2021). The *Drosophila* and human HDAC4 datasets from these two studies were compared to identify genes that were differentially expressed in both. Expression of both *Drosophila* and human HDAC4 resulted in downregulation of *kekkon 2* (*kek2*) and upregulation of *Niemann-Pick type C-2g* (*Npc2g*). *kek2* was also selected as it is expressed in the *Drosophila* central nervous system where it functions as a modulator of synapse growth (Musacchio & Perrimon, 1996), which is essential for LTM acquisition (Lamprecht & LeDoux, 2004). Although there is little known about the function of *Drosophila* Npc2g, this candidate was selected as mutations of its mammalian orthologue have been associated with Niemann Pick disease, a fatal neurodegenerative disease caused by cholesterol accumulation. Previous studies have shown that inhibition of HDAC4 results in a decrease of cholesterol levels (Nunes *et al.*, 2013), therefore, it was hypothesised that differential expression of HDAC4 could result in alterations to Npc2g levels leading to abnormal accumulation of cholesterol and neurodegenerative disease. An additional candidate gene was also selected from the HsHDAC4 dataset alone, *methuselah-like 8* (*mthl8*) as this was the most highly upregulated gene by both nuclear and cytoplasmic pools of HsHDAC4 (Main *et al.*, 2021) (Table 3.2).

Candidates were also chosen based on a wide literature review of proteins that may be involved with HDAC4, whether it be a confirmed physical interaction in a different tissue or organism, a functional relationship, or a predicted interaction based on conserved domain structures. These candidates selected include *forked*, *forkhead box, sub-group O* (*foxo*), *Kank*, *Lysine demethylase 5* (*Kdm5*), *Salt-inducible kinase 3* (*Sik3*), and *Thor* (Table 3.3).

A screening strategy was adopted for initial characterisation of the 16 candidate HDAC4-interactors. As the phenotypes resulting from HDAC4 overexpression in the eye and mushroom body have been extensively characterised (Hawley, 2020; Main *et al.*, 2021; Schwartz *et al.*,

2016; Tan *et al.*, 2024; Wilson, 2021) and can be assessed semi-quantitatively, the impact of knockdown of each candidate on eye and mushroom body development was examined. In addition to the above-mentioned analyses, for the genes in which green fluorescent protein (GFP) traps and/or GAL4 enhancer traps were available, the expression pattern in the brain was also characterised.

Table 3.1. Candidate gene selection based on a rough eye enhancer screen (Schwartz *et al.*, 2016)

Gene name	*Drosophila* molecular function/biological process	Rationale for gene selection
CG5846	Unknown	CG5846 is a homologue of mammalian RFXANK and ANKRA2, both of which contain a 5x ankyrin repeat domain (McKinsey *et al.*, 2006; Wang *et al.*, 2005). Both RFXANK and ANKRA2 directly bind the conserved putative PxLPxI/L motif in HDAC4 (Xu *et al.*, 2012), and a physical interaction between these proteins has been demonstrated in mammalian cell culture via yeast-two-hybrid (Wang *et al.*, 2005), co-immunoprecipitation (McKinsey *et al.*, 2006) and colocalisation studies (McKinsey *et al.*, 2006; Wang *et al.*, 2005).
cer	Lysosomal cysteine proteinase (cathepsin) inhibitor	Cer is an enzyme involved in the degradation of cathepsin (Tseng *et al.*, 2012) and has been associated with Alzheimer's disease, where increased levels of cathepsin messenger RNA (mRNA) are localised in regions of highly concentrated amyloid precursor protein (Comas *et al.*, 2004). Cer protein localises to the mushroom body lobes (Davis, 2005) and defects in long-term memory are observed on both overexpression and knockdown of Cer (Comas *et al.*, 2004).
kra	Translation inhibitor, regulator of axon midline repulsion	Kra is highly expressed in the central nervous system, where it localises to axons and glia. Kra physically interacts with Shot (F-actin crosslinker) to regulate translation as well as axon extension, guidance, and repulsion (Lee *et al.*, 2007). *Drosophila* Kra has high sequence similarity to human BZW1 which functions by activating histone H4 and is a co-regulator of transcription factors involved in cell cycle control (Mitra *et al.*, 2001) and carcinoma cell growth and proliferation (Li *et al.*, 2009).
NetB	Lamin related protein, regulator of axon extension and commissural axon guidance	NetB is expressed in midline glia (Guthrie, 1997) and mushroom body neurons (Kang *et al.*, 2019) and regulates commissural axon growth and extension (Mitchell *et al.*, 1996). NetB interacts with receptors Frazzled and Uncoupled-5 to regulate mushroom body axon extension. Overexpression of NetB results in β lobe fusion and knockdown of NetB in a *Drosophila* model of Fragile X syndrome ameliorated the associated defects in short-term memory (Kang *et al.*, 2019).
rogdi	Unknown	Rogdi is an orthologue of mammalian Rogdi. Loss-of-function mutations in *Rogdi* result in Kohlschutter-Tonz syndrome, which is a rare neurodegenerative disease, the predominant features of which are epilepsy and developmental delay (Huckert *et al.*, 2014; Mory *et al.*, 2014; Schossig *et al.*, 2017). Mammalian Rogdi is expressed in the central nervous system, largely in the brain and spinal cord (Kim *et al.*, 2017; Riemann *et al.*, 2017). *Drosophila* Rogdi has a role in sleep regulation via GABAergic control of dopaminergic signalling (Kim *et al.*, 2017) and has been implicated in epileptic seizures (Treiman, 2001). Rogdi mutants have also shown rapid tolerance to ethanol (Berger *et al.*, 2008) and significant long-term memory impairments (Dubnau *et al.*, 2003).
Scamp	Integral membrane protein	Scamp is involved in binding to transporters of neurotransmitters to regulate target destinations, thereby regulating membrane dynamics and potentials by Ca^{2+} induced synaptic vesicle recycling during neuronal signalling (Zheng *et al.*, 2014). *Drosophila* Scamp mutants have been implicated in synaptic transmission deficiencies in the larval neuromuscular junction (Fernandez-Chacon & Sudhof, 2000; Zhao *et al.*, 2009) and null mutants also exhibited deficits in survival, climbing ability, olfactory learning, and long-term memory (Zheng *et al.*, 2014).
shn	Transcription factor	Shn is a transcriptional repressor of decapentaplegic signalling-dependent genes which are required for *Drosophila* development (Arora *et al.*, 1995; Cai & Laughon, 2009; Gao *et al.*, 2005). Shn mutants have severely impaired long-term memory but normal learning (Dubnau *et al.*, 2003). These mutants also disrupt experience dependent plasticity in sleep patterning (Ganguly-Fitzgerald *et al.*, 2006).

Table 3.2. Candidate gene selection based on RNA-seq analyses (Main *et al.*, 2021; Schwartz *et al.*, 2016)

Gene name	Wild-type DmHDAC4		HsHDAC4^{L175A}		HsHDAC4^{3SA}		*Drosophila* molecular function/biological process	Rationale for gene selection
	Log^2 fold	Adj P	Log^2 fold	Adj P	Log^2 fold	Adj P		
kek2	-0.72	5E^{-5}	-2.28	4.55E^{-148}	-2.95	1.1E^{-11}	Transmembrane cell adhesion protein	Kek2 is expressed in the central nervous system as a neural activity-dependent modulator of synaptic growth (Musacchio & Perrimon, 1996), observed in puncta along the axis of axonal tracts and at the synaptic terminal of the neuromuscular junction. Under seizure conditions Kek2 expression levels increase in neuronal cell bodies and overexpression and knockdown studies show a reduction in synaptic growth (Guan *et al.*, 2005).
mthl8	n/a	n/a	11.49	2.54E^{-19}	11.15	2.93E^{-16}	G-Protein coupled receptor	Mthl8 is part of the secretin receptor family which play roles in larval development, lifespan, immunity, and oxidative stress resistance (Lin *et al.*, 1998). Mthl8 is expressed highly in the larval brain (Patel *et al.*, 2012), however, RNA-seq on RNA isolated from the *Drosophila* adult brain demonstrated that under basal conditions Mthl8 expression was undetectable (Wei Tan Jun, unpublished data). On the contrary, a previous *in situ* hybridisation study showed low levels of Mthl8 expression in neuronal cell bodies in the adult brain and that it is highly upregulated in a range of learning and memory mutants (Guan *et al.*, 2011).
Npc2g	0.8	5E^{-5}	0.68	3.11E^{-12}	1.11	0.015	Glycoprotein/ controlling homeostasis and steroid biosynthesis	The mammalian orthologue of Npc2g is Niemann-Pick Type C2 (NPC2), and mutations of NPC2 result in Niemann-Pick, a fatal hereditary neurodegenerative disease associated with abnormal cholesterol accumulation (Walterfang *et al.*, 2006). *Drosophila* Npc2g may participate in immune signaling (Shi *et al.*, 2012) and is expressed in the head mesoderm and fat body (Huang *et al.*, 2007).

n/a = not applicable.
HsHDAC4^{L175A} is a cytoplasmic restricted mutant of human HDAC4 with a lysine to alanine substitution (Lys^{175}) (Main *et al.*, 2021).
HsHDAC4^{3SA} is a nuclear restricted mutant of human HDAC4 with three serine to alanine substitutions (Ser^{246}, Ser^{467}, Ser^{623}) (Main *et al.*, 2021).

Table 3.3. Candidate gene selection based on literature mining

Gene name	*Drosophila* molecular function/biological process	Rationale for gene selection
forked	F-actin bundling, bristle formation	Forked is an ankyrin repeat containing protein (Hoover *et al.*, 1993) which was hypothesised to bind to the PxLPxI/L motif on HDAC4 (Xu *et al.*, 2012). Actin enriched microtubules and microfilaments play important roles in the morphogenesis of ommatidia and interommatidial mechanosensory bristles in the developing eye, where *forked* mutants often result in short, twisted bristles with a complete loss of fibre bundle formation (Hoover *et al.*, 1993; McLachlan, 1986; Perry, 1968; Petersen *et al.*, 1994).
foxo	Transcription factor/roles in insulin signaling, negative regulator of the cell cycle, cell growth and proliferation	Foxo is predominantly expressed in fat body cells and plays a role in insulin signaling by regulating cell number under conditions of reduced insulin (Jünger *et al.*, 2003). A *foxo* loss-of-function mutation has been implicated in regulating the circadian clock due to a sensitivity to oxidative stress (Zheng *et al.*, 2007). Foxo mutants display abnormal behavioral rhythms which are exacerbated due to an increase in oxidative stress from ageing. HDAC4 nuclear translocation results in Foxo activation which initiates downstream apoptotic target gene expression (Mihaylova *et al.*, 2011; Wang *et al.*, 2011). An interaction *in vivo* and *in vitro* has been established between Foxo, Kdm5, and HDAC4 in modulating oxidative stress by activating stress resistance genes (Liu *et al.*, 2014).
Kank	Regulator of actin polymerisation/unknown function in *Drosophila*	Kank is an ankyrin repeat containing protein that was found to be a potential tumor suppressor for renal cell carcinoma (Sarkar *et al.*, 2002). The *Drosophila* orthologue has been established to play a role in muscle-tendon attachment (Clohisey, 2013) and was hypothesised to bind to the PxLPxI/L motif in HDAC4 via its ankyrin repeat motif (Xu *et al.*, 2012). A large genomic deletion of the mammalian orthologue *Kank 1* is associated with the neurological disorder cerebral palsy spastic quadriplegic 2 syndrome (Chen *et al.*, 2018). Murine studies show weak expression of Kank 1 and 2 in the brain (Guo *et al.*, 2021) with predominant cytoplasmic localisation in TUHR14TKB cells (Zhu *et al.*, 2008).
Kdm5	Histone H3 lysine 4 demethylase/negative transcription regulator	Kdm5 has a broad expression pattern with predominant nuclear localisation in the ganglion mother cells and neuronal cell bodies required for axon morphogenesis (Hatch *et al.*, 2021; Zamurrad *et al.*, 2018). Kdm5 is essential for larval growth and development where it is required for appropriate synaptic morphology and neurotransmission (Belalcazar *et al.*, 2021). Introduction of a missense mutation of *Kdm5* results in intellectual disability in *Drosophila*. This mutation had little effect on mushroom body formation, however, had a significant detrimental impairment to memory formation (Zamurrad *et al.*, 2018). Kdm5 and Foxo both interact with HDAC4 to regulate oxidative stress resistance as co-expression of Kdm5 and Foxo is required for activation of stress resistance genes (Liu *et al.*, 2014).
Sik3	Serine/Threonine kinase/ phosphorylates HDAC4 in circadian clock regulation, glial nerve swelling	Knockdown and overexpression of Sik3 results in mild ommatidia alignment defects and disruption to bristle formation in the *Drosophila* eye. A *Sik3* null mutation causes lethality in early development, and in the larval eye disc, Sik3 localised to R3/R4 photoreceptor nuclei (Sahin *et al.*, 2020). HDAC4 is a phosphorylation target of Sik3 (Wang *et al.*, 2011), and Sik3 regulates the subcellular distribution of HDAC4 in glia, fat body cells, and clock neurons (Fujii *et al.*, 2017). Under basal conditions Sik3 promotes cytoplasmic retention of HDAC4, relieving inhibition of MEF2 resulting in upregulation of MEF2-dependent transcription (H. Li *et al.*, 2019). A loss of Sik3 results in dephosphorylation of HDAC4, leading to increased nuclear accumulation (Fujii *et al.*, 2017).
Thor	Eukaryotic 4E binding protein/regulator of translation	Foxo is a critical component of insulin signaling and under conditions of low insulin, upregulates transcription of Thor (Jünger *et al.*, 2003). Under basal conditions Thor is expressed in most tissues and is specifically localised to the embryonic nervous system (Bernal & Kimbrell, 2000), fat body, and salivary gland (Teleman *et al.*, 2005). Under conditions of amino acid starvation Foxo-dependent Thor expression is upregulated (Tettweiler *et al.*, 2005), and *Thor* null mutants have impaired survival (Teleman *et al.*, 2005).

3.2 Investigating the effect of candidate gene knockdown on mushroom body development

The *Drosophila* mushroom body is a bilateral symmetrical structure with dorsal and medial projecting lobes located on either side of the brain midline (Strausfeld *et al.*, 1998) (detailed in Section 1.3.1.1, Figure 1.2) and intact structural integrity of the mushroom body is essential for normal learning and memory formation (McBride *et al.*, 1999). Common mushroom body morphological defects are shown in Figure 3.1.

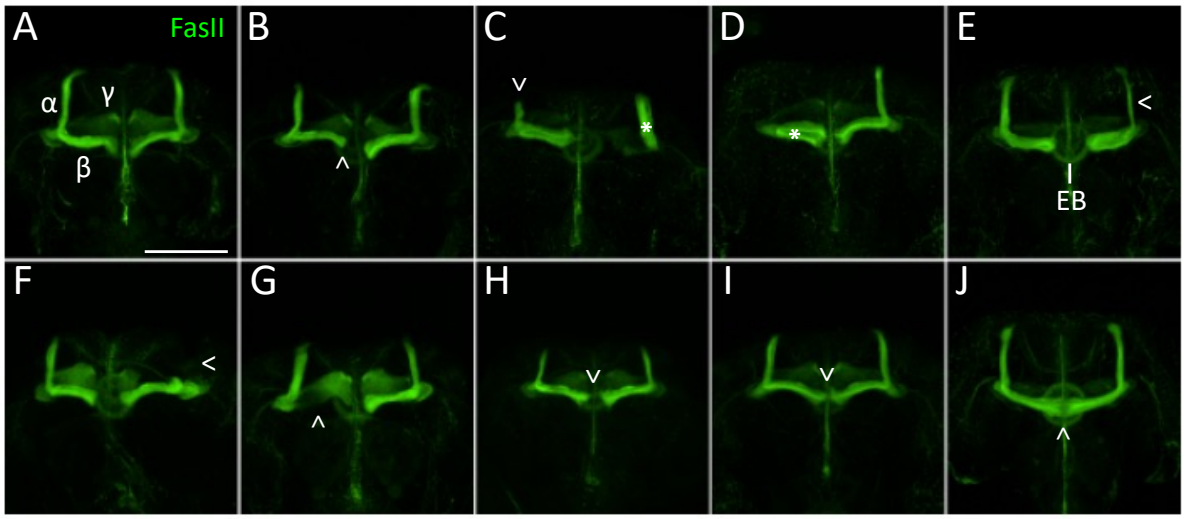

Figure 3.1. Examples of morphological defects of the mushroom body upon knockdown of candidate genes. Maximum anterior confocal projections of brains. Microdissected brains were processed for immunohistochemistry using anti-FasII to visualise the mushroom body lobes. A. Wild-type control brain showing the α, β and, γ mushroom body lobes. B-J. Representative images showing the range of abnormal mushroom body phenotypes. B. β lobe shortening (∧), C. α lobe shortening (∨) and β lobe guidance defect (*), D. α lobe guidance defect (*), E. thinned α lobe (<), F. missing α lobe (<), G. missing β lobe (∧), H. mild (∨), I. moderate (∨), and J. severe β lobe fusion (∧). Images taken using 40x objective lens in oil, 1 µm sections, scale bar = 100 µm. EB = ellipsoid body.

These include shortened and/or missing α and β lobes which can be attributed to a total or partial loss of axon extension signaling cues. Guidance defects, a result of misdirected axon growth and extension signaling, leading to the medial projection of the α lobe axons and dorsal projection of the β lobe axons. A thinned α lobe can be attributed to both guidance and missing lobe defects, as few bundled axons project in the correct manner, with the remainder of these axons either missing, due to extension defects, or projected in an aberrant direction. The β lobes project medially (Figure 3.2A) and fusion can be visualised as mild; where few axons project

and cross the midline from either one or both β lobes (Figure 3.2B), moderate; where only the top of the β lobes fuse at the midline (Figure 3.2C), or severe; where the entirety of both β lobes cross the midline and fuse as a single lobe (Figure 3.2D), hypothesised to be due to a loss of axon termination.

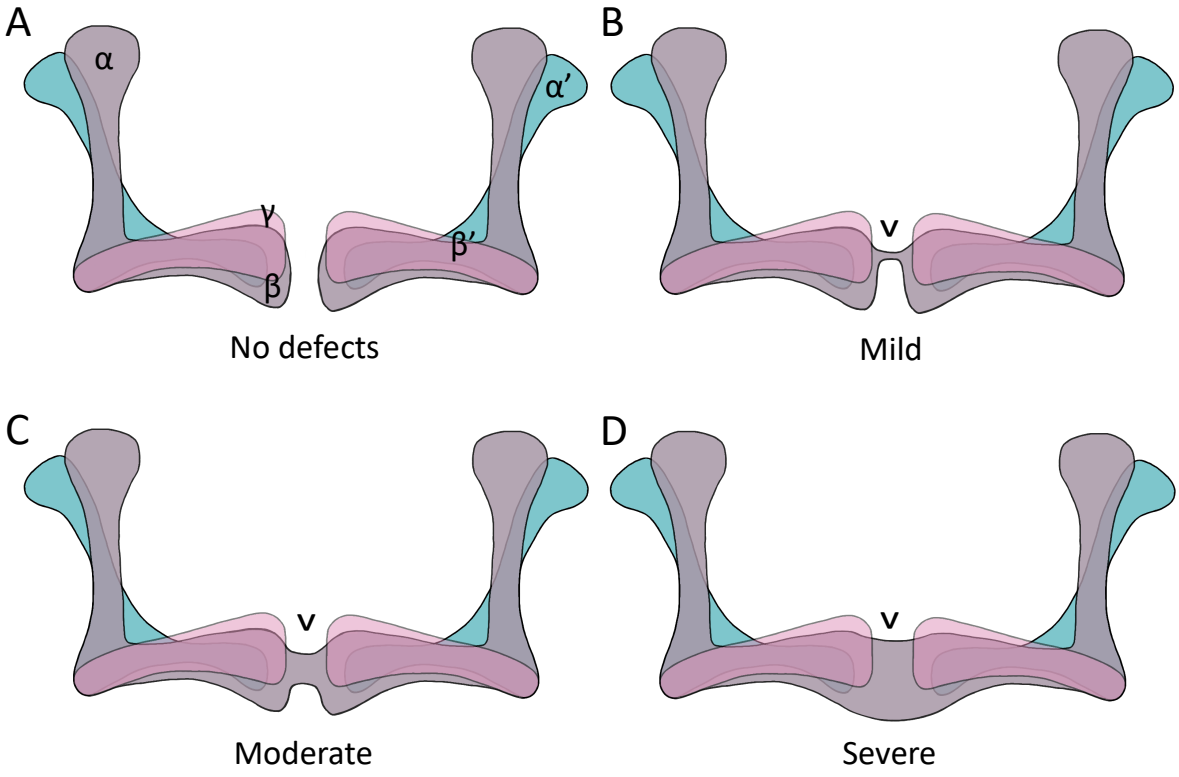

Figure 3.2. Cartoon figure demonstrating the different levels of β lobe fusion. A. The mushroom body is a symmetric bilateral structure that consists of five independent lobes, the vertical α and horizontal β lobes (purple), the vertical α' and horizontal β' lobes (blue), and the horizontal γ lobe (pink). Loss of axon termination in the β lobes result in B. mild (with few axons crossing the midline), C. moderate (the top half of the β lobe axon bundle crosses the midline), or D. severe fusion, where the entirety of both β lobe axon bundles cross the midline and fuse as one lobe.

Wild-type levels of HDAC4 are required for normal mushroom body formation, as overexpression and knockdown of DmHDAC4 or overexpression of HsHDAC4 resulted in abnormal axon morphogenesis. This was phenotypically observed as shortened, thinned or missing α and β lobes, as well as fusion of the β lobes (Hawley, 2020; Main *et al.*, 2021; Tan *et al.*, 2024). A more thorough analysis revealed that the most prevalent phenotype is β lobe fusion, with pan-neuronal overexpression of wild-type DmHDAC4 at 25°C resulting in fusion in 88% of brains, 67% of these a result of severe β lobe fusion (Tan *et al.*, 2024).

3.2.1 Approach to assessing and scoring alterations in axon morphogenesis

For each of the candidate genes, transgenic flies were obtained with genomic insertions of long inverted repeat hairpins downstream of UAS for RNAi-mediated tissue specific knockdown, with one line (*NetB*^{RNAi1}) consisting of a short hairpin RNA (Table 2.1), all lines are hereafter referred to as an "RNAi line". A total of 33 RNAi lines were procured from international stock centres to knock down expression of each of the 16 candidate genes. As previous studies utilised the mushroom body structure to visually assess whether overexpression of HDAC4 resulted in defects to brain development (Main *et al.*, 2021; Tan *et al.*, 2024), the mushroom body was also examined in this study to assess whether knockdown of a candidate gene resulted in similar defects to brain development, through the assessment of mushroom body axon morphogenesis. For the majority of genes, two or more independent RNAi lines were available. As it was of importance to compare the phenotypes induced by each of these candidate knockdowns to the phenotypes induced by the overexpression of HDAC4 (Main *et al.*, 2021; Tan *et al.*, 2024), males from each RNAi line were crossed to *elav-GAL4* virgin females to induce pan-neuronal knockdown of each candidate gene throughout all stages of development (Figure 8.6, Appendix 8.6) (Robinow & White, 1988). A single RNAi line (*Scamp*^{RNAi2}) was pupal lethal when expressed pan-neuronally, therefore, *Scamp*^{RNAi2} males were crossed to a virgin females of the mushroom body specific driver *OK107-GAL4*, which resulted in adult progeny survival. Immunohistochemistry was performed on whole brains of progeny using an anti-FasciclinII (anti-FasII) antibody to visualise the structure of the mushroom body (Section 2.2.4). FasII is a cell adhesion molecule that is highly expressed and localises to the α, β, and, γ lobes of the mushroom body, and is a commonly used maker for clear unobstructed observation of the mushroom body lobes (Cheng *et al.*, 2001). Z-projections were generated via confocal microscopy and maximum projections were processed using ImageJ software (Section 2.2.5).

A range of abnormal phenotypic defects in mushroom body development were observed and results were displayed in Table 3.4. Abnormalities include: shortening of the α and β lobes (Figure 3.1B, C), guidance defects (Figure 3.1C, D), α lobe thinning (Figure 3.1E), missing α (Figure 3.1F) and β lobes (Figure 3.1G), and β lobe fusion (Figure 3.1H, I, and J).

Table 3.4. Frequency of mushroom body phenotypes

	elav-GAL4/+	*OK107-GAL4/+*	*CG5846*^{RNAi1}	*CG5846*^{RNAi2}	*cer*^{RNAi1}	*cer*^{RNAi2}	*forked*^{RNAi1}	*forked*^{RNAi2}	*foxo*^{RNAi1}
α shortening (%)	-	-	-	-	-	5.0	-	-	-
β shortening (%)	-	-	3.7	-	-	-	-	5.0	4.8
α missing (%)	-	-	-	-	-	-	-	-	-
β missing (%)	-	-	-	-	-	-	-	-	-
α thinning (%)	-	-	-	-	-	-	-	-	-
Guidance (%)	-	-	3.7	2.9	-	-	-	-	-
Total β fusion (%)	-	10.0	11.1	5.9	-	-	5.0	5.0	14.4
Mild (%)	-	10.0	11.1	5.9	-	-	5.0	5.0	9.6
Moderate (%)	-	-	-	-	-	-	-	-	-
Severe (%)	-	-	-	-	-	-	-	-	4.8
n	20	20	27	34	18	20	20	20	21

	foxo^{RNAi2}	*Kank*^{RNAi}	*Kdm5*^{RNAi1}	*Kdm5*^{RNAi2}	*kek2*^{RNAi1}	*kek2*^{RNAi2}	*kra*^{RNAi1}	*kra*^{RNAi2}	*mthl8*^{RNAi1}
α shortening (%)	-	13.9	-	-	-	-	-	4.8	4.8
β shortening (%)	-	-	-	-	-	-	-	-	-
α missing (%)	-	-	-	-	5.0	-	-	-	-
β missing (%)	-	-	-	-	-	-	-	-	-
α thinning (%)	-	-	-	-	-	-	4.8	4.8	-
Guidance (%)	-	-	10.5	5.0	-	5.0	-	-	9.5
Total β fusion (%)	5.0	2.8	10.5	5.0	-	-	-	-	14.3
Mild (%)	-	2.8	-	-	-	-	-	-	14.3
Moderate (%)	-	-	10.5	-	-	-	-	-	-
Severe (%)	5.0	-	-	5.0	-	-	-	-	-
n	20	36	19	20	20	20	21	21	21

	mthl8^{RNAi2}	*NetB*^{RNAi1}	*NetB*^{RNAi2}	*Npc2g*^{RNAi1}	*Npc2g*^{RNAi2}	*Npc2g*^{RNAi3}	*rogdi*^{RNAi1}	*rogdi*^{RNAi2}	*Scamp*^{RNAi1}
α shortening (%)	-	-	9.5	6.5	2.4	-	5.0	-	-
β shortening (%)	-	-	-	-		-	-	-	-
α missing (%)	-	-	-	3.2	-	-	5.0	-	5.0
β missing (%)	-	-	-	-	2.4	-	-	-	-
α thinning (%)	-	-	4.8	-	-	-	-	-	-
Guidance (%)	19.0	-	9.5	3.2	4.8	2.8	-	-	5.0
Total β fusion (%)	57.2	-	71.4	3.2	2.4	19.6	-	15.0	50.0
Mild (%)	14.3	-	33.3	3.2	-	5.6	-	15.0	15.0
Moderate (%)	14.3	-	4.8	-	2.4	2.8	-	-	15.0
Severe (%)	28.6	-	33.3	-	-	5.6	-	-	20.0
n	21	21	21	31	42	36	20	20	20

	Scamp^{RNAi2*}	*shn*^{RNAi}	*Sik3*^{RNAi1}	*Sik3*^{RNAi2}	*Sik3*^{RNAi3}	*Thor*^{RNAi1}	*Thor*^{RNAi2}	*Thor*^{RNAi3}
α shortening (%)	-	-	4.5	-	-	-	5.0	-
β shortening (%)	-	-	-	-	-	-	-	-
α missing (%)	-	-	-	-	-	-	5.0	-
β missing (%)	-	5.0	-	-	-	-	-	-
α thinning (%)	10.0	-	-	-	-	-	-	-
Guidance (%)	5.0	-	-	-	-	10.0	5.0	-
Total β fusion (%)	70.0	25.0	13.6	4.5	15.0	5.0	15.0	-
Mild (%)	5.0	10.0	13.6	-	15.0	-	10.0	-
Moderate (%)	10.0	-	-	4.5	-	5.0	-	-
Severe (%)	55.0	15.0	-	-	-	-	5.0	-
n	20	20	22	22	20	20	20	19

* = RNAi line crossed to *OK107-GAL4*.

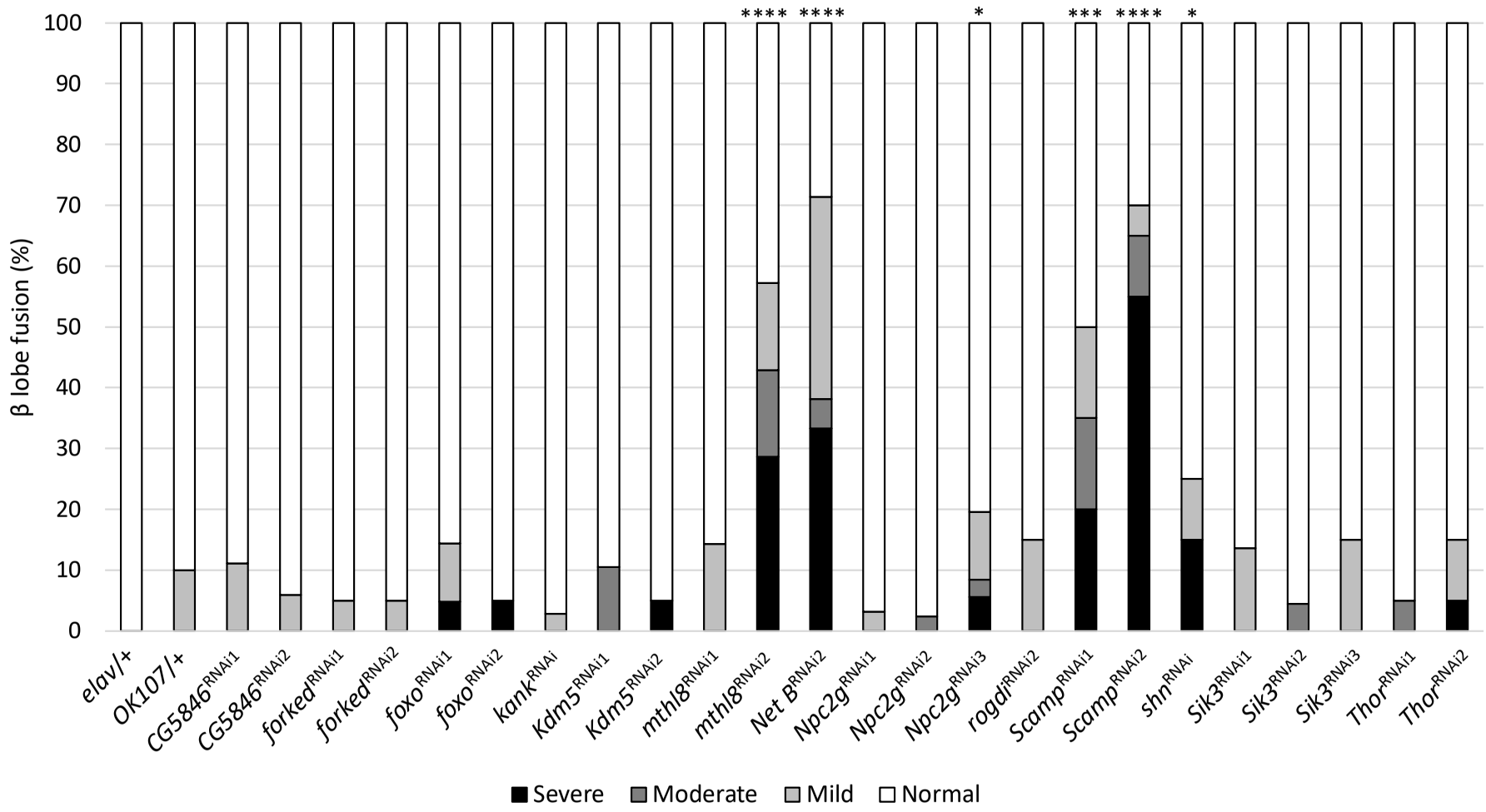

Figure 3.3. Penetrance of β lobe fusion following expression of each RNAi line. Each bar represents the percentage and level of β lobe fusion that was scored by a blinded observer in the mushroom body screen. Pan-neuronal expression of each RNAi construct was induced by *elav-GAL4* (*OK107-GAL4* used to induce $Scamp^{RNAi2}$), n≥18, (one-tailed Fisher's exact statistical test of total β lobe fusion compared to controls, *elav-GAL4/+* or *OK107-GAL4/+*,* = p<0.05, *** = p<0.001, **** = p<0.0001, *elav-GAL4/+* ; $mthl8^{RNAi2}$ = <0.0001, *elav-GAL4/+* ; $NetB^{RNAi2}$ = <0.0001, *elav-GAL4/+; Npc2g*^{RNAi3} = 0.036, *elavGAL4/+* ; $Scamp^{RNAi1}$ = 0.0002, *OK107-GAL4/+* ; $Scamp^{RNAi2}$ = <0.0001, *elav-GAL4/+* ; shn^{RNAi} = 0.0236). *elav* = *elav-GAL4*, *OK107* = *OK107-GAL4*.

Z-projections were quantitatively assessed and of the abnormal phenotypes observed, guidance defects and β lobe fusion were significantly more prevalent, with fewer incidences of axon elongation defects resulting in shortened, missing, and/or thinned lobes. As β lobe fusion is the most prevalent phenotype upon HDAC4 overexpression, the incidence of this phenotype following knockdown of each candidate was compared across all 16 genes (Figure 3.3).

Of all the RNAi lines that were screened, expression of six resulted in a significant incidence of β lobe fusion compared to controls (*mthl8*^{RNAi2}, *NetB*^{RNAi2}, *Npc2g*^{RNAi3} *Scamp*^{RNAi1}, *Scamp*^{RNAi2}, and *shn*^{RNAi}). Expression of *mthl8*^{RNAi2} resulted 19% of brains displaying guidance defects and 57.2% of brains displaying β lobe fusion defects, with 28.6% of these being severe fusion. Expression of *NetB*^{RNAi2} resulted in the highest level of total β lobe fusion (71.4%), the majority of which was moderate to severe. A small percentage of brains also displayed α lobe shortening (9.5%), α lobe thinning (4.8%), and guidance defects (9.5%), and expression of *Npc2g*^{RNAi3} resulted in 19.6% of brains displaying β lobe fusion. The β lobe fusion phenotypes induced by these three RNAi lines were however not observed with the additional RNAi lines that were also examined (*mthl8*^{RNAi1}, *NetB*^{RNAi1}, *Npc2g*^{RNAi1}, and *Npc2g*^{RNAi2}), which suggests that these phenotypes could either be a result of off-target effects or the efficacy of knockdown was lower in these additional RNAi lines. Although the targets of the inverted repeat hairpins were bioinformatically confirmed, not all RNAi lines provide efficient knockdown (Dietzl *et al.*, 2007) and some confer off-target effects. Reverse-transcriptase quantitative PCR (RT-qPCR) to determine the efficacy of knockdown and correct gene targeting of each of the RNAi lines would confirm this, however, these analyses were not performed given this was a preliminary screen to identify candidates for further investigation. *Scamp*^{RNAi1} resulted in a total of 50% of brains with fusion, with 20% being severe fusion. Pan-neuronal expression of *Scamp*^{RNAi2} driven by *elav-GAL4* resulted in lethality during the pupal stage, indicating that expression of Scamp during neurodevelopment is critical for survival. Expression of *elav* begins early in development, between 2-4 hours after fertilisation, and continues through to adulthood where it is expressed in all neurons in the brain (Hilgers *et al.*, 2011; Robinow & White, 1988). To circumvent this pupal lethal phenotype, *Scamp*^{RNAi2} was crossed to *OK107-GAL4*, restricting expression largely to the mushroom body. This resulted in viable F1 progeny, which were found to display a high level of β lobe fusion (70%) with the majority being severe fusion (55%). Expression of *shn*^{RNAi} resulted in a low albeit significant level of β lobe fusion, the majority of which was severe.

3.3 Investigating the effect of candidate gene knockdown on eye development

Overexpression of DmHDAC4 in all postmitotic photoreceptors driven by *GMR-GAL4* disrupts eye development and results in a rough eye phenotype due to misalignment and fusion of ommatidia, loss of normal bristle patterning, and depigmentation (Main *et al.*, 2021; Schwartz *et al.*, 2016; Tan *et al.*, 2024; Wilson, 2021). The term "rough eye" refers to the phenotypic combined disruption in the regular uniform organisation of ommatidia, due to misalignment and fusion of the ommatidia, a loss of normal bristle patterning, and in some instances a reduction of pigmentation (Basler *et al.*, 1990; Kaplow *et al.*, 2007). Overexpression of one copy of DmHDAC4 resulted in a mild rough eye phenotype with mild ommatidia disorganisation and few instances of multiple interommatidial mechanosensory bristles emerging from a single bristle pore (Schwartz *et al.*, 2016), which was exacerbated upon expression of a second copy of DmHDAC4 (Tan *et al.*, 2024).

3.3.1 Approach to assessing and scoring detriments in *Drosophila* compound eye development

To determine whether any of the candidate genes are required for eye development, males of each RNAi line were crossed to *GMR-GAL4* virgin females, to drive expression in all post-mitotic photoreceptor cells posterior to the morphogenetic furrow (Freeman, 1996). The F1 progeny eyes were then imaged using light microscopy (Section 2.4.1) and assessed for perturbations to the normal array of ommatidia, bristle organisation, and pigmentation disturbances using a simple rough eye phenotype scoring system (Table 2.6, Figure 3.4) that was previously established for characterising the HDAC4 overexpression-induced defects in eye development (Kaplow *et al.*, 2007; Schwartz *et al.*, 2016; Wilson, 2021).

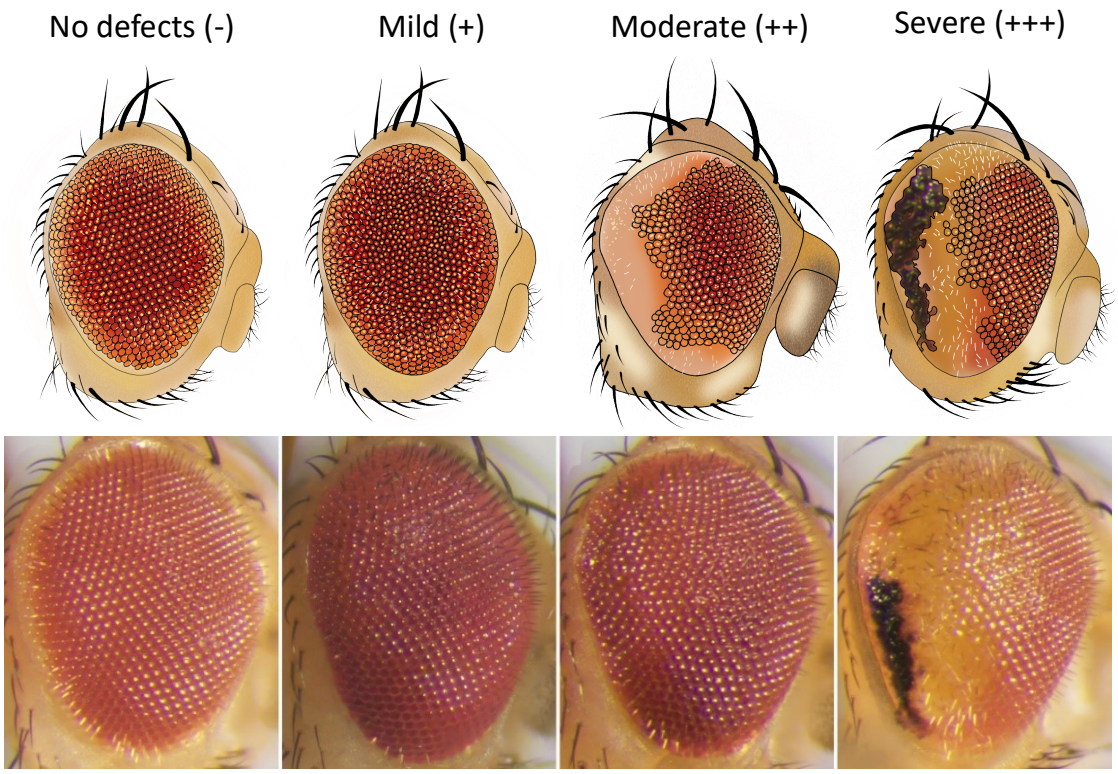

Figure 3.4. Examples demonstrating the different rough eye phenotype levels. Top: cartoon images depicting each level of phenotypic abnormalities. Bottom: Exemplar light microscopy images for each phenotypic level. No defects = normal eye. Mild = minimal ommatidia disorganisation. Moderate = ommatidial disorganisation, fusion and pigment loss. Severe = ommatidial disorganisation, fusion, pigment loss, and areas of necrosis.

3.3.2 Phenotypic evaluation of candidate contribution to eye development

A total of 20 eyes (10 female, 10 male) for each genotype were semi-quantitatively scored by a blinded observer and each eye was allocated an individual score. The results for those RNAi lines in which a rough eye phenotype was observed are displayed in Figure 3.5 and representative light microscopy images are shown in Figure 3.6.

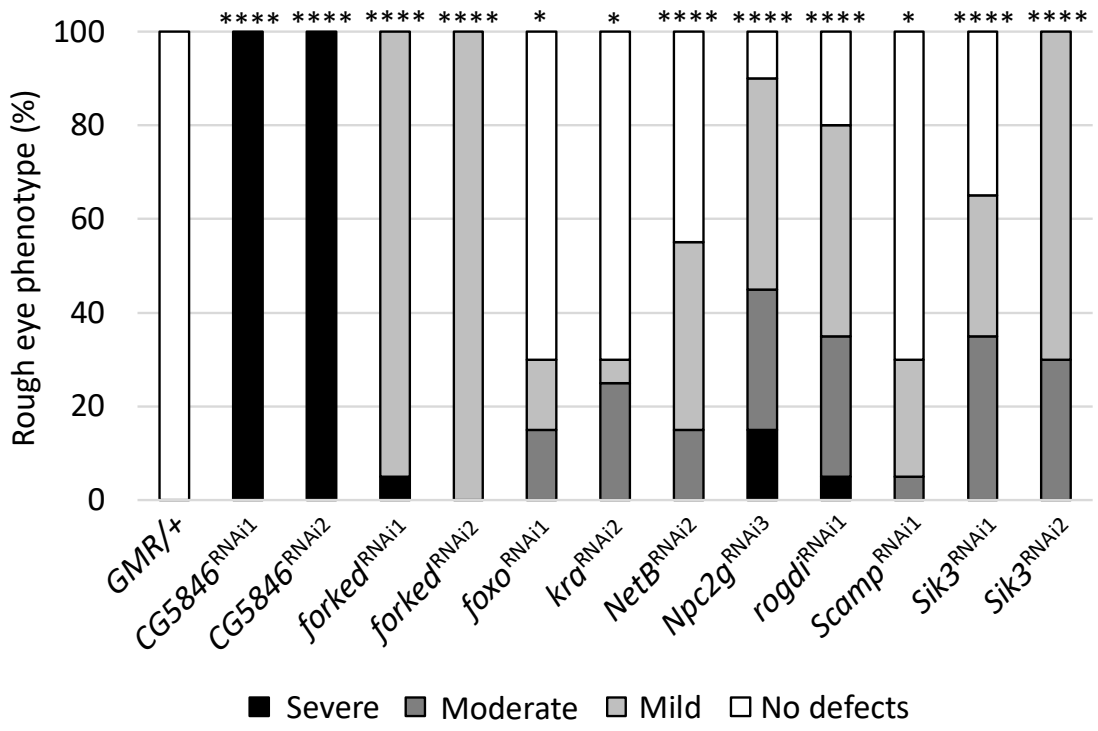

Figure 3.5. Penetrance of a rough eye phenotype with each RNAi line. Each bar represents the percentage of eyes displaying a rough eye phenotype at each level of severity, n=20, (one-tailed Fisher's exact statistical test of the total percentage of the rough eye phenotype compared to control, *GMR-GAL4*/+, * = p<0.05, **** = p<0.0001, *GMR-GAL4*/+ ; *CG5846*^{RNAi1} = <0.0001, *GMR-GAL4*/+ ; *CG5846*^{RNAi2} = <0.0001, *GMR-GAL4*/+ ; *forked*^{RNAi1} = <0.0001. *GMR-GAL4*/+ ; *forked*^{RNAi2} = <0.0001, *GMR-GAL4*/+ ; *foxo*^{RNAi1} = 0.0101, *GMR-GAL4*/+ ; *kra*^{RNAi2} = 0.0101, *GMR-GAL4*/+ ; *NetB*^{RNAi2} = <0.0001, *GMR-GAL4*/+ ; *Npc2g*^{RNAi3} = <0.0001, *GMR-GAL4*/+ ; *rogdi*^{RNAi1} = <0.0001, *GMR-GAL4*/+ ; *Scamp*^{RNAi1} = 0.0101, *GMR-GAL4*/+ ; *Sik3*^{RNAi1} = <0.0001, *GMR-GAL4*/+ ; *Sik3*^{RNAi2} = <0.0001). *GMR* = *GMR-GAL4*, *GMR/+* = Control.

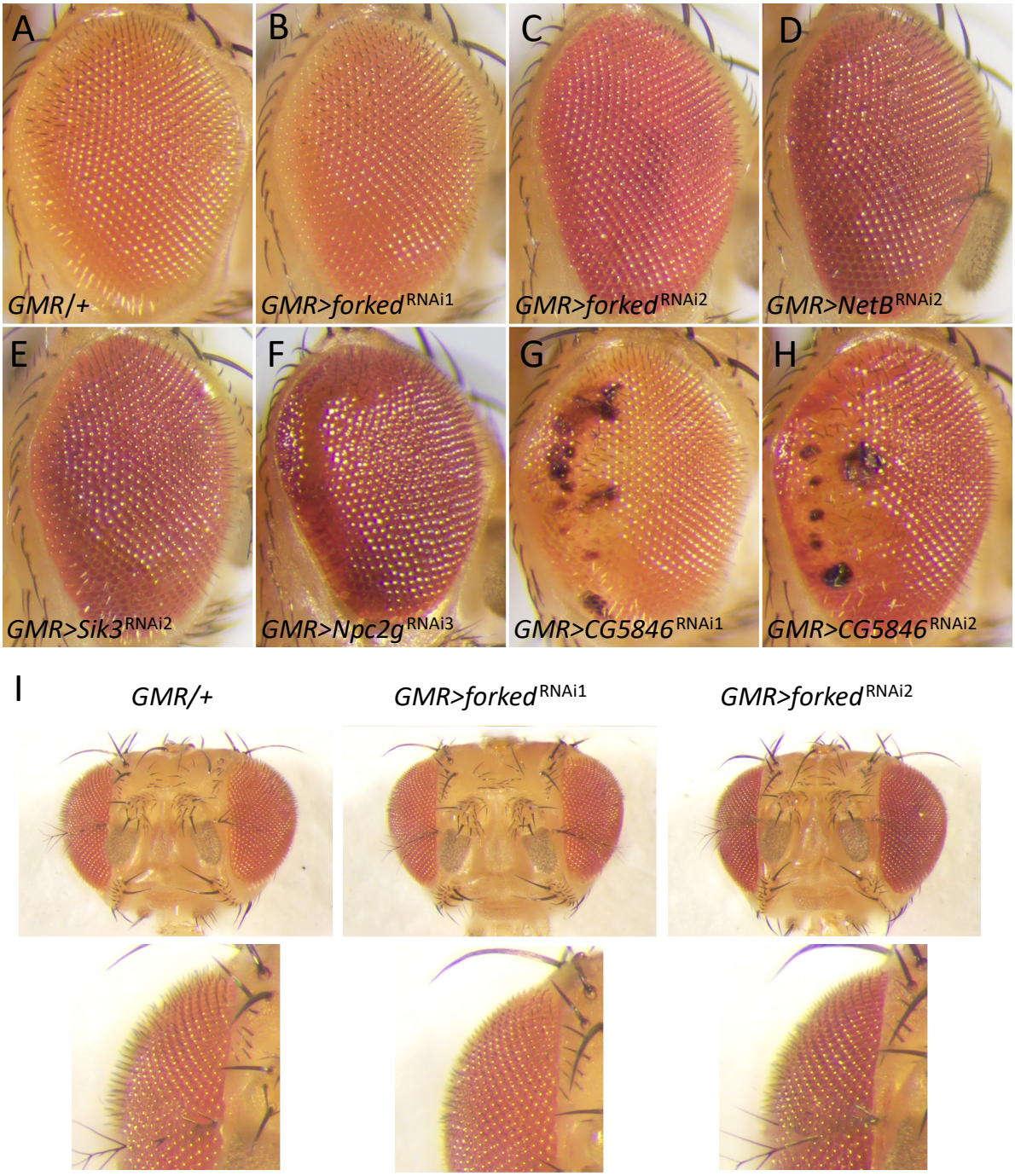

Figure 3.6. Representative images of some RNAi lines with phenotypic eye abnormalities. A. *GMR-GAL4*/+ (Control). B. *GMR-GAL4>forked*^{RNAi1} and C. *GMR-GAL4>forked*^{RNAi2} result in short, thick interommatidial bristles. D. *GMR-GAL4>NetB*^{RNAi2} and E. *GMR-GAL4>Sik3*^{RNAi2} result in ommatidial disorganisation. F. *GMR-GAL4>Npc2g*^{RNAi3} leads to ommatidial fusion, disorganisation, and loss of pigmentation. G. *GMR-GAL4>CG5846*^{RNAi1} and H. *GMR-GAL4>CG5846*^{RNAi2} result in ommatidia fusion, necrosis and, loss of pigmentation. I. Light microscopy images of *GMR-GAL4* driven *forked*^{RNAi1} and *forked*^{RNAi2} eyes compared to control showing differences in bristle phenotypes. *GMR-GAL4/+* have a normal interommatidial bristle pattern with long tapered bristles. *GMR-GAL4>forked*^{RNAi1} and *GMR-GAL4>forked*^{RNAi2} retain a normal bristle pattern with short thick stubble bristles. *GMR* = *GMR-GAL4*, *GMR/+* = Control.

Compared to the control (*GMR-GAL4/+*) (Figure 3.6A), knockdown of Forked resulted in bristle abnormalities in almost all eyes. The interommatidial mechanosensory bristles of the eye lack the growth and extension of a wild-type eye, resulting in short stubble-like bristles (Figure 3.6B, C). This phenotype was not unexpected, given that Forked has been shown to play a role in actin dynamics, specifically in bristle development and growth (Hoover *et al.*, 1993; Wulfkuhle *et al.*, 1998). To gain a better sense of how short and thick these stubble bristles were, light microscopy images were taken of the whole fly head from a dorsal position to show the difference in bristle length compared to control (Figure 3.6I). Expression of *NetB*^{RNAi2} resulted in deficits in 55% of eyes (Figure 3.5), which displayed a mild to moderate level of ommatidial disorganisation and a low level of ommatidial fusion (Figure 3.6D). *Sik3*^{RNAi1} and *Sik3*^{RNAi2} both resulted in abnormalities to eye development, with *Sik3*^{RNAi2} inducing a more severe phenotype in 100% of eyes (Figure 3.5), observed as mild to moderate ommatidial disorganisation (Figure 3.6E). Knockdown of *Npc2g*^{RNAi3} resulted in defects in 90% of eyes (Figure 3.5), with the most common phenotypic abnormality being ommatidial disorganisation. Furthermore, 15% of eyes displayed a severe level of ommatidial fusion paired with depigmentation, creating a glassy appearance (Figure 3.6F). Surprisingly, expression of both *Scamp*^{RNAi1} and *Scamp*^{RNAi2} significantly impaired mushroom body formation (Figure 3.3), however, only *Scamp*^{RNAi1} resulted in a mild rough eye phenotype (Figure 3.5) with *Scamp*^{RNAi2} resulting in an unperturbed eye. As only one of two RNAi's (*NetB*^{RNAi2}, *Npc2g*^{RNAi3}, and *Scamp*^{RNAi1}) or two of three RNAi's (*Sik*^{RNAi1} and *Sik*^{RNAi2}) resulted in a rough eye phenotype it is likely that these are a result of off-target effects. Although *mthl8*^{RNAi2} resulted in significant impairment in mushroom body development (Figure 3.3), eye development was normal. This suggests that there may be discordance between brain and eye development, where Mthl8 is required for normal formation of the mushroom body but not the eye, or the phenotype in the mushroom body induced by *mthl8*^{RNAi2} is due to an off-target effect.

The most striking phenotypes resulting from expression of the candidate genes were those induced by CG5846 knockdown. A severe rough eye phenotype was observed in 100% of eyes across both RNAi lines which were a result of ommatidial disorganisation, fusion, and loss of pigmentation, paired with the presence of dark necrotic lesions, some of which appear as a tumorigenic mass of dead cells peeling away from the eye (Figure 3.5, 3.6G, H). This severe eye phenotype demonstrates the discordance observed between the brain and the eye, upon tissue-specific RNAi-mediated knockdown, as mushroom body defects were minimal (Figure 3.3). This also shows that wild-type levels of CG5846 are required for maintenance of

ommatidial structure and cell survival. Upon closer observation, the areas displaying the severe phenotype were clustered at the posterior of the eye, which may suggest a positional and cell-type specific breakdown of development (Figure 3.6G, H). Curiously, from the vertical midline to the anterior edge, the eye, for the most part, remains wild-type in pigmentation, ommatidia organisation, and bristle patterning. Since CG5846 is yet to be characterised in *Drosophila*, these findings demonstrate the first indication of a role that CG5846 may play in eye development.

3.4 Characterising the expression patterns of candidate genes in the *Drosophila* brain

The expression pattern of endogenous HDAC4 has recently been characterised (Tan *et al.*, 2024; Wilson, 2021). As there is currently no antibody available for detection of DmHDAC4 *via* immunohistochemistry, an HDAC4::YFP trap line was utilised. This fly line contains an insertion of the yellow fluorescent protein (YFP) flanked by splice acceptor and donor sites into the second intron of the endogenous *HDAC4* gene, resulting in an internal fusion of YFP in the HDAC4 protein. Immunohistochemistry with an anti-GFP antibody demonstrated that HDAC4 is expressed throughout the brain, and appears highly concentrated in the antennal lobes, as well as the mushroom body, where it localises to cell bodies, the calyx (dendritic field), a subset of nuclei, and the bundled axons that form the α, β, and, γ lobes (Wilson, 2021). These data have since been validated by expression of HDAC4::EGFP, another protein trap line which consists of an insertion of enhanced GFP (EGFP) flanked by splice sites inserted into the second intron of the endogenous *HDAC4* gene (Tan *et al.*, 2024).

Both overexpression and knockdown of HDAC4 in the adult mushroom body results in impaired LTM formation (Fitzsimons *et al.*, 2013). If candidate genes are expressed in similar regions of the brain, this would provide preliminary support for a functional interaction with HDAC4, and if these proteins are expressed highly in the mushroom body, a potential role in memory formation, either independently or through an interaction with HDAC4.

3.4.1 The expression pattern of available GAL4 enhancer trap lines

GAL4 enhancer and GFP trap lines were available from stock centres for analysing the expression pattern of a select few candidate genes in the *Drosophila* brain. A GAL4 enhancer trap consists of an insertion of GAL4 within the enhancer of the gene, resulting in expression of GAL4 in the endogenous expression pattern of that gene (Brand & Perrimon, 1993). To visualise this expression pattern, the GAL4 trap line can be crossed to a reporter gene under UAS control, such as the *UAS-CD8*::*GFP* reporter. CD8::GFP localises to the plasma membrane and outlines the cell bodies and neuronal processes of the cells in which it is expressed (Figure 3.7) (Fitzsimons *et al.*, 2013; Lee *et al.*, 1999).

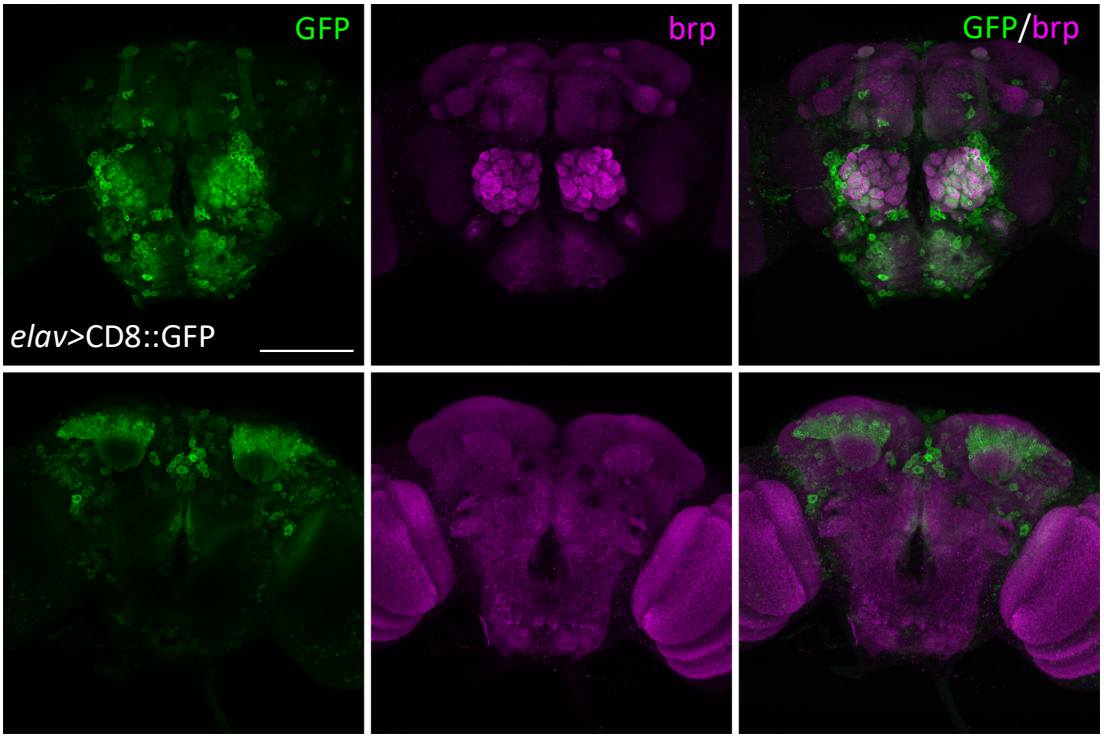

Figure 3.7. Pan-neuronal CD8::GFP expression pattern. CD8::GFP is a plasma membrane bound reporter and when expressed in the brain with the pan-neuronal *elav-GAL4* driver results in expression in all neurons in the brain. Anti-GFP (green) highlights CD8::GFP in the mushroom body lobes in the anterior of the brain (top panels). CD8::GFP localises to the Kenyon cell bodies clustered at the posterior of the brain surrounding the calyx (bottom panels). Anti-brp (magenta) was used as a counterstain to highlight the structure of the entire brain. Images were taken using the 40x objective lens in oil, 1 µm sections, scale bar = 100 µm. *elav* = *elav-GAL4*, CD8::GFP = *UAS-CD8::GFP*.

Of the 16 candidate genes, GAL4 enhancer trap lines were available for *Kank*, *kra,* and *mthl8*. Each of these lines were crossed to *UAS-CD8::GFP*, and the GFP signal was enhanced and visualised via immunohistochemistry with an anti-GFP antibody (Section 2.2.4).

3.4.1.1 *Kank-GAL4* drives expression in cells resembling descending neuron clusters

A wide albeit somewhat non-descript pattern of *Kank-GAL4* driven expression of CD8::GFP was observed in the adult *Drosophila* brain. In the anterior of the brain, *Kank-GAL4* drove expression in what appeared to be clusters of descending neurons (Figure 3.8A, top panel), including, the anterior optic tubercle (AOUT) cluster (Figure 3.8B, yellow), the anterior ventrolateral protocerebrum (AVLP) cluster (Figure 3.8B, orange), and the periesophageal (PENP) cluster (Figure 3.8B, blue) (Hsu & Bhandawat, 2016). There was a lack of CD8::GFP expression in the mushroom body, which could explain the minimal level of abnormal mushroom body phenotypes observed in the candidate mushroom body screen (Figure 3.3). In the posterior of the brain, CD8::GFP was also observed in cells in the lobular region between the midsection of the brain and the optic lobe and in cells resembling the gnathal ganglia (GNG) cluster of descending neurons (Figure 3.8C, pink) (Hsu & Bhandawat, 2016). Consistent with the lack of expression observed in the mushroom body lobes (the bundled axons of the Kenyon cells), no expression was observed in Kenyon cell bodies (Fig 3.8A, bottom panel).

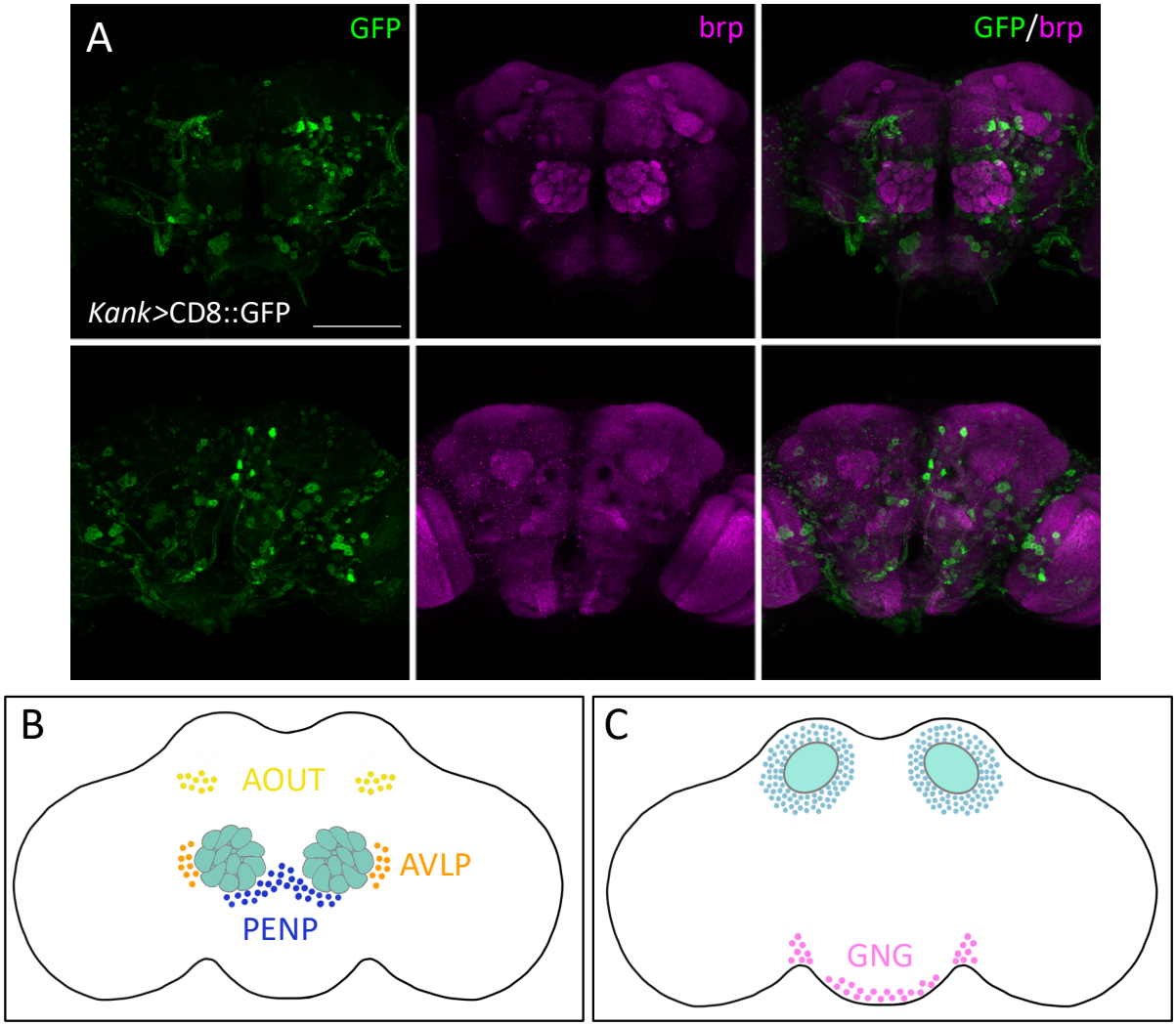

Figure 3.8 *Kank-GAL4* expression pattern in the adult brain using the CD8::GFP reporter. A. The endogenous distribution pattern of Kank was highlighted by expression of the CD8::GFP reporter using the *Kank-GAL4* driver and analysed using an anti-GFP antibody (green). In the anterior of the brain (top panels), CD8::GFP distribution resembled the distribution of clusters of descending neurons, *Kank-GAL4* also drove expression in a number of cells surrounding the antennal lobes. In the posterior of the brain (bottom panels) CD8::GFP was present in the lobular cells that lie between the midsection of the brain and the optic lobes. Anti-brp (magenta) was used as a counterstain to highlight the structure of the brain. Images were taken using the 40x objective lens in oil, 1 µm sections, scale bar = 100 µm. B. Schematic of the anterior of the brain demonstrating the distribution of descending neurons with a similar distribution pattern to Kank, AOUT (yellow), AVLP (orange), PENP (blue), and C. in the posterior of the brain, GNG (pink). *Kank* = *Kank-GAL4*, CD8::GFP = *UAS-CD8::GFP*.

3.4.1.2 *kra-GAL4* drives expression in cells resembling suboesophageal, descending and dopaminergic neuron clusters

In the anterior of the brain, *kra-GAL4* drove expression of CD8::GFP in the midline axons and a cluster of cells in the suboesophageal zone (SEZ) (Figure 3.9A, top panel), which is

responsible for feeding behaviour motor output based on gustatory sensory input (Figure 3.9B) (Kendroud *et al.*, 2018). In the posterior of the brain (Figure 3.9A, bottom panel), CD8::GFP was observed in posterior clusters of descending neurons (Hsu & Bhandawat, 2016), GNG (Figure 3.9C, pink), pars intercerebralis (PI) (Figure 3.9C, green), and the superior medial protocerebrum (SMP) cluster of neurons (Figure 3.9C, lavender). *kra-GAL4* driven CD8::GFP was also similarly distributed to clusters of dopaminergic neurons (Mao & Davis, 2009) which include those in the posterior superiomedial protocerebrum (PPM1) (Figure 3.9D, teal), posterior inferiomedial protocerebrum (PPM2) (Figure 3.9D, grey), posterior inferiolateral protocerebrum (PPL1) (Figure 3.9D, indigo), and the posterior lateral protocerebrum (PPL3) (Figure 3.9D, navy). Interestingly, Kra has previously been shown to be expressed in PPL1 neuronal cluster which are one of three dopaminergic clusters that innervate the mushroom body neuropil (Acebes *et al.*, 2011).

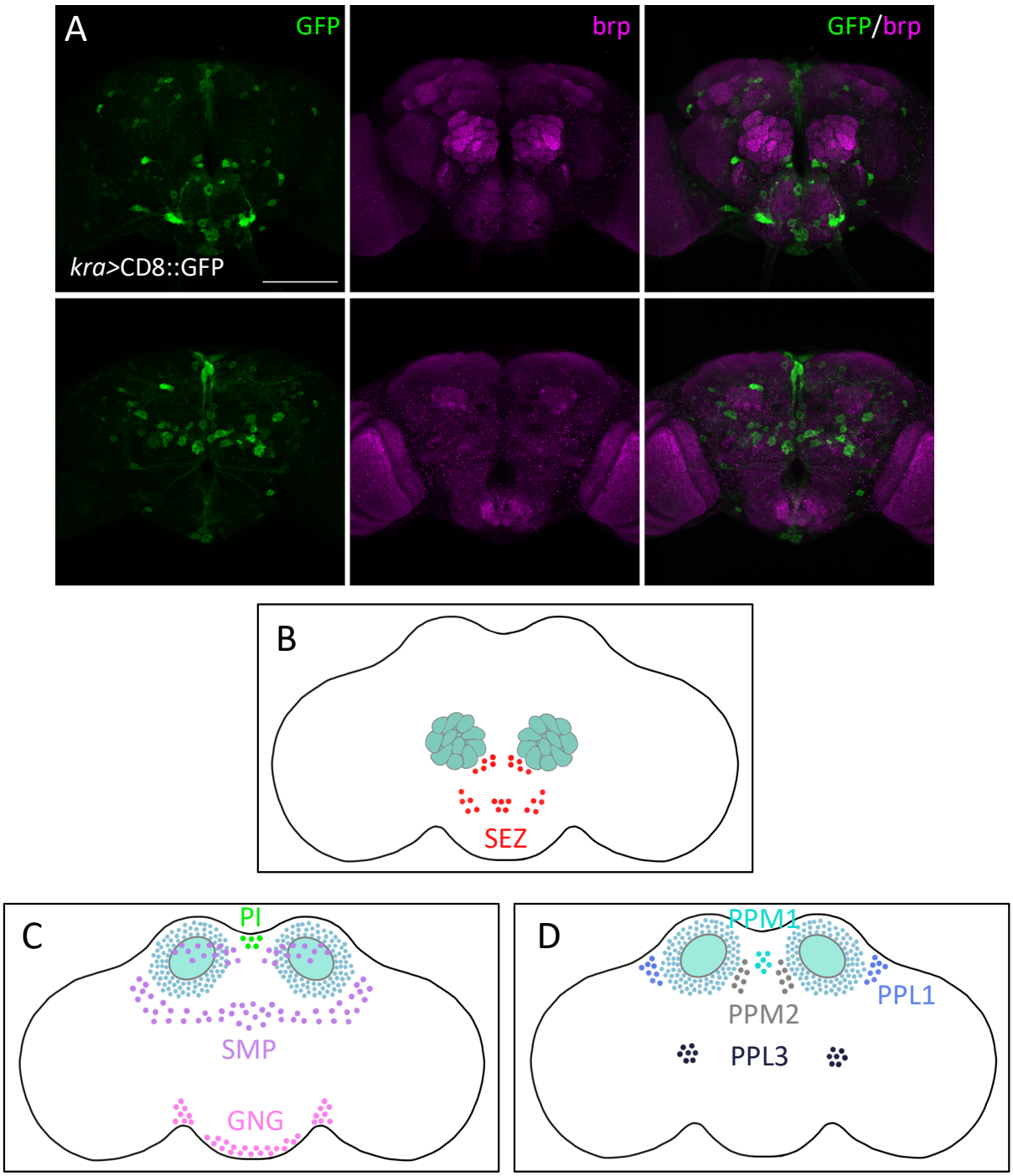

Figure 3.9 *kra-GAL4* expression pattern in the adult brain using the CD8::GFP reporter. A. The endogenous distribution pattern of Kra was highlighted by expression of the CD8::GFP reporter using the *kra-GAL4* driver and analysed using an anti-GFP antibody (green). In the anterior of the brain (top panels), CD8::GFP was localised to the midline axons and in cells within the subesophageal zone. In the posterior, cells expressing CD8::GFP resembled the distribution of clusters of descending and dopaminergic neurons. Anti-brp (magenta) was used as a counterstain to highlight the structure of the brain. Images were taken using the 40x objective lens in oil, 1 µm sections, scale bar = 100 µm. B. Schematic of the anterior of the brain demonstrating the SEZ (red). C. Schematic of the posterior of the brain demonstrating the distribution of descending neurons with a similar distribution pattern to Kra, GNG (pink), PI (green), SMP (lavender), and D. the distribution of dopaminergic neurons, PPM1 (teal), PPM2 (grey), PPL1 (indigo), PPL3 (navy). *kra* = *kra-GAL4*, CD8::GFP = *UAS-CD8::GFP*.

3.4.1.3 *mthl8-GAL4* driven expression is not detected in the adult brain

Mthl8 has been detailed to be highly expressed during larval development (Patel *et al.*, 2012) however little has been reported on adult brain expression. Previous RNA-seq data demonstrate that under basal conditions the levels of Mthl8 expression in the adult brain are undetectable (Wei Tan Jun, unpublished data). However, an *in situ* hybridisation assay showed low levels of Mthl8 in the brain, and upon expression of a range of well-established learning and memory mutants; Dunce, Rutabaga, and Amnesiac, expression was upregulated (Guan *et al.*, 2011). In the present study, the adult brain was analysed for the expression pattern of Mthl8, using an *mthl8-GAL4*, T2A-GAL4 driver line to drive expression of CD8::GFP in the Mthl8 endogenous distribution pattern. Interestingly, no specific staining was observed which could be consistent with the previous RNA-seq dataset (Wei Tan Jun, unpublished data) and *in situ* hybridisation analysis, which is more sensitive than immuunohistochemistry (Guan *et al.*, 2011), where under these conditions Mthl8 is expressed at an undetectable level in the adult brain (Figure 3.10).

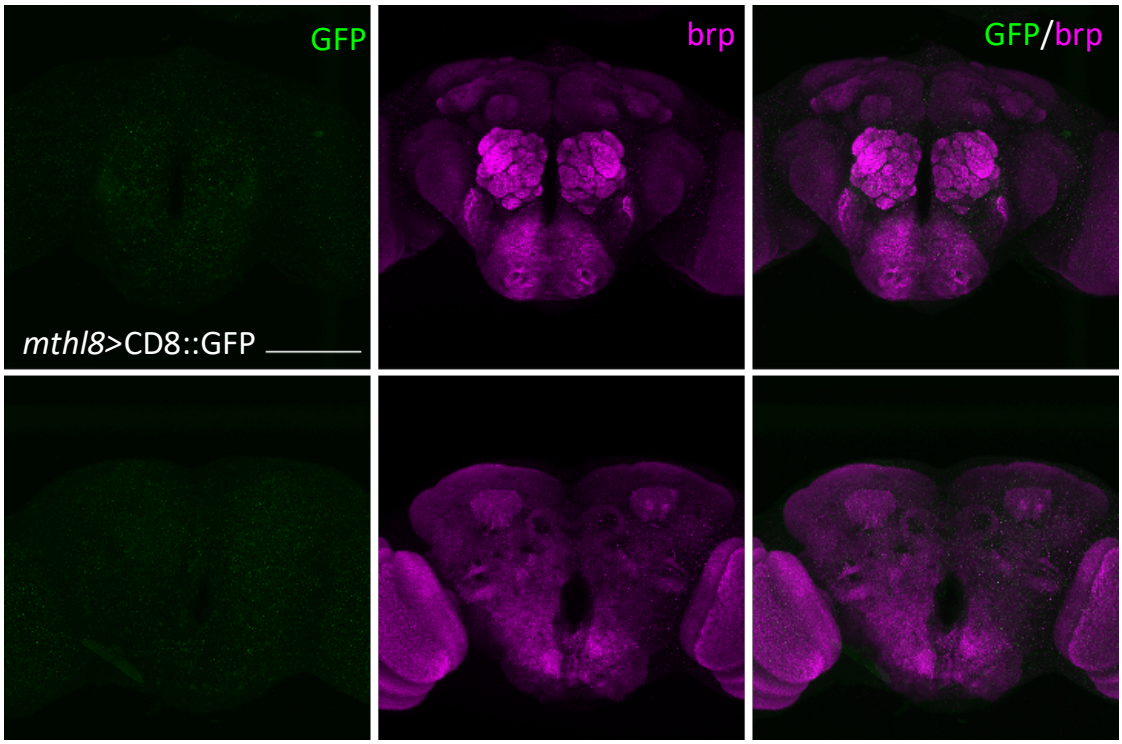

Figure 3.10. *mthl8-GAL4* expression pattern in the adult brain using the CD8::GFP reporter. Expression of the CD8::GFP reporter using *mthl8-GAL4* was not observed using an anti-GFP antibody (green). Expression was absent from both the anterior (top panel) and posterior of the brain (bottom panel). Anti-brp (magenta) was used as a counterstain to highlight the structure of the brain. Images were taken using the 40x objective lens in oil, 1 µm sections, scale bar = 100 µm. *mthl8* = *mthl8-GAL4*, CD8::GFP = *UAS-CD8::GFP*.

3.4.2 The expression pattern of available GFP trap lines

In addition to GAL4 traps, GFP trap lines were also available from stock centres for analysing endogenous expression. These GFP trap lines were generated similarly to the aforementioned HDAC4::YFP and HDAC4::EGFP lines (Section 3.4). Rather than GFP being expressed in the endogenous pattern of a gene by GAL4 trap, a GFP trap involves GFP tagging of the endogenous protein, which provides information not only about the expression pattern but also the subcellular distribution of the protein of interest. GFP was detected using an anti-GFP antibody to enhance protein visualisation. Of the 16 candidate genes GFP trap lines were available for Rogdi and Shn and the GFP signal was enhanced and visualised via immunohistochemistry with an anti-GFP antibody (Section 2.2.4).

3.4.2.1 Rogdi is expressed in the mushroom body

In the anterior of the brain, Rogdi was widely expressed throughout the brain, where it was predominantly localised to nuclei. In the mushroom body, low level Rogdi was detected in the lobes (Figure 3.11, top panel), similar to what has been previously observed (Dubnau *et al.*, 2003). Furthermore, a recent study demonstrated that wild-type Rogdi was evenly distributed between the cytoplasm and nucleus in both *Drosophila* S2 cells and in adult *Drosophila* neurons (Kim *et al.*, 2017), in the posterior of the brain, however, expression was very punctate and specific localisation was difficult to discern. Nuclear staining was not strongly detected in Kenyon cells, indicating that Rogdi is either present at a low level and/or that within the mushroom body, the subcellular distribution of Rogdi is different to other brain areas and is largely axonal (Figure 3.11, bottom panel).

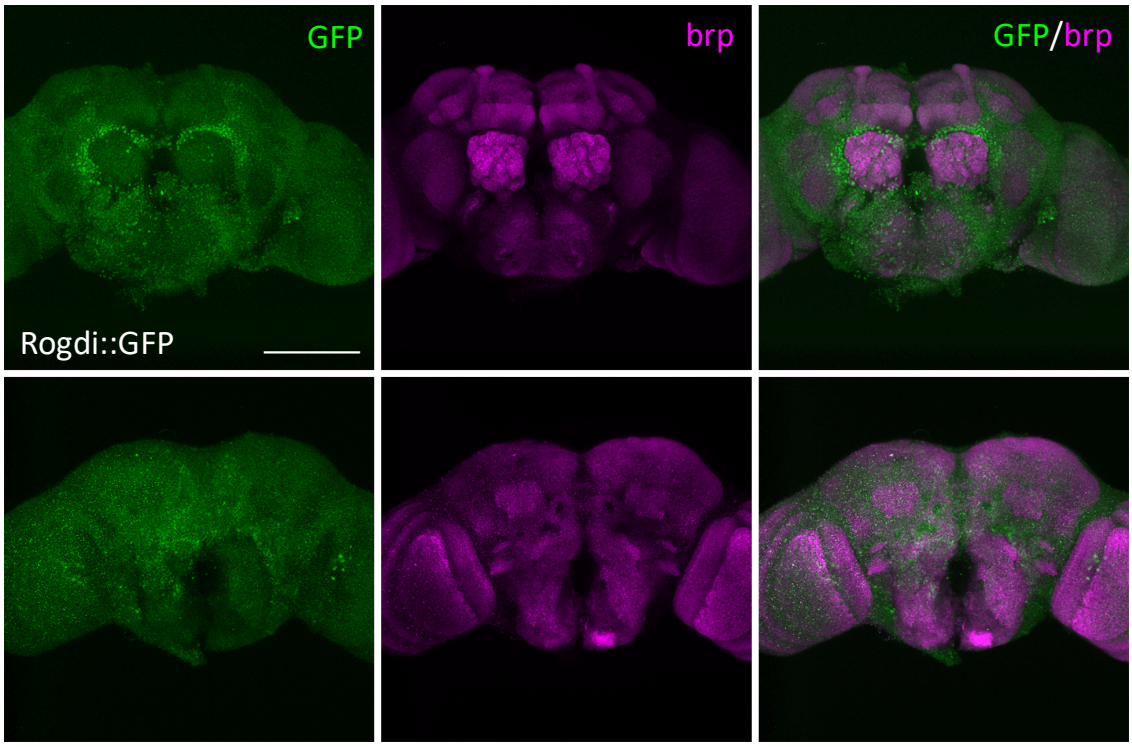

Figure 3.11. Rogdi::GFP expression pattern in the adult brain. Rodgi expression was analysed using an anti-GFP antibody (green). Anterior expression was mainly localised to cells surrounding the top of the antennal lobes with faint staining in the mushroom body lobes (top panel). Non-specific background staining was observed in the posterior (bottom panel). Anti-brp (magenta) was used as a counterstain to highlight the structure of the brain. Images were taken using the 40x objective lens in oil, 1 µm sections, scale bar = 100 µm.

3.4.2.2 Shn is not expressed in the adult brain

In both the anterior (Figure 3.12, top panel) and posterior (Figure 3.12, bottom panel) of the brain no specific Shn staining was observed. This was consistent with a previous study in which no expression was observed in the mushroom body (Dubnau *et al.*, 2003).

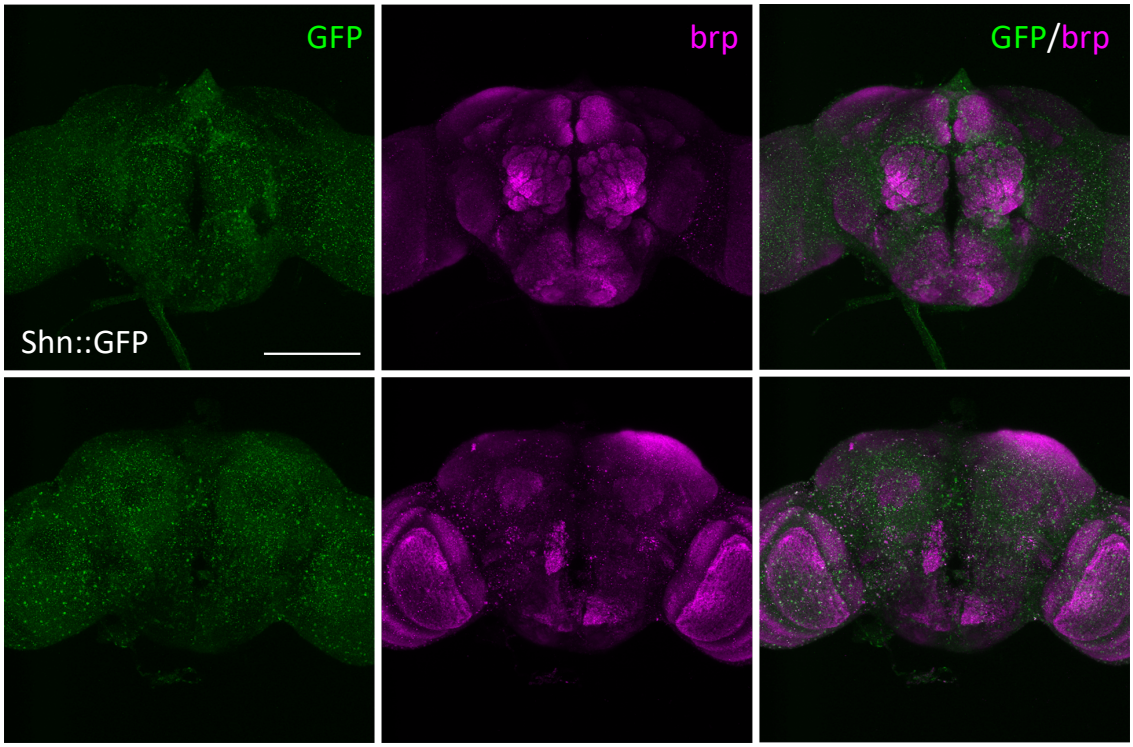

Figure 3.12. Shn::GFP expression pattern in the adult brain. Shn expression was analysed using an anti-GFP antibody (green), and no specific distribution was observed in either the anterior (top panel) or posterior (bottom panel) of the brain. Anti-brp (magenta) was used as a counterstain to highlight the structure of the brain. Images were taken using the 40x objective lens in oil, 1 µm sections, scale bar = 100 µm.

3.5 Rationale for the selection of CG5846 for further investigation

Several genes displayed similar phenotypes to those resulting from HDAC4 overexpression (Table 3.5). From this initial screen, CG5846 was selected for further analysis. Knockdown of CG5846 resulted in mild mushroom body defects and led to a severe rough eye phenotype, which was comprised of large areas of ommatidial fusion and depigmentation, reminiscent of the phenotype incurred by overexpression of two copies of HDAC4 (Tan *et al.*, 2024). The phenotypes observed in the eye upon HDAC4 overexpression are generic and common among many models of disease, therefore a definitive inference that HDAC4 and CG5846 act in similar molecular pathways cannot be deduced without further evidence, this screening approach did, however, provide justification to investigate a possible interaction between these two proteins. Furthermore, CG5846 knockdown in the eye lead to the appearance of necrotic lesions that varied in shape and size. These lesions were especially unique as they were clustered towards the posterior edge of the eye resulting in an unusual eye phenotype where the posterior region

was severely impaired and the anterior region consisted of a predominantly unperturbed array of ommatidia, making for an interesting phenotype to further delve into. As there was phenotypic consistency between the two independent *CG5846*^{RNAi} lines in both the mushroom body and eye, there was confidence that these phenotypes were not a result of off target effects.

Table 3.5 Summary of phenotypes observed for each candidate gene

Gene	Mushroom body (β lobe fusion%)	Compound eye %	Expression pattern (brain)
CG5846	11.1	100	ND
cer	-	-	ND
forked	5	100	ND
foxo	14.4	30*	ND
Kank	2.8	-	Expression resembles descending neuron clusters
Kdm5	10.5	-	ND
kek2	-	-	ND
kra	-	30*	Expression resembles suboesophageal, descending and dopaminergic neuron clusters
mthl8	57.2	-	No expression
NetB	71.4*	55*	ND
Npc2g	19.6	90*	ND
rogdi	15	80*	Mushroom body lobes and anterior cell nuclei
Scamp	70	30*	ND
shn	25	-	No expression
Sik3	15	100	ND
Thor	15	-	ND

The most severe phenotypic score has been displayed for simplicity.
* = A single RNAi line had a phenotype, the other/s had no defects.
ND = no data.

It was decided that focusing on one gene would allow for a more in-depth investigation of phenotypes to elucidate the molecular mechanisms that underlie its role in neural development and function. Given the severe unusual defects in the eye, CG5846 may play an important role in cell survival, therefore it was deemed to be of interest for further characterisation, and moreover, the nature of the interaction between CG5846 and HDAC4 warranted further investigation. As previously described in Section 1.7.2 the human CG5846 homologues, ANKRA2 and RFXANK, have been shown to physically interact with HsHDAC4 via the ankyrin repeats on ANKRA2 and RFXANK and the ankyrin repeat binding domain (PSLPNI

motif) on HDAC4 (McKinsey *et al.*, 2006; Wang *et al.*, 2005; Xu *et al.*, 2012). CG5846 also contains an ankyrin repeat region and therefore it was hypothesised that it too may physically interact with DmHDAC4 via the ankyrin repeat binding motif which is 100% conserved between human and *Drosophila* HDAC4 (Xu *et al.*, 2012).

Since CG5846 is currently uncharacterised and has no name, we chose to name it Peep, based on the posterior-localised necrotic phenotype in the eye upon knockdown. The remaining part of this chapter will take a peep at the interaction between HDAC4 and Peep. Chapter four describes the expression pattern of Peep and characterisation of Peep function via a range of phenotypic analyses. Chapter five describes an in-depth approach of how decreased levels of Peep affect eye development and an investigation of the molecular processes through which Peep operates.

3.6 Investigating the co-distribution of Peep and HDAC4 in Kenyon cells

Both vertebrate and *Drosophila* HDAC4 shuttle between the nucleus and cytoplasm, and dysregulation of this dynamic shuttling has been implicated in a number of neurological and neurodegenerative diseases (Herrup *et al.*, 2013; J. Li *et al.*, 2012; Shen *et al.*, 2016; Takahashi-Fujigasaki *et al.*, 2006; Takahashi-Fujigasaki & Fujigasaki, 2006).

Nuclear localisation and aggregation of HDAC4 have been observed in post-mortem hippocampal neurons of individuals diagnosed with Alzheimer's disease (Herrup *et al.*, 2013; Shen *et al.*, 2016). The components of these aggregates have not yet been characterised but are currently being assessed by another PhD candidate in this laboratory, as it is of importance to further understand dysregulation of HDAC4 in a disease context.

In mammalian COS cells, ectopic expression of HDAC4 resulted in a predominant nuclear distribution and the presence of nuclear aggregates. When ectopically expressed, ANKRA2 and RFXANK (the human homologues of Peep), were both localised to the nucleus, but on co-expression of HDAC4, both were re-distributed into nuclear aggregates of HDAC4 (McKinsey *et al.*, 2006). This interaction has been experimentally determined to be mediated by the ankyrin repeats on ANKRA2 and RFXANK that bind the PxLPxI motif on HDAC4. This motif is

conserved among species and also across other proteins that bind to ankyrin repeats (Nie *et al.*, 2015; Xu *et al.*, 2012). As the PSLPNI motif is 100% conserved between *Drosophila* and human HDAC4 (Xu *et al.*, 2012) it was of interest to determine whether the interaction between the ANKRA2 and RFXANK homologue Peep and HDAC4 was conserved in *Drosophila*, which was initially assessed by examining the co-distribution of Peep and HDAC4 in *Drosophila* Kenyon cells.

3.6.1 Generation and characterisation of the Peep overexpression construct

There are no Peep GFP trap lines nor antibodies available, therefore to initially examine the subcellular distribution of Peep in Kenyon cells and assess the interaction with HDAC4, an overexpression construct (GenBank accession Q9VL58) was synthesised with a 3x HA epitope-tag at the C-terminus (designed by Dr Helen Fitzsimons) and was henceforth denoted as Peep^{OE} (Section 2.1.2). This construct was subcloned into the fly transformation pUASTattB plasmid by GeneScript (New Jersey, USA) to generate the *UAS-peep*^{OE} construct. A plasmid DNA midi-prep was performed (Section 2.1.2.2) and the resulting plasmid DNA was sent to GenetiVision (Houston, TX, USA) where transgenic flies were generated (Venken *et al.*, 2006) (Section 2.1.2.3).

To verify expression of Peep^{OE}, *UAS-peep*^{OE} male flies were crossed to *elav-GAL4* virgin female flies to drive expression of Peep in all neurons. A western blot on whole cell lysates of heads with an antibody against the HA epitope tag (Section 2.3.8) confirmed expression of Peep at the expected size of approximately 38 kDa (Figure 3.13A). Additionally, immunohistochemistry on *elav-GAL4* driven *UAS-peep*^{OE} whole mount brains was carried out to determine the subcellular distribution of Peep (Section 2.2.4). Brains were counterstained with either anti-brp, to highlight the synaptic neuropil (Figure 3.13B), or anti-FasII to highlight the mushroom body lobes (Figure 3.13C). Peep was observed to localise predominantly to nuclei, with low level distribution in axons, as observed in the mushroom body lobes (Figure 3.13B, C). Given that this distribution is a result of overexpression, it is possible that the small amount of axonal Peep could be an artefact, and may be due to overspill from the nucleus. The predominant nuclear localisation of Peep does however correlate with the nuclear localisation of homologues ANKRA2 and RFXANK (McKinsey *et al.*, 2006).

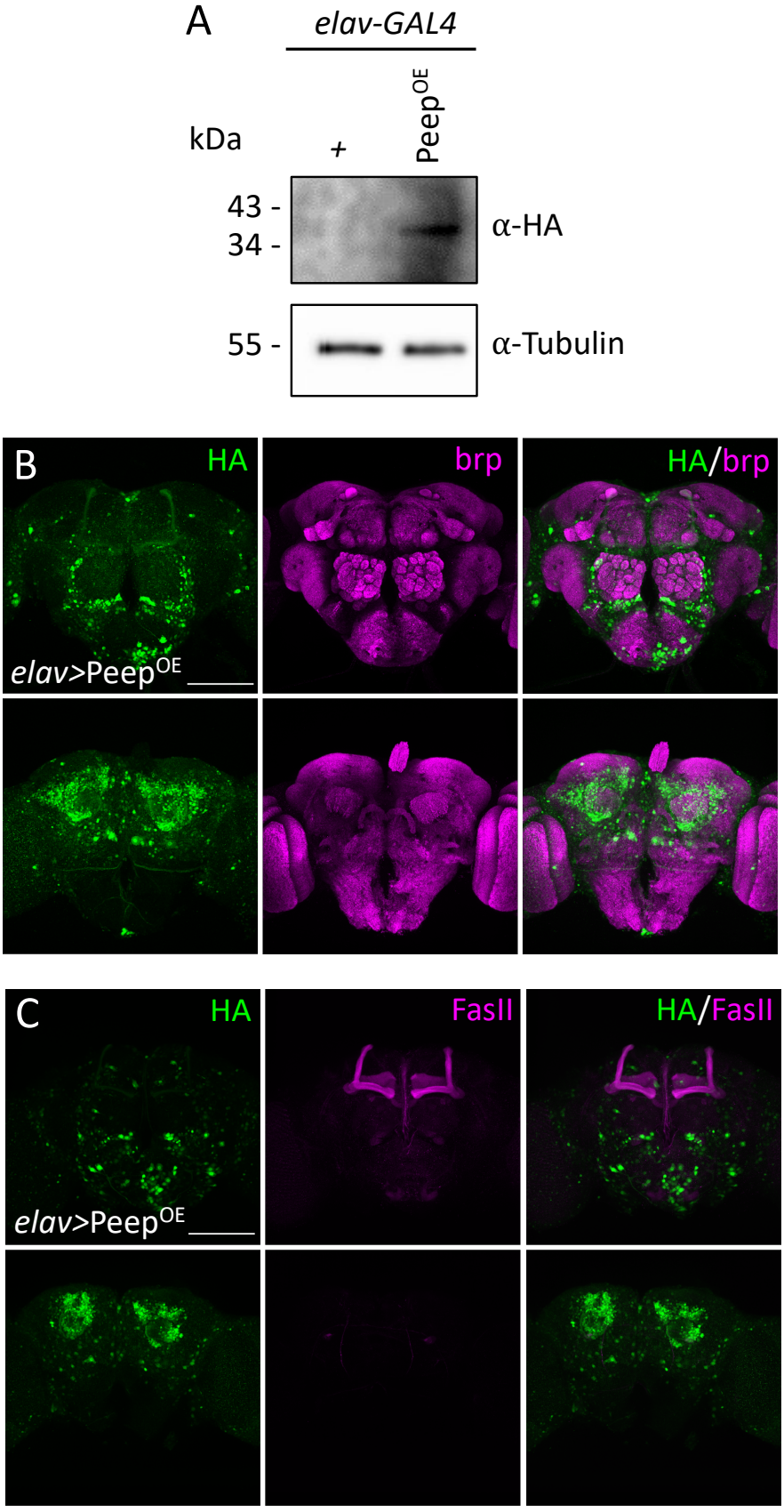

Figure 3.13. Verification of Peep^{OE} expression in the brain. A. Western blot confirming expression of the HA-tagged Peep^{OE} construct at approximately 38 kDa following pan-neuronal expression, 30 µg protein loaded, anti-Tubulin was used as a loading control. B. Pan-neuronal expression of HA-tagged

Peep^{OE} (green) showed localisation to the mushroom body axons and the nuclei of anterior neuronal subpopulations (top panel). In the posterior of the brain, Peep was observed in the nuclei of Kenyon cell neurons (bottom panel). Anti-brp (magenta) was used as a counterstain to highlight the structure of the brain. C. Localisation of Peep was to the mushroom body axons (green) which was confirmed by counterstaining with anti-FasII (magenta). Images taken using 40x objective lens in oil, 1 µm sections, scale bar = 100 µm. *elav* = *elav-GAL4*.

3.6.2 Generation of fly lines for analysis of the Peep-HDAC4 interaction

In order to examine the interaction between HDAC4 and Peep, *UAS-peep*^{OE} and an overexpression construct *UAS-HDAC4*-Myc (Main *et al.*, 2021; Tan *et al.*, 2024) henceforth denoted as HDAC4^{WT}, were combined into a single transgenic fly line. For experiments to demonstrate the nature of the interaction between the Peep ankyrin repeats and the ankyrin repeat binding motif (PSLPNI) on HDAC4, an overexpression Myc-tagged HDAC4 transgene with four alanine point mutations within the PSLPNI motif, HDAC4$^{\Delta Ank}$, was employed. These residues have been shown to be required for binding of both ANKRA2 and RFXANK to HsHDAC4 and are conserved in *Drosophila* (Xu *et al.*, 2012) (Figure 3.14).

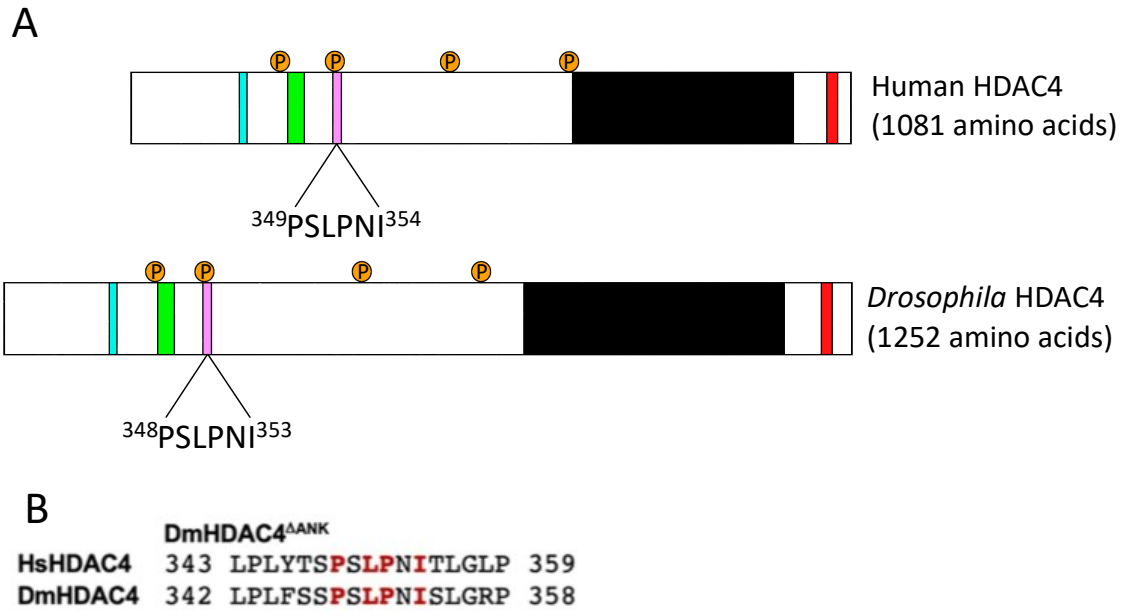

Figure 3.14. Generation of the HDAC4$^{\Delta Ank}$ transgenic fly line. A. Human (top) and *Drosophila* (bottom) HDAC4 construct. Highlighted in pink is the conserved ankyrin repeat binding domain (PSLPNI). Original artwork created with reference to Fitzsimons et al. (2013); Wilson (2021). B. Alignment of the amino acid sequence of the ankyrin repeat binding domain in human (top) and *Drosophila* (bottom) HDAC4 which is 100% conserved. The amino acids highlighted red were mutated to alanine to generate the HDAC4$^{\Delta Ank}$ mutant. *Image adapted from Tan et al. (2024) under Creative Commons Attribution 4.0 license http://creativecommons.org/licenses/by/4.0/.*

The HDAC4 transgene located on the third chromosome and the Peep transgene located on the second chromosome were recombined into a single fly line homozygous for both transgenes via standard genetic crosses depicted in Figure 8.7, Appendix 8.6. These lines could then be crossed to any GAL4 driver line of choice for UAS/GAL4 driven overexpression of Peep and/or HDAC4.

3.6.3 HDAC4 alters Peep nuclear distribution and sequesters it into nuclear aggregates

Peep was expressed with the mushroom body specific *OK107-GAL4* driver, which promotes strong expression (Hawley *et al.*, 2023). This driver was chosen as the Kenyon cell nuclei are clustered and easily visualised at the posterior of the brain. In addition, the expression pattern and subcellular distribution of $HDAC4^{WT}$ in these cells has been well characterised (Fitzsimons *et al.*, 2013; Main *et al.*, 2021; Tan *et al.*, 2024). As constitutive *OK107-GAL4* driven $HDAC4^{WT}$ overexpression induces a high level of nuclear punctate foci in a dose-dependent manner (Tan *et al.*, 2024), these flies were raised at 23°C to lower the level of HDAC4 overexpression-induced nuclear aggregate formation. Peep was observed in Kenyon cell nuclei with a relatively uniform distribution with a particular concentration around the periphery of the nucleus (Figure 3.15A). $HDAC4^{WT}$ was localised to both the nucleus and cytoplasm of neurons where cytoplasmic halos were observed and a large proportion of HDAC4 aggregated into punctate foci within nuclei (Figure 3.15B), as previously observed (Tan *et al.*, 2024). $HDAC4^{\Delta Ank}$ appeared slightly more nuclear (Figure 3.15D, panel 2) than $HDAC4^{WT}$ (Figure 3.15B, panel 2) as the aggregates were larger, the background nuclear staining was diminished and the cytoplasmic haloes were no longer visible as previously characterised (Tan *et al.*, 2024). This study confirmed that the ankyrin repeat motif of HDAC4 played a role in regulating subcellular distribution (Xu *et al.*, 2012). As described in Sections 1.5 and 1.6, several serine residues are critical to regulating the subcellular distribution of HDAC4 and are conserved in *Drosophila*. Phosphorylation of serine residues, Ser^{239}, Ser^{573}, and Ser^{748} in *Drosophila* (Ser^{246}, Ser^{467}, Ser^{632} in human) creates a docking site for 14-3-3, which exports HDAC4 from the nucleus (Bertos *et al.*, 2001; Chawla *et al.*, 2003; Grozinger & Schreiber, 2000; McKinsey *et al.*, 2001; Wang *et al.*, 2014). The PSLPNI motif contains a serine residue that is also phosphorylated and while it is not one of the three serine residues that are commonly mutated

to generate a nuclear-restricted mutant of HDAC4 (Bertos *et al.*, 2001; Chawla *et al.*, 2003; Grozinger & Schreiber, 2000; McKinsey *et al.*, 2001; Wang *et al.*, 2014), this serine has recently been shown to also recruit 14-3-3, where phosphorylation of this serine showed a binding partner switch from ANKRA2 to 14-3-3 (Xu *et al.*, 2012). Although the serine residue itself remained intact in the HDAC4$^{\Delta Ank}$ mutant (ASAANA), it cannot efficiently bind 14-3-3 as the surrounding residues (that are mutated in HDAC4$^{\Delta Ank}$) that normally provide the network of hydrogen bonds required for 14-3-3 docking are no longer present. This leads to reduced nuclear export thus resulting in a more nuclear distribution compared to HDAC4^{WT}.

When HDAC4^{WT} and Peep^{OE} were co-expressed, co-distribution of both proteins was observed whereby Peep was sequestered into a subset of HDAC4-containing nuclear aggregates. The number of HDAC4 aggregates that co-distributed with Peep were quantified, as was the number of aggregates that were devoid of Peep staining (Section 2.2.6). From this it was determined that Peep was sequestered into approximately 26% (Figure 3.15F) of these HDAC4 nuclear aggregates (Figure 3.15C), which is similar to what has previously been observed in COS cells co-expressing mammalian HDAC4 and ANKRA2 or RFXANK (McKinsey *et al.*, 2006). Upon co-expression of Peep, the total number of HDAC4-containing aggregates was not altered, but many of the aggregates were qualitatively assessed to be larger. These data suggest that under these specific conditions, Peep and HDAC4^{WT} may interact. To determine whether this interaction was mediated by the PSLPNI motif on HDAC4, HDAC4$^{\Delta Ank}$ was co-expressed with Peep^{OE} and surprisingly the co-distribution was maintained (Figure 3.15E) with approximately 35% of HDAC4 aggregates containing Peep (Figure 3.15F). This demonstrated that although there may be an interaction between HDAC4 and Peep, it appears to not be primarily mediated via the PSLPNI motif. This suggests that either other regions of HDAC4 bind Peep, there are unknown binding partners mediating this interaction, or this level of co-distribution is due to non-specific sequestration. HDAC4 was also co-expressed with *peep*^{RNAi} to determine whether loss of Peep had any impact on HDAC4 distribution. No change in the number of HDAC4 aggregates was observed on co-expression of either *peep*^{RNAi1} or *peep*^{RNAi2} (Figure 3.15G, H).

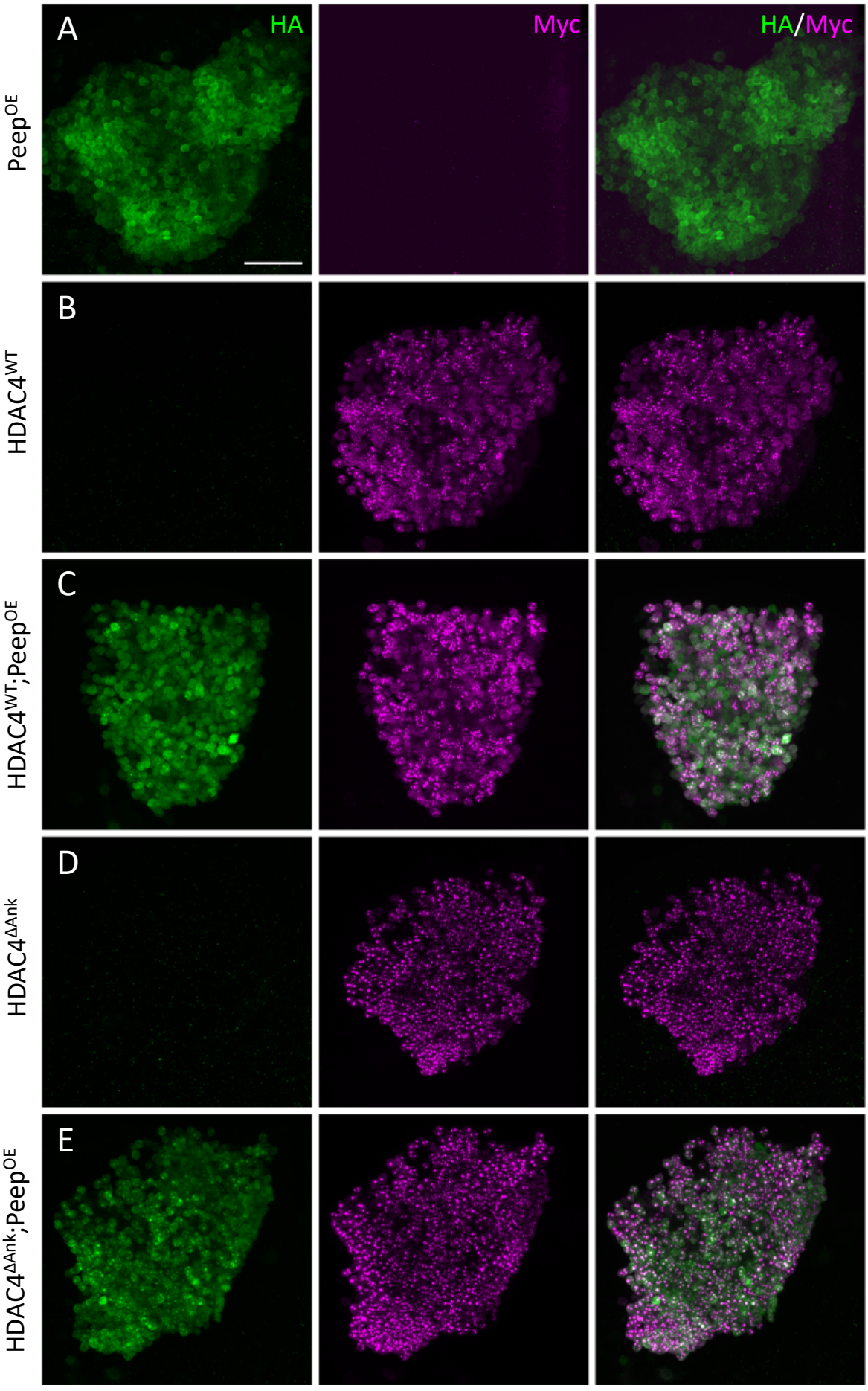
A
HA
Myc
HA/Myc
Peep^OE
B
HDAC4^WT
C
HDAC4^WT;Peep^OE
D
HDAC4^ΔAnk
E
HDAC4^ΔAnk;Peep^OE

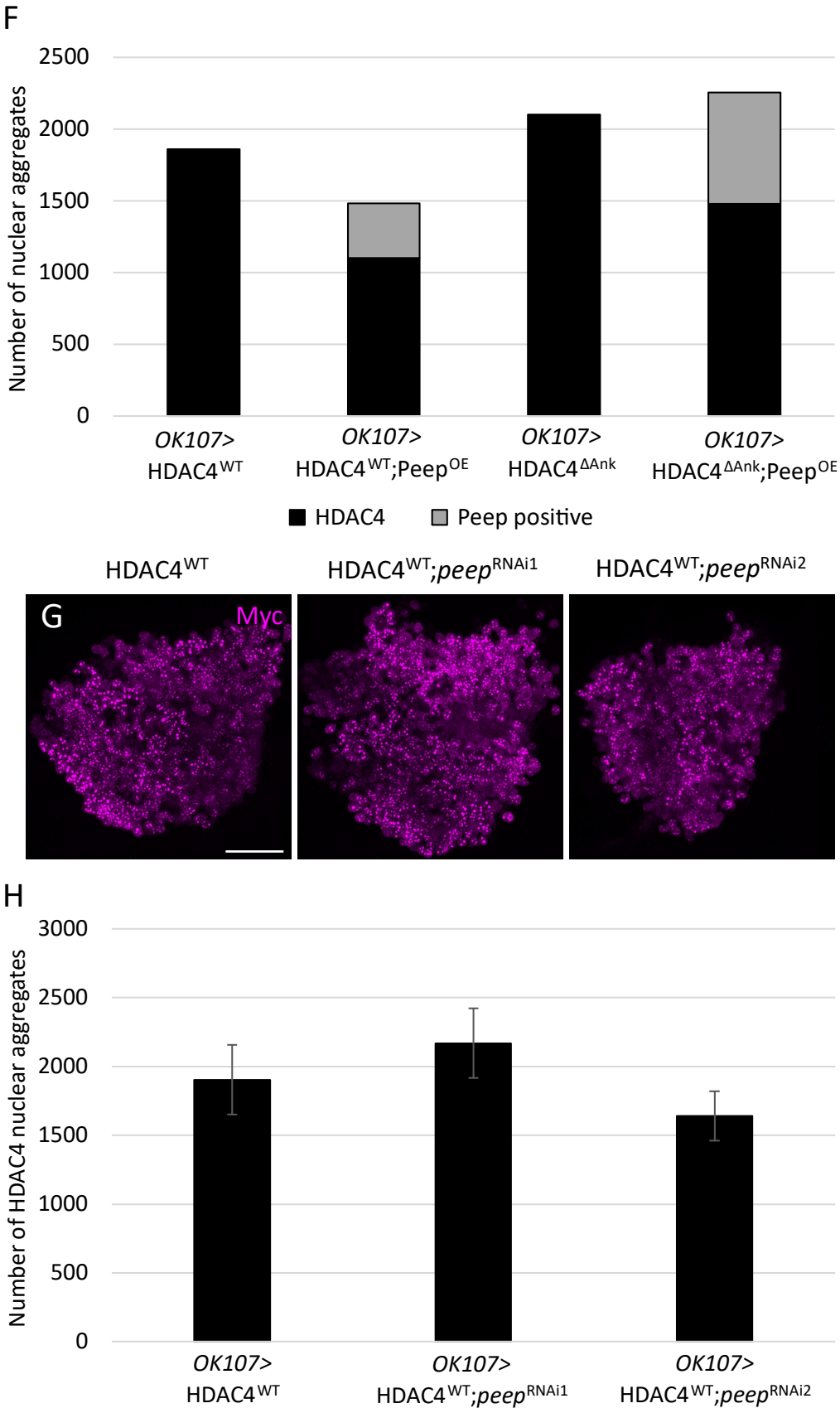

Figure 3.15. Peep co-distributes with HDAC4 nuclear aggregates in Kenyon cells. A. *OK107-GAL4* driven expression of Peep^{OE} showed a nuclear distribution using an anti-HA antibody (green) with a

particular distribution around the nuclear periphery. B. *OK107-GAL4* driven expression of $HDAC4^{WT}$ showed a predominant nuclear distribution with large nuclear protein aggregates and mild cytoplasmic halos using an anti-Myc antibody (magenta). C. *OK107-GAL4* driven co-expression of $Peep^{OE}$ and $HDAC4^{WT}$ demonstrated redistribution of Peep into HDAC4 nuclear aggregates (third panel, white speckles). D. *OK107-GAL4* driven expression of $HDAC4^{\Delta Ank}$ showed a nuclear aggregate distribution with a lack of cytoplasmic haloes using an anti-Myc antibody (magenta). E. *OK107-GAL4* driven co-expression of $Peep^{OE}$ and $HDAC4^{\Delta Ank}$ demonstrated redistribution of Peep into HDAC4 nuclear aggregates (third panel, white dots). Images taken using 40x objective lens in oil, Zoom 4x, 0.5 µm sections, scale bar = 20 µm. F. The total number of nuclear aggregates were quantified. Co-expression of $Peep^{OE}$ and $HDAC4^{WT}$ resulted in Peep co-distribution with HDAC4 in ~26% of nuclear aggregates, which was increased to ~35% on co-expression with $HDAC4^{\Delta Ank}$, n=4, (one-way ANOVA, post-hoc Tukey HSD, $f_{(3,15)} = 9.03$, no significant difference between treatments). G. *OK107-GAL4* driven expression of $HDAC4^{WT}$ with and without $peep^{RNAi}$ shows no difference in the number of HDAC4 nuclear aggregates. H. Quantitative analysis of the number of HDAC4 nuclear aggregates shows no difference upon Peep knockdown. Error bars indicate mean ± SEM, n=4, (one-way ANOVA, post-hoc Tukey HSD, $f_{(2,11)} = 0.984$, no significant difference between treatments). *OK107 = OK107-GAL4*.

Based on co-distribution in Kenyon cell aggregates, it was concluded that there may be an interaction between Peep and HDAC4, however this interaction was not reliant on an intact PSLPNI motif. Qualitative assessment demonstrated that aggregates containing Peep were larger, indicating that Peep may play a role in stabilising HDAC4 aggregate formation or sequestering additional factors, both of which would result in larger aggregates.

3.7 Co-immunoprecipitation of Peep and HDAC4

As Peep co-distributed with approximately 25% of HDAC4 nuclear aggregates, the interaction was further examined via co-immunoprecipitation. The co-immunoprecipitation protocol was optimised by another PhD candidate in this laboratory (Hannah Hawley, unpublished data) to determine the ideal conditions to maintain interactions and produce the highest capture efficiency.

3.7.1 Co-immunoprecipitation of GFP- and Myc-labelled HDAC4 provides a positive control

A positive control co-immunoprecipitation assay was initially performed to ensure the protocol was working successfully. Initial studies characterised that HsHDAC4 can self-interact and form tetramers and higher order complexes through a glutamine rich alpha helix N-terminal

domain (Guo *et al.*, 2007). A more recent study has shown that HDAC4 forms an antiparallel dimer through the glutamine rich region and binds two MEF2A dimers at the N-terminal MEF2 binding domain to mediate transcriptional repression (Dai *et al.*, 2024), (further described in Section 1.7.1.2). In order to provide a positive control co-immunoprecipitation result, two differently labelled constructs of wild-type DmHDAC4 were used, one with a C-terminal 6x Myc tag ($HDAC4^{WT}$) and one with an N-terminal fusion of GFP ($GFP\text{-}HDAC4^{WT}$) (Main *et al.*, 2021), which should form dimers and/or tetramers containing both of the labelled HDAC4 proteins. $GFP\text{-}HDAC4^{WT}$ and $HDAC4^{WT}$ were pan-neuronally co-expressed with *elav-GAL4* and whole heads were processed for immunoprecipitation (Section 2.3.9) using an anti-Myc antibody to capture $HDAC4^{WT}$ and all proteins that interact with it. The co-immunoprecipitation of $GFP\text{-}HDAC4^{WT}$ was detected using an anti-GFP antibody which showed a clear interaction between the two HDAC4 proteins, with the immunoprecipitation of $HDAC4^{WT}$ confirmed with anti-Myc (Figure 3.16). Each HDAC4 construct differed slightly in size as GFP adds 27 kDa to the 134 kDa HDAC4 protein whereas the 6x Myc tag adds 10 kDa.

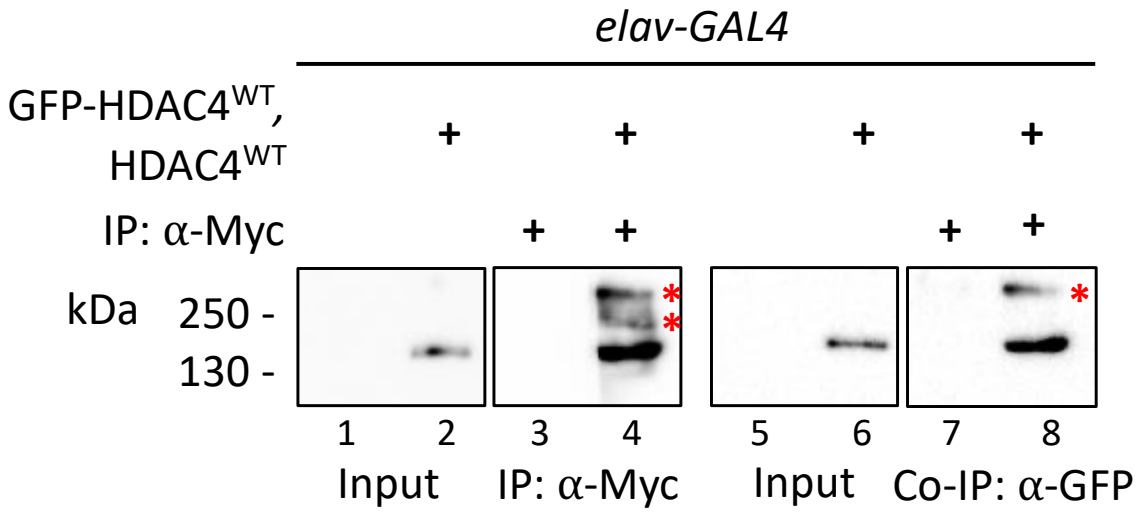

Figure 3.16. Co-immunoprecipitation of GFP- and Myc-labelled $HDAC4^{WT}$. C-terminal Myc-tagged HDAC4 and N-terminal GFP-fused HDAC4 were co-expressed pan-neuronally with *elav-GAL4*. Immunoprecipitation using an anti-Myc antibody captured the Myc-tagged HDAC4 as observed when probing with anti-Myc (lane 4). Co-immunoprecipitation using anti-GFP identified $GFP\text{-}HDAC4^{WT}$ which directly interacted with $HDAC4^{WT}$-Myc (lane 8). Immunoprecipitation samples were loaded alongside appropriate controls and 30 µg input samples. Lanes 1, 3, 5, and 7 were negative control lanes (*elav-GAL4/+*). Non-specific bands were observed in both immunoprecipitation samples (Asterix). IP = immunoprecipitation, Co-IP = co-immunoprecipitation.

3.7.2 A direct interaction was not detected between Peep and HDAC4

Following confirmation and validation of the co-immunoprecipitation protocol, $Peep^{OE}$ and $HDAC4^{WT}$ were pan-neuronally co-expressed and whole heads were processed for immunoprecipitation. If there was an interaction between Peep and HDAC4, similar to that observed between ANKRA2 or RFXANK and HDAC4, it would most likely be mediated through the PSLPNI motif on HDAC4 (McKinsey *et al.*, 2006; Wang *et al.*, 2005; Xu *et al.*, 2012). Although prior results in Kenyon cells (Section 3.6.3) suggest that any interaction between Peep and HDAC4 is not mediated through this domain, it is important to investigate via co-immunoprecipitation whether an interaction is abolished if the PSLPNI motif is mutated. Therefore, $Peep^{OE}$ was also co-expressed pan-neuronally with $HDAC4^{\Delta Ank}$, and whole heads were processed for immunoprecipitation (Section 2.3.9). An anti-Myc antibody was used to capture the Myc-tagged HDAC4 variants and all other bound proteins which were eluted off the beads and separated by SDS-PAGE (Section 2.3.8). The anti-Myc antibody was then used to ensure successful immunoprecipitation, with an anti-HA antibody used to detect the co-immunoprecipitation with HA-tagged Peep. No detectable interaction was observed between Peep and $HDAC4^{WT}$ (lane 7) or $HDAC4^{\Delta Ank}$ (lane 8) (Figure 3.17). The reverse co-immunoprecipitation was also performed and confirmed that under these conditions, no direct interaction via co-immunoprecipitation was detected between Peep and HDAC4 (Figure 8.10, Appendix 8.7). Inputs from each sample containing either Peep, $HDAC4^{WT}$, or $HDAC4^{\Delta Ank}$ independently or the co-expression of Peep with $HDAC4^{WT}$ or $HDAC4^{\Delta Ank}$ were run alongside the immunoprecipitation samples. Anti-Myc detected HDAC4 in all lanes containing HDAC4 (lanes 2-5), with no detection in the lane containing Peep alone. Anti-HA detected Peep in all lanes containing Peep (lanes 1, 4 and 5), with no detection in the lanes containing the HDAC4 variants alone (Figure 3.17).

Although Peep and $HDAC4^{WT}$ co-distributed in 26% of Kenyon cell nuclei using *OK107-GAL4* to drive expression in mushroom body neurons, a direct interaction via co-immunoprecipitation of co-expressed Peep and $HDAC4^{WT}$ or $HDAC4^{\Delta Ank}$ using the *elav-GAL4* pan-neuronal driver was not detected.

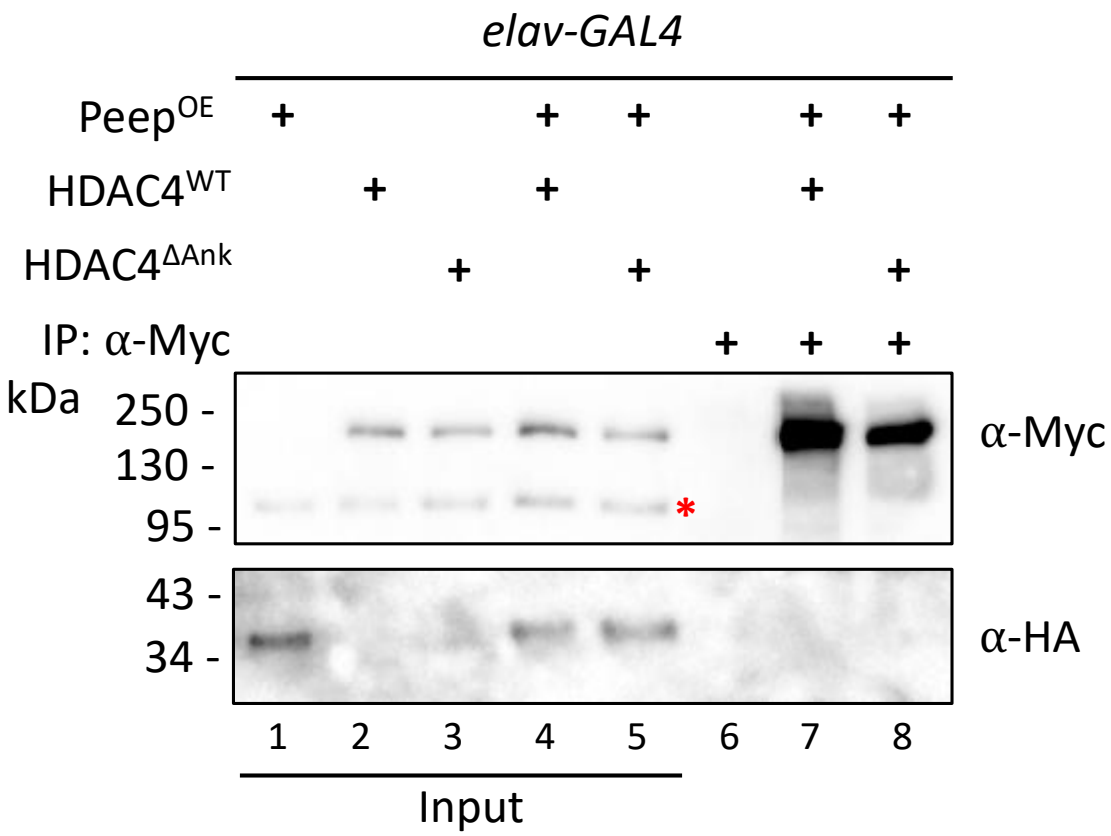

Figure 3.17. Peep and HDAC4 do not interact via co-immunoprecipitation. Lysates were processed from pan-neuronal (*elav-GAL4*) co-expression of Peep^{OE} and HDAC4^{WT} or HDAC4$^{\Delta Ank}$ and immunoprecipitation was performed using anti-Myc to capture HDAC4. Successful immunoprecipitation was observed when probing with anti-Myc, an interaction with Peep was not observed upon probing with anti-HA (lane 7). Co-expression of Peep^{OE} and HDAC4$^{\Delta Ank}$ also did not show an interaction (lane 8). Immunoprecipitation samples were loaded alongside a negative control (lane 6, *elav-GAL4/+*) and 30 µg input samples (lanes 1-5). A non-specific anti-Myc band was detected in all input lanes (Asterix). IP = immunoprecipitation.

3.8 Characterising the relationship between Peep and HDAC4 in mushroom body development

The prominent mushroom body phenotype induced by HDAC4 overexpression is β lobe fusion. Pan-neuronal overexpression of HDAC4^{WT} resulted in 67% of brains with severe β lobe fusion (Tan *et al.*, 2024), which is a result of axon termination failure before the midline of the brain, giving the appearance of fused β lobes (Figure 3.1H, I, J, Figure 3.2B, C, D).

Given that Peep and HDAC4^{WT} colocalised in Kenyon cell nuclei, and that knockdown of Peep resulted in a mild defect in mushroom body development, it was next investigated whether expression of Peep^{OE} altered the HDAC4-induced mushroom body defects. It was hypothesised

that if overexpression of HDAC4 disrupted normal Peep function, then Peep^{OE} would rescue the β lobe fusion phenotype caused by overexpression of HDAC4.

3.8.1 Peep^{OE} enhanced the HDAC4 induced β lobe fusion phenotype

For mushroom body analyses, transgene expression was driven pan-neuronally using the *elav-GAL4* driver and mushroom body morphology was visualised with anti-FasII. The mushroom body scoring system detailed in Section 3.2.1 with representative images in Figure 3.1, was followed. As the predominant phenotype upon overexpression of HDAC4^{WT} was β lobe fusion, this was the phenotype that was primarily focused on. As expected, expression of HDAC4^{WT} resulted in 90% of brains consisting of β lobe fusion, with 50% of these being severe fusion, caused by entire β lobe midline crossing, 15% moderate fusion where half of the β lobe axons have crossed the midline, and 25% mild fusion where few bundled β lobe axons breach and cross the midline (Table 3.6, Figure 3.18).

Table 3.6. Severity and incidence of β lobe fusion upon expression of HDAC4^{WT} or HDAC4$^{\Delta Ank}$ and Peep^{OE}

Genotype	***elav/+***	***elav> peep^{OE}***	***elav> HDAC4^{WT}***	***elav> HDAC4^{WT}; peep^{OE}***	***elav> HDAC4$^{\Delta Ank}$***	***elav> HDAC4$^{\Delta Ank}$; peep^{OE}***
Mild (%)	-	-	25	5	10	5
Moderate (%)	-	-	15	10	10	10
Severe (%)	-	-	50	75	55	80
No defects (%)	100	100	10	10	25	5
n	20	20	20	20	20	20

elav = elav-GAL4.

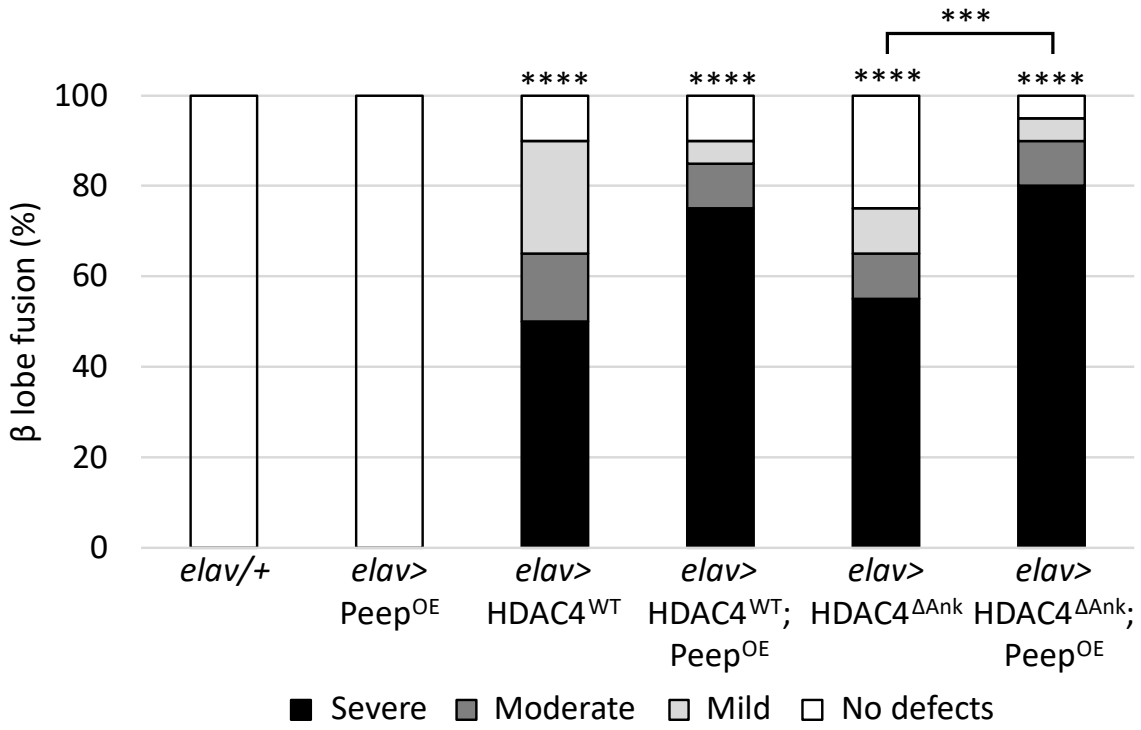

Figure 3.18. The percentage changes in HDAC4 β lobe fusion upon co-expression of Peep. Pan-neuronal co-expression of HDAC4^{WT} and Peep^{OE} does not increase β lobe fusion incidence compared to HDAC4^{WT} alone. Co-expression of HDAC4$^{\Delta Ank}$ and Peep^{OE} increases the incidence of β lobe fusion compared to HDAC4$^{\Delta Ank}$ alone, n=20, (one-tailed Fisher's exact statistical test, **** = p<0.0001, *** = p<0.001, *elav-GAL4/+* ; *elav-GAL4>HDAC4*^{WT} p= 0.00001, *elav-GAL4/+* ; *elav-GAL4>HDAC4*^{WT};*Peep*^{OE} p=0.00001, *elav-GAL4/+* ; *elav-GAL4>HDAC4*$^{\Delta Ank}$ p= 0.00001, *elav-GAL4/+* ; *elav-GAL4>HDAC4* $^{\Delta Ank}$;*Peep*^{OE} p= 0.00001, *elav-GAL4>HDAC4*$^{\Delta Ank}$; *elav-GAL4>HDAC4* $^{\Delta Ank}$;*Peep*^{OE} p= 0.0003). *elav* = *elav-GAL4, elav/+* = Control.

Overexpression of Peep alone had no impact on mushroom body development. Co-expression of HDAC4^{WT} and Peep^{OE} did not alter the total number of brains exhibiting β lobe fusion, but the severity of β lobe fusion was significantly increased (Figure 3.19).

HDAC4$^{\Delta Ank}$ alone resulted in a similar level of severe β lobe fusion as HDAC4^{WT} (55%), which was increased upon co-expression of Peep^{OE} where the overall number of brains exhibiting β lobe fusion increased significantly to 95% (Figure 3.18) as did the number with severe fusion to 80% (Figure 3.19) discussed in Section 3.10.2. This indicates that the modulation of the HDAC4 phenotype by Peep^{OE} is not dependent on the presence of the ankyrin repeat binding motif.

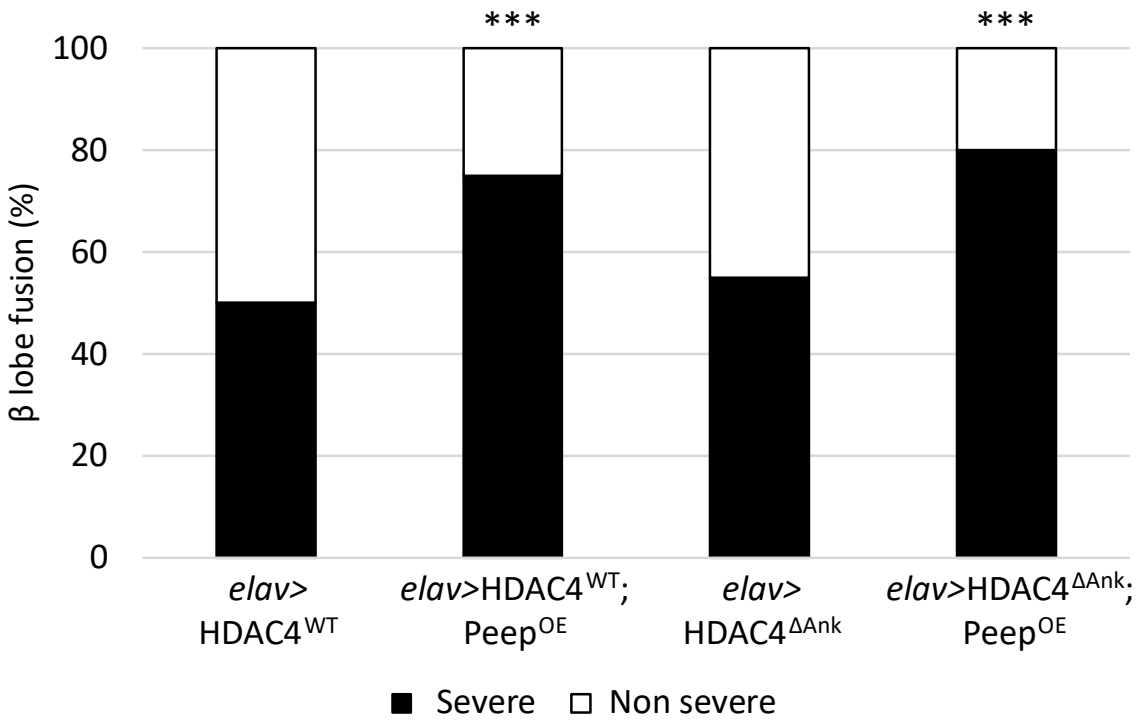

Figure 3.19. The percentage of severe β lobe fusion increases upon co-expression with Peep^{OE}. Pan-neuronal co-expression of HDAC4^{WT} and HDAC4$^{\Delta Ank}$ result in 50% and 55% severe β lobe fusion, respectively. Co-expression of Peep^{OE} increased the incidence of severe β lobe fusion to 75% and 80% respectively, n=20, (one-tailed Fishers exact test, *** = p<0.001, e*lav-GAL4>HDAC4*^{WT} ; *elav-GAL4>HDAC4*^{WT};*Peep*^{OE} = 0.0004, *elav-GAL4>HDAC4*$^{\Delta Ank}$; *elav-GAL4>HDAC4* $^{\Delta Ank}$;*Peep*^{OE} = 0.0003). *elav = elav-GAL4*.

Together, these data demonstrate that Peep^{OE} does not rescue the mushroom body β lobe fusion phenotype. Instead, HDAC4 redistributes Peep by sequestering it into 26% of nuclear aggregates and enhances the number of brains exhibiting severe β lobe fusion defects, both of which were not reliant on the ankyrin repeat binding motif.

3.9 Characterising the relationship between Peep and HDAC4 in eye development

Previously in this laboratory, a genetic rough eye enhancer genetic screen indicated a genetic interaction between *HDAC4* and *peep* (referred to as CG5846), in which knockdown of *peep* enhanced the *HDAC4*-induced rough eye phenotype (Schwartz *et al.*, 2016).

In that study a single RNAi construct was tested, which corresponded to *peep*^{RNAi2} in this study. Schwartz *et al.* (2016) excluded any genes from the screen that provoked more than a mild rough eye phenotype, and in the previous study *peep*^{RNAi2} was observed to only induce a mild rough eye phenotype as opposed to the severe rough eye phenotype observed in this present study. There was speculation that the fly line used in the prior study may not have been correct as it was not confirmed via PCR and a second RNAi construct was not analysed. It could also be speculated that if the flies were raised at a lower temperature, a less severe rough eye phenotype would have been produced, resulting in a lack of necrosis (Figure 3.20). The resolution from the light microscope that was used in the previous study was also lower and technical processing of images was limited, therefore the interpretation for scoring rough eye phenotype severity would have been different to what was used in this current study.

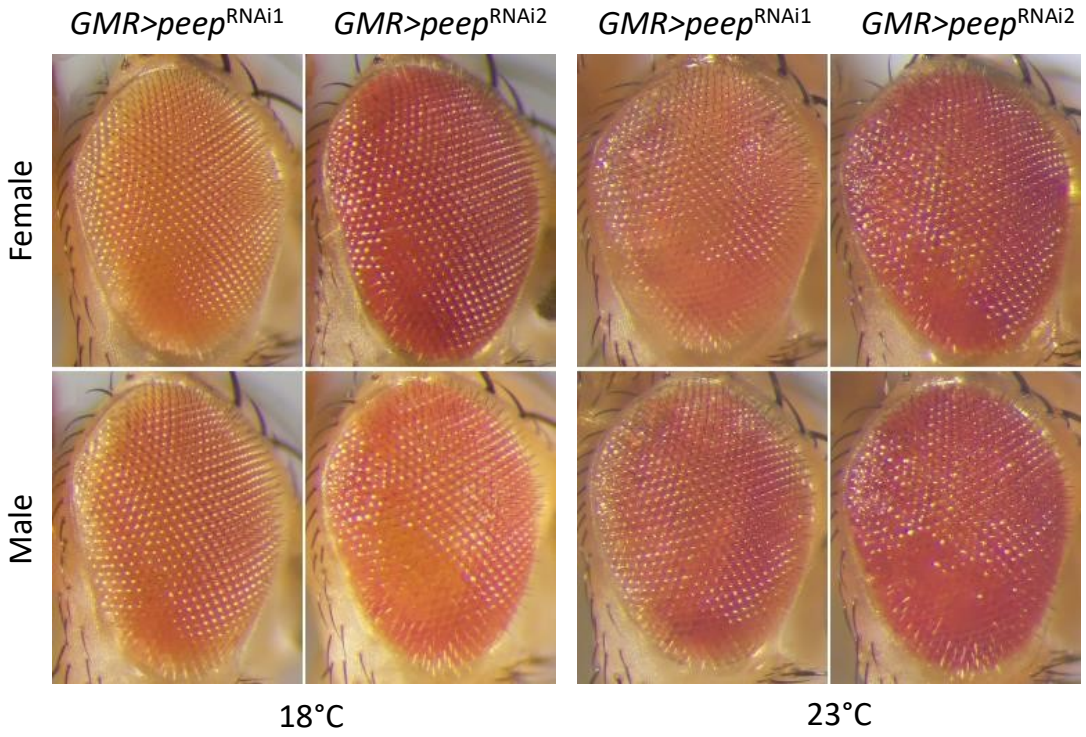

Figure 3.20. *peep*^{RNAi} does not induce a necrotic eye phenotype when raised at low temperatures. *GMR-GAL4* expression of *peep*^{RNAi1} resulted in a normal eye when raised at 18°C and a slight rough eye phenotype at 23°C. *GMR-GAL4* expression of *peep*^{RNAi2} resulted in a slight rough eye phenotype when raised at 18°C which was further exacerbated at 23°C, no necrosis was induced at these low temperatures. *GMR = GMR-GAL4.*

As observed during the initial candidate screen, *GMR-GAL4* expression of two independent *peep*^{RNAi} constructs resulted in a severe rough eye phenotype with areas of necrosis when raised at 25°C (Figures 3.5, 3.6). Therefore, a new scoring system was devised to tease apart small

differences specifically attributed to necrosis spread (Table 2.7). Peep^{OE} was also assessed, and strikingly, had no impact on eye development, with the eye appearing indistinguishable to the control (Figure 3.21A). Expression of HDAC4^{WT} resulted in a mild rough eye phenotype with misaligned bristles and co-expression of Peep^{OE} did not alter the HDAC4 overexpression-induced phenotype (Figure 3.21B).

Expression of *peep*^{RNAi1} resulted in a rough eye phenotype with areas of necrotic lesions at the posterior of the eye (Figure 3.21A), and an additive phenotype was elicited upon co-expression of HDAC4^{WT} (Figure 3.21B, E), with misalignment of ommatidia extending past the midline of the eye and into the anterior region. Even more strikingly, when HDAC4^{WT} was co-expressed with *peep*^{RNAi2}, progeny did not survive to adulthood as the flies did not emerge from their pupal casings, resulting from a pupal lethal phenotype. Co-expression of *peep*^{RNAi1} and HDAC4$^{\Delta Ank}$ resulted in a slightly more severe disruption to the alignment of ommatidia and an increased loss of pigmentation, attributed to the HDAC4$^{\Delta Ank}$ phenotype when expressed alone, but strikingly, there was an almost complete absence of necrosis, indicating that the necrotic phenotype induced by *peep*^{RNAi1} was rescued by the presence of HDAC4$^{\Delta Ank}$ (Figure 3.21C, Figure 3.22).When *peep*^{RNAi2} was co-expressed with HDAC4$^{\Delta Ank}$, pupal lethality remained. As shown in Figure 3.15D and by Tan *et al.* (2024), HDAC4$^{\Delta Ank}$ accumulates more highly in the nucleus compared to HDAC4^{WT} (Figure 3.15B), therefore, to determine whether the rescue of necrosis could be attributed to the increase in the nuclear pool of HDAC4 in the HDAC4$^{\Delta Ank}$ mutant, an HDAC4 mutant restricted to the nucleus was utilised. The HDAC4^{3SA} mutant contains substitutions of three serine residues (Ser^{239}, Ser^{573}, and Ser^{748}) important for 14-3-3 mediated nuclear export to alanine residues (Bertos *et al.*, 2001; Chawla *et al.*, 2003; Grozinger & Schreiber, 2000; McKinsey *et al.*, 2001; Wang *et al.*, 2014). This mutant has been shown to be restricted to the nuclei of Kenyon cells where it forms large aggregates and is absent from the axonal mushroom body lobes (Main *et al.*, 2021; Tan *et al.*, 2024).

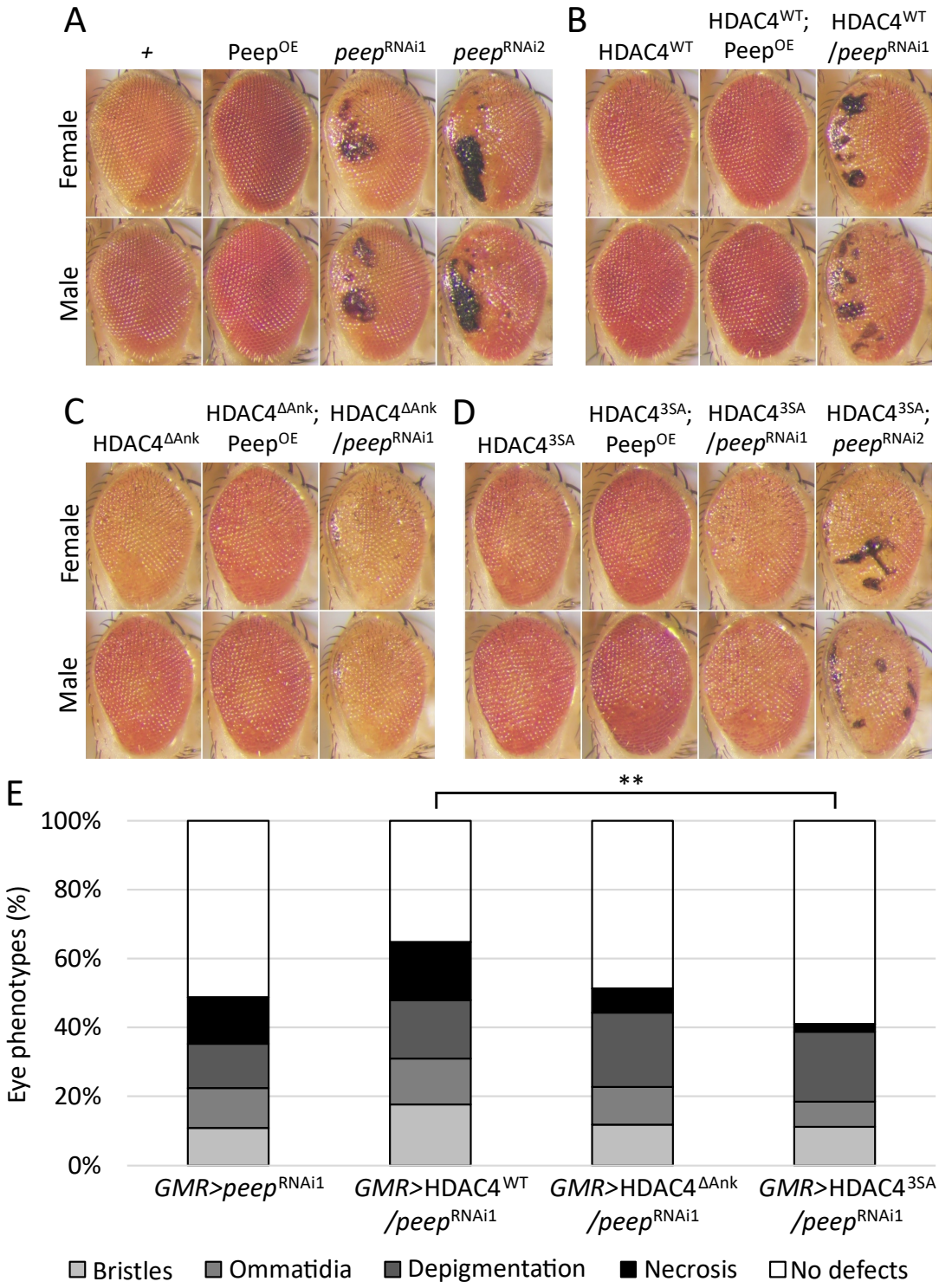

Figure 3.21. Peep did not rescue the HDAC4-induced eye phenotypes and HDAC4$^{\Delta Ank}$ minimised necrosis and HDAC4^{3SA} eliminated necrotic lesions induced by *peep*^{RNAi1}. A. *GMR-GAL4* expression of Peep^{OE} resulted in a normal eye. As previously examined, expression of both *peep*^{RNAi} constructs result in a severe rough eye phenotype with necrotic lesions localised to the posterior of the eye. B. *GMR-GAL4* driven co-expression of HDAC4^{WT} and Peep^{OE} did not rescue the HDAC4^{WT}-induced phenotype. Expression of HDAC4^{WT} was additive to the necrotic phenotype induced by *peep*^{RNAi1} by extending the rough eye phenotype to the anterior of the eye and co-expression with *peep*^{RNAi2} was pupal lethal. C. *GMR-GAL4* driven co-expression of HDAC4$^{\Delta Ank}$ and Peep^{OE} did not rescue the HDAC4$^{\Delta Ank}$-

induced phenotype. Expression of HDAC4$^{\Delta Ank}$ minimised the necrotic lesions induced by *peep*^{RNAi1} and co-expression with *peep*^{RNAi2} was pupal lethal. D. Co-expression of Peep^{OE} did not rescue the HDAC4^{3SA}-induced phenotype. Expression of HDAC4^{3SA} rescued the necrotic phenotype induced by *peep*^{RNAi1} and rescued the pupal lethal phenotype induced by *peep*^{RNAi2} that was observed in B and C. E. *peep*^{RNAi1} induces a range of phenotypic abnormalities including bristle and ommatidia disorganisation and areas of depigmentation and patches of necrosis. These defects increased upon co-expression of *HDAC4*^{WT}. *HDAC4*$^{\Delta Ank}$ reduced the level of necrosis and increased the level of depigmentation resulting in a similar level of defects to *peep*^{RNAi1} alone. *HDAC4*^{3SA} further reduced the level of necrosis thereby significantly decreasing the overall eye phenotypes compared to *HDAC4*^{WT}, n≥18, (one-tailed Fisher's exact test, ** = p<0.01, *GMR-GAL4;HDAC4*^{WT}>*peep*^{RNAi1} ; *GMR-GAL4;HDAC4*^{3SA}>*peep*^{RNAi1} = 0.0011). *GMR* = *GMR-GAL4*. *GMR-GAL4* was recombined with HDAC4^{WT}, HDAC4$^{\Delta Ank}$, and HDAC4^{3SA} and crossed to Peep^{OE}, *peep*^{RNAi1}, and *peep*^{RNAi2}.

Overexpression of Peep alone did not alter the HDAC4^{3SA} phenotype, however, co-expression of HDAC4^{3SA} with *peep*^{RNAi1} resulted in a slight increase in disruption to ommatidial alignment and loss of pigmentation, attributed to the HDAC4^{3SA} phenotype when expressed alone, and an almost complete rescue of the necrotic phenotype (Figure 3.21D, E). Co-expression of HDAC4^{3SA} with *peep*^{RNAi2} also rescued the pupal lethal phenotype. There was not a complete rescue of the necrotic phenotype, however, the necrosis observed was less severe at the posterior edge of the eye and was not restricted to this region, instead the necrosis was distributed in small patches across the entire eye field (Figure 3.21D).

The total volume of the eye containing necrotic lesions were also quantified for eyes expressing *peep*^{RNAi1} and each of the HDAC4 mutants (Section 2.4.4). It was evident that the total area of necrosis negatively correlated with the level of nuclear HDAC4 (Figure 3.22).

These data demonstrate that expression of *peep*^{RNAi} leads to two separate phenotypes, a developmental rough eye phenotype resulting in ommatidial misalignment and bristle abnormalities and a later onset necrotic phenotype, hypothesised as a result of cell death. The rough eye phenotype resulting from co-expression of HDAC4 mutants and *peep*^{RNAi} appear to be additive, however the necrotic phenotype was rescued, which was dependent on the relative levels of nuclear HDAC4.

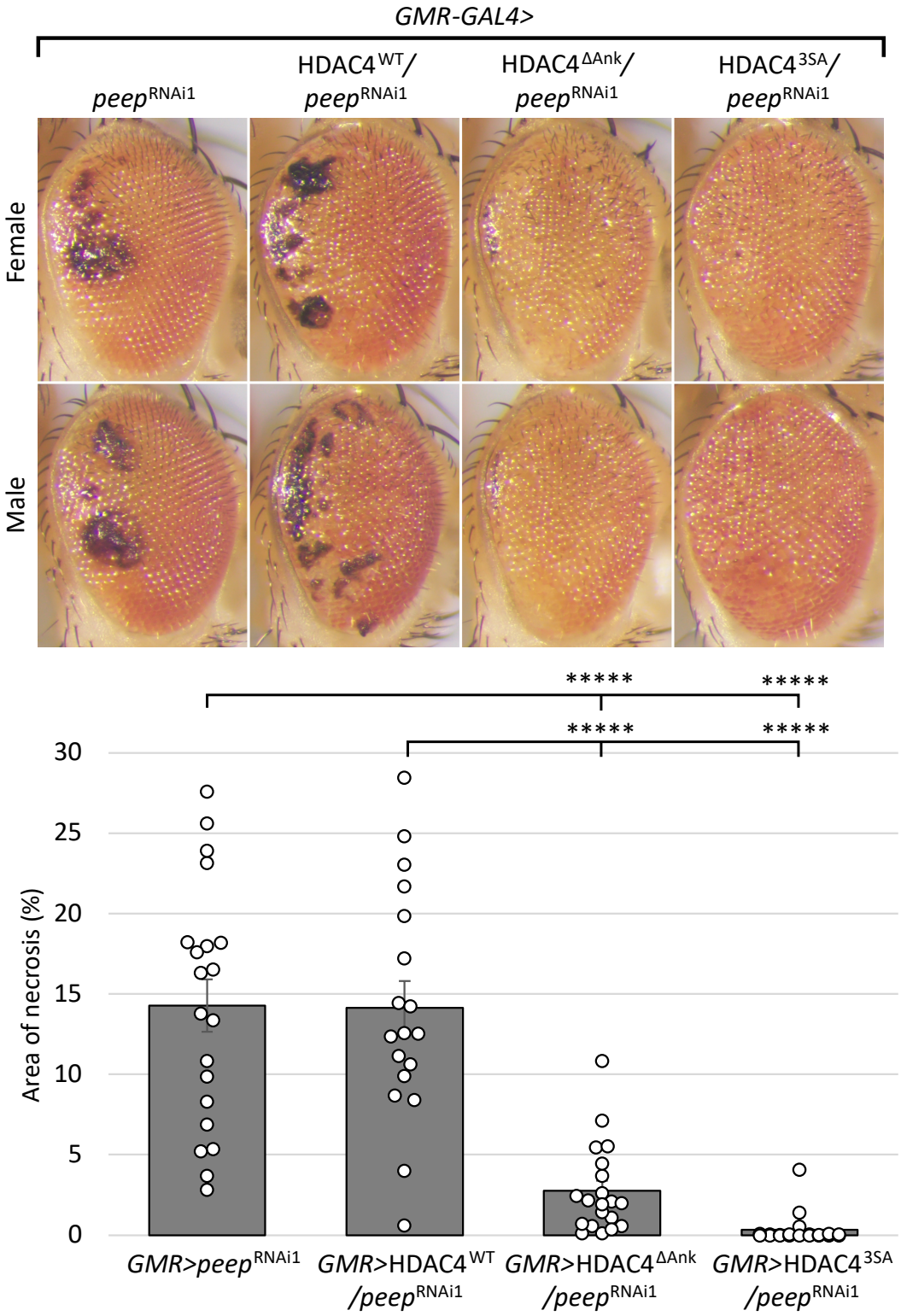

Figure 3.22. Increased nuclear HDAC4 rescued the *peep*^{RNAi}-induced necrotic phenotype. Co-expression of HDAC4$^{\Delta Ank}$ and HDAC4^{3SA} decreased the average area of necrosis induced by *peep*^{RNAi1}. Error bars indicate mean ± SEM, n≥18, (one-way ANOVA, post-hoc Tukey HSD, $f_{(3,77)} = 37$, ***** = p<0.00001, *GMR-GAL4>peep*^{RNAi1} ; *GMR-GAL4;HDAC4*$^{\Delta Ank}$*>peep*^{RNAi1} = 1.46E^{-8}, *GMR-GAL4>peep*^{RNAi1} ; *GMR-GAL4;HDAC4*^{3SA}*>peep*^{RNAi1} = 0, *GMR-GAL4;HDAC4*^{WT}*>peep*^{RNAi1} ; *GMR-GAL4;HDAC4*$^{\Delta Ank}$*>peep*^{RNAi1} = 4.2E^{-8}, *GMR-GAL4;HDAC4*^{WT}*>peep*^{RNAi1} ; *GMR-GAL4;HDAC4*^{3SA}*>peep*^{RNAi1} = 4.07E^{-11}). *GMR = GMR-GAL4, GMR-GAL4* was recombined with HDAC4^{WT}, HDAC4$^{\Delta Ank}$, and HDAC4^{3SA} and crossed to *peep*^{RNAi1}.

3.10 Discussion

HDAC4 has been implicated in a wide range of neurological and neurodegenerative diseases, some of which result from deletions (Morris *et al.*, 2012; Pigna *et al.*, 2019; Williams *et al.*, 2010), or missense mutations (Wakeling *et al.*, 2021) within the HDAC4 coding region and others in which increased nuclear abundance of HDAC4 has been observed in either post-mortem brains or in animal models (Herrup *et al.*, 2013; J. Li *et al.*, 2012; Shen *et al.*, 2016; Takahashi-Fujigasaki *et al.*, 2006; Takahashi-Fujigasaki & Fujigasaki, 2006). It was previously shown in *Drosophila* that the overexpression of HDAC4 results in large nuclear aggregate punctate foci within nuclei, and this was associated with impaired neurodevelopment (Main *et al.*, 2021; Tan *et al.*, 2024) and LTM (Fitzsimons *et al.*, 2013). The mechanisms through which increased nuclear HDAC4 acts to impair neurological function remains elusive, and therefore, a candidate approach was taken to identify genes that, when reduced in expression, result in similar phenotypes to HDAC4 overexpression, with the rationale that they may act in the same molecular pathways as HDAC4, and if HDAC4 was acting by impairing the function of the candidate then overexpression of the candidate should overcome the pathway disruption and rescue the HDAC4-induced phenotypes.

3.10.1 Several candidate RNAi lines conferred similar phenotypes to those induced by HDAC4 overexpression

RNAi lines were sourced from *Drosophila* stock centres for the 16 selected candidate genes, and these were screened for phenotypes similar to those induced by the overexpression of HDAC4 in both the mushroom body and the compound eye.

A significant β lobe fusion defect was observed following knockdown of Mthl8 with one of the two RNAi lines available, however no defects were observed in the eye. These results suggest a tissue specific phenotypic discordance and possible off-target effects induced by $mthl8^{RNAi2}$ resulting in the defects observed in the mushroom body. To alleviate questions regarding both RNAi efficacy and correct gene targeting, RT-qPCR could be performed. Some phenotype discordance between the brain and eye has also been observed with $HDAC4^{WT}$ (Main *et al.*, 2021; Tan *et al.*, 2024) resulting in a severe β lobe fusion defect in the mushroom body and mild ommatidial misalignment in the eye. As the mushroom body phenotypic defects could be

due to off-target effects, there was no abnormal phenotype observed in the eye and the low level of expression detected in the adult *Drosophila* brain via *in situ* hybridisation (Guan *et al.*, 2011) was unable to be recapitulated in this study with Mthl8 driven expression of CD8::GFP without further signal amplification, further studies of an interaction with HDAC4 would be difficult and potentially fruitless.

Knockdown of NetB with *NetB*^{RNAi2} resulted in a high level of β lobe fusion defects, similar to what has previously been observed for HDAC4^{WT} (Hawley, 2020; Main *et al.*, 2021; Tan *et al.*, 2024) and a moderate eye phenotype. Although there was little discordance between tissues with *NetB*^{RNAi2}, there were major discrepancies between independent RNAi lines and *NetB*^{RNAi2} was detailed to possibly confer off-target effects, therefore the efficacy and correct gene targeting of the knockdown should be assessed by RT-qPCR. Netrins are a family of lamin-related proteins with roles in midline axonal guidance and growth (Mitchell *et al.*, 1996). NetB is expressed in a variety of midline glia (Guthrie, 1997) and endogenous promoter expression of a tagged membrane tethered construct of NetB displayed expression in mushroom body lobes (Kang *et al.*, 2019). NetB expression analyses in Kenyon cell bodies has not yet been detailed, therefore, it is unknown whether NetB and HDAC4 would co-distribute in these cells in the adult brain.

Knockdown of Npc2g resulted in a range of ommatidial defects, with moderate levels of β lobe fusion in the mushroom body. The phenotypic defects in the eye and brain were similar to those observed upon overexpression of HDAC4 (Hawley, 2020; Main *et al.*, 2021; Schwartz *et al.*, 2016; Tan *et al.*, 2024; Wilson, 2021), however these defects were predominantly restricted to a single RNAi construct. Although phenotypes in the brain and eye elicited from *Npc2g*^{RNAi3} were similar to those induced by HDAC4^{WT} (Main *et al.*, 2021; Tan *et al.*, 2024), these were not recapitulated with the other two RNAi lines, therefore, the identities, gene targets, and relative efficacies of all RNAi lines require further investigation via PCR on genomic DNA and RT-qPCR. Little is known about *Drosophila* Npc2g aside from its expression in the head mesoderm and fat body (Huang *et al.*, 2007), and that mutations in the mammalian homologue NPC2, result in fatal Niemann-Pick disease due to abnormal cholesterol accumulation (Walterfang *et al.*, 2006).

Knockdown of Scamp resulted in a consistent high degree of β lobe fusion across the two independent RNAi lines, making Scamp a promising candidate for further investigation, however as pan-neuronal expression of *Scamp*^{RNAi2} was lethal, expression was restricted to the

mushroom body with *OK107-GAL4*, implicating a new driver related variable and therefore was unable to be compared to mushroom body defects induced by pan-neuronal overexpression of HDAC4. Furthermore, the mild rough eye phenotype induced by *Scamp*^{RNAi1} was not recapitulated with *Scamp*^{RNAi2}.

A single Mthl8, NetB, Npc2g, and Scamp RNAi line resulted in similar phenotypes to HDAC4^{WT} in the mushroom body and/or eye, however as there were discrepancies between the independent RNAi lines, which were not further investigated, it was possible that these induced defects were due to off-target effects by the RNAi, therefore, these candidates were not selected for further investigation.

3.10.2 Varied expression patterns were observed among select candidates

The CD8::GFP expression pattern when driven by either *Kank-GAL4* or *kra-GAL4* was also examined. These studies did not give information on the subcellular distribution of each protein but gave insight into the cellular expression pattern in the brain.

kank-GAL4 driven CD8::GFP was localised to cells resembling the descending neuron clusters, with a lack of expression in the anterior mushroom body lobes and posterior Kenyon cell bodies. Descending neurons are those that convey signals from the brain to the ventral nerve chord and are therefore important in most complex behaviours (Guo *et al.*, 2022). *kra-GAL4* driven CD8::GFP showed expression in cells resembling suboesophageal, descending, and dopaminergic neuron clusters, with no detectable expression in the mushroom body lobes and Kenyon cell bodies. The subesophageal neuron cluster processes inputs from the sensilla, which are small hair structures located on the head and mouth parts of the *Drosophila*, and these gustatory inputs control feeding behaviour movements (Gendre *et al.*, 2004). The dopaminergic neuron cluster, similar to descending neurons, play an important role in the brain by regulating behavioural processes related to reward and stress (Baik, 2020). The knockdown of either Kank or Kra resulted in few mushroom body defects, indicating that knockdown of Kank in descending neurons and knockdown of Kra in suboesophageal, descending, and dopaminergic neuron clusters does not have a cell non-autonomous effect on neuronal Kenyon cell axon development, and a minimal eye phenotype, and thus Kank and Kra were not selected for further investigation.

GFP trap lines were available from stock centres for Rogdi and Shn which gave insight into not only the expression pattern of the endogenous protein but also its subcellular distribution.

Previous studies have shown Rogdi expression in the mushroom body lobes (Dubnau *et al.*, 2003) and equal distribution between the nucleus and cytoplasm in adult *Drosophila* brain neurons and S2 cells (Kim *et al.*, 2017). In this current study Rogdi was localised to neuronal nuclei in the anterior of the brain, with minimal expression in the mushroom body lobes. Expression of either *rogdi*^{RNAi} line resulted in minimal mushroom body defects, however expression of *rogdi*^{RNAi1} resulted in defects to 80% of eyes, most of which consisted of mild to moderate ommatidial disruption. As no eye phenotype was induced by *rogdi*^{RNAi2}, these eye defects could be due to off-target effects and further investigation of RNAi efficiency and gene targeting via RT-qPCR would be required. For these reasons, Rogdi was not selected for further investigation into an interaction with HDAC4.

Shn expression was not detected in the brain which coincided with a previous study that reported no Shn expression in the mushroom body, although Shn was identified in a genetic screen for genes that impair LTM formation, which showed that Shn mutants had normal learning but significantly impaired LTM (Dubnau *et al.*, 2003). A single *shn*^{RNAi} construct was available and resulted in a mild to moderate level of β lobe fusion, most of which was severe, however no eye defects were observed. As there was no endogenous expression in the brain and no eye phenotype similar to that of HDAC4^{WT}, and a second RNAi line was not available to confirm the mushroom body phenotype, Shn was not selected for further investigation into an interaction with HDAC4.

3.10.3 Peep (CG5846) was selected for further investigation into the interaction with HDAC4

In the interest of thorough characterisation, a single gene *CG5846*, which was named *peep*, was selected to investigate the nature of an interaction with HDAC4, which was hypothesised to be mediated by the ankyrin repeats on Peep and the ankyrin repeat binding domain on HDAC4.

Knockdown of Peep resulted in a mild mushroom body phenotype but a strikingly severe unique eye phenotype. The two *peep*^{RNAi} lines induced similar phenotypes within either the brain or eye, providing consistent and reliable results. There was discordance between the brain and eye

with regard to phenotype severity, suggesting that Peep is involved in different tissue specific processes. A mild mushroom body phenotype was observed, with a small percentage of brains displaying β lobe fusion defects. The severe eye phenotype upon *peep*^{RNAi} resulted in ommatidial disorganisation and fusion, both of which are observed upon HDAC4 overexpression (Schwartz *et al.*, 2016; Tan *et al.*, 2024; Wilson, 2021), however expression of *peep*^{RNAi} also resulted in necrotic lesions that were restricted to the posterior edge of the eye and has rarely been observed. Peep is the sole *Drosophila* homologue of ANKRA2 and RFXANK and shares 32.3% sequence identity and 47.9% similarity with ANKRA2 and 33.6% identity and 47.8% similarity with RFXANK (Pairwise Sequence Alignment, EMBOSS Water). Peep also contains an C-terminal stretch of ankyrin repeats that are predicted to bind to the conserved ankyrin repeat binding domain on HDAC4 (McKinsey *et al.*, 2006; Wang *et al.*, 2005; Xu *et al.*, 2012). Although RFXANK plays an essential role in adaptive immune support through transcriptional regulation of MHC genes, and *Drosophila* do not harbour an adaptive immune system, it remains of interest to determine the nature of the interaction between Peep and HDAC4 in neuronal development. Peep was therefore selected for further investigation into the nature of its interaction with HDAC4, by co-distribution and co-immunoprecipitation in the brain and analysis of an interaction in the eye.

3.10.4 The PSLPNI motif does not mediate the interaction between HDAC4 and Peep in the brain

Although mushroom body phenotypes induced by *peep*^{RNAi} were mild, the most common phenotype observed was β lobe fusion, which is the prominent phenotype resulting from HDAC4 overexpression (Hawley, 2020; Main *et al.*, 2021; Tan *et al.*, 2024). As these result in a similar phenotype, it was hypothesised that if increased HDAC4 was acting to impair Peep function, then overexpression of Peep may rescue the HDAC4 overexpression-induced β lobe fusion phenotype.

A low level of ubiquitous Peep expression has been established via both large scale Microarray (Robinson *et al.*, 2013) and RNA-seq (Krause *et al.*, 2022) analyses. Furthermore, recent single cell-RNA-seq in the adult *Drosophila* showed moderate to low Peep expression in all cell types (Li *et al.*, 2022), however no studies have characterised expression at the protein level, nor the In the current study Peep was observed to localise to the nucleus (Section 3.6.3). Although this

was under overexpression conditions, expression was almost exclusively limited to the nucleus, with overexpression artefacts normally resulting from expression overspill into other cellular regions in which the protein is not normally expressed in. Co-expression of $Peep^{OE}$ and $HDAC4^{WT}$ in mushroom body neurons did not alter the HDAC4 overexpression-induced distribution in Kenyon cells, however Peep was sequestered into approximately 26% of the HDAC4 nuclear aggregates. These results indicate that there may be an interaction between Peep and HDAC4, and it was further investigated whether this interaction was mediated by the ankyrin repeat binding domain on HDAC4 with the $HDAC4^{\Delta Ank}$ mutant. Surprisingly, Peep was still sequestered into approximately 35% of $HDAC4^{\Delta Ank}$ nuclear aggregates. Although the number of nuclear aggregates was not increased upon co-expression of $Peep^{OE}$, aggregate size was increased in those that sequestered Peep, indicating that Peep may play a role in stabilising aggregate formation, either through increasing HDAC4 accumulation or sequestering other proteins that, under basal conditions are not normally recruited into these punctate nuclear foci. It is, however, important to note that these experiments were used to prove that an interaction in nuclei between these two proteins was physically possible, however as both were overexpressed, the resulting interactions may be due to increased expression rather than a reflection of the normal nature of the endogenous proteins.

As Peep was similarly sequestered into nuclear aggregates following mutation of the ankyrin repeat binding motif, it was hypothesised that if an interaction endogenously occurs, it may not be predominantly mediated by this motif. Instead Peep binding may be mediated by other binding partners or Peep may preferentially bind to a secondary region on HDAC4. Previous studies that have examined the interaction between RFXANK and HDAC4 (McKinsey *et al.*, 2006) showed a secondary binding site on HDAC4 for RFXANK (Wang *et al.*, 2005). As detailed in Section 1.7.2, an *in vitro* binding assay identified an RFXANK binding region between residues 118-279 on HDAC4 (Wang *et al.*, 2005) and a follow up *in vivo* co-immunoprecipitation assay identified a second RFXANK binding region between residues 315-666 (Wang *et al.*, 2005) which overlaps with the PSLPNI motif (residues 349-354) identified by Xu *et al.* (2012). The putative PSLPNI motif has since been characterised as the main binding site for ANKRA2 and RFXANK. Aside from HDAC4, ANKRA2 also binds to Megalin via this motif and RFXANK binds to RFX5, although the motif is not 100% conserved for these interactions, the binding pockets and weak hydrogen bond network allows for these interactions to remain favourable (Xu *et al.*, 2012). Furthermore, an N-terminal truncation comprised of residues 189-1084 showed a significantly stronger interaction between RFXANK and HDAC4

than full length HDAC4, however mutant 146-1084 showed a reduced level of binding. This indicated that there is an RFXANK autoinhibitory domain located within residues 146-189 which inhibits binding of RFXANK to the downstream region between residues 315-666. These results show that there are two different binding sites on HDAC4 for RFXANK, however there are limitations to the results of this study as some analyses were not replicated *in vitro* if they were performed *in vivo* and vice versa. It also remains to be determined whether one binding site is preferred and if the autoinhibitory region functions only to inhibit binding of RFXANK downstream or whether it also inhibits binding of RFXANK within the same region (Wang *et al.*, 2005). For these reasons it is not unprecedented that Peep may also bind to HDAC4 via a secondary binding region due to its homology with RFXANK.

Pan-neuronal overexpression of Peep did not result in any mushroom body abnormalities and was also unable to rescue the $HDAC4^{WT}$-induced severe β lobe fusion phenotype, and instead further exacerbated the frequency at which this phenotype was observed. Similarly to the observation that overexpression of Peep in mushroom body neurons increases the size of the HDAC4 nuclear aggregates, a result of either stabilisation or further protein sequestration, the pan-neuronal overexpression of Peep may also be altering the normal function of proteins required for normal mushroom body development resulting in a further increase in morphological defects on top of those induced by $HDAC4^{WT}$. A recent study from this laboratory showed that the ability of HDAC4 to impair mushroom body development relied on the presence of the MEF2 transcription factor. MEF2 is also sequestered into HDAC4-containing nuclear aggregates, and a mutant of HDAC4 that was unable to bind MEF2 could no longer induce β lobe fusion. In contrast, upon overexpression of MEF2 in the presence of HDAC4, the frequency of severe β lobe fusion increased (Tan *et al.*, 2024) (Section 1.7.1.2). It would be worth investigating whether $Peep^{OE}$ increased the expression of MEF2 and/or the sequestration of MEF2 into aggregates, thereby, enhancing the $HDAC4^{WT}$-induced β lobe fusion phenotype. On the contrary, the increase in fusion frequency could also be due to the propensity for Peep to interact with HDAC4 and block binding of other HDAC4 binding partners which may normally suppress the fusion phenotype.

Co-immunoprecipitation revealed no detectable interaction between HDAC4 and Peep. Although approximately 26% of HDAC4 nuclear aggregates were seen to co-distribute with Peep, these data were from co-expression with the *OK107-GAL4* driver, which promotes high expression in the mushroom body Kenyon cells (Hawley *et al.*, 2023). The co-

immunoprecipitation assay however, was performed on whole heads following pan-neuronal expression using *elav-GAL4* which drives much weaker expression in the mushroom body Kenyon cells (Hawley *et al.*, 2023). It is likely that with lower levels of expression in Kenyon cells, there would be lower incidence of co-distribution of HDAC4 and Peep resulting in a low level of interaction that was undetectable by co-immunoprecipitation. The interaction could also be indirect or transient or too weak to be maintained throughout the co-immunoprecipitation process, therefore, a prior crosslinking step could be introduced to preserve the interaction. To further this, co-immunoprecipitation could then be performed on fractionated nuclear extracts from dissected brains following mushroom body driven co-expression of $HDAC4^{WT}$ or $HDAC4^{\Delta Ank}$ and $Peep^{OE}$ to maximise the amount of Peep-HDAC4 protein complexes.

3.10.5 Nuclear HDAC4 ameliorates the necrotic phenotype induced by *peep*^{RNAi} in the eye

A previous genetic screen to identify candidate genes that enhance the HDAC4 overexpression-induced rough eye phenotype, suggestive of a genetic interaction, identified *peep* (Schwartz *et al.*, 2016). As knockdown of Peep enhanced the HDAC4 overexpression phenotype in this previous study, it was hypothesised that $Peep^{OE}$ may rescue the phenotype. This, however, did not occur which indicated that the $HDAC4^{WT}$ rough eye phenotype was not due to a loss of Peep activity. On the contrary, increased nuclear accumulation of HDAC4 rescued the necrotic phenotype upon Peep knockdown, while the rough eye phenotype remained similar to that of each HDAC4 mutant when expressed independently. This showed that the developmental rough eye phenotype and the necrotic lesion phenotype, result from disruption of two different pathways. Changes in expression levels of Peep did not rescue the developmental rough eye phenotype induced by HDAC4, however the necrotic phenotype induced by Peep depletion was rescued by increasing the nuclear pool of HDAC4, the mechanism by which remains unknown.

Nuclear accumulation of HDAC4 correlates with increased cell death in Parkinson's disease (Wu *et al.*, 2017), impaired cognitive function in Alzheimer's disease (Herrup *et al.*, 2013; Shen *et al.*, 2016), and neurodegeneration in ataxia telangiectasia (J. Li *et al.*, 2012). However, as nuclear HDAC4 rescues retinal necrotic damage induced by Peep knockdown, it is important to note that nuclear HDAC4 also plays a neuroprotective role under certain circumstances by

regulating neuronal death and modulating synaptic plasticity, a process that is specifically important during stroke recovery (Kong *et al.*, 2018).

Nuclear HDAC4 also confers a neuroprotective role during mouse eye development. In the mouse model of retinitis pigmentosa, expression of a short N-terminal fragment of HDAC4 played a neuroprotective role in preserving rod and cone photoreceptors through the suppression of apoptosis-related genes, resulting in partial restoration of visual function (Guo *et al.*, 2015). It is therefore possible that apoptosis in the eye may be the leading cause of the necrosis induced by depletion of Peep; if so, it may be likely that nuclear HDAC4 rescues the phenotype by suppressing expression of pro-apoptotic genes.

The following chapters attempt to further the limited understanding of the role that Peep plays in *Drosophila* development and neural function. Chapter four establishes the expression pattern of Peep and further investigates the phenotypes and behavioural role that Peep plays through a battery of well-established analyses. Chapter five includes an in-depth approach to understand the role of Peep in eye development. This approach led to potential pathways that may be disrupted upon knockdown of Peep, all of which warrant further investigation.

4 Characterising the importance of Peep in neural function via a battery of well-established behavioural and morphological analyses in *Drosophila*

In the previous chapter, Peep was identified as a potential interactor of HDAC4, which suggested it could be involved in the regulation of the HDAC4-induced phenotypes in both the eye and mushroom body. It was hypothesised that the overexpression of Peep would rescue the HDAC4-induced phenotypes, however this was not observed.

As there is currently little known about this gene, and given the severe developmental defects and cell death in the eye resulting from Peep knockdown, the role that Peep plays in both neuronal and non-neuronal function warrants further investigation. This chapter examines the expression of Peep during development in different tissues via immunohistochemistry and western blot. These studies were then followed by confirmation of the specificity and efficiency of the $peep^{RNAi}$, which was then utilised to determine the impact that Peep knockdown had on survival, longevity, brain morphogenesis, and learning and memory. The role that Peep plays in eye development will be further investigated in Chapter five.

4.1 Peep is endogenously expressed at low levels both spatially and temporally

Little is known about the temporal or spatial pattern or level of expression of Peep. Previous large scale Microarray (Robinson *et al.*, 2013) and RNA-seq (Krause *et al.*, 2022) data show relatively low expression of Peep in both adult and larval tissues, including the brain and eye. Recent adult-specific single cell-RNA-seq data demonstrates moderately low expression in both neurons and all glia with only 1% of these cells having detectable expression (Li *et al.*, 2022).

There is currently a lack of available tools to validate these previous analyses and further examine the endogenous expression pattern of Peep due to its uncharacterised nature. To

remedy this, a polyclonal antibody targeting a Peep epitope was generated (Genscript), however this failed to detect Peep via either immunohistochemistry or western blot. An alternative strategy was then devised in which two transgenic lines were generated to analyse expression driven by the endogenous *peep* promoter. There are two isoforms of *peep* (RA and RB) which are in the antisense orientation. The longer 5' untranslated region (UTR) of the *peep-RB* isoform overlaps with the 5' UTR of the neighbouring gene locus *CG4658* isoform RD which is in the sense orientation (Figure 8.3, Appendix 8.3). The *peep* promoter region that was used included the 5' region of *CG4658* up to the start codon and the overlapping 5' UTR of both *peep* isoforms (Figure 8.4, Appendix 8.4 and Figure 8.5, Appendix 8.5). For the first line, a construct was generated in which the *peep* promoter was fused upstream of the sequence encoding the *peep* gene, minus the stop codon, after which a 6x Myc tag was fused followed by a stop codon. This *peep*-Promoter-*Peep-Myc* (Peep-Myc) construct therefore drives Peep expression under the direct control of the endogenous *peep* promoter and allows for detection of Peep with an antibody against the Myc-tag (Section 2.1.2, Figure 8.4, Appendix 8.4). A *peep-GAL4* driver was also generated in which the *peep* promoter was fused upstream of GAL4 (Section 2.1.2, Figure 8.5, Appendix 8.5). Transgenic flies were generated via PhiC31-mediated homologous recombination into the VK22 landing site, which facilitates robust transgene expression (Main *et al.*, 2021; Tan *et al.*, 2024; Wilson *et al.*, 2023).

To characterise the endogenous pattern of distribution in the *Drosophila* adult brain, immunohistochemistry using an anti-Myc antibody was carried out following isolation of brains from Peep-Myc flies (Section 2.2.4), however no specific signal was detected (Figure 4.1A). This was compared to a negative Canton Special (CS) control (Figure 4.1B) and positive control containing *elav-GAL4* driven Myc tagged HDAC4^{3SA}, which is localised specifically to the Kenyon cells at the posterior of the brain (Figure 4.1C (bottom panel)), as has previously been established (Tan *et al.*, 2024).

peep-GAL4 flies were crossed to the *UAS-CD8::GFP* line, and anti-GFP immunohistochemistry was carried out on brains of the progeny (Section 2.2.4). While not directly detecting Peep, any detection of GFP would indicate regions in which Peep was endogenously expressed, as was performed previously in Section 3.4.1, however, no staining was observed (Figure 4.2A). This was compared to the negative CS control (Figure 4.2B) and positive control containing *elav-GAL4* driven *UAS-CD8::GFP* (Figure 4.2C). These results suggest that Peep was either too lowly expressed to be detected, or that the promoter was missing important tissue-specific enhancer regions.

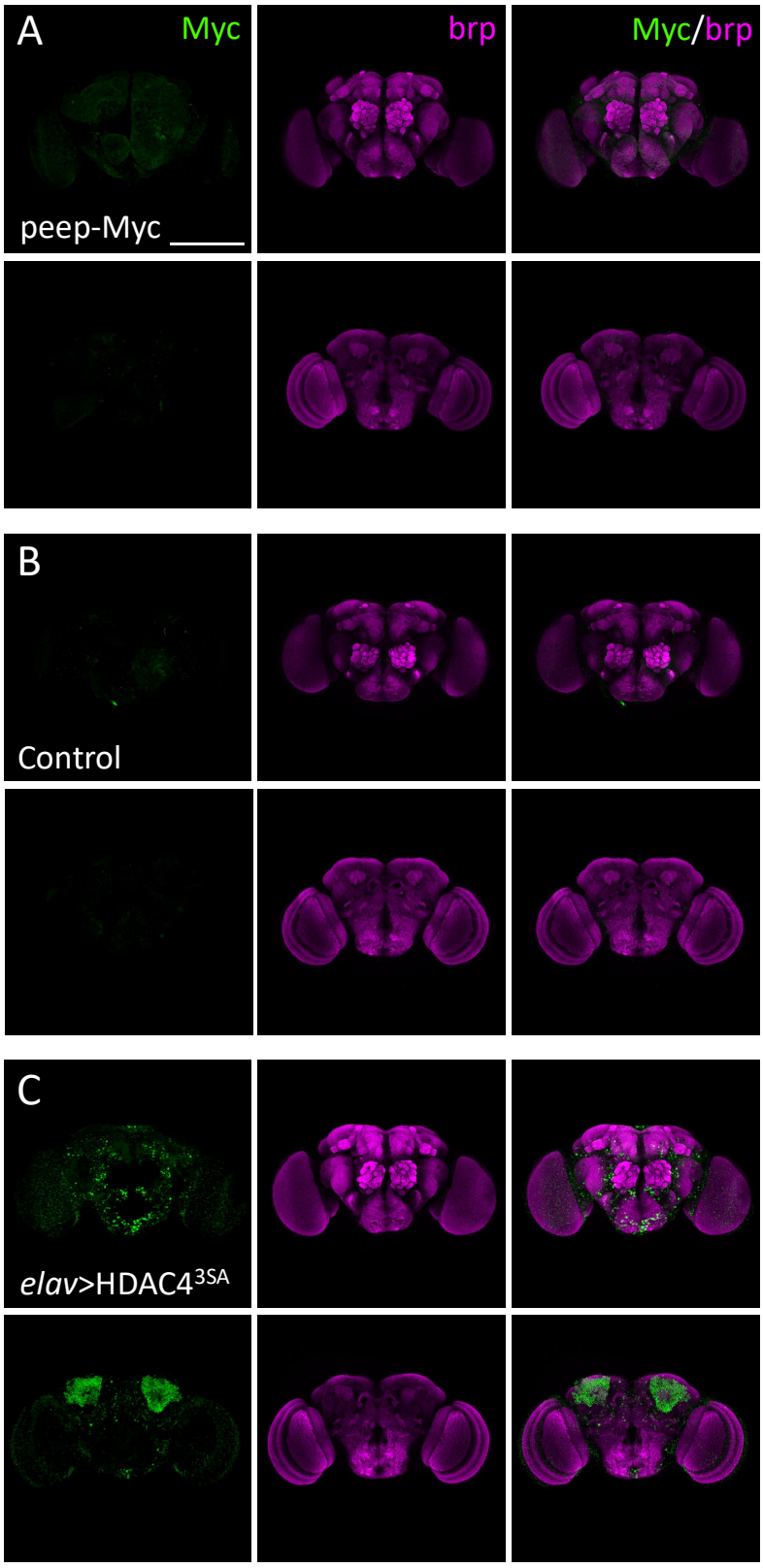

Figure 4.1. Peep-Myc was not detected via immunohistochemistry. Microdissected brains were subject to immunohistochemistry using an anti-Myc antibody (green) and counterstained with anti-brp (magenta) to highlight the structure of the brain. A. Peep-Myc showed faint, non-descript staining in the anterior of the brain (top panels). B. The negative CS control showed no Myc staining. C. *elav-GAL4* crossed to HDAC4^{3SA} was used as an anti-Myc antibody positive control and showed predominant localisation to neuronal nuclei in the anterior of the brain (top panels) and specific localisation to Kenyon

cell nuclei (bottom panels). Images were taken using 20x objective, 1 µm sections, scale bar = 100 µm. Anterior = top panels. Posterior = bottom panels. Control = CS.

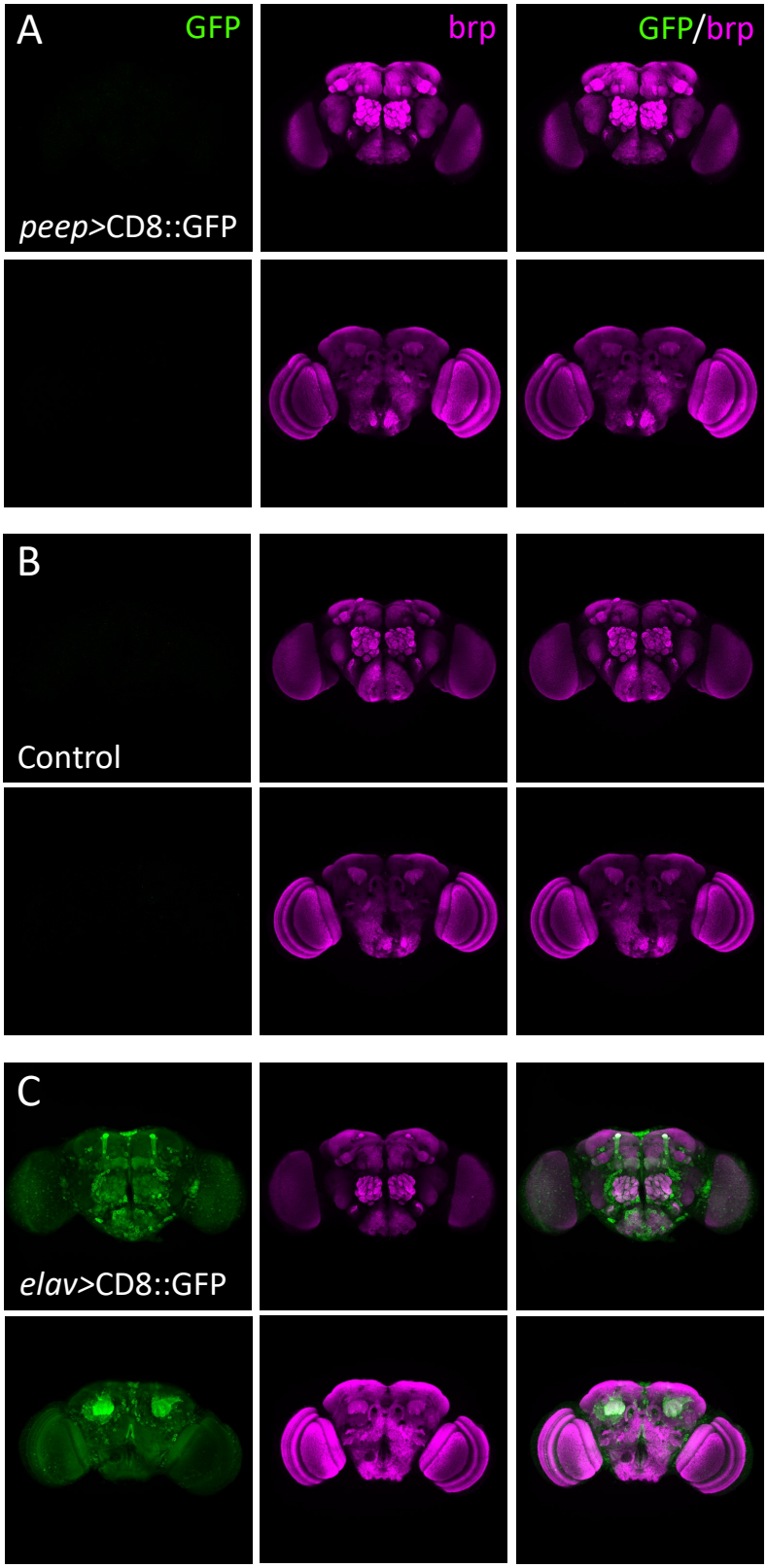

Figure 4.2. *peep-GAL4* driven CD8::GFP was not detected via immunohistochemistry. Microdissected brains were subject to immunohistochemistry using an anti-GFP antibody (green) and

counterstained with anti-brp (magenta) to highlight the structure of the brain. A. *peep-GAL4* crossed to *UAS-CD8::GFP* showed no CD8::GFP staining. B. The negative CS control showed no GFP staining. C. *elav-GAL4* crossed to *UAS-CD8::GFP* was used as an anti-GFP antibody positive control and showed predominant CD8::GFP localisation to the mushroom body axons in the anterior of the brain (top panels) and specific localisation to Kenyon cell bodies (bottom panels), as was established in Figure 3.7. Images were taken using 20x objective, 1 µm sections, scale bar = 100 µm. Anterior = top panels. Posterior = bottom panels. *peep* = *peep-GAL4,* Control = CS.

As western blotting is more sensitive than immunohistochemistry, tissues were dissected from Peep-Myc flies and whole cell lysates were generated. Peep expression was detected in the 0-2-hour old embryo (Section 2.3.2) via western blot with anti-Myc (Figure 4.3, left panel). Peep was also detected in the dissected larval eye/brain complex as well as the adult brain following microdissection of these tissues (Sections 2.3.3, 2.3.4). Furthermore, Peep expression in the whole pupa 48-hours APF (Section 2.3.5), the isolated adult eye (Section 2.3.6), head, and body (Section 2.3.1) were all independently confirmed (Figure 4.3, right panel). These results show that the promoter elements that drive Peep expression in each tissue were present, albeit at low levels, which is consistent with what was previously observed via Microarray (Robinson *et al.*, 2013) and RNA-seq (Krause *et al.*, 2022). This was evidenced by the appearance of non-specific protein bands present in both the control and Peep-Myc lanes, which are routinely observed following prolonged exposure and in the absence of highly expressed proteins. Anti-Tubulin was used as a loading control, however the whole-pupa and adult body samples both showed reduced Tubulin expression, indicative of low or unequal protein loading, however, this can be attributed to irregularities in BCA protein quantification. In a previous study it was shown that lipids in the presence of BCA produce an absorbance peak not too dissimilar to that of proteins, and therefore samples containing high proportions of lipids would cause errors in protein quantification (Kessler & Fanestil, 1986). The whole-pupa and adult body both contain large quantities of fats (ie. lipids), and therefore the protein quantification for these samples was disproportionately increased. This unknowingly led to comparatively less protein loaded resulting in a lower level of Tubulin detection which was consistent between the negative control and Peep-Myc samples.

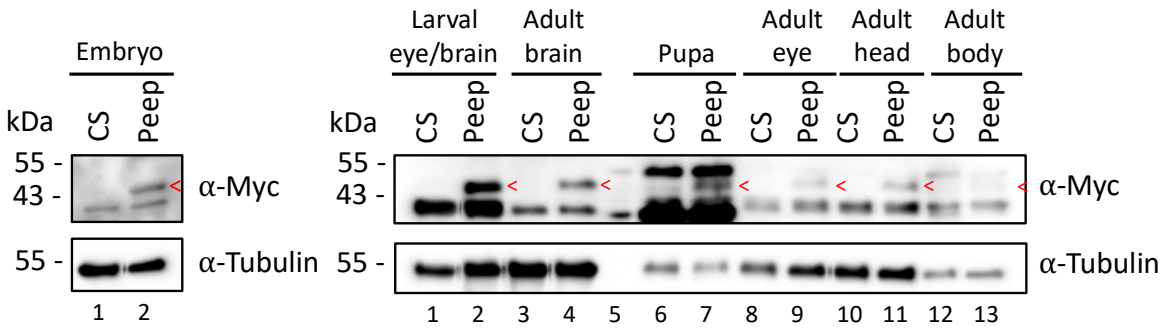

Figure 4.3. Western blot showing endogenous expression of Peep. Peep-Myc was expressed using the endogenous *peep* promoter and showed low level of expression in several tissues and developmental stages, and the protein was detected at approximately 47 kDa. On the left, Peep was expressed in the 0-2 hour embryo. On the right, Peep was expressed in the third instar larval eye/brain complex (lane 2) as well as the adult brain (lane 4) following isolation of dissected tissues. Lane 5 was a gap between samples. Peep was also expressed in the whole isolated pupa (lane 7), isolated adult eye (lane 9), isolated adult head (lane 11) and body (lane 13) (red arrowheads), 30 µg protein loaded, anti-Tubulin was used as a loading control.

Collectively these data show the first validation that Peep is endogenously expressed in both the adult brain and eye as well as in embryos, and the third instar larval eye/brain complex, however the expression level in all tissues remains low.

4.2 *peep*^{RNAi} efficiently targets *peep* mRNA to reduce Peep protein levels

Prior to investigating whether Peep is important for *Drosophila* survival, development, and brain function, the efficacy of the two RNAi constructs was evaluated. Since Peep expression was detected at an extremely low level, and it would be difficult to assess a further reduction in expression, therefore, the efficacy of knocking down the HA-tagged Peep^{OE} construct was tested. Peep^{OE} alone or in combination with either *peep*^{RNAi1} or *peep*^{RNAi2} was expressed in the eye with *GMR-GAL4*, followed by western blotting (Section 2.3.8) on whole cell lysates of eyes dissected from the progeny (Section 2.3.6). A significant reduction of Peep^{OE} was observed similarly between both RNAi constructs, with little protein detected following prolonged exposure, demonstrating that both *peep*^{RNAi} constructs target and efficiently knock down *peep* mRNA (Figure 4.4A).

It should be noted that the necrotic eye phenotype was unable to be rescued by co-expression of Peep^{OE} with either *peep*^{RNAi} (Figure 4.4B, C (*peep*^{RNAi1} was shown for simplicity)), which was unsurprising as *peep*^{RNAi} almost entirely eliminated Peep^{OE} protein expression (Figure 4.4A). In order to show a rescue in the necrotic eye phenotype, a Peep^{OE} construct with silent mutations within the *peep*^{RNAi} target region would have to be generated. This would render the RNAi inefficient in knocking down expression of Peep^{OE} and therefore the phenotype may be rescued. Furthermore, an uncharacterised homozygous lethal Peep mutant is available from BDSC (CG5846^{G3334}) which could be characterised and utilised for rescue experiments with either Peep^{OE} or Peep-Myc. Given that *peep*^{RNAi1} was verified by PCR (Section 2.8.4), and *peep*^{RNAi2} confers a similar phenotype in both the brain and eye, and both lines efficiently reduced Peep expression (Figure 4.4A), there is confidence in concluding that the eye phenotypes induced by these two RNAi lines are a direct result of Peep knockdown, and not due to off-target effects.

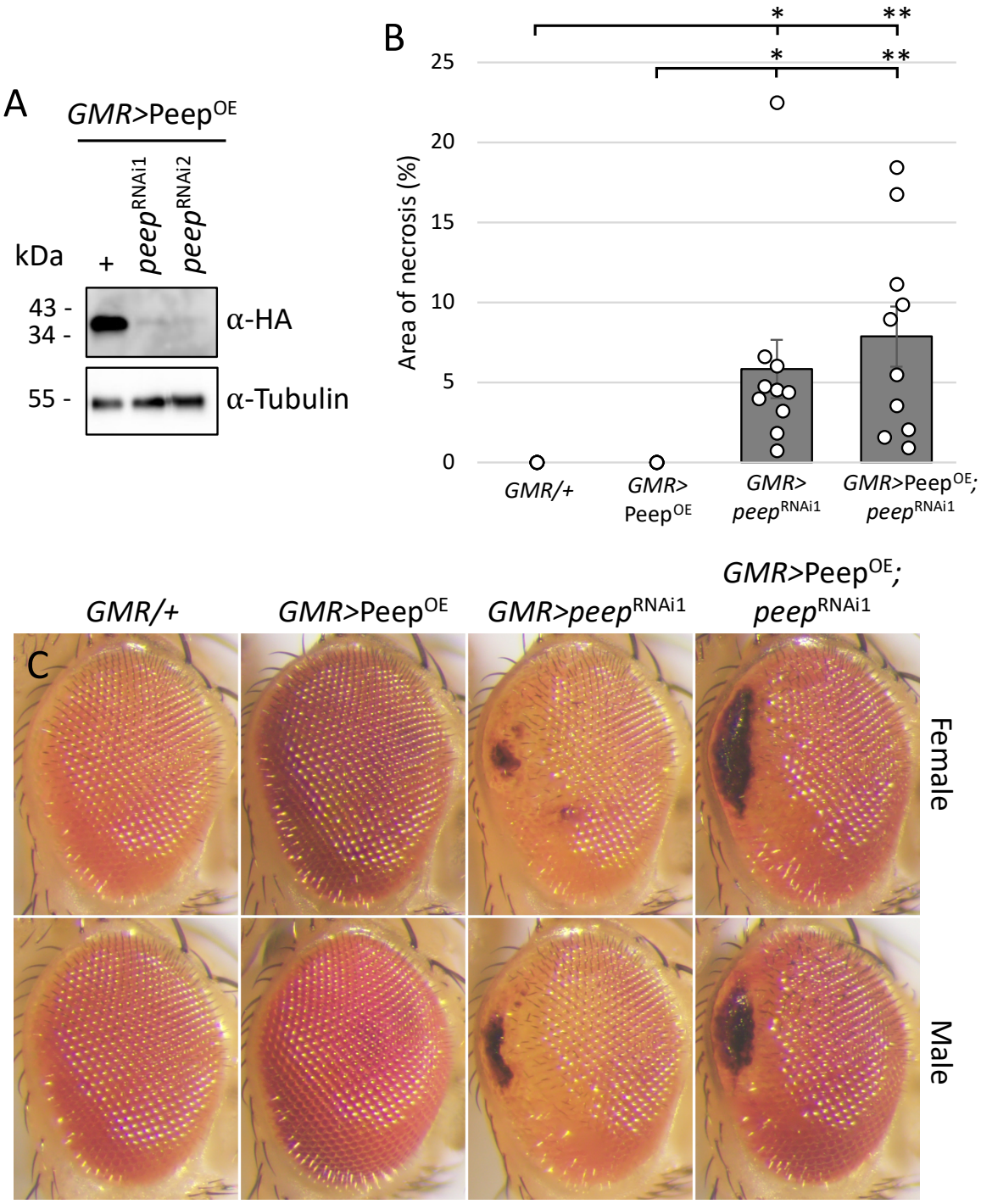

Figure 4.4. *peep*^{RNAi} efficiently targets *peep* mRNA to decrease Peep protein levels. A. Western blot showing the efficiency of *peep*^{RNAi1} and *peep*^{RNAi2} to degrade HA-tagged Peep^{OE} in the *Drosophila* eye, 30 µg protein loaded, anti-Tubulin was used as a loading control. B. Co-expression of Peep^{OE} and *peep*^{RNAi1} in the eye with *GMR-GAL4* result in a rough eye phenotype with a similar level of necrosis compared to *peep*^{RNAi1} expression alone. The area of necrosis was measured for each genotype and the percentage of the eye with necrosis was plotted to show a significant level of necrosis observed upon knockdown of Peep and no significant difference upon co-expression with Peep^{OE}. Error bars indicate mean ± SEM, n=10, (one-way ANOVA, post-hoc Tukey HSD, * = $p<0.05$, ** = $p<0.01$, *GMR-GAL4/+ ; GMR-GAL4>peep*^{RNAi1} = 0.02467, *GMR-GAL4>Peep*^{OE} *; GMR-GAL4>peep*^{RNAi1} = 0.02467, *GMR-GAL4/+ ; GMR-GAL4/Peep*^{OE}*>peep*^{RNAi1} = 0.001537, *GMR-GAL4>Peep*^{OE} *; GMR-GAL4/Peep*^{OE}*>peep*^{RNAi1} = 0.001537). C. Representative light microscopy images of the eyes quantified

for B. *GMR* = *GMR-GAL4*. *GMR/+* = Control. *GMR-GAL4* was recombined with Peep^{OE} and crossed to *peep*^{RNAi1}.

4.3 Functional analysis of the importance of Peep in survival, development, motor function, and behaviour

The Peep mutant, CG5846^{G3334} is homozygous lethal, which suggests that *peep* is an essential gene for survival, however, as this mutant remains uncharacterised, it is also possible that this fly line may contain other mutations that are important for survival. The importance of Peep in survival as well as development, motor function, and behaviour, therefore, requires further investigation.

Motor function and coordination relies on a tightly regulated series of processes and actions that are important for survival of higher-class organisms. In *Drosophila*, these movements include walking, flying, feeding, courtship, and eclosion, all of which involve a number of muscle groups and neuronal circuitries to deliver the desired responses. Motor neurons and neuropeptides are at the centre of these neuronal circuitries and are reorganised during metamorphosis to establish new neural connections throughout the different stages of development. Remodelling of neural circuitries have been well studied in the holometabolous insect *Manduca sexta*, a tobacco hornworm which proceeds through a similar lifecycle to *Drosophila* with an embryonic stage, a range of larval stages, as well as a pupal and adult stage. These studies show nervous system reorganisation in larvae prior to metamorphosis (Levine & Truman, 1982). Similar studies have been shown in the *Drosophila* larval abdomen, where early remodelling events at the neuromuscular junction result in muscle patterning through motor neuron innervation to their target muscles (Currie & Bate, 1991; Hebbar *et al.*, 2006). This circuitry and patterning was then altered again upon metamorphosis into the adult fly through a coordinated process of muscle destruction and regeneration (Kimura & Truman, 1990; Wasser *et al.*, 2007). Similar remodelling of the mushroom body occurs during pupal development (Technau & Heisenberg, 1982). The γ Kenyon cells are first to form during the early third instar larval stage where the axons bifurcate to form both a dorsal and medial projecting lobe. Immediately upon pupation the number of larval γ Kenyon cell axons drops by 40%, however the Kenyon cell bodies remain intact and regeneration and medial extension of these axons 24 hours into pupal development has been established (Armstrong *et al.*, 1998; Technau & Heisenberg, 1982).

4.3.1 Peep is required for adult survival

To initially investigate whether Peep is required for survival, the ubiquitous *arm-GAL4* driver was selected. Armadillo is a transcription factor that plays a role in cell adhesion, is an important component in wingless signalling (Orsulic & Peifer, 1996), and is a homologue of β-catenin, which is a central player of cell proliferation and differentiation (Liu *et al.*, 2022). Based on previous RNA-seq data, Armadillo is expressed highly and ubiquitously throughout all stages of development and into adulthood with the highest expression observed in the larval central nervous system and the adult brain (Krause *et al.*, 2022). A reporter assay in the adult fly was performed using the *arm-GAL4* driver which showed moderate expression in the adult brain (Legan *et al.*, 2008). Furthermore, Armadillo expression has been localised to the mushroom body lobes, calyx, and antennal lobes of the brain (Tan *et al.*, 2013) with much weaker expression in the ventral nerve cord, salivary glands, and muscles (Legan *et al.*, 2008). A previous study performed in this laboratory demonstrated the widespread expression pattern of *arm-GAL4* driven expression of CD8::GFP throughout the larval, pupal, and adult stages of life (Figure 4.5) (Hura, 2018).

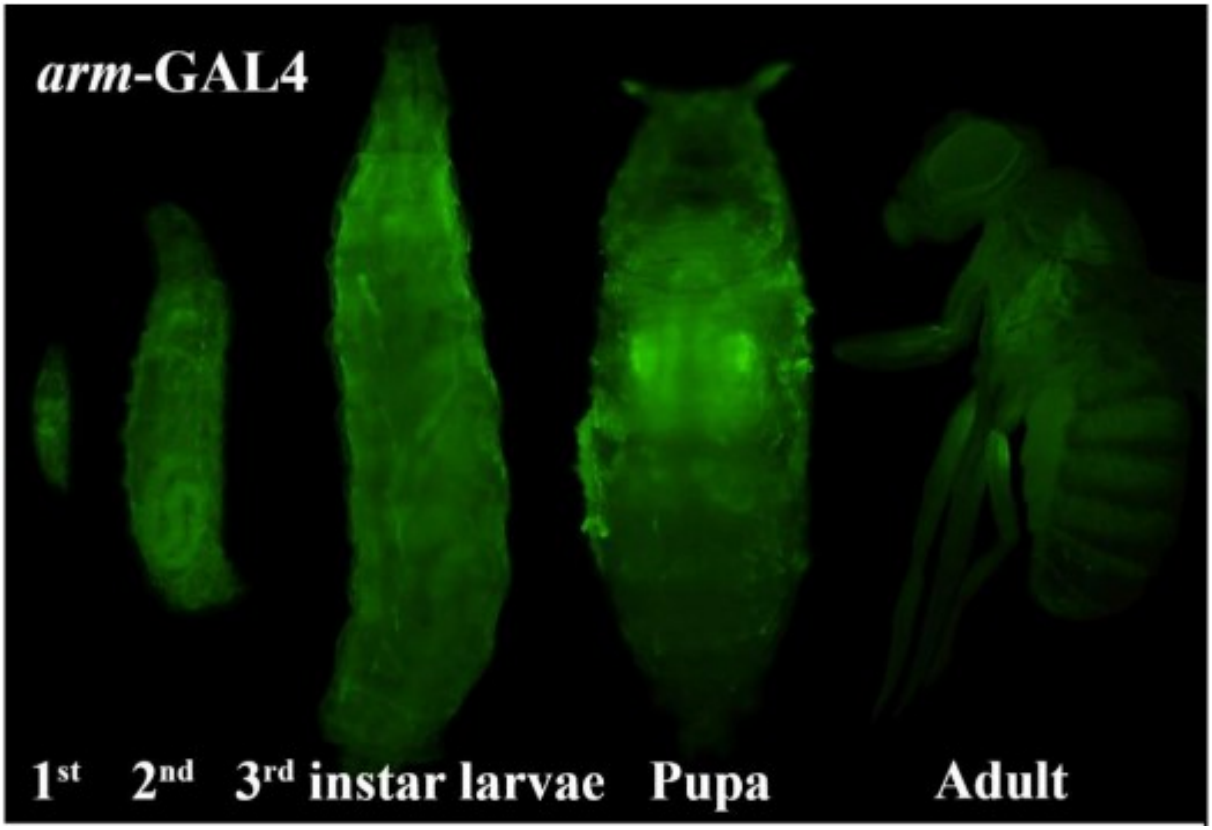

Figure 4.5. Expression pattern of the ubiquitous *arm-GAL4* driver. *arm-GAL4* crossed to *UAS-CD8::GFP* showed ubiquitous expression in all stages of development. *Image modified and reproduced with permission from Hura (2018).*

arm-GAL4 is homozygous infertile, therefore the stock was maintained over a chromosome balancer which contains multiple inversions to block crossing over and recombination events, and recessive mutations whereby only progeny heterozygous for these mutations survive (Miller *et al.*, 2019). Most balancer chromosomes also contain a dominant phenotypic marker. *arm-GAL4* is maintained over the third multiple (*TM3*) chromosome with the dominant markers *Sb* (*Stubble*) and *Ser* (*Serrate*), meaning that fertile heterozygotes will have stubble bristles and a serrated wing phenotype. *arm-GAL4* virgin females were crossed to *peep*^{RNAi1} (located on the third chromosome) (Figure 4.6) or *peep*^{RNAi2} (located on the second chromosome) in a preliminary study to determine whether ubiquitous expression of Peep is required for survival (Section 2.5.1). If *arm-GAL4* driven expression of *peep*^{RNAi} had no effect on survival, equal numbers of stubble Sb and non-Sb progeny would be expected.

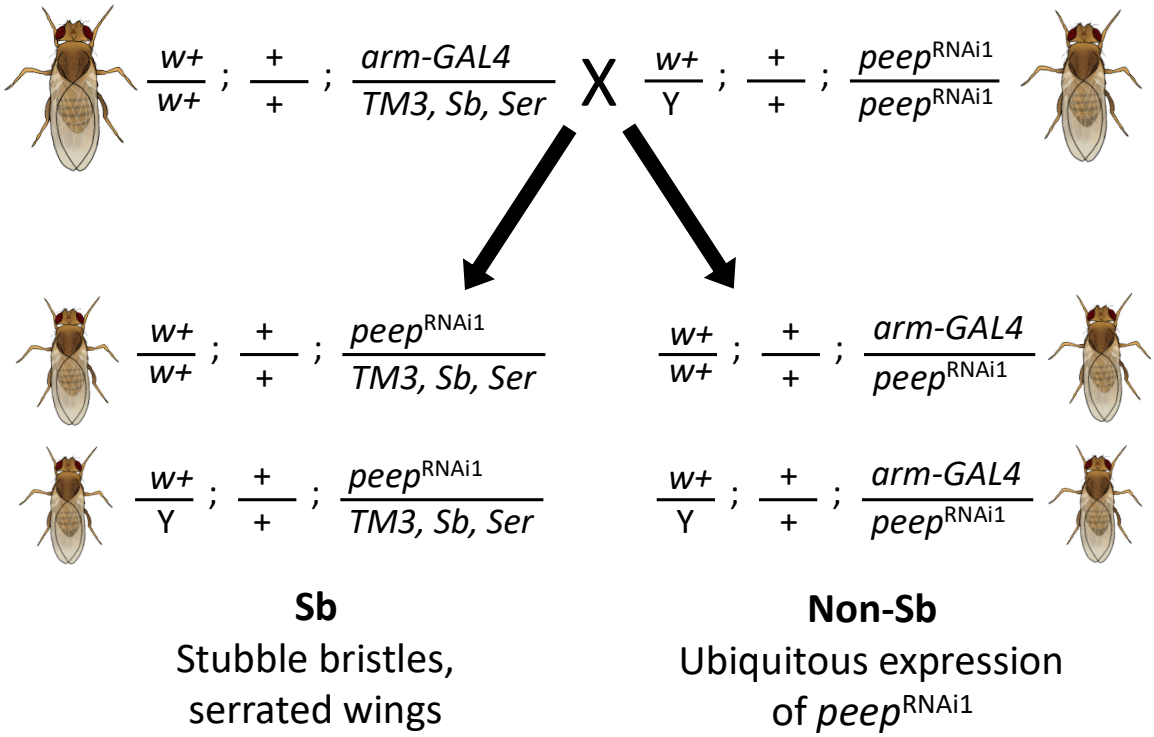

Figure 4.6. Crossing scheme for *arm-GAL4* to *peep*^{RNAi1}. *arm-GAL4* is homozygous infertile therefore is maintained as a heterozygote over the *TM3, Sb, Ser* balancer chromosome. *arm-GAL4* virgin females were crossed to males homozygous for *peep*^{RNAi1}. Half of the progeny is expected to carry one copy of the *peep*^{RNAi1} gene over the *TM3, Sb, Ser* balancer (Sb). These progeny will have stubble bristles and serrated wings, and *peep*^{RNAi1} is not expressed as the *arm-GAL4* driver is not present. The other half of the progeny is expected to carry the *arm-GAL4* driver and one copy of the *peep*^{RNAi1} gene, therefore driving expression of *peep*^{RNAi} (Non-Sb). *w+* = mini-*white, TM3* = *Third Multiple 3*, *Sb* = *Stubble*, *Ser* = *Serrated.*

A slightly higher number of progeny expressing either *peep*^{RNAi1} or *peep*^{RNAi2} (Non-Sb) emerged as compared to the Sb control, indicating that survival to adulthood was unaffected

upon ubiquitous reduction of Peep (Figure 4.7), and no gross phenotypic abnormalities were observed. Furthermore, there were no obvious differences between the number of surviving female progeny compared to male progeny.

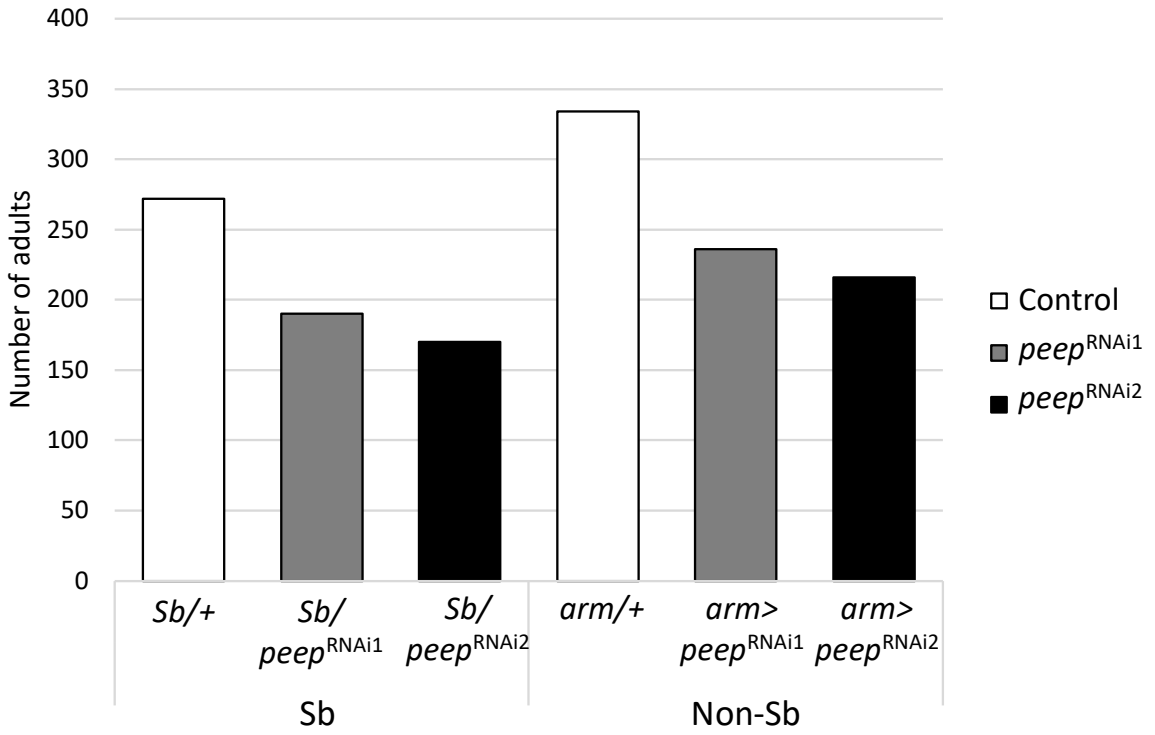

Figure 4.7. Ubiquitous expression of *peep*^{RNAi} with *arm-GAL4* does not affect adult survival. *arm-GAL4* is homozygous infertile, therefore heterozygous females carrying a single copy of *arm-GAL4* over a *TM3, Sb, Ser* balancer were crossed to *w(CS10)* (control) or *peep*^{RNAi} males in a preliminary study. Similar numbers of adult flies survived harbouring either the transgene alone (Sb) or with *arm-GAL4* driving *peep*^{RNAi} (Non-Sb). *Sb = Stubble, arm = arm-GAL4*, *arm/+* = Control.

Given that *arm-GAL4* is a relatively weak driver, this experiment was replicated with the stronger *da-GAL4* driver (Legan *et al.*, 2008). Daughterless is a nuclear transcription factor expressed in all developmental stages (Cronmiller & Cummings, 1993) specifically in the brain, where it is more highly expressed than Armadillo (Legan *et al.*, 2008), and during photoreceptor determination (Brown *et al.*, 1996). A previous study performed in this laboratory demonstrated the widespread expression pattern of *da-GAL4* driven expression of CD8::GFP throughout the larval, pupal, and adult stages of life (Figure 4.8), which was increased compared to *arm-GAL4* (Figure 4.5) (Hura, 2018).

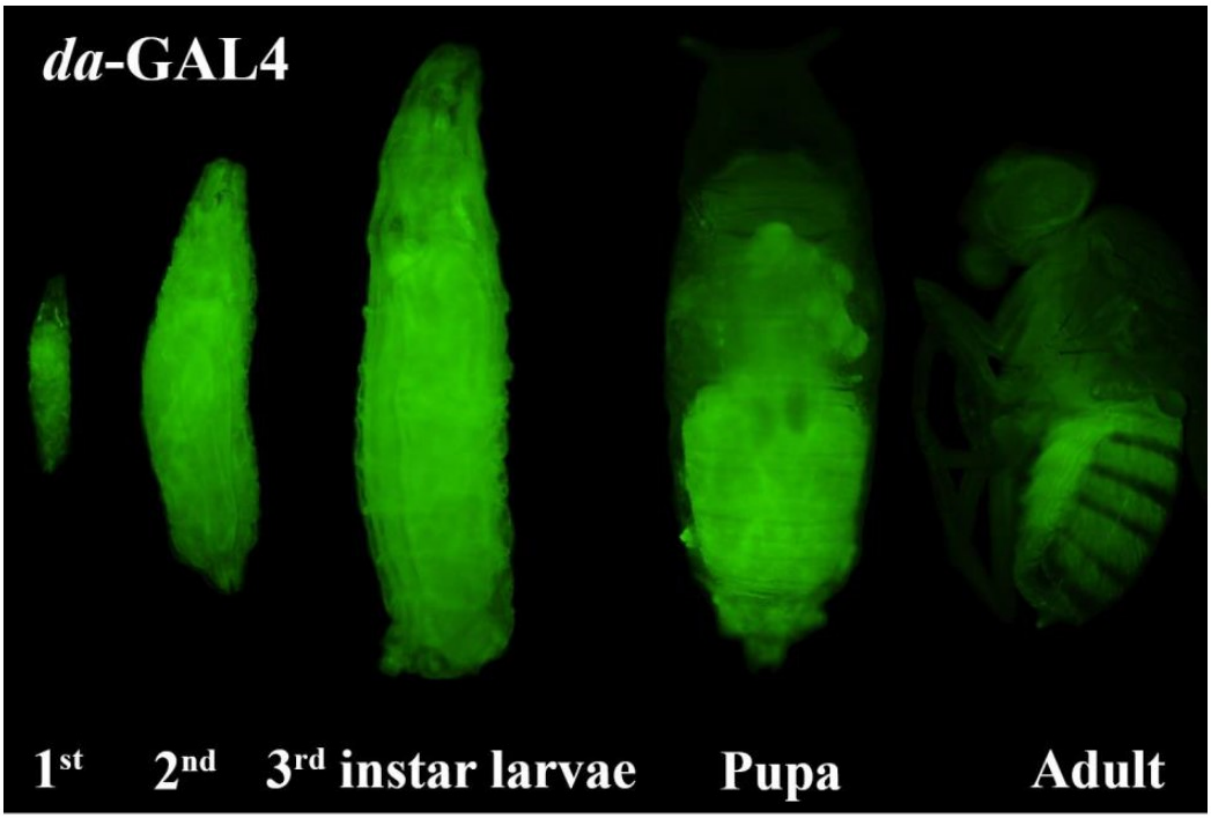

Figure 4.8. Expression pattern of the ubiquitous *da-GAL4* driver. *da-GAL4* crossed to *UAS-CD8::GFP* showed increased ubiquitous expression in all stages of development, compared to *arm-GAL4* (Figure 4.5). *Image modified and reproduced with permission from Hura (2018).*

The *da-GAL4* driver was crossed to either *UAS-Peep*^{OE} or *UAS-peep*^{RNAi} to investigate whether Peep is required for survival. Overexpression of Peep did not affect adult survival as compared to control, however upon knockdown of Peep there was a significant decrease in progeny survival, with expression of *peep*^{RNAi1} resulting in almost a complete loss of adult survival (Figure 4.9). Similar to *arm-GAL4* there were no obvious differences in the number of surviving female progeny compared to male progeny.

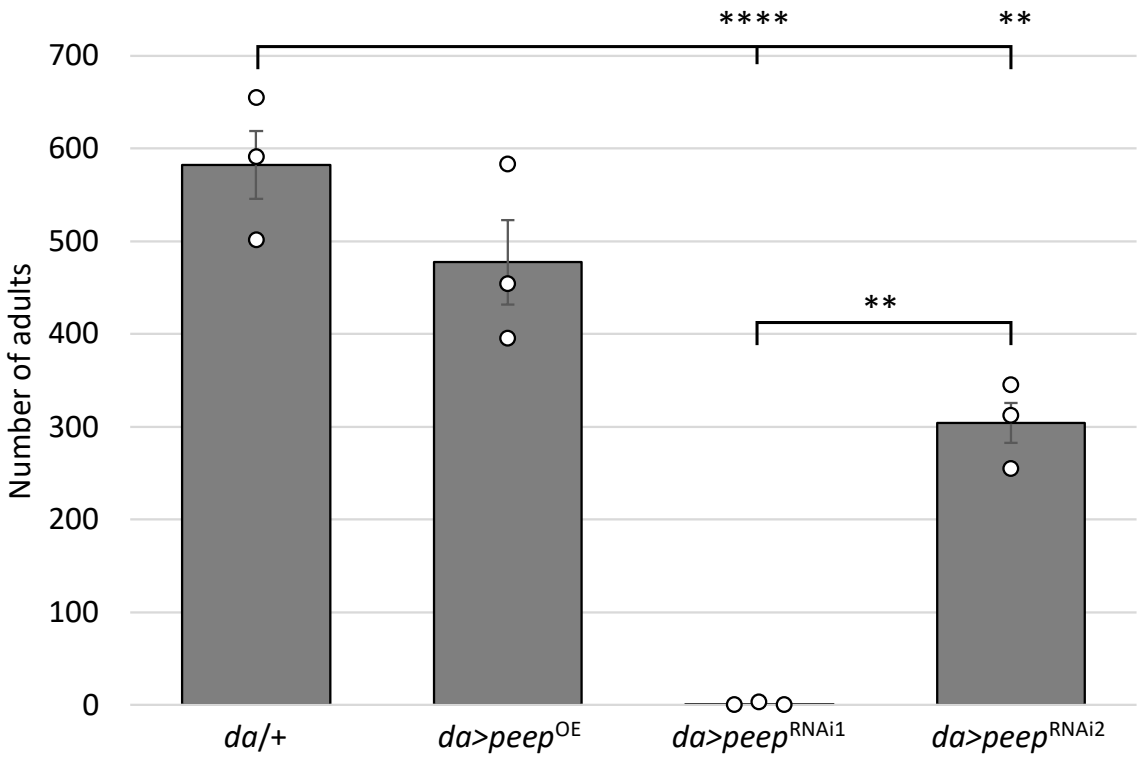

Figure 4.9. Ubiquitous expression of *peep*^{RNAi} with *da-GAL4* significantly affects adult survival. *da-GAL4* was crossed to either *UAS-Peep*^{OE} or *UAS-peep*^{RNAi} and the number of eclosed adult flies were tallied. Knockdown of Peep with *peep*^{RNAi2} resulted in a significant decrease in the number of adults, and knockdown with *peep*^{RNAi1} resulted in an almost complete loss of survival. Error bars indicate mean ± SEM, n=3, (one-way ANOVA, post-hoc Tukey HSD, $f_{(3,11)} = 44.79$, ** = $p<0.01$, **** = $p<0.0001$, *da-GAL4/+ ; da-GAL4>peep*^{RNAi1} = 0.00002, *da-GAL4/+ ; da-GAL4>peep*^{RNAi2} = 0.0037, *da-GAL4>peep*^{RNAi1} ; *da-GAL4>peep*^{RNAi2} = 0.0022). *da* = *da-GAL4*, *da/+* = Control.

To determine at which point during development reduced expression resulted in lethality (*peep*^{RNAi1}) or partial lethality (*peep*^{RNAi2}), both eclosed (empty) pupal casings and dead pupae were quantified (Section 2.5.1) and it was observed that the significant reduction in adult survival (Figure 4.10A) was a result of death at the pupal stage (Figure 4.10B, red arrowhead).

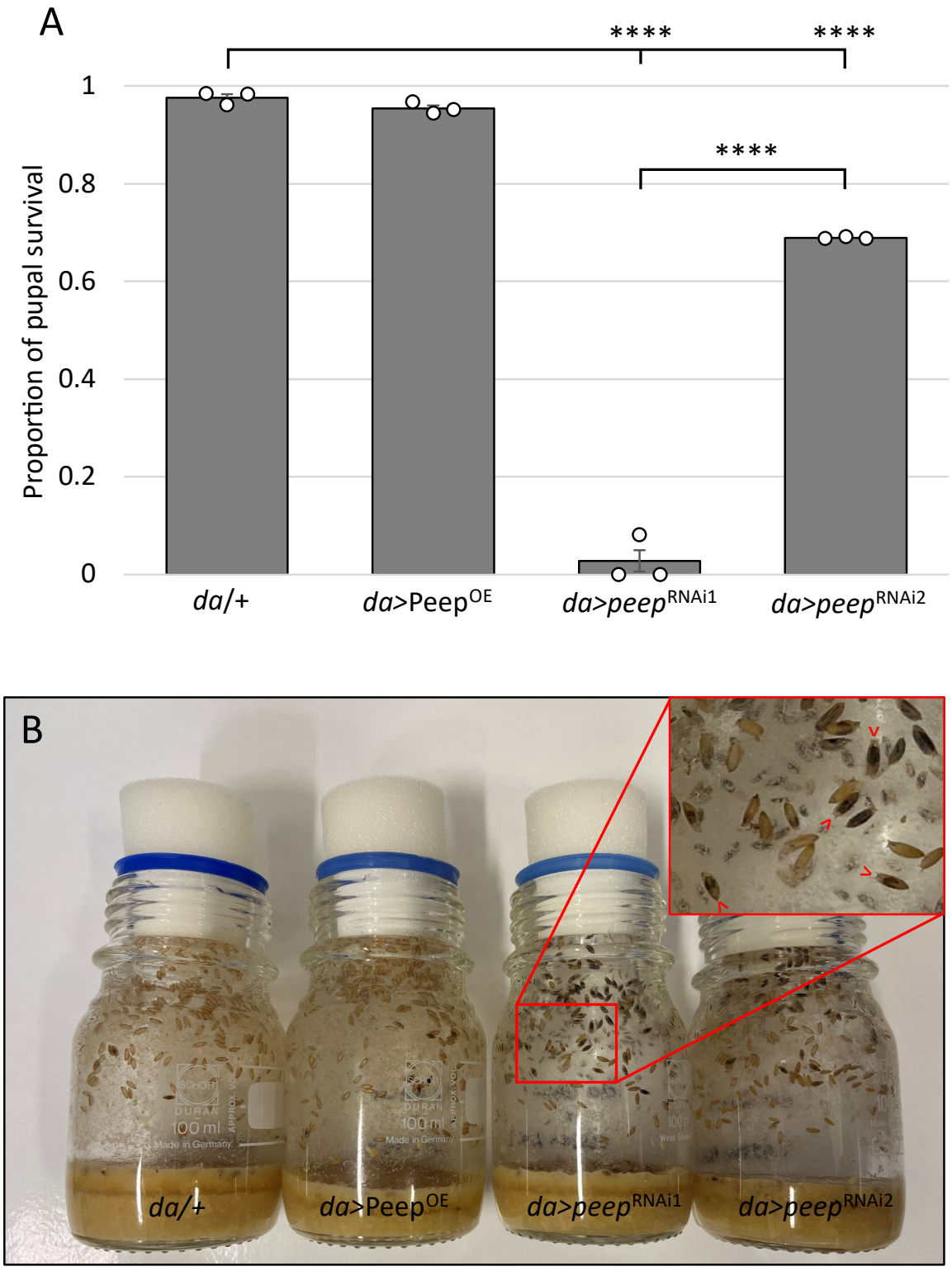

Figure 4.10. Widespread knockdown of Peep results in a significant reduction in pupal survival. A. Overexpression of Peep with the *da-GAL4* driver resulted in no difference in pupal survival, however *peep*^{RNAi1} resulted in almost complete pupal lethality, and a slightly less severe pupal lethal phenotype was observed upon *peep*^{RNAi2}, both of which had significantly reduced pupal survival compared to the *da/+* control. Error bars indicate mean ± SEM, n=3, (one-way ANOVA, post-hoc Tukey HSD, $f_{(3,11)}$ = 941.64, ***** = p<0.00001, *da-GAL4/+ ; da-GAL4>peep*^{RNAi1} = 3.33E^{-10}, *da-GAL4/+ ; da-GAL4>peep*^{RNAi2} = 3.01E^{-6}, *da-GAL4>peep*^{RNAi1} ; *da-GAL4>peep*^{RNAi2} = 7.16F^{-9}). B. Image showing pupal casings following eclosion of the vast majority of adult control progeny (left). A significant

proportion of dead pharate adults inside their pupal casings were observed following Peep knockdown (rightmost two bottles). Inset: close up of the dead pharate adults that do not have heads extended towards the anterior portion of the pupal casing (red arrowhead). *da* = *da-GAL4, da/+* = Control.

In addition, a preliminary study was performed with *tub-GAL4*, the strongest ubiquitous driver (Legan *et al.*, 2008). The *tub-GAL4* driver line is homozygous lethal and was therefore maintained as a heterozygous stock over the *TM3, Sb, Ser* balancer chromosome. As *tub-GAL4* is a weak stock, duplicate crosses were set in vials for analysis. If *tub-GAL4* driven expression of $peep^{RNAi}$ has no effect on survival, approximately equal numbers of non-Sb (ie. expressing $peep^{RNAi}$) and Sb (control) progeny would be expected, (see Figure 4.6 where *arm-GAL4* can be substituted for *tub-GAL4* on the third chromosome). Knockdown of Peep with both $peep^{RNAi}$ lines, resulted in no adult progeny and furthermore, no dead pupae or larvae were observed indicating death during embryogenesis.

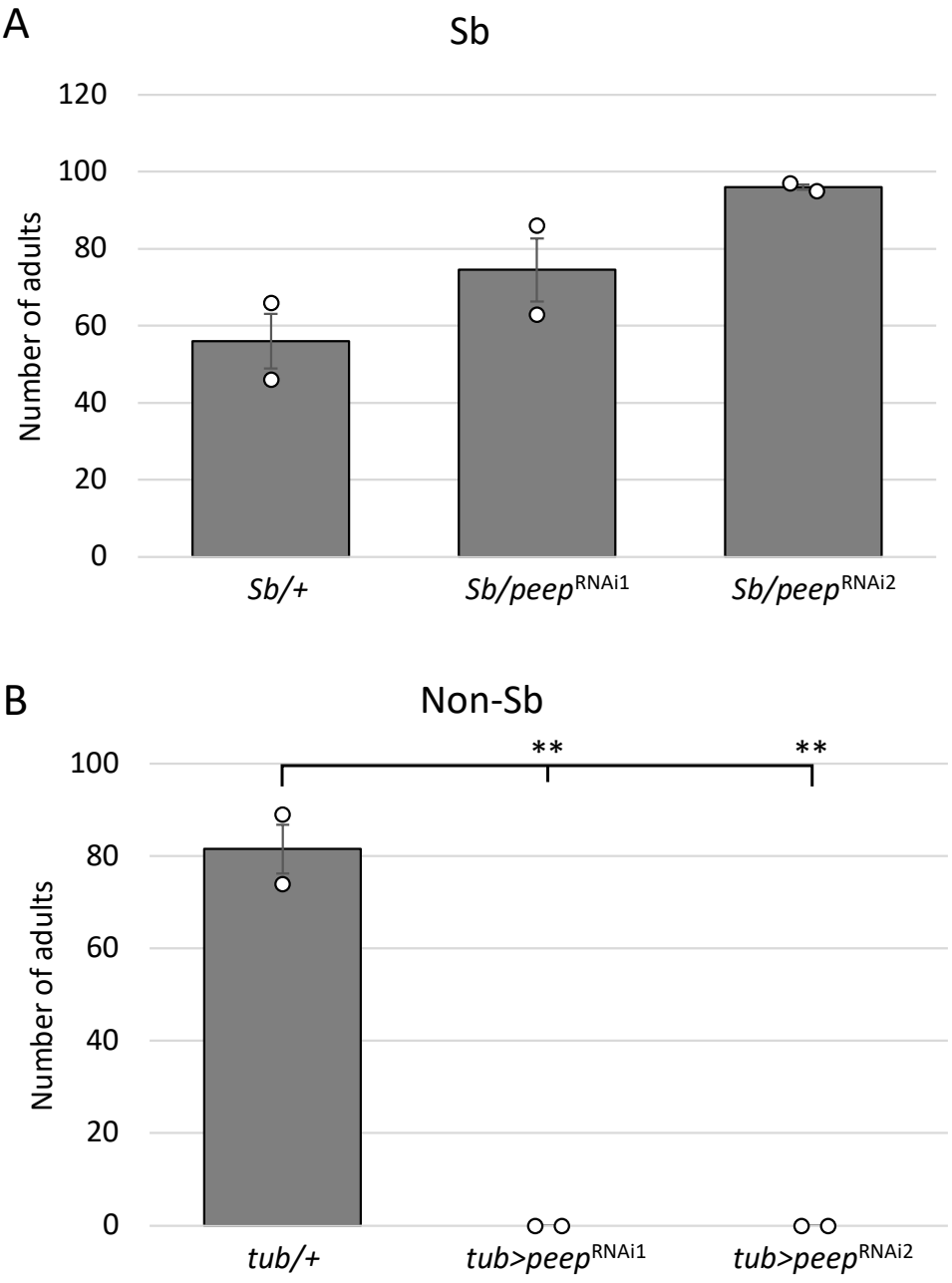

Figure 4.11. Ubiquitous expression of *peep*^{RNAi} with *tub-GAL4* significantly affects adult survival. *tub-GAL4* is homozygous lethal, therefore heterozygote females carrying a single copy of *tub-GAL4* over a *TM3, Sb, Ser* balancer were crossed to *w(CS10)* (Control) or *peep*^{RNAi} males in a preliminary study. A. The number of adults that do not harbour *tub-GAL4* (Sb). Error bars indicate mean ± SEM, n=2 (one-way ANOVA, post-hoc Tukey HSD, $f_{(2,3)} = 5.15$, $p = 0.107$). B. Knockdown of Peep with both *peep*^{RNAi} lines (Non-Sb) resulted in a no adult progeny, a result of an embryonic lethal phenotype. Error bars indicate mean ± SEM, n=2, (one-way ANOVA, post-hoc Tukey HSD, $f_{(2,3)} = 118.08$, ** = $p<0.01$, *tub-GAL4/+ ; tub-GAL4>peep*^{RNAi1} = 0.0019, *tub-GAL4/+ ; tub-GAL4>peep*^{RNAi2} = 0.0019). *Sb* = *Stubble, tub* = *tub-GAL4*, *tub/+* = Control.

These data demonstrate that Peep is an essential protein for survival. Furthermore, an advantage of an RNAi approach that does not result in a complete knockout is that some progeny survive

through to adulthood and can be utilised for further studies. As *da-GAL4* driven knockdown of Peep resulted in a significant pupal lethal phenotype, which could be due to defects in eclosion behaviour, it was of importance to utilise the survivors for further investigation into the importance of Peep in motor function (Section 4.3.2).

4.3.1.1 Expression of Peep in neurons is not required for survival

tub-GAL4, *da-GAL4*, and *arm-GAL4* all drive expression in many different cell types and since survival of eclosion requires neural function through reorganisation and development of neural circuitry as well as neuronal function specifically for motor coordinated muscle contraction, it was examined whether the reduced survival phenotype observed with both *da-GAL4* and *tub-GAL4* could be attributed to reduced expression of Peep in neurons and/or glia.

Pan-neuronal expression of $peep^{RNAi}$ was induced by either *elav-GAL4* or *nSyb-GAL4*. While both drive pan-neuronal expression, *nSyb-GAL4* drives approximately 2.5 fold higher expression in the brain than *elav-GAL4* (Hawley *et al.*, 2023). Knockdown of Peep with *nSyb-GAL4* (Figure 4.12A) or *elav-GAL4* (Figure 4.12B) did not result in a significant decrease in the total number of adult survivors. It should also be noted that expression of $peep^{RNAi2}$ with *elav-GAL4* did result in a significant decrease specifically in the number of male progeny, with an increase in female progeny (Figure 4.12C). These results show that a depletion of Peep in neurons can be tolerated and collective adult survival was unaffected.

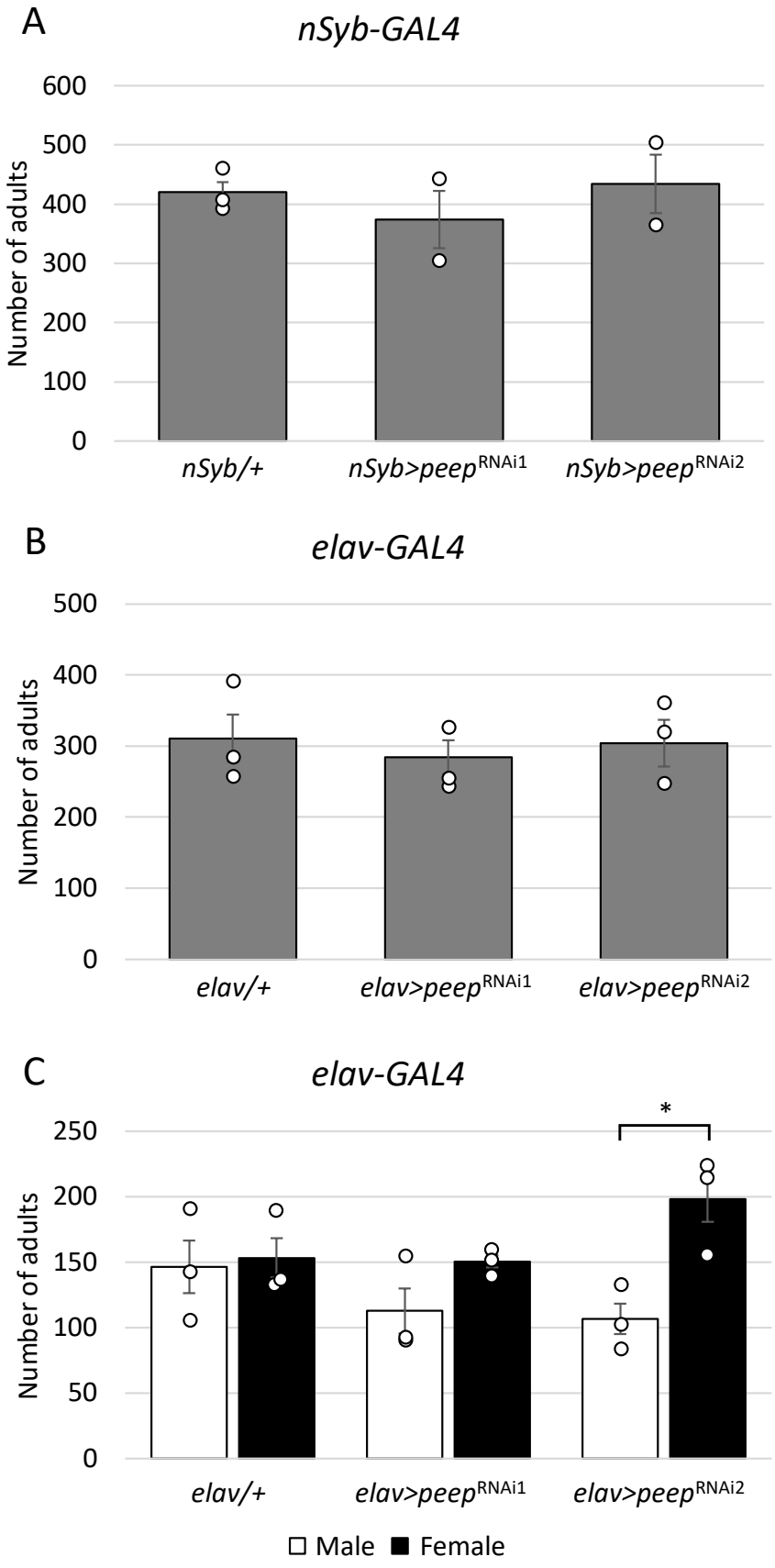

Figure 4.12. Pan-neuronal knockdown of Peep does not affect adult survival. A. *nSyb-GAL4* driven expression of *peep*^{RNAi} did not affect the total number of surviving adult progeny. Error bars indicate ±

SEM, n≥2, (one-way ANOVA, post-hoc Tukey HSD, $f_{(2,6)} = 0.38$, $p = 0.71$). B. *elav-GAL4* driven expression of *peep*^{RNAi} did not affect the total number of surviving adult progeny. Error bars indicate ± SEM, n=3, (one-way ANOVA, post-hoc Tukey HSD, $f_{(2,8)} = 0.36$, $p = 0.71$). C. *elav-GAL4* driven expression of *peep*^{RNAi2} resulted in a significant decrease in the number of male progeny compared to female progeny, indicating a mild male toxic phenotype. Error bars indicate ± SEM, n=3, (one-way ANOVA, post-hoc Tukey HSD, $f_{(5,17)} = 3.15$, * = $p<0.05$, *elav-GAL4>peep*^{RNAi2} (male) *; elav-GAL4>peep*^{RNAi2} (female) = 0.0405). *nSyb* = *nSyb-GAL4*, *nSyb/+* = Control, *elav* = *elav-GAL4*, *elav/+* = Control.

4.3.1.2 Expression of Peep in glia is required for embryonic survival

Glial cells have not been directly investigated for their role in ecdysis and adult eclosion, however, defects in glial cell function have been associated with defects in motor coordination and function, which could contribute to ecdysis and eclosion, as they play an essential role in supporting neurons, specifically motor neurons. Neuroglioblast progenitor cells generate both neurons and glia, and in a recent study it was shown that in *Drosophila*, neuroglioblasts simultaneously give rise to both leg motoneurons and the surrounding neuropil glia (Enriquez *et al.*, 2018), highlighting how closely intertwined neurons and glia are and how they may be essential in the processes of ecdysis and adult eclosion. Ensheathing glia, which have similar functions to mammalian oligodendrocytes and Schwann cells (Yildirim *et al.*, 2019), migrate to the peripheral nervous system to engulf and insulate the abdominal and thoracic motoneuron and sensory neuron axons in the *Drosophila* larvae (Matzat *et al.*, 2015). These play central roles in coordinating muscle movements in ecdysis through larval stages and may persist through to adult eclosion. Defects in glial function have been implicated in a variety of behavioural traits in the adult fly, including circadian rhythm. Period (Per) is essential in maintaining the circadian clock as it determines the length of rhythmicity. Per was found to be expressed in both neurons and glia, and glial expression was deemed sufficient for the upkeep of rhythmicity (Ewer *et al.*, 1992). As circadian rhythm plays a role in adult eclosion, it could be hypothesised that glial defects could cause deficiencies in both motor neurons and muscle connectivity as well as circadian rhythm, resulting in eclosion deficits.

With the exception of midline glia, all central nervous system derived lateral glia express the nuclear homeodomain transcription factor Repo (Halter *et al.*, 1995; Xiong *et al.*, 1994), therefore, *repo-GAL4* is an ideal driver to investigate glial function.

To determine whether the reduction of Peep in glia had an effect on survival and/or eclosion, Peep was knocked down in all glial cells with *repo-GAL4*. The *repo-GAL4* driver line is

homozygous lethal and was therefore maintained as a heterozygote over the *TM3, Sb, Ser* balancer. Similarly to *arm-GAL4* and *tub-GAL4*, if *repo-GAL4* driven expression of *peep*^{RNAi} had no effect on survival, approximately equal numbers of non-Sb (ie. expressing *peep*^{RNAi}) and Sb (control) progeny would be expected, (see Figure 4.6 where *arm-GAL4* can be substituted with *repo-GAL4* on the third chromosome). Expression of *peep*^{RNAi1} resulted in a significant reduction in adult survival, which was further exacerbated, with few surviving female flies, upon expression of *peep*^{RNAi2} (Figure 4.13).

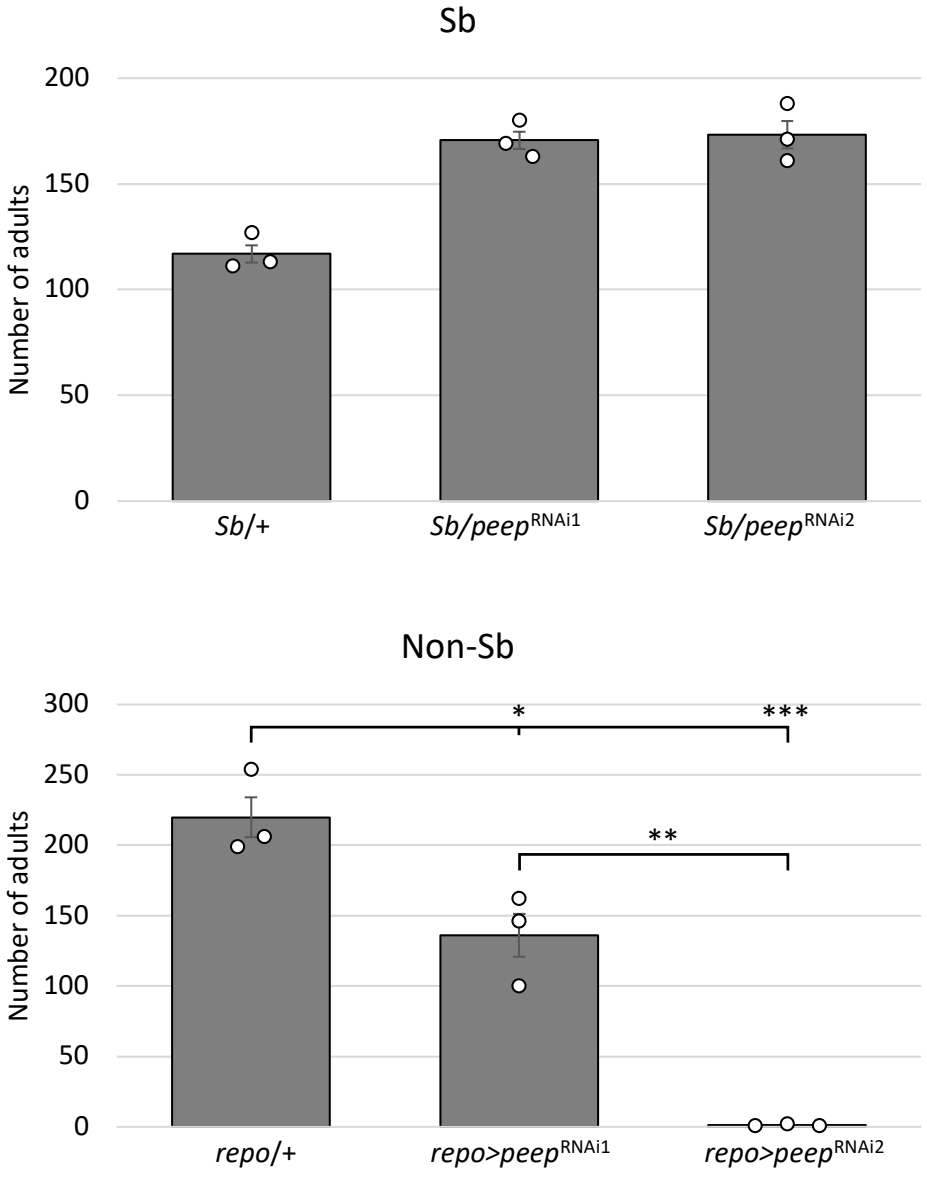

Figure 4.13. Glial specific expression of *peep*^{RNAi} results in a significant reduction in adult eclosion. The pan-glial driver *repo-GAL4* is homozygous lethal and therefore maintained as a heterozygous stock over a *TM3, Sb, Ser* balancer. The average number of progeny without *repo-GAL4* are indicated and have stubble bristles (Sb) (top graph) and the average number of progeny with *repo-GAL4* driven

expression are indicated and do not have stubble bristles (Non-Sb) (bottom graph). *repo-GAL4* driven *peep*^{RNAi1} resulted in fewer surviving adult progeny, which was exacerbated upon expression of *peep*^{RNAi2}. Bars indicate mean ± SEM, n=3, (one-way ANOVA, post-hoc Tukey HSD, $f_{(2,8)} = 56.51$, * = $p<0.05$, ** = $p<0.01$, *** = $p<0.001$, *repo-GAL4/+* ; *repo-GAL4/peep*^{RNAi1} = 0.016, *repo-GAL4/+ ; repo-GAL4/peep*^{RNAi2} = 0.00011, *repo-GAL4/peep*^{RNAi1} ; *repo-GAL4/peep*^{RNAi2} = 0.0015). *Sb = Stubble*, *repo = repo-GAL4*.

Taken together, depletion of Peep in neurons with the strong pan-neuronal *nSyb-GAL4* driver had no effect on development, eclosion, and pharate adult survival, whereas reduced expression of Peep in glia was almost entirely lethal (*peep*^{RNAi2}), demonstrating that Peep is essential in glia for survival. Unlike ubiquitous expression with *da-GAL4*, there were few dead pupae and no dead larvae as a result of knockdown with either *peep*^{RNAi} construct, indicating that glial-specific knockdown of Peep is predominantly embryonic lethal.

In summary, Peep plays an essential role in *Drosophila* survival (Table 4.1). It was of importance to note that there is a difference in knockdown efficiency between RNAi lines, when expressed with different GAL4 drivers. With *da-GAL4*, *peep*^{RNAi1} resulted almost no adult survival, whereas with *repo-GAL4*, *peep*^{RNAi2} resulted in almost no adult survival. In both instances the alternative RNAi line induced a significant decrease in survival, indicating that the phenotypes exhibited by each RNAi are the same, however, have differing levels of efficiency, depending on the tissue in which it is being expressed. As experiments to test efficacy were performed in the eye with *GMR-GAL4*, which is a strong driver (Section 4.2), in order to assess the efficiency of each GAL4-dependent RNAi knockdown, additional efficacy testing via western blot or RT-qPCR is required.

Table 4.1. Summary of *peep*^{RNAi} on adult survival

	Ubiquitous			**Pan-neuronal**		**Glial**
	arm-GAL4	***da-GAL4***	***tub-GAL4***	***elav-GAL4***	***nSyb-GAL4***	***repo-GAL4***
peep^{RNAi1}	No effect	Mostly pupal lethal	Entirely embryonic lethal	No effect	No effect	Partially embryonic lethal
peep^{RNAi2}	No effect	Partially pupal lethal	Entirely embryonic lethal	Less male progeny, more female progeny	No effect	Mostly embryonic lethal

4.3.1.3 Overexpression of Peep extends lifespan

As ubiquitous expression of *peep*^{RNAi} using the *arm-GAL4* driver resulted in viable progeny, this allowed a longevity assay to be performed to determine whether overexpression or knockdown of Peep affects a flies' lifespan. As outlined in Section 2.5.2, a total of three independent replicate crosses were generated for each genotype with 25 males and 25 females collected per replicate at one-day old. The data shown is a collective survival plot containing the data from all replicates, resulting in a starting total of 150 flies. Death was tallied every two-three days over the course of the experiment until all flies were dead. Interestingly, knockdown of Peep did not significantly impact lifespan, however increased expression of Peep resulted in enhanced longevity where over 100 flies were alive at day 80 compared to 70 flies in the control (*arm-GAL4*/+) (Figure 4.14).

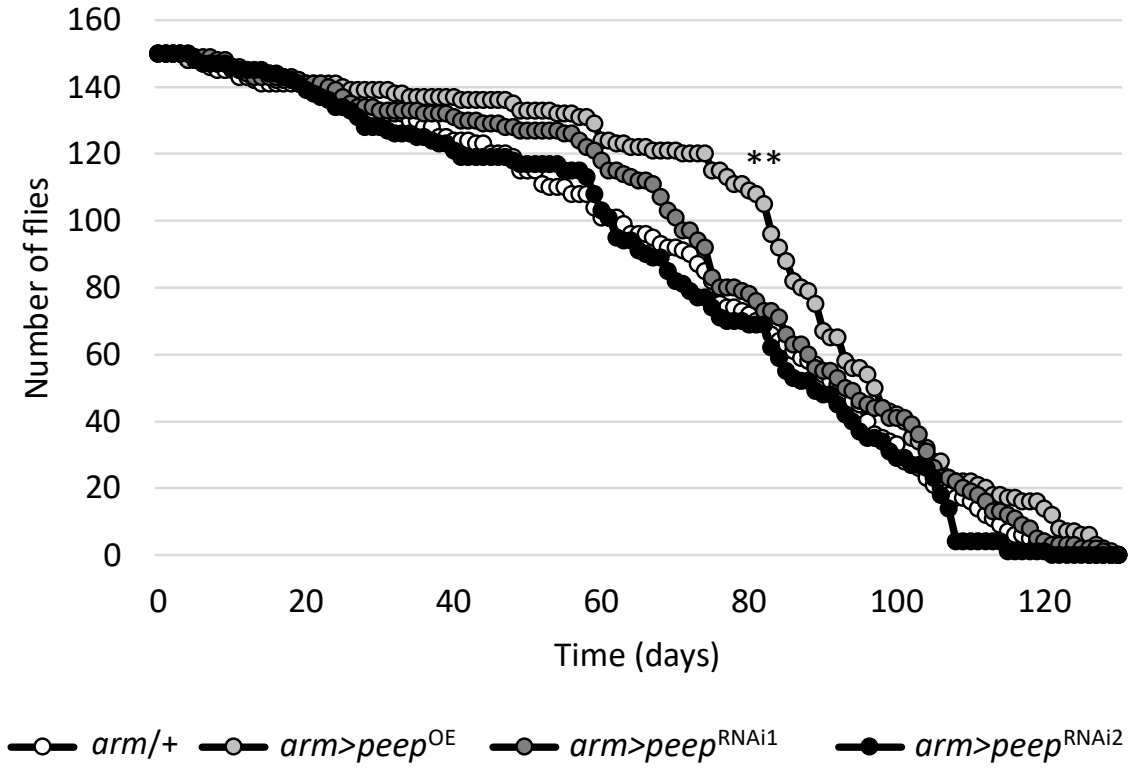

Figure 4.14. Overexpression of Peep enhances the flies lifespan. Ubiquitous knockdown of Peep with *arm-GAL4* did not affect the flies lifespan, however ubiquitous overexpression of Peep did significant enhance longevity, n=150, **(**log rank test, post-hoc Bonferrroni, ** = p<0.01, *arm-GAL4/+ ; arm-GAL4>peep*^{OE} = 0.005). *arm = arm-GAL4, arm/+* = Control.

These results show that following ubiquitous knockdown of Peep with the relatively weak *arm*-GAL4 driver, which does not result in a sufficient knockdown to result in embryonic lethality or eclosion defects (Section 4.3.1), flies have normal lifespans. Furthermore, increased expression of Peep extended the flies lifespan, further indicating a pro-survival role for Peep.

4.3.2 Peep is dispensable for adult locomotor function

Vertebrate motor function deteriorates with age and is also accelerated in diseases such as Parkinson's disease (Mazzoni *et al.*, 2012), spinocerebellar ataxia (Smeets & Verbeek, 2016), and motor neuron disease (Talbot, 2009). The locomotor function of a fly can be tested using the negative geotaxis climbing assay, as the innate response of a fly is to escape through directional movement against gravitational cues by climbing to the top of a vial (Inagaki *et al.*, 2010; Kamikouchi *et al.*, 2009; Sun *et al.*, 2009).

As described in Section 4.3.1, ubiquitous knockdown of Peep using the *da-GAL4* driver resulted in severe eclosion defects in $peep^{RNAi1}$ progeny, where insufficient flies eclosed for analysing locomotor function. Knockdown with $peep^{RNAi2}$ resulted in a 69% survival rate and escapers were able to be assessed further in a negative geotaxis assay (Section 2.5.3). The climbing ability of five-day-old flies was measured at ten intervals with a four-minute rest period between each interval. The proportion of flies that climbed to 5 cm or above were deemed to have intact climbing ability. From these results, both $Peep^{OE}$ and $peep^{RNAi2}$ maintained intact climbing ability as compared to the control (Figure 4.15), demonstrating that Peep was dispensable for normal locomotor function.

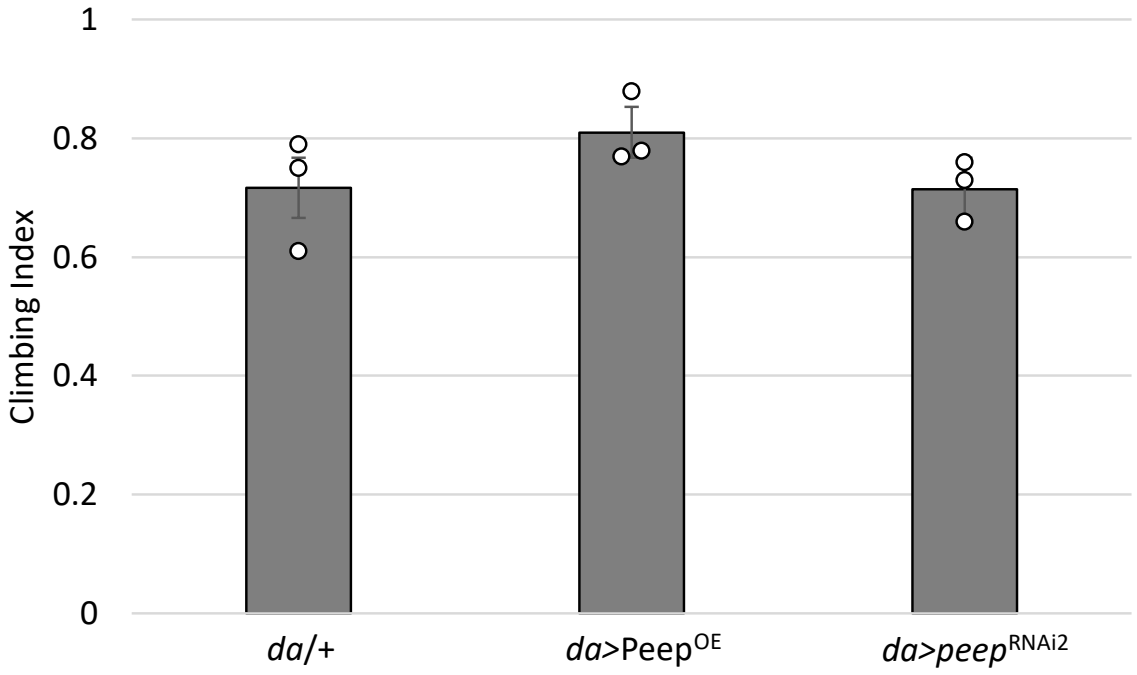

Figure 4.15. Ubiquitous knockdown of Peep does not decrease climbing proficiency. A negative geotaxis climbing assay to assess motor coordination was performed on flies with *da-GAL4* driven Peep^{OE} and *peep*^{RNAi2}. Error bars indicate mean ± SEM, n=3 independent crosses, 10 flies per cross, (One-way ANOVA, post-hoc Tukey HSD, $f_{(2,8)} = 1.71$, $p = 0.26$). *da* = *da-GAL4*, *da/+* = Control.

4.3.3 Peep is required for mushroom body development

The importance of mushroom body development has been described in Section 1.3.1.1, detailing how normal axonal projection is important for learning and memory acquisition (McBride *et al.*, 1999). It was determined in Section 3.2.1 that the pan-neuronal knockdown of Peep with *elav-GAL4* resulted in modest mushroom body defects (Table 3.4) with less than 15% of total brains having β lobe fusion (Figure 3.3). Additional mushroom body abnormalities were observed in a small proportion of brains, including β lobe shortening and axon guidance defects. These defects induced by pan-neuronal *elav-GAL4* were minimal, however *elav-GAL4* is a relatively weak driver (Hawley *et al.*, 2023). Dicer-2, which cleaves long inverted repeat hairpins (Elbashir *et al.*, 2001; Lee *et al.*, 2004; Schwarz *et al.*, 2003), is moderately expressed in neurons (Li *et al.*, 2022), therefore, the efficacy of Peep knockdown was enhanced upon pan-neuronal overexpression of Dicer-2.

4.3.3.1 Increased efficacy of pan-neuronal Peep knockdown results in more severe mushroom body defects

The transgenic lines imported from VDRC for RNAi knockdown contain long inverted repeat hairpin RNAs designed to target *peep* mRNA. The UAS/GAL4 bipartite system allows for tissue specific expression of these RNAi fragments which are enzymatically cleaved by Dicer-2 to generate siRNAs (Elbashir *et al.*, 2001; Lee *et al.*, 2004; Schwarz *et al.*, 2003) (discussed in Section 1.3.4.3). It has previously been shown that co-expression of Dicer-2 enhances the potency of the RNAi (Dietzl *et al.*, 2007), therefore, to determine whether a more efficient knockdown increases the mushroom body defects induced by $peep^{RNAi}$, Dicer-2 was overexpressed. *elav-GAL4*;Dicer-2 virgin females were crossed to males carrying either of the $peep^{RNAi}$ constructs, followed by immunohistochemistry using anti-FasII to highlight the mushroom body lobes for quantification (Section 2.2.4). Pan-neuronal overexpression of Dicer-2 alone did not disrupt mushroom body development, and the total proportion of mushroom body defects was increased when Dicer-2 was co-expressed with each $peep^{RNAi}$ (Figure 4.16). This increase in defects was predominantly attributed to an increase in β lobe fusion (Table 4.2), with some instances of short or missing α or β lobes. Together these data demonstrate that Peep is required in neurons for normal mushroom body axon elongation and termination.

Table 4.2. Overexpression of Dicer-2 increases mushroom body defects induced by knockdown of Peep

Genotype	*elav*> $peep^{RNAi1}$	*elav*> $peep^{RNAi2}$	*elav*>Dicer-2; $peep^{RNAi1}$	*elav*>Dicer-2/ $peep^{RNAi2}$
Short α lobe (%)	-	-	5	5
Short β lobe (%)	3.7	-	5	-
Missing α lobe (%)	-	-	5	-
Missing β lobe (%)	-	-	10	-
Guidance (%)	3.7	2.9	5	-
Total β lobe fusion (%)	10	5.9	20	25
No defects (%)	81	91	60	70
n	27	34	20	20

elav = elav-GAL4.

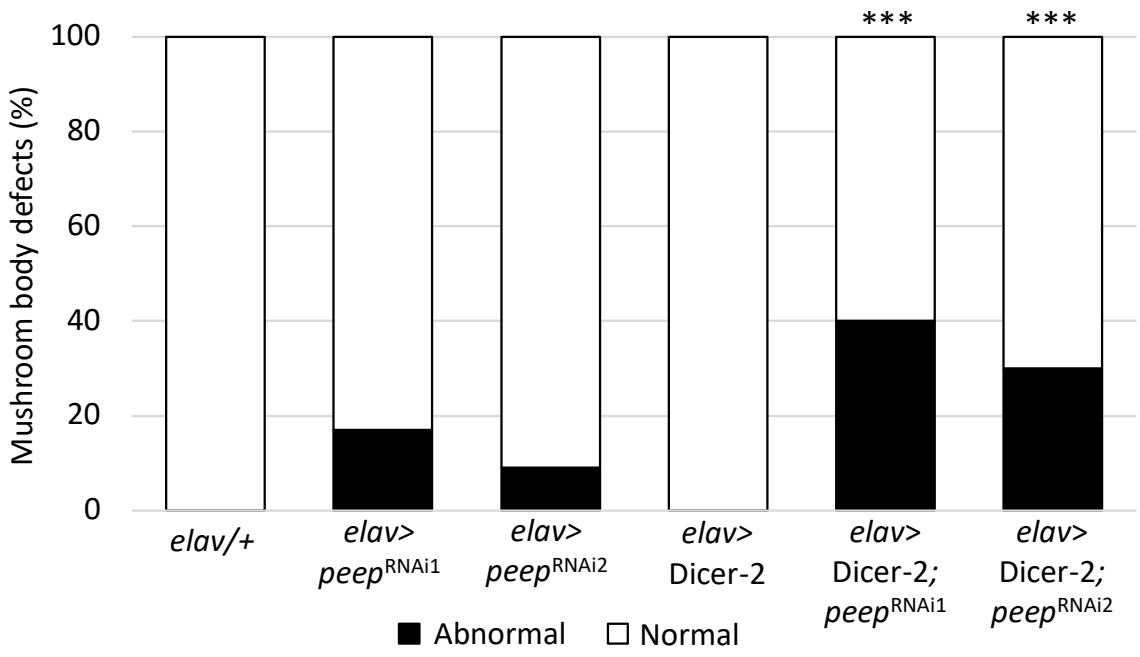

Figure 4.16. Percentage of brains displaying mushroom body defects. Pan-neuronal overexpression of Dicer-2 enhanced *peep*^{RNAi} efficiency which significantly increased the proportion of mushroom body defects, n≥19, (one-tailed Fisher's exact test- *** = p<0.001- *elav-GAL4>peep*^{RNAi1} ; *elav-GAL4;Dicer-2>peep*^{RNAi1} = 0.0003, *elav-GAL4>peep*^{RNAi2} ; *elav-GAL4;Dicer-2>peep*^{RNAi2} = 0.0001). *elav* = *elav-GAL4*, *elav/+* = Control, *elav-GAL4>*Dicer-2 = Dicer-2 control.

4.3.3.2 Reduced expression of Peep in glia results in severe mushroom body defects

Given that Peep is required in neurons for normal mushroom body development, and that expression of Peep in glia is important for overall survival, the role of glial-specific Peep in mushroom body development was also assessed. As there were a small number of adult survivors following glial-specific knockdown of Peep (Section 4.3.1.2), a preliminary immunohistochemistry study on brains isolated from these adults was performed. Brains were stained with either an anti-repo antibody to investigate differences in the number and distribution of glia in the brain, or with anti-brp to analyse defects to the structure of the brain (Section 2.2.4). Upon both overexpression and knockdown of Peep, a qualitative assessment of the brains showed no obvious differences in the number of glial cells observed.

These glia were localised to the external surface of the brain which were predicted to be surface glia, and also throughout the cortex region which were predicted to be cortex glia (further discussed in Section 1.3.1.2). The only point of interest was that the single brain that was isolated and imaged from *repo-GAL4* driven *peep*^{RNAi2} was smaller in overall brain volume

compared to the control, which could be attributed to a loss of structural integrity, as the brain was fragile, tacky, and easy to tear during the dissection process (Figure 4.17).

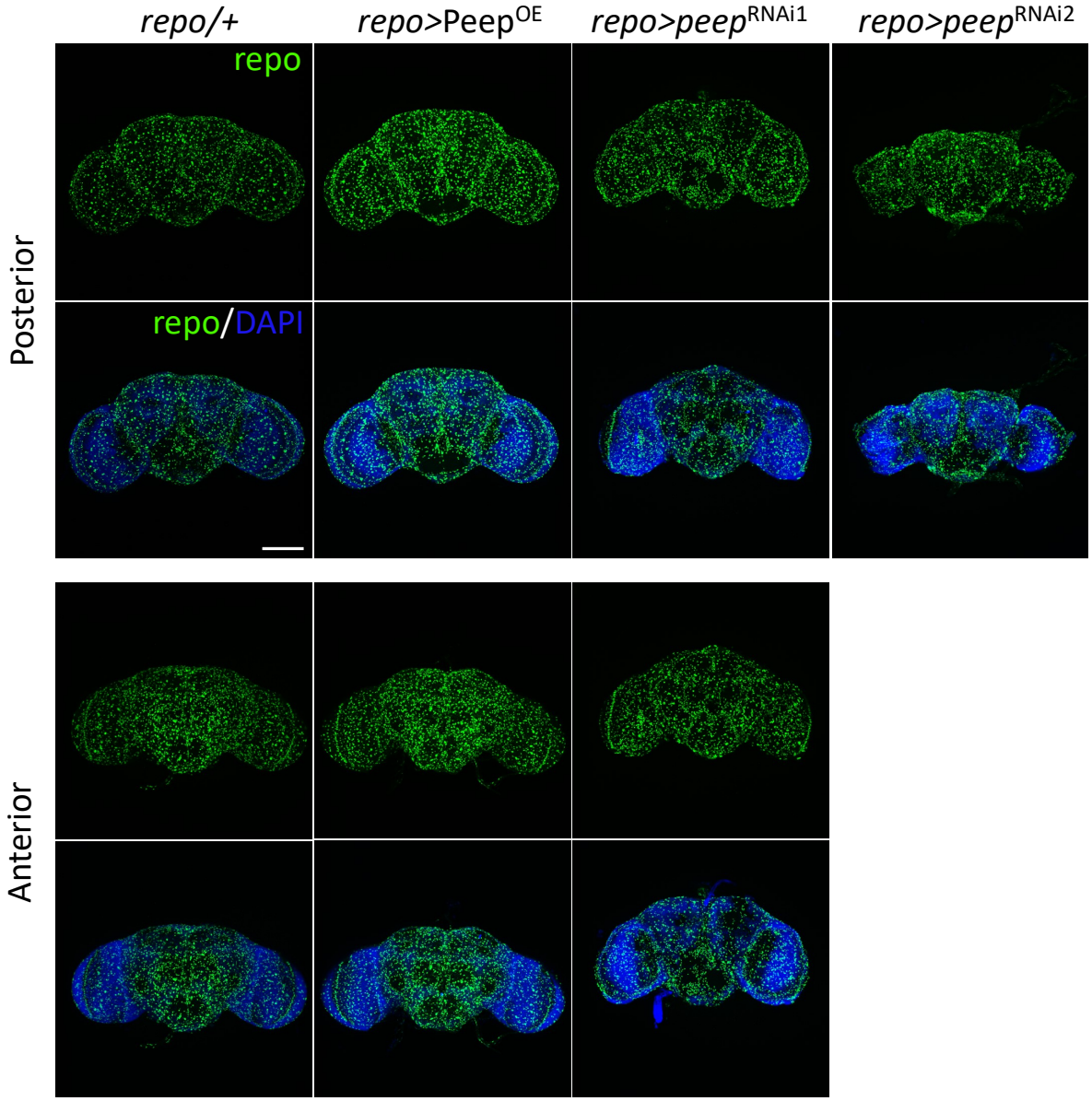

Figure 4.17. The distribution of glia in the brain remained unchanged upon *repo-GAL4* driven *peep*^{RNAi}. Both overexpression and knockdown of Peep in glia resulted in no obvious alterations to the distribution of glial cells, identified by anti-repo staining (green) in the posterior (top panels) or anterior (bottom panels) of the adult brain. Brains were counterstained with DAPI (blue) to highlight the structure of the brain and analyse brain volume. A single *peep*^{RNAi2} brain was isolated, therefore an anterior brain was unable to be imaged, however the posterior-imaged brain appeared to be smaller in brain volume. Images taken using 20x objective lens, 1 µm sections, scale bar = 100 µm. *repo* = *repo-GAL4*, *repo/+* = Control.

Anti-brp highlights the synaptic neuropil, which includes the axonal mushroom body projections. No overall gross structural brain defects were observed in either the posterior

(Figure 4.18A) or anterior (Figure 4.18B) maximum projections. However, analysis of the optical sections through the medially projecting β lobes showed that knockdown of Peep resulted in 100% severe β lobe fusion in the five brains analysed (Figure 4.18C, white arrowhead, Figure 4.18 insets C', C'' white arrowhead). These results show that Peep expression in glia is required for embryonic survival and that any adult escapers display severe defects in mushroom body development, demonstrating the requirement of glia, and Peep expression in glia for neurodevelopment and survival, both of which warrants further investigation.

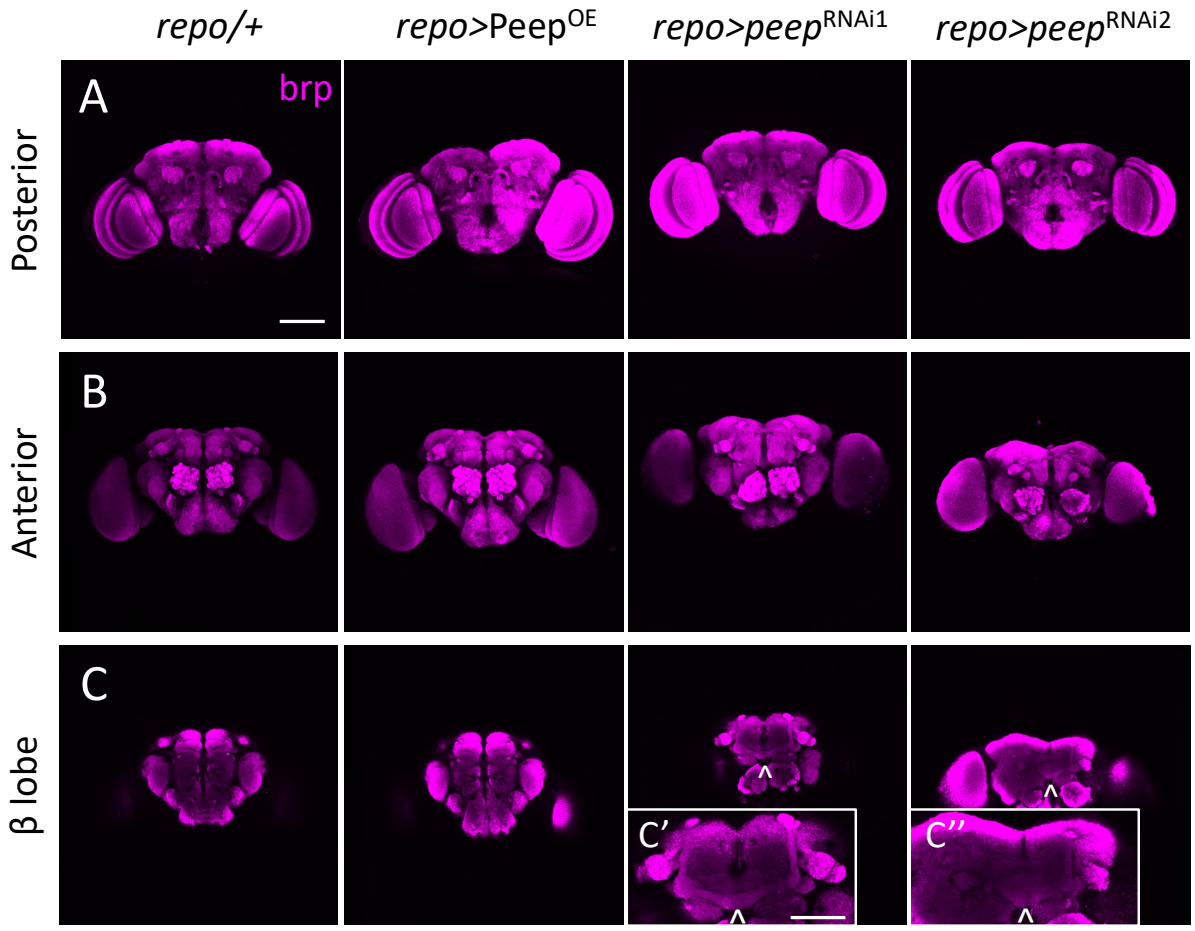

Figure 4.18. Pan-glial reduction of Peep results in a severe β lobe fusion defect. Using an antibody that highlights the synaptic neuropil (anti-brp), the structure of the dissected adult brain can be analysed. Upon depletion of Peep there were no gross morphological defects observed A. through the posterior of the brain, or B. to the overall structure of the anterior of the brain, aside from C. overextension and fusion of the β lobes (white arrowhead), was normal. C', C'' insets display a magnified view of the mushroom body, highlighting the fused β lobes (white arrowhead). Images are maximum projections through the whole brain and isolated sections (C) using the 20x objective lens, Zoom 1.25x, 1 µm sections, scale bar = 100 µm. Insets are cropped, magnified projections of the mushroom body, scale bar = 50 µm. *repo* = *repo-GAL4*, *repo/+* = Control.

4.3.4 Peep is not required for courtship learning or memory

Knockdown of Peep, similarly to overexpression of HDAC4, knockdown of Ankyrin2, and mutation of Moesin, all result in significant mushroom body defects, which is an important structure for learning and memory formation (McBride *et al.*, 1999). Overexpression of HDAC4, knockdown of Ankryin2, and mutation of Moesin all also affect long-term courtship memory formation when expressed in the adult brain (Fitzsimons *et al.*, 2013; Freymuth & Fitzsimons, 2017; Wilson *et al.*, 2023), it was therefore hypothesised that Peep may also play a role in learning and/or memory processes. In order to assess whether Peep is required for learning or memory, the courtship suppression assay was employed. This involves a classical conditioning process whereby a male fly learns and remembers experience-dependent rejection behaviours to suppress efforts to mate with a non-receptive female. Male courtship behaviour involves a distinct set of ritualistic behaviours performed to attract a mate and result in successful breeding, further discussed in Section 1.3.3.1 (Figure 1.7). The type of courtship behaviour and memory tested in this present study involved the male-specific cVA pheromone. Pairing olfactory processing of cVA with female rejection behaviour by an unreceptive, mated female to a male's courtship advances post-copulation by another male, results in suppression of male courtship further described in Section 1.3.3.1.

Mushroom body ablation has been shown to impair both short-term and long-term courtship memory (McBride *et al.*, 1999), therefore, to avoid developmental mushroom body defects induced by *peep*^{RNAi} (Section 3.2.1), the TARGET system was employed to restrict pan-neuronal Peep knockdown to the adult brain. The TARGET system allows for temporal control of gene expression (McGuire *et al.*, 2004) and was further described in Section 1.3.4.2. All fly lines used for courtship behaviour testing were outcrossed for five generations into the *w(CS10)* genetic background. Virgin females harbouring the *elav-GAL4* driver and *tubP-GAL80*^{ts} (*elav-GAL80*^{ts}) were crossed to *UAS-peep*^{RNAi} males. To control for learning and memory defects attributed to GAL80^{ts} and GAL4 expression, a control cross was set between *elav-GAL80*^{ts} virgin females and CS (Control) males. To control for learning and memory defects induced by the presence of *peep*^{RNAi}, virgin CS females were crossed to *UAS-peep*^{RNAi} males. All flies were raised at 19°C (McGuire *et al.*, 2004) and virgin male progeny to be trained and/or tested were immediately housed, following eclosion, in separate vials containing standard fly media for up to four days before being transferred to 30°C for 72-hours to induce transgene expression in the adult brain (Section 2.7).

4.3.4.1 Courtship activity and learning remained intact following adult-specific knockdown of Peep

Following 72-hours of *peep*^{RNAi} induction at 30°C, courtship suppression activity and learning was assayed. A single mated wild-type female was placed with each male to be tested (Section 2.7.1) and the first (pre-training) and final (post-training) 10 minutes of the hour were analysed for the proportion of time the male displayed any courtship behaviours previously described in Section 1.3.3.1 (Figure 1.7). A male with intact learning would court the unreceptive female for less time during the final post-training 10-minutes of the hour based on his learning of courtship rejection behaviours and olfactory processing of cVA. Courtship activity itself was first analysed because if Peep altered courtship behaviours, the courtship suppression assay would not be appropriate to measure learning and memory, as any defects could be attributed to alterations to courtship ability. There were no significant differences in courtship activity during pre-training across genotypes (Figure 4.19A), indicating that Peep is dispensable for courtship activity.

To assess courtship learning capabilities, the proportion of time the male spent performing courtship behaviours toward the mated female during the final (post-training) 10-minutes was compared to the proportion of time the male spent courting during the first (pre-training) 10-minutes. A learning index of zero would indicate no learning (ie. males did not reduce courtship activity during post-training compared to pre-training), and the higher the index, the better the male learnt to associate cVA with failure to mate and thus reduced his courtship efforts (Section 2.7.2). There were no significant differences in courtship learning following adult-induced Peep knockdown (Figure 4.19B), indicating that Peep is also dispensable for learning of cVA-dependent courtship suppression.

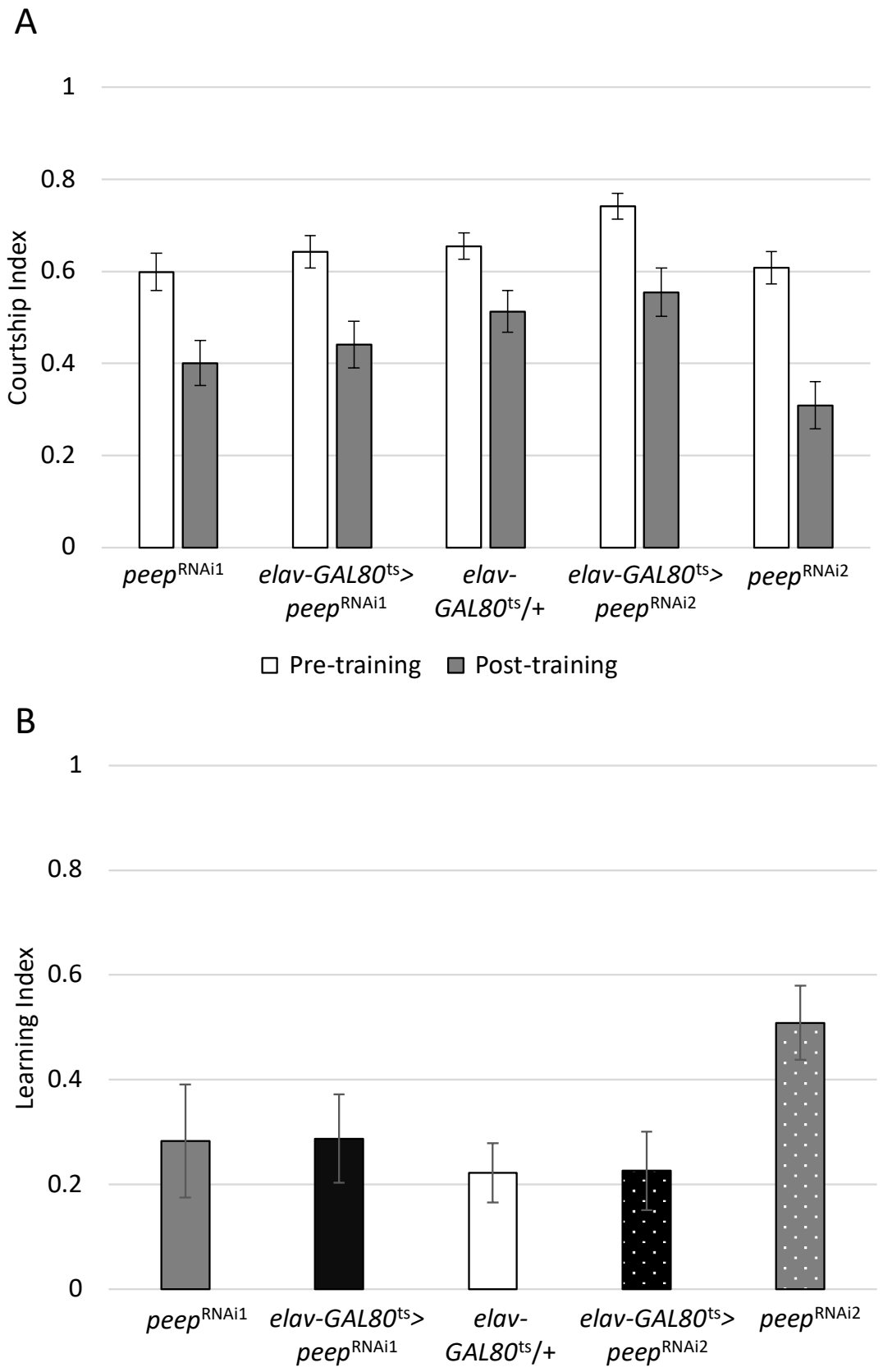

Figure 4.19. Courtship activity and learning remain intact following adult-induced knockdown of Peep. A. Knockdown of Peep in the adult brain did not impair courtship activity. Error bars indicate mean ± SEM, n≥19, (one-way ANOVA, post-hoc Tukey HSD, $f_{(9,197)} = 8.36$. No significant difference on arcsine-transformed data between both controls; transgene control (*peep*^{RNAi1} or *peep*^{RNAi2}), and driver

control (*elav-GAL80*^{ts}/+), and the driver-induced transgene knockdown (*elav-GAL80*^{ts}>*peep*^{RNAi1} or *elav-GAL80*^{ts}>*peep*^{RNAi2})). B. Knockdown of Peep in the adult brain also did not impair learning of cVA-dependent courtship suppression. Error bars indicate mean ± SEM, n≥19, (one-way ANOVA, post-hoc Tukey HSD, $f_{(4,98)} = 1.7$, $p = 0.157$. No significant difference on arcsine-transformed data between both controls; transgene control (*peep*^{RNAi1} or *peep*^{RNAi2}), and driver control (*elav-GAL80*^{ts}/+), and the driver-induced transgene knockdown (*elav-GAL80*^{ts}>*peep*^{RNAi1} or *elav-GAL80*^{ts}>*peep*^{RNAi2})). *elav-GAL80*^{ts} = *elav-GAL4;tub-GAL80*^{ts}.

4.3.4.2 Short-term and long-term courtship memory remained intact following adult-specific knockdown of Peep

Following 72-hours of *peep*^{RNAi} induction, both short-term and long-term courtship training was performed (Section 2.7.3). To examine memory, two groups of flies were tested, one group were trained, while the other group remained naïve (sham). For training, a mated wild-type female and a male of the genotype to be tested were transferred and housed in a training chamber at 30°C for one-hour for STM or seven hours for LTM. Simultaneously, sham males were housed alone in a training chamber, under identical conditions. For STM testing, following one-hour of training, the males were immediately removed from the training chamber and transferred into a testing chamber containing a new freshly mated wild-type female, and courtship behaviour was analysed over a 10-minute period. For LTM testing, females were removed and discarded, and all males were incubated at 30°C overnight in the training chamber. After 24 hours, each male was placed with a new freshly mated wild-type female in a testing chamber and courtship activity was measured over a 10-minute period. The courtship behaviour of sham males should be similar to that of males pre-training in the learning assay (Section 4.3.4.1), whereas a trained male with intact short-term and/or long-term memory would reduce his courtship behaviour due to experience-dependent learning and memory. A memory index was calculated by comparing the proportion of time each trained male spent courting verses the proportion of time each sham male spent courting. A low memory index score of zero indicates impaired memory that is no better than that of a sham male, whereas a memory index closer to one indicates intact memory acquisition. Adult-specific Peep knockdown did not significantly impair short-term (Figure 4.20A) or long-term courtship memory (Figure 4.20B).

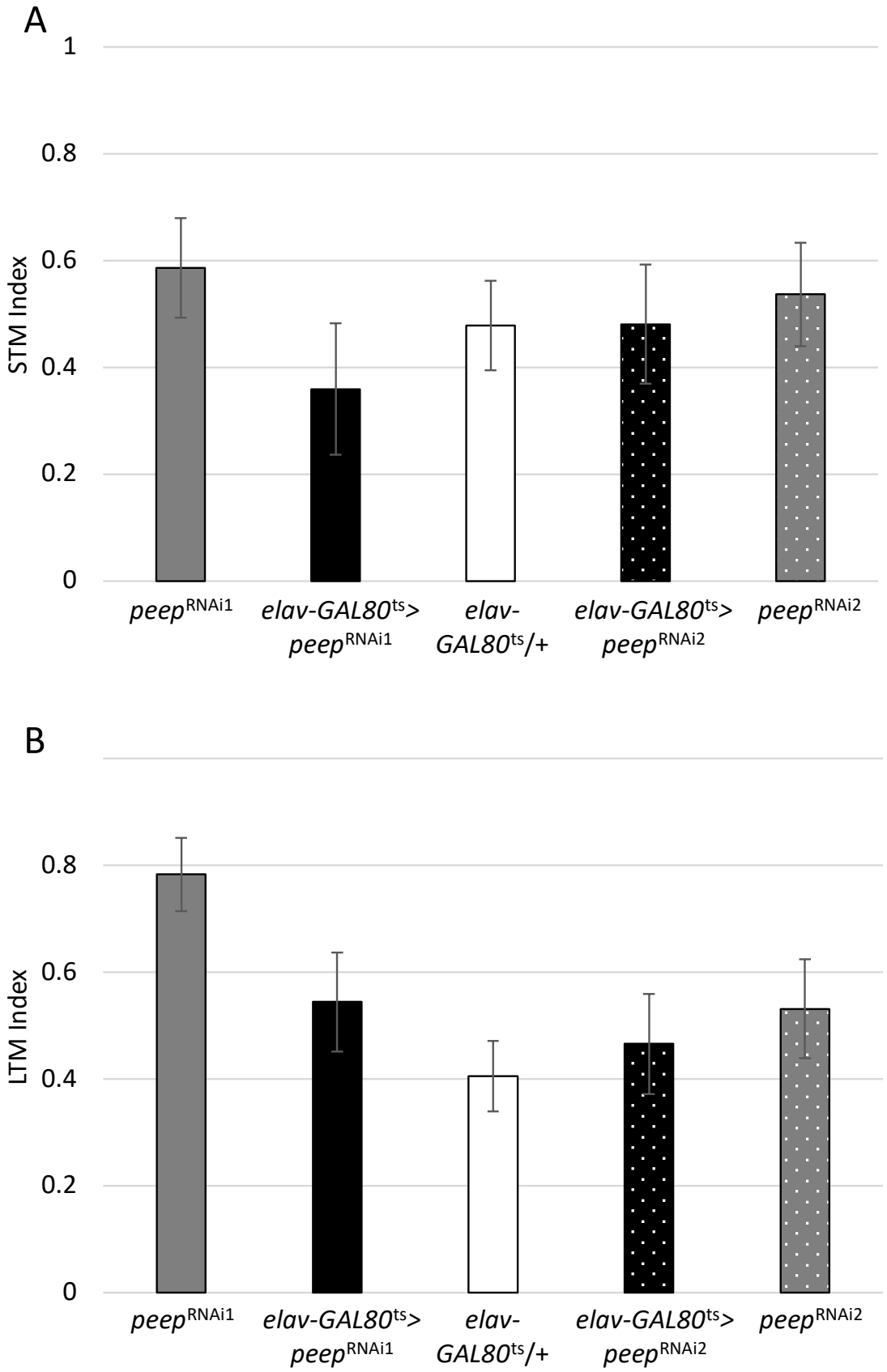

Figure 4.20. cVA-retrievable courtship memory remained intact upon adult-induced knockdown of Peep. A. Knockdown of Peep in the adult brain did not impair STM following courtship conditioning. Error bars indicate mean ± SEM, n≥19, (one-way ANOVA, post-hoc Tukey HSD, $f_{(4,98)} = 0.485$, p =

0.746. No significant difference on arcsine-transformed data between both controls; transgene control (*peep*^{RNAi1} or *peep*^{RNAi2}), and driver control (*elav-GAL80*^{ts}/+), and the driver-induced transgene knockdown (*elav-GAL80*^{ts}>*peep*^{RNAi1} or *elav-GAL80*^{ts}>*peep*^{RNAi2})). B. Knockdown of Peep in the adult brain did not impair long-term memory following courtship conditioning. Error bars indicate mean ± SEM, n≥19, (one-way ANOVA, post-hoc Tukey HSD, $f_{(4,98)} = 1.92$, $p = 0.113$. No significant difference on arcsine-transformed data between both controls; transgene control (*peep*^{RNAi1} or *peep*^{RNAi2}), and driver control (*elav-GAL80*^{ts}/+), and the driver-induced transgene knockdown (*elav-GAL80*^{ts}>*peep*^{RNAi1} or *elav-GAL80*^{ts}>*peep*^{RNAi2})). *elav-GAL80*^{ts} = *elav-GAL4;tub-GAL80*^{ts}.

Although knockdown of Peep results in morphological defects to the developing mushroom body, pan-neuronal knockdown of Peep in the adult brain does not affect cVA-retrievable courtship learning or memory, indicating that Peep is not essential for these behavioural processes.

4.3.5 Peep is dispensable for wing development

Drosophila imaginal discs make for ideal models to study development and growth, with the larval eye disc being further investigated in Section 5.1.1. The wing imaginal disc in third instar larvae do not contain neurons, however immediately following pupation a number of neurons are born and play an important role in creating the adult wing hinge, and the sensory bristles which disperse around the periphery of the wing (Jan *et al.*, 1985). The wing disc and developed adult wing structure are therefore often used as a model for neurodegeneration due to the large number of sensory neurons that reside in the wing vein with axons that project towards the central nervous system (Ghysen, 1978, 1980). Neural axon injury can be studied in this model through non-lethal ablation, and the wing, similar to the eye, is easily perturbed and live imaging can be utilised to study axonal degeneration (Fang *et al.*, 2012).

The *en-GAL4* driver was used in a preliminary study to determine whether Peep is involved in wing development. Engrailed is a transcription factor that plays an important role in neuronal development with specific localisation to cells in the posterior compartments of tissues, and in *Drosophila* was first established as a regulator of body segmentation (Kornberg, 1981). *en-GAL4* has been detailed to have an extensive expression pattern in the adult fly, with strong expression in the antennae, proboscis, and ocelli as well as in all leg segments, halteres, and in the posterior hindgut and genitalia, as well as in the wing hinge and the posterior wing veins (Blagburn, 2008). As there is strong expression in the wing, this driver was used to overexpress

and knockdown Peep and assess the requirement of Peep for adult wing development. Wings were imaged and assessed (Section 2.4.5) and compared to control wings (*en*/+), no defects to wing development and vein patterning were observed (Figure 4.21). These data indicate that Peep is likely not required for wing development.

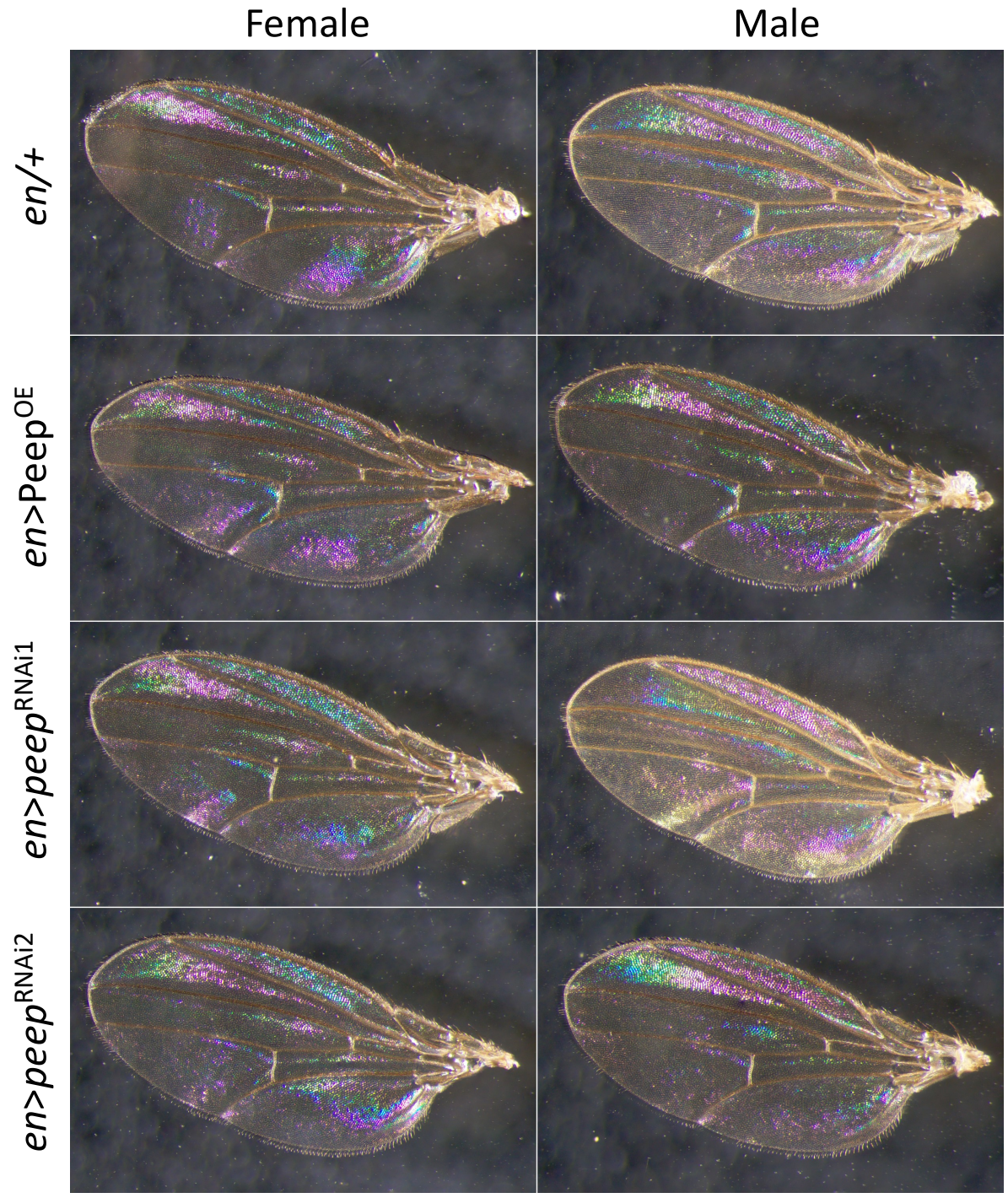

Figure 4.21. Wing morphology was normal upon overexpression and knockdown of Peep. *en-GAL4* expression of Peep^{OE} and *peep*^{RNAi} does not affect wing morphology and vein patterning. *en* = *en-GAL4*, *en*/+ = Control.

4.4 Discussion

This chapter involved characterisation of Peep expression and its contribution to normal development and adult function via a battery of well-established behavioural and morphological analyses.

Peep was found to be endogenously expressed throughout different stages of development and in a range of tissues, albeit at a very low level, including in the adult retina and adult brain. Ubiquitous depletion of Peep with *tub-GAL4* was lethal during embryogenesis, indicating that Peep plays an essential role in embryogenesis. Peep is also required at later stages of development as knockdown with *da-GAL4*, which drives widespread expression but at a lower level than *tub-GAL4* (Legan *et al.*, 2008), allowed survival through embryogenesis but was lethal at the pupal stage. The motor function of adult escapers, however, was not affected. Post-developmental, pan-neuronal depletion of Peep did not affect courtship learning and memory acquisition. In contrast, glial expression of Peep was required for survival through embryogenesis and interestingly, adult escapers, displayed severe developmental defects in the mushroom body, which warrants further investigation.

4.4.1 Peep is required for survival through eclosion

Drosophila eclosion begins during the last 10-hours of adult development where the area between the pupal cuticle and pharate adult fills with a moulting fluid and over the course of approximately three-hours this fluid is reabsorbed, which changes the appearance of the head area of the pupal cuticle from a smooth texture to a grainy wrinkled texture. Within an hour, the newly formed adult trachea fills with air and expands causing extension of the ptilinum, a membranous sac, that breaches the anterior portion of the pupal casing. These events are followed by a 40-minute quiescent period before eclosion proceeds (Kimura & Truman, 1990; McNabb *et al.*, 1997). Eclosion relies on the precise coordination of motor neurons and muscles, and takes place in three main stages, the first being movement of the pharate adult further towards the anterior portion of the pupal case followed by a series of head expansions to break open the operculum. The second stage involves head thrashing movements and thoracic and abdominal contractions to propel the pharate adult forward to push the head out through the operculum. During the third and final stage, the remainder of the fly is propelled out of the

pupal casing, which occurs through large bouts of abdominal contractions (McNabb *et al.*, 1997).

Knockdown of Peep with *da-GAL4* resulted in a significant decrease in adult survival due to either defects in ecdysis or pharate adult development, with expression of *peep*^{RNAi1} or *peep*^{RNAi2} resulting in 97.3% and 31.1% pupal lethality respectively. The pupal lethal phenotype was not observed upon knockdown with the weaker ubiquitous driver *arm-GAL4*, thus the use of drivers that confer different temporal and spatial expression profiles and expression levels is important for determining the role that Peep plays at different developmental stages and in different tissues. Overall, these results show that wild-type levels of Peep are not required for survival into adulthood (ie. a modest level of knockdown was tolerated), as knockdown with *arm-GAL4* did not alter survival. It would therefore be of interest to examine the hallmark processes that occur during eclosion, including hormone production, circadian rhythm, and motor neuron function and coordination, to assess whether the pupal lethality resulting from *da-GAL4* driven Peep knockdown could be attributed to a failure of one or more of these processes during eclosion itself, or whether other processes during the final stages of pupal development or physiological defects, unrelated to ecdysis and eclosion, result in death prior to initiation of eclosion.

Eclosion is a timed process that is regulated by pulses of the steroid hormone ecdysone (Baehrecke, 1996). The precise timing of events is closely related to circadian rhythm and the presence of three additional hormones. The *Drosophila* ecdysis-triggering hormone (Eth) shares similarities with the *Manduca* (Park *et al.*, 1999; Zitnan *et al.*, 1996) and is only expressed in the epitracheal Inka cells which persist throughout development and into adulthood (Meiselman *et al.*, 2017). Eth plays a pivotal role in regulating eclosion, and its activation is achieved through the ecdysone receptor and pulses of ecdysone hormone release. Eth hormone expression has been shown to be important for both cuticle loosening (pre-ecdysis) and shedding (ecdysis) throughout development, as a reduction results in a high degree of lethality (Zitnan *et al.*, 1996). The eclosion hormone (Eh) was first identified in the silkmoth (Truman & Riddiford, 1970) and was shown to be instrumental in all ecdyses throughout larval and adult development in holometabolous insects (Truman *et al.*, 1981). There are two pairs of ventral medial (VM) neurons that secrete Eh and their cell bodies are located in the brain and their axons extend the length of the central nervous system (Truman & Copenhaver, 1989). Interestingly, ablation of Eh producing neurons in *Drosophila* lead to a significant reduction in adult eclosion due to a failure of tracheal inflation, with one-third surviving (McNabb *et al.*,

1997), indicating that while the Eh can be required for ecdysis, it is not necessary. The Eh targets the Inka cells to release Eth resulting in Eth targeting of the VM neurons to release Eh, therefore, the precise timing and release of these hormones generates a positive feedback loop for ecdysis control (Ewer *et al.*, 1992), whereby, a loss of either hormone leads to early lethality (McNabb *et al.*, 1997; Zitnan *et al.*, 1996). The Crustacean cardioactive peptide (CCAP) is expressed in a small subset of neurons in the ventral nervous system and is believed to be the master control peptide that turns on ecdysis motor function. Ablation of CCAP neurons prior to larval ecdysis was not lethal, however the pre-ecdysis period was significantly longer than the control, indicating that CCAP expression is not essential for survival (Park *et al.*, 2003), but may be of importance for the execution of ecdysis (Kim *et al.*, 2006). CCAP ablation prior to pupal ecdysis, which occurs upon head eversion in during which time the imaginal disc appendages take on their adult form, resulted in the majority of pharate adults dead within their pupal cases, which was due to failure of adult body expansion, including extension of the head, legs, and wings, rather than a defect in the ecdysis motor function or eclosion. Ablation of CCAP post-eclosion resulted in only a small proportion of flies with inflated wings, indicating that CCAP is also required post-ecdysis (Park *et al.*, 2003).

To determine whether Peep is required for hormone signalling during eclosion, Peep could be knocked down in cells that express hormones required for eclosion and/or ecdysis (Scott *et al.*, 2020), and the resulting hormone levels in these cells could be measured.

The circadian clock is another main player in the process of eclosion as it gatekeeps and promotes eclosion during specific windows of time. Eclosion for most insects occurs at dawn or dusk due to the circadian clock, and flies are normally raised in a 12-hour light/dark cycle (Mark *et al.*, 2021). Interestingly, wild-type flies under constant darkness retain their internal clock and eclose at 24-hour intervals even when there is no light exposure. However, flies with a non-functional circadian clock eclose at any time throughout the day and night. The circadian clock has been shown to control the final stages of metamorphosis in order to initiate adult ecdysis and eclosion in a daily 24-hour rhythm (Mark *et al.*, 2021). Knockout of either Eh or CCAP, by using an Eh or CCAP cell-specific enhancer to induce expression of pro-apoptotic genes *reaper* (*rpr*) or *hid* to ablate these cells, did not disrupt circadian rhythm (McNabb *et al.*, 1997; Park *et al.*, 2003). However, Eh knockouts failed to respond to rapid bursts of light, known as the lights-on response which normally results in a rapid increase of eclosion as light is an important environmental cue for eclosion timing (McNabb *et al.*, 1997), furthermore, CCAP mutants had abnormal timing of eclosion events throughout the day (Park *et al.*, 2003).

Peep has previously been shown to be regulated by the circadian clock in the fat body (Xu *et al.*, 2011), therefore further studies of whether Peep plays a role in circadian rhythm in neurons could be performed. Pupae lacking Peep could be monitored throughout the regular 12-hour light/dark cycle to determine whether *peep*^{RNAi} induces an abnormal circadian rhythm resulting in abnormal eclosion timing, leading to a pupal lethal phenotype.

Upon closer inspection, the dead pharate adult heads were not in close proximity to the operculum (Figure 4.10B, inset), and therefore movement towards the anterior portion of the pupal casing may be defective, which implicates muscle coordination, motoneuron circuitry, and hormone signalling. It does however require mention that the positioning of the pharate head may either be the cause of eclosion failure, or consequence of late-stage pupal death, the latter would result in degradation and shrinkage of the pharate adult inside the pupal casing. Aside from this, no obvious phenotypic defects were observed, and visually the pharate adults appeared to be fully developed. Analysing survival upon Peep knockdown with the motor neuron driver *D42-GAL4* (Parkes *et al.*, 1998; Sanyal, 2009) would be of interest to determine the requirement of Peep in motor neurons.

4.4.2 Peep is dispensable for adult motor function

To identify whether depletion of Peep affected motor function, the negative geotaxis climbing assay was performed to evaluate the motor function of adult flies. This assay is quantitative and reproducible (Hura, 2018; Patel & Tamanoi, 2006) and has been used to evaluate motor function in *Drosophila* models of Parkinson's and Alzheimer's diseases (Song *et al.*, 2017; Zhang *et al.*, 2017). Following overexpression and knockdown of Peep with *da-GAL4* no deficits in climbing ability were observed, indicating that Peep is not an important contributor to motor strength and/or coordination required for climbing. However, a limitation to this study is that there is internal bias towards escapers that had the capacity to eclose in the first place, meaning that if *peep*^{RNAi} impaired motor function, it is likely that eclosion would be affected. This suggests incomplete penetrance such that if the pharate adult can survive pupal development and the eclosion process, then motor function of the adult fly would be sufficiently intact. Therefore, from these results it is impossible to discern whether knockdown of Peep affects motor skills involved in eclosion and post-developmental climbing ability. It would be informative to repeat this experiment using a motor neuron driver such as *D42-GAL4* (Parkes

et al., 1998; Sanyal, 2009) as it is possible that although *da-GAL4* is expressed in motor neurons, the level of expression may not be high and may not include all important motor neurons required for both eclosion and climbing. Furthermore, these results also require repetition with a pan-neuronal driver (*elav-GAL4* or *nSyb-GAL4*) as a previous study has shown that clusters of dopaminergic neurons that innervate the mushroom body modulate startle-induced negative geotaxis (Sun *et al.*, 2018)

Further experiments could include investigating muscle expansion and contraction in third instar larvae. Analysing larval locomotion may reveal early indications of motor control dysfunction, and offer insight into whether the pupal lethal phenotype is due to motor dysfunction, resulting in eclosion failure. Similarly, dissection of pharate adult progeny from pupal casings at the normal time of eclosion to first, determine whether these adults survive, and second, analyse climbing behaviour. These analyses would further shed light on whether defects in eclosion behaviour are due to motor coordination and muscle function.

4.4.3 Peep expression in glia but not neurons is essential for embryonic survival

Glia are non-neuronal cells of the central and peripheral nervous systems that maintain and support neuronal function by providing cues through the secretion of neurotropic factors for neuronal conduction, axon guidance, neurotransmitter recycling, cell morphology, and the overall maintenance of homeostasis (Rahman *et al.*, 2022) (Section 1.1.1). Glia play a critical role in early development and survival, specifically during the development of the embryonic central nervous system, where neuronal survival relies on the presence of glia, as impaired glial function or ablation has been shown to result in neuronal death (Booth *et al.*, 2000).

In the current study, expression of Peep in glia was determined to be essential for embryonic survival. The embryonic lethal phenotype was also observed when Peep was knocked down with *tub-GAL4*, but not the weaker *da-GAL4* driver. Although Daughterless is expressed in glia, *da-GAL4* may not drive expression in all glia and/or to as high of a level as *repo-GAL4* (which drives expression in all glia). If this is the case, it would provide a possible explanation as to why knockdown with *da-GAL4* result in progeny that survive through to the pupal stage, whereas knockdown with *repo-GAL4* is embryonic lethal. Although Peep expression in glia is essential for embryonic development, it is as yet unclear whether the pupal lethal phenotype

induced by *da-GAL4*-driven knockdown of Peep is a result of reduced Peep in glia. It is possible that knockdown of Peep in other *da-GAL4*-expressing cell types is responsible for this phenotype, and further delineating the specific cell types in which Peep expression is required during pupal development would be informative.

Peep has been shown in single cell RNA-seq data to be lowly expressed in glia (Li *et al.*, 2022), however its endogenous expression in different glial subtypes is yet to be explored. From these data it is likely that Peep is expressed in glia early in development, and reduced expression may impair normal glial function in shaping the central nervous system.

Given these results, it would be important to determine the glial subtypes in which Peep is expressed, to elucidate the role that Peep plays in glia during early development and embryonic survival, discussed further in Section 6.1.

Pan-neuronal knockdown of Peep with *elav-GAL4* or *nSyb-GAL4* drivers resulted in predominantly normal survival. As *nSyb-GAL4* drives 2.5-fold higher expression than *elav-GAL4*, it can be concluded that flies can tolerate a large depletion of Peep in neurons and survive (Hawley *et al.*, 2023). However, while the overall total number of progeny was not reduced, *elav-GAL4* driven knockdown of Peep resulted in a reduced number of male survivors. This could be due to a difference in survival fitness as there is limited capacity for progeny due to space and resources. This means that if females are physically fitter, they would outcompete the males, resulting in less male progeny and more female progeny. The temporal expression patterns of the two pan-neuronal drivers differ, whereby *elav* gene expression turns on earlier than *nSyb* (DiAntonio *et al.*, 1993; Robinow & White, 1988), and there is variation in the spatial patterns of expression in the brain (Hawley *et al.*, 2023). As stated above, *nSyb-GAL4* drives a higher overall level of expression, but there are some brain areas in which *elav-GAL4* expression is higher. To that end, it is possible that reduced expression of Peep is less tolerated in one (or more) of the cell types in which *elav-GAL4* is expressed more highly. This could also be due to dosage compensation which is a mechanism specific to male *Drosophila* to balance gene expression related to the unequal distribution of sex chromosomes. A male *Drosophila* will double the expression of genes residing on the X chromosome (Muller, 1932) and as *elav-GAL4* is located on the X chromosome males will express twice as much GAL4 which can often result in lethality. This experiment should be repeated to determine whether the male lethality result is reproducible.

In order to examine the importance of Peep in survival of both glia and neurons throughout development, a comprehensive analysis of the expression pattern of Peep during embryogenesis, larval, and pupal development should be performed, following the generation and validation of a new Peep antibody, or using fluorescence *in situ* hybridisation. Furthermore, tissue-specific conditional knockout studies using CRISPR/Cas9 to knockout Peep expression in all neurons and also in specific subsets of central nervous system glia could be compared to the current knockdown studies. This would indicate whether the phenotypes are further exacerbated upon complete loss of Peep, to determine which cells are specifically important for development and survival through to adulthood.

4.4.4 Peep expression is required for mushroom body development but is not required for learning and memory

4.4.4.1 Peep depletion in neurons results in mushroom body morphological defects

While neuronal Peep is required for mushroom body development, it does not appear to be required in neurons for the formation and/or storage of courtship memory. The mushroom body morphological defects resulting from pan-neuronal Peep knockdown that were initially observed in Section 3.2.1, were exacerbated upon overexpression of Dicer-2 (Dietzl *et al.*, 2007). The phenotypes induced by Peep knockdown with Dicer-2 included reduced elongation of α and β lobes with the predominant phenotype attributed to β lobe fusion.

The mushroom body is comprised of the extending axonal processes from the neuronal Kenyon cell bodies that are clustered at the posterior of the brain. These mushroom body axons extend through the pedunculus and bifurcate to form bisymmetric dorsal and medial projecting neuropil structures (Section 1.3.1.1) (Crittenden *et al.*, 1998).

To further understand the requirement of Peep in each Kenyon cell neuronal subgroup, GAL4 drivers that drive expression in each of the different Kenyon cell subgroups (α/β, α'/β', or γ) could be utilised (Aso *et al.*, 2009). These drivers are not fully restricted to these cells, as expression is also often observed in the ellipsoid body, subesophageal ganglion, and lobula plate in the optic lobes (Aso *et al.*, 2009). Therefore, to avoid confounding non-specific defects induced by Peep depletion, the Split-GAL4 system could be utilised. GAL4 is comprised of two domains, the DNA binding domain (DBD) and the AD. The DBD binds directly to the

UAS, positioned upstream of the transgene of interest, and the AD drives transgene transcription. The traditional UAS/GAL4 system employs a tissue-specific promoter to drive GAL4 (consisting of a DBD and AD) expression of a UAS transgene in a tissue-specific manner (Brand & Perrimon, 1993) (Figure 1.8). The Split-GAL4 system is an alternative approach for manipulating gene expression targeted to a specific subset of cells and removing background expression (Luan *et al.*, 2006). The DBD and AD are independently targeted by two different promoters and transgene expression will only occur if the DBD and AD are at overlapping expression zones where a DBD-AD heterodimer can form through a leucine zipper (Luan *et al.*, 2006). There are Split-GAL4 drivers available for α/β, α'β', and γ Kenyon cell neurons, and these were recently validated by expression of UAS-GFP, and the expression pattern in the mushroom body of each Split-GAL4 driver was specific to its intended cell type (Tan, 2022). Peep knockdown in specific Kenyon cell neurons would demonstrate the requirement of Peep in each subgroup and demonstrate whether a reduction of Peep in one set of Kenyon cell neurons non-autonomously regulates the growth and extension of axons from other Kenyon cell populations.

The processes involved in guiding mushroom body axonal growth involve chemotropic guidance cues, cell-cell contact and adhesion, and cytoskeletal regulator proteins.

NetB was a candidate in the initial mushroom body and eye screen to identify genes that interact with HDAC4 and was selected from a previously performed rough eye phenotype screen (Schwartz *et al.*, 2016). Netrins guide axon growth through chemotropic repulsion cues (Colamarino & Tessier-Lavigne, 1995), and NetB, one of two *Drosophila* homologues, is highly expressed in the mushroom body and has been shown to regulate mushroom body morphogenesis, where knockdown of NetB resulted in severe β lobe shortening (Kang *et al.*, 2019), the phenotype of which was unable to be recapitulated in this current study (Table 3.4). Frazzled and Uncoordinated-5 are *Drosophila* Netrin receptors and knockdown of either results in short α lobes and short α and β lobes respectively, however an interaction with NetB has not been identified, indicating that the axonal defects induced by NetB reduction may not be mediated by these receptors (Kang *et al.*, 2019),

The L1 cell adhesion molecule (L1-CAM) *Drosophila* homologue Neuroglian (Bieber *et al.*, 1989) is required for mushroom body development (Goossens *et al.*, 2011) specifically in regulating axon extension by mediating protein-protein and axon-axon interactions (Siegenthaler *et al.*, 2015). A neuroglian mutant lacking the capacity for intracellular protein-

protein interactions resulted in a loss α/α' and β/β' projection into the pedunculus. Furthermore, Neuroglian mediates an interaction between different axon populations during navigation into the pedunculus for normal axonal projection and guidance (Siegenthaler *et al.*, 2015).

Moesin and Ankyrin2 (Ank2) are both cytoskeletal proteins that have also been shown to play a role in mushroom body axon regulation (Freymuth & Fitzsimons, 2017; Wilson *et al.*, 2023). Both Moesin and Ank2 knockdown disrupts mushroom body morphology resulting in a number of deficits, including guidance defects, missing lobes, and β lobe fusion (Freymuth & Fitzsimons, 2017; Siegenthaler *et al.*, 2015; Wilson *et al.*, 2023), and both have been shown to interact with Neuroglian. The Ank2-Neuroglian interaction is important for synapse growth (Enneking *et al.*, 2013) and the Ank2-Moesin-Neuroglian interaction is important for guidance of mushroom body axons (Siegenthaler *et al.*, 2015).

Moesin is part of the ezrin-radixin-moesin (ERM) family of proteins and has been characterised as an adaptor protein with roles in signal regulation and synaptic development (Seabrooke & Stewart, 2008) as well as cell shape maintenance, by playing a crucial part in cytoskeletal rearrangement (Edwards *et al.*, 1997) and regulating photoreceptor morphology (Karagiosis & Ready, 2004). Ank2 is part of the ankyrin family of proteins that contain an N-terminal ankyrin repeat domain and shares homology with human ANK3, which has been implicated in a number of neurological disorders (Bi *et al.*, 2012; Iqbal *et al.*, 2013; Morgan *et al.*, 2008; Tesli *et al.*, 2011). Ank2 has also been characterised as an adaptor protein with roles in mediating the link between the actin cytoskeleton, ion channels, and cell adhesion signalling molecules, a process that involves cytoskeletal rearrangement (Cunha & Mohler, 2009). Rearrangement of the actin cytoskeleton promotes structural changes and synaptic plasticity, both of which are required for neuronal morphogenesis and memory formation (Lamprecht & LeDoux, 2004).

Genetic interaction studies during mushroom body development between *peep* and the above-mentioned genes would provide further insight into whether Peep acts in similar molecular pathways in regulating normal axon growth and guidance. Identification of regulator pathways and Peep interacting proteins is further discussed in Section 6.3.

4.4.4.2 Peep depletion in glia results in mushroom body morphological defects

Preliminary immunohistochemistry studies on the brains of progeny that survived to adulthood following pan-glial knockdown of Peep showed severe β lobe fusion, which requires further investigation using an anti-FasII antibody and quantifying mushroom body lobe defects. As the mushroom body is comprised of neuronal Kenyon cell axon projections (Crittenden *et al.*, 1998), Peep knockdown in glia results in non-autonomous mushroom body defects. It is therefore important to determine which glia Peep expression is specifically required in during mushroom body development, discussed further in Section 6.1.

Memory testing following post-developmental pan-glial Peep knockdown could give further insight into the function of Peep in non-neuronal cells. These analyses would further the understanding of the requirement of glial cells and the role that Peep plays in mushroom body morphogenesis and the processes of learning and memory. Thus far few studies have investigated the requirement of glia in mushroom body development, however it has been shown that ensheathing glia are more concentrated around mushroom body axons and extend their processes to the ellipsoid body and antennal lobes. Furthermore, cortex glia are concentrated at the posterior of the brain and extend their processes to the neuronal cell bodies (Ou *et al.*, 2016). A glial-specific Smad E3 ubiquitin protein ligase SMURF has been shown to induce Hedgehog signalling to suppress the proliferation of neuronal mushroom body neuroblasts, which sheds light on the communication between neurons and glia in mushroom body cell proliferation (Yang *et al.*, 2021). The immunoglobulin transmembrane protein Plum is required to regulate axon pruning of the mushroom body γ lobes (Yu *et al.*, 2013) and regulate β lobe midline termination, as a loss-of-function mutation and knockdown of Plum resulted in midline crossing of β lobe axons (Marmor-Kollet *et al.*, 2019). These studies demonstrate the importance of glia in maintaining mushroom body structure, in a cell non-autonomous manner. In examining the processes of learning and memory, most studies focus on synaptic plasticity and activity-dependent transcriptional changes in neurons with little reported on the requirement of glia. One study however, showed that during olfactory associative LTM there was an acute increase in *repo* transcription in glia which was necessary for the formation of memories, suggesting a role for glia in LTM formation (Matsuno *et al.*, 2015). These data from this current study demonstrate that Peep expression in glia is important for maintaining normal mushroom body morphology, as the pan-glial knockdown of Peep resulted in fusion of the β lobes, suggesting that Peep, similarly to Plum, may also play an important role in the processes

involved in learning and memory. To that end, additional studies into the non-neuronal role of Peep in learning and memory could be analysed using the *repo-GAL4* driver or other subtype specific glial-GAL4 drivers (Jenett *et al.*, 2012; Kremer *et al.*, 2017) (Section 6.1).

The following Chapter will delve further into understanding the importance of Peep for normal eye development, specifically in ommatidial patterning and cell survival, as previously established in Section 3.3.2. The role that Peep plays in the developing eye will be investigated by analysing the structure and organisation of the larval, pupal, and adult eye followed by an analysis of potential pathways implicated as a result of Peep knockdown, using the eye as a model.

5 Functional dissection of the role that Peep plays in the *Drosophila* compound eye

The *Drosophila* eye is an ideal model for dissecting the molecular mechanisms underlying neuronal processes. The eye is comprised of 800 individual facets called ommatidia, each containing both neuronal and non-neuronal cells that are organised into 32-34 vertical columns. The lattice structure of the eye is highly organised, whereby disruptions are easily identified, resulting in a "rough" appearance, often a result of structural defects where the precise boundaries separating ommatidia are lost. Each ommatidium is comprised of eight photoreceptor neurons, four lens secreting cone cells and two primary pigment cells. Surrounding these, each ommatidium shares six secondary pigment cells as well as three tertiary pigment cells and three bristle cell groups which are present at alternating interommatidial vertices (Figure 1.5B, B') providing structure to the ommatidial lattice (Ready *et al.*, 1976). Cone and pigment cells are derived from non-neuronal cell types and function as intrinsic glia (Charlton-Perkins & Cook, 2010; Chaturvedi *et al.*, 2014) similarly to those in the honeybee compound eye (Baumann, 1992) (Section 1.3.2.2).

As previously observed in Section 3.3.2, disruption to ommatidial patterning as well as severe necrosis were observed when Peep was knocked down in the developing eye by two independent *peep*^{RNAi} constructs. The aims of this Chapter were to determine the cell types in which Peep is required for normal eye development, by investigating whether Peep is required at the larval, pupal and/or adult stages, and to further characterise the developmental and necrotic defects resulting from a loss of Peep, to determine the pathway(s) in which Peep acts to promote normal eye development and cell survival, and protect against necrosis.

5.1 The role of Peep in the developing *Drosophila* eye

The *GMR-GAL4* driver promotes expression in all cells posterior to the morphogenetic furrow (Freeman, 1996) therefore it was important to determine whether Peep is required in specific cell types in the developing eye. As previously shown in Section 3.3.2, *GMR-GAL4* driven Peep knockdown resulted in defects in ommatidial patterning, loss of pigmentation and necrosis along the posterior side of the adult eye (Figure 5.1A). As opposed to *GMR-GAL4, eyeless-*

GAL4 (*ey-GAL4*) drives expression in undifferentiated cells anterior to the morphogenetic furrow, and expression of *peep*^{RNAi} with *ey-GAL4* (Figure 5.1B) resulted in no change in the adult eye phenotype as compared to control. These results demonstrate that Peep expression is not required in the undifferentiated cells anterior to the morphogenetic furrow (Section 1.3.2.1) for normal ommatidial patterning, therefore Peep may not be essential for growth and proliferation, which occurs anterior to the furrow, but may play an important role during cell differentiation, which occurs posterior to the furrow.

GMR-GAL4 drives expression in the developing larval eye disc and also throughout pupal development and in the adult retina (Escobedo *et al.*, 2021), therefore it was important to determine at which stage(s) of development Peep is required in order for normal development of the adult eye.

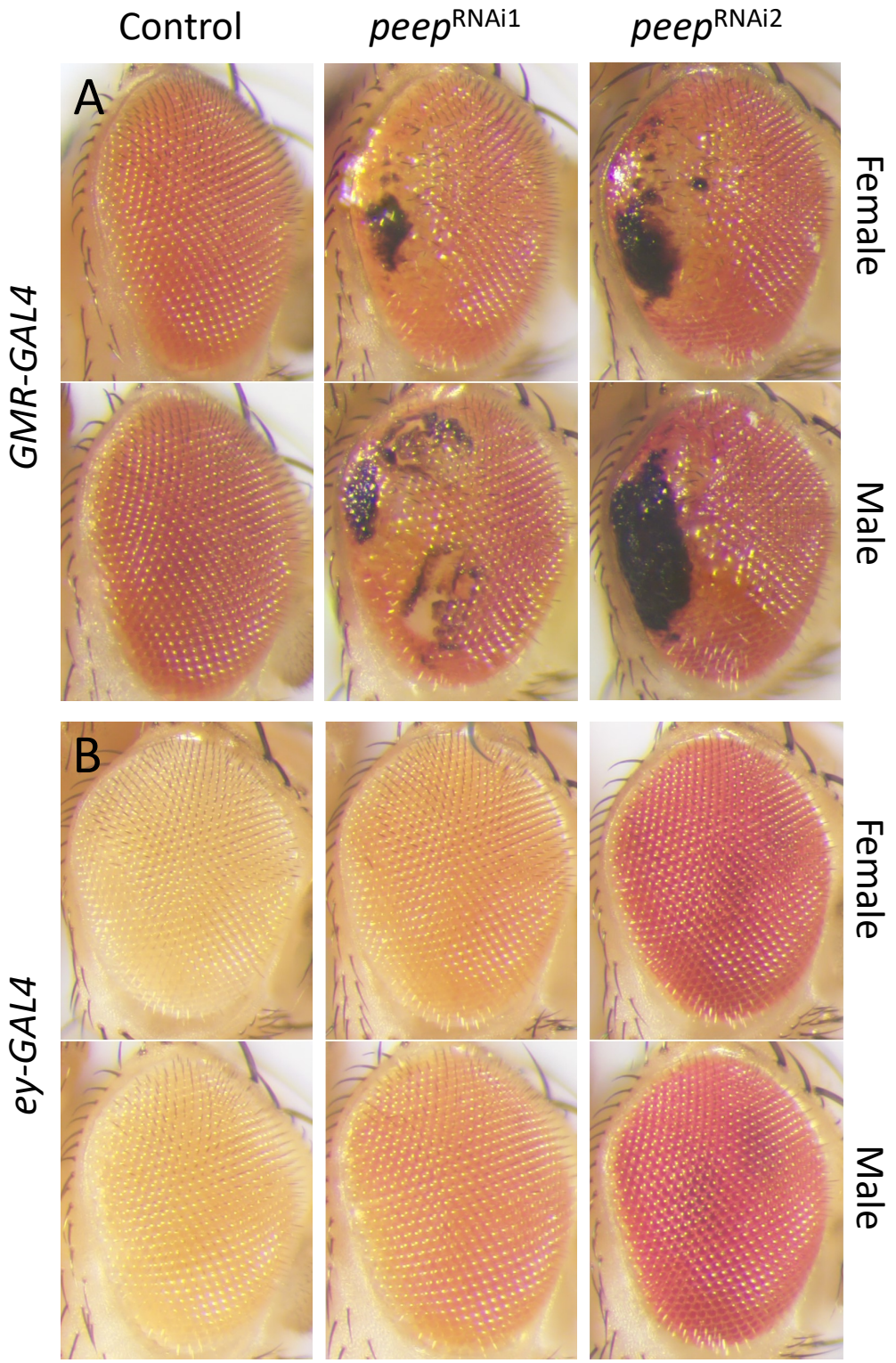

Figure 5.1. Peep expression is required posterior and not anterior to the morphogenetic furrow. A. *GMR-GAL4* expression of *peep*^{RNAi} in all differentiating cells posterior to the morphogenetic furrow induces a severe rough eye phenotype with large areas of necrotic lesions. B. *ey-GAL4* expression of *peep*^{RNAi} in undifferentiated cells anterior to the morphogenetic furrow resulted in an unperturbed eye. There is a significant difference in eye colour between the *ey-GAL4* control and *ey-GAL4* driven *peep*^{RNAi} eyes, which is unrelated to expression of Peep itself. The *ey-GAL4* control progeny were generated by crossing the driver to the *w(CS10)* control which is mutant for the *white* gene (ie has white eyes), and the *ey-GAL4* driven *peep*^{RNAi} progeny were generated by crossing the driver to the RNAi line

which contains an additional copy of the mini *white* gene, resulting in a darker red eye. All images were attained seven days post-eclosion.

5.1.1 Knockdown of Peep does not alter the gross structure of the larval eye disc

It was of interest to examine whether Peep is required for the correct development of the third instar larval eye imaginal disc in which the adult eye develops from. To do this, following knockdown of Peep with *GMR-GAL4*, the organisation of the differentiating cells posterior to the morphogenetic furrow and overall eye disc structure was analysed using two different markers, anti-FasII and anti-disc-large 1 (Dlg-1). Dlg-1 is a tumor suppressor member of the membrane-associated guanylate kinases which have roles in cell-cell contact junctions (Bilder *et al.*, 2000). FasII is expressed in differentiating cells posterior to the morphogenetic furrow, with stronger expression observed immediately posterior to the furrow (Mao & Freeman, 2009) (Figure 5.2A, panel 1 and 2) and also localises to the photoreceptor axons that descend basally before projecting posteriorly through the optic stalk (data not shown), while Dlg-1 localises to the cell membrane of all cells (Figure 5.2A, panel 3). Staining with FasII and Dlg-1, therefore, allows for visualisation of the structure and organisation of the cell population within the eye-antennal disc, and upon knockdown of Peep, there were no gross cellular array abnormalities (Figure 5.2B, C). On closer inspection, FasII staining of the cone cell membranes (see Figure 5.2A, panel 2 inset) at the apical surface revealed no defects to cone cell clusters or in the organisation of ommatidial columns (Figure 5.2B, C, panel 2). Similarly, using Dlg-1 as a second membrane-associated marker of cells across the entire eye disc, no overall structural defects to the eye disc upon knockdown of Peep were observed (Figure 5.2B, C, panel 3). These results demonstrate that Peep does not affect the gross structure and cellular organisation of the larval eye disc.

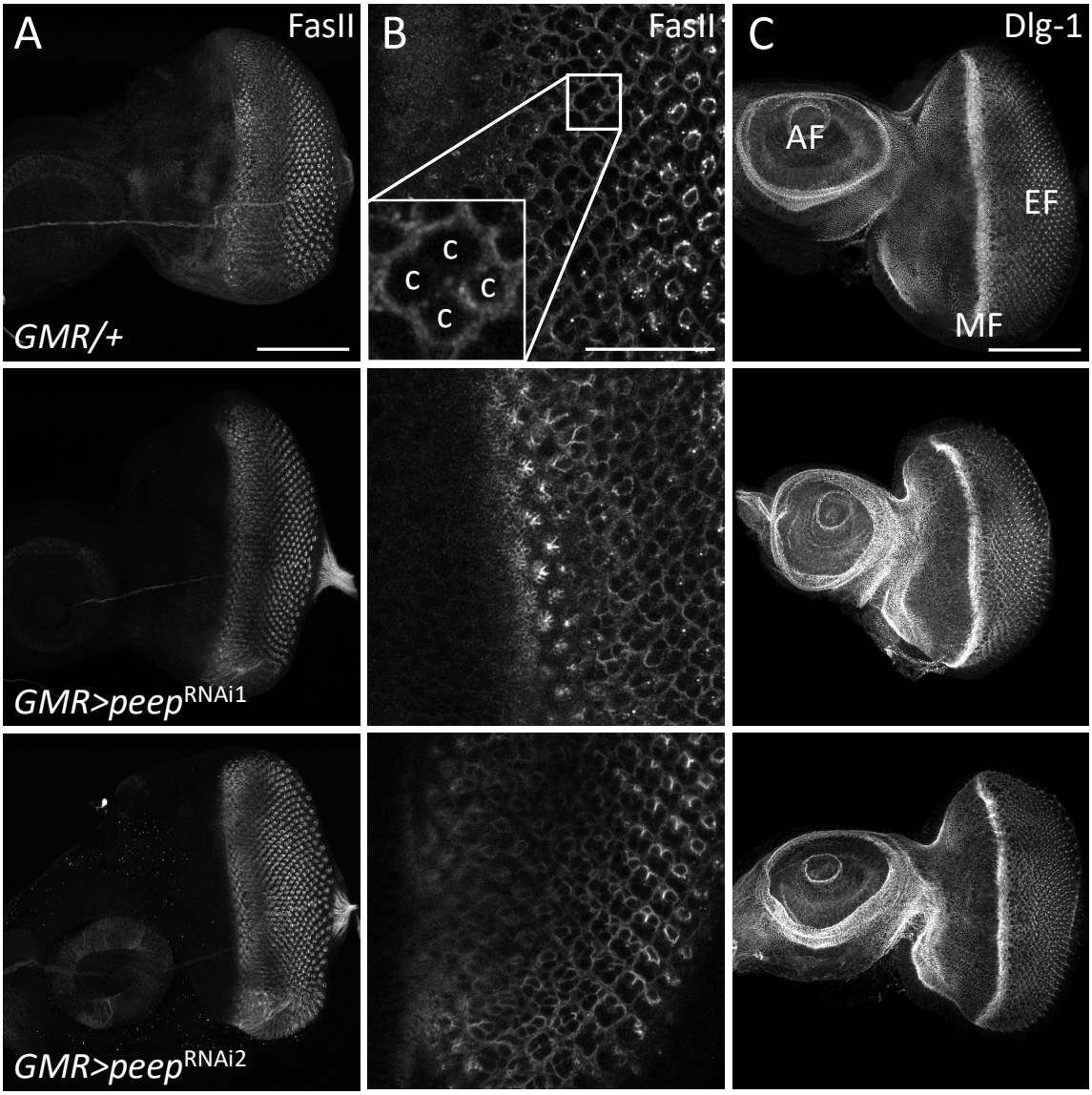

Figure 5.2. *peep*^{RNAi} in the larval eye disc does not induce gross structural and organisational defects. A. Using anti-FasII as a membrane marker of cells posterior to the morphogenetic furrow and photoreceptor axonal projections, a stacked maximum projection through the apical region of the eye disc shows no structural or organisational defects. Images taken using 40x objective lens in oil, 1 µm sections, scale bar = 100 µm. B. Single slice images through the apical region with anti-FasII highlights the cone cell membranes and demonstrated no obvious defects to cone cell clusters and ommatidial column organisation, inset shows one cone cell cluster. Images taken using 63x objective lens in oil, Zoom 3x, scale bar = 30 µm. C. Stacked maximum projections through the entire eye-antennal disc using anti-Dlg-1 as a membrane associated marker of all cells shows no structural or organisational defects to the eye disc following Peep knockdown. Images taken using 40x objective lens in oil, 1 µm sections, scale bar = 100 µm. *GMR = GMR-GAL4, GMR/+* = Control, C = cone cell, AF = antennal field, MF = morphogenetic furrow, EF = eye field.

5.1.1.1 Peep is required for retinal basal glia development and/or migration

The retinal basal glia are a subset of glia that populate the larval eye disc and are comprised of carpet, surface, and ensheathing glia. Ensheathing glia are important for ensheathment of

photoreceptor axons for projection and guidance through the optic stalk to innervate the brain (Rangarajan *et al.*, 1999) and therefore play an important role in maintaining neuronal complexities (Section 1.3.2.1.1). *GMR-GAL4* drives expression in all differentiating cells posterior to the morphogenetic furrow (Freeman, 1996), however as glial cells migrate into the eye disc in order to populate it, *GMR-GAL4* does not express in these cells (Velarde *et al.*, 2021). To examine whether Peep plays a non-autonomous role in the development and/or migration of the retinal basal glia, following *GMR-GAL4* knockdown, glial cells in the third instar larval eye disc were labelled using an anti-repo antibody, which highlights the nucleus of almost all glia. In the control group the number of retinal basal glia were quantified and revealed to contain up to two carpet glia (mean = 186), which were identified based on their large nuclei. Upon overexpression of Peep, there was a significant decrease in the number of glial cells (mean = 120), and a further significant decrease resulted from knockdown of Peep, $peep^{RNAi1}$ (mean = 62) and $peep^{RNAi2}$ (mean = 43) (Figure 5.3A, B). The identity of the glial cells populating the eye disc is unknown, however it is likely these are surface glia. A lack of surface glia suggests there could be defects in carpet glial migration or function (Silies *et al.*, 2007) (Section 1.3.2.1.1). Although the carpet glial membranes have not been stained in this study, their membranes have been detailed to spread and cover the differentiating field posterior to the morphogenetic furrow providing contact points for surface glia migration and ultimate proliferation (Ho *et al.*, 2019; Silies *et al.*, 2007). If there is a loss of this carpet glial membrane spread, the surface glia would not migrate correctly into the eye field which could potentially affect downstream proliferation. When there is a complete loss of these carpet glial cells, the migration of surface glia into the eye field is not controlled, whereby the surface glia migrate randomly ahead of the differentiating photoreceptors (Silies *et al.*, 2007). Interestingly, under conditions of increased and decreased expression of Peep, the large carpet glia at the posterior of the eye disc were not observed (Figure 5.3A), but migration remained unaffected.

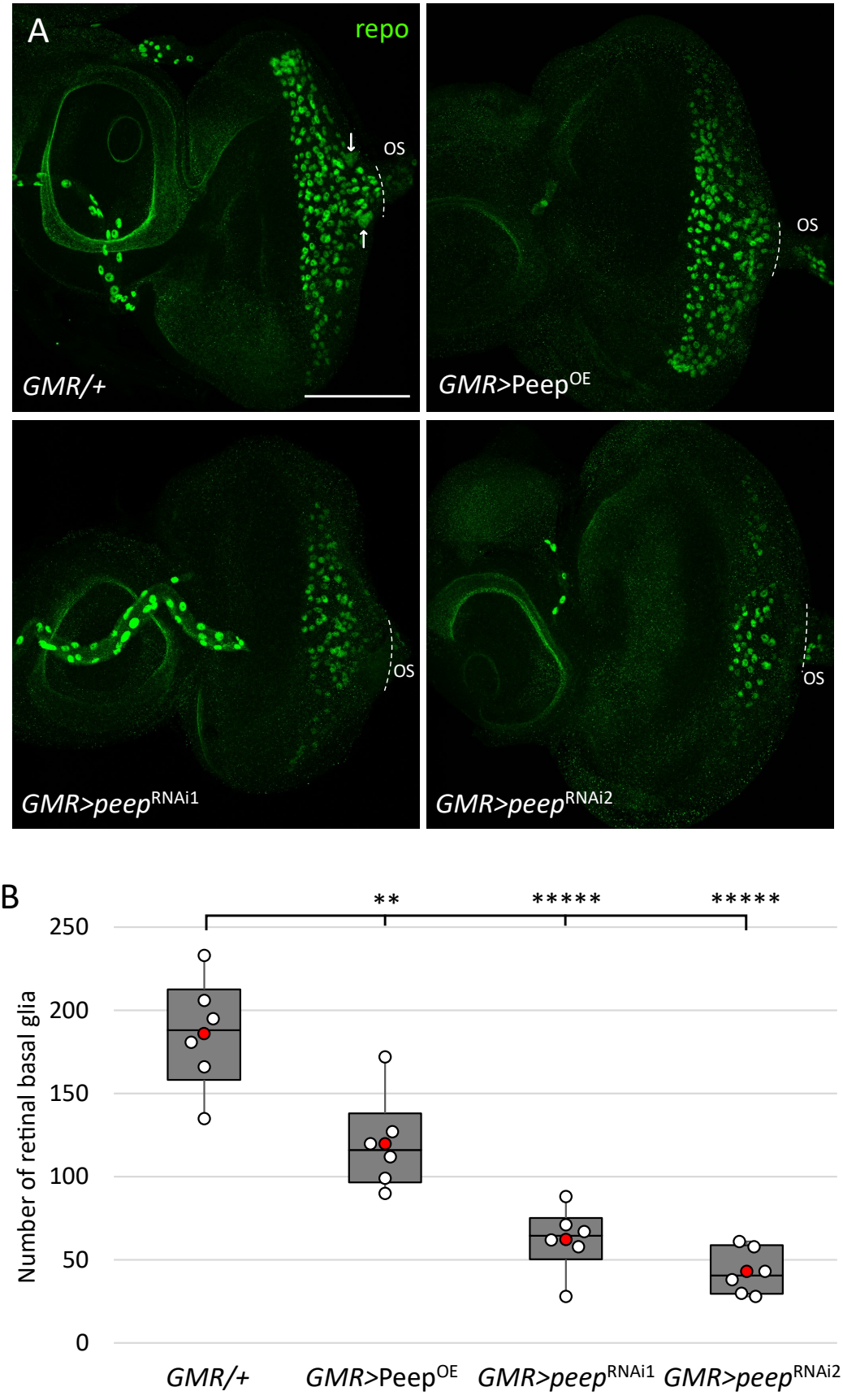

Figure 5.3. Both Peep^{OE} and *peep*^{RNAi} induce a decrease in retinal basal glia counts in the larval eye disc. A. An anti-repo antibody was used to label retinal basal glia in the third instar larval eye disc.

Glia are localised posterior to the morphogenetic furrow and both Peep^{OE} and *peep*^{RNAi} result in reduced glial numbers. *GMR/+* controls contain up to two large carpet glia (white arrow) close to the OS. Images are maximum projections through the larval eye disc using the 40x objective lens in oil, 0.5 µm sections, scale bar = 100 µm. B. Box-and-whisker plot showing the number of retinal basal glia (excluding glia in the OS) (red datapoint shows the mean). A significant reduction in glia was observed upon both Peep^{OE} and *peep*^{RNAi}, n=6, (one-way ANOVA, post-hoc Tukey HSD, $f_{(3,23)} = 38.86$, ** = $p<0.01$, ***** = $p<0.00001$, *GMR-GAL4/+ ; GMR-GAL4>peep*^{OE} = 0.0011, *GMR-GAL4/+ ; GMR-GAL4>peep*^{RNAi1} = $2.72E^{-7}$, *GMR-GAL4/+ ; GMR-GAL4>peep*^{RNAi2} = $2.58E^{-8}$). OS = optic stalk, *GMR = GMR-GAL4, GMR/+* = Control.

Based on these results in the larval eye, knockdown or overexpression of Peep with *GMR-GAL4* does not result in overall gross structural defects, however these do significantly reduce the number of retinal basal glial cells in a non-autonomous manner.

5.1.2 Peep is required for pupal eye development

The pupal eye was next examined to determine whether altered expression of Peep disrupts its development. The pupal eye is comprised of hexagonal ommatidia, each consisting of a collection of accessory cells including, four cone cells surrounded by two primary pigment cells, encased by six secondary pigment cells with three tertiary pigment cells and three bristle cells positioned at alternating vertices (Cagan & Ready, 1989a) (Figure 1.5B, B'). The secondary and tertiary pigment cells are collectively known as the interommatidial pigment cells (IPCs), as they are shared by either two or three ommatidia (Johnson & Cagan, 2009). Perturbations to the pupal ommatidial lattice are easily visualised and could result from defects in photoreceptor or accessory cell development, which may contribute to the adult rough and necrotic eye phenotype. Although there is minimal evidence of retinal basal glia function following larval eye disc development, the pupal ommatidium is comprised of both neuronal and glial-like cells. To investigate the requirement of Peep during pupal eye development, the highly organised and structured glial-like cone and pigment accessory cells can be assessed for perturbations (Charlton-Perkins *et al.*, 2017).

At 48-hours APF the pupal eye was isolated (Section 2.2.3) and the apical accessory cells membranes were visualised with anti-Dlg-1 as maintenance of the apical pupal eye structure is important in generating the adult retinal structure, which was severely disrupted in Peep knockdown flies. *GMR-GAL4*, controls when raised at the permissive temperature of 25°C, result in no adult eye phenotype when observed under light microscopy, minus the few

instances of misplaced bristles. Upon investigation of the pupal eye, if a bristle cell was not formed at the correct vertex and was instead formed where a tertiary pigment cell would normally reside, a tertiary pigment cell would be generated in the bristle cell place (Figure 5.4A). Although there were some minor abnormalities in accessory cell number, for consistency and clarity the *GMR-GAL4* control eye was scored as 'normal'. Overexpression of Peep resulted in minimal defects to accessory cell number, similarly to the control, with the overall ommatidial lattice remaining intact (Figure 5.4B). Upon knockdown of Peep there was a significant difference in the number of accessory cells per ommatidium. *peep*^{RNAi1} induced numerous accessory cell defects, most of which were a result of abnormal numbers of IPCs, which resulted in some ommatidia with more accessory cells than controls, and also some with fewer (Table 5.1, Figure 5.4E). In addition, some ommatidia displayed additional primary pigment cells within a cluster (Figure 5.4C, red arrowhead). Expression of *peep*^{RNAi2} resulted in a more widespread distribution of accessory cell number than *peep*^{RNAi1} (Figure 5.4E), which was also attributed to abnormal numbers of IPCs as well as abnormal numbers of cone cells (Figure 5.4D, red arrowhead). Ommatidia were analysed and quantified from four regions within each eye, anterior, posterior, dorsal, and ventral. It was surprising to note that there were no noticeable differences in the number of accessory cells per ommatidium in one region over another, indicating that the observed pupal eye phenotype may not be the primary contributor to the posterior-localised adult eye phenotype.

Table 5.1 Table showing the proportion of ommatidia per genotype with fewer, normal, and excess numbers of accessory cells

Number of accessory cells	***GMR/+***	***GMR*>Peep^{OE}**	***GMR>peep^{RNAi1}***	***GMR>peep^{RNAi2}***
Fewer (≤17)	0.01	0.05	0.10	0.11
Normal (18)	0.82	0.84	0.38	0.40
Excess (≥19)	0.17	0.11	0.52	0.49
Ommatidia (n)	352	393	344	437

GMR = GMR-GAL4.

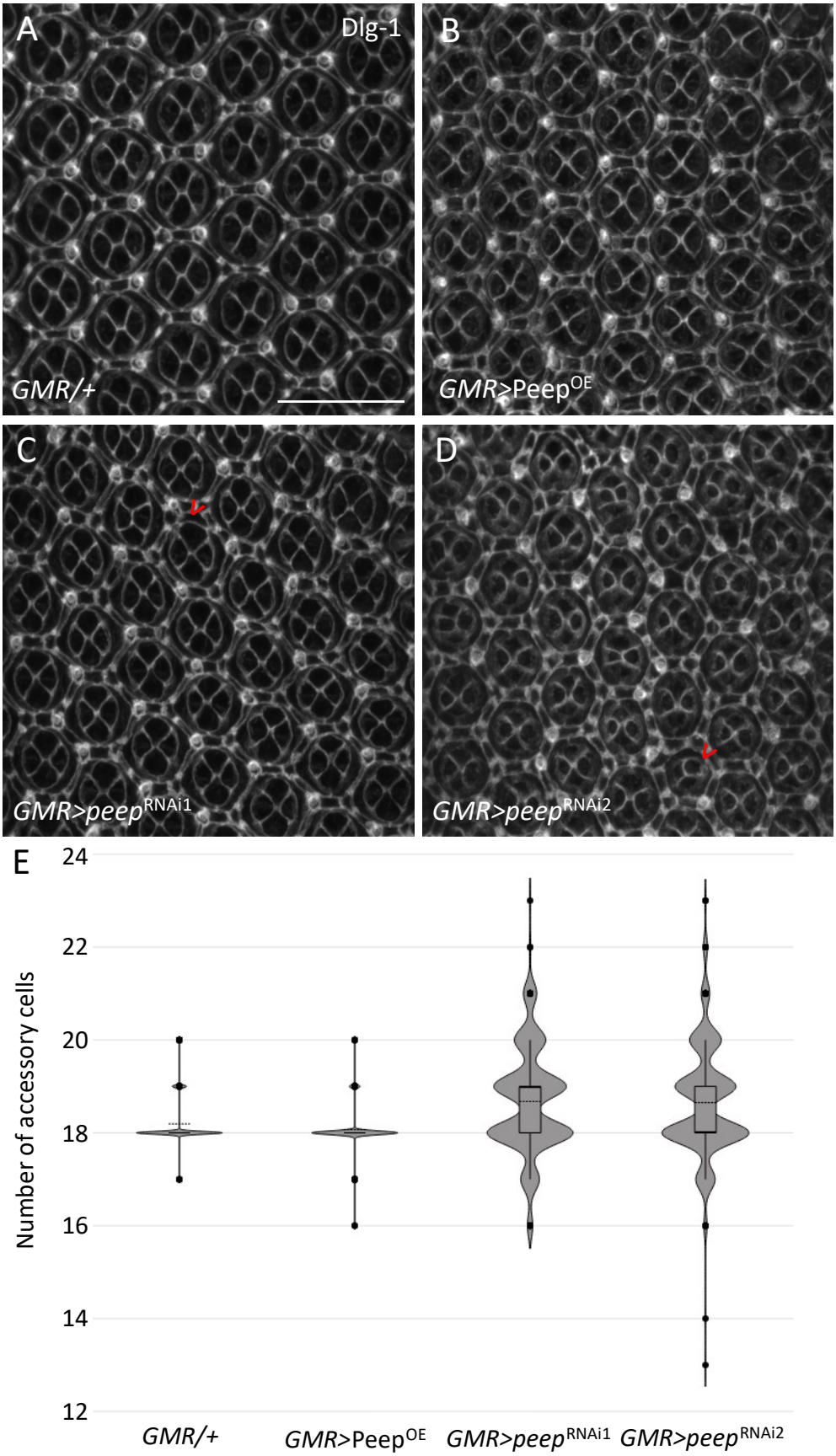

Figure 5.4. *GMR-GAL4* driven *peep*^{RNAi} induces abnormal accessory cell numbers in the pupal eye. Pupal eyes dissected 48-hours APF display an organised ommatidial lattice. Cell membranes were

labelled with anti-Dlg-1 and the number of accessory cells from four regions of each eye (anterior, posterior, dorsal, and ventral) were quantified. A. The 'normal' control pupal ommatidial lattice. B. The lattice remains unchanged upon overexpression of Peep. C. *peep*^{RNAi1} resulted in abnormal numbers of accessory cells with some instances of extra primary pigment cells (red arrowhead). D. *peep*^{RNAi2} resulted in a similar lattice array to C. with some abnormalities attributed to defects in cone cell numbers (red arrowhead showing a missing cone cell). Images were maximum projections taken using the 40x objective lens in oil, Zoom 8x, 0.5 µm sections, scale bar = 20 µm. E. Violin plot showing the distribution in the number of accessory cells per ommatidium, n≥344 ommatidia from four regions of the eye with four independent eyes per genotype. *GMR* = *GMR-GAL4*, *GMR/+* = Control.

These data show that knockdown of Peep results in dysregulation in the number of accessory cells. Under basal conditions excess interommatidial potentials are born and subsequently cleared if the correct cell-cell contacts are not generated, suggesting that Peep may play a role in regulating clearance of excess cells via apoptosis. The cone cells and primary pigment cells are specified and defined from the late larval/early pupal stage and are therefore not targeted for degradation. The secondary and tertiary pigment cell lattice, however, forms during mid pupal development prior to the two waves of apoptosis, in which DIAP1 plays an essential role. Hid represses DIAP1 in order to activate downstream caspase cleavage pathways (S. L. Wang *et al.*, 1999), to rid the lattice of excess interommatidial potentials that make minimal cell contacts and are therefore insufficient to terminally differentiate as secondary and tertiary pigment cells. Given the role that DIAP1 plays in regulating apoptosis, the phenotype resulting from expression of DIAP1 in the eye was compared to the phenotypes resulting from Peep knockdown.

Overexpression of DIAP1 in the eye inhibits apoptosis, blocking the clearance of extra interommatidial potentials, often resulting in three cells at each tertiary pigment vertex which have equal potential to be maintained in the final lattice following apoptosis, and at least two cells equally fated to become secondary pigment cells (Figure 5.5B), as compared to the control where apoptosis eliminates excess interommatidial potentials (Figure 5.5A). Overexpression of DIAP1, therefore, results in an average of 23 accessory cells when the normal number of accessory cells is 18 (Figure 5.5C). Although there was an increase in IPCs upon overexpression of DIAP1 the overall lattice organisation remains intact, as the rows of ommatidia are all neatly aligned, with the excess cells changing their defined elongated shape to tightly pack together.

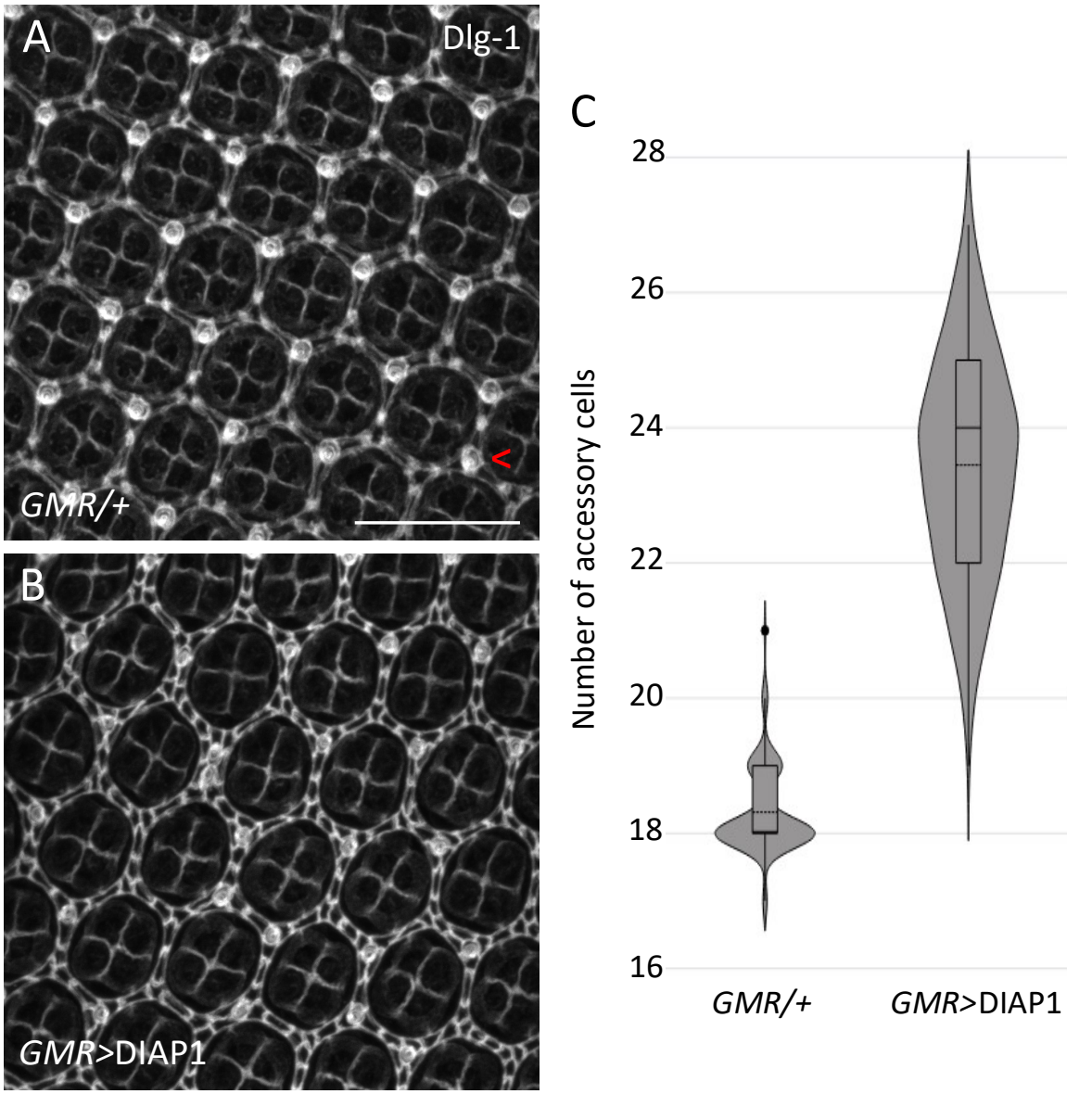

Figure 5.5. Overexpression of DIAP1 resulted in an increase in interommatidial pigment cells. Pupal eyes dissected 48-hours APF display an organised ommatidial lattice. Cell membranes were highlighted with anti-Dlg-1 and four regions of each eye (anterior, posterior, dorsal, and ventral) were quantified. A. The 'normal' control pupal ommatidial lattice with few misplaced bristle cells (red arrowhead). B. Overexpression of DIAP1 resulted in an overabundance of accessory cells, predominantly IPCs. Images were maximum projections taken using the 40x objective lens in oil, Zoom 8x, 0.5 µm sections, scale bar = 20 µm. C. Violin plot showing the distribution in the number of accessory cells per ommatidium, n≥256 ommatidia from four regions of the eye with four independent eyes per genotype. *GMR* = *GMR-GAL4*, *GMR/+* = Control.

5.1.2.1 Peep overexpression does not rescue the DIAP1-induced increase in interommatidial pigment cells

Reduced expression of Peep resulted in an increase in the number of accessory cells in approximately 50% of ommatidia. Given the similarities in phenotypes, it was hypothesised

that if Peep acts upstream of DIAP1 to repress its activity, then overexpression of Peep may reduce the DIAP1-induced overexpression phenotype in the pupal eye through inhibition, resulting in caspase cleavage mediated apoptosis of excess interommatidial potentials.

This experimental protocol involved comparison of pupal eyes expressing DIAP1 in the presence and absence of Peep^{OE}. Given that expression of both DIAP1 and Peep^{OE} is induced by GAL4, it is possible that if GAL4 is not sufficiently in excess, there may be more GAL4 available to bind *UAS-DIAP1* when expressed alone, compared to when co-expressed with *UAS-peep*^{OE}, which may result in a higher level of DIAP1 protein when expressed independently, which would confound the interpretation of the results. Therefore, to avoid any GAL4 titration-mediated differences in phenotype, flies were generated that carried both *GMR-GAL4* and either benign *UAS-GFP* (GFP) or *UAS-peep*^{OE} to ensure an equal number of transgenes were expressed between the controls and testing groups. *GMR-GAL4* driven expression of GFP resulted in no difference in ommatidial array (Figure 5.6A) or the number of accessory cells compared to the *GMR-GAL4* control (compare Figure 5.4E and Figure 5.6E). Overexpression of Peep resulted in a similar ommatidial pattern and number of accessory cells when compared to previous results (compare Figure 5.4B, E to Figure 5.6B, E). In addition, overexpression of DIAP1 resulted in a similar pattern and distribution of excess IPCs as compared to previous results (compare Figure 5.5B, C to Figure 5.6C, E). Co-expression of Peep with DIAP1 however, did not reduce the DIAP1-induced increase in IPCs (Figure 5.6C, D). Although there was a slight decrease in the mean accessory cell number (Figure 5.6E), these data indicate that Peep does not interact with DIAP1 to regulate the number of interommatidial cells in the pupal eye. Therefore, the increased number of accessory cells resulting from knockdown of Peep in the pupal eye may not be due to defects in the regulation of DIAP1-controlled apoptosis of interommatidial potentials.

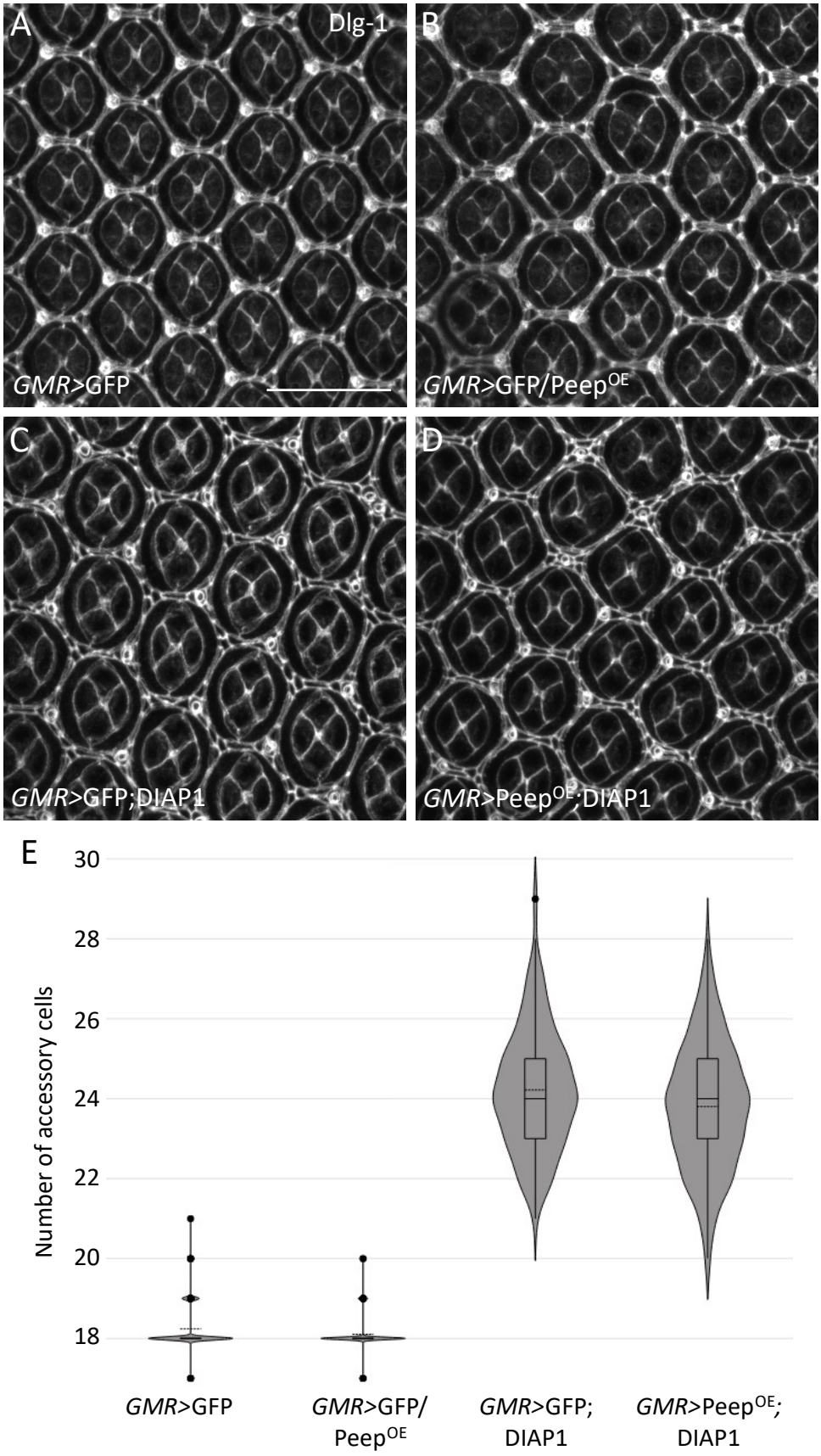

Figure 5.6. Peep overexpression does not rescue the DIAP1-induced increase in interommatidial pigment cells. Pupal eyes were dissected 48-hours APF. Cell membranes were labelled with anti-Dlg-

1 and four regions of each eye (anterior, posterior, dorsal, and ventral) were quantified. A. The normal pupal ommatidial lattice remained unchanged upon expression of *UAS-GFP*. B. Co-expression of Peep and GFP resulted in a similar phenotype to what was previously observed (Figure 5.4B, E). C. Co-expression of DIAP1 and GFP resulted in a similar phenotype to what was previously observed (Figure 5.4B, C). D. Co-expression of Peep and DIAP1 did not rescue the DIAP1-induced increase of IPCs. Images were maximum projections taken using the 40x objective lens in oil, Zoom 8x, 0.5 µm sections, scale bar = 20 µm. E. Violin plot showing the distribution in the number of accessory cells per ommatidium, n≥239 ommatidia from four regions of the eye with four independent eyes per genotype. *GMR = GMR-GAL4.*

5.1.3 Peep is required for cell survival in the adult eye

Thus far these data demonstrate that depletion of Peep in the eye did not result in obvious structural defects in third instar larvae, but resulted in major defects in the pupal eye, with individual ommatidia displaying both increased and decreased numbers of IPCs. This demonstrates that the structural integrity of the eye is likely reduced during pupal development, however there is discordance with the adult eye, as the defects in the adult eye are localised to the posterior region whereas the pupal eye defects were observed across the entire eye. Given this, it was hypothesised that the pupal eye defects may only play a part in contributing to the rough and necrotic adult eye phenotype, and other yet unknown defects result in the posterior placement of these adult eye phenotypic abnormalities.

To determine the requirement of Peep in neuronal photoreceptors, Peep was knocked down in the developed R3, R4, and R7 photoreceptor neurons with the *sevenless-GAL4* (*sev-GAL4*) driver (Bowtell *et al.*, 1989), and no adult eye phenotype was observed (Figure 5.7), indicating that Peep expression in these photoreceptors once terminally differentiated is not required for normal adult eye development.

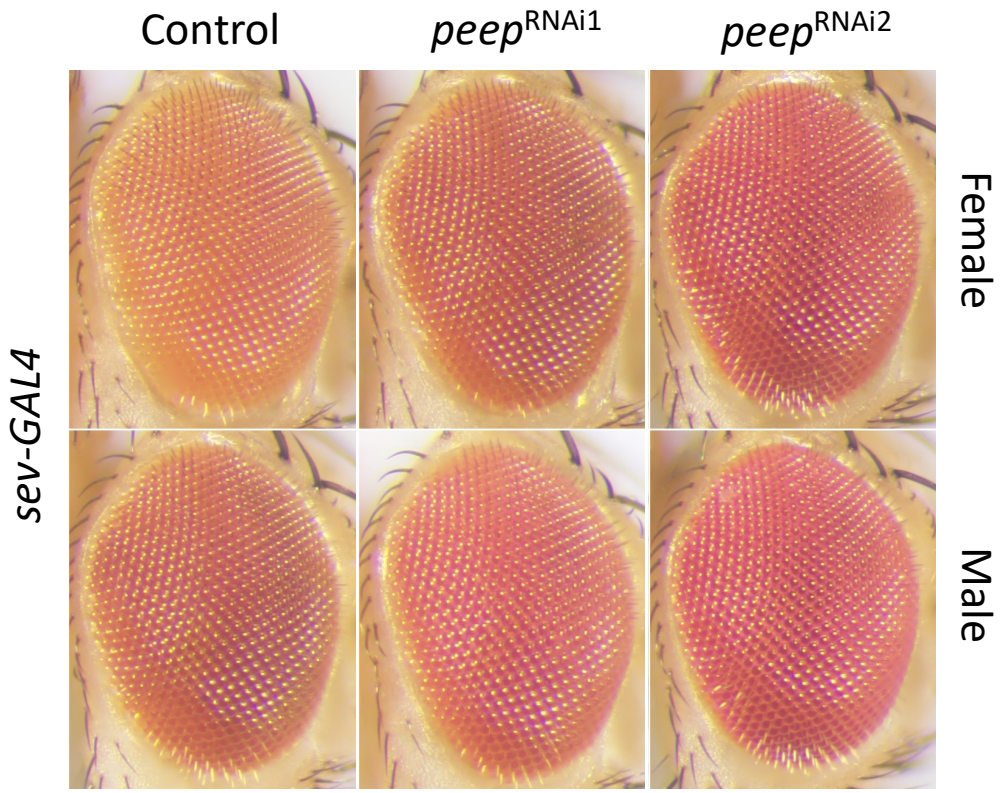

Figure 5.7. Peep expression in few terminally differentiated photoreceptors is dispensable for normal adult eye development. Expression of *peep*^{RNAi} with *sev-GAL4*, which expresses in R3, R4, and R7 terminally differentiated photoreceptor neurons, does not affect adult eye development.

Since *GMR-GAL4* induces expression in all photoreceptor cells (Escobedo *et al.*, 2021), this driver was employed to examine the impact of Peep overexpression and knockdown on the presence and structure of all photoreceptors in the adult eye. The formation and structure of the R1-R7 rhabdomeres, which are an apical specialised compartment of the photoreceptor neuron (Section 1.3.2.2) was visualised using Nile Red as a marker (Moulton *et al.*, 2021) (Section 2.2.7). R8 was not analysed as it lies below R7 and therefore is not in the same focal plane. As expected, overexpression of Peep (Figure 5.8B) did not alter the normal array of ommatidia column organisation and all seven rhabdomeres that could be visualised from the apical surface, were all of normal shape and displayed in a uniform trapezoid arrangement, similar to that of the control (Figure 5.8A). Upon knockdown of Peep, the ommatidial arrangement was compromised, which appeared to be attributed to a loss of structural integrity which may be a result of abnormal IPC numbers. Interestingly, *peep*^{RNAi1} did not appear to have a detrimental effect on the shape and organisation of R1-R7 rhabdomeres, however, it must be noted that although a number of R7 rhabdomeres were not visualised, this may not indicate missing rhabdomeres, rather that, due to the curvature of the retina, these rhabdomeres may have been

positioned above or below the plane of focus and therefore not imaged (Figure 5.8C). *peep*^{RNAi2} resulted in misshapen rhabdomeres (white arrowhead) and impaired the organisation of photoreceptors, generating a loose trapezoid cluster of rhabdomeres (Figure 5.8D). The size of each rhabdomere was measured (Section 2.2.7.1) and the combined average area was significantly reduced upon knockdown with either RNAi line (Figure 5.8E). These data demonstrate that Peep is required for normal rhabdomere formation in the adult eye. Consideration, however, of the validity of rhabdomere size should be taken into account, as the overall structural integrity of the adult retina upon *peep*^{RNAi} was compromised. This means, the retina may not have remained convex following mounting on a glass microscope slide and instead may have been flattened which would result in rhabdomeres in these eyes sitting lower in the plane of focus, compared to the control eyes, which remained convex, leading to the appearance of smaller rhabdomeres.

Overall, these data demonstrate that Peep is required for normal eye development, as a reduction throughout development resulted in defects in ommatidial patterning and necrosis in the adult eye. No gross structural defects were observed in the third instar larval eye disc, however there was a non-autonomous reduction in retinal basal glia upon aberrant expression of Peep. Furthermore, knockdown of Peep resulted in abnormalities in the number of accessory cells in the 48-hour pupal eye lattice, which was predominantly attributed to abnormal numbers of IPCs. Peep however was shown to not play a role in regulating the DIAP1-induced inhibition of caspase cleavage mediated programmed cell death in the pupal eye, indicating that the abnormal numbers of IPCs upon a reduction of Peep may not be due to apoptosis failure. As the abnormal accessory cell numbers were observed across the entire pupal eye, it is unlikely that these are the primary cause of the posterior-localised adult eye phenotype, and instead some other additional unknown mechanism dysfunction induced by Peep knockdown is at play. Adult rhabdomeres were misshapen upon Peep reduction, however it remains unclear whether this spans the entire eye due to difficulties in rhabdomere imaging based on the convex curvature of the retina, therefore the images attained were from the centre of the eye. Furthermore, it also remains unknown whether the rhabdomeres were smaller in eyes with a knockdown of Peep, due to the lack of structural integrity of these eyes, resulting in what appear to be smaller rhabdomeres.

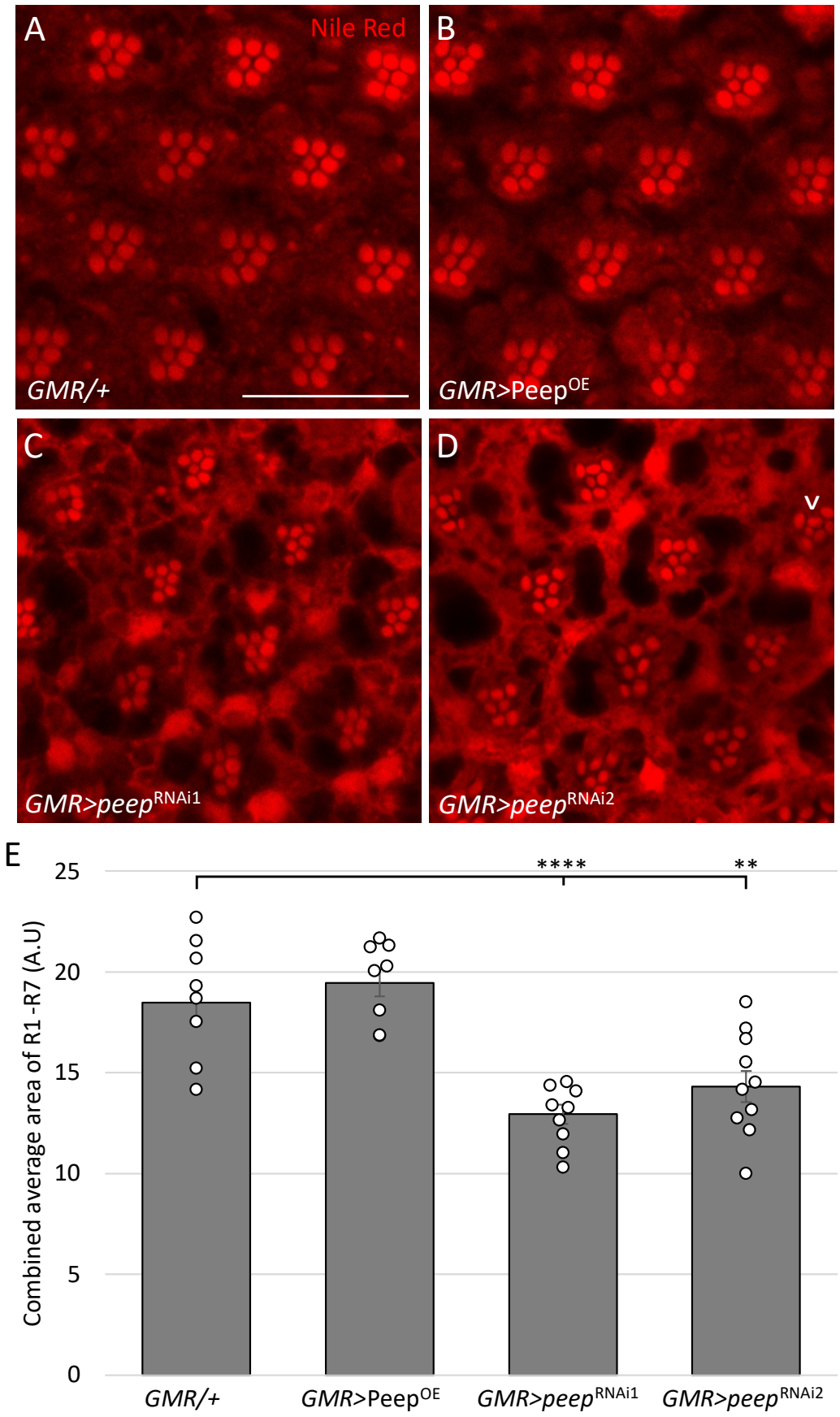

Figure 5.8. *GMR-GAL4* driven *peep*^{RNAi} resulted in ommatidial disruption and misshapen rhabdomeres. Nile Red staining of rhabdomeres was performed on dissected adult retina. Images

captured R1-R7 rhabdomeres, R8 was excluded as it lies below the plane of focus. A. *GMR/+* control eye displaying the normal trapezoid organisation of R1-R7 rhabdomeres and a highly uniform ommatidial array. B. Peep^{OE} showed no changes to rhabdomere formation and organisation. C. Expression of *peep*^{RNAi1} and D. *peep*^{RNAi2} result in abnormal ommatidial organisation with large gaps between rhabdomere clusters. The normal trapezoid arrangement of rhabdomeres was observed, however these rhabdomeres appeared smaller than the controls and there were few that were misshapen, displayed as oval and heart shaped (white arrowhead) in D. Single optical section images were attained with the 40x objective lens in oil, Zoom 8x, scale bar = 20 µm. E. Graph showing the combined average area of R1-R7 rhabdomeres in *peep*^{RNAi} samples is significantly reduced. Error bars indicate mean ± SEM, n≥8, (one-way ANOVA, post hoc Tukey HSD, $f_{(3,34)} = 16.73$, ** = p<0.01, **** = p<0.0001, *GMR-GAL4/+ ; GMR-GAL4>peep*^{RNAi1} = 0.00007, *GMR-GAL4/+ ; GMR-GAL4>peep*^{RNAi2} = 0.003). *GMR = GMR-GAL4, GMR/+* = Control.

5.2 The role of Peep in adult eye degeneration

These results demonstrate that Peep is required during eye development for normal ommatidial patterning in the pupal and adult eye, and for survival of cells in the posterior of the adult eye. Accidental cell death through internal or external factors results in necrosis, which is the morphological resting state of the cell after it has died, however the processes that predate this final resting state are often unknown. Necrosis in the eye resulting in physically smaller eyes due to mass peripheral cell death, a result of tumour necrosis factor (TNF) induced c-Jun N-terminal kinase (JNK) caspase-dependent and independent cell death (M. Li *et al.*, 2019; Li *et al.*, 2020; Wu *et al.*, 2015; Yang *et al.*, 2013), has been widely studied, however large necrotic lesions within an area of fused ommatidia on an otherwise normal eye have not been so well studied, and therefore the pathways involved are yet to be elucidated.

Although it is not yet understood how this necrosis occurs, it was hypothesised that there may be a degenerative element to these lesions as necrosis often affects neighbouring cells due to the uncontrollable release of toxic factors (Yang *et al.*, 2013). To determine whether the necrosis observed on the adult eye was progressive, *peep*^{RNAi} was driven in the eye with *GMR-GAL4* throughout development and necrosis progression was imaged and documented at different timepoints post-eclosion (Section 2.4.3). The *GMR-GAL4* control eyes appeared unaffected at all time points (Figure 5.9A). Over the course of seven to 14 days, the necrotic lesions induced by *peep*^{RNAi1} grew significantly, with only minor regions of necrosis one day post-eclosion (Figure 5.9B, D). As *peep*^{RNAi2} induced large areas of necrosis during the final stages of pupal development, which was visually observed through the pupal casing, there was no significant progression in these lesions over the 14 days post-eclosion (Figure 5.9C, D).

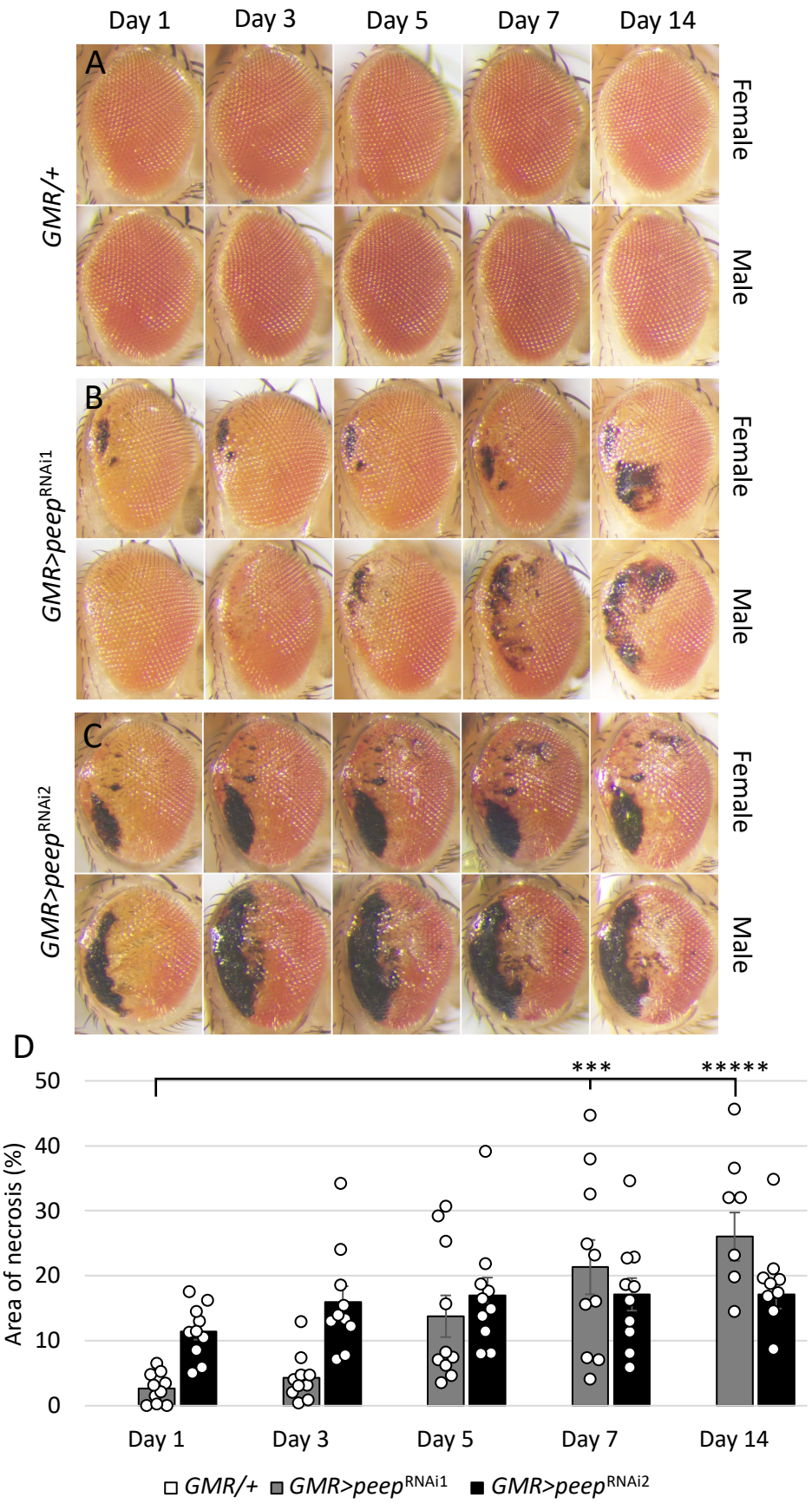

Figure 5.9. Peep knockdown resulted in a degenerative necrotic lesion phenotype. Over the course of seven days, individual flies were imaged every two days to analyse degeneration across the eye and were again imaged at 14 days post-eclosion. A. *GMR/+* control showed no sign of necrosis. B.

Expression of *peep*^{RNAi1} with *GMR-GAL4* showed a minimal area of necrosis one day post-eclosion which progressively spread over the course of 14 days. C. Expression of *peep*^{RNAi2} with *GMR-GAL4* induced a severe necrotic phenotype late in pupal development resulting in one day old adult progeny with large areas of necrosis which progressed modestly over 14 days. D. Graph showing the percent increase in necrotic lesion area over the span of 14 days. Error bars indicate mean ± SEM, n≥7, (one-way ANOVA, post-hoc Tukey HSD, $f_{(9,95)} = 7.58$, *** = p<0.001, ***** = p<0.00001, *GMR-GAL4>peep*^{RNAi1} (Day 1) ; *GMR-GAL4>peep*^{RNAi1} (Day 7) = 0.0001, *GMR-GAL4>peep*^{RNAi1} (Day 1) ; *GMR-GAL4>peep*^{RNAi1} (Day 14) = $3.92E^{-7}$). *GMR* = *GMR-GAL4, GMR/+* = Control.

It is of interest to note that the progressive phenotype induced by *peep*^{RNAi1} surpassed that of *peep*^{RNAi2} at 14 days post-eclosion (Figure 5.9D), and although this was not to an overall significant level, the phenotype in some individual eyes was largely more severe, due to incomplete penetrance. Furthermore, at day 14, the necrotic lesions induced by both *peep*^{RNAi1} and *peep*^{RNAi2} extended past the vertical midline of the eye, encroaching on the anterior region of the eye, demonstrating that the necrosis continued to spread across the eye and is not exclusively restricted to the posterior of the eye as was previously observed. In addition, as opposed to the control in which all flies were alive, by day 14, three flies harbouring *peep*^{RNAi1} and one fly harbouring *peep*^{RNAi2} were dead.

Since it has been demonstrated that Peep is important during development, it was next determined whether expression of Peep was required for cell survival in the adult eye post-eclosion. *GMR-GAL4* expresses not only during third instar larval development but also in photoreceptors, interommatidial accessory cells, and bristle groups in the pupal and adult retina (Escobedo *et al.*, 2021; Plautz *et al.*, 1996). To that effect, in order to restrict RNAi expression to the adult eye, the TARGET system (Section 1.3.4.2) was employed, with virgin female flies harbouring *GMR-GAL4* and *tubP-GAL80*^{ts}. As a control, a subset of flies were maintained at 19°C for 72 hours following eclosion and imaged without expression of *peep*^{RNAi}. The remainder of the flies were moved to 30°C to induce GAL4-mediated Peep knockdown for 72 hours or seven days. No necrosis was observed in control eyes (Figure 5.10A), nor on expression of either *peep*^{RNAi} transgene for either 72 hours (Figure 5.10B) or seven days (Figure 5.10C)

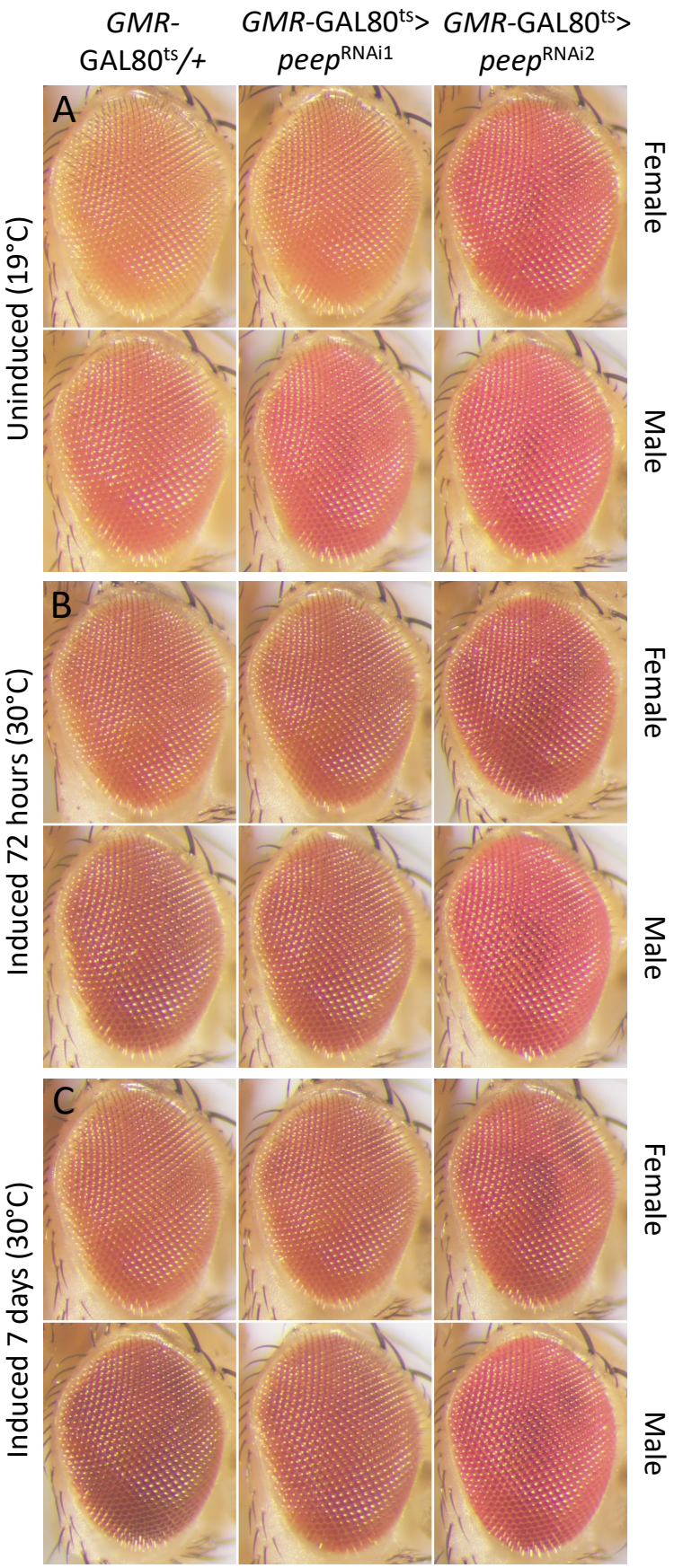

Figure 5.10. Adult-specific knockdown of Peep did not affect the adult eye. The TARGET system was employed to restrict expression of *peep*^{RNAi} to adulthood. Flies were raised at 19°C, once emerged,

flies were either A. maintained at 19°C for 72 hours before being processed or B. transferred to 30°C for 72 hours before being processed or C. transferred to 30°C for seven days before being processed. A rough eye phenotype was not observed upon any treatment. *GMR-GAL80*^{ts} = *GMR-GAL4,tub-GAL80*^{ts}, *GMR-GAL4,tubGAL80*^{ts}/+ = Control.

These data show that Peep may not be required for maintenance of the retina post-eclosion, demonstrating that specific expression of Peep in the eye during development is important for cell survival, specifically those in the posterior of the eye. To further these conclusions it would be of interest to further utilise the TARGET system and induce Peep knockdown during larval development and silence the knockdown from pupal development onwards to further analyse the requirement of Peep during larval and pupal development.

5.2.1 Necrosis was reduced by expression of factors that improve mitochondrial function, reduce apoptosis and reduce the production of reactive oxygen species

As necrotic cell death is an end product of cellular dysfunction resulting from cellular inflammation and lysis that can be induced via a range of different mechanisms, it was of importance to highlight the potential pathways through which Peep acts to prevent the necrosis originating at the posterior of the eye. Mitochondrial dysfunction, apoptosis and increases in ROS are all interconnected, and all have implications in necrotic cell death. Apoptosis or programmed cell death is a normal cellular process in which old or defective cells are degraded via caspase cleavage (Parrish *et al.*, 2013). Apoptosis can be initiated by mitochondrial dysfunction which can result from a loss of mitochondrial integrity, furthermore, mitochondrial dysfunction can be attributed to a loss of membrane dynamics and increases in oxidative stress, often a result of increased ROS (Misrani *et al.*, 2021).

One source of ROS is the electron transport chain (ETC) which is located at the mitochondria and generates oxidative adenine triphosphate (ATP) as an energy source via oxidative phosphorylation, during which time oxygen is reduced to water (Zhao *et al.*, 2019). Superoxide radicals are produced by electron leakage at complex I and III whereby the transference of an electron to an oxygen molecule generates a superoxide radical. These superoxide radicals are highly reactive and under basal conditions are quickly converted to non-reactive H_2O_2 through mitochondrial expressed superoxide dismutase 1 (SOD1), the pool of H_2O_2 is then detoxified by Catalase into water molecules. ROS are therefore a by-product of normal cell activity and

have an important role in long-term potentiation, synaptic plasticity, and memory formation, as observed in mouse models (Levin *et al.*, 1998; Thiels *et al.*, 2000).

Both SOD1 and Catalase are conserved among species and are involved in the decomposition of highly reactive superoxide radicals to less reactive H_2O_2, and further breakdown of H_2O_2 into water, respectively (Nandi *et al.*, 2019; Wang *et al.*, 2018). High concentrations of superoxide radicals and H_2O_2 are a result of dysregulation induced oxidative stress, and often cause irreversible cell damage and death (McCord & Fridovich, 1968, 1969). Mitochondrial dynamics are important for maintaining organelle shape and connectivity networks. Mitochondrial morphological changes occur during the processes of fission, to divide and regenerate, and fusion, to combine two mitochondria for the transfer of metabolites and DNA to repair respiratory machinery, with both processes being important for mitochondrial maintenance (Green *et al.*, 2022). These processes are undertaken by a range of GTPases Mitofusin 1 and Mitofusin 2 which play an essential role in outer membrane mitochondrial fusion. The *Drosophila* homologue Mitochondrial associated regulatory factor (Marf) has also been shown to also be required for mitochondrial fusion, as a loss of Marf results in mitochondrial morphological defects (Katti *et al.*, 2021) and impairments to neuromuscular junction synaptic transmission (Sandoval *et al.*, 2014). Marf reduction early in muscle development results in decreased muscle function (Katti *et al.*, 2021) as mitochondria are the main source of ATP, which is essential for muscle movement. Furthermore, ubiquitous ablation of Marf was larval lethal (Debattisti *et al.*, 2014) suggesting that a loss of mitochondria fusion, leading to mitochondrial dysfunction, ultimately results in death. As previously detailed in Section 1.3.2.2, in *Drosophila,* expression of the pro-apoptotic gene, *hid*, as well as *grim*, and *rpr* results in repression of DIAP1, leading to activation of the caspase initiator Dronc, which in turn regulates expression of caspases Drice and Dcp-1 resulting in degradation of target cells (Muro *et al.*, 2002; S. L. Wang *et al.*, 1999). Apoptosis relies on phagocytes to engulf and eliminate apoptotic bodies containing cellular components from caspase-mediated cleavage. If scavenging fails, these apoptotic bodies lose membrane integrity resulting in rupture and leakage of pro-inflammatory contents which is referred to as secondary necrosis, demonstrating the pathway disruption in which apoptosis can result in necrosis (Poon *et al.*, 2014). It has been shown that during third instar larval eye development, differentiating photoreceptor neurons accumulate DIAP1 in order to escape apoptosis under increased expression of Hid (Fan & Bergmann, 2014), demonstrating how DIAP1 can rescue cells from ectopic induction of apoptosis.

In order to identify new avenues for investigating the role that Peep plays during eye development, Catalase, SOD1, Marf, and DIAP1, all of which have all been shown to promote cell survival (hereafter called survival factors), were co-expressed with *peep*^{RNAi} to determine whether rescue of the *peep*^{RNAi}-induced necrosis could be achieved.

To co-express *peep*^{RNAi} with each of the survival factors, the *UAS-peep*^{RNAi} transgenes were first recombined with *GMR-GAL4,tub-GAL80*^{ts} to maintain a homozygous stock that when raised at low temperatures, facilitated low expression of *peep*^{RNAi} (Figures 8.8 and 8.9, Appendix 8.6). This was required for stock maintenance as constitutive expression of *peep*^{RNAi} with *GMR-GAL4* was semi-lethal (Section 5.2.2).

This homozygous line was then crossed to lines carrying each survival gene under UAS control. Flies were initially raised at 30°C, however, this temperature induced a total pupal lethal phenotype in flies with a knockdown of Peep, therefore, flies were raised at 27°C. At this temperature there was adequate pupal survival however under these conditions the expression of *peep*^{RNAi1} was not sufficient to induce large areas of necrosis (Figure 8.11, Appendix 8.7), therefore the experiment was only carried out with *peep*^{RNAi2}. Expression of Catalase, DIAP1, and SOD1 did not individually induce a rough eye phenotype, however, expression of Marf resulted in a very mild rough eye phenotype consisting of depigmentation and ommatidial misalignment (Figure 5.11A). As expected, expression of *peep*^{RNAi2} alone induced a posterior localised moderate rough eye phenotype with a region of necrosis along the posterior edge of the eye. Upon co-expression with Catalase, DIAP1, Marf, or SOD1 there was no obvious improvement to the rough eye phenotype, however the area of necrosis was significantly reduced (Figure 5.11B, C). This indicated that the knockdown of Peep triggers a necrotic phenotype which occurs as a result of apoptosis dysregulation, mitochondrial dysfunction, and increased levels of ROS as overexpression of each of these survival factors rescued the necrotic eye phenotype.

An additional control was later tested to account for any GAL4 titration differences upon knockdown of Peep and expression of survival genes, whereby *GMR-GAL4,tub-GAL80*^{ts},*peep*^{RNAi2} was crossed to a benign transgene, *UAS-GFP* (GFP). A similar level of necrosis was observed, however due to the incomplete penetrance induced by *peep*^{RNAi2}, the severity of necrosis varied between individual eyes (Figure 5.11D).

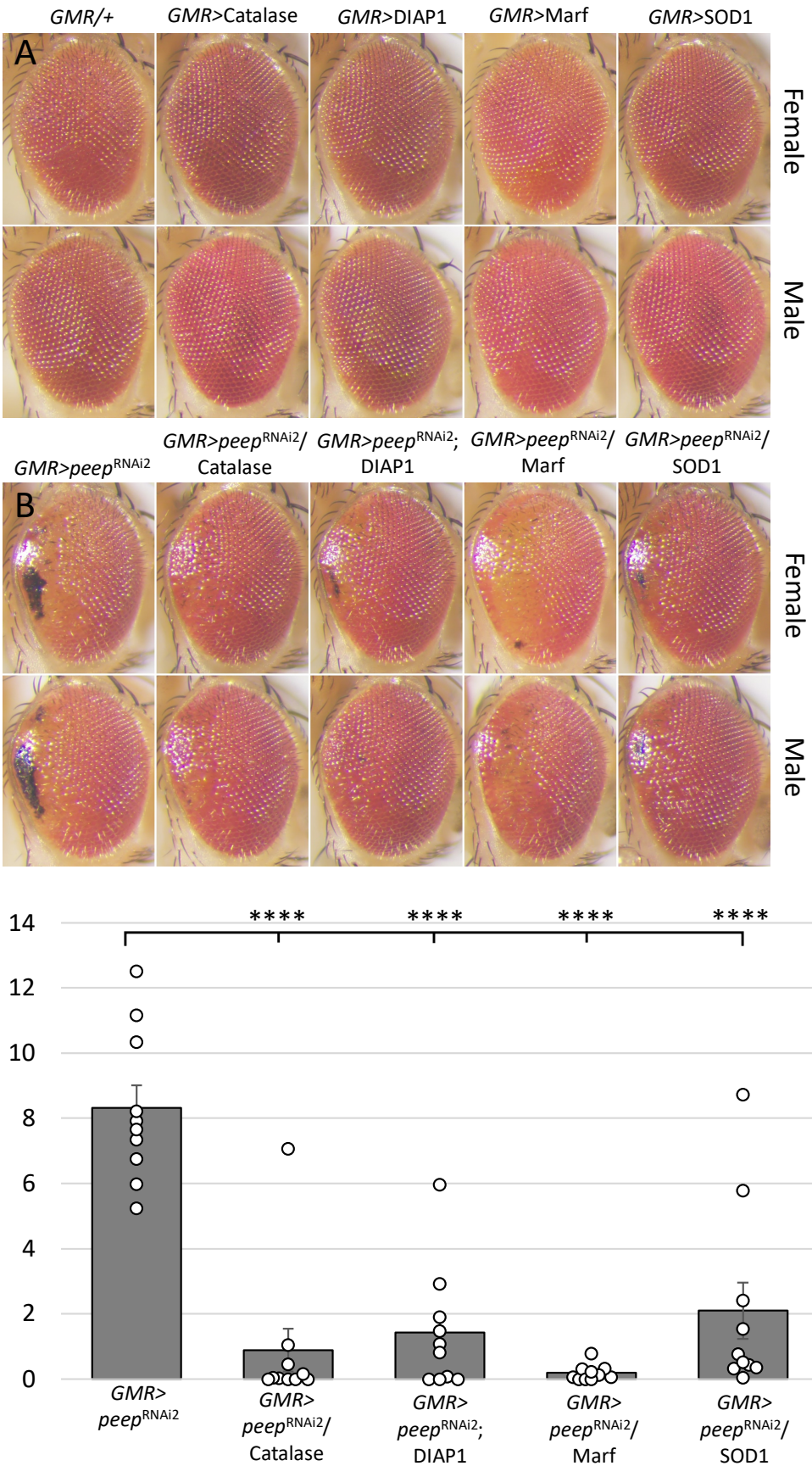
GMR/+
GMR>Catalase
GMR>DIAP1
GMR>Marf
GMR>SOD1
A
Female
Male
GMR>peepRNAi2
GMR>peepRNAi2/ Catalase
GMR>peepRNAi2; DIAP1
GMR>peepRNAi2/ Marf
GMR>peepRNAi2/ SOD1
B
Female
Male
C
Area of necrosis (%)
0
2
4
6
8
10
12
14
****
****
****
****
GMR> peepRNAi2
GMR> peepRNAi2/ Catalase
GMR> peepRNAi2; DIAP1
GMR> peepRNAi2/ Marf
GMR> peepRNAi2/ SOD1

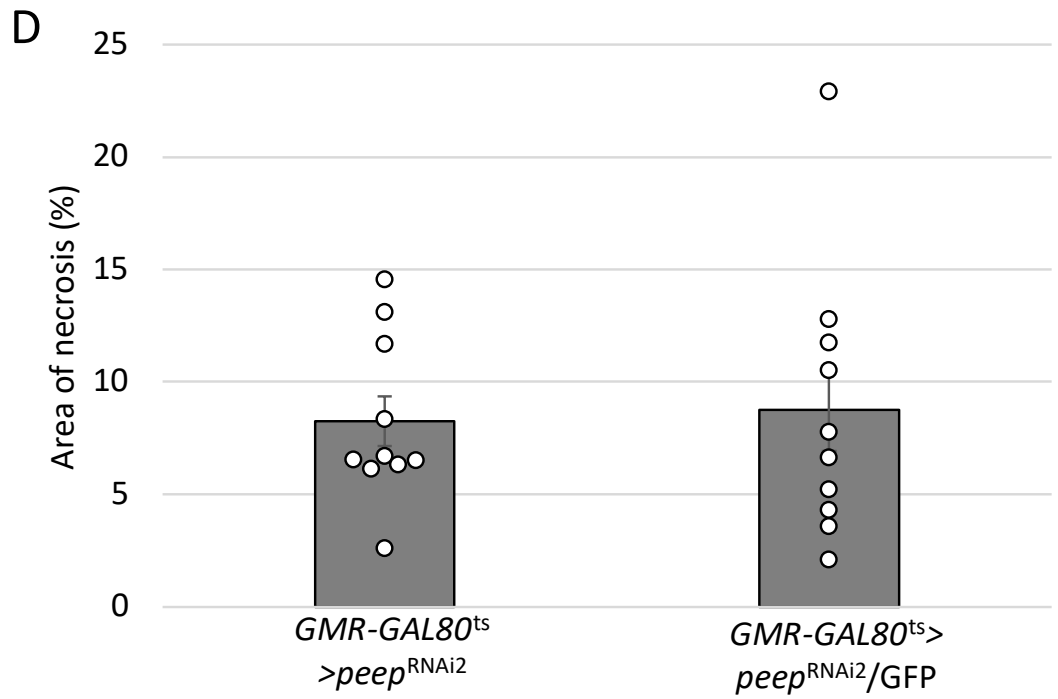

Figure 5.11. Genes involved in maintaining cell survival, rescue *peep*^{RNAi}-induced necrotic lesions on the adult eye. All flies were raised at 27°C throughout development to induce a necrotic phenotype upon Peep reduction. A. *GMR-GAL4,tub-GAL80*^{ts} was crossed to overexpression constructs of genes involved in the breakdown of ROS (*Catalase* and *SOD1*), mitochondrial function (*Marf*), and apoptosis inhibition (*DIAP1*). All, excluding Marf, lacked a rough eye phenotype. B. *GMR-GAL4,tub-GAL80*^{ts}*,peep*^{RNAi2} was crossed to Catalase, DIAP1, Marf, and SOD1 and all maintain the rough eye phenotype but reduce the area of necrosis. C. The area of necrosis was measured using ImageJ and was represented as a percentage proportion of the total eye area. All overexpressed survival genes significantly reduced the area of necrosis. Error bars indicate mean ± SEM, n=10, (one way ANOVA, post-hoc Tukey HSD, $f_{(4,49)} = 24.3$, **** = $p<0.0001$, *GMR-GAL4,tub-GAL80*^{ts}*,peep*^{RNAi2}/+ ; *GMR-GAL4,tub-GAL80*^{ts}*,peep*^{RNAi2}*>Catalase* = $4.827E^{-9}$ *GMR-GAL4,tub-GAL80*^{ts}*,peep*^{RNAi2}/+ ; *GMR-GAL4,tub-GAL80*^{ts}*,peep*^{RNAi2}*>DIAP1* = $3.393E^{-8}$ *GMR-GAL4,tub-GAL80*^{ts}*,peep*^{RNAi2}/+ ; *GMR-GAL4,tub-GAL80*^{ts}*,peep*^{RNAi2}*>Marf* = $4.323E^{-10}$ *GMR-GAL4,tub-GAL80*^{ts}*,peep*^{RNAi2}/+ ; *GMR-GAL4,tub-GAL80*^{ts}*,peep*^{RNAi2}*>SOD1* = $3.803E^{-7}$). D. *GMR-GAL80*^{ts}-driven expression of two transgenes (*peep*^{RNAi2} and *GFP*) resulted in a similar level of necrosis on the eye as *GMR-GAL80*^{ts}-driven expression of one transgene (*peep*^{RNAi2}). *GMR* = *GMR-GAL4,tub-GAL80*^{ts}.

To link these results back to the structure of the pupal eye (Section 5.1.2), it was of interest to note that DIAP1 expression in the adult retina resulted in an uncompromised ommatidial array (Figure 5.11A) yet during pupal development there was a significant increase in the number of IPCs (Figure 5.5B). This demonstrates that in this case an excessive number of accessory cells does not induce an adult rough eye phenotype, which provides further evidence that the pupal eye phenotype resulting in abnormal numbers of accessory cells on knockdown of Peep, is not necessarily causative of the adult rough and necrotic eye phenotype.

5.2.2 H_2O_2 exposure does not affect the severity of the necrotic eye phenotype

Based on these data it appears that expression of Catalase and SOD1, both of which are involved in the breakdown of superoxide radicals and H_2O_2 into non-reactive water molecules, represses the necrotic lesion phenotype induced by *peep*^{RNAi2}, leading to the hypothesis that Peep may be involved in the regulation and/or clearance of ROS in the eye and that the necrotic lesions observed are, at least in part, due to increased levels of ROS.

As stated earlier, *GMR-GAL4* driven expression of *peep*^{RNAi} was semi-lethal, as a significant number of pharate adults were dead inside their pupal cases (Figure 5.12A). Upon dissection of these dead adults, it was observed that the insides of the pupal casings encapsulating the head remained adhered to the large necrotic lesions on the eyes, which indicated that if the fully developed pharate adult eyes have significantly large areas of necrosis prior to eclosion, these flies become stuck and die inside of their pupal casings.

As the *GMR-GAL4* driven *peep*^{RNAi2}-induced necrosis on the eye was rescued by both Catalase and SOD1, whose primary function is the breakdown and removal of ROS, it was hypothesised that if the levels of ROS were enhanced by exposure to exogenous H_2O_2, the level of pupal lethality would indirectly increase, which may be attributed to ROS-induced increases in the onset and/or spreading of eye necrosis prior to eclosion, resulting in fewer surviving adults with an enhanced necrotic phenotype. To induce necrosis, Peep must be knocked down in the eye throughout development, therefore, the fly media was supplemented with 1% H_2O_2 resulting in *peep*^{RNAi2} expressing progeny ingesting H_2O_2 in order to increase internal levels of ROS (Section 2.6.1). Upon exposure to H_2O_2 there was a significant increase in the proportion of pupal lethality upon expression of *peep*^{RNAi2} compared to the *peep*^{RNAi2} control raised on standard media (Figure 5.12B). This, however, cannot be confirmed to be a direct result of increased spreading or earlier onset necrosis as there was also an increased proportion of pupal lethality in the driver control (*GMR-GAL4/+*) (Figure 5.12B), indicating that exposure to H_2O_2 results in increased pupal death regardless of genetic makeup. Interestingly, exposure of H_2O_2 had a close to significant decrease in the average total number of pupae (ie a count of the total number of larvae that pupated regardless of whether they emerged from their pupal cases or not) in the *GMR-GAL4/+* control compared to the *GMR-GAL4/+* control raised on standard media (Figure 5.12C). Upon closer inspection, this was attributed to a number of first and second instar larvae that were dead on the walls of the bottles (Figure 5.12D), which was only observed in the *GMR-GAL4/+* control. There was however a comparable number of total pupae

upon expression of *peep*^{RNAi2} when raised on standard media and H_2O_2 supplemented media (Figure 5.12C), therefore, it could be concluded that knockdown of Peep may result in flies that are more susceptible to increases in ROS specifically during pupal development through exposure of H_2O_2, leading to an increase in pupal lethality. These flies, however, were protected against the H_2O_2-induced larval lethality that was observed in the *GMR-GAL4/+* control (Figure 5.12C, D). The eye phenotype from adult escapers upon knockdown of Peep was not obviously more severe following exposure of H_2O_2 (Figure 8.12, Appendix 8.7), and as there was also an increase in pupal lethality in the *GMR-GAL4/+* control it is unlikely that knockdown of Peep upon exposure to H_2O_2 increased pupal lethality through an increase in necrotic lesions. Instead it could be hypothesised that similar to the *GMR-GAL4/+* control, increased ROS may be affecting other eclosion related processes, leading to an increase in pupal death.

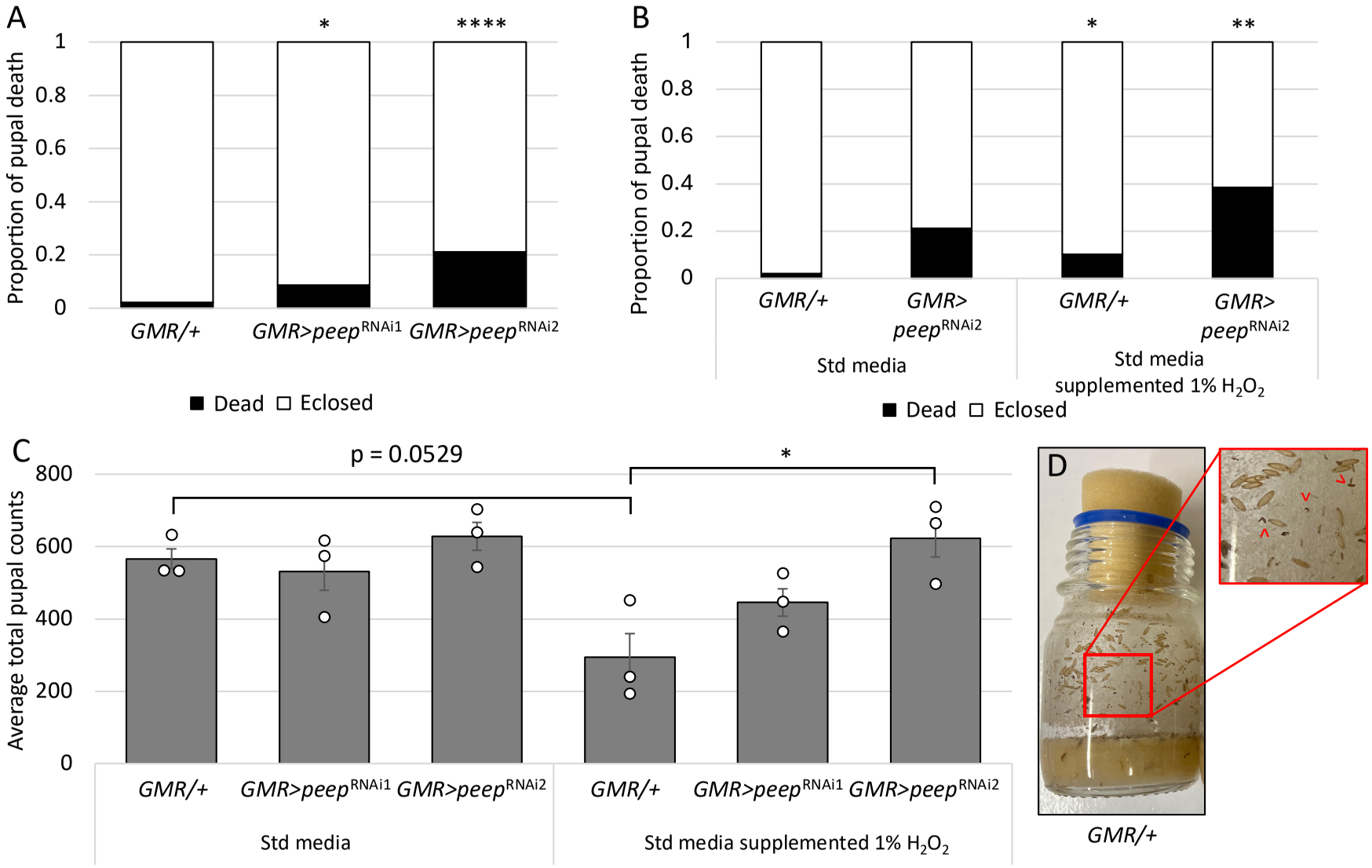

Figure 5.12. Exposure to 1% H_2O_2 increased pupal lethality. A. *GMR-GAL4* driven expression of *peep*^{RNAi} resulted in a significant increase in pupal death when raised on standard fly media, n=3, (One-tailed Fisher's exact test, * = p<0.05, **** = p<0.0001, *GMR-GAL4/+* ; *GMR-GAL4>peep*^{RNAi1} = 0.0291, *GMR-*

GAL4/+ ; *GMR-GAL4>peep*^{RNAi2} = 0.0001). B. The proportion of pupal death was significantly increased upon H_2O_2 exposure in both control flies and flies expressing *peep*^{RNAi2}, n=3, (one-tailed Fisher's exact test, * = p<0.05, ** = p<0.01, *GMR-GAL4/+* (std) ; *GMR-GAL4/+* (1% H_2O_2) = 0.165, *GMR-GAL4>peep*^{RNAi2} (std) ; *GMR-GAL4>peep*^{RNAi2}(1% H_2O_2) = 0.0064). C. The total number of pupae (eclosed and dead) show a decrease in larval propagation to the pupal stage in the *GMR-GAL4* driver control when exposed to H_2O_2 compared to the *GMR-GAL4* driver control raised on standard media. There are similar total pupal counts for *peep*^{RNAi2} between standard media and H_2O_2 supplemented media. Error bars indicate mean ± SEM, n=3, (one-way ANOVA, post-hoc Tukey HSD, $f_{(5,17)} = 4.84$, * = p<0.05, *GMR-GAL4/+* (std) *; GMR-GAL4/+* (1% H_2O_2) = 0.0529, *GMR-GAL4/+* (1% H_2O_2) *; GMR-GAL4>peep*^{RNAi2} = 0.0163). D. Image showing larval death upon H_2O_2 exposure in *GMR-GAL4* driver control flies. Inset: close-up showing death of first and second instar larvae (red arrowheads). *GMR* = *GMR-GAL4, GMR/+* = Control, std = standard, H_2O_2 = hydrogen peroxide.

5.2.2.1 *peep*^{RNAi2} post-developmental survival is reduced upon H_2O_2 exposure

An alternative approach was taken to assess susceptibility to increases in ROS, by analysing survival rates following ubiquitous knockdown or overexpression of Peep with *arm-GAL4*. To measure longevity, three-to-four-day old adult progeny driving ubiquitous knockdown or overexpression of Peep were placed in empty plastic vials, and a long strip of Whatman filter paper soaked with 5% sucrose and 1% H_2O_2 was added to each vial as a fly media substitute (Section 2.6.2). Fly death counts were recorded each day until all flies were dead. Total death occurred by the end of day 22, with accelerated death occurring between days five and ten. A statistically significant difference in death rate in the presence of H_2O_2 occurred between the control and *peep*^{RNAi2}, however this was not observed with *peep*^{RNAi1} (Figure 5.13A). This death rate could be attributed to increased oxidative stress as a control assay was performed in conjunction where flies were fed 5% sucrose, and no differences in mortality was observed between *peep*^{RNAi1} or *peep*^{RNAi2} and the control (Figure 5.13B). This assay requires replication to determine whether there is a reproducible difference in survival capacity between RNAi lines. Surprisingly, there was also a significant increase in the rate of death in the presence of H_2O_2 in flies overexpressing Peep compared to the control (Figure 5.13A), however, in the control assay, where flies were fed only sucrose, there was also a significant increase in the rate of death in flies overexpressing Peep compared to the control (Figure 5.13B). These results indicate that the increased death rate upon overexpression of Peep, when exposed to H_2O_2, is likely not due to increases in oxidative stress, rather this accelerated death could be due nutrient deprivation.

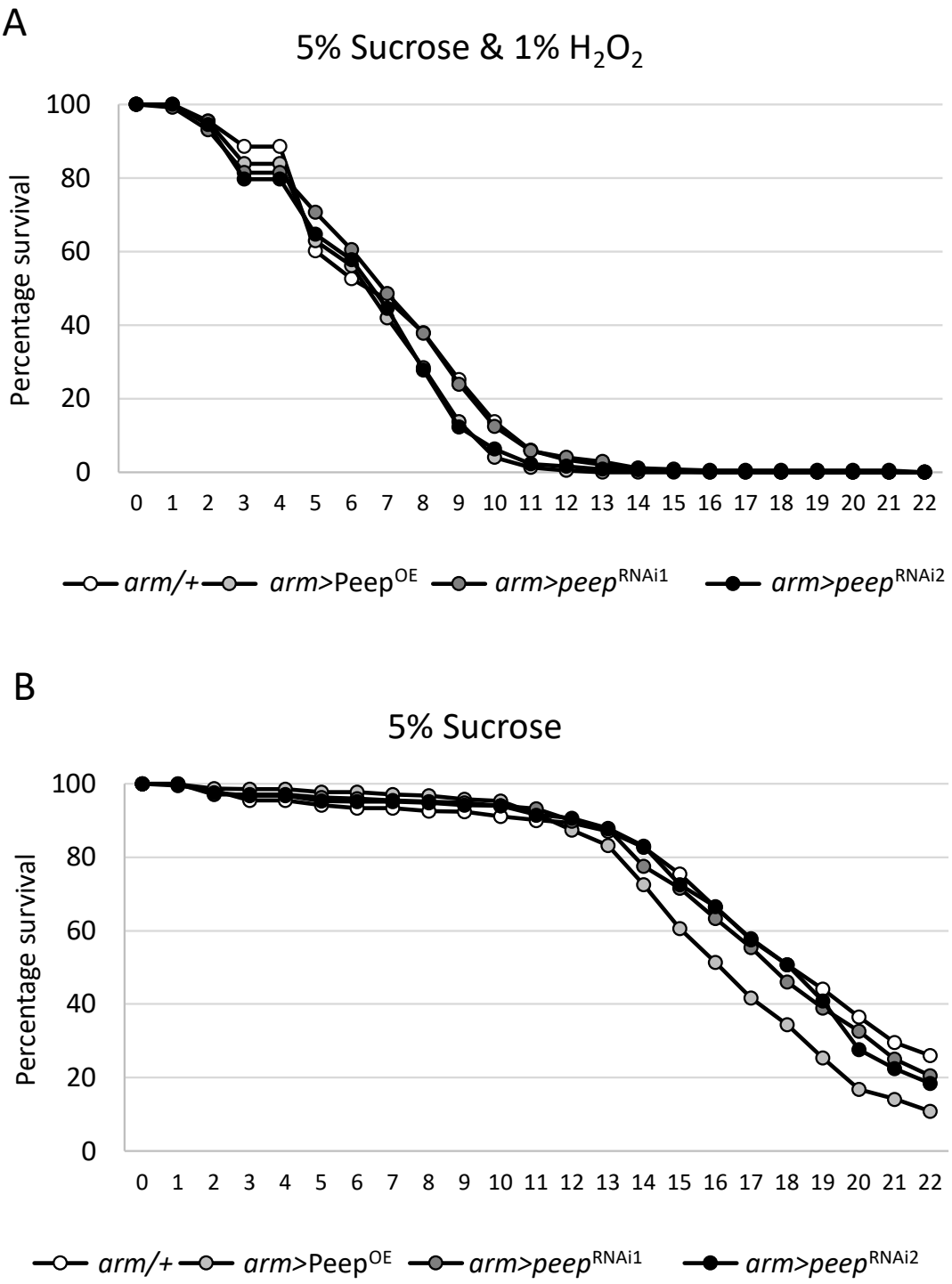

Figure 5.13. Ubiquitous *peep*^{RNAi2} increased the death rate upon exposure to H_2O_2. A. Ubiquitous expression of Peep^{OE} or *peep*^{RNAi2} resulted in rapid death upon increased levels of ROS via feeding adult flies 5% sucrose supplemented with 1% H_2O_2, n≥276, housed at a maximum of 20 per vial, (log rank test, Bonferroni correction, ** = p<0.01, *** = p<0.001, *arm-GAL4/+ ; arm-GAL4>peep*^{OE} = 0.0002, *arm-GAL4/+ ; arm-GAL4>peep*^{RNAi2} = 0.0034). B. Ubiquitous expression of Peep^{OE} had an enhanced death rate upon feeding adult flies 5% sucrose, n≥267, housed at a maximum of 20 per vial, (log rank test, Bonferroni correction, ***** = p<0.00001, *arm-GAL4/+ ; arm-GAL4>peep*^{OE} = 0). *arm = arm-GAL4, arm/+* = Control, H_2O_2 = hydrogen peroxide.

5.2.3 Proteasome activity was reduced upon knockdown of Peep

The confinement of the rough and necrotic eye phenotypes to the posterior region of the eye is unusual and unique and an extensive literature review failed to find many examples of this phenotype. Interestingly, however, the few reports that were found involved proteasomal subunit mutants (Fernandez-Cruz *et al.*, 2020; Muller *et al.*, 2006; Tonoki *et al.*, 2009; Velentzas *et al.*, 2013).

The 26S proteasome is an ATP-dependent protease complex which functions to degrade ubiquitin tagged proteins and is comprised of two multi-subunit complexes. The 20S catalytic core contains four stacked rings two inner β rings and two outer α rings. Each ring is comprised of seven individual subunits (α1-α7, β1-β7). The outer α rings act as gate keepers to block untagged substrate entrance into the catalytic inner β ring core. There are three catalytic active sites within the catalytic chamber, all of which contain different substrate specificities and hydrolytic properties. β1 contains caspase-like activity, β2 contains trypsin-like activity, and β5 contains chymotrypsin-like activity. The 19S complex forms from two smaller complexes, the base and the lid, which are located on either end of the outer α rings and contain either Regulatory particle of triple-ATPase (Rpt) subunits or Regulatory particle of non-ATPase (Rpn) subunits or both. α, β, Rpt, and Rpn are all systematic nomenclature and are referred to by different nomenclature depending on the organism. The lid is comprised of nine Rpn subunits that differ from those in the base (Rpn3, Rpn5-Rpn9, Rpn11, Rpn12, and Rpn 15) which form a semi-circle structure and function by removing the ubiquitin tag from proteins that are targeted for degradation by the proteasome. The base contains six Rpt (Rpt1-Rpt6) and four Rpn (Rpn1, Rpn2, Rpn10, and Rpn13) subunits which form a ring, and function as ubiquitin receptors and therefore recognise and capture ubiquitin tagged proteins. The base also uses ATP hydrolysis for protein unfolding and transfer facilitation into the catalytic core (Livneh *et al.*, 2016) (Figure 5.14).

Protein degradation via the ubiquitin-proteasome pathway is an important quality control process for basic cell function, however there is both age-related decline in assembly and function as well as early-onset aberrant degradation which contributes to a variety of diseases, resulting from accumulation of unfolded and misfolded proteins (McNaught *et al.*, 2003; McNaught *et al.*, 2002; Tonoki *et al.*, 2009).

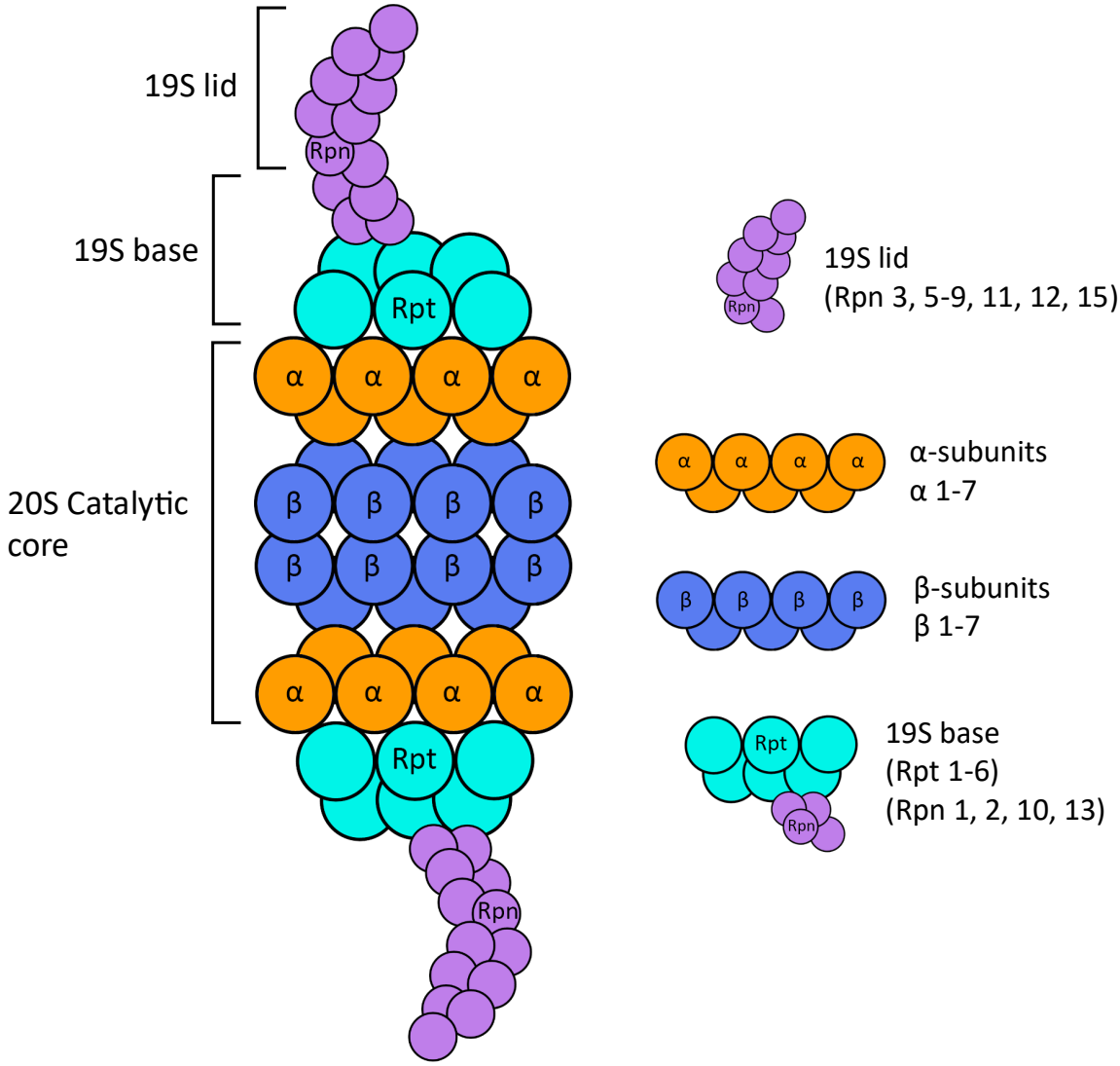

Figure 5.14. The components of the 26S proteasome. The proteasome is comprised of the 20S catalytic core which contains four stacked rings of seven outer α-subunits and seven inner β-subunits. The β subunits packed in the centre generate the catalytic core. Stacked on the α-subunit rings are the 19S base, comprised of the Rpt 1-6 and Rpn 1, 2, 10, and 13 subunits, which is capped by the 19S lid, comprised of the Rpn 3, 5-9, 11, 12, and 15 subunits.

ROS have been shown to lead to proteasomal dysfunction, where increases in internal ROS levels results in a decrease in 20S subunit generation (Parajuli, 2019) and dissociation of the 26S proteasome complex, ultimately leading to reduced proteasomal activity, all of which were reversible on reduction of ROS (Livnat-Levanon *et al.*, 2014). Proteasome dysfunction, via oxidative damage, loss of subunit production, or mutations to the polyubiquitination process result in increases in mitochondrial ROS and accumulation of poly-ubiquitinated proteins in mitochondria (Livnat-Levanon *et al.*, 2014; Maharjan *et al.*, 2014; Parajuli, 2019). These

studies show the cyclic nature of mitochondrial and proteasomal dysfunction in the production of ROS, which often ultimately results in cell death.

Both Muller *et al.* (2006) and Fernandez-Cruz *et al.* (2020) showed that a reduction in the 19S base subunit Rpt2, which is highly conserved from yeast to humans (Hölzl *et al.*, 2000), resulted in a posterior-localised rough eye phenotype with areas of necrosis. In *Drosophila*, Rpt2 reduction specifically in the dopaminergic neurons resulted in a shortened lifespan, reduced locomotion, disordered sleep, and degeneration of dopaminergic neuron clusters (Fernandez-Cruz *et al.*, 2020). Additional subunits of the 19S base, Rpn1 and Rpn2 also result in a posterior localised rough and necrotic eye phenotype upon depletion (Velentzas *et al.*, 2013).

Rpn11, a subunit of the 19S lid is also important for proteasome function and its reduction also resulted in a rough and necrotic posterior-localised eye phenotype. In addition, rhabdomeres were shown to degenerate over a ten-day timeframe and the Rpn11 reduction resulted in a decrease in chymotrypsin-like activity which led to premature accumulation of poly-ubiquitinated proteins. Furthermore, the normal age-related decline of proteasome assembly and subsequent activity, was mitigated by overexpression of Rpn11 (Tonoki *et al.*, 2009).

Knockdown of the α5, β5, and β6 subunits of the 20S proteasome also induced a rough necrotic phenotype in the posterior of the eye (Velentzas *et al.*, 2013), and targeted depletion of β5 resulted in a decrease in protein degradation (Kisselev *et al.*, 2006), which was unsurprising as the chymotrypsin-like active site resides within the β5 subunit. These results show that subunits of both the 19S and 20S proteasome, including those that comprise the catalytic core are required for normal eye development, as defects to proteasome assembly and function result in severe impairments.

As the adult eye phenotypes induced following reduction of proteasomal subunits mirrors those induced by *peep*^{RNAi}, it was hypothesised that Peep may play an important role in proteasomal function, and that reduced expression of Peep may result in impairments to proteasome activity. The chymotrypsin-like proteolytic activity of the proteasome was assessed by measuring the fluorescence of the N-succinyl-leucine-leucine-valine-tyrosine-7-amino-4-methylcoumarin (Suc-LLVY-AMC) substrate. AMC is a fluorescent probe, where conjugation via its amino terminal to a chymotrypsin targeted peptide (Suc-LLVY) quenches the fluorescence (Zimmerman *et al.*, 1977; Zimmerman *et al.*, 1976) (Section 2.9). Chymotrypsin enzymes have an affinity for aromatic amino acids due to a hydrophobic pocket (Bergmann & Fruton, 1937;

Fruton & Bergmann, 1942), therefore cleavage of the Suc-LLVY-AMC peptide occurs at the tyrosine residue of the peptide, in turn releasing the fluorescent AMC probe to be detected at 355 nm/460 nm (ex/em). Proteasome activity was first measured in the eye using *GMR-GAL4* to drive expression of *peep*^{RNAi}. Whole fly heads were homogenised and incubated with Suc-LLVY-AMC. Fluorescence readings from the cleaved AMC probe were recorded on a fluorogenic plate reader, and the change in fluorescence per minute per µg of protein was determined, and a significant reduction in chymotrypsin-like activity following expression of *peep*^{RNAi2} in the eye was observed. *peep*^{RNAi1}, which induces a less severe necrotic phenotype upon adult eclosion, also resulted in a decrease in activity, however not significantly (Figure 5.15A). These results suggest that Peep plays a role in regulating proteasomal activity in the eye.

To examine whether Peep is required for proteasome activity in other tissues, Peep was ubiquitously knocked down with *arm-GAL4,* and proteasome activity was assayed on whole fly lysates, however no significant change in proteasome activity was observed, although there was a general decreasing trend (Figure 5.15B).

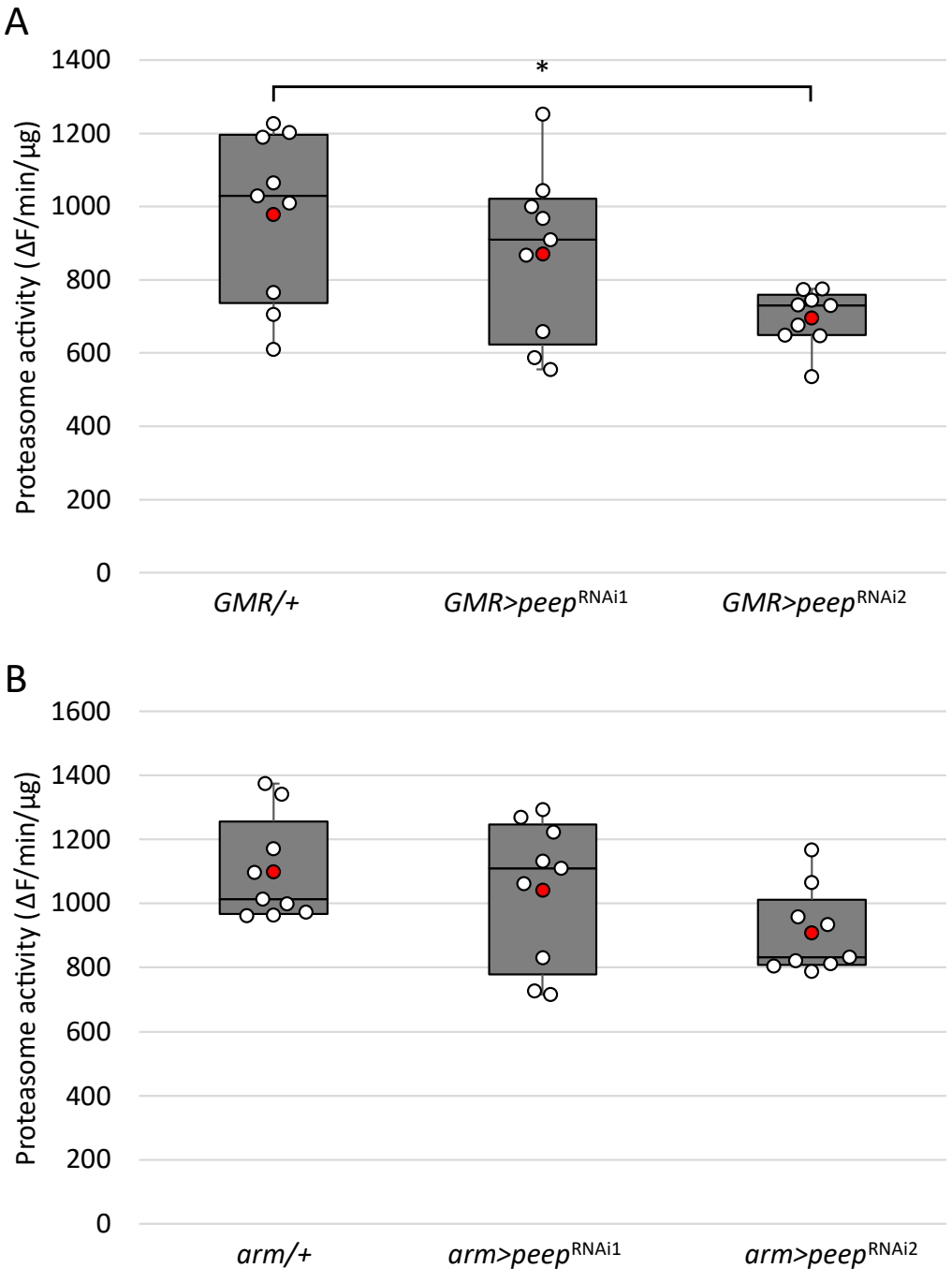

Figure 5.15. Box-and-whisker plots showing the reduction in chymotrypsin-like activity upon eye specific induction of *peep*^{RNAi2}. Chymotrypsin-like proteasome activity was measured through the cleavage of a fluorescent peptide (Suc-LLVY-AMC). Each biological replicate was measured in triplicate and a proteasome inhibitor (MG132) was measured alongside each replicate. A. *peep*^{RNAi1} and *peep*^{RNAi2} were expressed in the eye with *GMR-GAL4*, whole heads were assayed, and *peep*^{RNAi2} significantly reduced chymotrypsin-like proteasome activity, n=9 samples from three independent crosses, mean is shown in red, (One-way ANOVA, post-hoc Tukey HSD, $f_{(2,26)} = 4.88$, * = $p<0.05$, *GMR-GAL4/+ ; GMR-GAL4>peep*^{RNAi2} = 0.0132). B. *peep*^{RNAi1} and *peep*^{RNAi2} were expressed ubiquitously with *arm-GAL4* and raised at 23°C, whole flies were assayed, and no difference in activity was observed between samples, n=9 samples from three independent crosses, mean is shown in red, (One-way ANOVA, post-hoc Tukey HSD, $f_{(2,26)} = 2.68$, $p = 0.089$).

5.3 Discussion

Depletion of Peep with *GMR-GAL4* resulted in a non-autonomous reduction in the number of retinal basal glia in the larval eye disc and an alteration in the number of accessory cells in the pupal eye, suggestive of a role for Peep in the regulation of apoptosis. These findings combined with the observation that reduced expression of Peep results in necrosis in the adult eye, led to the hypothesis that Peep is acting as a survival factor. To provide insight into the pathways in which Peep may be acting, genes involved in apoptosis inhibition, mitochondrial function, and oxidative stress resistance were co-expressed with $peep^{RNAi}$ and expression of all four survival genes rescued the necrotic phenotype, induced by $peep^{RNAi}$, suggesting that Peep may play a pro-survival role in each of these pathways. The unique posterior-localised necrotic eye phenotype was found to be similar to that induced by reduction of proteasomal subunit components, and $peep^{RNAi2}$ in the eye resulted in a decrease in proteasomal activity, indicative of a role for Peep in regulating proteasomal protein degradation in the eye.

5.3.1 Reduced expression of Peep in the developing eye results in a range of deficits

Expression of Peep in the differentiating cells posterior to the morphogenetic furrow was shown to be essential for normal pupal and adult eye development and for the general survival of cells at the posterior edge of the adult eye, as knockdown with *GMR-GAL4,* induced a severe rough and necrotic eye phenotype. Peep expression both anterior to the morphogenetic furrow and in a subset of photoreceptor cells was dispensable for normal eye development as knockdown of Peep with *ey-GAL4* and *sev-GAL4* both resulted in a normal eye with no morphological defects.

5.3.1.1 Peep is required for glial proliferation and/or migration

As the rough eye necrotic phenotype was apparent immediately following eclosion, these defects were attributed to developmental impairments. The structural organisation of cells in the larval, pupal, and adult eye were further investigated to identify the developmental timeframe at which expression of Peep is necessary for normal eye development.

As previously mentioned, (Section 1.3.2.1) the eye-antennal imaginal disc provides the framework for generating head structures including, the antennae, compound eye, and ocelli (de Bruyne *et al.*, 1999; Nayak & Singh, 1985; Venkatesh & Singh, 1984). As post-developmental Peep knockdown did not induce a rough eye phenotype, it was hypothesised that Peep expression during either larval and/or pupal development is important for the generation of a normal adult eye. The gross structure and cell organisation posterior to the morphogenetic furrow was investigated using markers to highlight cell membranes, and no obvious defects were observed. For the most part, in the present study, many experimental approaches were neuron focused with few experiments performed on non-neuronal cell types. Glia have been demonstrated to be instrumental in the central nervous system for modulating neuronal activity (Doherty *et al.*, 2009; Hakim *et al.*, 2014; Paolicelli & Gross, 2011; Tasdemir-Yilmaz & Freeman, 2014) and have been implicated in neurodevelopmental (Zhan *et al.*, 2014) and neurodegenerative disease (Cinar *et al.*, 2022; Zhang *et al.*, 2021) (Sections 1.1.1, 1.3.1.2).

In the previous chapter, reduced expression of Peep in all glia was predominantly embryonic lethal and the brains of those flies that survived to adulthood displayed severely fused β lobes which warrants further investigation to uncover the part that glial Peep plays in the *Drosophila* brain, specifically in a learning and memory capacity. In this chapter it was shown that Peep is required in the larval eye disc for normal retinal basal glia proliferation and/or migration. The data presented demonstrated that both increased and reduced expression of Peep with *GMR-GAL4*, in all cells posterior to the morphogenetic furrow, results in a decrease of repo-expressing retinal basal glia, indicating that loss of wild-type levels of Peep disrupts either proliferation and/or migration of glia. As glial precursors do not reside in the eye disc and instead migrate from the optic stalk to populate and proliferate posterior to the morphogenetic furrow, *GMR-GAL4* does not express in these cells (Velarde *et al.*, 2021), therefore Peep acts non-autonomously to regulate glial cell proliferation and/or migration in the eye disc. Although this is yet to be confirmed, it also appears as though aberrant Peep expression also results in a potential loss, or the generation of non-functional carpet glia.

There are two carpet glia, identifiable by their large nucleus, which migrate through the optic stalk and reside at the anterior-most part of the larval eye disc and extend their membranes posterior to the morphogenetic furrow. It was previously shown that removal of carpet glia, by expressing the pro-apoptotic gene *hid* specifically in carpet cells, resulted in over migration of surface glia (Silies *et al.*, 2007), however, this was not what was observed in this current study.

This, therefore, may indicate that these carpet glia are in fact present, however these glia may be smaller and indistinguishable from surface and ensheathing glia when using an anti-repo antibody to identify glial cells. If these carpet glia are present but non-functional, surface glia proliferation may be repressed resulting in an overall loss of in total glia populating the eye field, yet the carpet glial membranes may remain intact allowing for normal coordinated migration of the few glial cells that are born. The small sample size in this present study may also play a role in not observing these carpet glia as it has previously been shown that 30% of wild-type controls do not have two identifiable carpet glial cells with 10% containing none at all (Torres-Oliva *et al.*, 2018).

Further, as rhabdomeres were identified, and ommatidia in the anterior region of the eye remained intact, it was hypothesised that the photoreceptor axons were encapsulated by ensheathing glia, which would suggest that there were some surface glia that migrate into the eye field and differentiate to generate the pool of ensheathing glia. As the identification of these glia in the eye disc are yet to be determined, it remains unknown which glial cells are non-autonomously affected by the knockdown of Peep.

It also remains unclear whether this loss of in glia plays a part in generating the rough and necrotic adult eye phenotype, however *repo-GAL4* driven *peep*^{RNAi} did not induce any noticeable adult eye phenotypes (data not shown). As *repo-GAL4* is homozygous lethal and is therefore maintained as a heterozygous stock over a balancer chromosome with adult phenotypic traits, phenotypic abnormalities due to Peep depletion during larval eye development require *repo-GAL4* to be heterozygous over a balancer chromosome with a larval phenotypic marker or recombined with a fluorescent marker to indicate the presence of *repo-GAL4* driven expression. Any defects induced by Peep knockdown could then be analysed to determine whether Peep is also required in glia for larval eye development and proliferation/migration of the retinal basal glia in the eye disc.

Future experiments to further understand the requirement of Peep expression for glial development and glial-mediated eye development are described in Sections 6.1 and 6.1.1.

5.3.1.2 Peep is required for development of the pupal eye lattice

To further investigate the role that Peep plays in eye development, the pupal eye was also analysed for structural defects which may give rise to the rough and necrotic adult eye phenotype.

Pupation follows the third instar larval stage in the *Drosophila melanogaster* life cycle and occurs through the hardening and conversion of the final larval cuticle into the puparium exoskeleton which covers and protects the pupa during pupal development. The mechanical properties of extracellular matrix regulating proteins can be attributed to the drastic changes in the shape that the pupa undergoes during the first few hours of pupal formation. The longitudinal axis shrinks while the lateral axis widens to allow for metamorphosis from larvae to pharate adult (Tajiri *et al.*, 2017). The *Drosophila* pupal eyes are oval and connected to the optic lobes of the pupal brain via the optic stalk. It has been illustrated that the final ommatidial lattice at the apical region of the eye consists of four lens secreting cone cells, two primary pigment cells, six secondary pigment cells, and three bristle and three tertiary pigment cells at alternating vertices (Figure 1.5B, B'), and is complete at approximately 40 hours APF when raised at 25°C (DeAngelis & Johnson, 2019; Tea *et al.*, 2014) and 60 hours APF when raised at 20°C (Cagan & Ready, 1989a). In pupal eye development, an overabundance of cells are differentiated in the wake of the morphogenetic furrow, however, not all form the correct cell-cell contacts to terminally differentiate as a specified accessory cell. These cells, called potentials, are then targeted for degradation via caspase-cleavage directed programmed cell death (Cagan & Ready, 1989a) (Section 1.3.2.2). To be certain that the final lattice formation was imaged and that all excess cells were removed by apoptosis, pupal eyes were analysed at 48 hours APF when raised at 25°C. Knockdown of Peep in the pupal eye had a significant effect on the number and position of bristle cells and IPCs, which include the secondary and tertiary pigment cells, and was not localised to a specific region of the eye, rather these defects were spread across the entire eye. As the phenotype was not restricted to the posterior of the eye, it is unlikely that the observed pupal eye phenotype is the primary contributor to the adult posterior localised rough and necrotic eye phenotype. The total number of accessory cells per ommatidia were quantified and although on average the same number of total accessory cells per ommatidia were present as in controls, there were numerous instances of excess or too few accessory cells upon knockdown of Peep. The excess accessory cell phenotype was reminiscent of the phenotype induced by overexpression of DIAP1; therefore it was hypothesised that Peep

may be regulating accessory cell number by inhibiting DIAP1 during apoptosis of interommatidial potentials. Co-expression, however, of Peep and DIAP1 did not show a regulatory interaction, as Peep did not inhibit or rescue the DIAP1 overexpression-induced increase in IPCs.

Interestingly, although pupa were staged and dissected at the same point in the developmental timeline, some pupal eyes with a knockdown of Peep displayed excess IPCs that were of similar size and shape of those at an earlier developmental timepoint, prior to one or both waves of apoptosis (Johnson & Cagan, 2009). Given this, it would be of interest to examine the lattice formation at multiple different timepoints throughout pupal development to determine whether Peep knockdown affects cell adhesion or signal transduction, leading to more than one interommatidial potential generating the necessary contacts to escape apoptosis and terminally differentiate as an extra IPC.

To further our understanding of the function of Peep in the developing eye and the role that glia play, both increased and decreased expression of Peep could be driven in pigment cell glia with the *54C-GAL4* driver (Liu *et al.*, 2017) or in the cone cells, which express the homeoprotein cut, with the *cut-GAL4* driver (Kumar *et al.*, 2015). Expression in these specific accessory cells would aid in elucidating whether the adult necrotic eye phenotype is due to Peep expression in these specific glial-like cells, and whether a knockdown results a similar phenotype to that observed following depletion with *GMR-GAL4.*

Based on the pupal eye phenotype induced by Peep knockdown it was hypothesised that Peep may be an important regulator of IPC patterning via cell adhesion or signalling as studies have shown that the Notch, Dpp, and DE-cadherin signalling pathways are all important for IPC patterning (Bao, 2014; Cagan & Ready, 1989b; Cordero *et al.*, 2004; Cordero *et al.*, 2007). Notch signalling is conserved among species (Zhou *et al.*, 2022) and during *Drosophila* eye development, Notch plays a vital role in regulating cell fate through cell-cell contacts, adhesion, and cell death (Bao, 2014; Cagan & Ready, 1989b; Cordero *et al.*, 2004). Dpp, is part of the Bone morphogenetic protein (BMP) family of proteins important for cell growth, patterning, and stabilising cell-cell contacts during *Drosophila* development (Arora *et al.*, 1995; Dai *et al.*, 2000; Gao *et al.*, 2005). Downregulation of Dpp in the eye results in similar phenotypes to that observed upon Peep knockdown and have been attributed to defects in IPC patterning, including deficits in IPC cell-cell contacts, misplaced bristle groups, and incorrect secondary/tertiary pigment cell placement (Cordero *et al.*, 2007).

DE-cadherin and Armadillo are integral components of adherens junctions that mediate cellular rearrangement and cell-cell adhesion (Bauer *et al.*, 2006; Cox *et al.*, 1996; Peifer *et al.*, 1992). DE-cadherin, encoded by the gene *shotgun*, regulates *roughest* during active cell rearrangement (Cordero *et al.*, 2007). Roughest is expressed in the junction between primary pigment cells and IPCs and mediates cell movement in the eye (Reiter *et al.*, 1996). Mutant DE-cadherin prevents Roughest expression which results in improper cell sorting and persistence of interommatidial potentials (Grzeschik & Knust, 2005). Roughest mutants with a deletion of the C-terminal domain, impair cell sorting and block apoptosis, resulting in a rough eye phenotype (Reiter *et al.*, 1996).

IPC organisation has been shown to require a finely tuned balance between Roughest and Dpp signalling to generate the regular ommatidial array, where Roughest directs cell movement and Dpp stabilises the cell-cell contacts (Cordero *et al.*, 2007). As Peep knockdown impairs IPC organisation, it is hypothesised that Peep may be implicated in one or more of these interlocking pathways involved in regulation of IPC patterning. A genetic interaction screen in the eye could be employed to determine whether *peep* interacts with any of the known components implicated in regulating IPC patterning. To further this, if Peep is shown to interact in the same molecular pathway as any of the selected candidates, it would be important to determine whether this is in a transcriptional capacity via RNA-seq or whether Peep physically interacts with these proteins via co-immunoprecipitation coupled mass spectrometry (discussed further in Section 6.3).

5.3.1.3 Peep is required for adult eye development

Knockdown of Peep results in fewer glial cells populating the third instar larval eye disc and abnormal numbers of accessory cells in the pupal eye 48 hours APF. These defects, however, are yet to be linked to the rough and necrotic eye phenotypes in the adult eye. Curiously, the pupal phenotype was not restricted to the posterior region of the eye and was instead spread across the entire eye, suggesting that the defects observed in the pupal eye may not be the primary contributor of the adult eye phenotype and instead, additional as of yet unknown dysfunctional mechanisms may play a part in restricting this phenotype to the posterior edge of the eye. To further assess the defects in the adult eye below the necrotic surface, an investigation of the appearance and organisation of photoreceptors was performed. Adult eyes in which Peep

had been knocked down with *GMR-GAL4* were isolated and stained with Nile Red, which highlights the rhabdomeres of the R1-R7 photoreceptor cells, which all lie within the same plane of focus, therefore R8 photoreceptor morphology was not assessed. The areas in which necrosis had covered the eye were devoid of any Nile red staining, indicating in these regions, the photoreceptor cells were dead. Rhabdomeres in regions of the eye without necrosis were slightly misshapen and the neatly arranged boundaries between photoreceptor clusters were no longer present, which was reflective of ommatidial fusion localised to the posterior of the eye around the necrotic patches. Strikingly, there was a significant reduction of the quantified total area of the seven visible rhabdomeres. However, it should be noted when retina were prepared for imagining and analysis, the eye remains convex as it is when it is attached on either side of the head capsule, and images were taken at the centre apex of the eye in order to gain maximal ommatidia in the same focal plane. Rough and necrotic eyes are fragile and easily torn when microdissected. It is likely that the fragility of the necrotic eyes resulted in retina squishing, leading to images of an eye that was no longer convex, meaning that the plane of focus would be further away resulting in what appeared to be smaller rhabdomeres. It was therefore difficult to discern whether *peep*^{RNAi} results in a reduction in rhabdomere size and whether this contributes to the external rough and necrotic eye phenotype, therefore, further studies to assess photoreceptor degeneration are warranted as discussed in Section 6.2.

These results show that Peep expression is required for normal larval, pupal, and adult eye development. Both overexpression and knockdown of Peep resulted in a non-autonomous decrease in retinal basal glial cells in the developing larval eye disc and a knockdown of Peep lead to both excess and reduced numbers of accessory cells across the entire pupal eye and abnormally shaped adult rhabdomeres in non-necrotic areas of the adult eye. Knockdown of Peep anterior to the morphogenetic furrow and in a subset of terminally differentiated photoreceptor neurons as well as post-eclosion all led to a normal adult eye, further indicating that Peep is essential from larval development in all differentiating cells posterior to the morphogenetic furrow for the generation of a normal eye.

5.3.2 The necrotic eye phenotype induced by *peep*^{RNAi} is degenerative and can be rescued by expression of factors involved in mitochondrial function, apoptosis inhibition and the removal of reactive oxygen species

The exact cause of the necrotic lesions observed on the adult eye are yet to be determined, however it was concluded that this phenotype is dependent on the knockdown of Peep during eye development and once necrosis has been established at the posterior of the eye, the surrounding cells become affected, resulting in necrosis spreading and retinal neural cell degeneration.

Uncontrollable cell death or necrosis can be induced by a range of different mechanisms, through primary necrosis or apoptotic induced secondary necrosis, where necrosis instead of apoptosis is responsible for spreading cell death across the eye disc (Yang *et al.*, 2013). The necrotic lesion phenotype is unique and not well documented, proving difficult to determine how these lesions occur. Necrosis can be induced by defects in programmed cell death which is an essential tightly regulated process required for cell growth and proliferation and also by oxidative stress through elevated levels of ROS (Wu *et al.*, 2015; Yang *et al.*, 2013).

Independent expression of four different 'survival factor' genes which play roles in oxidative stress resistance, mitochondrial function, and inhibition of apoptosis rescued the necrotic eye phenotype, however the ommatidial patterning and fusion defects that comprise the rough eye phenotype remained, further indicating that the rough eye phenotype induced at the posterior of the eye is the result of different pathway disruptions to that of the necrotic cell death phenotype. These results show that Peep is implicated in the regulation of apoptosis, oxidative stress response, and mitochondrial function.

5.3.2.1 Investigating the role of Peep in oxidative stress response

To further the understanding of whether increases in oxidative stress contributes to the necrotic phenotype in the eye and elucidate the role that Peep plays in regulating oxidative stress, eclosion survival and adult longevity was examined. As previously discussed, oxidative stress can be induced by increases in ROS, including non-reactive H_2O_2, a product of superoxide radicals. It was of interest to determine whether increasing the level of ROS by exposure to

supplemented H_2O_2 in the fly resulted in a more severe eye phenotype upon knockdown of Peep in the eye, which was analysed by quantifying eclosion rate.

Throughout these studies, it was observed that constitutive expression of *peep*^{RNAi} in the eye was semi-pupal lethal, and upon dissection a possible explanation for this was observed, as the eyes of the pharate adults with significant areas of necrosis, prior to eclosion, were adhered to the insides of their pupal cases, restricting the adult fly from eclosing, resulting in pupal death. This occurred in a low but significant proportion of flies as the area and severity of the necrosis varied due to incomplete penetrance of the RNAi. It was hypothesised that if the necrosis was a result of increased oxidative stress, then further increasing the level of H_2O_2 would result in an increase in phenotype severity which could lead to an exacerbated rate of pupal lethality. As it has previously been stated, the necrotic phenotype arises due to a depletion of Peep during development of the eye with *GMR-GAL4*, as post-developmental adult-induced Peep knockdown did not affect the appearance of the adult eye. Given this, H_2O_2 was supplemented into the standard fly media in order for progeny to ingest H_2O_2 to increase internal ROS levels. Exposing H_2O_2 to flies expressing *peep*^{RNAi2} resulted in an increase in pupal death when compared to *peep*^{RNAi2} flies raised on standard media, however as an increase in pupal lethality was also observed in the control, it cannot be concluded that this increase in pupal death is due to an exacerbated necrotic eye phenotype. Interestingly, H_2O_2 exposure resulted in larval lethality in control flies, a phenotype that was mitigated by a depletion of Peep, indicating a potential lethal role for Peep during larval development in the presence of exogenous H_2O_2. *GMR-GAL4* has been shown to express in a variety of third instar larval tissues including the eye disc, wing disc, and trachea (W. Z. Li *et al.*, 2012), therefore it is possible that the knockdown of Peep, which rescues the larval lethal phenotype in the control, during early larval development is driven in a wide range of cells, not just in the eye disc. Of those controls that survived larval development, pupation and eclosion appeared normal, as normal Peep expression during pupal development is required for the development of a normal eye.

As exposure to H_2O_2 resulted in an increase in pupal death regardless of genetic makeup, and a high level of larval death in the controls, these variables made it difficult to draw conclusions about the requirement of Peep in the eye under conditions of increased oxidative stress. Therefore, an additional study to examine the effect of increased H_2O_2 on adult lifespan was administered to elucidate the role that Peep plays in oxidative stress response. These results showed that *peep*^{RNAi2} and Peep^{OE} had reduced lifespans compared to control when exposed to H_2O_2. *peep*^{RNAi} and Peep^{OE} were ubiquitously expressed, and following eclosion, flies were

maintained on a diet of either sucrose alone or sucrose supplemented with H_2O_2. Interestingly, regardless of whether flies were exposed to H_2O_2 or not, overexpression of Peep showed a significant reduction in lifespan, compared to the negative control, indicating that H_2O_2 was not the primary cause of reduced survival in these flies, and instead premature death may be due to nutrient-deprivation.

It is also possible that the reduced longevity upon exposure to increased levels of H_2O_2 may in fact be due to external factors like food aversion. A recent study in adult flies by Harrison *et al.* (2020) showed that certain metabolic pathways play crucial roles in survival under stress-induced conditions, specifically when exposed to H_2O_2. Genes involved in nutrient signalling in both glycogen and folate metabolism are implicated in survival, where glycogen reserves may be depleted in response to stress, resulting in death via stress-induced starvation. It is important to keep in mind that food aversion and nutrient content can play major roles in early death when supplementing a flies diet, which as a result, cannot be entirely attributed to increased oxidative stress via exposure to H_2O_2. Therefore, these results could be attributed to metabolic stress resistance pathway failure and/or food aversion-induced starvation. In addition, motor neurons are not only important in eclosion and climbing behaviour (Sections 4.4.1, 4.4.2), but also in feeding behaviour as motor neurons have been shown to innervate the muscles involved in proboscis extension and retraction, which is part of the sensory-motor taste circuitry, whereby the proboscis is used as the feeding organ (Schwarz *et al.*, 2017). Therefore, if Peep is important in motor neuron function, when ubiquitously knocked down, this may induce feeding defects, resulting in premature death.

There were also limitations to the statistical testing used for analysing these data. The log rank statistical test uses the area under the curve to measure differences in survival. When the curve is extended, due to increased survival, and analyses are not taken through to when all flies are dead, like what was observed for those maintained on sucrose alone, the differences in survival become less accurate. It would therefore be necessary to repeat these analyses and account for the death of all flies (H_2O_2 supplemented and sucrose alone) over the entire survival period to gain more robust statistical data.

Together these preliminary data suggest a possible role for Peep in oxidative stress resistance, however due to limitations in both assays, further investigation is warranted to fully elucidate whether Peep is involved in regulating levels of oxidative stress in the fly and whether the

necrotic phenotype is attributed, at least in part, to increases in ROS, which was further detailed in Section 6.2.

5.3.3 Peep may play a role in proteasome function

To further uncover the cause of the necrotic eye phenotype upon Peep knockdown, the proteasome was investigated as mutations in proteasomal subunits have been demonstrated to result in a similar posterior localised necrotic eye phenotype.

The proteasome fluorogenic peptide assay was performed on two different tissue types to test chymotrypsin-like activity. Peep was first knocked down in the eye and a significant decrease in chymotrypsin-like activity was observed following knockdown with *peep*^{RNAi2} compared to control, with a more modest reduction upon knockdown with *peep*^{RNAi1}. Given that *peep*^{RNAi1} induces a more degenerative phenotype, the time at which the flies were harvested may have resulted in different levels of proteasome dysfunction. Necrosis is a result of total cell death, which is hypothesised to result in a decrease of proteasome activity. Therefore, if the loss of proteasome activity is directly correlated with the area of necrosis, *peep*^{RNAi2}, which induces an larger areas of necrosis immediately post-eclosion, would result in a larger decrease in proteasome activity as compared to *peep*^{RNAi1}, which induces little necrosis immediately post-eclosion. This proteasome dysfunction could be further assessed by isolating retina, rather than whole heads, as the remainder of the head capsule and brain tissues may have diluted out the eye specific decrease in chymotrypsin-like activity, leading to a more mild decrease in activity. MG132 was used to eliminate background fluorescence emission induced by eye pigment, to generate a more robust study. Chymotrypsin-like activity was shown to be reduced by 98% upon addition of 10 μM MG132, both trypsin- and caspase-like proteolytic activities were also reduced, albeit, to a lower level in the mouse liver and two human cancer cell lines, A549 and HL60 (Wu *et al.*, 2013). MG132 can also inhibit the growth of tumours through cell cycle regulation and apoptosis induction via ROS formation (Han & Park, 2010), which generates a link between proteasome dysfunction, apoptosis, and the formation of ROS. Further, as previously described in Section 5.2.3, mitochondrial dysregulation and increases in ROS can cause proteasomal dysfunction, and proteasomal dysfunction can result in increases in ROS and lead to mitochondrial dysfunction (Livnat-Levanon *et al.*, 2014; Maharjan *et al.*, 2014; Parajuli, 2019), therefore Peep may play a role in one or all aforementioned processes.

Parkinson's disease as discussed in (Section 1.5.1) is a progressive neurodegenerative disorder that is associated with the loss of dopaminergic neurons in the substantial nigra, appearance of Lewy bodies and accumulation of α-synuclein inclusions (Spillantini *et al.*, 1998), resulting in a loss of mobility and onset of dementia. Autosomal recessive early-onset Parkinson's disease has been attributed to mutations in the *PTEN-induced kinase 1* (*pink1*) gene (Valente *et al.*, 2004), and pink1 plays a role in mitochondrial dynamics (Deng *et al.*, 2008; Yang *et al.*, 2008). Knockdown of pink1 results in a posterior localised necrotic eye phenotype and loss of dopaminergic neuron clusters. Expression of SOD1 rescued this loss of dopaminergic neurons, indicating that knockdown of pink1 results in an increase in ROS (Wang *et al.*, 2006). This current study shows that as the necrotic eye phenotypes are similar between pink1 and Peep knockdown, and if similarly, to pink1, Peep knockdown decreased the number of dopaminergic neurons in the brain, this may suggest a role for Peep in regulating mitochondrial dynamics and mitigating Parkinson's disease-like phenotypes, which may or may not be attributed to increased ROS through regulation of pink1. This opens a new avenue of investigation as to whether Peep is important for the regulation and maintenance of the dopaminergic neuron clusters in the brain.

Interestingly, when β5, the subunit in the proteasome catalytic core which harbours the active site for chymotrypsin-like activity, is knocked down, a posterior localised rough and necrotic eye phenotype results (Velentzas *et al.*, 2013), similar to $peep^{RNAi}$, and likely reduces chymotrypsin-like activity, similar to $peep^{RNAi}$. It can therefore be hypothesised that Peep may regulate transcription, either directly or indirectly of the β5 subunit, to regulate proteasome assembly and activity in the eye.

From these initial investigations, Peep is required for proteasomal function specifically in the eye, as chymotrypsin-like activity was decreased upon knockdown of Peep with *GMR-GAL4*, however activity was maintained upon ubiquitous knockdown with *arm-GAL4*. It is however, yet to be determined whether these results are a direct effect on the proteasome or a downstream result due to disruption of other cellular pathways. It would, therefore, be of interest to also determine whether the decrease in proteasomal function results in an accumulation of poly-ubiquitinated proteins, as observed in other proteasomal mutants (Fernandez-Cruz *et al.*, 2020; Muller *et al.*, 2006; Tonoki *et al.*, 2009; Velentzas *et al.*, 2013), increases in ROS, and mitochondrial dysfunction, further discussed in Section 6.2.

6 Summary and Future Directions

In an effort to further the understanding of the underlying molecular mechanisms through which HDAC4 regulates neurological processes, an RNAi-based candidate screening approach was taken to identify potential HDAC4 interacting proteins, which when knocked down display similar phenotypes to that of HDAC4 overexpression in the mushroom body and eye (Main *et al.*, 2021; Tan *et al.*, 2024). A similar phenotype would indicate that this candidate and HDAC4 may function in similar molecular pathways and therefore overexpression of the candidate may rescue the HDAC4 overexpression-induced phenotype by overcoming the molecular pathway disruption. Based on similar phenotypes in the brain and eye, a single uncharacterised candidate (CG5846, named Peep) was selected for further investigation of the functional relationship with HDAC4.

Co-distribution studies in the brain and a genetic screen in the eye demonstrated that Peep did not mitigate the HDAC4 overexpression-induced phenotypes and instead, HDAC4 regulated the subcellular distribution of Peep and rescued the eye phenotype induced by Peep depletion. Furthermore, no interaction was observed following co-immunoprecipitation. Based on these results it was considered that pursuing a more thorough characterisation of the function of Peep in *Drosophila* would be more fruitful than further investigating the interaction with HDAC4.

A battery of well-established analyses were performed and Peep was shown to be essential in glia for survival, as well as for normal development of mushroom body morphology, and in neurons during mushroom body and compound eye development. Peep depletion in the eye resulted in a unique severe posterior-localised necrotic phenotype, which was rescued by expression of proteins with roles in regulating apoptosis, oxidative stress response, and mitochondrial function. In addition, this unique eye phenotype has been reported in mutants of the proteasome, and Peep was observed to be important in maintaining proteasomal function (Figure 6.1).

Based on these analyses, the main findings of this thesis and future directions, based on questions that have arisen to further the functional characterisation of Peep, are summarised and described below.

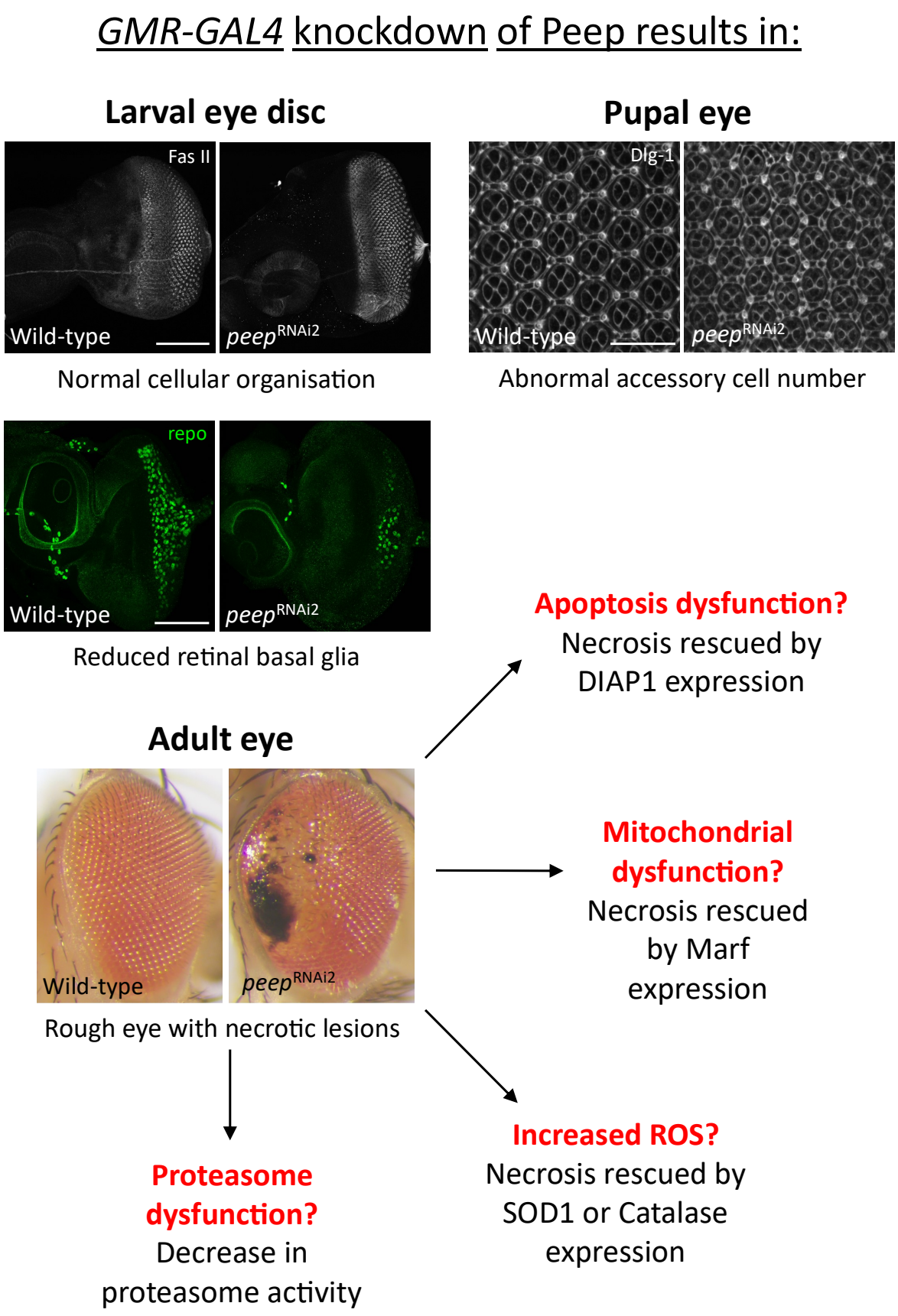

Figure 6.1. Summary of the phenotypes and pathways in which Peep functions. Knockdown of Peep in the eye using the *GMR-GAL4* driver resulted in a variety of phenotypes at different stages of development. In the third instar larval eye disc there were no perturbations to the regular cellular

organisation as shown with anti-FasII, however there was a non-autonomous significant decrease in the population of retinal basal glia, labelled with anti-repo. Peep knockdown in the pupal eye resulted in abnormal accessory cell numbers, often a result of both increased and decreased interommatidial pigment cells. In the adult eye, Peep knockdown induced a unique severe necrotic eye phenotype which was rescued by expression of DIAP1, Marf, SOD1, and Catalase. Eye-specific Peep knockdown also resulted in a decrease in proteasome activity, indicating that Peep plays an important role in regulating proteasomal and mitochondrial function, apoptosis, and oxidative stress.

6.1 Peep expression in glia is essential for embryonic survival of *Drosophila* and for normal development of the mushroom body

Pan-glial knockdown of Peep resulted in an embryonic lethal phenotype, indicative of a role for Peep in glial-mediated development from embryogenesis. Furthermore, of those adult escapers, the requirement for Peep in glia extended to the formation of the mushroom body, which resulted in total fusion of the β lobes and a novel γ lobe fusion phenotype, a phenotype which has not previously been reported. Further investigation into the identity of the specific glial cell subtypes in which Peep expression is essential is required to further the understanding of the requirement of glia and the role that Peep plays during *Drosophila* development.

A panel of glial GAL4 drivers have recently been reported to express in all types of glia including perineurial, subperineurial, cortex, astrocyte-like, and ensheathing glia, some of which have little to no expression in neurons (Jenett *et al.*, 2012; Kremer *et al.*, 2017). Each glial subtype could be fluorescently labelled for identification, and either following the generation of a new Peep specific antibody or by utilising fluorescence *in situ* hybridisation for Peep identification, expression patterns of Peep could be analysed. Furthermore, to determine the requirement of Peep in each glial subtype, knockdown could be induced with each of the glial-GAL4 drivers and survival measured. In addition, any escapers could be assessed for climbing impairments, to determine the requirement of Peep expression in glia for motor function, and learning and memory impairments, with brains also being dissected for assessment of mushroom body morphology.

6.1.1 Aberrant Peep expression in differentiating cells in the eye non-autonomously regulate the population of retinal basal glia in third instar larvae

Both overexpression and knockdown of Peep with *GMR-GAL4* resulted in a non-autonomous decrease in the number of retinal basal glia populating the larval eye disc, hypothesised to be attributed to dysfunction in carpet cell-mediated migration and subsequent proliferation. A GAL4 driver line (*moody-GAL4*), which drives expression specifically in carpet cell glia in the larval optic stalk (Silies *et al.*, 2007), could be used to investigate the requirement of Peep specifically in this subtype of glia to examine the downstream effects induced by both overexpression and knockdown of Peep on retinal basal glial cell migration in the larval eye disc and the resulting adult phenotypes.

6.2 Peep plays a role in cell survival by regulating mitochondrial and proteasomal function, apoptosis and oxidative stress

Thus far, a candidate approach has been taken to identify molecular pathways in which Peep is involved. Investigation of these pathways was initiated through a search of the literature for pathways where dysfunction resulted in necrosis, and therefore could be causative of the posterior-localised necrotic eye phenotype. Expression of DIAP1 (inhibitor of apoptosis) (S. L. Wang *et al.*, 1999), SOD1 and Catalase (regulators of oxidative stress) (Nandi *et al.*, 2019; Wang *et al.*, 2018), and Marf (regulator of mitochondrial function) (Katti *et al.*, 2021; Sandoval *et al.*, 2014), all rescued the necrotic eye phenotype induced by Peep knockdown, indicating that Peep may play a role in each of these processes, and that the necrotic phenotype may be caused due to dysfunction of one or all of these processes. Apoptosis, levels of ROS, and mitochondrial function could all be assessed in the eye following knockdown of Peep. Apoptosis can be measured by caspase activity using the GFP-based variant of caspase 3-like proteases activity indicator (GC3Ai) apoptosis sensor in the larval eye disc which utilises a GFP reporter that fluoresces upon caspase cleavage (Schott *et al.*, 2017). Mitochondrial function and ROS levels in different stages of eye development can be measured using dihydroethidium, a redox-sensitive fluorescent probe that detects the presence of superoxide radicals (Zhao *et al.*, 2003). Coenzyme Q8 (Coq8) is the *Drosophila* homologue of human Coenzyme Q8A, which is essential for the synthesis of Coenzyme Q10, an important component of the ETC (Hayashi

et al., 2014), mutations of which have been associated with onset of intellectual disability and cerebellar ataxia (Jacobsen *et al.*, 2018; Traschütz *et al.*, 2020). A recent study staining *Drosophila* retina, following knockdown of Coq8 which results in a centrally-localised necrotic eye phenotype, with dihydroethidium, indicated an increase in ROS in the eye (Hura *et al.*, 2022). Furthermore, assessing rhabdomere integrity in the adult eye with Nile Red or Phalloidin staining could be performed over time to investigate photoreceptor degeneration, as the necrosis on the eye becomes progressively worse. Studies have shown that degeneration of rhabdomeres can occur with the external surface of the eye remaining unperturbed (Richard *et al.*, 2022), therefore, although the external surface of the anterior region of the eye, following Peep depletion, remains normal, there may be photoreceptor degeneration occurring below the surface. To assess mitochondrial function the fluorescent *MitoTimer* reporter gene can be used which targets mitochondria, and upon mitochondrial stress the fluorescent output shifts from green to red (Laker *et al.*, 2014).

The posterior-localised necrotic eye phenotype has been previously observed in proteasomal subunit mutants (Fernandez-Cruz *et al.*, 2020; Kisselev *et al.*, 2006; Muller *et al.*, 2006; Tonoki *et al.*, 2009; Velentzas *et al.*, 2013), and knockdown of Peep in the eye resulted in a decrease in chymotrypsin-like proteasomal activity via a fluorogenic peptide assay. An additional study to assess the role of Peep in proteasome function, would be to analyse the level of poly-ubiquitinated proteins via western blot with an anti-ubiquitin antibody in a sample of eyes following knockdown of Peep. In addition, immunohistochemistry with an anti-ubiquitin antibody on eyes at different stages of development could be assessed, as an accumulation of poly-ubiquitinated proteins has been associated with defects in proteasomal activity (Fernandez-Cruz *et al.*, 2020; Kisselev *et al.*, 2006; Muller *et al.*, 2006; Tonoki *et al.*, 2009; Velentzas *et al.*, 2013).

6.3 Identification of Peep interacting proteins and further identification of Peep-mediated regulatory pathways

As discussed in Section 6.2, the Peep associated molecular pathways that have been established have utilised a candidate approach to identify pathway dysfunction that may cause the necrotic eye phenotype. Additional notable phenotypes associated with Peep depletion included abnormal interommatidial pigment cell number in the pupal eye lattice and defects in mushroom

body axon growth and guidance. Genetic interaction studies in the mushroom body and in the eye with genes that have unequivocally been shown to be involved in axon extension, interommatidial pigment cell dynamics, and adult eye development would shed light on the involvement of Peep in any of these processes. In addition, RNA-seq on larval brains and pupal or adult eyes would establish whether an interaction between *peep* and these genes involved in these processes is regulated at a transcription level or whether the interaction occurs on a protein level via co-immunoprecipitation coupled mass spectrometry.

6.4 Characterising the functional relationship between Peep in *Drosophila* and its human homologues RFXANK and ANKRA2

RFXANK and ANKRA2 are the closest homologues to Peep as they share homology across the ankyrin repeat regions, however as Peep contains no other characterised domains, there is little other sequence similarity. In order to further characterise the role that Peep plays in *Drosophila*, it is important to determine whether Peep is functionally similar to RFXANK and ANKRA2. ANKRA2 interacts with Megalin a member of the low-density lipoprotein receptor family (Rader *et al.*, 2000), and CCDC8 which when mutated, results in the 3M growth disorder (Nie *et al.*, 2015). RFXANK is an essential component of the RFX group which is responsible for regulating transcription of MHC genes, the proteins of which are involved in regulating adaptive immunity (Maternak *et al.*, 1998). As there is no *Drosophila* homologue of CCDC8 and *Drosophila* do not contain an adaptive immune system, rescue experiments of the necrotic eye phenotype by overexpression of either RFXANK and ANKRA2 could be carried out to determine whether supplementing the function of ANKRA2 or RFXANK can overcome the pathway disruptions induced by Peep depletion. If there are functional similarities between these proteins, the conclusions drawn in the current study may shed light on potential uncharacterised functions of both RFXANK and ANKRA2 in humans.

RFXANK interacts with RFX5, which contains a DNA binding domain that specifically targets an X-box sequence in the promoter of MHC class II genes (Maternak *et al.*, 1998), and ANKRA2 interacts with Megalin (Rader *et al.*, 2000). As both of these interactions are mediated by the ankyrin repeats on RFXANK and ANKRA2 and the ankyrin repeat binding domain on RFX5 and Megalin, it could be of interest to select *Drosophila* candidates which may interact similarly with Peep.

There is a *Drosophila* homologue of human Megalin (GenBank accession P98164), which is *Drosophila* Megalin (GenBank accession A8JTM7), and these proteins share 56.9% sequence similarity (Pairwise Sequence Alignment, EMBOSS Water). There are also *Drosophila* regulatory factor X (Rfx) homologues of human RFX proteins. *Drosophila* Rfx, is a transcription factor that plays an essential function in ciliated sensory neurons which are required for signalling processes in sensory organs and is orthologous to human RFX1 (Dubruille *et al.*, 2002). RFX1 is expressed in neurons and plays a role in regulating brain tumour cell proliferation (Ohashi *et al.*, 2004) and shares similarity with *Drosophila* Rfx through the DNA binding domain (Dubruille *et al.*, 2002). *Drosophila* Rfx2 has no known mammalian homologue and has not been mapped to the *Drosophila* genome as it is hypothesised to be present in heterochromatin. One study has shown that expression of just the DNA binding domain of *Drosophila* Rfx2 in the eye resulted in disruptions in cell cycle progression and induction of apoptosis (Otsuki *et al.*, 2004). *Drosophila* CG9727 is orthologous to human RFX5, which plays an important role in regulating MHC class II gene expression (Maternak *et al.*, 1998), with similarities in both the DNA binding domain and also contains a conserved ankyrin repeat binding domain. CG9727, however, is yet to be characterised, although single cell-RNA-seq has established that CG9727 is expressed in neurons and glia in the adult fly (Li *et al.*, 2022). Candidate investigation with *Drosophila* Megalin, Rfx, Rfx2, and CG9727 to explore additional binding partners of Peep could give further insight into the role that Peep plays in neural function and also further establish and characterise the roles that these candidates play in *Drosophila* neural function.

In conclusion, Peep does not regulate the HDAC4-mediated phenotypes induced in the brain and eye, and therefore the molecular mechanisms underlying the processes in which HDAC4 regulates neurological dysfunction remain unknown. Peep, however, has been characterised to play an essential role in cell survival by regulating mitochondrial and proteasomal function, apoptosis, and oxidative stress. These studies provide the first documentation of the functional role that Peep plays in *Drosophila* neural development and provide the basis for further investigation into the underlying molecular mechanisms involved in brain and eye development.

7 References

Acebes, A., Martin-Pena, A., Chevalier, V., & Ferrus, A. (2011). Synapse loss in olfactory local interneurons modifies perception. *J Neurosci*, *31*(8), 2734-2745. https://doi.org/10.1523/JNEUROSCI.5046-10.2011

Adams, M. D., Celniker, S. E., Holt, R. A., Evans, C. A., Gocayne, J. D., Amanatides, P. G., Scherer, S. E., Li, P. W., Hoskins, R. A., Galle, R. F., George, R. A., Lewis, S. E., Richards, S., Ashburner, M., Henderson, S. N., Sutton, G. G., Wortman, J. R., Yandell, M. D., Zhang, Q., . . . Venter, J. C. (2000). The genome sequence of *Drosophila melanogaster*. *Science*, *287*(5461). https://doi.org/10.1126/science.287.5461.2185

Alberini, C. M. (2011). The role of reconsolidation and the dynamic process of long-term memory formation and storage. *Frontiers in Behavioral Neuroscience*, *5*(12), 1-10. https://doi.org/10.3389/fnbeh.2011.00012

Alharby, E., Obaid, M., Elamin, M. A. O., Almuntashri, M., Bakhsh, I., Samman, M., Peake, R. W. A., Alasmari, A., & Almontashiri, N. A. M. (2021). Progressive Ataxia and Neurologic Regression in RFXANK-Associated Bare Lymphocyte Syndrome. *Neurol Genet*, *7*(3), e586. https://doi.org/10.1212/NXG.0000000000000586

Alonso, A. D. C., Grundke-Iqbal, I., & Iqbal, K. (1996). Alzheimer's disease hyperphosphorylated tau sequesters normal tau into tangles of filaments and disassembles microtubules. *Nature Medicine*, *2*(7), 783-787. https://doi.org/10.1038/nm0796-783

Alzheimer, A. (1907). Über eine eigenartige Erkrankung der Hirnrinde. *Allgemeine Zeitschrift fur Psychiatrie und Psychisch-gerichtliche Medizin*, 146-148.

American Psychiatric Association. (2013). *DSM-5 Development* (5 ed.).

Anholt, R. R. H., O'Grady, P., Wolfner, M. F., & Harbison, S. T. (2020). Evolution of Reproductive Behavior. *Genetics*, *214*(1), 49-73. https://doi.org/10.1534/genetics.119.302263

Armstrong, G. A. B., Xiao, C., Krill, J. L., Seroude, L., Dawson-Scully, K., & Robertson, R. M. (2011). Glial Hsp70 Protects K+ Homeostasis in the Drosophila Brain during Repetitive Anoxic Depolarization. *PLoS One*, *6*(12). https://doi.org/10.1371/journal.pone.0028994

Armstrong, J. D., de Belle, J. S., Wang, Z., & Kaiser, K. (1998). Metamorphosis of the Mushroom Bodies; Large-Scale Rearrangements of the Neural Substrates for Associative Learning and Memory in Drosophila. *Learn Mem*, *5*, 102-114. https://doi.org/https://doi.org/10.1101/lm.5.1.102

Arora, K., Dai, H., Kazuko, S. G., Jamal, J., O'Connor, M. B., Letsou, A., & Warrior, R. (1995). The *Drosophila schnurri* gene acts in the Dpp/TGFβ signalling pathway and encodes a transcription factor homologous to the human MBP family. *Cell*, *81*(5), 781-790. https://doi.org/10.1016/0092-8674(95)90539-1

Aso, Y., Grübel, K., Busch, S., Friedrich, A. B., Siwanowicz, I., & Tanimoto, H. (2009). The mushroom body of adult Drosophila characterized by GAL4 drivers. *J Neurogenet*, *23*(1-2), 156-172. https://doi.org/10.1080/01677060802471718

Aso, Y., Sitaraman, D., Ichinose, T., Kaun, K. R., Vogt, K., Belliart-Guerin, G., Placais, P. Y., Robie, A. A., Yamagata, N., Schnaitmann, C., Rowell, W. J., Johnston, R. M., Ngo, T. T., Chen, N., Korff, W., Nitabach, M. N., Heberlein, U., Preat, T., Branson, K. M., . . . Rubin, G. M. (2014). Mushroom body output neurons encode valence and guide memory-based action selection in *Drosophila*. *Elife*, *3*, e04580. https://doi.org/10.7554/eLife.04580

Atkin, G., & Paulson, H. (2014). Ubiquitin pathways in neurodegenerative disease. *Front Mol Neurosci*, *7*, 63. https://doi.org/10.3389/fnmol.2014.00063

Bach, M. E., Hawkins, R. D., Osman, M., Kandel, E. R., & Mayford, M. (1995). Impairment of spatial but not contextual memory in CaMKII mutant mice with a selective loss of hippocampal LTP in the range of the θ frequency. *Cell*, *81*(6). https://doi.org/10.1016/0092-8674(95)90010-1

Baehrecke, E. H. (1996). Ecdysone signaling cascade and regulation ofDrosophila metamorphosis. *Archives of Insect Biochemistry and Physiology*, *33*(3-4), 231-244. https://doi.org/10.1002/(sici)1520-6327(1996)33:3/4<231::Aid-arch5>3.0.Co;2-v

Baik, J. H. (2020). Stress and the dopaminergic reward system. *Exp Mol Med*, *52*(12), 1879-1890. https://doi.org/10.1038/s12276-020-00532-4

Bailey, C., & Kandel, E. R. (1993). Structural changes accompanying memory storage. *Annual Review of Physiology*, *55*, 397-426. https://doi.org/10.1146/annurev.ph.55.030193.002145

Ballard, P. A., Tetrud, J. W., & Langston, J. W. (1985). Permanent human parkinsonism due to 1-methyl-4-phenyl-1,2,3,6-tetrahydropyridine (MPTP): seven cases. *Neurology*, *35*(7), 949-956. https://doi.org/10.1212/wnl.35.7.949

Bao, S. (2014). Notch controls cell adhesion in the Drosophila eye. *PLoS Genet*, *10*(1), e1004087. https://doi.org/10.1371/journal.pgen.1004087

Barbagallo, B., & Garrity, P. A. (2015). Temperature sensation in Drosophila. *Curr Opin Neurobiol*, *34*, 8-13. https://doi.org/10.1016/j.conb.2015.01.002

Barco, A., Bailey, C. H., & Kandel, E. R. (2006). Common molecular mechanisms in explicit and implicit memory. *J Neurochem*, *97*(6), 1520-1533. https://doi.org/10.1111/j.1471-4159.2006.03870.x

Basler, K., Yen, D., Tomlinson, A., & Hafen, E. (1990). Reprogramming cell fate in the developing *Drosophila* retina: transforamtion of R7 cells by ectopic expression of *rough*. *Genes & Development*, *4*(5), 728-739. https://doi.org/10.1101/gad.4.5.728

Bates, K. E., Sung, C. S., & Robinow, S. (2010). The unfulfilled gene is required for the development of mushroom body neuropil in Drosophila. *Neural Dev*, *5*, 4. https://doi.org/10.1186/1749-8104-5-4

Bauer, R., Weimbs, A., Lechner, H., & Hoch, M. (2006). DE-cadherin, a core component of the adherens junction complex modifies subcellular localization of the Drosophila gap junction protein innexin2. *Cell Commun Adhes*, *13*(1-2), 103-114. https://doi.org/10.1080/15419060600631839

Baumann, O. (1992). Submembrane cytoskeleton of pigmented glial cells, primary pigment cells and crystalline cone cells in the honeybee compound eye. *Cell and Tissue Research*, *270*(2), 353-363. https://doi.org/10.1007/BF00328019

Beira, J. V., & Paro, R. (2016). The legacy of Drosophila imaginal discs. *Chromosoma*, *125*(4), 573-592. https://doi.org/10.1007/s00412-016-0595-4

Belalcazar, H. M., Hendricks, E. L., Zamurrad, S., Liebl, F. L. W., & Secombe, J. (2021). The histone demethylase KDM5 is required for synaptic structure and function at the *Drosophila* neuromuscular junction. *Cell Rep*, *34*(7). https://doi.org/10.1016/j.celrep.2021.108753

Berger, K. H., Kong, E. C., Dubnau, J., Tully, T., Moore, M. S., & Heberlein, U. (2008). Ethanol sensitivity and tolerance in long-term memory mutants of *Drosophila melanogaster*. *Alcohol Clin Exp Res*, *32*(5), 895-908. https://doi.org/10.1111/j.1530-0277.2008.00659.x

Bergles, D. E., & Richardson, W. D. (2015). Oligodendrocyte Development and Plasticity. *Cold Spring Harb Perspect Biol*, *8*(2), a020453. https://doi.org/10.1101/cshperspect.a020453

Bergmann, M., & Fruton, J. S. (1937). On Proteolytic Enzymes. *Journal of Biological Chemistry*, *118*(2), 405-415. https://doi.org/10.1016/s0021-9258(18)74495-5

Bernal, A., & Kimbrell, D. A. (2000). *Drosophila Thor* participates in host immune defense and connects a translational regulator with innate immunity. *PNAS*, *97*(11), 6019-6024. https://doi.org/10.1073/pnas.100391597

Bertos, N. R., Wang, A. H., & Yang, X.-J. (2001). Class II histone deacetylases: Structure, function, and regulation. *Biochemistry and Cell Biology*, *79*(3), 243-252. https://doi.org/10.1139/bcb-79-3-243

Bi, C., Wu, J., Jiang, T., Liu, Q., Cai, W., Yu, P., Cai, T., Zhao, M., Jiang, Y. H., & Sun, Z. S. (2012). Mutations of ANK3 identified by exome sequencing are associated with autism susceptibility. *Human Mutation*, *33*(12), 1635-1638. https://doi.org/10.1002/humu.22174

Bieber, A. J., Snow, P. M., Hortsch, M., Patel, N. H., Jacobs, J. R., Traquina, Z. R., Schilling, J., & Goodman, C. S. (1989). *Drosophila* neuroglian: A member of the immunoglobulin superfamily with extensive homology to the vertebrate neural adhesion molecule L1. *Cell*, *59*(3), 447-460. https://doi.org/10.1016/0092-8674(89)90029-9

Bilder, D., Li, M., & Perrimon, N. (2000). Cooperative regulation of cell polarity and growth by Drosophila tumor suppressors. *Science*, *289*(5476), 113-116. https://doi.org/10.1126/science.289.5476.113

Blagburn, J. M. (2008). Engrailed expression in subsets of adult Drosophila sensory neurons: an enhancer-trap study. *Invert Neurosci*, *8*(3), 133-146. https://doi.org/10.1007/s10158-008-0074-6

Blakemore, W. F. (1975). Remyelination by Schwann cells of axons demyelinated by intraspinal injection of 6-aminonicotinamide in the rat. *J Neurocytol*, *4*(6), 745-757. https://doi.org/10.1007/bf01181634

Bolger, T. A., & Yao, T. P. (2005). Intracellular trafficking of histone deacetylase 4 regulates neuronal cell death. *J Neurosci*, *25*(41), 9544-9553. https://doi.org/10.1523/JNEUROSCI.1826-05.2005

Booth, G. E., Kinrade, E. F., & Hidalgo, A. (2000). Glia maintain follower neuron survival during Drosophila CNS development. *Development*, *127*(2), 237-244. https://doi.org/10.1242/dev.127.2.237

Borghi, S., Molinari, S., Razzini, G., Parise, F., Battini, R., & Ferrari, S. (2001). The nuclear localization domain of the MEF2 family of transcription factors shows member-specific features and mediates the nuclear import of histone deacetylase 4. *J Cell Sci*, *114*(Pt 24), 4477-4483. https://doi.org/10.1242/jcs.114.24.4477

Bowtell, D. D., Kimmel, B. E., Simon, M. A., & Rubin, G. M. (1989). Regulation of the complex pattern of sevenless expression in the developing Drosophila eye. *Proc Natl Acad Sci U S A*, *86*(16), 6245-6249. https://doi.org/10.1073/pnas.86.16.6245

Brand, A. H., & Perrimon, N. (1993). Targeted gene expression as a means of altering cell fates and generating dominant phenotypes. *Development*, *118*(2), 401-415. https://doi.org/10.1242/dev.118.2.401

Brothers, H. M., Gosztyla, M. L., & Robinson, S. R. (2018). The physiological roles of amyloid-beta peptide hint at new ways to treat Alzheimer's disease. *Front Aging Neurosci*, *10*, 118. https://doi.org/10.3389/fnagi.2018.00118

Brown, N. L., Paddock, S. W., Sattler, C. A., Cronmiller, C., Thomas, B. J., & Carroll, S. B. (1996). daughterless is required for Drosophila photoreceptor cell determination, eye morphogenesis, and cell cycle progression. *Dev Biol*, *179*(1), 65-78. https://doi.org/10.1006/dbio.1996.0241

Budson, A. E. (2009). Understanding memory dysfunction. *Neurologist*, *15*(2), 71-79. https://doi.org/10.1097/NRL.0b013e318188040d

Cagan, R. (2009). Principles of Drosophila eye differentiation. *Curr Top Dev Biol*, *89*, 115-135. https://doi.org/10.1016/S0070-2153(09)89005-4

Cagan, R. L., & Ready, D. F. (1989a). The emergence of order in the Drosophila pupal retina. *Dev Biol*, *136*(2), 346-362. https://doi.org/10.1016/0012-1606(89)90261-3

Cagan, R. L., & Ready, D. F. (1989b). Notch is required for successive cell decisions in the developing Drosophila retina. *Genes Dev*, *3*(8), 1099-1112. https://doi.org/10.1101/gad.3.8.1099

Cai, Y., & Laughon, A. (2009). The *Drosophila* Smad cofactor Schnurri engages in redundant and synergistic interactions with multiple corepressors. *Biochim Biophys Acta*, *1789*(3), 232-245. https://doi.org/10.1016/j.bbagrm.2009.01.001

Cajal, S. R. y. (1894). *The croonian lecture - La fine structure des centres nerveux*.

Cameron, S., Chen, Y., & Rao, Y. (2016). Borderless regulates glial extension and axon ensheathment. *Dev Biol*, *414*(2), 170-180. https://doi.org/10.1016/j.ydbio.2016.04.020

Campos-Ortega, J. A., & Strausfeld, N. J. (1972). The columnar organization of the second synaptic region of the visual system of Musca domestica. L. I. Receptor terminals in the medulla. *Z Zellforsch Mikrosk Anat*, *124*(4), 561-585. https://doi.org/10.1007/bf00335258

Chakraborty, R., Vepuri, V., Mhatre, S. D., Paddock, B. E., Miller, S., Michelson, S. J., Delvadia, R., Desai, A., Vinokur, M., Melicharek, D. J., Utreja, S., Khandelwal, P., Ansaloni, S., Goldstein, L. E., Moir, R. D., Lee, J. C., Tabb, L. P., Saunders, A. J., & Marenda, D. R. (2011). Characterization of a Drosophila Alzheimer's disease model: pharmacological rescue of cognitive defects. *PLoS One*, *6*(6), e20799. https://doi.org/10.1371/journal.pone.0020799

Chang, Y. C., Tsao, C. K., & Sun, Y. H. (2018). Temporal and spatial order of photoreceptor and glia projections into optic lobe in Drosophila. *Sci Rep*, *8*(1), 12669. https://doi.org/10.1038/s41598-018-30415-8

Chanut, F., & Heberlein, U. (1997). Role of decapentaplegic in initiation and progression of the morphogenetic furrow in the developing Drosophila retina. *Development*, *124*(2), 559-567. https://doi.org/10.1242/dev.124.2.559

Charlton-Perkins, M., & Cook, T. A. (2010). Building a fly eye: Terminal differentiation events of the retina, corneal lens, and pigmented epithelia. *Current Topics in Developmental Biology*, *93*, 129-173. https://doi.org/10.1016/B978-0-12-385044-7.00005-9

Charlton-Perkins, M. A., Sendler, E. D., Buschbeck, E. K., & Cook, T. A. (2017). Multifunctional glial support by Semper cells in the Drosophila retina. *PLoS Genet*, *13*(5), e1006782. https://doi.org/10.1371/journal.pgen.1006782

Chaturvedi, R., Reddig, K., & Li, H. S. (2014). Long-distance mechanism of neurotransmitter recycling mediated by glial network facilitates visual function in Drosophila. *Proc Natl Acad Sci U S A*, *111*(7), 2812-2817. https://doi.org/10.1073/pnas.1323714111

Chawla, S., Vanhoutte, P., Arnold, F. J. L., Huang, C. L. H., & Bading, H. (2003). Neuronal activity-dependent nucleocytoplasmic shuttling of HDAC4 and HDAC5. *Journal of Neurochemistry*, *85*(1), 151-159. https://doi.org/10.1046/j.1471-4159.2003.01648.x

Chen, N. P., Sun, Z., & Fassler, R. (2018). The Kank family proteins in adhesion dynamics. *Curr Opin Cell Biol*, *54*, 130-136. https://doi.org/10.1016/j.ceb.2018.05.015

Chen, Y., Cameron, S., Chang, W. T., & Rao, Y. (2017). Turtle interacts with borderless in regulating glial extension and axon ensheathment. *Mol Brain*, *10*(1), 17. https://doi.org/10.1186/s13041-017-0299-6

Cheng, Y., Endo, K., Wu, K., Rodan, A. R., Heberlein, U., & Davis, R. L. (2001). *Drosophila fasciclinII* is required for the formation of odor memories and for normal sensitivity to alcohol. *Cell*, *105*(6), 757-768. https://doi.org/10.1016/s0092-8674(01)00386-5

Cheung, G., To, E., Rivera-Rodriguez, C., Ma'u, E., Chan, A. H. Y., Ryan, B., & Cullum, S. (2022). Dementia prevalence estimation among the main ethnic groups in New Zealand: a population-based descriptive study of routinely collected health data. *BMJ Open*, *12*(9), e062304. https://doi.org/10.1136/bmjopen-2022-062304

Chiang, A. S., Lin, C. Y., Chuang, C. C., Chang, H. M., Hsieh, C. H., Yeh, C. W., Shih, C. T., Wu, J. J., Wang, G. T., Chen, Y. C., Wu, C. C., Chen, G. Y., Ching, Y. T., Lee, P. C., Lin, C. Y., Lin, H. H., Wu, C. C., Hsu, H. W., Huang, Y. A., . . . Hwang, J. K. (2011). Three-dimensional reconstruction of brain-wide wiring networks in *Drosophila* at single-cell resolution. *Current Biology*, *21*(1), 1-11. https://doi.org/10.1016/j.cub.2010.11.056

Chiaravalloti, N. D., & DeLuca, J. (2008). Cognitive impairment in multiple sclerosis. *Lancet Neurol*, *7*(12), 1139-1151. https://doi.org/10.1016/s1474-4422(08)70259-x

Cho, Y., Griswold, A., Campbell, C., & Min, K. T. (2005). Individual histone deacetylases in *Drosophila* modulate transcription of distinct genes. *Genomics*, *86*(5), 606-617. https://doi.org/10.1016/j.ygeno.2005.07.007

Choi, K. W., & Benzer, S. (1994). Migration of glia along photoreceptor axons in the developing Drosophila eye. *Neuron*, *12*(2), 423-431. https://doi.org/10.1016/0896-6273(94)90282-8

Cinar, E., Tel, B. C., & Sahin, G. (2022). Neuroinflammation in Parkinson's Disease and its Treatment Opportunities. *Balkan Med J*, *39*(5), 318-333. https://doi.org/10.4274/balkanmedj.galenos.2022.2022-7-100

Clohisey, S. (2013). *KANK: A novel EB1 interactor and Drosophila orthologue of a conserved tumour suppressor* University of Edinburgh].

Colamarino, S. A., & Tessier-Lavigne, M. (1995). The axonal chemoattractant netrin-1 is also a chemorepellent for trochlear motor axons. *Cell*, *81*(4), 621-629. https://doi.org/10.1016/0092-8674(95)90083-7

Comas, D., Petit, F., & Preat, T. (2004). *Drosophila* long-term memory formation involves regulation of cathepsin activity. *Nature*, *430*(6998), 460-463. https://doi.org/10.1038/nature02726

Cordero, J., Jassim, O., Bao, S., & Cagan, R. (2004). A role for *wingless* in an early pupal cell death event that contributes to patterning the *Drosophila* eye. *Mechanisms of Development*, *121*(12), 1523-1530. https://doi.org/10.1016/j.mod.2004.07.004

Cordero, J. B., Larson, D. E., Craig, C. R., Hays, R., & Cagan, R. (2007). Dynamic decapentaplegic signaling regulates patterning and adhesion in the Drosophila pupal retina. *Development*, *134*(10), 1861-1871. https://doi.org/10.1242/dev.002972

Cox, R. T., Kirkpatrick, C., & Peifer, M. (1996). Armadillo is required for adherens junction assembly, cell polarity, and morphogenesis during Drosophila embryogenesis. *J Cell Biol*, *134*(1), 133-148. https://doi.org/10.1083/jcb.134.1.133

Crittenden, J. R., Skoulakis, E. M., Han, K. A., Kalderon, D., & Davis, R. L. (1998). Tripartite mushroom body architecture revealed by antigenic markers. *Learn Mem*, *5*(1-2), 38-51.

Cronmiller, C., & Cummings, C. A. (1993). The daughterless gene product in Drosophila is a nuclear protein that is broadly expressed throughout the organism during development. *Mech Dev*, *42*(3), 159-169. https://doi.org/10.1016/0925-4773(93)90005-i

Crowther, D. C., Page, R., Chandraratna, D., & Lomas, D. A. (2006). A *Drosophila* Model of Alzheimer's Disease. In *Amyloid, Prions, and Other Protein Aggregates, Part B* (pp. 234-255). https://doi.org/10.1016/s0076-6879(06)12015-7

Cunha, S. R., & Mohler, P. J. (2009). Ankyrin protein networks in membrane formation and stabilization. *Journal of Cellular and Molecular Medicine*, *13*(11-12), 4364-4376. https://doi.org/10.1111/j.1582-4934.2009.00943.x

Currie, D. A., & Bate, M. (1991). The development of adult abdominal muscles in Drosophila: myoblasts express twist and are associated with nerves. *Development*, *113*(1), 91-102. https://doi.org/10.1242/dev.113.1.91

Dai, H., Hogan, C., Gopalakrishnan, B., Torres-Vazquez, J., Nguyen, M., Park, S., Raftery, L. A., Warrior, R., & Arora, K. (2000). The zinc finger protein schnurri acts as a Smad partner in mediating the transcriptional response to decapentaplegic. *Dev Biol*, *227*(2), 373-387. https://doi.org/10.1006/dbio.2000.9901

Dai, S., Guo, L., Dey, R., Guo, M., Zhang, X., Bates, D., Cayford, J., Jiang, L., Wei, H., Chen, Z., Zhang, Y., Chen, L., & Chen, Y. (2024). Structural insights into the HDAC4-MEF2A-DNA complex and its implication in long-range transcriptional regulation. *Nucleic Acids Res*. https://doi.org/10.1093/nar/gkae036

Darcy, M. J., Calvin, K., Cavnar, K., & Ouimet, C. C. (2010). Regional and subcellular distribution of HDAC4 in mouse brain. *The Journal of Comparative Neurology*, *518*(5), 722-740. https://doi.org/10.1002/cne.22241

Davis, R. L. (2005). Olfactory memory formation in *Drosophila*: from molecular to systems neuroscience. *Annu Rev Neurosci*, *28*, 275-302. https://doi.org/10.1146/annurev.neuro.28.061604.135651

de Bruyne, M., Clyne, P. J., & Carlson, J. R. (1999). Odor coding in a model olfactory organ: the Drosophila maxillary palp. *J Neurosci*, *19*(11), 4520-4532. https://doi.org/10.1523/jneurosci.19-11-04520.1999

DeAngelis, M. W., & Johnson, R. I. (2019). Dissection of the Drosophila Pupal Retina for Immunohistochemistry, Western Analysis, and RNA Isolation. *J Vis Exp*(145). https://doi.org/10.3791/59299

Debattisti, V., Pendin, D., Ziviani, E., Daga, A., & Scorrano, L. (2014). Reduction of endoplasmic reticulum stress attenuates the defects caused by Drosophila mitofusin depletion. *J Cell Biol*, *204*(3), 303-312. https://doi.org/10.1083/jcb.201306121

Delgado, M. G., Oliva, C., Lopez, E., Ibacache, A., Galaz, A., Delgado, R., Barros, L. F., & Sierralta, J. (2018). Chaski, a novel Drosophila lactate/pyruvate transporter required in glia cells for survival under nutritional stress. *Sci Rep*, *8*(1), 1186. https://doi.org/10.1038/s41598-018-19595-5

Dementia economic impact report 2016. (2017). D. T. T. Ltd.

Deng, H., Dodson, M. W., Huang, H., & Guo, M. (2008). The Parkinson's disease genes pink1 and parkin promote mitochondrial fission and/or inhibit fusion in Drosophila. *Proc Natl Acad Sci U S A*, *105*(38), 14503-14508. https://doi.org/10.1073/pnas.0803998105

DiAntonio, A., Burgess, R. W., Chin, A. C., Deitcher, D. L., Scheller, R. H., & Schwarz, T. L. (1993). Identification and characterization of Drosophila genes for synaptic vesicle proteins. *J Neurosci*, *13*(11), 4924-4935. https://doi.org/10.1523/jneurosci.13-11-04924.1993

Dietzl, G., Chen, D., Schnorrer, F., Su, K. C., Barinova, Y., Fellner, M., Gasser, B., Kinsey, K., Oppel, S., Scheiblauer, S., Couto, A., Marra, V., Keleman, K., & Dickson, B. J. (2007). A genome-wide transgenic RNAi library for conditional gene inactivation in *Drosophila*. *Nature*, *448*(7150), 151-156. https://doi.org/10.1038/nature05954

Doherty, J., Logan, M. A., Tasdemir, O. E., & Freeman, M. R. (2009). Ensheathing glia function as phagocytes in the adult Drosophila brain. *J Neurosci*, *29*(15), 4768-4781. https://doi.org/10.1523/JNEUROSCI.5951-08.2009

Dos Santos, S. E., Medeiros, M., Porfirio, J., Tavares, W., Pessoa, L., Grinberg, L., Leite, R. E. P., Ferretti-Rebustini, R. E. L., Suemoto, C. K., Filho, W. J., Noctor, S. C., Sherwood, C. C., Kaas, J. H., Manger, P. R., & Herculano-Houzel, S. (2020). Similar Microglial Cell Densities across Brain Structures and Mammalian Species: Implications for Brain Tissue Function. *J Neurosci*, *40*(24), 4622-4643. https://doi.org/10.1523/JNEUROSCI.2339-19.2020

Dubnau, J., Chiang, A. S., Grady, L., Barditch, J., Gossweiler, S., McNeil, J., Smith, P., Buldoc, F., Scott, R., Certa, U., Broger, C., & Tully, T. (2003). The *staufen/pumilio* pathway is involved in *Drosophila* long-term memory. *Curr Biol*, *13*, 286-296. https://doi.org/10.1016/s0960-9822(03)00064-2

Dubruille, R., Laurencon, A., Vandaele, C., Shishido, E., Coulon-Bublex, M., Swoboda, P., Couble, P., Kernan, M., & Durand, B. (2002). Drosophila regulatory factor X is necessary for ciliated sensory neuron differentiation. *Development*, *129*(23), 5487-5498. https://doi.org/10.1242/dev.00148

Dukas, R. (2008). Evolutionary biology of insect learning. *Annual Review Entomology*, *53*, 145-160. https://doi.org/10.1146/annurev.ento.53.103106.093343

Dumstrei, K., Wang, F., & Hartenstein, V. (2003). Role of DE-Cadherin in Neuroblast Proliferation, Neural

Morphogenesis, and Axon Tract Formation in Drosophila

Larval Brain Development. *The Journal of Neuroscience*, *23*(8), 3325-3335. https://doi.org/https://doi.org/10.1523/JNEUROSCI.23-08-03325.2003

Edwards, K. A., Demsky, M., Montague, R. A., Weymouth, N., & Kiehart, D. P. (1997). GFP-moesin illuminates actin cytoskeleton dynamics in living tissue and demonstrates cell shape changes during morphogenesis in Drosophila. *Dev Biol*, *191*(1), 103-117. https://doi.org/10.1006/dbio.1997.8707

Ejima, A., Smith, B. P., Lucas, C., van der Goes van Naters, W., Miller, C. J., Carlson, J. R., Levine, J. D., & Griffith, L. C. (2007). Generalization of courtship learning in Drosophila is mediated by cis-vaccenyl acetate. *Curr Biol*, *17*(7), 599-605. https://doi.org/10.1016/j.cub.2007.01.053

Elbashir, S. M., Lendeckel, W., & Tuschl, T. (2001). RNA interference is mediated by 21- and 22-nucleotide RNAs. *Genes Dev*, *15*(2), 188-200. https://doi.org/10.1101/gad.862301

Enneking, E. M., Kudumala, S. R., Moreno, E., Stephan, R., Boerner, J., Godenschwege, T. A., & Pielage, J. (2013). Transsynaptic coordination of synaptic growth, function, and stability by the L1-type CAM neuroglian. *PLoS Biology*, *11*(4), e1001537. https://doi.org/10.1371/journal.pbio.1001537

Enriquez, J., Rio, L. Q., Blazeski, R., Bellemin, S., Godement, P., Mason, C., & Mann, R. S. (2018). Differing Strategies Despite Shared Lineages of Motor Neurons and Glia to Achieve Robust Development of an Adult Neuropil in Drosophila. *Neuron*, *97*(3), 538-554 e535. https://doi.org/10.1016/j.neuron.2018.01.007

Escobedo, S. E., Shah, A., Easton, A. N., Hall, H., & Weake, V. M. (2021). Characterizing a gene expression toolkit for eye- and photoreceptor-specific expression in Drosophila. *Fly (Austin)*, *15*(1), 73-88. https://doi.org/10.1080/19336934.2021.1915683

Evans, R. C., Morera-Herreras, T., Cui, Y., Du, K., Sheehan, T., Kotaleski, J. H., Venance, L., & Blackwell, K. T. (2012). The effects of NMDA subunit composition on calcium influx and spike timing-dependent plasticity in striatal medium spiny neurons. *PLoS Comput Biol*, *8*(4). https://doi.org/10.1371/journal.pcbi.1002493

Ewer, J., Frisch, B., Hamblen-Coyle, M. J., Rosbash, M., & Hall, J. C. (1992). Expression of the period clock gene within different cell types in the brain of Drosophila adults and mosaic analysis of these cells' influence on circadian behavioral rhythms. *J Neurosci*, *12*(9), 3321-3349. https://doi.org/10.1523/jneurosci.12-09-03321.1992

Fan, Y., & Bergmann, A. (2014). Multiple mechanisms modulate distinct cellular susceptibilities toward apoptosis in the developing Drosophila eye. *Dev Cell*, *30*(1), 48-60. https://doi.org/10.1016/j.devcel.2014.05.007

Fang, Y., Soares, L., Teng, X., Geary, M., & Bonini, N. M. (2012). A novel Drosophila model of nerve injury reveals an essential role of Nmnat in maintaining axonal integrity. *Curr Biol*, *22*(7), 590-595. https://doi.org/10.1016/j.cub.2012.01.065

Feany, M. B., & Bender, W. W. (2000). A *Drosophila* model of Parkinson's disease. *Nature*, *404*, 394-398. https://doi.org/10.1038/35006074

Fernandez-Chacon, R., & Sudhof, T. C. (2000). Novel SCAMPs lacking NPF repeats: Ubiquitous and synaptic vesicle-specific forms implicate SCAMPs in multiple membrane-trafficking functions. *Journal of Neuroscience*, *20*(21), 7941-7950. https://doi.org/10.1523/JNEUROSCI.20-21-07941.2000

Fernandez-Cruz, I., Sanchez-Diaz, I., Narvaez-Padilla, V., & Reynaud, E. (2020). Rpt2 proteasome subunit reduction causes Parkinson's disease like symptoms in Drosophila. *IBRO Rep*, *9*, 65-77. https://doi.org/10.1016/j.ibror.2020.07.001

Fischle, W., Kiermer, V., Dequiedt, F., & Verdin, E. (2001). The emerging role of class II histone deacetylases. *Biochemistry and Cell Biology*, *79*(3), 337-348. https://doi.org/10.1139/bcb-79-3-337

Fitzsimons, H. L., Schwartz, S., Given, F. M., & Scott, M. J. (2013). The histone deacetylase HDAC4 regulates long-term memory in *Drosophila*. *PLoS One*, *8*(12). https://doi.org/10.1371/journal.pone.0083903

Foglietti, C., Filocamo, G., Cundari, E., De Rinaldis, E., Lahm, A., Cortese, R., & Steinkuhler, C. (2006). Dissecting the biological functions of *Drosophila* histone deacetylases by RNA interference and transcriptional profiling. *Journal of Biological Chemistry*, *281*(26), 17968-17976. https://doi.org/10.1074/jbc.M511945200

Foust, A., Popovic, M., Zecevic, D., & McCormick, D. A. (2010). Action potentials initiate in the axon initial segment and propagate through axon collaterals reliably in cerebellar purkinje neurons. *The Journal of Neuroscience*, *30*(20), 6891-6902. https://doi.org/10.1523/JNEUROSCI.0552-10.2010

Freeman, M. (1996). Reiterative use of the EGF receptor triggers differentiation of all cell types in the *Drosophila* eye. *Cell*, *87*(4), 651-660. https://doi.org/10.1016/S0092-8674(00)81385-9

Freeman, M. R. (2015). Drosophila Central Nervous System Glia. *Cold Spring Harb Perspect Biol*, *7*(11). https://doi.org/10.1101/cshperspect.a020552

Freymuth, P. S., & Fitzsimons, H. L. (2017). The ERM protein moesin is essential for neuronal morphogenesis and long-term memory in *Drosophila*. *Molecular Brain*, *10*(1), 41. https://doi.org/10.1186/s13041-017-0322-y

Frohman, E. M., Racke, M. K., & Raine, C. S. (2006). Multiple sclerosis--the plaque and its pathogenesis. *N Engl J Med*, *354*(9), 942-955. https://doi.org/10.1056/NEJMra052130

Fruton, J. S., & Bergmann, M. (1942). The Multiple Specificity of Chymotrypsin. *Journal of Biological Chemistry*, *145*(1), 253-265. https://doi.org/10.1016/s0021-9258(18)45029-6

Fujii, S., Emery, P., & Amrein, H. (2017). SIK3-HDAC4 signaling regulates *Drosophila* circadian male sex drive rhythm via modulating the DN1 clock neurons. *Proc Natl Acad Sci U S A*, *114*(32), E6669-E6677. https://doi.org/10.1073/pnas.1620483114

Gallinari, P., Di Marco, S., Jones, P., Pallaoro, M., & Steinkuhler, C. (2007). HDACs, histone deacetylation and gene transcription: from molecular biology to cancer therapeutics. *Cell Res*, *17*(3), 195-211. https://doi.org/10.1038/sj.cr.7310149

Ganguly-Fitzgerald, I., Donlea, J., & Shaw, P. J. (2006). Waking experience affects sleep need in *Drosophila*. *Science*, *313*(5794), 1775-1781. https://doi.org/10.1126/science.1130408

Gao, J., & Xu, C. (2020). Structural basis for the recognition of RFX7 by ANKRA2 and RFXANK. *Biochem Biophys Res Commun*, *523*(1), 263-266. https://doi.org/10.1016/j.bbrc.2019.12.059

Gao, S., Steffen, J., & Laughon, A. (2005). Dpp-responsive silencers are bound by a trimeric Mad-Medea complex. *J Biol Chem*, *280*(43), 36158-36164. https://doi.org/10.1074/jbc.M506882200

Garcia-Bellido, A., & Merriam, J. R. (1969). Cell lineage of the imaginal discs in *Drosophila gynandromorphs*. *Journal of Experimental Zoology*, *170*(1). https://doi.org/10.1002/jez.1401700106

Gauthier, S., Rosa-Neto, P., Morais, J. A., & Webster, C. (2021). *World Alzheimer Report*. A. D. International.

Gendre, N., Luer, K., Friche, S., Grillenzoni, N., Ramaekers, A., Technau, G. M., & Stocker, R. F. (2004). Integration of complex larval chemosensory organs into the adult nervous system of Drosophila. *Development*, *131*(1), 83-92. https://doi.org/10.1242/dev.00879

Ghosh, R., Roy, D., Dubey, S., Das, S., & Benito-Leon, J. (2022). Movement Disorders in Multiple Sclerosis: An Update. *Tremor Other Hyperkinet Mov (N Y)*, *12*, 14. https://doi.org/10.5334/tohm.671

Ghysen, A. (1978). Sensory neurones recognise defined pathways in Drosophila central nervous system. *Nature*, *274*(5674), 864-872. https://doi.org/10.1038/274869a0

Ghysen, A. (1980). The projection of sensory neurons in the central nervous system of Drosophila: choice of the appropriate pathway. *Dev Biol*, *78*(2), 521-541. https://doi.org/10.1016/0012-1606(80)90351-6

Giasson, B. I., Duda, J. E., Murray, I. V. J., Chen, Q., Souza, J. M., Hurtig, I. H., Ischiropoulos, H., Trojanowski, J. Q., & Lee, V. M.-Y. (2000). Oxidative damage linked to seurodegeneration by selective α-synuclein nitration in synucleinopathy lesions. *Science*, *290*, 985-989. https://doi.org/10.1126/science.290.5493.985

Gibson, M. C., & Schubiger, G. (2001). Drosophila peripodial cells, more than meets the eye? *Bioessays*, *23*(8), 691-697. https://doi.org/10.1002/bies.1098

Goguel, V., Belair, A. L., Ayaz, D., Lampin-Saint-Amaux, A., Scaplehorn, N., Hassan, B. A., & Preat, T. (2011). Drosophila amyloid precursor protein-like is required for long-term memory. *J Neurosci*, *31*(3), 1032-1037. https://doi.org/10.1523/JNEUROSCI.2896-10.2011

Goossens, T., Kang, Y. Y., Wuytens, G., Zimmermann, P., Callaerts-Vegh, Z., Pollarolo, G., Islam, R., Hortsch, M., & Callaerts, P. (2011). The Drosophila L1CAM homolog neuroglian signals through distinct pathways to control different aspects of mushroom body axon development. *Development*, *138*(8), 1595-1605. https://doi.org/10.1242/dev.052787

Green, A., Hossain, T., & Eckmann, D. M. (2022). Mitochondrial dynamics involves molecular and mechanical events in motility, fusion and fission. *Front Cell Dev Biol*, *10*, 1010232. https://doi.org/10.3389/fcell.2022.1010232

Greenwood, S., & Struhl, G. (1999). Progression of the morphogenetic furrow in the Drosophila eye: the roles of Hedgehog, Decapentaplegic and the Raf pathway. *Development*, *126*(24), 5795-5808. https://doi.org/10.1242/dev.126.24.5795

Gregoire, S., & Yang, X. J. (2005). Association with class IIa histone deacetylases upregulates the sumoylation of MEF2 transcription factors. *Mol Cell Biol*, *25*(6), 2273-2287. https://doi.org/10.1128/MCB.25.6.2273-2287.2005

Grozinger, C. M., Hassig, C. A., & Schreiber, S. L. (1999). Three proteins define a class of human histone deacetylases releated to yeast Hda1p. *Proc Natl Acad Sci U S A*, *96*(9), 4868-4873. https://doi.org/10.1073/pnas.96.9.4868

Grozinger, C. M., & Schreiber, S. L. (2000). Regulation of histone deacetylase 4 and 5 and transcriptional activity by 14-3-3-dependent cellular localization. *PNAS*, *97*(14), 7835-7840. https://doi.org/10.1073/pnas.140199597

Grozinger, C. M., & Schreiber, S. L. (2002). Deacetylase enzymes: biological functions and the use of small-molecule inhibitors. *Chemistry & Biology*, *9*(1), 3-16. https://doi.org/10.1016/s1074-5521(02)00092-3

Grzeschik, N. A., & Knust, E. (2005). IrreC/rst-mediated cell sorting during Drosophila pupal eye development depends on proper localisation of DE-cadherin. *Development*, *132*(9), 2035-2045. https://doi.org/10.1242/dev.01800

Gu, X. L., Long, C. X., Sun, L., Xie, C., Lin, X., & Cai, H. (2010). Astrocytic expression of Parkinson's disease-related A53T alpha-synuclein causes neurodegeneration in mice. *Mol Brain*, *3*, 12. https://doi.org/10.1186/1756-6606-3-12

Guan, Z., Buhl, L. K., Quinn, W. G., & Littleton, J. T. (2011). Altered gene regulation and synaptic morphology in Drosophila learning and memory mutants. *Learn Mem*, *18*(4), 191-206. https://doi.org/10.1101/lm.2027111

Guan, Z., Giustetto, M., Lomvardas, S., Kim, J.-H., Miniaci, M. C., Schwartz, J., H., Thanos, D., & Kandel, E. R. (2002). Integration of long-term-memory-related synaptic plasticity involves bidirectional regulation of gene expression and chromatin structure. *Cell*, *111*(4), 483-493. https://doi.org/10.1016/s0092-8674(02)01074-7

Guan, Z., Saraswati, S., Adolfsen, B., & Littleton, J. T. (2005). Genome-wide transcriptional changes associated with enhanced activity in the *Drosophila* nervous system. *Neuron*, *48*(1), 91-107. https://doi.org/10.1016/j.neuron.2005.08.036

Guenther, M. G., Barak, O., & Lazar, M. A. (2001). The SMRT and N-CoR corepressors are activating cofactors for histone deacetylase 3. *Mol Cell Biol*, *21*(18), 6091-6101. https://doi.org/10.1128/MCB.21.18.6091-6101.2001

Guo, L., Han, A., Bates, D. L., Cao, J., & Chen, L. (2007). Crystal structure of a conserved N-terminal domain of histone deacetylase 4 reveals functional insights into glutamine-rich domains. *Proceedings of the National Academy of Sciences of the United States of America*, *104*(11), 4297-4302. https://doi.org/10.1073/pnas.0608041104

Guo, L., Zhang, N., & Simpson, J. H. (2022). Descending neurons coordinate anterior grooming behavior in Drosophila. *Curr Biol*, *32*(4), 823-833 e824. https://doi.org/10.1016/j.cub.2021.12.055

Guo, S. S., Seiwert, A., Szeto, I. Y. Y., & Fassler, R. (2021). Tissue distribution and subcellular localization of the family of Kidney Ankyrin Repeat Domain (KANK) proteins. *Exp Cell Res*, *398*(1). https://doi.org/10.1016/j.yexcr.2020.112391

Guo, X., Wang, S. B., Xu, H., Ribic, A., Mohns, E. J., Zhou, Y., Zhu, X., Biederer, T., Crair, M. C., & Chen, B. (2015). A short N-terminal domain of HDAC4 preserves photoreceptors and restores visual function in retinitis pigmentosa. *Nat Commun*, *6*, 8005. https://doi.org/10.1038/ncomms9005

Guthrie, S. (1997). Axon guidance: netrin receptors are revealed. *Dispatch*, *7*(1), 6-9. https://doi.org/10.1016/S0960-9822(06)00007-8

Hakim, Y., Yaniv, S. P., & Schuldiner, O. (2014). Astrocytes play a key role in Drosophila mushroom body axon pruning. *PLoS One*, *9*(1), e86178. https://doi.org/10.1371/journal.pone.0086178

Halter, D. A., Urban, J., Rickert, C., Ner, S. S., Ito, K., Travers, A. A., & Technau, G. M. (1995). The homeobox gene repo is required for the differentiation and maintenance of glia function in the embryonic nervous system of Drosophila melanogaster. *Development*, *121*(2), 317-332. https://doi.org/10.1242/dev.121.2.317

Han, S., Gim, Y., Jang, E. H., & Hur, E. M. (2022). Functions and dysfunctions of oligodendrocytes in neurodegenerative diseases. *Front Cell Neurosci*, *16*, 1083159. https://doi.org/10.3389/fncel.2022.1083159

Han, Y. H., & Park, W. H. (2010). MG132, a proteasome inhibitor decreased the growth of Calu-6 lung cancer cells via apoptosis and GSH depletion. *Toxicol In Vitro*, *24*(4), 1237-1242. https://doi.org/10.1016/j.tiv.2010.02.005

Handy, D. E., Castro, R., & Loscalzo, J. (2011). Epigenetic modifications: basic mechanisms and role in cardiovascular disease. *Circulation*, *123*(19), 2145-2156. https://doi.org/10.1161/CIRCULATIONAHA.110.956839

Harrison, B. R., Wang, L., Gajda, E., Hoffman, E. V., Chung, B. Y., Pletcher, S. D., Raftery, D., & Promislow, D. E. L. (2020). The metabolome as a link in the genotype-phenotype map for peroxide resistance in the fruit fly, Drosophila melanogaster. *BMC Genomics*, *21*(1), 341. https://doi.org/10.1186/s12864-020-6739-1

Hatch, H. A. M., Belalcazar, H. M., Marshall, O. J., & Secombe, J. (2021). A KDM5-Prospero transcriptional axis functions during early neurodevelopment to regulate mushroom body formation. *Elife*, *10*. https://doi.org/10.7554/eLife.63886

Hawley, H. R. (2020). *Investigating the role of HDAC4 aggregation in neuronal development in Drosophila melanogaster: a thesis presented in partial fulfilment of the requirements for the degree of Bachelor of Science (Honours) in Biochemistry at Massey University, Manawatu, New Zealand*.

Hawley, H. R., Roberts, C. J., & Fitzsimons, H. L. (2023). Comparison of neuronal GAL4 drivers along with the AGES (auxin-inducible gene expression system) and TARGET (temporal and regional gene expression targeting) systems for fine tuning of neuronal gene expression in Drosophila. *MicroPubl Biol*, *2023*. https://doi.org/10.17912/micropub.biology.000885

Hayashi, K., Ogiyama, Y., Yokomi, K., Nakagawa, T., Kaino, T., & Kawamukai, M. (2014). Functional conservation of coenzyme Q biosynthetic genes among yeasts, plants, and humans. *PLoS One*, *9*(6), e99038. https://doi.org/10.1371/journal.pone.0099038

Haynie, J. L., & Bryant, P. J. (1986). Development of the eye-antenna imaginal disc and morphogenesis of the adult head in Drosophila melanogaster. *J Exp Zool*, *237*(3), 293-308. https://doi.org/10.1002/jez.1402370302

Hebbar, S., Hall, R. E., Demski, S. A., Subramanian, A., & Fernandes, J. J. (2006). The adult abdominal neuromuscular junction of Drosophila: a model for synaptic plasticity. *J Neurobiol*, *66*(10), 1140-1155. https://doi.org/10.1002/neu.20279

Herrup, K., Li, J., & Chen, J. (2013). The role of ATM and DNA damage in neurons: upstream and downstream connections. *DNA Repair (Amst)*, *12*(8), 600-604. https://doi.org/10.1016/j.dnarep.2013.04.012

Heslop-Harrison, J. S., & Schwarzacher, T. (2013). Nucleosomes and centromeric DNA packaging. *Proc Natl Acad Sci U S A*, *110*(50), 19974-19975. https://doi.org/10.1073/pnas.1319945110

Hildmann, C., Wegener, D., Riester, D., Hempel, R., Schober, A., Merana, J., Giurato, L., Guccione, S., Nielsen, T. K., Ficner, R., & Schwienhorst, A. (2006). Substrate and inhibitor specificity of class 1 and class 2 histone deacetylases. *Journal of Biotechnology*, *124*(1), 258-270. https://doi.org/10.1016/j.jbiotec.2006.01.030

Hilgers, V., Perry, M. W., Hendrix, D., Stark, A., Levine, M., & Haley, B. (2011). Neural-specific elongation of 3' UTRs during *Drosophila* development. *Proc Natl Acad Sci U S A*, *108*(38), 15864-15869. https://doi.org/10.1073/pnas.1112672108

Ho, T. Y., Wu, W. H., Hung, S. J., Liu, T., Lee, Y. M., & Liu, Y. H. (2019). Expressional Profiling of Carpet Glia in the Developing Drosophila Eye Reveals Its Molecular Signature of Morphology Regulators. *Front Neurosci*, *13*, 244. https://doi.org/10.3389/fnins.2019.00244

Hölzl, H., Kapelari, B., Kellermann, J., Seemüller, E., Sümegi, M., Udvardy, A., Medalia, O., Sperling, J., Müller, S. A., Engel, A., & Baumeister, W. (2000). The regulatory complex of Drosophila melanogaster 26S proteasomes. Subunit composition and localization of a deubiquitylating enzyme. *J Cell Biol*, *150*(1), 119-130. https://doi.org/10.1083/jcb.150.1.119

Hoover, K. K., Chien, A. J., & Corces, V. G. (1993). Effects of transposable elements on the expression of the *forked* gene of *Drosophila melanogaster*. *Genetics*, *135*(2), 507-526. https://doi.org/10.1093/genetics/135.2.507

Hsu, C. T., & Bhandawat, V. (2016). Organization of descending neurons in Drosophila melanogaster. *Sci Rep*, *6*, 20259. https://doi.org/10.1038/srep20259

Huang, X., Warren, J. T., Buchanan, J., Gilbert, L. I., & Scott, M. P. (2007). *Drosophila* Niemann-Pick type C-2 genes control sterol homeostasis and steroid biosynthesis: a model of human neurodegenerative disease. *Development*, *134*(20), 3733-3742. https://doi.org/10.1242/dev.004572

Huang, Y. C., Wang, C. T., Su, T. S., Kao, K. W., Lin, Y. J., Chuang, C. C., Chiang, A. S., & Lo, C. C. (2018). A single-cell level and connectome-derived computational model of the *Drosophila* brain. *Frontiers in Neuroinformatics*, *12*, 99. https://doi.org/10.3389/fninf.2018.00099

Huber, K. M., Gallagher, S. M., Warren, S. T., & Bear, M. F. (2002). Altered synaptic plasticity in a mouse model of fragile X mental retardation. *Proc Natl Acad Sci U S A*, *99*(11), 7746-7750. https://doi.org/10.1073/pnas.122205699

Huckert, M., Mecili, H., Laugel-Haushalter, V., Stoetzel, C., Muller, J., Flori, E., Laugel, V., Maniere, M. C., Dollfus, H., & Bloch-Zupan, A. (2014). A novel mutation in the ROGDI gene in a patient with Kohlschutter-Tonz Syndrome. *Mol Syndromol*, *5*(6), 293-298. https://doi.org/10.1159/000366252

Hura, A. (2018). *Functional characterisation of coq8 in Drosophila: a thesis presented in partial fulfilment of the requirements for the degree of Master of Science in Genetics at Massey University, Manawatu, New Zealand.*

Hura, A. J., Hawley, H. R., Tan, W. J., Penny, R. J., Jacobsen, J. C., & Fitzsimons, H. L. (2022). Loss of Drosophila Coq8 results in impaired survival, locomotor deficits and photoreceptor degeneration. *Mol Brain*, *15*(1), 15. https://doi.org/10.1186/s13041-022-00900-3

Ichinose, T., Aso, Y., Yamagata, N., Abe, A., Rubin, G. M., & Tanimoto, H. (2015). Reward signal in a recurrent circuit drives appetitive long-term memory formation. *Elife*, *4*. https://doi.org/10.7554/eLife.10719

Ikeda, A., Nishioka, K., Meng, H., Takanashi, M., Hasegawa, I., Inoshita, T., Shiba-Fukushima, K., Li, Y., Yoshino, H., Mori, A., Okuzumi, A., Yamaguchi, A., Nonaka, R., Izawa, N., Ishikawa, K. I., Saiki, H., Morita, M., Hasegawa, M., Hasegawa, K., . . . Hattori, N. (2019). Mutations in CHCHD2 cause alpha-synuclein aggregation. *Hum Mol Genet*, *28*(23), 3895-3911. https://doi.org/10.1093/hmg/ddz241

Imai, S.-I., Armstrong, C. M., Kaeberlein, M., & Guarente, L. (2000). Transcriptional silencing and longevity protein Sir2 is an NAD-sependent histone deacetylase. *Nature*, *403*, 795-800. https://doi.org/10.1038/35001622

Inagaki, H. K., Kamikouchi, A., & Ito, K. (2010). Methods for quantifying simple gravity sensing in Drosophila melanogaster. *Nat Protoc*, *5*(1), 20-25. https://doi.org/10.1038/nprot.2009.196

Iqbal, Z., Vandeweyer, G., van der Voet, M., Waryah, A. M., Zahoor, M. Y., Besseling, J. A., Roca, L. T., Vulto-van Silfhout, A. T., Nijhof, B., Kramer, J. M., Van der Aa, N., Ansar, M., Peeters, H., Helsmoortel, C., Gilissen, C., Vissers, L. E., Veltman, J. A., de Brouwer, A. P., Frank Kooy, R., . . . Rooms, L. (2013). Homozygous and heterozygous disruptions of ANK3: at the crossroads of neurodevelopmental and psychiatric disorders. *Human Molecular Genetics*, *22*(10), 1960-1970. https://doi.org/10.1093/hmg/ddt043

Ito, K., Awano, W., Suzuki, K., Hiromi, Y., & Yamamoto, D. (1997). The Drosophila mushroom body is a quadruple structure of clonal units each of which contains a virtually identical set of neurones and glial cells. *Development*, *124*(4), 761-771. https://doi.org/10.1242/dev.124.4.761

Ito, K., Suzuki, K., Estes, P., Ramaswami, M., Yamamoto, D., & Strausfeld, N. J. (1998). The organization of extrinsic neurons and their implications in the functional roles of the mushroom bodies in *Drosophila melanogaster* meigen. *Learning & Memory*, *5*(1-2), 52-77. https://doi.org/10.1101/lm.5.1.52

Jacobsen, J. C., Whitford, W., Swan, B., Taylor, J., Love, D. R., Hill, R., Molyneux, S., George, P. M., Mackay, R., Robertson, S. P., Snell, R. G., & Lehnert, K. (2018). Compound Heterozygous Inheritance of Mutations in Coenzyme Q8A Results in Autosomal Recessive Cerebellar Ataxia and Coenzyme Q(10) Deficiency in a Female Sib-Pair. *JIMD Rep*, *42*, 31-36. https://doi.org/10.1007/8904_2017_73

Jaenisch, R., & Bird, A. (2003). Epigenetic regulation of gene expression: how the genome integrates intrinsic and environmental signals. *Nature Genetics*, *33*, 245-254. https://doi.org/10.1038/ng1089

Jan, Y. N., Ghysen, A., Christoph, I., Barbel, S., & Jan, L. Y. (1985). Formation of neuronal pathways in the imaginal discs of Drosophila melanogaster. *J Neurosci*, *5*(9), 2453-2464. https://doi.org/10.1523/jneurosci.05-09-02453.1985

Jenett, A., Rubin, G. M., Ngo, T.-T. B., Shepherd, D., Murphy, C., Dionne, H., Pfeiffer, B. D., Cavallaro, A., Hall, D., Jeter, J., Iyer, N., Fetter, D., Hausenfluck, J. H., Peng, H., Trautman, E. T., Svirskas, R., Myers, E. W., Iwinski, Z. R., Aso, Y., . . . Zugates, C. T. (2012). A GAL4-driver line resource for *Drosophila* neurobiology. *Cell Reports*, *2*(4), 991-1001. https://doi.org/10.1016/j.celrep.2012.09.011

Johnmark, N., & Kinyi, H. W. (2021). Amaranth leaf extract protects against hydrogen peroxide induced oxidative stress in Drosophila melanogaster. *BMC Res Notes*, *14*(1), 188. https://doi.org/10.1186/s13104-021-05603-x

Johnson, R. I., & Cagan, R. L. (2009). A quantitative method to analyze Drosophila pupal eye patterning. *PLoS One*, *4*(9), e7008. https://doi.org/10.1371/journal.pone.0007008

Jünger, M. A., Rintelen, F., Stocker, H., Wasserman, J. D., Végh, M., Radimerski, T., Greenberg, M. E., & Hafen, E. (2003). The *Drosophila* Forkhead transcription factor FOXO mediates the reduction in cell number associated with reduced insulin signaling. *Journal of Biology*, *2*(3). https://doi.org/10.1186/1475-4924-2-20

Juusola, M., & Hardie, R. C. (2001). Light adaptation in Drosophila photoreceptors: I. Response dynamics and signaling efficiency at 25 degrees C. *J Gen Physiol*, *117*(1), 3-25. https://doi.org/10.1085/jgp.117.1.3

Kalmus, H. (1943). The optomotor responses of some eye mutants of Drosophila. *Journal of Genetics*, *45*, 206-213. https://doi.org/10.1007/BF02982936

Kamikouchi, A., Inagaki, H. K., Effertz, T., Hendrich, O., Fiala, A., Gopfert, M. C., & Ito, K. (2009). The neural basis of Drosophila gravity-sensing and hearing. *Nature*, *458*(7235), 165-171. https://doi.org/10.1038/nature07810

Kandel, E. R., Dudai, Y., & Mayford, M. R. (2014). The molecular and systems biology of memory. *Cell*, *157*(1), 163-186. https://doi.org/10.1016/j.cell.2014.03.001

Kang, H., Zhao, J., Jiang, X., Li, G., Huang, W., Cheng, H., & Duan, R. (2019). *Drosophila* Netrin-B controls mushroom body axon extension and regulates courtship-associated learning and memory of a *Drosophila* fragile X syndrome model. *Mol Brain*, *12*(1), 52. https://doi.org/10.1186/s13041-019-0472-1

Kao, H.-Y., Downes, M., Ordentlich, P., & Evans, R. M. (1999). Isolation of a novel histone deacetylase reveals that class I and class II deacetylases promote SMRT-mediated repression. *Genes & Development*, *14*(1), 55-66. https://doi.org/10.1101/gad.14.1.55

Kaplow, M. E., Mannava, L. J., Pimentel, A. C., Fermin, H. A., Hyatt, V. J., Lee, J. J., & Venkatesh, T. R. (2007). A genetic modifier screen identifies multiple genes that interact with *Drosophila* Rap/Fzr and suggests novel cellular roles. *J Neurogenet*, *21*(3), 105-151. https://doi.org/10.1080/01677060701503140

Karagiosis, S. A., & Ready, D. F. (2004). Moesin contributes an essential structural role in *Drosophila* photoreceptor morphogenesis. *Development*, *131*(4), 725-732. https://doi.org/10.1242/dev.00976

Kato, A., Ohta, K., Okanoya, K., & Kazama, H. (2023). Dopaminergic neurons dynamically update sensory values during olfactory maneuver. *Cell Rep*, *42*(10), 113122. https://doi.org/10.1016/j.celrep.2023.113122

Katti, P., Rai, M., Srivastava, S., D'Silva, P., & Nongthomba, U. (2021). Marf-mediated mitochondrial fusion is imperative for the development and functioning of indirect flight muscles (IFMs) in drosophila. *Exp Cell Res*, *399*(2), 112486. https://doi.org/10.1016/j.yexcr.2021.112486

Keleman, K., Kruttner, S., Alenius, M., & Dickson, B. J. (2007). Function of the Drosophila CPEB protein Orb2 in long-term courtship memory. *Nat Neurosci*, *10*(12), 1587-1593. https://doi.org/10.1038/nn1996

Keleman, K., Vrontou, E., Kruttner, S., Yu, J. Y., Kurtovic-Kozaric, A., & Dickson, B. J. (2012). Dopamine neurons modulate pheromone responses in Drosophila courtship learning. *Nature*, *489*(7414), 145-149. https://doi.org/10.1038/nature11345

Kendroud, S., Bohra, A. A., Kuert, P. A., Nguyen, B., Guillermin, O., Sprecher, S. G., Reichert, H., VijayRaghavan, K., & Hartenstein, V. (2018). Structure and development of the subesophageal zone of the Drosophila brain. II. Sensory compartments. *J Comp Neurol*, *526*(1), 33-58. https://doi.org/10.1002/cne.24316

Kennedy, M. B. (2013). Synaptic signaling in learning and memory. *Cold Spring Harbor Perspective Biology*, *8*(2). https://doi.org/10.1101/cshperspect.a016824

Kessler, R. J., & Fanestil, D. D. (1986). Interference by lipids in the determination of protein using bicinchoninic acid. *Anal Biochem*, *159*(1), 138-142. https://doi.org/10.1016/0003-2697(86)90318-0

Kim, M., Jang, D., Yoo, E., Oh, Y., Sonn, J. Y., Lee, J., Ki, Y., Son, H. J., Hwang, O., Lee, C., Lim, C., & Choe, J. (2017). Rogdi defines GABAergic control of a wake-promoting dopaminergic pathway to sustain sleep in *Drosophila*. *Sci Rep*, *7*(1). https://doi.org/10.1038/s41598-017-11941-3

Kim, M. S., Akhtar, M. W., Adachi, M., Mahgoub, M., Bassel-Duby, R., Kavalali, E. T., Olson, E. N., & Monteggia, L. M. (2012). An essential role for histone deacetylase 4 in synaptic plasticity and memory formation. *The Journal of Neuroscience*, *32*(32), 10879-10886. https://doi.org/10.1523/JNEUROSCI.2089-12.2012

Kim, Y. J., Zitnan, D., Cho, K. H., Schooley, D. A., Mizoguchi, A., & Adams, M. E. (2006). Central peptidergic ensembles associated with organization of an innate behavior. *Proc Natl Acad Sci U S A*, *103*(38), 14211-14216. https://doi.org/10.1073/pnas.0603459103

Kimura, K. I., & Truman, J. W. (1990). Postmetamorphic cell death in the nervous and muscular systems of Drosophila melanogaster. *J Neurosci*, *10*(2), 403-401. https://doi.org/10.1523/jneurosci.10-02-00403.1990

Kisselev, A. F., Callard, A., & Goldberg, A. L. (2006). Importance of the different proteolytic sites of the proteasome and the efficacy of inhibitors varies with the protein substrate. *J Biol Chem*, *281*(13), 8582-8590. https://doi.org/10.1074/jbc.M509043200

Kolodziejczyk, A., Sun, X., Meinertzhagen, I. A., & Nassel, D. R. (2008). Glutamate, GABA and acetylcholine signaling components in the lamina of the Drosophila visual system. *PLoS One*, *3*(5), e2110. https://doi.org/10.1371/journal.pone.0002110

Kong, Q., Hao, Y., Li, X., Wang, X., Ji, B., & Wu, Y. (2018). HDAC4 in ischemic stroke: mechanisms and therapeutic potential. *Clin Epigenetics*, *10*(1), 117. https://doi.org/10.1186/s13148-018-0549-1

Kornberg, T. (1981). Engrailed: a gene controlling compartment and segment formation in Drosophila. *Proc Natl Acad Sci U S A*, *78*(2), 1095-1099. https://doi.org/10.1073/pnas.78.2.1095

Kozlov, E. N., Tokmatcheva, E. V., Khrustaleva, A. M., Grebenshchikov, E. S., Deev, R. V., Gilmutdinov, R. A., Lebedeva, L. A., Zhukova, M., Savvateeva-Popova, E. V., Schedl, P., & Shidlovskii, Y. V. (2023). Long-Term Memory Formation in Drosophila Depends on the 3'UTR of CPEB Gene orb2. *Cells*, *12*(2). https://doi.org/10.3390/cells12020318

Krause, S. A., Overend, G., Dow, J. A. T., & Leader, D. P. (2022). FlyAtlas 2 in 2022: enhancements to the Drosophila melanogaster expression atlas. *Nucleic Acids Res*, *50*(D1), D1010-D1015. https://doi.org/10.1093/nar/gkab971

Kremer, M. C., Jung, C., Batelli, S., Rubin, G. M., & Gaul, U. (2017). The glia of the adult Drosophila nervous system. *Glia*, *65*(4), 606-638. https://doi.org/10.1002/glia.23115

Kruttner, S., Stepien, B., Noordermeer, J. N., Mommaas, M. A., Mechtler, K., Dickson, B. J., & Keleman, K. (2012). Drosophila CPEB Orb2A mediates memory independent of Its RNA-binding domain. *Neuron*, *76*(2), 383-395. https://doi.org/10.1016/j.neuron.2012.08.028

Kruttner, S., Traunmuller, L., Dag, U., Jandrasits, K., Stepien, B., Iyer, N., Fradkin, L. G., Noordermeer, J. N., Mensh, B. D., & Keleman, K. (2015). Synaptic Orb2A Bridges Memory Acquisition and Late Memory Consolidation in Drosophila. *Cell Rep*, *11*(12), 1953-1965. https://doi.org/10.1016/j.celrep.2015.05.037

Kumar, J. P. (2018). The fly eye: Through the looking glass. *Dev Dyn*, *247*(1), 111-123. https://doi.org/10.1002/dvdy.24585

Kumar, J. P. (2020). *Catching the Next Wave: Patterning of the Drosophila Eye by the Morphogenetic Furrow*. Springer, Charm. https://doi.org/10.1007/978-3-030-42246-2_3

Kumar, S. R., Patel, H., & Tomlinson, A. (2015). Wingless mediated apoptosis: How cone cells direct the death of peripheral ommatidia in the developing Drosophila eye. *Dev Biol*, *407*(2), 183-194. https://doi.org/10.1016/j.ydbio.2015.09.017

Kupfermann, I., & Kandel, E. R. (1969). Neuronal controls of a behavioural response mediated by the abdominal ganglion of aplysia. *Science*, *164*(3881), 847-850. https://doi.org/10.1126/science.164.3881.847

Kurada, P., & White, K. (1998). Ras promotes cell survival in Drosophila by downregulating hid expression. *Cell*, *95*(3), 319-329. https://doi.org/10.1016/s0092-8674(00)81764-x

Kurtovic, A., Widmer, A., & Dickson, B. J. (2007). A single class of olfactory neurons mediates behavioural responses to a Drosophila sex pheromone. *Nature*, *446*(7135), 542-546. https://doi.org/10.1038/nature05672

Lahm, A., Paolini, C., Pallaoro, M., Nardi, M. C., Jones, P., Neddermann, P., Sambucini, S., Bottomley, S., Surdo, P. L., Carfi, A., Koch, U., Francesco, R. D., Steinkuler, C., & Gallinari, P. (2007). Unraveling the hidden catalytic activity of vertebrate class IIa histone deacetylases. *Proc Natl Acad Sci U S A*, *104*(44). https://doi.org/10.1073/pnas.0706487104

Laker, R. C., Xu, P., Ryall, K. A., Sujkowski, A., Kenwood, B. M., Chain, K. H., Zhang, M., Royal, M. A., Hoehn, K. L., Driscoll, M., Adler, P. N., Wessells, R. J., Saucerman, J. J., & Yan, Z. (2014). A novel MitoTimer reporter gene for mitochondrial content, structure, stress, and damage in vivo. *J Biol Chem*, *289*(17), 12005-12015. https://doi.org/10.1074/jbc.M113.530527

Lamprecht, R., & LeDoux, J. (2004). Structural plasticity and memory. *Nature Reviews Neuroscience*, *5*(1), 45-54. https://doi.org/10.1038/nrn1301

Lawson, L. J., Perry, V. H., Dri, P., & Gordon, S. (1990). Heterogeneity in the distribution and morphology of microglia in the normal adult mouse brain. *Neuroscience*, *39*(1), 151-170. https://doi.org/10.1016/0306-4522(90)90229-w

Lazarczyk, M. J., Kemmler, J. E., Eyford, B. A., Short, J. A., Varghese, M., Sowa, A., Dickstein, D. R., Yuk, F. J., Puri, R., Biron, K. E., Leist, M., Jefferies, W. A., & Dickstein, D. L. (2016). Major Histocompatibility Complex class I proteins are critical for maintaining neuronal structural complexity in the aging brain. *Sci Rep*, *6*. https://doi.org/10.1038/srep26199

Le Bourg, E., & Lints, F. A. (1992). Hypergravity and aging in Drosophila melanogaster. 4. Climbing activity. *Gerontology*, *38*(1-2), 59-64. https://doi.org/10.1159/000213307

Lee, S., Nahm, M., Lee, M., Kwon, M., Kim, E., Zadeh, A. D., Cao, H., Kim, H. J., Lee, Z. H., Oh, S. B., Yim, J., Kolodziej, P. A., & Lee, S. (2007). The F-actin-microtubule crosslinker Shot is a platform for Krasavietz-mediated translational regulation of midline axon repulsion. *Development*, *134*(9), 1767-1777. https://doi.org/10.1242/dev.02842

Lee, T., Lee, A., & Luo, L. (1999). Development of the *Drosophila* mushroom bodies: Sequential generation of three distinct types of neurons from a neuroblast. *Development*, *126*, 4065-4076. https://doi.org/10.1242/dev.00466

Lee, Y. S., Nakahara, K., Pham, J. W., Kim, K., He, Z., Sontheimer, E. J., & Carthew, R. W. (2004). Distinct roles for *Drosophila* dicer-1 and dicer-2 in the siRNA/miRNA silencing pathways. *Cell*, *117*(1), 69-81. https://doi.org/10.1016/S0092-8674(04)00261-2

Legan, S. K., Rebrin, I., Mockett, R. J., Radyuk, S. N., Klichko, V. I., Sohal, R. S., & Orr, W. C. (2008). Overexpression of glucose-6-phosphate dehydrogenase extends the life span of Drosophila melanogaster. *J Biol Chem*, *283*(47), 32492-32499. https://doi.org/10.1074/jbc.M805832200

Levin, E. D., Brady, T. C., Hochrein, E. C., Oury, T. D., Jonsson, L. M., Marklund, S. L., & Crapo, J. D. (1998). Molecular manipulations of extracellular superoxide dismutase: functional importance for learning. *Behav Genet*, *28*(5), 381-390. https://doi.org/10.1023/a:1021673703129

Levine, R. B., & Truman, J. W. (1982). Metamorphosis of the insect nervous system: changes in morphology and synaptic interactions of identified neurones. *Nature*, *299*(5880), 250-252. https://doi.org/10.1038/299250a0

Li, C., & Gotz, J. (2017). Somatodendritic accumulation of Tau in Alzheimer's disease is promoted by Fyn-mediated local protein translation. *EMBO J*, *36*(21), 3120-3138. https://doi.org/10.15252/embj.201797724

Li, H., Janssens, J., De Waegeneer, M., Kolluru, S. S., Davie, K., Gardeux, V., Saelens, W., David, F. P. A., Brbic, M., Spanier, K., Leskovec, J., McLaughlin, C. N., Xie, Q., Jones, R. C., Brueckner, K., Shim, J., Tattikota, S. G., Schnorrer, F., Rust, K., . . . Zinzen, R. P. (2022). Fly Cell Atlas: A single-nucleus transcriptomic atlas of the adult fruit fly. *Science*, *375*(6584), eabk2432. https://doi.org/10.1126/science.abk2432

Li, H., Russo, A., & DiAntonio, A. (2019). SIK3 suppresses neuronal hyperexcitability by regulating the glial capacity to buffer K(+) and water. *J Cell Biol*, *218*(12), 4017-4029. https://doi.org/10.1083/jcb.201907138

Li, J., Chen, J., Ricupero, C. L., Hart, R. P., Schwartz, M. S., Kusnecov, A., & Herrup, K. (2012). Nuclear accumulation of HDAC4 in ATM deficiency promotes neurodegeneration in ataxia telangiectasia. *Nature Medicine*, *18*(5), 783-790. https://doi.org/10.1038/nm.2709

Li, J., Wang, J., Wang, J., Nawaz, Z., Liu, J. M., Qin, J., & Wong, J. (2000). Both corepressor proteins SMRT and N-CoR exist in large protein complexes containing HDAC3. *EMBO J*, *19*(16), 4342-4350. https://doi.org/10.1093/emboj/19.16.4342

Li, M., Sun, S., Priest, J., Bi, X., & Fan, Y. (2019). Characterization of TNF-induced cell death in Drosophila reveals caspase- and JNK-dependent necrosis and its role in tumor suppression. *Cell Death Dis*, *10*(8), 613. https://doi.org/10.1038/s41419-019-1862-0

Li, S., Chai, Z., Li, Y., Liu, D., Bai, Z., Li, Y., Li, Y., & Situ, Z. (2009). BZW1, a novel proliferation regulator that promotes growth of salivary muocepodermoid carcinoma. *Cancer Lett*, *284*(1), 86-94. https://doi.org/10.1016/j.canlet.2009.04.019

Li, S., Li, Y., Carthew, R. W., & Lai, Z. C. (1997). Photoreceptor cell differentiation requires regulated proteolysis of the transcriptional repressor Tramtrack. *Cell*, *90*(3), 469-478. https://doi.org/10.1016/s0092-8674(00)80507-3

Li, W. Z., Li, S. L., Zheng, H. Y., Zhang, S. P., & Xue, L. (2012). A broad expression profile of the GMR-GAL4 driver in Drosophila melanogaster. *Genet Mol Res*, *11*(3), 1997-2002. https://doi.org/10.4238/2012.August.6.4

Li, Y., Shen, M., Stockton, M. E., & Zhao, X. (2019). Hippocampal deficits in neurodevelopmental disorders. *Neurobiol Learn Mem*, *165*, 106945. https://doi.org/10.1016/j.nlm.2018.10.001

Li, Z., Wu, C., Ding, X., Li, W., & Xue, L. (2020). Toll signaling promotes JNK-dependent apoptosis in Drosophila. *Cell Div*, *15*, 7. https://doi.org/10.1186/s13008-020-00062-5

Lilly, B., Zhao, B., Ranganayakulu, G., Paterson, B. M., Schulz, R. A., & Olson, E. N. (1995). Requirement of MADS domain transcription factor D-MEF2 for muscle formation in Drosophila. *Science*, *267*(5198), 688-693. https://doi.org/10.1126/science.7839146

Lin, Y.-J., Seroude, L., & Benzer, S. (1998). Extended life-span and stress resistance in the *Drosophila* mutant methuselah. *Science*, *282*(5390), 943-946. https://doi.org/10.1126/science.282.5390.943

Linford, N. J., Bilgir, C., Ro, J., & Pletcher, S. D. (2013). Measurement of lifespan in Drosophila melanogaster. *J Vis Exp*(71). https://doi.org/10.3791/50068

Liu, J., Xiao, Q., Xiao, J., Niu, C., Li, Y., Zhang, X., Zhou, Z., Shu, G., & Yin, G. (2022). Wnt/beta-catenin signalling: function, biological mechanisms, and therapeutic opportunities. *Signal Transduct Target Ther*, *7*(1), 3. https://doi.org/10.1038/s41392-021-00762-6

Liu, L., MacKenzie, K. R., Putluri, N., Maletić-Savatić, M., & Bellen, H. J. (2017). The Glia-Neuron Lactate Shuttle and Elevated ROS Promote Lipid Synthesis in Neurons and Lipid Droplet Accumulation in Glia via APOE/D. *Cell Metab*, *26*(5), 719-737.e716. https://doi.org/10.1016/j.cmet.2017.08.024

Liu, X., Greer, C., & Secombe, J. (2014). KDM5 interacts with Foxo to modulate cellular levels of oxidative stress. *PLoS Genet*, *10*(10). https://doi.org/10.1371/journal.pgen.1004676

Livnat-Levanon, N., Kevei, E., Kleifeld, O., Krutauz, D., Segref, A., Rinaldi, T., Erpapazoglou, Z., Cohen, M., Reis, N., Hoppe, T., & Glickman, M. H. (2014). Reversible 26S proteasome disassembly upon mitochondrial stress. *Cell Rep*, *7*(5), 1371-1380. https://doi.org/10.1016/j.celrep.2014.04.030

Livneh, I., Cohen-Kaplan, V., Cohen-Rosenzweig, C., Avni, N., & Ciechanover, A. (2016). The life cycle of the 26S proteasome: from birth, through regulation and function, and onto its death. *Cell Res*, *26*(8), 869-885. https://doi.org/10.1038/cr.2016.86

Lloyd, T. E., & Taylor, J. P. (2010). Flightless flies: *Drosophila* models of neuromuscular disease. *Annals of the New York Academy of Sciences*, *1184*(1). https://doi.org/10.1111/j.1749-6632.2010.05432.x

Luan, H., Peabody, N. C., Vinson, C. R., & White, B. H. (2006). Refined spatial manipulation of neuronal function by combinatorial restriction of transgene expression. *Neuron*, *52*(3), 425-436. https://doi.org/10.1016/j.neuron.2006.08.028

Ma'u, E., Saeed, F., Yates, S., Oulaghan, B., Whittington, R., Coomarasamy, C., Cheung, G., & Cullum, S. (2022). Do Māori and Pacific Peoples Living with Dementia in New Zealand Receive Equitable Long-Term Care Compared with New Zealand Europeans? *Journal of Long Term Care*, 222-233. https://doi.org/10.31389/jltc.148

MacDonald, M. E., Ambrose, C. M., Duyao, M. P., Myers, R. H., Lin, C., Srinidhi, L., Barnes, G., Taylor, S. A., James, M., Groot, N., MacFarlane, H., Jenkins, B., Anderson, M. A., Wexler, N. S., & Gusella, J. F. (1993). A novel gene containing a trinucleotide repeat that is expanded and unstable on Huntington's disease chromosomes. *Cell*, *72*(6), 971-983. https://doi.org/10.1016/0092-8674(93)90585-E

Mach, B., Steimle, V., Martinez-Soria, E., & Reith, W. (1996). Regulation of MHC class II genes: lessons from a disease. *Annu Rev Immunol*, *14*, 301-331. https://doi.org/10.1146/annurev.immunol.14.1.301

Madabattula, S. T., Strautman, J. C., Bysice, A. M., O'Sullivan, J. A., Androschuk, A., Rosenfelt, C., Doucet, K., Rouleau, G., & Bolduc, F. (2015). Quantitative Analysis of Climbing Defects in a Drosophila Model of Neurodegenerative Disorders. *J Vis Exp*(100), e52741. https://doi.org/10.3791/52741

Maharjan, S., Oku, M., Tsuda, M., Hoseki, J., & Sakai, Y. (2014). Mitochondrial impairment triggers cytosolic oxidative stress and cell death following proteasome inhibition. *Sci Rep*, *4*, 5896. https://doi.org/10.1038/srep05896

Mahmoud, S., Gharagozloo, M., Simard, C., & Gris, D. (2019). Astrocytes Maintain Glutamate Homeostasis in the CNS by Controlling the Balance between Glutamate Uptake and Release. *Cells*, *8*(2). https://doi.org/10.3390/cells8020184

Main, P., Tan, W. J., Wheeler, D., & Fitzsimons, H. L. (2021). Increased abundance of nuclear HDAC4 impairs neuronal development and long-term memory. *Front Mol Neurosci*, *14*. https://doi.org/10.3389/fnmol.2021.616642

Mandaravally, M. M., & Schneiderman, H. A. (1977). Histological analysis of the dynamics of growth of imaginal discs and histoblast nests during the larval development ofDrosophila melanogaster. *Wilhelm Roux's archives of Developmental Biology*, *183*(4), 269-305. https://doi.org/10.1007/BF00848459

Mao, Y., & Freeman, M. (2009). Fasciclin 2, the Drosophila orthologue of neural cell-adhesion molecule, inhibits EGF receptor signalling. *Development*, *136*(3), 473-481. https://doi.org/10.1242/dev.026054

Mao, Z., & Davis, R. L. (2009). Eight different types of dopaminergic neurons innervate the Drosophila mushroom body neuropil: anatomical and physiological heterogeneity. *Front Neural Circuits*, *3*, 5. https://doi.org/10.3389/neuro.04.005.2009

Mark, B., Bustos-Gonzalez, L., Cascallares, G., Conejera, F., & Ewer, J. (2021). The circadian clock gates Drosophila adult emergence by controlling the timecourse of metamorphosis. *Proc Natl Acad Sci U S A*, *118*(27). https://doi.org/10.1073/pnas.2023249118

Marmor-Kollet, N., Gutman, I., Issman-Zecharya, N., & Schuldiner, O. (2019). Glial Derived TGF-beta Instructs Axon Midline Stopping. *Front Mol Neurosci*, *12*, 232. https://doi.org/10.3389/fnmol.2019.00232

Martin, K. C., Michael, D., Rose, J. C., Barad, M., Casadio, A., Zhu, H., & Kandel, E. R. (1997). MAP kinase translocates into the nucleus of the presynaptic cell and is required for long-term facilitation of *Aplysia*. *Neuron*, *18*, 899-912. https://doi.org/10.1016/S0896-6273(00)80330-X

Masrori, P., & Van Damme, P. (2020). Amyotrophic lateral sclerosis: a clinical review. *Eur J Neurol*, *27*(10), 1918-1929. https://doi.org/10.1111/ene.14393

Maternak, K., Barras, E., Zufferey, M., Conrad, B., Corthals, G., Aebersold, R., Sanchez, J.-C., Hochstrasser, D. F., Mach, B., & Reith, W. (1998). A gene encoding a novel RFX-associated transactivator is mutated in the majority of MHC class II deficiency patients. *Nature Genetics*, *20*(3), 273-277. https://doi.org/10.1038/3081

Matsuno, M., Horiuchi, J., Yuasa, Y., Ofusa, K., Miyashita, T., Masuda, T., & Saitoe, M. (2015). Long-term memory formation in Drosophila requires training-dependent glial transcription. *J Neurosci*, *35*(14), 5557-5565. https://doi.org/10.1523/JNEUROSCI.3865-14.2015

Matzat, T., Sieglitz, F., Kottmeier, R., Babatz, F., Engelen, D., & Klambt, C. (2015). Axonal wrapping in the Drosophila PNS is controlled by glia-derived neuregulin homolog Vein. *Development*, *142*(7), 1336-1345. https://doi.org/10.1242/dev.116616

Mavromatakis, Y. E., & Tomlinson, A. (2016). R7 Photoreceptor Specification in the Developing Drosophila Eye: The Role of the Transcription Factor Deadpan. *PLoS Genet*, *12*(7), e1006159. https://doi.org/10.1371/journal.pgen.1006159

Mazzoni, P., Shabbott, B., & Cortes, J. C. (2012). Motor control abnormalities in Parkinson's disease. *Cold Spring Harb Perspect Med*, *2*(6), a009282. https://doi.org/10.1101/cshperspect.a009282

McBride, S. M., Choi, C. H., Wang, Y., Liebelt, D., Braunstein, E., Ferreiro, D., Sehgal, A., Siwicki, K. K., Dockendorff, T. C., Nguyen, H. T., McDonald, T. V., & Jongens, T. A. (2005). Pharmacological rescue of synaptic plasticity, courtship behavior, and mushroom body defects in a Drosophila model of fragile X syndrome. *Neuron*, *45*(5), 753-764. https://doi.org/10.1016/j.neuron.2005.01.038

McBride, S. M. J., Giuliani, G., Choi, C., Krause, P., Correale, D., Watson, K., Baker, G., & Siwicki, K. K. (1999). Mushroom body ablation impairs short-term and long-term memory of courtship conditioning in *Drosophila melanogaster*. *Neuron*, *24*(4), 967-977. https://doi.org/10.1016/s0896-6273(00)81043-0

McClure, K. D., & Schubiger, G. (2005). Developmental analysis and squamous morphogenesis of the peripodial epithelium in Drosophila imaginal discs. *Development*, *132*(22), 5033-5042. https://doi.org/10.1242/dev.02092

McCord, J. M., & Fridovich, I. (1968). The reduction of cytochrome c by milk xanthine oxidase. *J Biol Chem*, *243*(21), 5753-5760.

McCord, J. M., & Fridovich, I. (1969). Superoxide dismutase. An enzymic function for erythrocuprein (hemocuprein). *J Biol Chem*, *244*(22), 6049-6055.

McGuire, S. E., Mao, Z., & Davis, R. L. (2004). Spatiotemporal gene expression targeting with the TARGET and gene-switch systems in *Drosophila*. *Sci STKE*, *2004*(220). https://doi.org/10.1126/stke.2202004pl6

McKinsey, T. A., Kuwahara, K., Bezprozvannaya, S., & Olson, E. N. (2006). Class II histone deacetylases confer signal responsiveness to the ankyrin-repeat proteins ANKRA2 and RFXANK. *Molecular Biology of the Cell*, *17*(1), 438-447. https://doi.org/10.1091/mbc.e05-07-0612

McKinsey, T. A., Zhang, C. L., & Olson, E. N. (2001). Identification of a signal-responsive nuclear export sequence in class II histone deacetylases. *Mol Cell Biol*, *21*(18), 6312-6321. https://doi.org/10.1128/mcb.21.18.6312-6321.2001

McLachlan, A. (1986). *Drosophila* forked locus. *Molecular and Cellular Biology*, *6*(1), 1-6. https://doi.org/10.1128/mcb.6.1.1

McNabb, S. L., Baker, J. D., Agapite, J., Steller, H., Riddiford, L. M., & Truman, J. W. (1997). Disruption of a behavioral sequence by targeted death of peptidergic neurons in Drosophila. *Neuron*, *19*(4), 813-823. https://doi.org/10.1016/s0896-6273(00)80963-0

McNaught, K. S., Belizaire, R., Isacson, O., Jenner, P., & Olanow, C. W. (2003). Altered proteasomal function in sporadic Parkinson's disease. *Exp Neurol*, *179*(1), 38-46. https://doi.org/10.1006/exnr.2002.8050

McNaught, K. S., Belizaire, R., Jenner, P., Olanow, C. W., & Isacson, O. (2002). Selective loss of 20S proteasome alpha-subunits in the substantia nigra pars compacta in Parkinson's disease. *Neurosci Lett*, *326*(3), 155-158. https://doi.org/10.1016/s0304-3940(02)00296-3

Meiselman, M., Lee, S. S., Tran, R. T., Dai, H., Ding, Y., Rivera-Perez, C., Wijesekera, T. P., Dauwalder, B., Noriega, F. G., & Adams, M. E. (2017). Endocrine network essential for reproductive success in Drosophila melanogaster. *Proc Natl Acad Sci U S A*, *114*(19), E3849-E3858. https://doi.org/10.1073/pnas.1620760114

Michel, C. I., Kraft, R., & Restifo, L. L. (2004). Defective neuronal development in the mushroom bodies of Drosophila fragile X mental retardation 1 mutants. *J Neurosci*, *24*(25), 5798-5809. https://doi.org/10.1523/JNEUROSCI.1102-04.2004

Mihaylova, M. M., Vasquez, D. S., Ravnskjaer, K., Denechaud, P. D., Yu, R. T., Alvarez, J. G., Downes, M., Evans, R. M., Montminy, M., & Shaw, R. J. (2011). Class IIa histone deacetylases are hormone-activated regulators of FOXO and mammalian glucose homeostasis. *Cell*, *145*(4), 607-621. https://doi.org/10.1016/j.cell.2011.03.043

Miller, D. E., Cook, K. R., & Hawley, R. S. (2019). The joy of balancers. *PLoS Genet*, *15*(11), e1008421. https://doi.org/10.1371/journal.pgen.1008421

Miller, D. L., I.A., P., Styles, J., Bobin, S. A., Lin, Y. Y., Biemann, K., & Iqbal, K. (1993). Peptide compositions of the cerebrovascular and senile plaque core amyloid deposits of Alzheimer's disease. *Archives of Biochemistry and Biophysics*, *301*(1), 41-52. https://doi.org/https://doi.org/10.1006/abbi.1993.1112

Miquel, J., Lundgren, P. R., Bensch, K. G., & Atlan, H. (1976). Effects of temperature on the life span, vitality and fine structure of Drosophila melanogaster. *Mech Ageing Dev*, *5*(5), 347-370. https://doi.org/10.1016/0047-6374(76)90034-8

Miska, E. A., Karlsson, C., Langley, E., Nielson, S. J., Pines, J., & Kouzarides, T. (1999). HDAC4 deacetylase associates with and represses the MEF2 transcription factor. *The EMBO Journal*, *18*(18), 5099-5107. https://doi.org/10.1093/emboj/18.18.5099

Misrani, A., Tabassum, S., & Yang, L. (2021). Mitochondrial Dysfunction and Oxidative Stress in Alzheimer's Disease. *Front Aging Neurosci*, *13*, 617588. https://doi.org/10.3389/fnagi.2021.617588

Mitchell, K. J., Doyle, J. L., Serafini, T., Kennedy, T. E., Tessier-Lavigne, M., Goodman, C. S., & Dickson, B. J. (1996). Genetic analysis of *Netrin* genes in *Drosophila*: Netrins guide CNS commissural axons and peripheral motor axons. *Neuron*, *17*(2), 203-215. https://doi.org/10.1016/s0896-6273(00)80153-1

Mitra, P., Vaughan, P. S., Stein, J. L., Stein, G. S., & van Wijnen, A. J. (2001). Purification and functional analysis of a novel leucine-zipper/nucleotide-fold protein, BZAP45, stimulating cell cycle regulated histone H4 gene transcription. *Biochemistry*, *40*, 10693-10699. https://doi.org/10.1021/bi010529o

Morgan, A. R., Hamilton, G., Turic, D., Jehu, L., Harold, D., Abraham, R., Hollingworth, P., Moskvina, V., Brayne, C., Rubinsztein, D. C., Lynch, A., Lawlor, B., Gill, M., O'Donovan, M., Powell, J., Lovestone, S., Williams, J., & Owen, M. J. (2008). Association analysis of 528 intra-genic SNPs in a region of chromosome 10 linked to late onset Alzheimer's disease. *American Journal of Medical Genetics Part B (Neuropsychiatric Genetics)*, *147B*(6), 727-731. https://doi.org/10.1002/ajmg.b.30670

Morgan, T. H. (1911). The origin of five mutations in eye color in *Drosophila* and their modes of inheritance. *Science*, *33*(849), 534-537.

Morris, B., Etoubleau, C., Bourthoumieu, S., Reynaud-Perrine, S., Laroche, C., Lebbar, A., Yardin, C., & Elsea, S. H. (2012). Dose dependent expression of HDAC4 causes variable expressivity in a novel inherited case of brachydactyly mental retardation syndrome. *American Journal of Medical Genetics A*, *158A*(8), 2015-2020. https://doi.org/10.1002/ajmg.a.35463

Morris, M. J., & Monteggia, L. M. (2013). Unique functional roles for class I and class II histone deacetylases in central nervous system development and function. *Int J Dev Neurosci*, *31*(6), 370-381. https://doi.org/10.1016/j.ijdevneu.2013.02.005

Mory, A., Dagan, E., Shahor, I., Mandel, H., Illi, B., Zolotushko, J., Kurolap, A., Chechik, E., Valente, E. M., Amselem, S., & Gershoni-Baruch, R. (2014). Kohlschutter-Tonz syndrome: clinical and genetic insights gained from 16 cases deriving from a close-knit village in Northern Israel. *Pediatr Neurol*, *50*(4), 421-426. https://doi.org/10.1016/j.pediatrneurol.2014.01.006

Mosavi, L. K., Cammett, T. J., Desrosiers, D. C., & Peng, Z. Y. (2004). The ankyrin repeat as molecular architecture for protein recognition. *Protein Sci*, *13*(6), 1435-1448. https://doi.org/10.1110/ps.03554604

Moulton, M. J., Barish, S., Ralhan, I., Chang, J., Goodman, L. D., Harland, J. G., Marcogliese, P. C., Johansson, J. O., Ioannou, M. S., & Bellen, H. J. (2021). Neuronal ROS-induced glial lipid droplet formation is altered by loss of Alzheimer's disease-associated genes. *Proc Natl Acad Sci U S A*, *118*(52). https://doi.org/10.1073/pnas.2112095118

Muller, D., Nagel, A. C., Maier, D., & Preiss, A. (2006). A molecular link A molecular link between Hairless and Pros26.4, a member of the AAA-ATPase subunits of the proteasome 19S regulatory particle in Drosophila. *J Cell Sci*, *119*(Pt 2), 250-258. https://doi.org/10.1242/jcs.02743

Muller, H. J. (1932). Further studies on the nature and causes of gene mutations. *Proc. 6th Int. Cong. Genet*, *1*, 213-255.

Murakami, S., Umetsu, D., Maeyama, Y., Sato, M., Yoshida, S., & Tabata, T. (2007). Focal adhesion kinase controls morphogenesis of the Drosophila optic stalk. *Development*, *134*(8), 1539-1548. https://doi.org/10.1242/dev.001529

Muro, I., Hay, B. A., & Clem, R. J. (2002). The Drosophila DIAP1 protein is required to prevent accumulation of a continuously generated, processed form of the apical caspase DRONC. *J Biol Chem*, *277*(51), 49644-49650. https://doi.org/10.1074/jbc.M203464200

Musacchio, M., & Perrimon, N. (1996). The *Drosophila kekkon* genes: novel members of both the leucine-rich repeat and immunoglobulin superfamilies expressed in the CNS. *Developmental Biology*, *178*(1), 63-76. https://doi.org/10.1006/dbio.1996.0198

Nandi, A., Yan, L. J., Jana, C. K., & Das, N. (2019). Role of Catalase in Oxidative Stress- and Age-Associated Degenerative Diseases. *Oxid Med Cell Longev*, *2019*, 9613090. https://doi.org/10.1155/2019/9613090

National ethnic population projections, by age and sex, 2018(base)-2043. (2021). Stats NZ. https://nzdotstat.stats.govt.nz/wbos/Index.aspx?DataSetCode=TABLECODE8613#

Nayak, S. V., & Singh, R. N. (1985). Primary sensory projections from the labella to the brain of Drosophila melanogaster Meigen (Diptera : Drosophilidae). *International Journal of Insect Morphology and Embryology*, *14*(2), 115-129. https://doi.org/10.1016/0020-7322(85)90051-0

Neugroschl, J., & Wang, S. (2011). Alzheimer's disease: diagnosis and treatment across the spectrum of disease severity. *Mt Sinai Journal of Medicine*, *78*(4), 596-612. https://doi.org/10.1002/msj.20279

Nie, J., Xu, C., Jin, J., Aka, J. A., Tempel, W., Nguyen, V., You, L., Weist, R., Min, J., Pawson, T., & Yang, X. J. (2015). Ankyrin repeats of ANKRA2 recognize a PxLPxL motif on the 3M syndrome protein CCDC8. *Structure*, *23*(4), 700-712. https://doi.org/10.1016/j.str.2015.02.001

Nowak, S. J., & Corces, V. G. (2004). Phosphorylation of histone H3: a balancing act between chromosome condensation and transcriptional activation. *Trends in Genetics*, *20*(4), 214-220. https://doi.org/10.1016/j.tig.2004.02.007

Nunes, M. J., Moutinho, M., Gama, M. J., Rodrigues, C. M., & Rodrigues, E. (2013). Histone deacetylase inhibition decreases cholesterol levels in neuronal cells by modulating key genes in cholesterol synthesis, uptake and efflux. *PLoS One*, *8*(1). https://doi.org/10.1371/journal.pone.0053394

O'Donnell, M., Chance, R. K., & Bashaw, G. J. (2009). Axon growth and guidance: receptor regulation and signal transduction. *Annu Rev Neurosci*, *32*, 383-412. https://doi.org/10.1146/annurev.neuro.051508.135614

Ohashi, Y., Ueda, M., Kawase, T., Kawakami, Y., & Toda, M. (2004). Identification of an epigenetically silenced gene, RFX1, in human glioma cells using restriction landmark genomic scanning. *Oncogene*, *23*(47), 7772-7779. https://doi.org/10.1038/sj.onc.1208058

Oortveld, M. A., Keerthikumar, S., Oti, M., Nijhof, B., Fernandes, A. C., Kochinke, K., Castells-Nobau, A., van Engelen, E., Ellenkamp, T., Eshuis, L., Galy, A., van Bokhoven, H., Habermann, B., Brunner, H. G., Zweier, C., Verstreken, P., Huynen, M. A., & Schenck, A. (2013). Human intellectual disability genes form conserved functional modules in *Drosophila*. *PLoS Genet*, *9*(10). https://doi.org/10.1371/journal.pgen.1003911

Orsulic, S., & Peifer, M. (1996). An in vivo structure-function study of armadillo, the beta-catenin homologue, reveals both separate and overlapping regions of the protein required for cell adhesion and for wingless signaling. *J Cell Biol*, *134*(5), 1283-1300. https://doi.org/10.1083/jcb.134.5.1283

Otsuki, K., Hayashi, Y., Kato, M., Yoshida, H., & Yamaguchi, M. (2004). Characterization of dRFX2, a novel RFX family protein in Drosophila. *Nucleic Acids Res*, *32*(18), 5636-5648. https://doi.org/10.1093/nar/gkh895

Ou, J., Gao, Z., Song, L., & Ho, M. S. (2016). Analysis of Glial Distribution in Drosophila Adult Brains. *Neurosci Bull*, *32*(2), 162-170. https://doi.org/10.1007/s12264-016-0014-0

Pandey, U. B., & Nichols, C. D. (2011). Human disease models in *Drosophila melanogaster* and the role of the fly in therapeutic drug discovery. *Pharmacological Reviews*, *63*(2), 411-436. https://doi.org/10.1124/pr.110.003293

Paolicelli, R. C., & Gross, C. T. (2011). Microglia in development: linking brain wiring to brain environment. *Neuron Glia Biol*, *7*(1), 77-83. https://doi.org/10.1017/S1740925X12000105

Parajuli, N. (2019). A Cycle of Altered Proteasome and Reactive Oxygen Species Production in Renal Proximal Tubular Cells. *Toxicol Forensic Med*, *4*(1), 13-17. https://doi.org/10.17140/tfmoj-4-128

Park, J. H., Schroeder, A. J., Helfrich-Forster, C., Jackson, F. R., & Ewer, J. (2003). Targeted ablation of CCAP neuropeptide-containing neurons of Drosophila causes specific defects in execution and circadian timing of ecdysis behavior. *Development*, *130*(12), 2645-2656. https://doi.org/10.1242/dev.00503

Park, Y., Zitnan, D., Gill, S. S., & Adams, M. E. (1999). Molecular cloning and biological activity of ecdysis-triggering hormones in Drosophila melanogaster. *FEBS Lett*, *463*(1-2), 133-138. https://doi.org/10.1016/s0014-5793(99)01622-1

Parkes, T. L., Elia, A. J., Dickinson, D., Hilliker, A. J., Phillips, J. P., & Boulianne, G. L. (1998). Extension of Drosophila lifespan by overexpression of human SOD1 in motorneurons. *Nat Genet*, *19*(2), 171-174. https://doi.org/10.1038/534

Paroni, G., Cernotta, N., Dello Russo, C., Gallinari, P., Pallaoro, M., Foti, C., Talamo, F., Orsatti, L., Steinkuhler, C., & Brancolini, C. (2008). PP2A regulates HDAC4 nuclear import. *Mol Biol Cell*, *19*(2), 655-667. https://doi.org/10.1091/mbc.e07-06-0623

Parrish, A. B., Freel, C. D., & Kornbluth, S. (2013). Cellular mechanisms controlling caspase activation and function. *Cold Spring Harb Perspect Biol*, *5*(6). https://doi.org/10.1101/cshperspect.a008672

Patel, M. V., Hallal, D. A., Jones, J. W., Bronner, D. N., Zein, R., Caravas, J., Husain, Z., Friedrich, M., & Vanberkum, M. F. (2012). Dramatic expansion and developmental expression diversification of the methuselah gene family during recent *Drosophila* evolution. *J Exp Zool B Mol Dev Evol*, *318*(5), 368-387. https://doi.org/10.1002/jez.b.22453

Patel, P. H., & Tamanoi, F. (2006). Increased Rheb-TOR signaling enhances sensitivity of the whole organism to oxidative stress. *J Cell Sci*, *119*(Pt 20), 4285-4292. https://doi.org/10.1242/jcs.03199

Patterson, C. (2018). *World Alzheimer report 2018. The state of the art of dementia research: New frontiers*. A. D. International.

Peifer, M., McCrea, P. D., Green, K. J., Wieschaus, E., & Gumbiner, B. M. (1992). The vertebrate adhesive junction proteins beta-catenin and plakoglobin and the Drosophila segment polarity gene armadillo form a multigene family with similar properties. *J Cell Biol*, *118*(3), 681-691. https://doi.org/10.1083/jcb.118.3.681

Perez-Perez, J. M., Candela, H., & Micol, J. L. (2009). Understanding synergy in genetic interactions. *Trends in Genetics*, *25*(8), 368-376. https://doi.org/10.1016/j.tig.2009.06.004

Perry, M. M. (1968). Further studies on the development of the eye of *Drosophila melanogaster*. I. The ommatidia. *Journal of Morphology*, *124*(2), 227-247. https://doi.org/10.1002/jmor.1051240208

Petersen, N. S., Lankenau, D.-H., Mitchell, H. K., Young, P., & Corces, V. G. (1994). *forked* proteins are components of fibre bundles present in developming bristles of *Drosophila melanogaster*. *Genetics*, *136*(1), 173-182. https://doi.org/10.1093/genetics/136.1.173

Petrova, N. S., Zenkova, M. A., & Chernolovskaya, E. L. (2013). Structure-functions relations in small interfering RNAs. *Pract. Appl. Biomed. Eng*. https://doi.org/10.5772/53945

Pigna, E., Simonazzi, E., Sanna, K., Bernadzki, K. M., Proszynski, T., Heil, C., Palacios, D., Adamo, S., & Moresi, V. (2019). Histone deacetylase 4 protects from denervation and skeletal muscle atrophy in a murine model of amyotrophic lateral sclerosis. *EBioMedicine*, *40*, 717-732. https://doi.org/10.1016/j.ebiom.2019.01.038

Plautz, J. D., Day, R. N., Dailey, G. M., Welsh, S. B., Hall, J. C., Halpain, S., & Kay, S. A. (1996). Green fluorescent protein and its derivatives as versatile markers for gene expression in living Drosophila melanogaster, plant and mammalian cells. *Gene*, *173*(1 Spec No), 83-87. https://doi.org/10.1016/0378-1119(95)00700-8

Polymeropoulos, M. H., Lavedan, C., Leroy, E., Ide, S. E., Dehejia, A., Dutra, A., Pike, B., Root, H., Rubenstein, J., Boyer, R., Stenroos, E. S., Chandrasekharappa, S., Athanassiadou, A., Papapetropoulos, T., Johnson, W. G., Lazzarini, A. M., Duvoisin, R. C., Di lorio, G., Golbe, L. I., & Nussbaum, R. L. (1997). Mutation in the α-synuclein gene identified in families with Parkinson's disease. *Science*, *276*(5321), 2045-2047. https://doi.org/10.1126/science.276.5321.2045

Poon, I. K., Lucas, C. D., Rossi, A. G., & Ravichandran, K. S. (2014). Apoptotic cell clearance: basic biology and therapeutic potential. *Nat Rev Immunol*, *14*(3), 166-180. https://doi.org/10.1038/nri3607

Przedborski, S. (2005). Pathogenesis of nigral cell death in Parkinson's disease. *Parkinsonism Relat Disord*, *11 Suppl 1*, S3-7. https://doi.org/10.1016/j.parkreldis.2004.10.012

Rader, K., Orlando, R. A., Lou, X., & Farquhar, M. G. (2000). Characterisation of ANKRA, a novel ankyrin repeat protein that interacts with the cytoplasmic domain of megalin. *J Am Soc Nephrol*, *11*(12), 2167-2178. https://doi.org/10.1681/ASN.V11122167

Rahman, M. M., Islam, M. R., Yamin, M., Islam, M. M., Sarker, M. T., Meem, A. F. K., Akter, A., Emran, T. B., Cavalu, S., & Sharma, R. (2022). Emerging Role of Neuron-Glia in Neurological Disorders: At a Glance. *Oxid Med Cell Longev*, *2022*, 3201644. https://doi.org/10.1155/2022/3201644

Raji, J. I., & Potter, C. J. (2021). The number of neurons in *Drosophila* and mosquito brains. *PLoS One*, *16*(5). https://doi.org/10.1371/journal.pone.0250381

Rangarajan, R., Gong, Q., & Gaul, U. (1999). Migration and function of glia in the developing Drosophila eye. *Development*, *126*(15), 3285-3292. https://doi.org/10.1242/dev.126.15.3285

Raun, N., Jones, S., & Kramer, J. M. (2021). Conditioned courtship suppression in Drosophila melanogaster. *J Neurogenet*, *35*(3), 154-167. https://doi.org/10.1080/01677063.2021.1873323

Ray, M., & Lakhotia, S. C. (2015). The commonly used eye-specific sev-GAL4 and GMR-GAL4 drivers in Drosophila melanogaster are expressed in tissues other than eyes also. *J Genet*, *94*(3), 407-416. https://doi.org/10.1007/s12041-015-0535-8

Ready, D. F., Hanson, T. E., & Benzer, S. (1976). Development of the *Drosophila* retina, a neurocrystalline lattice. *Developmental Biology*, *53*(2), 217-240. https://doi.org/0.1016/0012-1606(76)90225-6

Reece, J. B., Meyers, N., Urry, L. A., Cain, M. L., Wasserman, S. A., Minorsky, P. V., Jackson, R. B., & Cooke, B. N. (2014). Animal form and function. In *Campbell biology* (10 ed., pp. 1090-1103). Pearson Education Inc.

Reiter, C., Schimansky, T., Nie, Z., & Fischbach, K. F. (1996). Reorganization of membrane contacts prior to apoptosis in the Drosophila retina: the role of the IrreC-rst protein. *Development*, *122*(6), 1931-1940. https://doi.org/10.1242/dev.122.6.1931

Reiter, L. T., Potocki, L., Chien, S., Gribskov, M., & Bier, E. (2001). A systematic analysis of human disease-associated gene sequences in *Drosophila melanogaster*. *Genome Research*, *11*(6), 1114-1125. https://doi.org/10.1101/gr.169101

Richard, M., Doubkova, K., Nitta, Y., Kawai, H., Sugie, A., & Tavosanis, G. (2022). A Quantitative Model of Sporadic Axonal Degeneration in the Drosophila Visual System. *J Neurosci*, *42*(24), 4937-4952. https://doi.org/10.1523/JNEUROSCI.2115-21.2022

Ridley, R. M., Frith, C. D., Farrer, L. A., & Conneally, P. M. (1991). Patterns of inheritance of the symptoms of Huntington's disease suggestive of an effect of genomic imprinting. *J Med Genet*, *28*, 224-231. https://doi.org/10.1136/jmg.28.4.224

Riemann, D., Wallrafen, R., & Dresbach, T. (2017). The Kohlschutter-Tonz syndrome associated gene Rogdi encodes a novel presynaptic protein. *Sci Rep*, *7*(1). https://doi.org/10.1038/s41598-017-16004-1

Robinow, S., & White, K. (1988). The locus *elav* in *Drosophila melanogaster* is expressed in neurons at all developmental stages. *Developmental Biology*, *126*(2), 294-303. https://doi.org/10.1016/0012-1606(88)90139-x

Robinson, S. W., Herzyk, P., Dow, J. A., & Leader, D. P. (2013). FlyAtlas: database of gene expression in the tissues of Drosophila melanogaster. *Nucleic Acids Res*, *41*(Database issue), D744-750. https://doi.org/10.1093/nar/gks1141

Rosen, L. B., & Greenberg, M. E. (1996). Stimulation of growth factor receptor signal transduction bu activation of voltage-sensitive calcium channels. *Proc Natl Acad Sci U S A*, *93*(3), 1113-1118. https://doi.org/10.1073/pnas.93.3.1113

Roumier, A., Bechade, C., Poncer, J. C., Smalla, K. H., Tomasello, E., Vivier, E., Gundelfinger, E. D., Triller, A., & Bessis, A. (2004). Impaired synaptic function in the microglial KARAP/DAP12-deficient mouse. *J Neurosci*, *24*(50), 11421-11428. https://doi.org/10.1523/JNEUROSCI.2251-04.2004

Sahin, H. B., Sayin, S., Holder, M., Bugra, K., & Celik, A. (2020). Salt inducible kinases as novel Notch interactors in the developing *Drosophila* retina. *PLoS One*, *15*(6). https://doi.org/10.1371/journal.pone.0234744

Salma, J., & McDermott, J. C. (2012). Suppression of a MEF2-KLF6 survival pathway by PKA signaling promotes apoptosis in embryonic hippocampal neurons. *J Neurosci*, *32*(8), 2790-2803. https://doi.org/10.1523/JNEUROSCI.3609-11.2012

Sando, R., 3rd, Gounko, N., Pieraut, S., Liao, L., Yates, J., 3rd, & Maximov, A. (2012). HDAC4 governs a transcriptional program essential for synaptic plasticity and memory. *Cell*, *151*(4), 821-834. https://doi.org/10.1016/j.cell.2012.09.037

Sandoval, H., Yao, C. K., Chen, K., Jaiswal, M., Donti, T., Lin, Y. Q., Bayat, V., Xiong, B., Zhang, K., David, G., Charng, W. L., Yamamoto, S., Duraine, L., Graham, B. H., & Bellen, H. J. (2014). Mitochondrial fusion but not fission regulates larval growth and synaptic development through steroid hormone production. *Elife*, *3*. https://doi.org/10.7554/eLife.03558

Sanyal, S. (2009). Genomic mapping and expression patterns of C380, OK6 and D42 enhancer trap lines in the larval nervous system of Drosophila. *Gene Expr Patterns*, *9*(5), 371-380. https://doi.org/10.1016/j.gep.2009.01.002

Sarkar, S., Roy, B. C., Hatano, N., Aoyagi, T., Gohji, K., & Kiyama, R. (2002). A novel ankyrin repeat-containing gene (Kank) located at 9p24 is a growth suppressor of renal cell carcinoma. *J Biol Chem*, *277*(39), 36585-36591. https://doi.org/10.1074/jbc.M204244200

Scharfman, H. E. (2007). The CA3 "backprojection" to the dentate gyrus. *Prog Brain Res*, *163*, 627-637. https://doi.org/10.1016/S0079-6123(07)63034-9

Schlumm, F., Mauceri, D., Freitag, H. E., & Bading, H. (2013). Nuclear calcium signaling regulates nuclear export of a subset of class IIa histone deacetylases following synaptic activity. *The Journal of Biological Chemistry*, *288*(12), 8074-8084. https://doi.org/10.1074/jbc.M112.432773

Schossig, A., Bloch-Zupan, A., Lussi, A., Wolf, N. I., Raskin, S., Cohen, M., Giuliano, F., Jurgens, J., Krabichler, B., Koolen, D. A., de Macena Sobreira, N. L., Maurer, E., Muller-Bolla, M., Penzien, J., Zschocke, J., & Kapferer-Seebacher, I. (2017). SLC13A5 is the second gene associated with Kohlschutter-Tonz syndrome. *J Med Genet*, *54*(1), 54-62. https://doi.org/10.1136/jmedgenet-2016-103988

Schott, S., Ambrosini, A., Barbaste, A., Benassayag, C., Gracia, M., Proag, A., Rayer, M., Monier, B., & Suzanne, M. (2017). A fluorescent toolkit for spatiotemporal tracking of apoptotic cells in living Drosophila tissues. *Development*, *144*(20), 3840-3846. https://doi.org/10.1242/dev.149807

Schwartz, S., Truglio, M., Scott, M. J., & Fitzsimons, H. L. (2016). Long-term memory in *Drosophila* is influenced by histone deacetylase HDAC4 interacting with SUMO-conjugating enzyme Ubc9. *Genetics*, *203*(3), 1249-1264. https://doi.org/10.1534/genetics.115.183194

Schwarz, D. S., Hutvágner, G., Du, T., Xu, Z., Aronin, N., & Zamore, P. D. (2003). Asymmetry in the assembly of the RNAi enzyme complex. *Cell*, *115*(2), 199-208. https://doi.org/10.1016/s0092-8674(03)00759-1

Schwarz, O., Bohra, A. A., Liu, X., Reichert, H., VijayRaghavan, K., & Pielage, J. (2017). Motor control of Drosophila feeding behavior. *Elife*, *6*. https://doi.org/10.7554/eLife.19892

Scott, R. L., Diao, F., Silva, V., Park, S., Luan, H., Ewer, J., & White, B. H. (2020). Non-canonical Eclosion Hormone-Expressing Cells Regulate Drosophila Ecdysis. *iScience*, *23*(5), 101108. https://doi.org/10.1016/j.isci.2020.101108

Seabrooke, S., & Stewart, B. A. (2008). Moesin helps to restrain synaptic growth at the *Drosophila* neuromuscular junction. *Developmental Neurobiology*, *68*(3), 379-391. https://doi.org/10.1002/dneu.20595

Sen, T., & Sen, N. (2016). Isoflurane-induced inactivation of CREB through histone deacetylase 4 is responsible for cognitive impairment in developing brain. *Neurobiol Dis*, *96*, 12-21. https://doi.org/10.1016/j.nbd.2016.08.005

Shen, X., Chen, J., Li, J., Kofler, J., & Herrup, K. (2016). Neurons in vulnerable regions of the Alzheimer's disease brain display reduced ATM signaling. *eNeuro*, *3*(1), 1-18. https://doi.org/10.1523/ENEURO.0124-15.2016

Shi, X. Z., Zhong, X., & Yu, X. Q. (2012). *Drosophila melanogaster* NPC2 proteins bind bacterial cell wall components and may function in immune signal pathways. *Insect Biochem Mol Biol*, *42*(8), 545-556. https://doi.org/10.1016/j.ibmb.2012.04.002

Sidiropoulou, K., Pissadaki, E. K., & Poirazi, P. (2006). Inside the brain of a neuron. *EMBO Reports*, *7*(9), 886-892. https://doi.org/10.1038/sj.embor.7400789

Siegel, R. W., & Hall, J. C. (1979). Conditioned responses in courtship behavior of normal and mutant Drosophila. *Proc Natl Acad Sci U S A*, *76*(7), 3430-3434. https://doi.org/10.1073/pnas.76.7.3430

Siegenthaler, D., Enneking, E. M., Moreno, E., & Pielage, J. (2015). L1CAM/neuroglian controls the axon-axon interactions establishing layered and lobular mushroom body architecture. *The Journal of Cell Biology*, *208*(7), 1003-1018. https://doi.org/10.1083/jcb.201407131

Silies, M., Yuva, Y., Engelen, D., Aho, A., Stork, T., & Klambt, C. (2007). Glial cell migration in the eye disc. *J Neurosci*, *27*(48), 13130-13139. https://doi.org/10.1523/JNEUROSCI.3583-07.2007

Smeets, C. J., & Verbeek, D. S. (2016). Climbing fibers in spinocerebellar ataxia: A mechanism for the loss of motor control. *Neurobiol Dis*, *88*, 96-106. https://doi.org/10.1016/j.nbd.2016.01.009

Sokolowski, M. B. (2001). *Drosophila*: Genetics meets behaviour [Review Article]. *Nat Rev Genet*, *2*, 879. https://doi.org/10.1038/35098592

Somoza, J. R., Skene, R. J., Katz, B. A., Mol, C., Ho, J. D., Jennings, A. J., Luong, C., Arvai, A., Buggy, J. J., Chi, E., Tang, J., Sang, B. C., Verner, E., Wynands, R., Leahy, E. M., Dougan, D. R., Snell, G., Navre, M., Knuth, M. W., . . . Tari, L. W. (2004). Structural snapshots of human HDAC8 provide insights into the class I histone deacetylases. *Structure*, *12*(7), 1325-1334. https://doi.org/10.1016/j.str.2004.04.012

Song, L., He, Y., Ou, J., Zhao, Y., Li, R., Cheng, J., Lin, C. H., & Ho, M. S. (2017). Auxilin Underlies Progressive Locomotor Deficits and Dopaminergic Neuron Loss in a Drosophila Model of Parkinson's Disease. *Cell Rep*, *18*(5), 1132-1143. https://doi.org/10.1016/j.celrep.2017.01.005

Spillantini, M. G., Crowther, R. A., Jakes, R., Hasegawa, M., & Goedert, M. (1998). α-synuclein in filamentous inclusions of Lewy bodies from Parkinson's disease and dementia with Lewy bodies. *Proc Natl Acad Sci U S A*, *95*(11), 6469-6473. https://doi.org/10.1073/pnas.95.11.6469

Sterner, D. E., & Berger, S. L. (2000). Acetylation of histones and transcription-related factors. *Microbiology and Molecular Biology Reviews*, *64*(2), 435-459. https://doi.org/10.1128/mmbr.64.2.435-459.2000

Strausfeld, N. J., Hansen, L., Li, Y., Gomez, R. S., & Ito, K. (1998). Evolution, discovery and interpretations of arthropod mushroom bodies. *Learning & Memory*, *5*(1), 11-37. https://doi.org/10.1101/lm.5.1.11

Sudhof, T. C., & Malenka, R. C. (2008). Understanding synapses: past, present, and future. *Neuron*, *60*(3), 469-476. https://doi.org/10.1016/j.neuron.2008.10.011

Sun, J., Xu, A. Q., Giraud, J., Poppinga, H., Riemensperger, T., Fiala, A., & Birman, S. (2018). Neural Control of Startle-Induced Locomotion by the Mushroom Bodies and Associated Neurons in Drosophila. *Front Syst Neurosci*, *12*, 6. https://doi.org/10.3389/fnsys.2018.00006

Sun, Y., Liu, L., Ben-Shahar, Y., Jacobs, J. S., Eberl, D. F., & Welsh, M. J. (2009). TRPA channels distinguish gravity sensing from hearing in Johnston's organ. *Proc Natl Acad Sci U S A*, *106*(32), 13606-13611. https://doi.org/10.1073/pnas.0906377106

Suster, M. L., Seugnet, L., Bate, M., & Sokolowski, M. B. (2004). Refining GAL4-driven transgene expression in *Drosophila* with a GAL80 enhancer-trap. *Genesis*, *39*(4), 240-245. https://doi.org/10.1002/gene.20051

Tajiri, R., Ogawa, N., Fujiwara, H., & Kojima, T. (2017). Mechanical Control of Whole Body Shape by a Single Cuticular Protein Obstructor-E in Drosophila melanogaster. *PLoS Genet*, *13*(1), e1006548. https://doi.org/10.1371/journal.pgen.1006548

Takahashi-Fujigasaki, J., Arai, K., Funata, N., & Fujigasaki, H. (2006). SUMOylation substrates in neuronal intranuclear inclusion disease. *Neuropathol Appl Neurobiol*, *32*(1), 92-100. https://doi.org/10.1111/j.1365-2990.2005.00705.x

Takahashi-Fujigasaki, J., & Fujigasaki, H. (2006). Histone deacetylase (HDAC) 4 involvement in both Lewy and Marinesco bodies. *Neuropathol Appl Neurobiol*, *32*(5), 562-566. https://doi.org/10.1111/j.1365-2990.2006.00733.x

Talbot, K. (2009). Motor neuron disease: the bare essentials. *Pract Neurol*, *9*(5), 303-309. https://doi.org/10.1136/jnnp.2009.188151

Tan, W. J. (2022). *Investigating the role of HDAC4 in Drosophila neuronal function: a thesis presented in partial fulfilment of the requirements for the degree of Doctor of Philosophy at Massey University, Manawatu, New Zealand.*

Tan, W. J., Hawley, H. R., Wilson, S. J., & Fitzsimons, H. L. (2024). Deciphering the roles of subcellular distribution and interactions involving the MEF2 binding region, the ankyrin repeat binding motif and the catalytic site of HDAC4 in Drosophila neuronal morphogenesis. *BMC Biol*, *22*(1), 2. https://doi.org/10.1186/s12915-023-01800-1

Tan, Y., Yu, D., Busto, G. U., Wilson, C., & Davis, R. L. (2013). Wnt signaling is required for long-term memory formation. *Cell Rep*, *4*(6), 1082-1089. https://doi.org/10.1016/j.celrep.2013.08.007

Tang, A. H., Neufeld, T. P., Kwan, E., & Rubin, G. M. (1997). PHYL acts to down-regulate TTK88, a transcriptional repressor of neuronal cell fates, by a SINA-dependent mechanism. *Cell*, *90*(3), 459-467. https://doi.org/10.1016/s0092-8674(00)80506-1

Tasaki, I. (1939). The electro-saltatory transmission of the nerve impulse and the effect of narcosis upon the nerve fiber. *The American Journal of Physiology*, *127*(2), 211-227. https://doi.org/10.1152/ajplegacy.1939.127.2.211

Tasdemir-Yilmaz, O. E., & Freeman, M. R. (2014). Astrocytes engage unique molecular programs to engulf pruned neuronal debris from distinct subsets of neurons. *Genes Dev*, *28*(1), 20-33. https://doi.org/10.1101/gad.229518.113

Taylor, J. P., Hardy, J., & Fischbeck, K. H. (2002). Toxic proteins in neurodegenerative disease. *Science*, *296*, 1991-1995. https://doi.org/10.1126/science.1067122

Tea, J. S., Cespedes, A., Dawson, D., Banerjee, U., & Call, G. B. (2014). Dissection and mounting of Drosophila pupal eye discs. *J Vis Exp*(93), e52315. https://doi.org/10.3791/52315

Technau, G., & Heisenberg, M. (1982). Neural reorganization during metamorphosis of the corpora pedunculata in *Drosophila melanogaster*. *Nature*, *295*(5848), 405-407. https://doi.org/10.1038/295405a0

Teleman, A. A., Chen, Y. W., & Cohen, S. M. (2005). 4E-BP functions as a metabolic brake used under stress conditions but not during normal growth. *Genes Dev*, *19*(16), 1844-1848. https://doi.org/10.1101/gad.341505

Tesli, M., Koefoed, P., Athanasiu, L., Mattingsdal, M., Gustafsson, O., Agartz, I., Rimol, L. M., Brown, A., Wirgenes, K. V., Smorr, L. L., Kahler, A. K., Werge, T., Mors, O., Mellerup, E., Jonsson, E. G., Melle, I., Morken, G., Djurovic, S., & Andreassen, O. A. (2011). Association analysis of *ANK3* gene variants in nordic bipolar disorder and schizophrenia case-control samples. *American Journal of Medical Genetics. Part B Neuropsychiatric Genetics*, *156B*(8), 969-974. https://doi.org/10.1002/ajmg.b.31244

Tettweiler, G., Miron, M., Jenkins, M., Sonenberg, N., & Lasko, P. F. (2005). Starvation and oxidative stress resistance in *Drosophila* are mediated through the eIF4E-binding protein, d4E-BP. *Genes Dev*, *19*(16), 1840-1843. https://doi.org/10.1101/gad.1311805

Thiels, E., Urban, N. N., Gonzalez-Burgos, G. R., Kanterewicz, B. I., Barrionuevo, G., Chu, C. T., Oury, T. D., & Klann, E. (2000). Impairment of long-term potentiation and associative memory in mice that overexpress extracellular superoxide dismutase. *J Neurosci*, *20*(20), 7631-7639. https://doi.org/10.1523/jneurosci.20-20-07631.2000

Tomlinson, A. (1985). The cellular dynamics of pattern formation in the eye of Drosophila. *J Embryol Exp Morphol*, *89*, 313-331.

Tomlinson, A. (2012). The origin of the Drosophila subretinal pigment layer. *J Comp Neurol*, *520*(12), 2676-2682. https://doi.org/10.1002/cne.23063

Tomlinson, A., & Ready, D. F. (1987). Neuronal differentiation in the *Drosophila* ommatidium. *Developmental Biology*, *120*(2), 366-376. https://doi.org/10.1016/0012-1606(87)90239-9

Tonoki, A., Kuranaga, E., Tomioka, T., Hamazaki, J., Murata, S., Tanaka, K., & Miura, M. (2009). Genetic evidence linking age-dependent attenuation of the 26S proteasome with the aging process. *Mol Cell Biol*, *29*(4), 1095-1106. https://doi.org/10.1128/MCB.01227-08

Torres-Oliva, M., Schneider, J., Wiegleb, G., Kaufholz, F., & Posnien, N. (2018). Dynamic genome wide expression profiling of Drosophila head development reveals a novel role of Hunchback in retinal glia cell development and blood-brain barrier integrity. *PLoS Genet*, *14*(1), e1007180. https://doi.org/10.1371/journal.pgen.1007180

Traschütz, A., Schirinzi, T., Laugwitz, L., Murray, N. H., Bingman, C. A., Reich, S., Kern, J., Heinzmann, A., Vasco, G., Bertini, E., Zanni, G., Durr, A., Magri, S., Taroni, F., Malandrini, A., Baets, J., de Jonghe, P., de Ridder, W., Bereau, M., . . . Synofzik, M. (2020). Clinico-Genetic, Imaging and Molecular Delineation of COQ8A-Ataxia: A Multicenter Study of 59 Patients. *Ann Neurol*, *88*(2), 251-263. https://doi.org/10.1002/ana.25751

Trazzi, S., Fuchs, C., Viggiano, R., De Franceschi, M., Valli, E., Jedynak, P., Hansen, F. K., Perini, G., Rimondini, R., Kurz, T., Bartesaghi, R., & Ciani, E. (2016). HDAC4: a key factor underlying brain developmental alterations in CDKL5 disorder. *Hum Mol Genet*, *25*(18), 3887-3907. https://doi.org/10.1093/hmg/ddw231

Treiman, D. M. (2001). GABAergic mechanisms in epilepsy. *Epilepsia*, *42*(3), 8-12. https://doi.org/10.1046/j.1528-1157.2001.042suppl.3008.x

Trujillo-Cenóz, O. (1965). Some aspects of the structural organization of the intermediate retina of dipterans. *J Ultrastruct Res*, *13*(1), 1-33. https://doi.org/10.1016/s0022-5320(65)80086-7

Truman, J. W., & Copenhaver, P. F. (1989). The Larval Eclosion Hormone Neurones in Manduca Sexta:Identification of the Brain-Proctodeal Neurosecretory System. *Journal of Experimental Biology*, *147*(1), 457-470. https://doi.org/10.1242/jeb.147.1.457

Truman, J. W., & Riddiford, L. M. (1970). Neuroendocrine control of ecdysis in silkmoths. *Science*, *167*(3925), 1624-1626. https://doi.org/10.1126/science.167.3925.1624

Truman, J. W., Taghert, P. H., Copenhaver, P. F., Tublitz, N. J., & Schwartz, L. M. (1981). Eclosion hormone may control all ecdyses in insects. *Nature*, *291*(5810), 70-71. https://doi.org/10.1038/291070a0

Tsao, C. K., Huang, Y. F., & Sun, Y. H. (2020). Early lineage segregation of the retinal basal glia in the Drosophila eye disc. *Sci Rep*, *10*(1), 18522. https://doi.org/10.1038/s41598-020-75581-w

Tseng, T. S., Cheng, C. S., Chen, D. J., Shih, M. F., Liu, Y. N., Hsu, S. T., & Lyu, P. C. (2012). A molten globule-to-ordered structure transition of *Drosophila melanogaster* crammer is required for its ability to inhibit cathepsin. *Biochem J*, *442*(3), 563-572. https://doi.org/10.1042/BJ20111360

Turner, G. C., Bazhenov, M., & Laurent, G. (2008). Olfactory representations by *Drosophila* mushroom body neurons. *Journal of Neurophysiology*, *99*(2), 734-746. https://doi.org/10.1152/jn.01283.2007

Valente, E. M., Abou-Sleiman, P. M., Caputo, V., Muqit, M. M., Harvey, K., Gispert, S., Ali, Z., Del Turco, D., Bentivoglio, A. R., Healy, D. G., Albanese, A., Nussbaum, R., González-Maldonado, R., Deller, T., Salvi, S., Cortelli, P., Gilks, W. P., Latchman, D. S., Harvey, R. J., . . . Wood, N. W. (2004). Hereditary early-onset Parkinson's disease caused by mutations in PINK1. *Science*, *304*(5674), 1158-1160. https://doi.org/10.1126/science.1096284

van der Kloot, W., & Kita, H. (1974). Mechanisms for neurotransmitter release. *Oxford Journals*, *24*(1), 13-17. https://doi.org/10.1016/S0074-7742(08)60544-9

Vega, R. B., Matsuda, K., Oh, J., Barbosa, A. C., Yang, X., Meadows, E., McAnally, J., Pomajzl, C., Shelton, J. M., Richardson, J. A., Karsenty, G., & Olson, E. N. (2004). Histone deacetylase 4 controls chondrocyte hypertrophy during skeletogenesis. *Cell*, *119*(4), 555-566. https://doi.org/10.1016/j.cell.2004.10.024

Velarde, S. B., Quevedo, A., Estella, C., & Baonza, A. (2021). Dpp and Hedgehog promote the glial response to neuronal apoptosis in the developing Drosophila visual system. *PLoS Biol*, *19*(8), e3001367. https://doi.org/10.1371/journal.pbio.3001367

Velentzas, P. D., Velentzas, A. D., Mpakou, V. E., Antonelou, M. H., Margaritis, L. H., Papassideri, I. S., & Stravopodis, D. J. (2013). Detrimental effects of proteasome inhibition activity in Drosophila melanogaster: implication of ER stress, autophagy, and apoptosis. *Cell Biol Toxicol*, *29*(1), 13-37. https://doi.org/10.1007/s10565-012-9235-9

Venkatesh, S., & Singh, R. N. (1984). Sensilla on the third antennal segment of Drosophila melanogaster meigen (Diptera : Drosophilidae). *International Journal of Insect Morphology and Embryology*, *13*(1), 51-63. https://doi.org/10.1016/0020-7322(84)90032-1.

Venken, K. J., He, Y., Hoskins, R. A., & Bellen, H. J. (2006). P[acman]: a BAC transgenic platform for targeted insertion of large DNA fragments in D. melanogaster. *Science*, *314*(5806), 1747-1751. https://doi.org/10.1126/science.1134426

Verdone, L., Caserta, M., & Di Mauro, E. (2005). Role of histone acetylation in the control of gene expression. *Biochem Cell Biol*, *83*(3), 344-353. https://doi.org/10.1139/o05-041

Verreault, A. (2000). De novo nucleosome assembly: new pieces in an old puzzle. *Genes & Development*, *14*(12), 1430-1438. https://doi.org/10.1101/gad.14.12.1430

Wake, H., Moorhouse, A. J., Jinno, S., Kohsaka, S., & Nabekura, J. (2009). Resting microglia directly monitor the functional state of synapses in vivo and determine the fate of ischemic terminals. *J Neurosci*, *29*(13), 3974-3980. https://doi.org/10.1523/JNEUROSCI.4363-08.2009

Wakeling, E., McEntagart, M., Bruccoleri, M., Shaw-Smith, C., Stals, K. L., Wakeling, M., Barnicoat, A., Beesley, C., Study, D. D. D., Hanson-Kahn, A. K., Kukolich, M., Stevenson, D. A., Campeau, P. M., Ellard, S., Elsea, S. H., Yang, X. J., & Caswell, R. C. (2021). Missense substitutions at a conserved 14-3-3 binding site in HDAC4 cause a novel intellectual disability syndrome. *HGG Adv*, *2*(1). https://doi.org/10.1016/j.xhgg.2020.100015

Walterfang, M., Fietz, M., Fahey, M., Sullican, D., Leane, P., Lubman, D. I., & Velakoulis, D. (2006). The neuropsychiatry of Niemann-Pick Type C disease in adulthood. *J Neuropsychiatry Clin Neurosci*, *18*(2), 158-170. https://doi.org/10.1176/jnp.2006.18.2.158

Wang, A. H., Bertos, N. R., Vezmar, M., Pelletier, N., Crosato, M., Heng, H. H., Th'ng, J., Han, J., & Yang, X.-J. (1999). HDAC4, a human histone deacetylase related to yeast HDA1, is a transcriptional corepressor. *Molecular and Cellular Biology*, *19*(11), 7816-7827. https://doi.org/10.1128/mcb.19.11.7816

Wang, A. H., Gregoire, S., Zika, E., Xiao, L., Li, C. S., Li, H., Wright, K. L., Ting, J. P., & Yang, X. J. (2005). Identification of the ankyrin repeat proteins ANKRA and RFXANK as novel partners of class IIa histone deacetylases. *The Journal of Biological Chemistry*, *280*(32), 29117-29127. https://doi.org/10.1074/jbc.M500295200

Wang, A. H., & Yang, X. J. (2001). Histone deacetylase 4 possesses intrinsic nuclear import and export signals. *Molecular and Cellular Biology*, *21*(17), 5992-6005. https://doi.org/10.1128/mcb.21.17.5992-6005.2001

Wang, B., Moya, N., Niessen, S., Hoover, H., Mihaylova, M. M., Shaw, R. J., Yates, J. R., 3rd, Fischer, W. H., Thomas, J. B., & Montminy, M. (2011). A hormone-dependent module regulating energy balance. *Cell*, *145*(4), 596-606. https://doi.org/10.1016/j.cell.2011.04.013

Wang, D., Qian, L., Xiong, H., Liu, J., Neckameyer, W. S., Oldham, S., Xia, K., Wang, J., Bodmer, R., & Zhang, Z. (2006). Antioxidants protect PINK1-dependent dopaminergic neurons in Drosophila. *Proc Natl Acad Sci U S A*, *103*(36), 13520-13525. https://doi.org/10.1073/pnas.0604661103

Wang, H., & Zeng, X. (2000). Analysing protein–protein interactions using a GST-fusion protein to pull down the interacting target from the cell lysate. *Technical Tips Online*, *5*(1), 26-30. https://doi.org/10.1016/s1366-2120(08)70153-3

Wang, S. L., Hawkins, C. J., Yoo, S. J., Müller, H. A., & Hay, B. A. (1999). The Drosophila caspase inhibitor DIAP1 is essential for cell survival and is negatively regulated by HID. *Cell*, *98*(4), 453-463. https://doi.org/10.1016/s0092-8674(00)81974-1

Wang, Y., Branicky, R., Noe, A., & Hekimi, S. (2018). Superoxide dismutases: Dual roles in controlling ROS damage and regulating ROS signaling. *J Cell Biol*, *217*(6), 1915-1928. https://doi.org/10.1083/jcb.201708007

Wang, Z., Qin, G., & Zhao, T. C. (2014). Histone deacetylase 4 (HDAC4): mechanism of regulation and biological functions. *Epigenomics*, *6*(1), 139-150. https://doi.org/10.2217/epi.13.73

Warren, J., & Kumar, J. P. (2023). Patterning of the Drosophila retina by the morphogenetic furrow. *Front Cell Dev Biol*, *11*, 1151348. https://doi.org/10.3389/fcell.2023.1151348

Wasser, M., Bte Osman, Z., & Chia, W. (2007). EAST and Chromator control the destruction and remodeling of muscles during Drosophila metamorphosis. *Dev Biol*, *307*(2), 380-393. https://doi.org/10.1016/j.ydbio.2007.05.001

Weasner, B. P., & Kumar, J. P. (2022). The early history of the eye-antennal disc of Drosophila melanogaster. *Genetics*, *221*(1). https://doi.org/10.1093/genetics/iyac041

Weasner, B. P., Weasner, B. M., & Kumar, J. P. (2020). *Ghost in the Machine: The Peripodial Epithelium*. Springer, Charm. https://doi.org/10.1007/978-3-030-42246-2_4

Weaver, L. N., Ma, T., & Drummond-Barbosa, D. (2020). Analysis of Gal4 Expression Patterns in Adult Drosophila Females. *G3 Genes|Genomes|Genetics*, *10*(11), 4147-4158. https://doi.org/10.1534/g3.120.401676

Weinhard, L., di Bartolomei, G., Bolasco, G., Machado, P., Schieber, N. L., Neniskyte, U., Exiga, M., Vadisiute, A., Raggioli, A., Schertel, A., Schwab, Y., & Gross, C. T. (2018). Microglia remodel synapses by presynaptic trogocytosis and spine head filopodia induction. *Nat Commun*, *9*(1), 1228. https://doi.org/10.1038/s41467-018-03566-5

Williams, S. R., Aldred, M. A., Der Kaloustian, V. M., Halal, F., Gowans, G., McLeod, D. R., Zondag, S., Toriello, H. V., Magenis, R. E., & Elsea, S. H. (2010). Haploinsufficiency of HDAC4 causes brachydactyly mental retardation syndrome, with brachydactyly type E, developmental delays, and behavioral problems. *The American Journal of Human Genetics*, *87*(2), 219-228. https://doi.org/10.1016/j.ajhg.2010.07.011

Wilson, S. (2021). *Teasting apart the interaction between Ankyrin2 and HDAC4 in Drosophila neuronal function: a thesis presented in partial fulfilment of the requirements for the degree of Master of Science Biochemistry at Massey University, Manawatu, New Zealand.*

Wilson, S. J., Schwartz, S., Hale, T. K., & Fitzsimons, H. L. (2023). Ankyrin2 is essential for neuronal morphogenesis and long-term courtship memory in Drosophila. *Mol Brain*, *16*(1), 42. https://doi.org/10.1186/s13041-023-01026-w

Wolff, T., & Ready, D. F. (1991). Cell death in normal and rough eye mutants of Drosophila. *Development*, *113*(3), 825-839. https://doi.org/10.1242/dev.113.3.825

Wolff, T., & Ready, D. F. (1993). *Pattern formation in the Drosophila retina* (Vol. 2). Cold Spring Harbor Laboratory Press.

Wu, C., Chen, C., Dai, J., Zhang, F., Chen, Y., Li, W., Pastor-Pareja, J. C., & Xue, L. (2015). Toll pathway modulates TNF-induced JNK-dependent cell death in Drosophila. *Open Biol*, *5*(7), 140171. https://doi.org/10.1098/rsob.140171

Wu, J., Harrison, J. K., Dent, P., Lynch, K. R., Weber, M. J., & Sturgill, T. W. (1993). Identification adn charaterization of a new mammalian mitogen-activated protein kinase kinase, MKK2. *Molecular and Cellular Biology*, *13*(8), 4539-4548. https://doi.org/10.1128/mcb.13.8.4539-4548.1993

Wu, Q., Yang, X., Zhang, L., Zhang, Y., & Feng, L. (2017). Nuclear accumulation of histone deacetylase 4 (HDAC4) exerts neurotoxicity in models of Parkinson's disease. *Molecular Neurobiology*, *54*(9), 6970-6983. https://doi.org/10.1007/s12035-016-0199-2

Wu, Y. X., Sato, E., Kimura, W., & Miura, N. (2013). Baicalin and scutellarin are proteasome inhibitors that specifically target chymotrypsin-like catalytic activity. *Phytother Res*, *27*(9), 1362-1367. https://doi.org/10.1002/ptr.4878

Wulfkuhle, J. D., Petersen, N. S., & Otto, J. J. (1998). Changes in the F-actin cytoskeleton during neurosensory bristle development in *Drosophila*: the role of singed and forked proteins. *Cell Motil Cytoskeleton*, *40*(2), 119-132. https://doi.org/10.1002/(SICI)1097-0169(1998)40:2<119::AID-CM2>3.0.CO;2-A

Xiong, W. C., Okano, H., Patel, N. H., Blendy, J. A., & Montell, C. (1994). repo encodes a glial-specific homeo domain protein required in the Drosophila nervous system. *Genes Dev*, *8*(8), 981-994. https://doi.org/10.1101/gad.8.8.981

Xu, C., Jin, J., Bian, C., Lam, R., Tian, R., Weist, R., You, L., Nie, J., Bochkarev, A., Tempel, W., Tan, C. S., Wasney, G. A., Vedadi, M., Gish, G. D., Arrowsmith, C. H., Pawson, T., Yang, X.-J., & Min, J. (2012). Sequence-specific recognition of a PxLPxI/L motif by an ankyrin repeat tumbler lock. *Science Signaling*, *5*(226). https://doi.org/10.1126/scisignal.2002979

Xu, K., DiAngelo, J. R., Hughes, M. E., Hogenesch, J. B., & Sehgal, A. (2011). The circadian clock interacts with metabolic physiology to influence reproductive fitness. *Cell Metab*, *13*(6), 639-654. https://doi.org/10.1016/j.cmet.2011.05.001

Yamagata, N., Ichinose, T., Aso, Y., Placais, P. Y., Friedrich, A. B., Sima, R. J., Preat, T., Rubin, G. M., & Tanimoto, H. (2015). Distinct dopamine neurons mediate reward signals for short- and long-term memories. *Proc Natl Acad Sci U S A*, *112*(2), 578-583. https://doi.org/10.1073/pnas.1421930112

Yamamoto, K. K., Gonzalez, G. A., Biggs, W. H., & Montminy, M. R. (1988). Phosphorylation-induced binding and transcriptional efficacy of nuclear factor CREB. *Nature*, *334*, 494-498. https://doi.org/10.1038/334494a0

Yang, I., Han, S. J., Kaur, G., Crane, C., & Parsa, A. T. (2010). The role of microglia in central nervous system immunity and glioma immunology. *J Clin Neurosci*, *17*(1), 6-10. https://doi.org/10.1016/j.jocn.2009.05.006

Yang, M., Wang, H., Chen, C., Zhang, S., Wang, M., Senapati, B., Li, S., Yi, S., Wang, L., Zhang, M., Yin, S., He, Y., Xue, L., Lin, S., & Ho, M. S. (2021). Glia-derived temporal signals orchestrate neurogenesis in the Drosophila mushroom body. *Proc Natl Acad Sci U S A*, *118*(23). https://doi.org/10.1073/pnas.2020098118

Yang, Y., Hou, L., Li, Y., Ni, J., & Liu, L. (2013). Neuronal necrosis and spreading death in a Drosophila genetic model. *Cell Death Dis*, *4*(7), e723. https://doi.org/10.1038/cddis.2013.232

Yang, Y., Ouyang, Y., Yang, L., Beal, M. F., McQuibban, A., Vogel, H., & Lu, B. (2008). Pink1 regulates mitochondrial dynamics through interaction with the fission/fusion machinery. *Proc Natl Acad Sci U S A*, *105*(19), 7070-7075. https://doi.org/10.1073/pnas.0711845105

Yildirim, K., Petri, J., Kottmeier, R., & Klambt, C. (2019). Drosophila glia: Few cell types and many conserved functions. *Glia*, *67*(1), 5-26. https://doi.org/10.1002/glia.23459

Yin, J. C., & Tully, T. (1996). CREB and the formation of long-term memory. *Curr Opin Neurobiol*, *6*(2), 264-268. https://doi.org/10.1016/s0959-4388(96)80082-1

Yu, X. M., Gutman, I., Mosca, T. J., Iram, T., Ozkan, E., Garcia, K. C., Luo, L., & Schuldiner, O. (2013). Plum, an immunoglobulin superfamily protein, regulates axon pruning by facilitating TGF-beta signaling. *Neuron*, *78*(3), 456-468. https://doi.org/10.1016/j.neuron.2013.03.004

Zamurrad, S., Hatch, H. A. M., Drelon, C., Belalcazar, H. M., & Secombe, J. (2018). A *Drosophila* model of intellectual disability caused by mutations in the histone demethylase KDM5. *Cell Rep*, *22*(9), 2359-2369. https://doi.org/10.1016/j.celrep.2018.02.018

Zawistowski, S., & Richmond, R. C. (1986). Inhibition of courtship and mating of Drosophila melanogaster by the male-produced lipid, cis-vaccenyl acetate. *Journal of Insect Physiology*, *32*(3), 189-192. https://doi.org/10.1016/0022-1910(86)90057-0

Zhan, Y., Paolicelli, R. C., Sforazzini, F., Weinhard, L., Bolasco, G., Pagani, F., Vyssotski, A. L., Bifone, A., Gozzi, A., Ragozzino, D., & Gross, C. T. (2014). Deficient neuron-microglia signaling results in impaired functional brain connectivity and social behavior. *Nat Neurosci*, *17*(3), 400-406. https://doi.org/10.1038/nn.3641

Zhang, G., Wang, Z., Hu, H., Zhao, M., & Sun, L. (2021). Microglia in Alzheimer's Disease: A Target for Therapeutic Intervention. *Front Cell Neurosci*, *15*, 749587. https://doi.org/10.3389/fncel.2021.749587

Zhang, P., Sun, Q., Zhao, C., Ling, S., Li, Q., Chang, Y. Z., & Li, Y. (2014). HDAC4 protects cells from ER stress induced apoptosis through interaction with ATF4. *Cellular Signalling*, *26*(3), 556-563. https://doi.org/10.1016/j.cellsig.2013.11.026

Zhang, X., Wang, W. A., Jiang, L. X., Liu, H. Y., Zhang, B. Z., Lim, N., Li, Q. Y., & Huang, F. D. (2017). Downregulation of RBO-PI4KIIIalpha Facilitates Abeta(42) Secretion and Ameliorates Neural Deficits

in Abeta(42)-Expressing Drosophila. *J Neurosci*, *37*(19), 4928-4941. https://doi.org/10.1523/JNEUROSCI.3567-16.2017

Zhang, Y., & Reinberg, D. (2001). Transcription regulation by histone methylation: interplay between different covalent modifications of the core histone tails. *Genes & Development*, *15*(18), 2343-2360. https://doi.org/10.1101/gad.927301

Zhao, H., Kalivendi, S., Zhang, H., Joseph, J., Nithipatikom, K., Vasquez-Vivar, J., & Kalyanaraman, B. (2003). Superoxide reacts with hydroethidine but forms a fluorescent product that is distinctly different from ethidium: potential implications in intracellular fluorescence detection of superoxide. *Free Radic Biol Med*, *34*(11), 1359-1368. https://doi.org/10.1016/s0891-5849(03)00142-4

Zhao, H., Zheng, X., Yuan, X., Wang, L., Wang, X., Zhong, Y., Xie, Z., & Tully, T. (2009). *ben* Functions with *Scamp* during synaptic transmission and long-term memory formation in *Drosophila*. *The Journal of Neuroscience*, *29*(2), 414-424. https://doi.org/10.1523/JNEUROSCI.5036-07.2009

Zhao, R. Z., Jiang, S., Zhang, L., & Yu, Z. B. (2019). Mitochondrial electron transport chain, ROS generation and uncoupling (Review). *Int J Mol Med*, *44*(1), 3-15. https://doi.org/10.3892/ijmm.2019.4188

Zhao, X., Sternsdorf, T., Bolger, T. A., Evans, R. M., & Yao, T. P. (2005). Regulation of MEF2 by histone deacetylase 4- and SIRT1 deacetylase-mediated lysine modifications. *Molecular and Cellular Biology*, *25*(19), 8456-8464. https://doi.org/10.1128/MCB.25.19.8456-8464.2005

Zheng, J. C., Tham, C. T., Keatings, K., Fan, S., Liou, A. Y., Numata, Y., Allan, D., & Numata, M. (2014). Secretory carrier membrane protein (SCAMP) deficiency influences behavior of adult flies. *Frontiers in Cell and Developmental Biology*, *2*, 64. https://doi.org/10.3389/fcell.2014.00064

Zheng, X., Yang, Z., Yue, Z., Alvarez, J. D., & Sehgal, A. (2007). FOXO and insulin signalling regulate sensitivity of the circadian clock to axidative stress. *PNAS*, *104*(40), 15899-15904. https://doi.org/10.1073/pnas.0701599104

Zhou, B., Lin, W., Long, Y., Yang, Y., Zhang, H., Wu, K., & Chu, Q. (2022). Notch signaling pathway: architecture, disease, and therapeutics. *Signal Transduct Target Ther*, *7*(1), 95. https://doi.org/10.1038/s41392-022-00934-y

Zhu, Y., Kakinuma, N., Wang, Y., & Kiyama, R. (2008). Kank proteins: a new family of ankyrin-repeat domain-containing proteins. *Biochim Biophys Acta*, *1780*(2), 128-133. https://doi.org/10.1016/j.bbagen.2007.09.017

Zimmerman, M., Ashe, B., Yurewicz, E. C., & Patel, G. (1977). Sensitive assays for trypsin, elastase, and chymotrypsin using new fluorogenic substrates. *Anal Biochem*, *78*(1), 47-51. https://doi.org/10.1016/0003-2697(77)90006-9

Zimmerman, M., Yurewicz, E., & Patel, G. (1976). A new fluorogenic substrate for chymotrypsin. *Anal Biochem*, *70*(1), 258-262. https://doi.org/10.1016/s0003-2697(76)80066-8

Zirin, J., Hu, Y., Liu, L., Yang-Zhou, D., Colbeth, R., Yan, D., Ewen-Campen, B., Tao, R., Vogt, E., VanNest, S., Cavers, C., Villalta, C., Comjean, A., Sun, J., Wang, X., Jia, Y., Zhu, R., Peng, P., Yu, J., . . . Perrimon, N. (2020). Large-scale transgenic *Drosophila* resource collections for loss- and gain-of-function studies. *Genetics*, *214*(4), 755-767. https://doi.org/10.1534/genetics.119.302964

Zitnan, D., Kingan, T. G., Hermesman, J. L., & Adams, M. E. (1996). Identification of ecdysis-triggering hormone from an epitracheal endocrine system. *Science*, *271*(5245), 88-91. https://doi.org/10.1126/science.271.5245.88

Zovkic, I. B., Guzman-Karlsson, M. C., & Sweatt, J. D. (2013). Epigenetic regulation of memory formation and maintenance. *Learn Mem*, *20*(2), 61-74. https://doi.org/10.1101/lm.026575.112

8 Appendix

8.1 pUAST plasmid for transgenic fly transformation

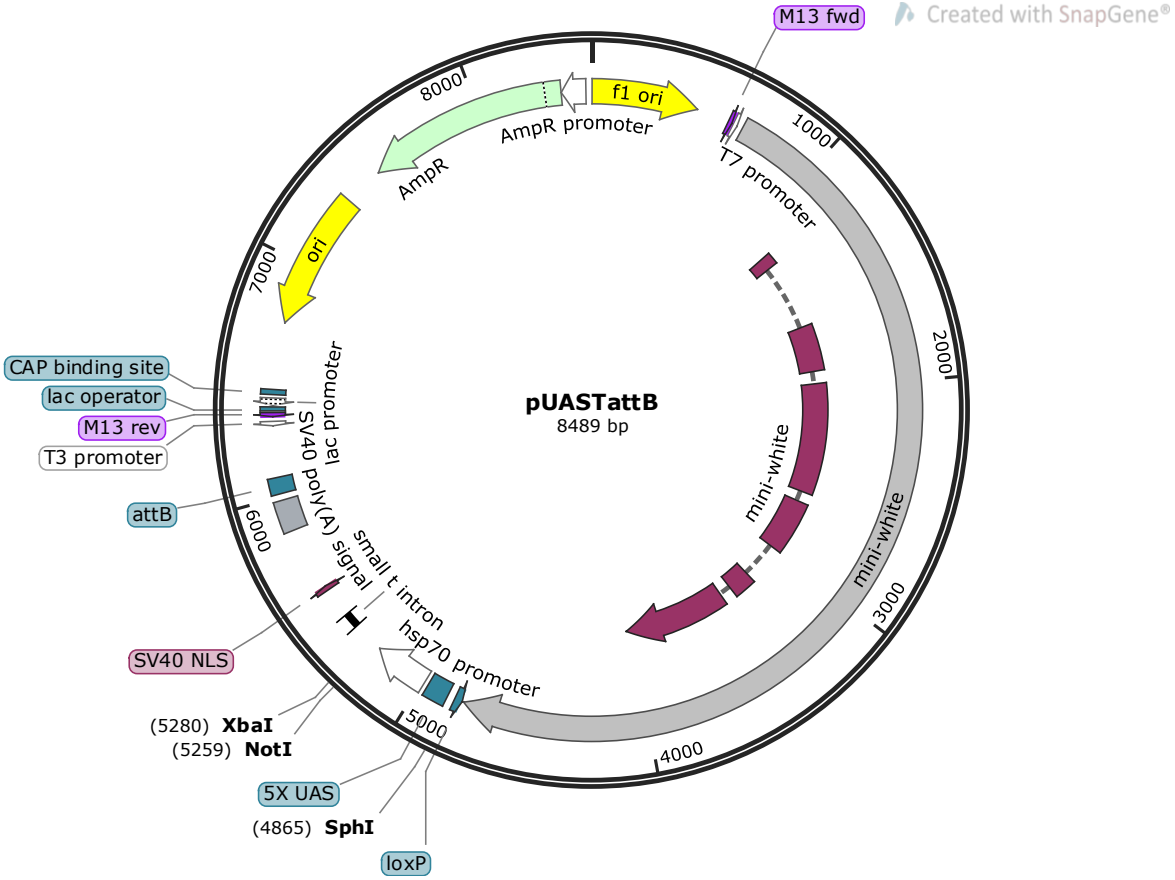

Figure 8.1. pUASTattB plasmid map. The pUASTattB plasmid was used for fly transformations. Features of the plasmid are highlighted, including the 5X UAS located upstream to promote expression of the transgene inserted into the XbaI and NotI restriction sites. The SphI restriction site is also highlighted which in combination with the NotI site removes the UAS allowing for the insertion of a different promoter sequence.

8.2 *CG5846-HA* sequence

```
5′
gcg gcc gcc aac atg gtg gca cca gca aac aca atc caa act aat gcg aat tcc gac gac
              M   V   A   P   A   N   T   I   Q   T   N   A   N   S   D   D
gat gag gga gtg cgg tcg gcg cct acc tcc atg ctg gtg ctg gac gcc aag cgg aag agc
 D   E   G   V   R   S   A   P   T   S   M   L   V   L   D   A   K   R   K   S
gcc ttc ttg ccg tac cgc ccc cag tcc acc gtg ctg acc aac ttg cag cgc ggc aat acg
 A   F   L   P   Y   R   P   Q   S   T   V   L   T   N   L   Q   R   G   N   T
gag gcc acc ttt tgc ccc gtc gaa gtt tcg ctc tcc ttt cac gaa cgc gct ggc caa ggc
 E   A   T   F   C   P   V   E   V   S   L   S   F   H   E   R   A   G   Q   G
gag atc acg gag gag cag gtg gca gcg gaa aga gcg cgt cag cag aac att gat tac aag
 E   I   T   E   E   Q   V   A   A   E   R   A   R   Q   Q   N   I   D   Y   K
gat gca cat ggt ttc aca gcc tta cat tgg gca gcc tcc tac ggt caa ctg gtt tcc gtg
 D   A   H   G   F   T   A   L   H   W   A   A   S   Y   G   Q   L   V   S   V
cag ctc ctc gtc gcg gct ggt gcc aat gtg aac act atg gct cca gat ttg att agt cct
 Q   L   L   V   A   A   G   A   N   V   N   T   M   A   P   D   L   I   S   P
cta ctc cta gct gcc gcc ggt ggg cat aac gag atc gtc cgc ttc ttg ctg gaa cac ggc
 L   L   L   A   A   A   G   G   H   N   E   I   V   R   F   L   L   E   H   G
gct gat tcg ggc cac atg gac atc gtt gga aac acg gcg ctt atg tac gca gcg gcc ggc
 A   D   S   G   H   M   D   I   V   G   N   T   A   L   M   Y   A   A   A   G
aat cat ccg cat act tgc aac gag ctc ctg gcc aaa gac ctg gat cta agt gcc acc aac
 N   H   P   H   T   C   N   E   L   L   A   K   D   L   D   L   S   A   T   N
gag gac gga gac acg gcc tac tcg ctg gcc gta gag cat ggg gct cat ctg gcg cag gcg
 E   D   G   D   T   A   Y   S   L   A   V   E   H   G   A   H   L   A   Q   A
cta ctg gag cag tac atg acg gcc ata atc aca gcg gga gcc ttc ggt agt att ggc gga
 L   L   E   Q   Y   M   T   A   I   I   T   A   G   A   F   G   S   I   G   G
ggc tac cca tac gat gtt cct gac tat gcg ggc tat ccc tat gac gtc ccg gac tat gca
 G   Y   P   Y   D   V   P   D   Y   A   G   Y   P   Y   D   V   P   D   Y   A
gga tcc tat cca tat gac gtt cca gat tac gct tag tct aga
 G   S   Y   P   Y   D   V   P   D   Y   A   -       3′
```

Figure 8.2. Annotated sequence of *CG5846-HA*. 5’ NotI (pink) and 3’ XbaI (purple) restriction sites flank the *CG5846* open reading frame (ORF) and allow for insertion into the NotI and XbaI restriction sites on the pUASTattB downstream of the 5X UAS. A Kozak consensus sequence (orange) was added just upstream of the *CG5846* start site (green) which directs the pre-initiation complex to promote translation. At the 3’ end of the *CG5846* ORF is a 3x glycine linker (blue) followed by a 3x HA tag (bold black) with the stop codon (red) just upstream of the 3’ XbaI restriction site.

8.3 *CG5846* promoter region

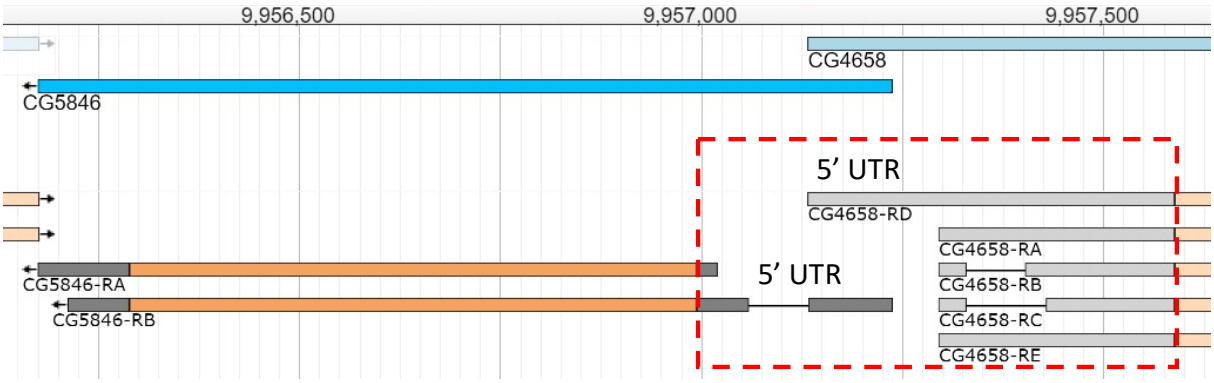

Figure 8.3. The *CG5846* promoter region. There are two isoforms of *CG5846* (RA and RB) which are in the antisense orientation. The *CG5846-RB* isoform contains a longer 5' UTR (dark grey) which overlaps with the 5' UTR (light grey) of the neighbouring gene *CG4658* which is in the sense orientation. The boxed region indicates the promoter region that was included in *CG5846-Myc* and *CG5846-GAL4*.

8.4 *CG5846-Myc* sequence

```
5'
gca tgc ttg gtg atg ttt cga cgc taa ttt ggg gca gtg gaa acg tac aac gaa agg gca

taa aaa agg cca aac gca ggt ttg cac tga aaa caa att ggc gag gcg caa cag gtg cag

gga agt ttt ggc caa aga aac aac tgc gcc gcg tcg caa aac ctg tta tga aac aca caa

aca cag tgc taa caa atc ggg taa ata tat tta cat aat taa acg caa att aag ctt tga

aac gag aaa ata aaa aca aac caa tcg aat gtg acc gtg ctg gag ttg caa att aat gct

gat tac aat gtg gct tta cca cac cac aga aaa atc tac agc aac tag aag ata ggt gta

cca gtt ata tga tgc cct gtt att ttc tag ttt tat gat tat gtt agc gtt tga cat aaa

taa att ttt att tgt tta aaa tac gag aca ttt taa cgg taa atc aat ttt aaa ttt tat

att gaa aga att tat att aag atg gca ttt tat aat ctt gta tat cat taa gtt cga gct

att ata ccc ttt ggg gct tcc aat aca ggg tat taa tgg taa ata taa cca aaa caa atg
                                                                        M
gtg gca cca gca aac aca atc caa act aat gcg aat tcc gac gac gat gag gga gtg cgg
 V   A   P   A   N   T   I   Q   T   N   A   N   S   D   D   D   E   G   V   R
tcg gcg cct acc tcc atg ctg gtg ctg gac gcc aag cgg aag agc gcc ttc ttg ccg tac
 S   A   P   T   S   M   L   V   L   D   A   K   R   K   S   A   F   L   P   Y
cgc ccc cag tcc acc gtg ctg acc aac ttg cag cgc ggc aat acg gag gcc acc ttt tgc
 R   P   Q   S   T   V   L   T   N   L   Q   R   G   N   T   E   A   T   F   C
ccc gtc gaa gtt tcg ctc tcc ttt cac gaa cgc gct ggc caa ggc gag atc acg gag gag
 P   V   E   V   S   L   S   F   H   E   R   A   G   Q   G   E   I   T   E   E
cag gtg gca gcg gaa aga gcg cgt cag cag aac att gat tac aag gat gca cat ggt ttc
 Q   V   A   A   E   R   A   R   Q   Q   N   I   D   Y   K   D   A   H   G   F
```

```
aca gcc tta cat tgg gca gcc tcc tac ggt caa ctg gtt tcc gtg cag ctc ctc gtc gcg
 T   A   L   H   W   A   A   S   Y   G   Q   L   V   S   V   Q   L   L   V   A
gct ggt gcc aat gtg aac act atg gct cca gat ttg att agt cct cta ctc cta gct gcc
 A   G   A   N   V   N   T   M   A   P   D   L   I   S   P   L   L   L   A   A
gcc ggt ggg cat aac gag atc gtc cgc ttc ttg ctg gaa cac ggc gct gat tcg ggc cac
 A   G   G   H   N   E   I   V   R   F   L   L   E   H   G   A   D   S   G   H
atg gac atc gtt gga aac acg gcg ctt atg tac gca gcg gcc ggc aat cat ccg cat act
 M   D   I   V   G   N   T   A   L   M   Y   A   A   A   G   N   H   P   H   T
tgc aac gag ctc ctg gcc aaa gac ctg gat cta agt gcc acc aac gag gac gga gac acg
 C   N   E   L   L   A   K   D   L   D   L   S   A   T   N   E   D   G   D   T
gcc tac tcg ctg gcc gta gag cat ggg gct cat ctg gcg cag gcg cta ctg gag cag tac
 A   Y   S   L   A   V   E   H   G   A   H   L   A   Q   A   L   L   E   Q   Y
atg acg gcc ata atc aca gcg gga gcc ttc ggt agt att ggc gga ggc gag caa aag ctc
 M   T   A   I   I   T   A   G   A   F   G   S   I   G   G   G   E   Q   K   L
att tct gaa gag gac ttg aat gaa atg gag caa aag ctc att tct gaa gag gac ttg aat
 I   S   E   E   D   L   N   E   M   E   Q   K   L   I   S   E   E   D   L   N
gaa atg gag caa aag ctc att tct gaa gag gac ttg aat gaa atg gag caa aag ctc att
 E   M   E   Q   K   L   I   S   E   E   D   L   N   E   M   E   Q   K   L   I
tct gaa gag gac ttg aat gaa atg gag caa aag ctc att tct gaa gag gac ttg aat gaa
 S   E   E   D   L   N   E   M   E   Q   K   L   I   S   E   E   D   L   N   E
atg gag agc ttg ggc gac ctc acc atg gag caa aag ctc att tct gaa gag gac ttg tag
 M   E   S   L   G   D   L   T   M   E   Q   K   L   I   S   E   E   D   L   -
gcg gcc gc
 A   A   3'
```

Figure 8.4. Annotated sequence of *CG5846-Myc*. 5' SphI (teal) and 3' NotI (pink) restriction sites flank the promoter and coding region of the *CG5846* gene. The promoter includes the 5' region of the *CG4658* gene, which is in the sense orientation, up until the *CG4658* start codon (orange) and the *CG5846* 5' UTR (purple) of the *CG5846*-RB transcript (transcription start site in bold dark blue), see boxed region in Figure 8.3. The *CG5846*-RA transcript's 5' UTR is located within this promoter region (bold dark green). The start site of the *CG5846* ORF is indicated (green). A 3x glycine linker (blue) is inserted at the end of the ORF (minus the stop codon), followed by a 6x Myc tag (bold black) and a stop codon (red) just upstream of the 3' NotI restriction site.

8.5 *CG5846-GAL4* sequence

```
5′
gca tgc ttg gtg atg ttt cga cgc taa ttt ggg gca gtg gaa acg tac aac gaa agg gca

taa aaa agg cca aac gca ggt ttg cac tga aaa caa att ggc gag gcg caa cag gtg cag

gga agt ttt ggc caa aga aac aac tgc gcc gcg tcg caa aac ctg tta tga aac aca caa

aca cag tgc taa caa atc ggg taa ata tat tta cat aat taa acg caa att aag ctt tga

aac gag aaa ata aaa aca aac caa tcg aat gtg acc gtg ctg gag ttg caa att aat gct

gat tac aat gtg gct tta cca cac cac aga aaa atc tac agc aac tag aag ata ggt gta

cca gtt ata tga tgc cct gtt att ttc tag ttt tat gat tat gtt agc gtt tga cat aaa

taa att ttt att tgt tta aaa tac gag aca ttt taa cgg taa atc aat ttt aaa ttt tat

att gaa aga att tat att aag atg gca ttt tat aat ctt gta tat cat taa gtt cga gct

att ata ccc ttt ggg gct tcc aat aca ggg tat taa tgg taa ata taa cca aaa caa atg
                                                                          M
aag cta ctg tct tct atc gaa caa gcc tgc gat att tgc cga ctt aaa aag ctc aag tgc
 K   L   L   S   S   I   E   Q   A   C   D   I   C   R   L   K   K   L   K   C
tcc aaa gaa aaa ccg aag tgc gcc aag tgt ctg aag aac aac tgg gag tgt cgc tac tct
 S   K   E   K   P   K   C   A   K   C   L   K   N   N   W   E   C   R   Y   S
ccc aaa acc aaa agg tct ccg ctg act agg gca cat ctg aca gaa gtg gaa tca agg cta
 P   K   T   K   R   S   P   L   T   R   A   H   L   T   E   V   E   S   R   L
gaa aga ctg gaa cag cta ttt cta ctg att ttt cct cga gaa gac ctt gac atg att ttg
 E   R   L   E   Q   L   F   L   L   I   F   P   R   E   D   L   D   M   I   L
aaa atg gat tct tta cag gat ata aaa gca ttg tta aca gga tta ttt gta caa gat aat
 K   M   D   S   L   Q   D   I   K   A   L   L   T   G   L   F   V   Q   D   N
gtg aat aaa gat gcc gtc aca gat aga ttg gct tca gtg gag act gat atg cct cta aca
 V   N   K   D   A   V   T   D   R   L   A   S   V   E   T   D   M   P   L   T
ttg aga cag cat aga ata agt gcg aca tca tca tcg gaa gag agt agt aac aaa ggt caa
 L   R   Q   H   R   I   S   A   T   S   S   S   E   E   S   S   N   K   G   Q
aga cag ttg act gta tcg att gac tcg gca gct cat cat gat aac tcc aca att ccg ttg
 R   Q   L   T   V   S   I   D   S   A   A   H   H   D   N   S   T   I   P   L
gat ttt atg ccc agg gat gct ctt cat gga ttt gat tgg tct gaa gag gat gac atg tcg
 D   F   M   P   R   D   A   L   H   G   F   D   W   S   E   E   D   D   M   S
gat ggc ttg ccc ttc ctg aaa acg gac ccc aac aat aat ggg ttc ttt ggc gac ggt tct
 D   G   L   P   F   L   K   T   D   P   N   N   N   G   F   F   G   D   G   S
ctc tta tgt att ctt cga tct att ggc ttt aaa ccg gaa aat tac acg aac tct aac gtt
 L   L   C   I   L   R   S   I   G   F   K   P   E   N   Y   T   N   S   N   V
aac agg ctc ccg acc atg att acg gat aga tac acg ttg gct tct aga tcc aca aca tcc
 N   R   L   P   T   M   I   T   D   R   Y   T   L   A   S   R   S   T   T   S
cgt tta ctt caa agt tat ctc aat aat ttt cac ccc tac tgc cct atc gtg cac tca ccg
 R   L   L   Q   S   Y   L   N   N   F   H   P   Y   C   P   I   V   H   S   P
acg cta atg atg ttg tat aat aac cag att gaa atc gcg tcg aag gat caa tgg caa atc
 T   L   M   M   L   Y   N   N   Q   I   E   I   A   S   K   D   Q   W   Q   I
ctt ttt aac tgc ata tta gcc att gga gcc tgg tgt ata gag ggg gaa tct act gat ata
 L   F   N   C   I   L   A   I   G   A   W   C   I   E   G   E   S   T   D   I
gat gtt ttt tac tat caa aat gct aaa tct cat ttg acg agc aag gtc ttc gag tca ggt
 D   V   F   Y   Y   Q   N   A   K   S   H   L   T   S   K   V   F   E   S   G
 tcc ata att ttg gtg aca gcc cta cat ctt ctg tcg cga tat aca cag tgg agg cag aaa
 S   I   I   L   V   T   A   L   H   L   L   S   R   Y   T   Q   W   R   Q   K
aca aat act agc tat aat ttt cac agc ttt tcc ata aga atg gcc ata tca ttg ggc ttg
 T   N   T   S   Y   N   F   H   S   F   S   I   R   M   A   I   S   L   G   L
aat agg gac ctc ccc tcg tcc ttc agt gat agc agc att ctg gaa caa aga cgc cga att
 N   R   D   L   P   S   S   F   S   D   S   S   I   L   E   Q   R   R   R   I
```

```
tgg tgg tct gtc tac tct tgg gag atc caa ttg tcc ctg ctt tat ggt cga tcc atc cag
 W   W   S   V   Y   S   W   E   I   Q   L   S   L   L   Y   G   R   S   I   Q
ctt tct cag aat aca atc tcc ttc cct tct tct gtc gac gat gtg cag cgt acc aca aca
 L   S   Q   N   T   I   S   F   P   S   S   V   D   D   V   Q   R   T   T   T
ggt ccc acc ata tat cat ggc atc att gaa aca gca agg ctc tta caa gtt ttc aca aaa
 G   P   T   I   Y   H   G   I   I   E   T   A   R   L   L   Q   V   F   T   K
atc tat gaa cta gac aaa aca gta act gca gaa aaa agt cct ata tgt gca aaa aaa tgc
 I   Y   E   L   D   K   T   V   T   A   E   K   S   P   I   C   A   K   K   C
ttg atg att tgt aat gag att gag gag gtt tcg aga cag gca cca aag ttt tta caa atg
 L   M   I   C   N   E   I   E   E   V   S   R   Q   A   P   K   F   L   Q   M
gat att tcc acc acc gct cta acc aat ttg ttg aag gaa cac cct tgg cta tcc ttt aca
 D   I   S   T   T   A   L   T   N   L   L   K   E   H   P   W   L   S   F   T
aga ttc gaa ctg aag tgg aaa cag ttg tct ctt atc att tat gta tta aga gat ttt ttc
 R   F   E   L   K   W   K   Q   L   S   L   I   I   Y   V   L   R   D   F   F
act aat ttt acc cag aaa aag tca caa cta gaa cag gat caa aat gat cat caa agt tat
 T   N   F   T   Q   K   K   S   Q   L   E   Q   D   Q   N   D   H   Q   S   Y
gaa gtt aaa cga tgc tcc atc atg tta agc gat gca gca caa aga act gtt atg tct gta
 E   V   K   R   C   S   I   M   L   S   D   A   A   Q   R   T   V   M   S   V
agt agc tat atg gac aat cat aat gtc acc cca tat ttt gcc tgg aat tgt tct tat tac
 S   S   Y   M   D   N   H   N   V   T   P   Y   F   A   W   N   C   S   Y   Y
ttg ttc aat gca gtc cta gta ccc ata aag act cta ctc tca aac tca aaa tcg aat gct
 L   F   N   A   V   L   V   P   I   K   T   L   L   S   N   S   K   S   N   A
gag aat aac gag acc gca caa tta tta caa caa att aac act gtt ctg atg cta tta aaa
 E   N   N   E   T   A   Q   L   L   Q   Q   I   N   T   V   L   M   L   L   K
aaa ctg gcc act ttt aaa atc cag act tgt gaa aaa tac att caa gta ctg gaa gag gta
 K   L   A   T   F   K   I   Q   T   C   E   K   Y   I   Q   V   L   E   E   V
tgt gcg ccg ttt ctg tta tca cag tgt gca atc cca tta ccg cat atc agt tat aac aat
 C   A   P   F   L   L   S   Q   C   A   I   P   L   P   H   I   S   Y   N   N
agt aat ggt agc gcc att aaa aat att gtc ggt tct gca act atc gcc caa tac cct act
 S   N   G   S   A   I   K   N   I   V   G   S   A   T   I   A   Q   Y   P   T
ctt ccg gag gaa aat gtc aac aat atc agt gtt aaa tat gtt tct cct ggc tca gta ggg
 L   P   E   E   N   V   N   N   I   S   V   K   Y   V   S   P   G   S   V   G
cct tca cct gtg cca ttg aaa tca gga gca agt ttc agt gat cta gtc aag ctg tta tct
 P   S   P   V   P   L   K   S   G   A   S   F   S   D   L   V   K   L   L   S
aac cgt cca ccc tct cgt aac tct cca gtg aca ata cca aga agc aca cct tcg cat cgc
 N   R   P   P   S   R   N   S   P   V   T   I   P   R   S   T   P   S   H   R
tca gtc acg cct ttt cta ggg caa cag caa cag ctg caa tca tta gtg cca ctg acc ccg
 S   V   T   P   F   L   G   Q   Q   Q   Q   L   Q   S   L   V   P   L   T   P
tct gct ttg ttt ggt ggc gcc aat ttt aat caa agt ggg aat att gct gat agc tca ttg
 S   A   L   F   G   G   A   N   F   N   Q   S   G   N   I   A   D   S   S   L
tcc ttc act ttc act aac agt agc aac ggt ccg aac ctc ata aca act caa aca aat tct
 S   F   T   F   T   N   S   S   N   G   P   N   L   I   T   T   Q   T   N   S
caa gcg ctt tca caa cca att gcc tcc tct aac gtt cat gat aac ttc atg aat aat gaa
 Q   A   L   S   Q   P   I   A   S   S   N   V   H   D   N   F   M   N   N   E
atc acg gct agt aaa att gat gat ggt aat aat tca aaa cca ctg tca cct ggt tgg acg
 I   T   A   S   K   I   D   D   G   N   N   S   K   P   L   S   P   G   W   T
gac caa act gcg tat aac gcg ttt gga atc act aca ggg atg ttt aat acc act aca atg
 D   Q   T   A   Y   N   A   F   G   I   T   T   G   M   F   N   T   T   T   M
gat gat gta tat aac tat cta ttc gat gat gaa gat acc cca cca aac cca aaa aaa gag
 D   D   V   Y   N   Y   L   F   D   D   E   D   T   P   P   N   P   K   K   E
taa gcg gcc gc
 -   A   A   3'
```

Figure 8.5. Annotated sequence of *CG5846-GAL4*. 5' SphI (teal) and 3' NotI (pink) restriction sites flank the promoter region of the *CG5846* gene and GAL4 coding region. The promoter includes the 5' region of the *CG4658* gene, which is in the sense orientation, up until the *CG4658* start codon (orange) and the *CG5846* 5' UTR (purple) of the *CG5846*-RB transcript (transcription start site in bold dark blue), see boxed region in Figure 8.3. The *CG5846*-RA transcript's 5' UTR is located within this promoter region (bold dark green). The initiation codon (green) of the *GAL4* ORF which has an a to c substitution to remove an SphI site from the *GAL4* coding region, and changes the codon from gca to gcc, however does not change the amino acid sequence (blue). The *GAL4* stop codon is indicated (red), followed by the 3' NotI site.

8.6 Crossing schemes

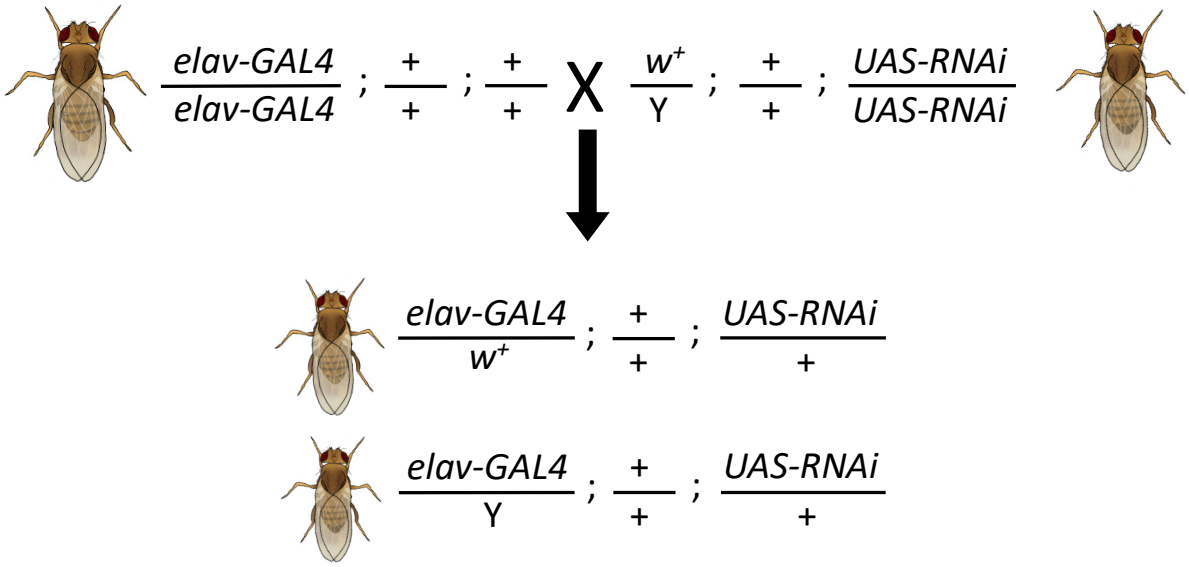

Figure 8.6. Simple genetic cross for the candidate mushroom body screen. *elav-GAL4* is located on the X chromosome. Homozygous virgin females were crossed to a homozygous *UAS-RNAi* line, in this example the RNAi is located on the third chromosome. F1 progeny are heterozygous for e*lav-GAL4* and *UAS-RNAi,* resulting in pan-neuronal expression of the RNAi. Both male and female progeny were dissected and quantified for mushroom body defects. w^+ = mini *white.*

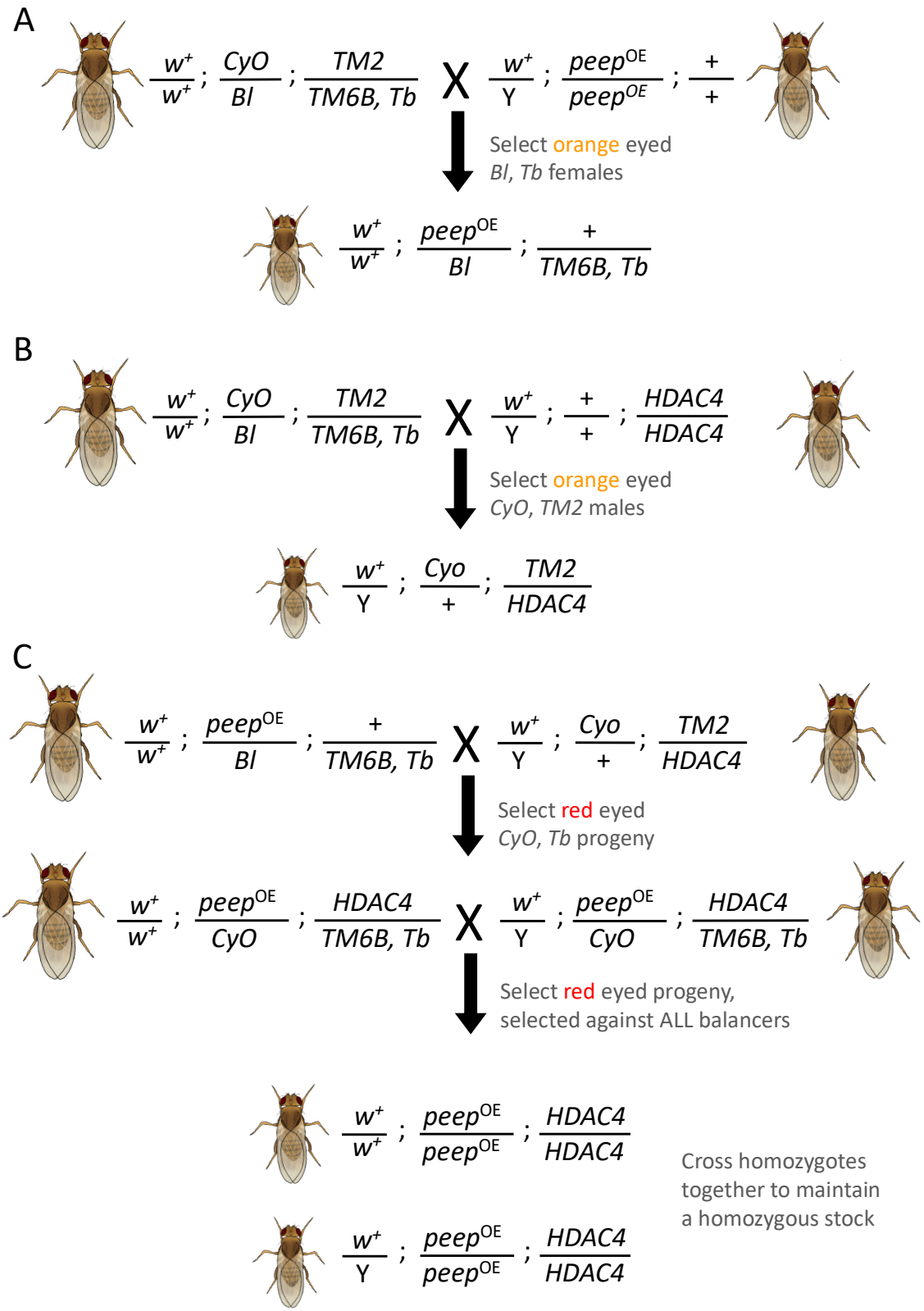

Figure 8.7. Crossing scheme to generate variant *HDAC4; Peep*^{OE} homozygotes. A. White eyed virgin females carrying *CyO/Bl* on second chromosome (with phenotypic markers of curly wings and short bristles) and *TM2/TM6B, Tb* on third chromosome (with phenotypic markers of ultrabithorax and tubby pupae), were crossed to male flies homozygous for *UAS-Peep*^{OE}, (indicated here as *Peep*^{OE}), on the second chromosome. Orange-eyed tubby virgin females with short bristles were collected. B. The same virgin females described in A were crossed to male flies homozygous for *UAS-HDAC4*^{WT},

(indicated as *HDAC4*) on the third chromosome. Orange-eyed males with curly wings and ultrabithorax were collected. C. Virgin females from the cross in A were crossed to males from cross in B, and red eyed tubby males and females with curly wings carrying one copy of *UAS-Peep*^{OE} on the second chromosome and one copy of *UAS-HDAC4*^{WT} on the third chromosome were selected for, and short bristles and ultrabithorax were selected against. Males and females were self-crossed and red eyed homozygous progeny were selected and crossed together to maintain a homozygous stock harbouring two copies of *UAS-Peep*^{OE} on the second chromosome and two copies of *UAS-HDAC4*^{WT} on the third chromosome. The same crossing scheme was performed to generate *UAS-HDAC4*$^{\Delta Ank}$; *UAS-Peep*^{OE}. w^+ = mini-*white, CyO = Curly of Oster*, *TM2 = Third Multiple 2, Bl = Bristle*, *TM6B = Third Multiple 6B, Tb = Tubby*.

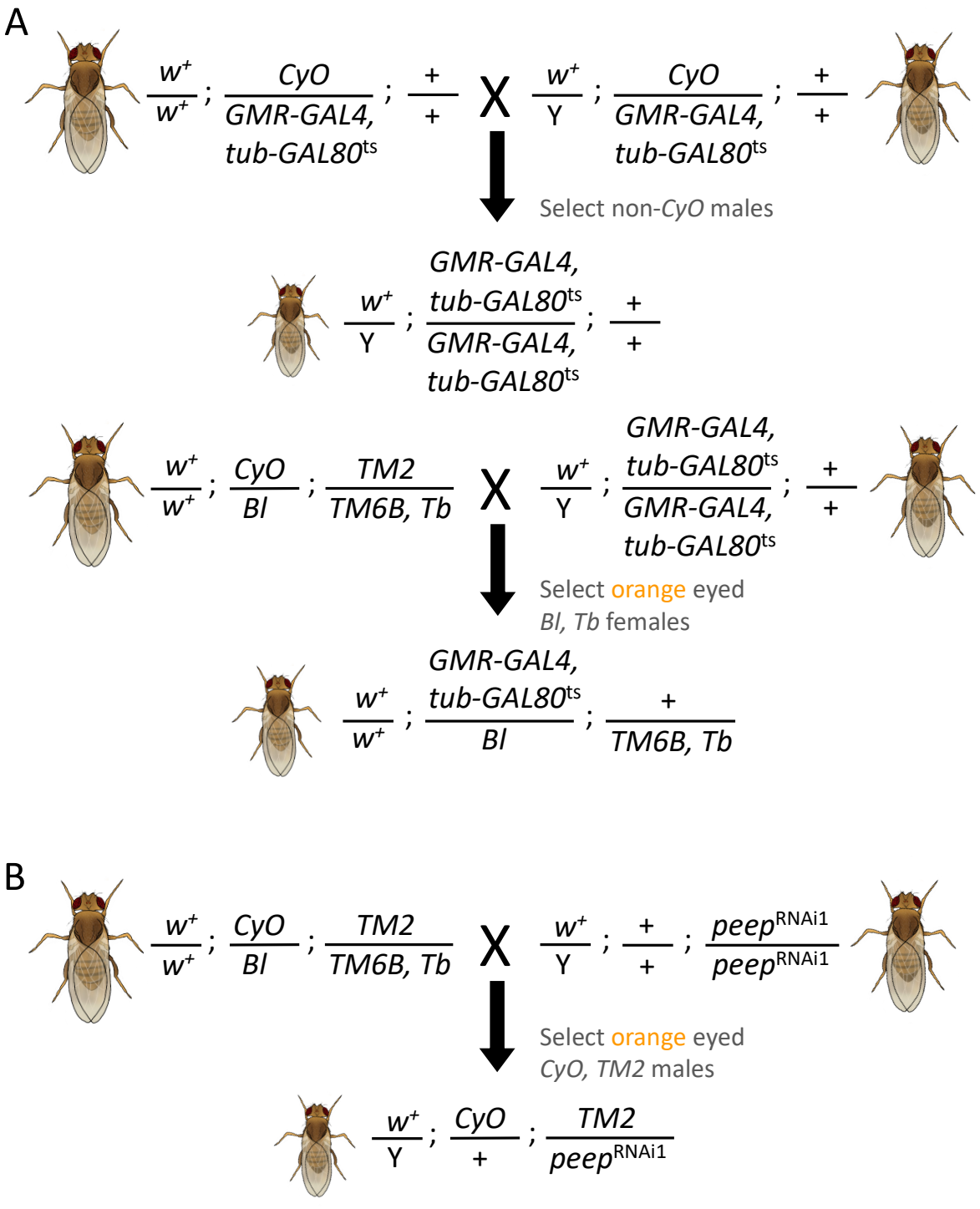

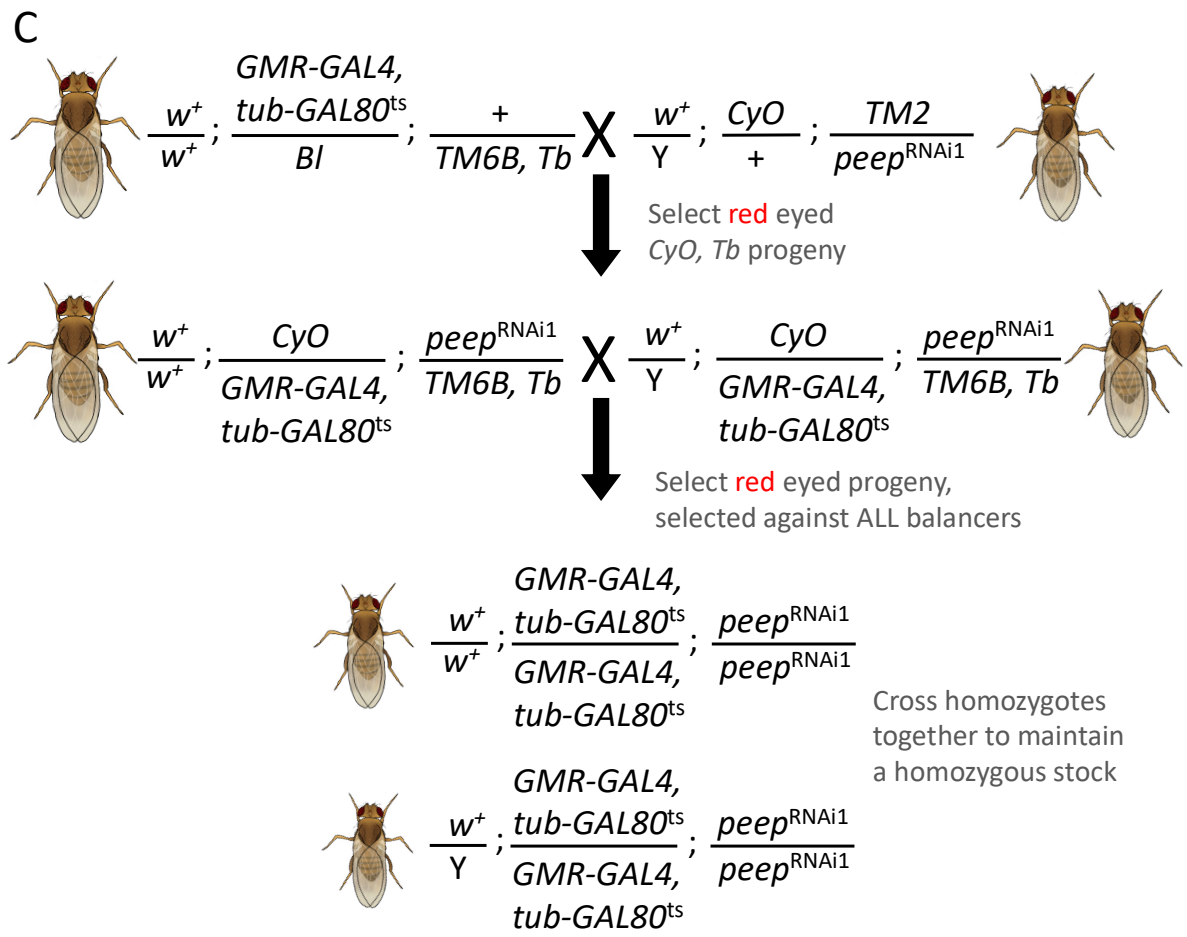

Figure 8.8. Crossing scheme to generate *GMR-GAL4,tub-GAL80^{ts};UAS-peep^{RNAi1}* homozygotes to cross to 'survival factors'. A. *GMR-GAL4,tub-GAL80^{ts}* heterozygotes balanced over the second chromosome balancer *CyO*, were crossed, and non-curly male *GMR-GAL4,tub-GAL80^{ts}* progeny were crossed to virgin *CyO/Bl;TM2/TM6B, Tb* females and orange eyed tubby females with short bristles were collected. B. *CyO/Bl;TM2/TM6B, Tb* virgin females were crossed to third chromosome *UAS-peep^{RNAi1}* (indicated here as *peep^{RNAi1}*) homozygotes and orange eyed males with curly wings and ultrabithorax were collected. C. Virgin females collected from A were crossed to males collected from B and red eyed tubby males and females with curly wings were collected, each carrying one copy each of *GMR-GAL4* and *tub-GAL80^{ts}* on the second chromosome and one copy of *UAS-peep^{RNAi1}* on the third chromosome. Males and females were crossed and red eyed homozygous progeny were selected and crossed together to maintain a homozygous stock harbouring two copies each of *GMR-GAL4* and *tub-GAL80^{ts}* on the second chromosome and two copies of *UAS-peep^{RNAi}* on the third chromosome. *w^+* = mini-*white, CyO = Curly of Oster*, *TM2 = Third Multiple 2, Bl = Bristle*, *TM6B = Third Multiple 6B, Tb = Tubby*.

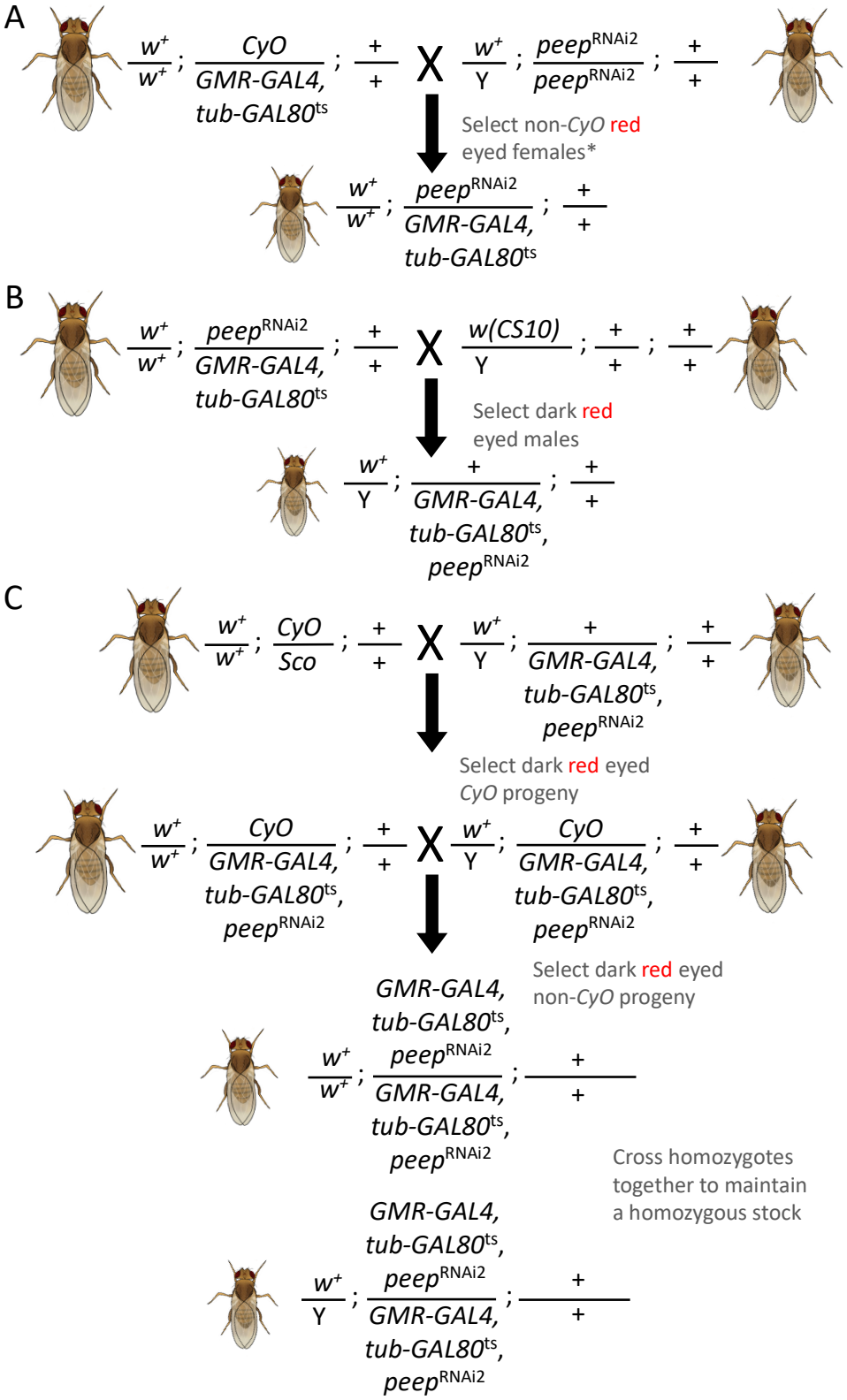

Figure 8.9. Crossing scheme to generate *GMR-GAL4,tub-GAL80*ts,*UAS-peep*^{RNAi2} homozygotes to cross to 'survival factors'. A. Virgin female *GMR-GAL4,tub-GAL80*^{ts} heterozygotes over the second chromosome *CyO* balancer were crossed to second chromosome homozygous *UAS-peep*^{RNAi2}(indicated here as *peep*^{RNAi2}) males. Red eyed non-curly virgin females were collected, and B. crossed to white eyed *w(CS10)* males. Flies in which a recombination event occurred to generate a chromosome carrying *GMR-GAL4,tub-GAL80*^{ts} and *UAS-peep*^{RNAi2} displayed darker red eyes due to the presence of three

copies of w^+. The darkest red eyed males were collected and crossed to virgin *w(CS10);CyO* females which phenotypically have curly wings and a loss of thoracic bristles (*Sco*). Dark red eyed progeny carrying one copy of each *GMR-GAL4*, *tub-GAL80*^{ts} and *UAS-peep*^{RNAi2} on the second chromosome over the *CyO* balancer were collected and males and virgin females were crossed and dark red eyed non-curly progeny were collected and crossed together to maintain a homozygous stock harbouring two copies each of *GMR-GAL4*, *tub-GAL80*^{ts} and *UAS-peep*^{RNAi2} on the second chromosome. w^+ =mini-*white, CyO = Curly of Oster, Sco = Scutoid.*

8.7 Supplementary data

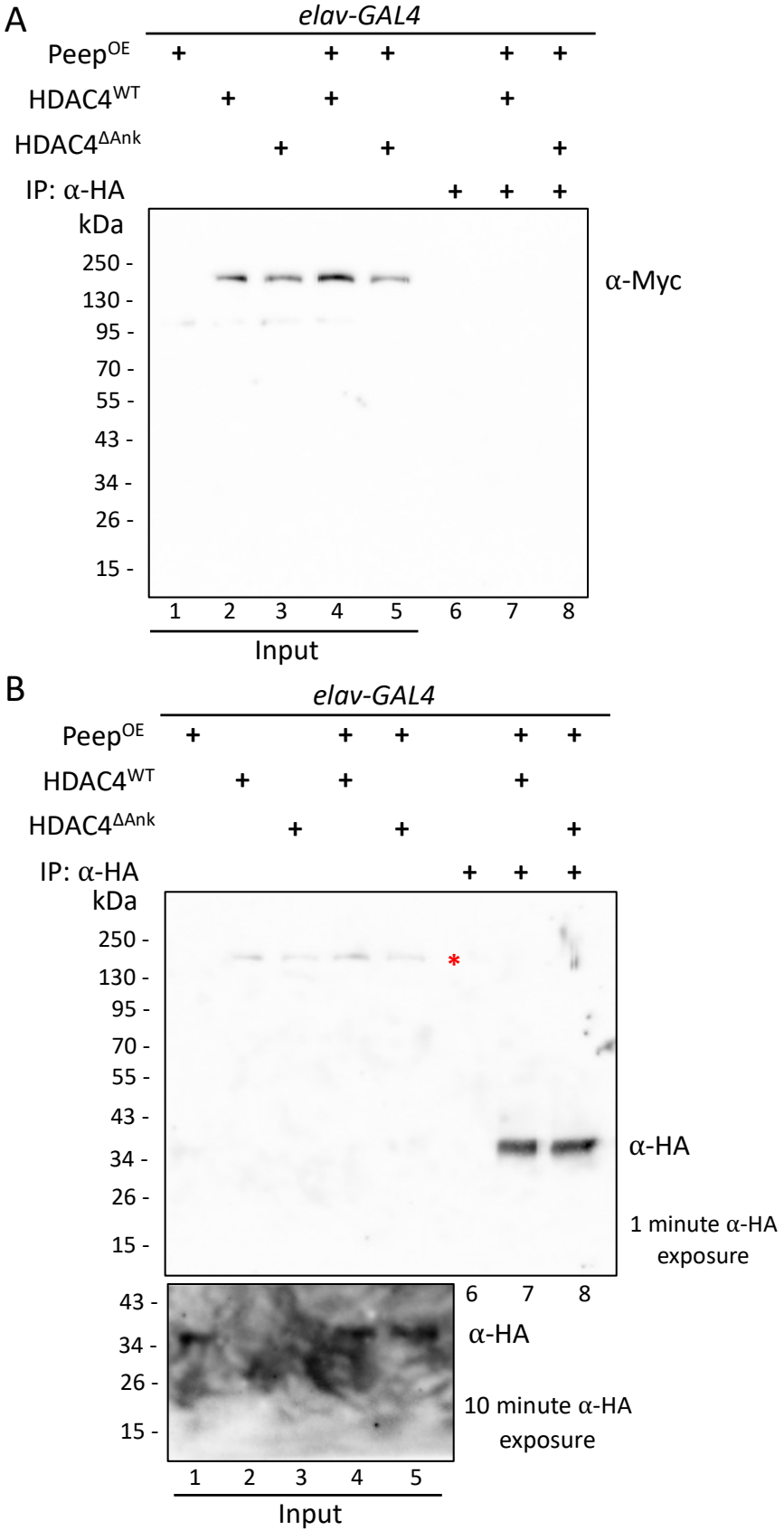

Figure 8.10. Full western blot of the reverse co-immunoprecipitation further demonstrating that Peep and HDAC4 do not interact. Lysates were processed from pan-neuronal (*elav-GAL4*) co-

expression of Peep^{OE} and HDAC4^{WT} and immunoprecipitation was performed using anti-HA to capture HA-tagged Peep^{OE}. A. Co-expression of Peep^{OE} and HDAC4^{WT} or HDAC4$^{\Delta Ank}$ did not show an interaction (lane 7 or 8, respectively). Immunoprecipitation samples were loaded alongside a control (lane 6) and 30 µg input samples (lanes 1-5). B. Successful immunoprecipitation was observed when probing with anti-HA (lanes 7 and 8). Immunoprecipitation samples were loaded alongside a control (lane 6). The immunoprecipitation detection with anti-HA was too bright to see the 30 µg input samples (lanes 1-5), therefore these immunoprecipitation lanes were removed, and a longer exposure was taken to detect the input bands (bottom panel).

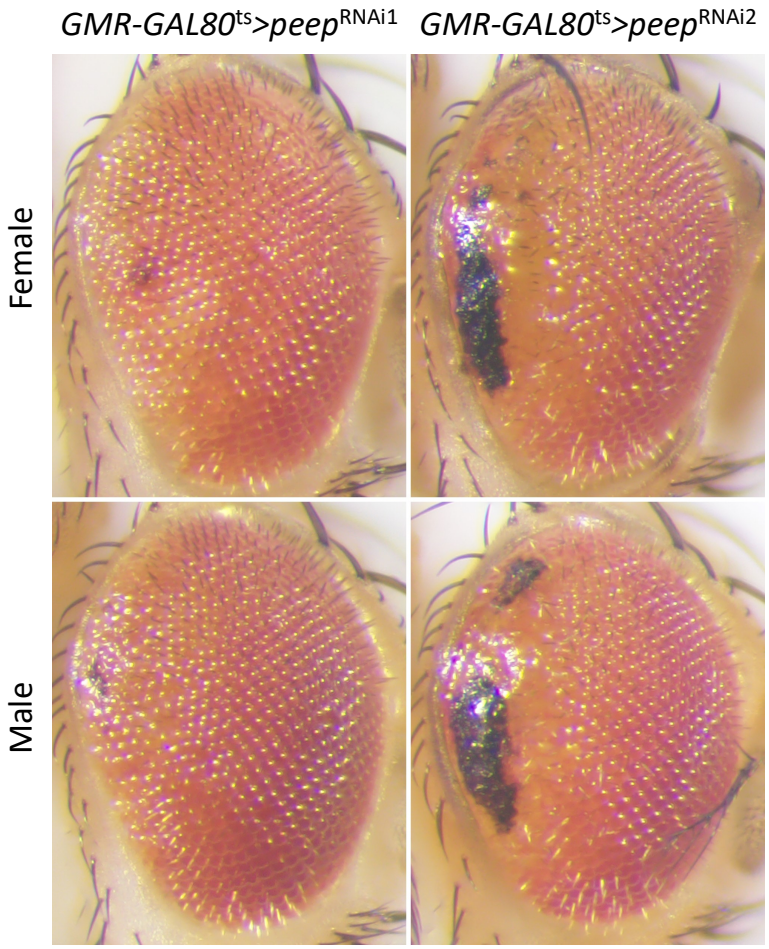

Figure 8.11. *GMR-GAL80*^{ts}-induced expression of *peep*^{RNAi1} resulted in minimal necrosis. Flies were raised at 27°C to induce expression of *peep*^{RNAi1}, and the area of necrosis was measured to determine whether co-expression of a 'survival factor' could rescue the *peep*^{RNAi} induced necrotic eye phenotype. As *peep*^{RNAi1} expression under these conditions was not sufficient to induce a high level of necrosis, quantitative analysis was only performed on eyes expressing *peep*^{RNAi2}. *GMR-GAL80*^{ts} = *GMR-GAL4,tub-GAL80*^{ts}.

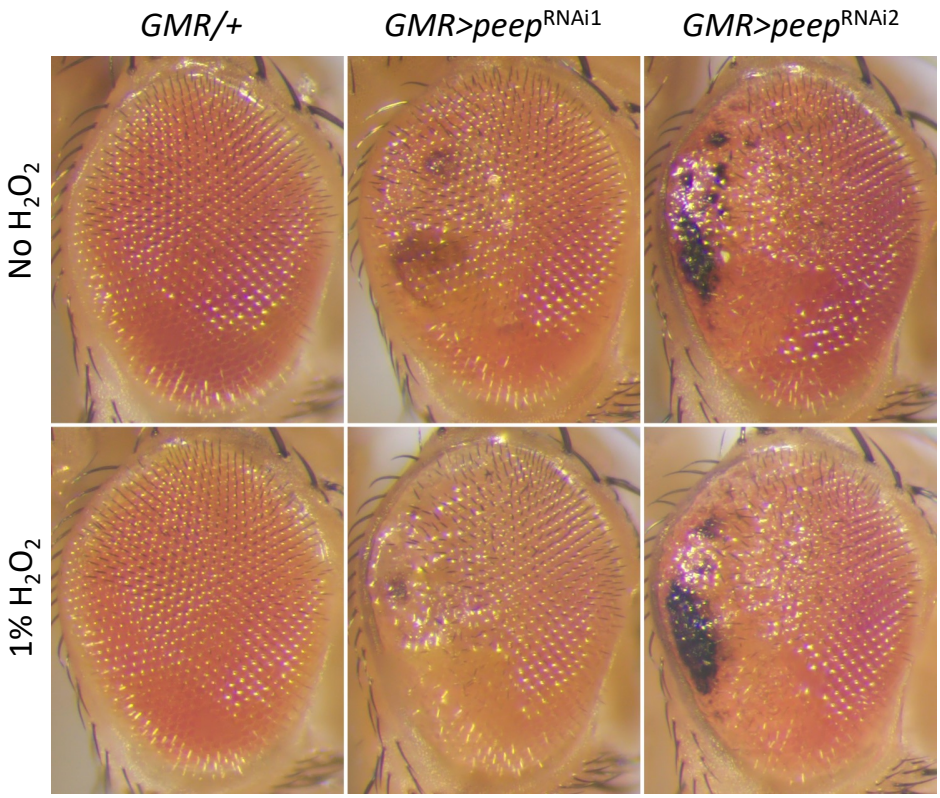

Figure 8.12. Exposure to H_2O_2 did not significantly affect the level of necrosis of escapers. When raised on standard fly media with no H_2O_2, *GMR-GAL4* expression of *peep*^{RNAi} resulted in a lower level of necrosis for *peep*^{RNAi1} compared to *peep*^{RNAi2}, as expected. Upon exposure to 1% H_2O_2 during development, this level of necrosis was unchanged from those adults that escaped pupal death. *GMR* = *GMR-GAL4*, *GMR/+* = Control.

8.8 Original western blot images

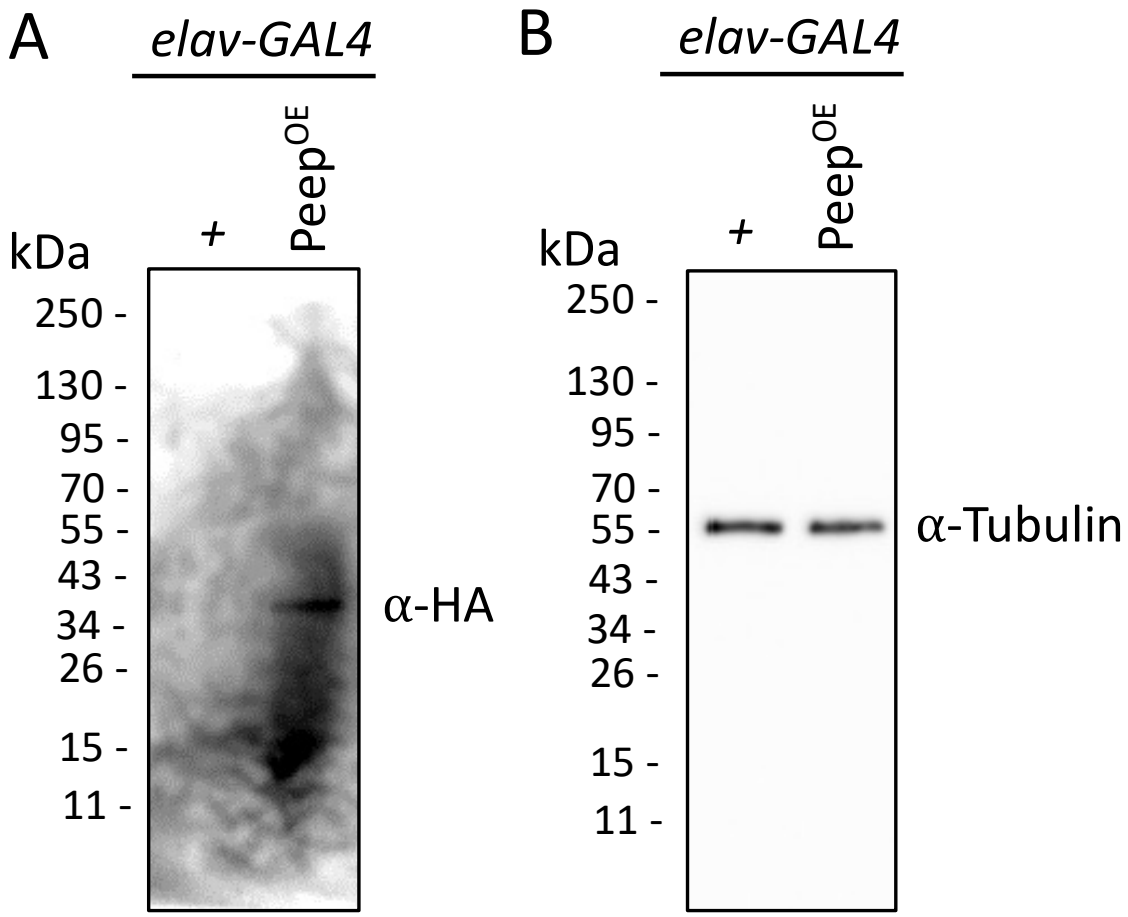

Figure 8.13. Original western blot verifying the Peep^{OE} construct. A. Confirming pan-neuronal expression of the HA-tagged Peep^{OE} construct at approximately 38 kDa. A total of 30 µg protein was loaded and B. Anti-Tubulin was used as a loading control and detected at 55 kDa.

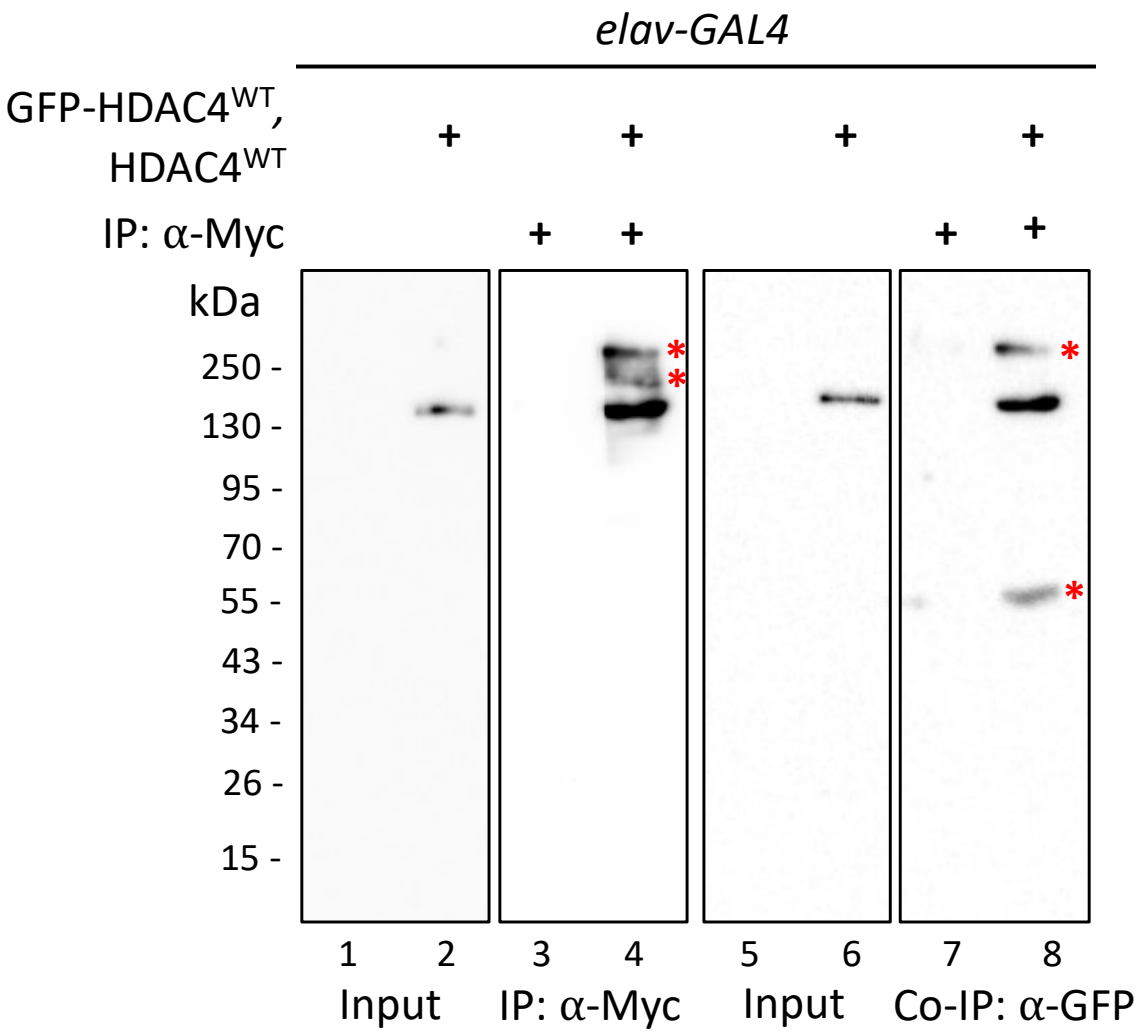

Figure 8.14. Original western blot of the co-immunoprecipitation of GFP- and Myc-labelled HDAC4^{WT}. C-terminal Myc-tagged HDAC4 and N-terminal GFP-fused HDAC4 were both overexpressed pan-neuronally with *elav-GAL4*. Immunoprecipitation using an anti-Myc antibody captured the Myc-tagged HDAC4 as observed when probing with anti-Myc (lane 4). Co-immunoprecipitation using anti-GFP identified GFP-HDAC4^{WT} which directly interacted with HDAC4^{WT}-Myc (lane 8). Immunoprecipitation samples were loaded alongside appropriate controls and 30 µg input samples. Lanes 1, 3, 5, and 7 were negative control lanes (*elav-GAL4/+*). Non-specific bands were observed in both immunoprecipitation samples (Asterix). IP = immunoprecipitation, Co-IP = co-immunoprecipitation.

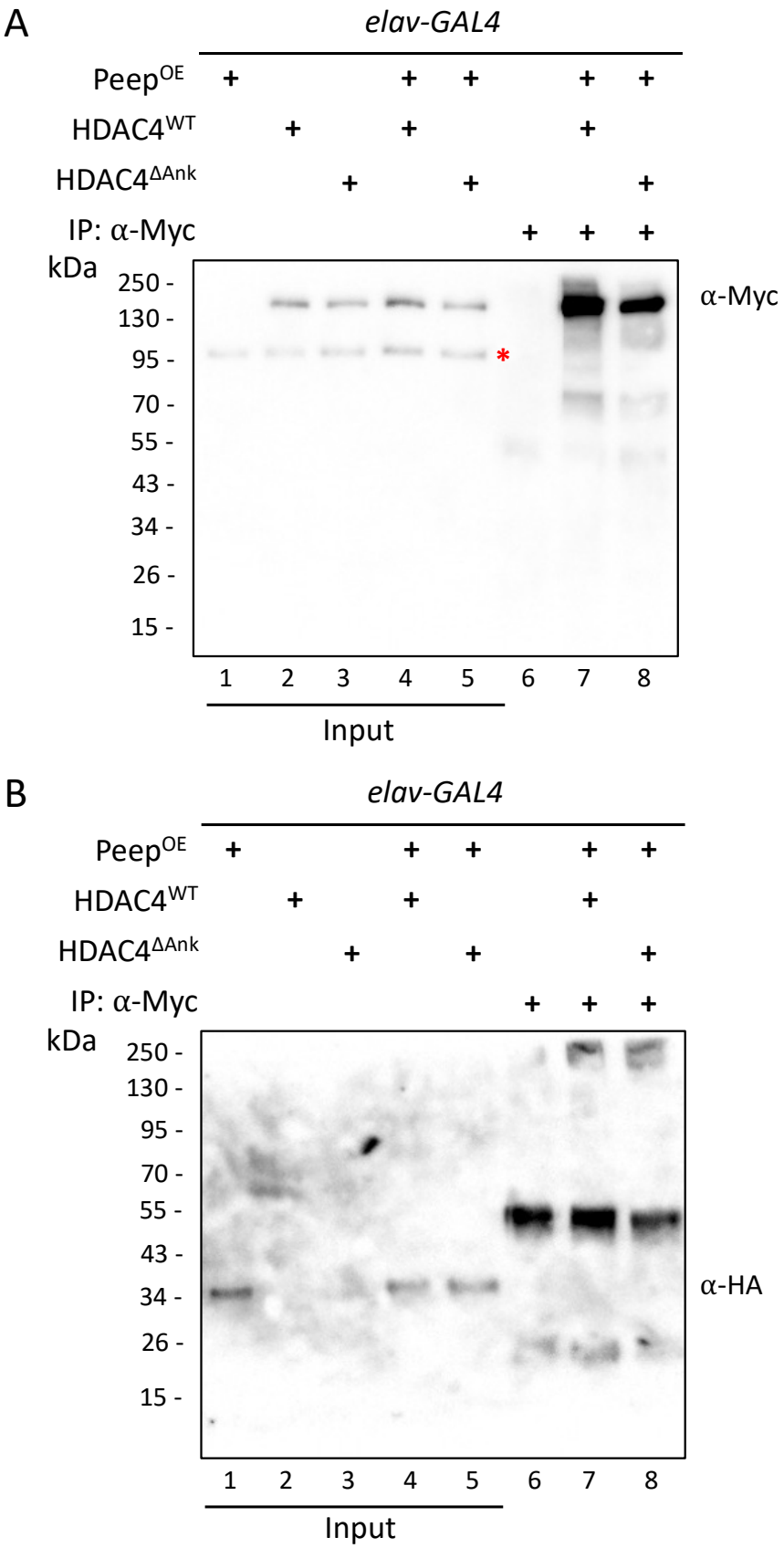

Figure 8.15. Original western blot showing Peep and HDAC4 do not interact via co-immunoprecipitation. Lysates were processed from pan-neuronal (*elav-GAL4*) co-expression of $Peep^{OE}$ and $HDAC4^{WT}$ or $HDAC4^{\Delta Ank}$. A. Immunoprecipitation was performed using anti-Myc to

capture HDAC4. Successful immunoprecipitation was observed when probing with anti-Myc (lanes 7 and 8) Immunoprecipitation samples were loaded alongside a negative control (lane 6, *elav-GAL4/+*) and 30 µg input samples (lanes 1-5). A non-specific anti-Myc band was detected in all input lanes (Asterix). B. An interaction between $Peep^{OE}$ and $HDAC4^{WT}$ was not observed upon probing with anti-HA (lane 7). Furthermore, co-expression of $Peep^{OE}$ and $HDAC4^{\Delta Ank}$ also did not show an interaction (lane 8). Immunoprecipitation samples were loaded alongside a negative control (lane 6, *elav-GAL4/+*) and 30 µg input samples (lanes 1-5). IP = immunoprecipitation.

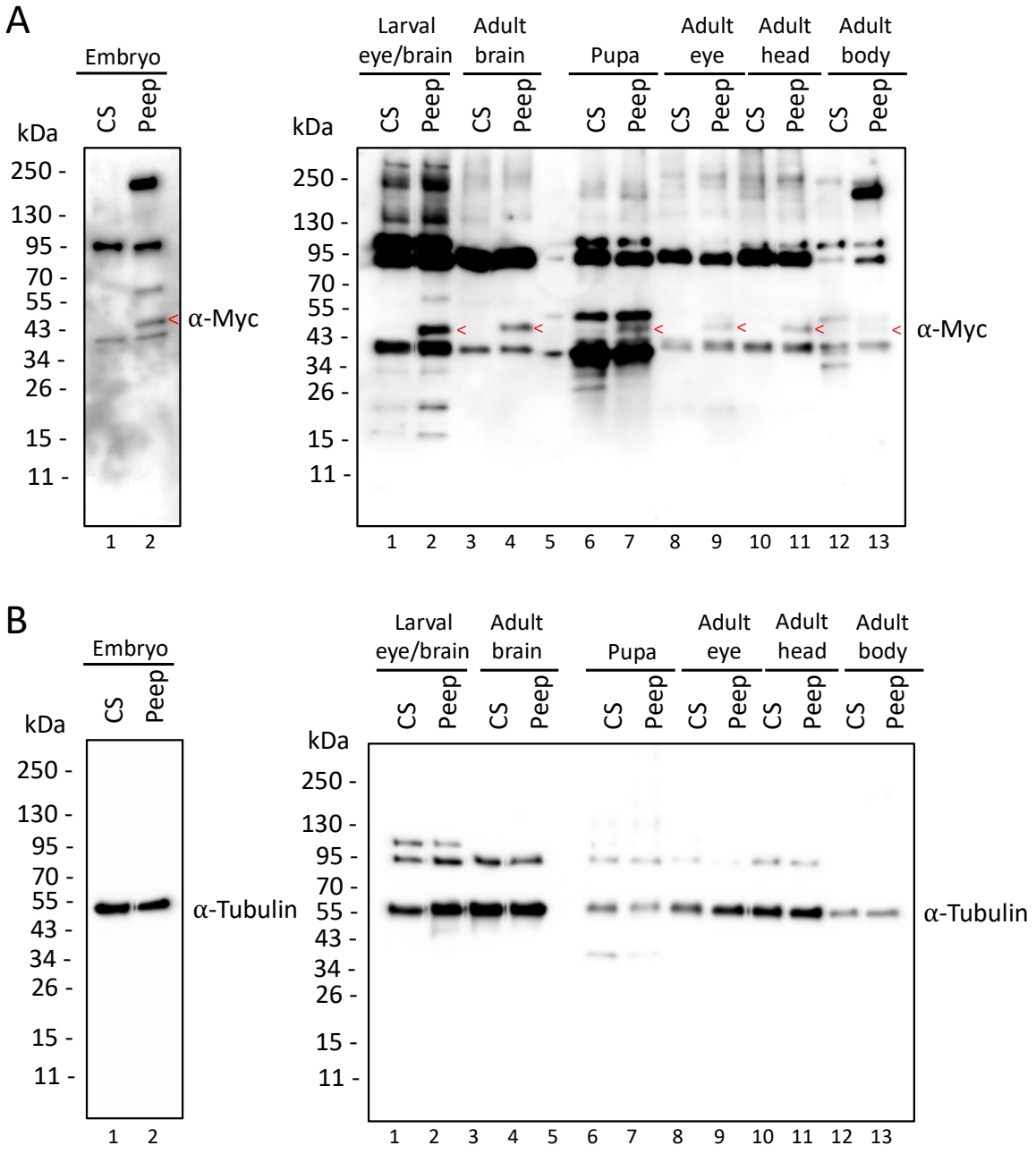

Figure 8.16. Original western blot showing endogenous expression of Peep. Peep-Myc was expressed using the endogenous *peep* promoter and showed low level of Peep expression in several tissues and developmental stages at approximately 47 kDa. A. On the left, Peep was expressed in the 0-2 hour embryo. On the right, Peep was expressed in the third instar larval eye/brain complex (lane 2) as well as the adult brain (lane 4) following isolation of dissected tissues. Lane 5 was a gap between samples. Peep was also expressed in the whole isolated pupa (lane 7), isolated adult eye (lane 9), isolated

adult head (lane 11) and body (lane 13) (red arrowheads). A total of 30 µg protein was loaded and B. Anti-Tubulin was used as a loading control and detected in all lanes at 55 kDa.

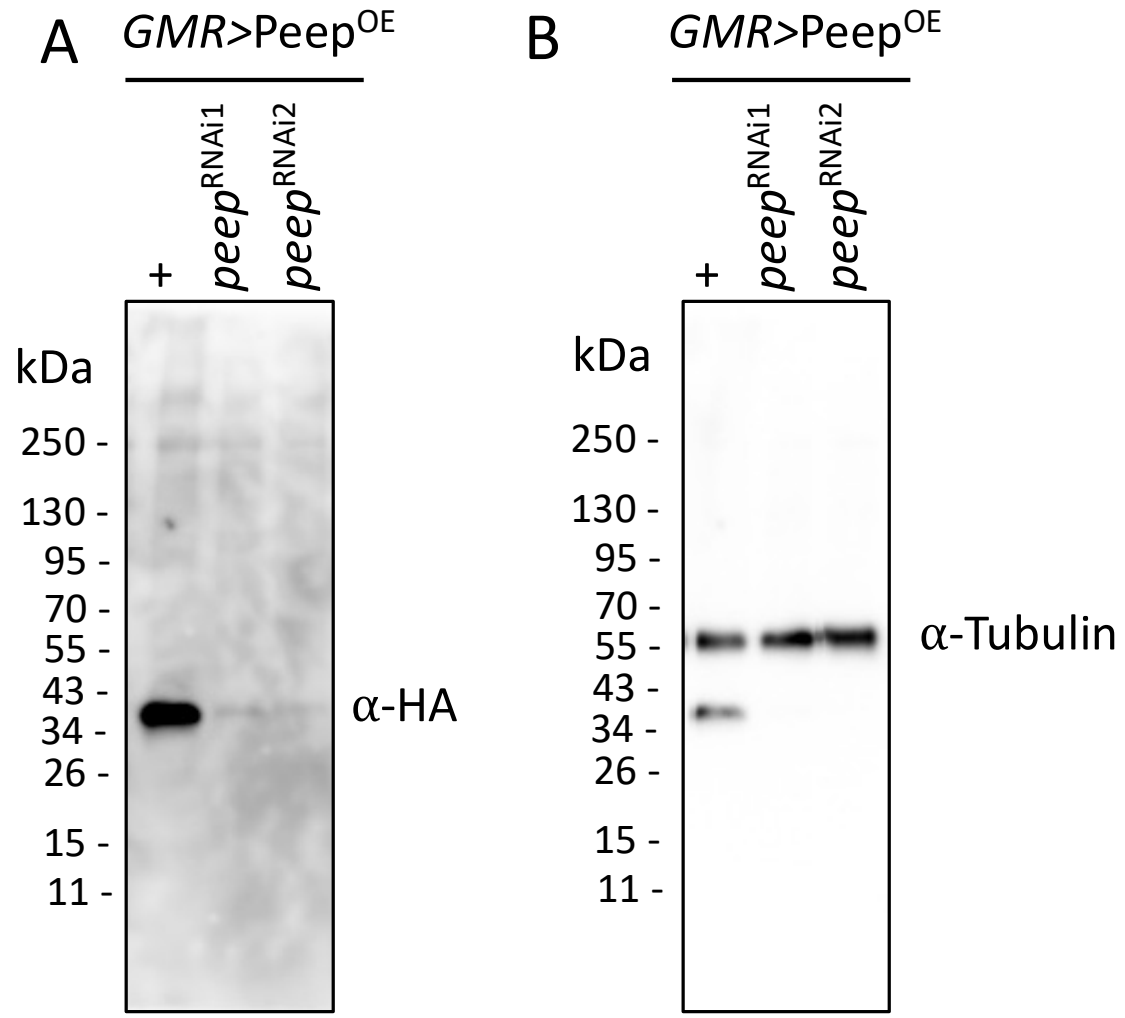

Figure 8.17. Original western blot showing *peep*^{RNAi} efficiently targets peep mRNA to decrease Peep protein levels. A. Western blot showing the efficiency of *peep*^{RNAi1} and *peep*^{RNAi2} to target and degrade HA-tagged Peep^{OE} in the *Drosophila* eye. A total of 30 µg protein was loaded and B. Anti-Tubulin was used as a loading control and detected at 55 kDa.